VALORIZATION OF BIOBASED FURFURALS BY CATALYTIC OXIDATIVE ESTERIFICATION

Dissertation

In partial fulfillment of the requirements for the degree of

Doctor rerum naturalium (Dr. rer.nat.)

At the University of Rostock

Faculty for Mathematics and Natural Sciences

Submitted by

Dipl. Chem. Abel David Salazar La Rosa

Born January 22nd 1990

In Caracas, Venezuela

Leibniz-Institute für Katalyse an der Universität Rostock

2020

Eidesstattliche Erklärung

Ich versichere hiermit an Eides statt, dass ich die vorgelegte Dissertation selbständig, ohne fremde Hilfe und ohne Benutzung anderer als die in der Arbeit angegebenen Hilfsmittel angefertigt habe.

Alle Stellen, die wörtlich oder sinngemäß aus veröffentlichen und nicht veröffentlichen Quellen entnommen wurden, sind ald solche in der Arbeit kenntlich gemacht.

Rostock, den 10.05.2020

_____

Abel David Salazar La Rosa

Die vorliegende Dissertation wurde von 04.04.2016 bis 30.07.2019 am Leibniz-Institut für Katalyse e.V. and der Universität Rostock unter Anleitung von Prof. Dr. Udo Kragl erstellt.

1. Gutachter: Prof. Udo Kragl, Universität Rostock
2. Gutachter: Prof. Johannes de Vries, Leibniz-Institut für Katalyse e.V.

Tag der mündlichen Prüfung: 15.07.2020

A mi madre, por hacerme la persona que soy

y por mostrarme el camino a seguir

"If you thought that science was certain – well,

that is just an error on your part."

Richard P. Feynman

Acknowledgements

Abstract

5-Hydroxymethylfurfural (HMF) has become a benchmark chemical as it can be obtained by the processing of renewable biomass, making its downstream modification an important topic both in industry and academia. Finding catalytic processes for the selective derivatization of HMF is challenging due to its reactivity, hence mild conditions are needed. Here is reported the selective oxidative esterification of HMF to methyl 5-(hydroxymethyl)furan-2-carboxylate and to dimethyl furan-2,5-carborxylate (FDCM) under mild conditions using oxygen (from air) as oxidant (in batch). A synergetic effect between the used catalysts, cobalt oxide over nitrogen-doped carbon, and ruthenium over carbon catalysts was observed by catalytic and electron paramagnetic resonance measurements. Kinetic analysis revealed a first order dependence on substrate for the cobalt catalyst and an apparent zero order for the ruthenium catalysts. The conversion rates were improved by the use of a perfluoroether as solvent, proving that the oxygen diffusion is the limiting factor in the system.

To run a continuous flow reactor and due to technical problems, a new series of nitrogen doped bimetallic Co/Ru heterogeneous catalysts had to be prepared. Two different supports were used. XRD, XPS and BET measurements showed that porosity of the materials and order of impregnation of metals to the carbon substrate lead to materials with different catalytic activities. Co_xO_y-N + RuO_x-N@C-irregular, which showed a mesoporous character, was the most suitable catalyst; achieving 98% conversion of HMF with selectivity of 57% to FDCM was obtained.

The synthesis of a new type of furan-based monomers was studied. Coupling of HMF and diols was made through NHC catalysis, more specifically by oxidative esterification. Catalysts, base, oxidant and solvent screening was made. NHC catalyzed upgrade of HMF proved to be challenging; the results and mechanistic studies suggest that different mechanisms operate at the same time, therefore control of the reaction is a difficult task. 6-hydroxyhexyl 5-(hydroxymethyl)furan-2-carboxylate was synthesized with 28% isolated yield and 6-hydroxyhexyl 5-methylfuran-2-carboxylate could be identified as a side product. A mechanistic proposal is made showing the cooperative catalysis between the NHC catalyst and the MnO_2. The formation of the side product is mostly due to the possible formation of a manganese ester. In the esterification of furfural, the reaction mechanism showed a dependence to the atmosphere used; oxygenative and oxidative mechanisms were identified. Esterification of benzaldehyde showed that electron withdrawing substituents on the aromatic ring foster the reaction also dependence on the alcohol used.

Exploring experiments on NHC catalyzed amidation of aldehydes showed, in general, low yields. In the case of primary amines, amidation and condensation to imines are competitive reactions. Tetrahydroisoquinoline as substrate gave the best amide yield (75%), on the contrary to pyrrolidine (0%), a secondary amine reduces suppress the formation of imine by condensation.

Table of contents

List of Schemes

List of Figures

List of Tables

List of Graphics

List of Abbreviations

Ac	Acetyl-
Bn	Benzyl-
Boc	Tert-butyloxycarbonyl
Bz	Benzoyl-
DBU	1,8-Diazabicyclo[5.4.0]undec-7-en
DCM	Dichloromethane
DMPO	5,5-dimethyl-1-pyrroline N-oxide
EG	Ethyleneglycol
El	Electrophile
ETM	Electron transfer mediator
EtOH	Ethanol
FDA	Food and Drug Administration (U.S. Federal Agency)
FDCA	2,5-furandicarboxylic acid
FDCM	dimethyl-2,5-furandicarboxylate
HMF	5-Hydroxymethylfurfural
iPrOH	Isopropanol
Me	Methyl-
MeOH	Methanol
Mesitylene	1,3,5-trimethylbenzene
MPBF	Methoxyperfluorobutane
nBuOH	1-Butanol
NHC	N-heterocyclic carbenes
Nu	Nucleophile
Ox.	Oxidant
PBF	Poly (1,4-butylene 2,5-furandicarboxylate)
PBT	Poly (1,4-butylene terephthalate)
PEF	Polyethylene furanoate
PET	Polyethylene terephthalate
PFC	Perfluorinated compounds
Piv	Pivaloyl-
SET	Single electron transfer
TBS	Tert-Butyldimethylsilyl-

TEMPO	(2,2,6,6-tetramethylpiperidin-1-yl)oxidanyl
THP	Tetrahydropyranyl
TPA	Terephtalic acid
Trityl	Triphenylmethyl-

1 Introduction

1.1 Need of biomass-based chemistry

The main task of basic chemical industry is to produce a broad range of raw materials that can be used to make consumer goods. Normally these raw materials are low-value chemicals with relatively simple structure, which are known as building blocks or platform chemicals. Traditionally the petrochemical industry has been the major provider of them. Crude Oil is rich in hydrocarbons and has a rather constant composition, from which after cracking and distillation a variety of platform chemicals can be obtained. Obviously, the petrochemical industry is much more complex and has his own challenges.[1]

The limited supply of fossil resources[2] forces us to find new ways toward fuels, energy and chemicals which are all part of our everyday life. In the past years, societal concerns about the changes of the ecosystem as a consequence of human activities have become an important topic.[3,4] Sustainability and ecological impact are today important criteria to achieve green engineering processes. Oil is a non-renewable resource, or at least not in the way that it can sustain the demand of it. The oil that is being consumed today took several hundred thousand of years to be formed. Due to the fast depletion of fossil resources biomass feedstocks are gaining attention. There is a constantly growing interest on biomass treatment and processing, which is reflected in the number of publications per year (see Graphic 1.1).
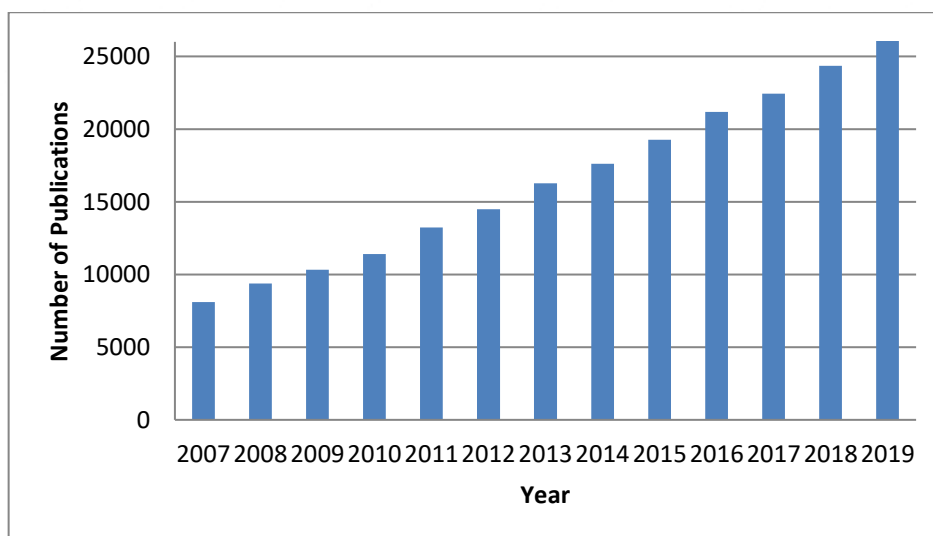
Graphic 1.1. Number of publications per year with the keyword biomass, as registered by Web of Science.

1.2 Circular economy

As a result of the growing environmental concerns, in December 2014 the European Commission withdraw a legislative proposal on waste, that was replaced next year with a more broad package which would cover not only waste reduction targets but also the full economic cycle; a proposal for circular economy.[5]

In comparison, a linear economy ignores the environmental impacts inherent to resource consumption and waste disposal, having therefore too much virgin extraction, pollution and waste. It starts with extraction of raw materials and ends in disposal of the goods once they reach their lifetime. Circular economy considers the environmental impact of resource consumption and waste disposal, creating a closed loop in which the resources move on (see Figure 1.1). The goal of a circular economy is to optimize the use of raw materials by reusing them after collecting them from used goods. This reduces the extraction of non-renewable materials (e.g. oil, precious metals, etc.), reduces pollution and waste. Nowadays the concept of circular economy is becoming the benchmark of sustainable development.[6]

Figure 1.1. Regenerative cycle for a Circular Economy.

1.3 Biorefineries

Therefore, the concept of biorefineries becomes valuable and a challenging strategy to reduce the impact of human activities in the environment, related to the chemical industry and its associated production chains. There is a huge variety of feedstocks for biorefineries. Grass and green plants, starch crops, sugar crops and grains for ethanol production; Oilseed crops and oil plants for vegetable oils and biodiesels; and finally forest harvesting residues, barks, sawdust, pulping liquors, fibers, agricultural wastes, crop residues, urban wood wastes and industrial organic wastes can be used in the production of fuels, energy, chemicals and materials.[7]

The term "waste" used by biorefineries refers to the secondary organic material left after the removal of the primary material, the original reason for which the plants were grown (e.g. rice straw, wheat straw, sugar cane bagasse, lignin from paper pulping, etc.). Almost all the waste has some value and is being used, for example to improve the soil in the fields or as fuel for power generation. But there is room to get higher value via conversion to chemicals.[8, 9] In comparison to oil as raw material for chemical production, biomass is a highly functionalized source of chemicals. Such functionalization is because it contains a high amount of oxygen (31-50 wt.%).[10, 11] Also sulfur content is lower (up to 0.13 wt.% in wheat straw)[12] in biomass than in oil (above 1.3 wt.% in OPEC-members).[13] A lower sulfur content means that potential sulfur emissions to the environment are reduced, hence, desulfurization methods might not be necessary and less investment is needed.

1.3.1   Lignocellulose

Here, non-edible lignocellulosic biomass, such as waste from agro and paper industry, constitutes a huge alternative resource.[14, 15] It is quite resistant to degradation under biological conditions, and it accumulates when other components of the plant are used as food, fodder or other applications. Its resistance to degradation is due to the lignin present in the structure, which forms a barrier that hinders the access to cellulose and hemicellulose, the source of sugars.[16, 17]

A wheat plant can be used as an example, in which only the spike contains the edible part. And it is also not completely edible. After the harvest, the roots and a small part of the stem remain in the soil. Most of the stem and the leaves are the main residues from harvesting wheat. And it contains from 65 to 89% of cellulose, hemicellulose and lignin combined.[18]

As mentioned before; cellulose, hemicellulose and lignin are the main components lignocellulosic biomass (See Figure 1.2). From the biologic point of view these are the components

of the cell walls of plants; and are present in a 4:3:3 ratio respectively. The ratio changes from plant to plant, and also depends on the function of the plant cells. Lignin content determines the hardness of the cell wall. From the chemical point of view, all three components are polymers; cellulose is independent from the other two, but hemicellulose and lignin are chemically bonded to each other. Cellulose is a linear polymer of D-glucose units (C6-sugar)[19], while hemicellulose is more complex; it can contain D-Xylose, D-Mannose, L-Arabinose, L-Galactose (C5 and C6-sugars) and glucuronic acid (glucose derivative) bonded in a nonlinear fashion.[20] On the other side, lignin is a polymer of phenylpropanoid derivatives bonded through ether bonds, giving it special characteristics.[21]
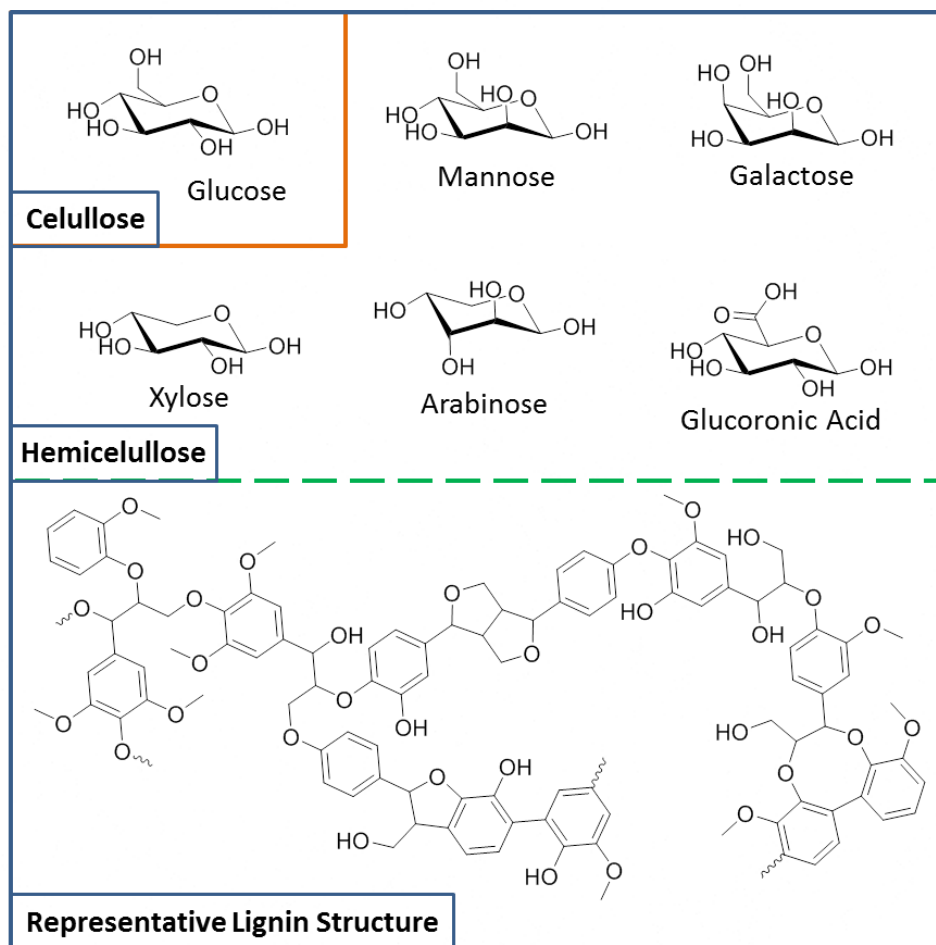
Figure 1.2. Main components of lignocellulose.[20, 21]

Unlike in traditional sugars sources (e.g. starch, sugar beets and sugarcane), the sugar precursors in lignocellulose are shielded by a matrix of lignin which complicate recovering them. The paper industry has dealt with this issue for long time[22], and several pulping methods were stablished with the goal to recover high quality cellulose. The Kraft[23], Sulfite[24], Alkaline[25] and Klason[26] process are

typical example of these methods, which heavily modify the structure of lignin by the extensive use of inorganic salts, base, or acid.

With the years, the potential in lignin as a source for aromatics was taken into account and more processes with mild structural modifications to lignin have been developed. The Björkman process[24], ionic liquid treatment[27] and the organosolv process are examples of them. The last one received more attention lately because is environmentally friendlier than the traditional pulping methods, it is easily tunable in terms of solvents (or mixtures) used, conditions (pressure, temperature, etc.); and also catalysts can be added to it.[28] Lignin has a huge potential for valorization, and its depolymerization represents a big challenge.[21, 29-33]

A lignocellulose based biorefinery must deal with several processes in different levels (see Scheme 1.1); the first will be breaking apart lignocellulose and isolate its main components. The second; depolymerization of cellulose and hemicellulose into sugars, and lignin into aromatic compounds. The third, processing of sugars into bulk chemicals. Depolymerization (hydrolysis) of cellulose to glucose can be performed under acidic conditions, as reported by Lavoie et al.[34] Hemicellulose hydrolysis is performed in similar conditions but leading to other sugars.[35]

After depolymerization of cellulose and hemicellulose, acidic dehydration of C6 and C5 sugars leads to the formation of 5-hydroxymethylfurfural (HMF, **1**) and Furfural (**2**) respectively.[36, 37] A lack of control in the previous reaction can lead to repolymerization of the desired products and form humins.[38]
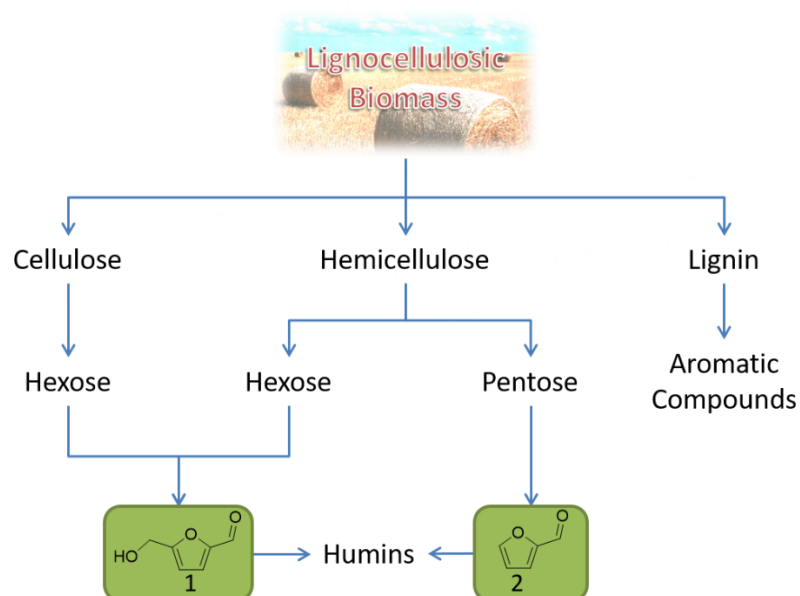
Scheme 1.1. Lignocellulose fractionation.[15]

1.4 5-Hydroxymethylfurfural

Furan compounds have been part of the human diet since humans started cooking their food. 5-Hydroxymethylfurfural (HMF, **1**) is formed during the thermal decomposition of carbohydrates (sugars) as an intermediate during caramelization[39] and in Maillard reactions[40, 41] HMF is formed as an intermediate. Studies show that HMF has positive pharmacological activity. Wei et al. reported the anti-inflammatory activity by inhibitory effects of nitric oxide and inflammatory cytokines production.[42] Also, protective effects against acute hypobaric hypoxia were demonstrated by Fan et al.[43] In vitro antioxidant activity have also been reported by Kim et al.[44] Although these and other several reports show the benefits of HMF, also cytotoxic activity at high concentrations is known and there is no consensus in the scientific community on what the tolerable daily intake should be, making it unclear if exposure to HMF represents a potential health risk.[45-48]

1.4.1   HMF synthesis and mechanism

HMF have been identified as a key intermediate for the transition from fossil-based to bio-based industrial chemistry.[49] There is increasing effort going on in the academic community focused on the synthesis and further modification of HMF, as it's reflected by the increasing number of publications per year (see Graphic 1.2). Dehydration of sugars is the most common way to synthesize HMF, and through the years different methodologies have been developed.[50]
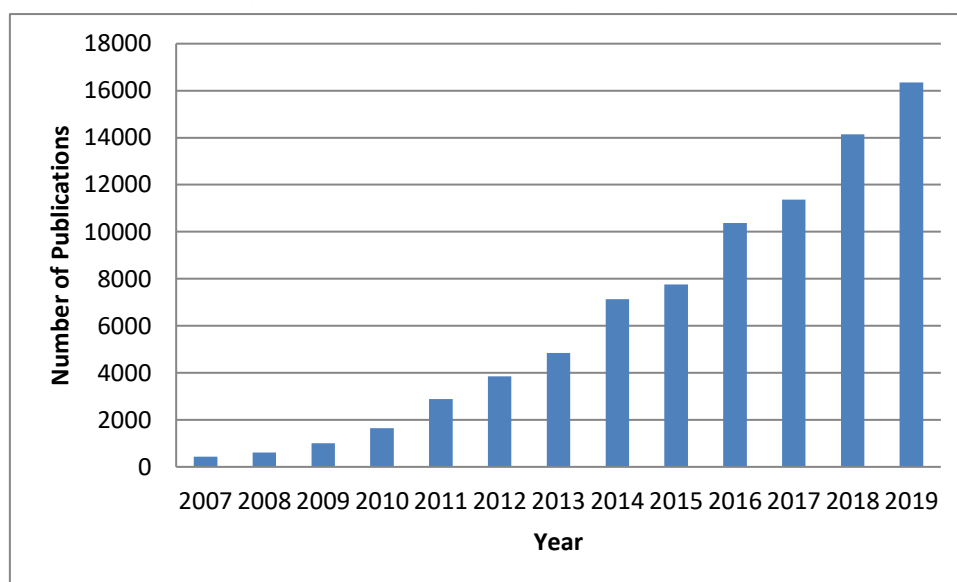
Graphic 1.2. Number of publications per year with the keyword 5-Hydroxymethylfurfural, as registered by Web of Science.

For a hexose to convert into HMF it must lose three water molecules. Two general mechanisms have been proposed, one in which the intermediaries are cyclic and other in which they are acyclic.[51] Riisager et al. proposed a mechanism for HMF synthesis promoted by boric acid in imidazolium chlorides. The mechanism starts with the isomerization of glucose to fructose followed by dehydration (see Scheme 1.2).[52]
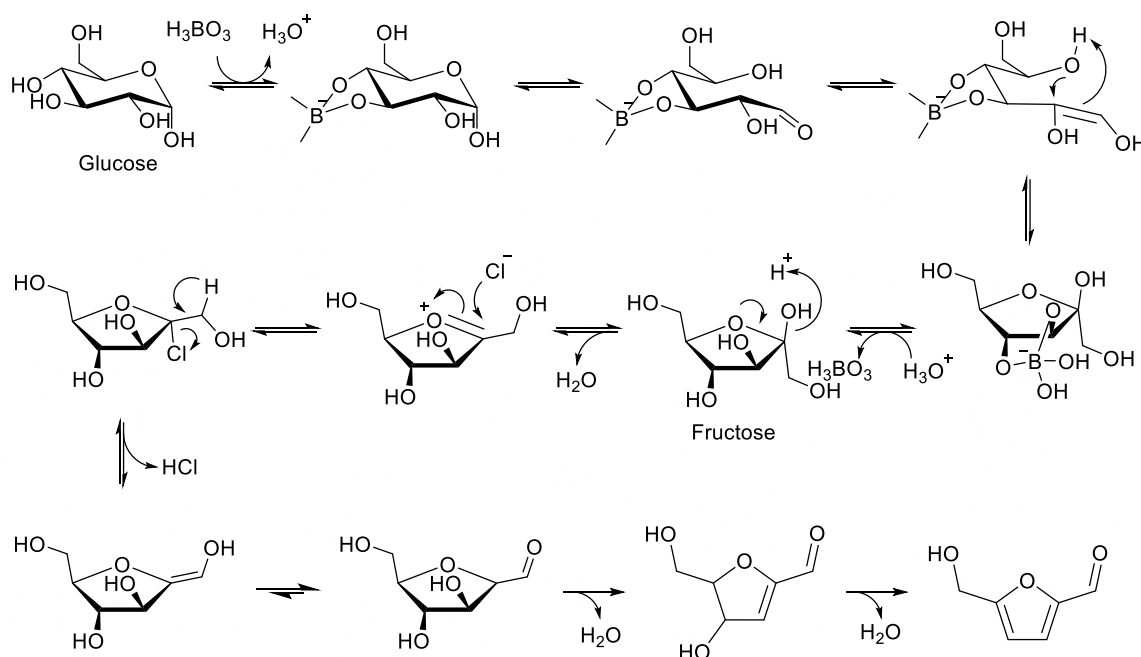
Scheme 1.2. Proposed mechanism for the boric acid promoted isomerization/dehydration of HMF.[52]

Moreau et al. proposed a mechanism for the dehydration of fructose over H-mordenites in which they observed the presence in small amounts of glucose and mannose. They attribute this to the intermediary 1,2-enediol from which both glucose and mannose isomerize to fructose. The same intermediary suffers the first dehydration to form 3-Deoxyhexosulose, which by further dehydration forms HMF and Furfural. Furfural is formed when a fast reverse-aldol cleavage occurs to an intermediary previous to the last dehydration step (see Scheme 1.3).[53]

Both cyclic and acyclic mechanism have been proposed as the most probable, but there is no consensus in the academic community about which one is the most plausible.[54] One clear thing is that fructose is the best starting substrate for the formation of HMF in terms of yields. In the calculations made by Nair et al. they support this assumption. The dehydration process is highly influenced by interactions with the solvent, and that is related to the intra and intermolecular hydrogen bonds formed between the intermediaries and the solvent. This plays an important role

and influences the mechanistic pathway of the reaction. They also conclude that a catalytic system that promotes glucose isomerization to fructose is ideal for HMF synthesis from glucose.[55]
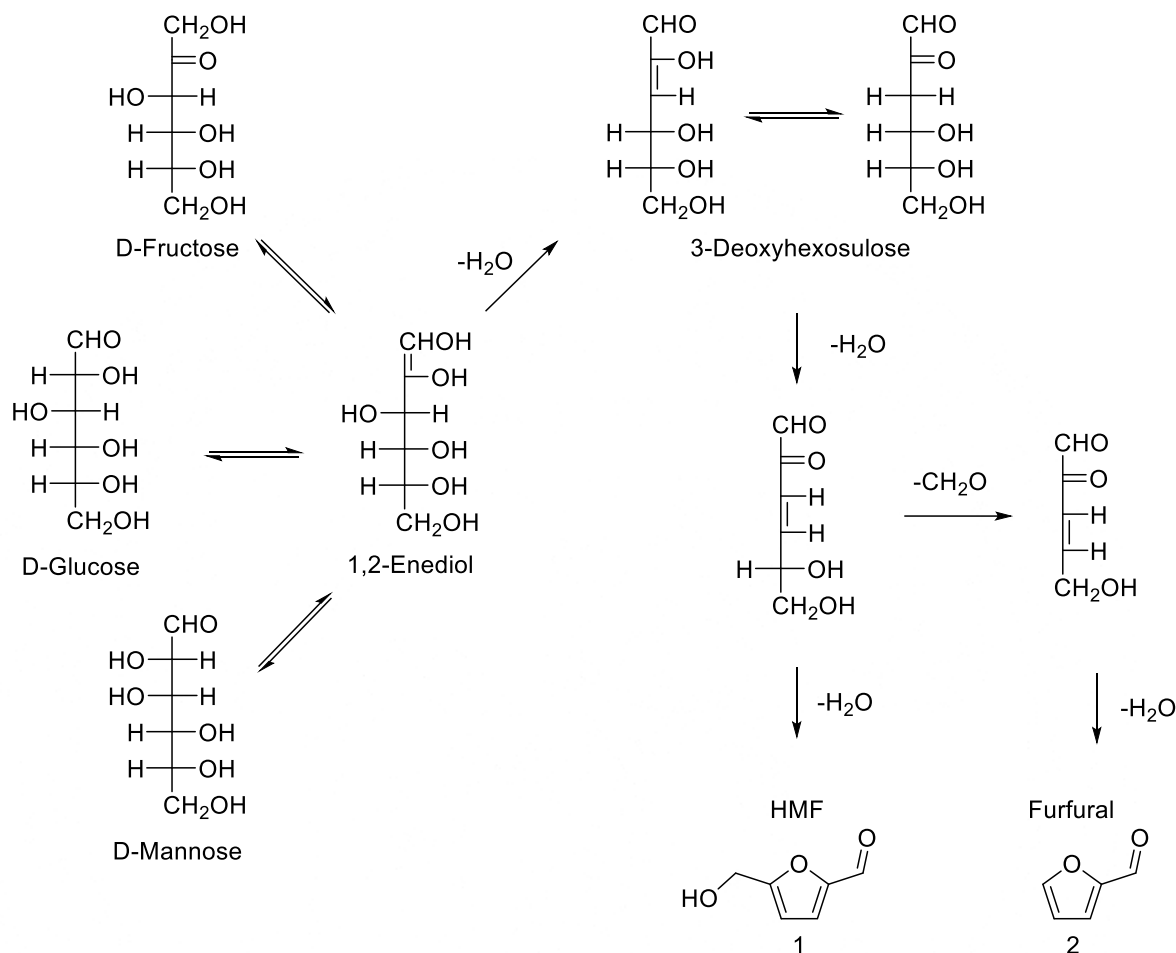
Scheme 1.3. Acyclic dehydration mechanism proposed by Moreau et al.[53]

HMF is unstable in low and high pH, at acidic conditions it repolymerize to form humins[56] and in alkaline, due to the Cannizzaro mechanism, the aldehyde functionality is lost by disproportion to form alcohols and acids.[57, 58] Also its oxidation derivatives show pH sensitivity.[59] HMF thermal degradation was reported by Nakajima et al. in which by heating HMF at 200 °C for 2 hours resulted in more than 80% decomposition.[60]

1.4.2   HMF as building block

HMF has become an important building block for a wide range of applications. It is the starting molecule for the furan-based polymer family[61] and also for other monomers like adipic acid, 1,6-hexanediol, caprolactone, caprolactame, etc. (See Scheme 1.4).
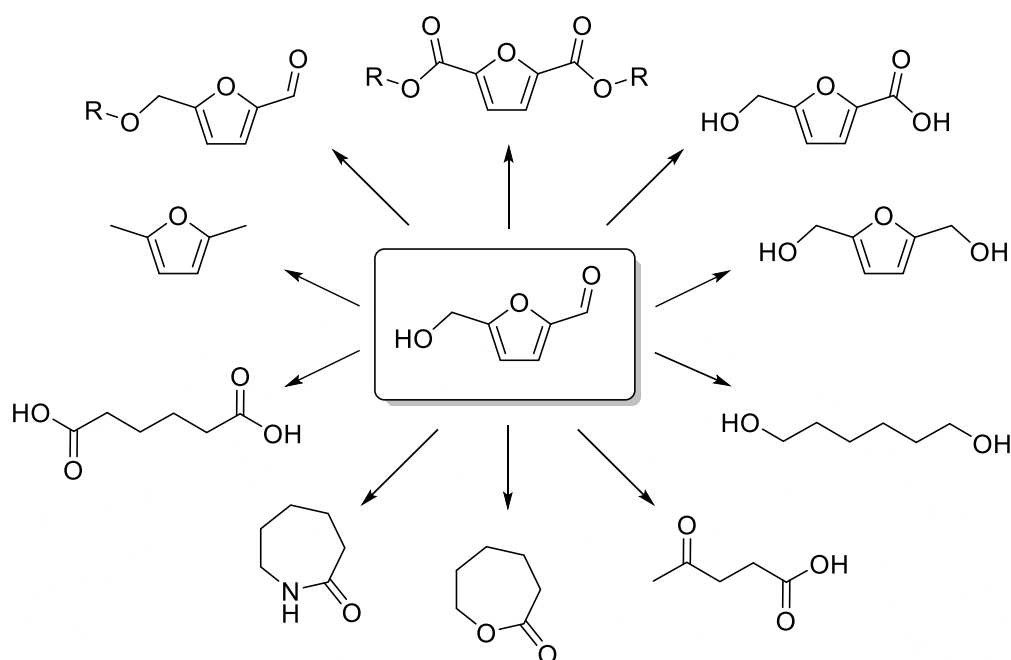
Scheme 1.4. HMF as platform chemical.[50]

HMF can be modified in two main different ways, modifications to the side groups and to the furan ring, which produces intermediaries for different applications. Reduction of it is one of the most studied reactions, since removal of oxygen is important to access to high performance fuels, new diol monomers and solvents. Oxidation of HMF to 2,5-furandicarboxylic acid (FDCA) and production of other monomers is important to material science applications because it provides the source of new polymers. Also different functionalization processes have been studied, like aldol reaction, nucleophilic additions, OH group modifications, reductive amination, ring transformations, C-H activation, preparation of MOFs and others.[50, 62]

1.4.2.1   *Reduction*

Reduction of HMF can be controlled and performed selectively (see Scheme 1.5). The synthesis of dihydroxymethylfurfural (**3**) (see Scheme 1.5 A) can be made by reduction under hydrogen atmosphere and a Ru@C catalyst at 150 °C.[63] It can also be synthesized by transfer hydrogenation using isopropanol as hydrogen source using a Cp*Ir(pyridinesulfonamide)Cl complex under base free conditions at 85 °C.[64] Reduction with stoichiometric NaBH$_4$ results in an almost quantitative yield.[65]
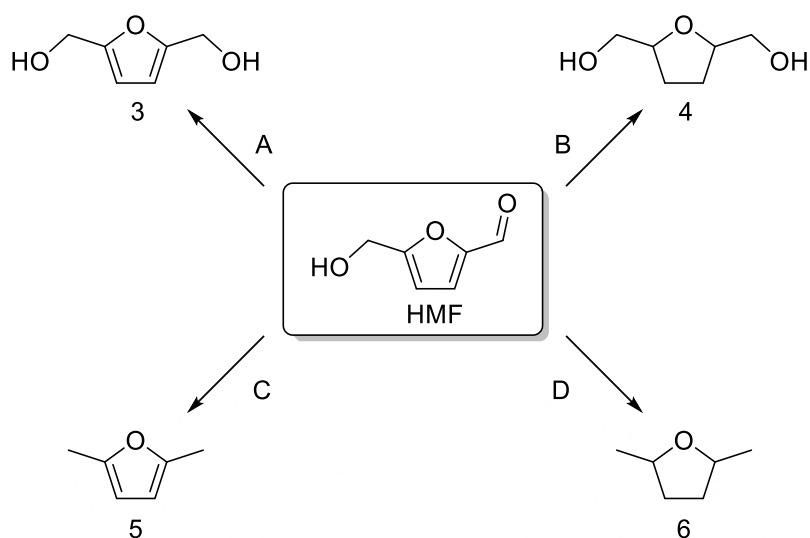
Scheme 1.5. Reduction of HMF

Reduction to dihydroxymethyltetrahydrofuran (**4**) (see Scheme 1.5 B) is achieved by reduction in hydrogen atmosphere at 50 Bar using Raney-Ni with methanol as solvent (62% yield).[66] Ruthenium catalysts have been used in different ways obtaining low to moderate yields (10-50%).[67,68] In a similar fashion Pd@C as catalyst, under hydrogen atmosphere at 80 Bar, water as solvent and temperature up to 180 °C yielded 96% of the desired product.[69]

Several systems using different catalysts have been reported for the synthesis of dimethylfuran (**5**) (see Scheme 1.5 C). Gorte et al. reported the hydrodeoxygenation of HMF using NiCu nanocrystals supported on carbon, 33 bar of hydrogen, isopropanol as solvent, at 180 °C under flow conditions with high conversion (>99%) and selectivity (>95%).[70] Kim et al. reported the one pot conversion of monosaccharides to dimethylfuran using Pd loaded Zr-MOF on sulfonated graphene oxide. The reaction starts with the isomerization of glucose to fructose, further dehydration to HMF and hydrogenation/hydrogenolysis to yield up to 45,3% dimethylfuran. When fructose was used as starting material, a maximum yield of 70,5% was achieved.[71] Rauchfuss et al. reported a tunable system in which dimethyltetrahydrofuran (**6**) can be obtained by reduction using Pd@C in up to 95% yield (see Scheme 1.5 D).[72]

Both **3** and **4** are used as monomers for polymers.[73] **5** is used in the biomass based production of the oil based Terephthalic acid for the production of polymers (e.g. PET).[74-76] **6** as a biobased fuel, which is superior to ethanol and has many of the desirable properties found in petroleum derived compounds.[77]

1.4.2.2   *Oxidation*

Oxidation of 1 to FDCA (**7**) represents the most studied reaction so far, because **7** is the main monomer to produce furan based based polymers. And as with the reduction, **7** and several intermediaries of oxidation can also be synthesized selectively (see Scheme 1.6). **7** and its oxidation intermediaries are mainly used as monomers in polymer research.[61, 73, 78-84]
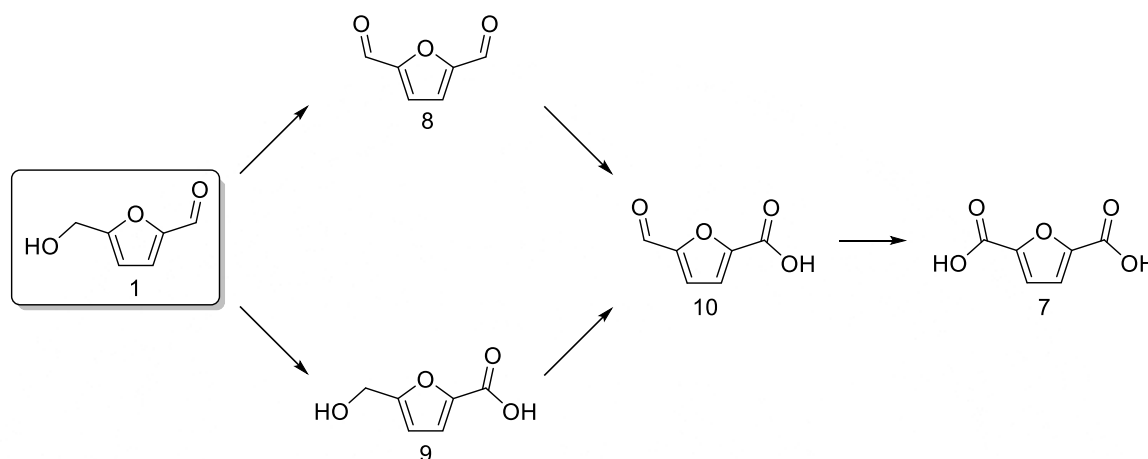
Scheme 1.6. Synthetic route pathway for the obtention of HMF through oxidation

Diformylfuran (**8**) is one of the first intermediaries formed in the oxidation pathway. Iborra et al. reported its selective synthesis with quantitative yields using a Fe-MOF in the presence of TEMPO as cocatalyst and $NaNO_2$ as additive.[72] Photoelectrocatalytic oxidation of HMF using TiO_2 modified electrodes, water as a solvent, oxygen as oxidant and UV light; with 40% yield to the desired product was reported by Yurdakal et al.[85] It is also possible to synthesize by oxidation with MnO_2 in toluene under reflux with up to 97% yield.[86]

Hydroxymethylfuroic acid (**9**) is another one of the first intermediaries. De Jongh et al. synthesize it with 93% yield using gold nanoparticles supported on high-surface area graphite, 10 bar of oxygen, water as solvent and $NaHCO_3$ as additive at 90 °C.[87] Li et al. developed whole-cell biocatalytic a selective approach using HMF-tolerant C. testosterone SC1588 cells in aqueous phosphate buffer a 30 °C, with up to 90% yield.[88] On the other side, the same group reported an enzymatic procedure in which they use horse liver alcohol dehydrogenase, hydrogen peroxide as oxidant in an aqueous phosphate buffer at 30 °C with 81% yield to hydroxymethylfuroic acid.[89]

Formylfuroic acid (**10**) is the last oxidation intermediary before FDCA formation. Wu et al. reported a system using Ru@C as catalyst, hydrogen peroxide as oxidant, using water as solvent and $NaHCO_3$ to synthesize formylfuroic acid with up to 92% yield.[90] Dibenedetto et al. proposed a

system using a mixture of MgO.CeO$_2$ using water as a solvent, 9 bar oxygen at 130 °C to obtain the desired product in up to 89% yield.[59] Liu et al. reported a enzymatic system in which a magnetic laccase catalyst in combination with TEMPO as mediator on an aqueous acetate buffer produce FFCA in 77% yield.[91]

1.4.2.3   *Other reactions*

Protection of HMF functional groups have been performed and reported, in order to achieve different synthetic transformations. Protection of the –OH group has been made with common groups like, Ac, TBS, Bn, trityl, THP, Boc, Bz, Piv and Me.[92-94] Protection of the carbonyl group with diols is common.[95] Also direct etherification of HMF under reductive conditions to yield bisalkoxymethylfuranes has been reported.[96]

As previously mentioned, HMF have been used as an electrophile in the aldol reactions as a way to increase the length of the carbon backbone chain to achieve higher hydrocarbons (see Scheme 1.7).
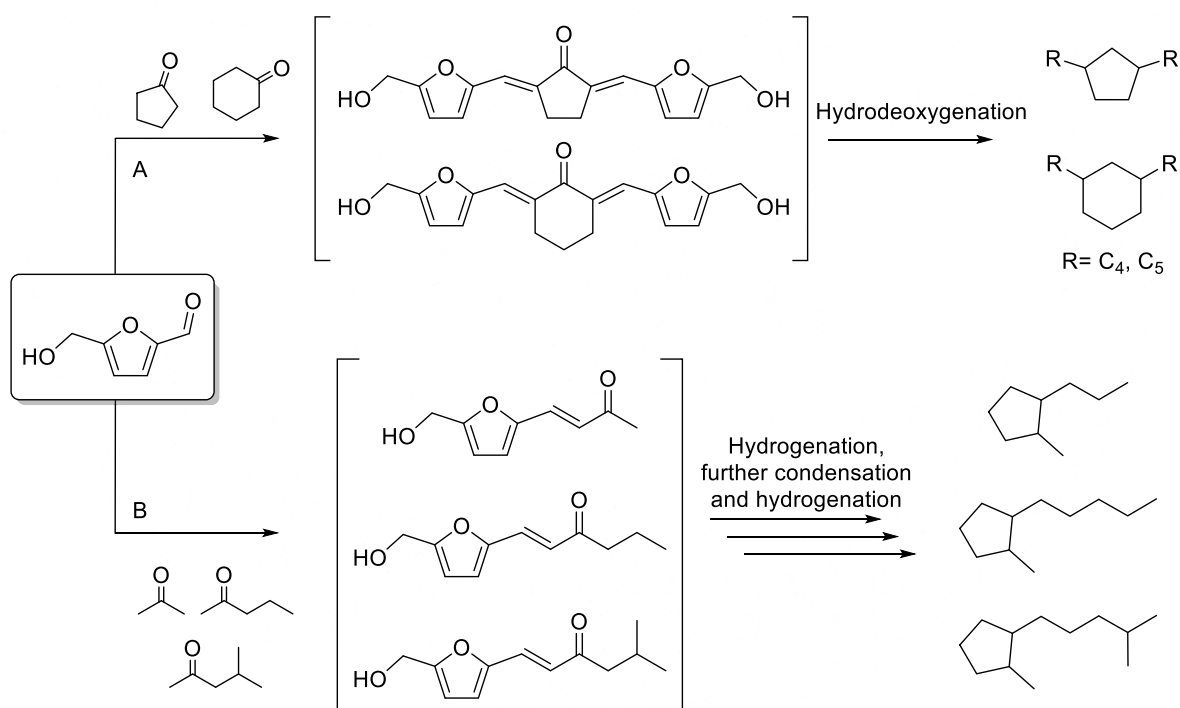
Scheme 1.7. Aldol condensation of HMF and ketones to synthesize full range cycloalkanes. [97, 98]

Ma et al. reported the condensation of furfural and HMF with cyclopentanone and cyclohexanone as a starting step to produce long chain (C$_{13}$-C$_{18}$) 1,3-substituted cycloalkanes (See scheme 1.7 path A).[97] Similarly, Zhang et al. reported the synthesis of jet-fuel range branched

cycloalkanes starting from HMF. The synthetic route starts with solvent free aldol condensation between HMF and methyl ketones, the intermediaries formed were hydrogenated in aqueous phase to produce linear triketones which after a second condensation and hydrogenation yielded the desired cycloalkanes (See scheme 1.7 path B).[98]

HMF can also be subjected to other modifications (see Scheme 1.8). The Wittig reaction can be made in order to introduce olefin functionality. Ji et al. reported the obtention of 5-hydroxymethyl-2-vinylfuran (**11**), which was then polymerized and used as an adhesive, showing a versatile behavior. Its performance was compared to commercial glues, outperforming polyvinylalcohol and epoxy resins; and behaving similar to cyanoacrylate. Also its use as bio-adhesive was assessed showing potential use in medical applications.[99]
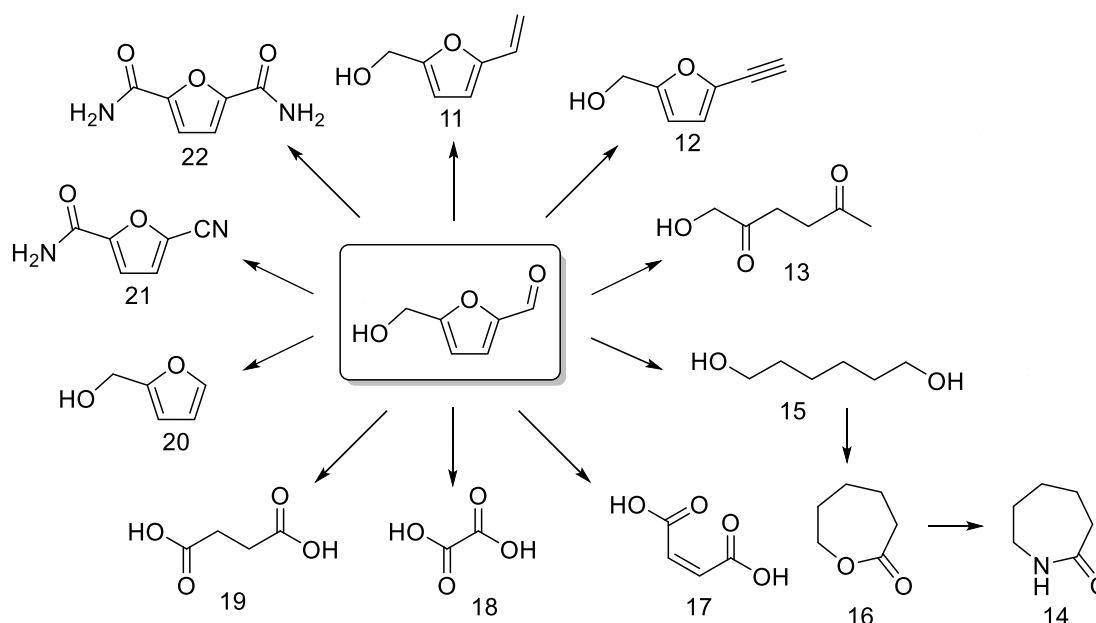
Scheme 1.8. Other HMF derivatives obtained from non- oxidation/reduction processes.

Alkynilation of HMF and derivatives was performed using the Oshira-Bestmann reaction obtaining mono (**12**) and bisacetylenic derivatives in almost quantitative yields. This allowed the implementation of traditional alkyne chemistry, like Sonogashira coupling, Glaser oxidation and Rh-catalyzed polymerization; to biobased furan compounds.[94]

Reductive ring opening has also been reported. Under harsh conditions HMF can be converted to 1-hydroxyhexane-2,5-dione (**13**) with moderate yields (69-74%); which is normally a synthetic intermediary.[100-102] De Vries et al. reported a whole synthetic pathway for the production of

caprolactam (**14**) from HMF. Reductive ring opening forms 1,6-Hexanediol (**15**), and further oxidation forms Caprolactone (**16**) as intermediaries.[103]

On the other side, HMF can be oxidatively cleaved to maleic acid (**17**) in high yields (up to 95%) using hydrogen peroxide in formic acid.[104] And by using an Fe@C-nanotubes under harsh conditions (10 Bar O_2 at 140 °C) oxalic (**18**) and succinic (**19**) acids can be synthesized with up to 48% and 18% yield respectively.[105]

In compressed CO_2 after 4h at 145 °C with Pd@Al_2O_3, furfuryl alcohol (**20**) can be synthesized from HMF by decarbonylation with high conversion and selectivity (>99% both).

Xu et al. reported that under oxidative conditions in the presence of ammonia in aqueous solution at 100 °C using manganese oxides, catalytic amidation proceeds to nitrile-amide (**21**) derivatives. The selectivity of the system is related to the type of manganese oxide (crystal structure) and solvent used.[106] Shortly after, the same group, reported the tandem selective aerobic ammoxidation-hydration of HMF to 2,5-furandicarboxamide (**22**) using Al-doped Cryptomelane as catalyst with 97% yield.[107]

Rehydration of HMF under acidic conditions leads to levulinic acid, which is regarded as the final product during biomass hydrolysis. It is another biobased building block with as much potential as HMF.[108]

1.5 Furan based polymers

As mentioned before, the increasing awareness of the environmental impact related to waste disposal and fossil based oil industry; research has focused on developing macromolecular materials in order to replace those obtained from non-renewable sources.[29, 49, 109-111] In this sense, FDCA (**7**) has emerged as a representative monomer for the synthesis of biobased polymers, as the increasing number of publications per year show (see graphic 1.3). Although the synthesis of **7** can be traced back to 1876 where Fittig and Heinzelman reported that by dehydration of galactaric acid with fuming hydrobromic acid it could be obtained[112], it only received high attention recently because of its resemblance to its petrochemical counterpart terephthalic acid (TPA). Due to that fact, the exchange to the biobased analog in the established TPA systems is simple and straightforward.
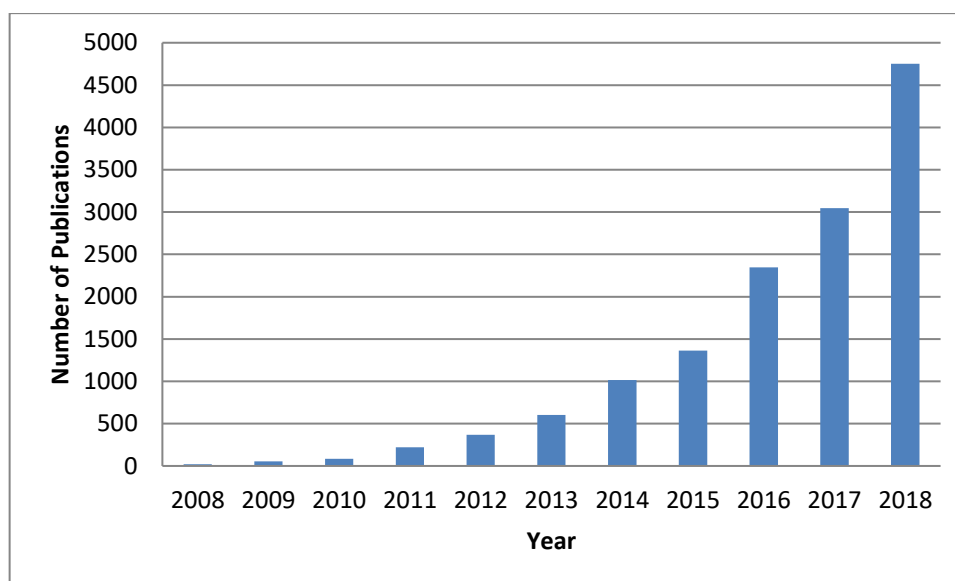
Graphic 1.3. Number of publications per year with the keyword 2,5-furandicarboxylic acid, as registered by Web of Science.

Different FDCA-based polyesters have been investigated, been the furanic-aliphatic family the one who got most of the research effort. The backbone of these polymers is furan and aliphatic units, and has been tailored by using different aliphatic monomers (linear and branched, from C2 to C18) and also rigid cyclic structures.[113-119] Also entirely aromatic polyesters with both furan and benzene rings in their backbone have been prepared. In both cases with the aim to obtain novel materials with enhanced thermal and mechanical properties. Lignin based aromatic monomers like vanillic, syringic, salicylic and 4-hydroxybenzoic acids have attracted particular attention because of its renewable nature.[120-122]

Also other FDCA-based polymers or resins[123, 124] have been prepared, such as polyamides,[125, 126] thermotropic polyesters,[121, 122] photodegraded polyesters,[121] branched furan based polyester resins,[127] linear and cross-linked poly(ester amide),[128, 129] epoxy resins,[130] poly(ester urethanes),[124] etc.

1.5.1 Polyethylenefuranoate (PEF)

The efforts to introduce bio-based renewable materials is a recent trend in comparison to the early reports of the synthesis of polyethylene furanoate (PEF), which date back to the late 1940s.[131] PEF is the so called "furan counterpart of polyethylene terephthalate (PET)".[132] Different routes for a renewable based production of PET has been proposed, using p-xylene as key intermediate; they are still limited by low yields which makes them non-viable for industrial scale up.[133-135] Therefore The Coca-Cola Company introduced a 30% renewable PET with the tradename PlantBottle[TM] which

is made with bio ethylene glycol (EG) and non-renewable TPA. [136] On the contrary to PET and its biobased alternatives, PEF is a 100% renewable based polymer with high performance properties that will potentially occupy the market belonging to PET nowadays. As an example of its environmental benefits, Patel et al. have shown that greenhouse gas emissions and non-renewable energy use can be reduced by 50-60% if PET is replaced by PEF, starting from corn-derived fructose and bio-ethylene glycol.[137]

PEF has been prepared in different ways. Several polycondensation and polytransesterification approaches have been tested using **7** or its dichloride-, dimethyl-, diethyl-, or bis(hydroxyethyl)-derivatives.[138, 139] A two stage polymerization was described, in which starting materials, reaction temperatures and catalysts influence the polymerization process and consequently the final product. Polymerization over 250 °C yields a colored (brown) polymer in reduced amounts, which is due to decarboxylation of **7**. Tin(IV)/Tin(II) catalyst systems are said to increase the molecular weights. There are still some issues, like long reaction times and poor mass transfer due to viscosity.[140] A third stage has been used aiming to increase the degree of polymerization by solid-state polycondensation during several days at temperatures between glass transition and melting point; resulting in molecular weight values up to 83000 g/mol, giving it industrial relevance.[140-142] Other methods like direct esterification with tetrabutyl titanate as catalyst,[143] ring opening polymerization of cyclic FDCA-based monomers[81] and the combination of melting polymerization and subsequent solid state post condensation[141] have been presented.

The better properties, compared to PET, have been reviewed and precisely described.[61, 119] All the evidence of the better performance of PEF indicates that the furan ring provides different molecular properties to the polymer. PEF possess increased chain rigidity, this related to the inhibition of the ring flipping motion due to the nonlinear rotation axis of the furan ring and the ring polarity; which is not the case for PET in which flipping rotation of the phenyl ring is free (see Scheme 1.9).

PET
free rotation

PEF
restricted rotation
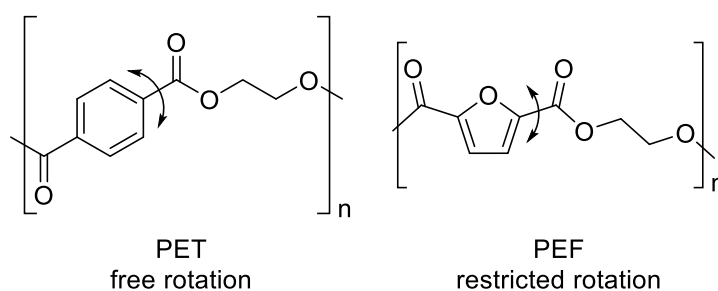
Scheme 1.9. Ring flipping motion differences in PET and PEF

This is particularly highlighted in the studies made by Koros et.al. in which they test PEF for packaging applications.[144-148] The oxygen sorption behavior of PEF is similar to PET at 35 °C, but showed a significant reduction in oxygen permeability (up to 11 times less than PET) could be assessed. More importantly, CO_2 permeability and diffusivity were respectively 19 and 31 times lower than PET. PEF showed a higher equilibrium water uptake due to higher affinity with the polar furan ring, and also exhibited an almost three-fold reduction in water permeability at 35 °C.

Although the synthesis process and final properties of PEF are comparable and better (e.g. barrier properties), some differences exist in terms of mechanical performance. PEF shows a brittle fracture behavior during stress-strain tests; it has a lower elastic modulus than PET, the elongation at break was 2.81%, much lower than PET (90-250%).[141] Such drawback has found some solutions like annealing[141] or blending it with PET[149] as way to enhance the mechanical properties.

In terms of recyclability of PEF both chemical and mechanical approaches have been investigated. PEF can be depolymerized via hydrolysis, methanolysis or glycolysis can be carried out in excess of water or alcohol using a base (e.g. metal alkoxides) in catalytic amounts as reported by Sipos et al.[150] PEF and PET were subjected to methanolysis, in which depolymerization of PEF proceeded faster than of PET. 52% of PEF could be dissolved in comparison to 2% of PET, recover **7** and dimethyl-2,5-furandicarboxylate (FDCM) was possible. Further use of the recovered depolymerization products was possible; they were used to prepare new furan-containing polymers, fuels or fuel additives. In order to use the established recycling system, PEF was added to the recycling streams. An addition of up to 5%wt was possible without detriment of the mechanical and physical properties of PET.[140] More recently, Pellis et al. reported the enzymatic hydrolysis of PEF.[151] In this study Cutinase 1 from *Thermobifida cellulosilytica* was selected due to its ability to hydrolyze several PET substrates.[152, 153] In the process, **7** and oligomers were liberated, showing its potential.

1.5.2   Other furan based polyesters

As mentioned, before, tailoring of the FDCA-based polyesters is made by use of different aliphatic diols (See figure 1.3 A). In 2012 Zhou et al.[143] reported a systematic study of the properties of polyesters prepared with diols that can be prepared via biological fermentation.[154, 155] PEF, Poly (1,3-propylene 2,5-furandicarboxylate), Poly (1,4-butylene 2,5-furandicarboxylate)(PBF) and Poly (1,6-hexylene 2,5-furandicarboxylate), Poly (1,8-octylene 2,5-furandicarboxylate) were prepared by direct esterification of **7**. They show similar thermal stabilities to its benzene-aromatic counterparts. Viscoelastic properties of the furan polyesters were also tested, showing that the

brittle behaviour seen in PEF decreases with the increase of methylene units in the aliphatic chain. Van Es et al. added to the previous list Poly (2,3-butylene 2,5-furandicarboxylate) and also compares polymers of different isomers of **7**, the 2,5-, 2,4-and 3,4- furandicarboxylic acids.[83] Additionally, Biriakis et al. report the synthesis of Poly (1,9-nonylene 2,5-furandicarboxylate), Poly (1,10-decylene 2,5-furandicarboxylate) and Poly (1,12-dodecylene 2,5-furandicarboxylate).[156] To the aliphatic based polyesters, cyclic diols (mainly 1,4:3,6-dianhydrohexitols) can be added as part of the studies made.
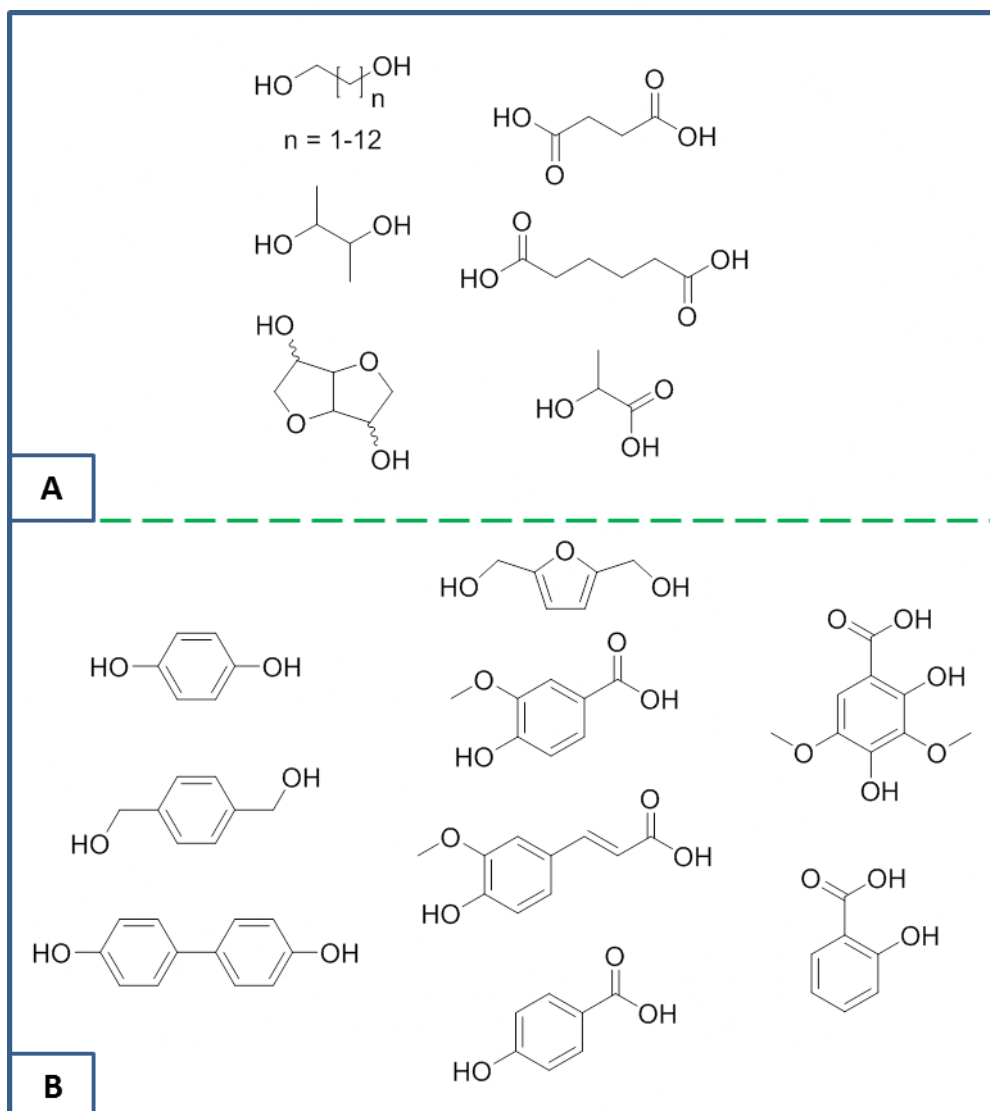
Figure 1.3. Representative aliphatic and aromatic monomers for FDCA-based polyesters.[61]

Fully aromatic polyesters have also been pursued. These incorporate both furan based and benzene rings in their backbone, or exclusively furan units. In this area lignin-based aromatics are

of interest due to their renewable nature. Also other HMF derivatives have been used in the synthesis of this type of polyesters (See figure 1.3 B).[61]

Between all the previous mentioned aliphatic polymers PBF has drawn the attention because of its similar properties to Poly (1,4-butylene terephthalate) (PBT). PBF (as PBT) is a highly crystalline material that has multiple melting behaviours depending on the thermal history of the material.[157, 158] It also showed thermal stability up 304-373 °C, which is similar as the one observed for PBT.[143, 159] Stress-strain tests for elongation at break and stress at break shows that the Young's modulus increases with increasing Mn, keeping a constant value starting 23000 g/mol. Those values match with the ones of commercial PBT.[160] Similarly, PBF fibres show matching properties to those of PBT.[158]

Following the trend, copolymerization of **7** and more than one aliphatic alcohol was made (see Scheme 1.10). Gandini et al. reported the synthesis of Poly (ethylene 2,5-furandicarboxylate)- co- Poly (1,3-propylene 2,5-furandicarboxylate) by polytransesterification. A random copolyester composed by 24% ethylene units and 76% propylene units was obtained showing properties more similar to PEF than to PPF.[138] In a same way Pang et al report the preparation of various copolyesters of Poly (ethylene 2,5-furandicarboxylate) and Poly (1,4- butylene 2,5-furandicarboxylate). In this work the authors demonstrate the possibility of tuning thermal properties by adjustment of the comonomer ratio in the polymers.[161]
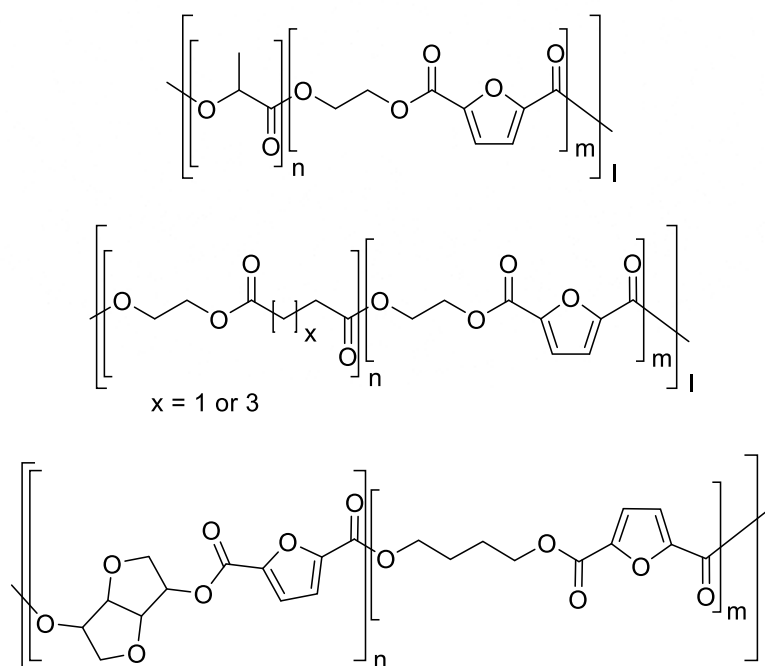
Scheme 1.10. Some copolyesters including FCDA in its backbone

The FDCA-based copolymers are not restricted to different diols. With the goal of tackle the lack of biodegradability also other monomers have been used. Sousa et al. reported the copolymerization of PEF and poly (lactic acid) (PLA). The obtained copolymers were stiff amorphous solids with improved degradability when compared to PEF. Only by the addition of 8% mol of lactic acid was enough to improve the biodegradability and to keep the thermal properties similar to PEF.[79] In general, copolyesters from FDCA can be prepared by either incorporating more than one aliphatic diols or introducing others diacids monomers. This opens the possibility to tune the biodegradability, thermal, mechanical and barrier properties of the polymers, just by choosing the ratio and correct monomers.[162-165]

The interest on furan based polymers derives from their renewable nature. In general, incorporating furan rings to the backbone improves the mechanical and thermal stability of the polymers. Although there is great variety of them, their use and application depend on the possibility of efficient, simple and inexpensive production of these valuable monomers.

1.6 Flow chemistry

Chemistry has long been perceived as a dangerous science and the word "chemical" a synonym of "toxic"; these days this perception is used as a marketing strategy to sell products "without chemistry" containing so-called nature derived ingredients making them less hazardous. Nowadays, the 12 principles of green chemistry are the guidelines to follow for the design and development of sustainable processes. They were presented by Anastas and Werner in 1998 as an integrated cohesive system for the design of safer chemicals and chemical transformations (see Table 1.1).[166] When a chemical process moves to the industrial scale, engineering comes into play. Other factors must be taken into account; both chemistry and engineering have to work in synergy to achieve the sustainability goals. In that sense, years later Anastas and Zimmerman presented the 12 principles of green engineering (see Table 1.1). Which main goals are not only to avoid the use/generation of toxic materials but also maximize efficiency, minimize waste and increase profitability.[167]

Within the combination of both green chemistry and engineering, continuous processing has been presented as the best option to achieve green and sustainable manufacturing.[168] Flow chemistry became popular in academia, and as expected it took longer to be adapted by the industry. The continuous manufacturing of active pharmaceutical ingredients is encouraged by

regulatory agencies like the FDA (Food and Drug Administration (U.S. Federal Agency)), giving to its implementation an incentive.[169]

Table 1.1. Principles of green chemistry and engineering[166, 167]

12 Principles of Green Chemistry	12 Principles of Green Engineering
1. Prevent waste	1. Inherent rather than circumstantial
2. Atom economy	2. Prevention instead of treatment
3. Less hazardous chemical synthesis	3. Design for separation
4. Designing safer chemicals	4. Maximize efficiency
5. Safer solvents and auxiliaries	5. Output-pulled vs. Input-pushed
6. Design for energy efficiency	6. Conserve complexity
7. Use of renewable feedstocks	7. Durability rather than inmortality
8. Reduce derivatives	8. Meet need, minimize excess
9. Catalysis	9. Minimize material diversity
10. Design for degradation	10. Integrate material and energy flows
11. Real-time analysis for pollution prevention	11. Design for commercial afterlife
12. Inherently safer chemistry for accident prevention	12. Renewable rather than depleting

To see the benefits of continuous flow processing, it has to be correlated with its batch equivalent. Safety is the main aspect that makes it attractive for manufacturing scale.[170] Smaller reactor can be used, meaning reduced volume of reagents used and finally a minimized severity in case of an accident. Hence, performing hazardous chemical synthetic routes becomes safer. Exothermic reactions can be controlled more efficiently due to high mass- and heat transfer rates. The slow additions or the need of dilution to control overheating are avoided; therefore, the energy costs are reduced. Additionally, efficient dosing and mixing of gases with a liquid stream can be achieved, making possible to perform multiphase reactions under safe conditions.[171] All these features allow the in-situ generation and immediate use of unstable or hazardous chemicals avoiding its storage; therefore reducing risks and providing a safe working place.[172] Although, high temperatures and pressures are not in correlation with the principles of green chemistry, thanks to the already mentioned small reactor volumes and excellent heat-exchange efficiency; these can be performed with less energy input. Also, re-optimization is reduced to the minimum in a scale-up process, making it less time consuming. In comparison, the investment of a batch reactor with comparable throughput compared to a continuous processing unit is 12 times higher[173].

1.6.1 Continuous flow upgrading of biobased chemicals

Many aspects of flow chemistry help chemists to develop new strategies to support the effort on the transition to a biobased chemical industry. Thanks to the survey released by the US department of energy in 2004, a list of biobased platform chemicals was on the focus of the chemical community. They were foreseen as a potential source of starting feedstock for the synthesis of traditional oil-based olefins and other building blocks. Although HMF was not listed, it became an attractive C6 platform. .[49, 174]

Bioresources become attractive when the processes to produce them are highly efficient, use low amount of solvents and are robust. Added to that, the potential scale production must satisfy a demand around hundreds of thousands of tons per year. As presented by Monbaliu et al. the research efforts for the application of flow technologies has focused mainly in Glycerol (**23**) and HMF, and to a lesser extent to succinic (**19**), fumaric and itaconic acid.[175]

Valorization of glycerol is the best example of what can be achieved by combining both biobased chemistry and continuous flow process (see Figure 1.4).
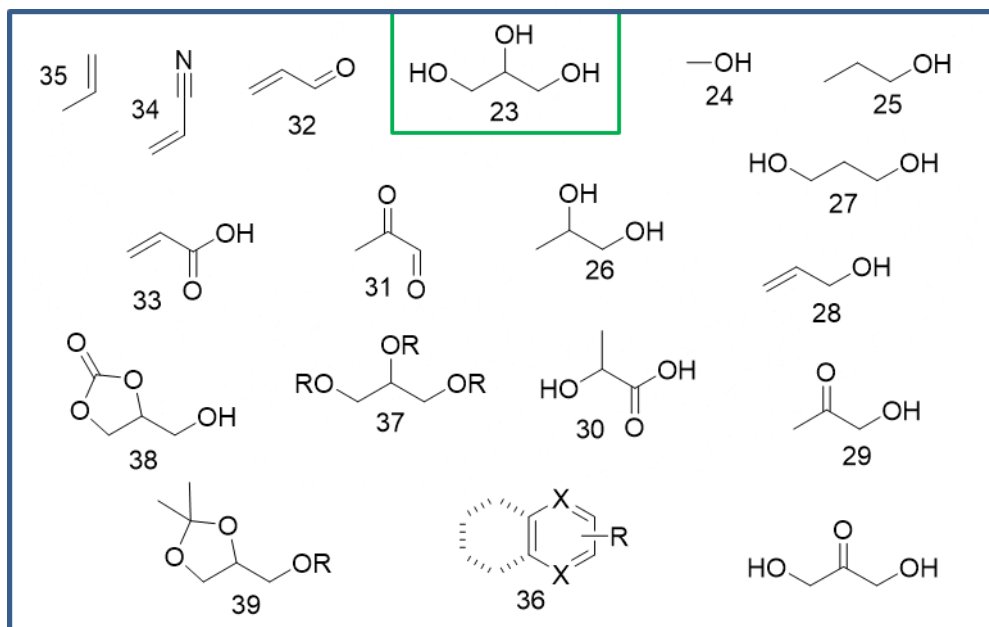
Figure 1.4. Building blocks obtained from glycerol under continuous flow conditions[175]

Bioglycerol is a byproduct/waste of biodiesel production, in Europe its production was expected to be up to 21 billion liters in 2018 and to increase even further.[176] By 2020 the EU aims to use of 10% biobased fuel for transportation means. The abundance of **23** made it the ideal raw material for C3 based molecules; it has to through a defunctionalization or functionalization processes. Reduction, oxidation, dehydration and cracking have been used to get methanol (**24**), propanol (**25**), propanediol (1,2- (**26**),1,3- (**27**)), allyl alcohol (**28**), hydroxyacetone (**29**), lactic acid (**30**), pyruvaldehyde (**31**), acrolein (**32**), acrylic acid (**33**), acrylonitrile(**34**), propene(**35**), etc. Aromatics (**36**) like quinoline, 2-methylpyrazine, pyridine and benzene were prepared through condensation, dehydro-cyclization, two-stage continuous dehydration/aromatization, gas phase aromatization, etc. Esterification (**37**), carbonation (**38**), ketalization (**39**) and etherification have been performed in order to keep the glycerol backbone in the product. [175]

There is a great potential in the use of glycerol as raw material for chemical production, all the processes mentioned before must deal with the variability in quality. Crude glycerol coming from the biodiesel industry can contain water, inorganic salts and lower alcohols (e.g. MeOH, EtOH), all in different amounts and ratios. [175]

Also, the valorization of succinic, fumaric and itaconic acids have been explored, but as mentioned before, to a lesser extent. Reduction of succinic acid to 1,4-butanediol was reported by Vardon et al.[177] And the upgrade of fumaric and itaconic acids to γ-butirolactones in lab- and pilot-scale has been studied by Monbaliu et al.[178]

1.6.1.1 *Valorization of HMF under flow conditions*

As mentioned in previous sections, HMF in an important intermediary in the production of biobased platform chemicals, and also modifications under flow conditions has been tested.

Hermans et al. reported the synthesis of dihydroxymethylfurfural (**3**), which was obtained by Cu-catalyzed hydrogenation/hydrolysis of HMF using 1,4-butanediol as H_2-source. Cu nanoparticles over AlO_x as heterogeneous catalyst converted HMF with 93% yield. The residence time was important, the previous conversion was achieved with 0.6 min residence time. With longer residence times (29 min) the hydrogenation proceeds further to dimethylfuran (**5**) with a 71% yield; also 1,4-butanediol was converted to γ-butyrolactone making the process more appealing.[179] Later that year, in a similar fashion the same group report the same reaction catalyzed by 2% wt $Pd@Fe_2O_3$ using iPrOH as H_2-source.[180] The use of gaseous hydrogen has also been reported. These

can be performed with noble (e.g.Ru, Pt, Pd), non-noble metals (e.g. Ni, Cu, Co, Fe, Zn, Zr, Mg) and mixtures of them.[181]

Barta et al. developed a tunable and highly selective method for the reduction of HMF using Copper-doped porous metal oxides as catalysts and H_2 gas. At 100 °C only the carbonyl functionality was reduced, and **3** could be obtained in 97% yield. At higher temperatures (220 °C) the molecule was further reduced to **5**, also to **6**.[182]

Hf-, Zr- and Sn-Beta and other zeolites were used as catalysts in the etherification of HMF to synthesize 2,5-Dialcoxymethylfurans. Román-Leshkov et al. demonstrated that these zeolites promote the transfer hydrogenation/etherification of HMF with primary and secondary alcohols. Hf- and Zr-Beta seemed to be more active in the Meerwin-Poondorf-Verley reduction, whereas Sn-Beta showed the highest stability and selectivity for etherification. 2-butanol proved to be a better H_2-source than ethanol. Using EtOH the etherification yields were in the range of 28-44% and with 2-BuOH 45-85%. [183] Gorte et al. studied how acidity of solid materials can affect the etherification of HMF under flow conditions, Lewis acids are able to carry out transfer hydrogenation of the aldehyde functionality and form a mono-ether. Strong Bronsted acidity catalyze the formation of mono-ethers without the hydrogenation of the carbonyl group. Weak Bronsted acidity is responsible for two step etherification/transfer hydrogenation. By the use of Sn-BEA a conversion of 69% could be obtained with a 86% selectivity towards the dietherificated product (2,5-bis(isopropoxymethyl)furan).[184]

Zheng et al. synthesized 1,6-hexanediol from HMF with 57.8% yield over double layered Pd/SiO$_2$ + Ir–ReO$_x$/SiO$_2$. The double layered catalyst showed better performance in improving product selectivity towards the desired diol. The volume ratios of water/THF used as solvent proved to have influence in the yields; a ratio 2:3 was the most suitable.[185]

In an interesting way, Li et al. coupled the synthesis of phenols and dimethylfuran (**5**). They developed bimetallic Ni-Cu nanocatalysts that allowed performing a formal transfer hydrogenation using cyclohexanol as the hydrogen source to reduce HMF. 99% conversion and >98% yield was observed for both the conversion of cyclohexanol to phenol and HMF to **5**.

More relevant to this work (See Table 1.2), the synthesis of FDCA under flow conditions has also been explored. In 2010, Lilga et al. reported the quantitative oxidation of HMF with a selectivity of 95-99% **7** using Pt@C under basic conditions at 100°C. pH effects were studied, at low pH and Pt@ZrO$_2$ as catalyst **8** was obtained; with 80-85% conversion and 67-70% selectivity.[186]

24

Table 1.2 HMF Oxidation under flow conditions

Entry	Ref.	Conditions	Conv./Select. (%)
1	[186]	- Pt@C, basic conditions, 100°C.	>99/95-99 **7**
		- Pt@ZrO$_2$, acid conditions	80-85/67-70 **8**
2	[187]	Silica-supported TEMPO, O$_2$ as oxidant, HNO$_3$ as co-oxidant	97/98 **8**
3	[188]	Hypervalent Iodine/TEMPO	89/61 **8**
4	[189]	Resin-supported Pt, base free, O$_2$ as oxidant, 120 °C	>99/99 **7**

Hermans et al. developed a straightforward continuous flow process for the oxidation of alcohols using Silica-supported TEMPO as catalyst. HMF was oxidized to **8** in the presence of O$_2$ as oxidant and HNO$_3$ as co-oxidant; 97% conversion and 98% selectivity were obtained. Elongated reaction time yielded **7** which also resulted in technical issues (e.g. clogging).[187] Wirth et al. reported the hypervalent Iodine/TEMPO mediated oxidation of alcohols in flow systems, with a HMF conversion of 89% and a selectivity towards **8** of 61%.[188]

More recently, Barbaro et al. reported the oxidation of HMF over heterogeneous resin-supported Pt catalysts in base free conditions and water as solvent. 99% yield of **7** was obtained at 120 °C, 303 s residence time, and 7.7 Bar of O$_2$ at 1.2 mL/min flow rate.[189]

1.7 Scope of the work and methodology

Based on the background presented previously, the main goal of this research is the development new catalytic systems for the valorization of furfural derivatives, with special focus on HMF. The processes should be controllable and the results reproducible. The oxidative esterification of HMF was taken as target upgrading reaction. Both heterogeneous and homogeneous catalyst systems were screened and tested. Traditional batch conditions as standard methodology was used. Also, the application of innovative flow chemistry conditions was explored. Application of the green chemistry and engineering principles has been a priority.
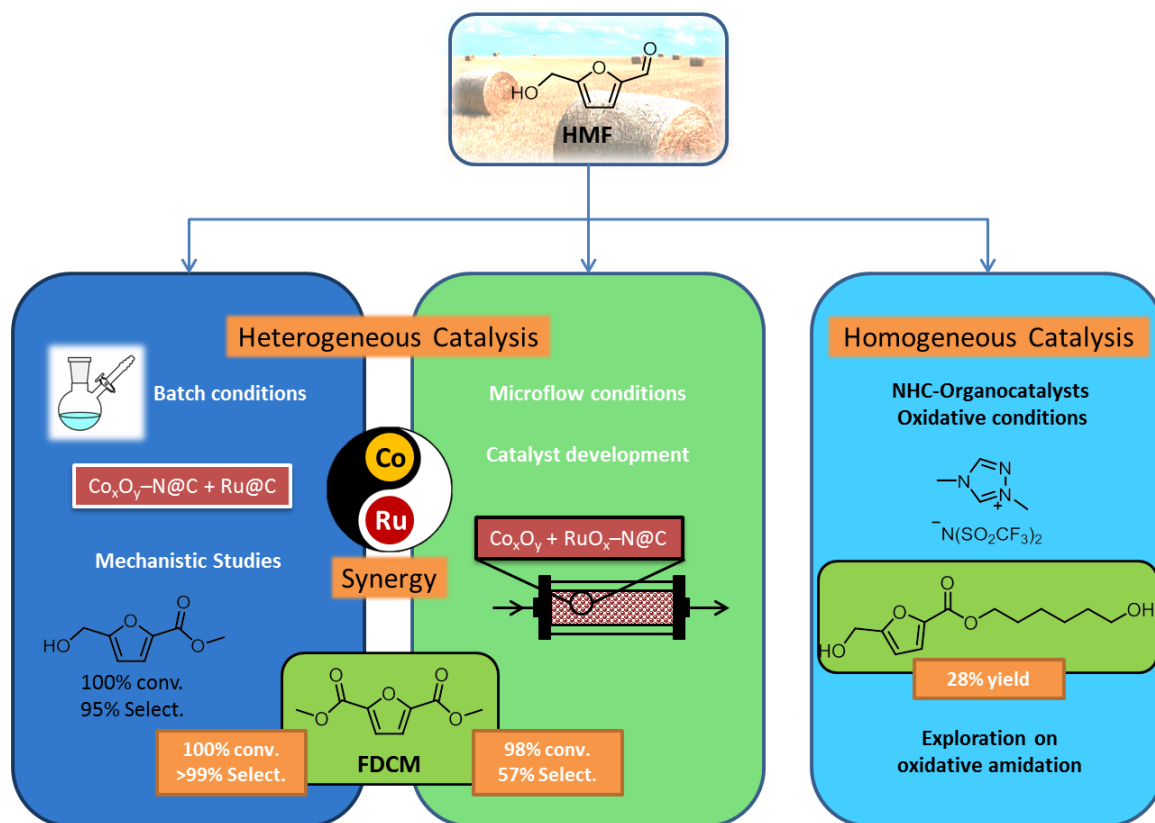
Figure 1.5. Scope of the work

The first part of the work focuses on the oxidative esterification of HMF in batch conditions and on the establishment of a new method to achieve high conversion and selectivity. All the influencing aspects of the system have been studied, to achieve the best possible and milder conditions.

Dimethyl-2,5-furandicarboxylate (FDCM) was taken as synthtic target, and a screening of catalyst was done and compared to the state of the art. Optimization of the catalytic system was performed. Mechanistic aspects were investigated to reveal the role of each component of the reaction (e.g. solvent, temperature, catalyst loading, reagents, etc.).

The second part follows with the applications of micro flow conditions to the previously studied batch reactions. Technical issues lead to the modification and the development of new catalyst with ideal properties to operate under continuous regime (e.g. change of support, development of a new bimetallic catalyst, etc.).

In the final part, a different approach was also studied; which focused on the synthesis of diols that can be lately used as biobased monomers. HMF upgrade by NHC organocatalytic esterification of aldehydes was studied. Efforts to optimize and understand the working mechanism has also been adressed.

26

2 Synergetic Bimetallic Oxidative Esterification of 5-Hydroxymethylfurfural (HMF) under mild conditions[a]

2.1 Introduction

The use of biomass-derived chemicals it's nowadays a very relevant topic, since these, coming from renewable sources, can be incorporated in a circular, sustainable economy.[190] Special focus has been given to the conversion of agricultural waste into useful chemical commodities.[191] Among these products, 5-hydroxymethylfurfural (HMF, **1**) is of special interest; it can be synthesized by dehydration of C_6-sugars (eg. fructose or glucose), which in turn can be obtained from lignocellulose materials from the agro and food industries (Scheme 2.1).[192] Among other applications, HMF is the precursor of 2,5-furandicarboxylic acid (FDCA, **7**) and its methyl ester derivative (FDCM, **40**).[15] Both can be used as monomers for the production of furan-based polyesters,[80] like poly-ethylene-furanoate (PEF), which is the furan based analogue of Poly-ethylene-terephthalate (PET).[61] There is special interest in PEF as it has shown better gas containing properties than PET, an advantage in the storage of CO_2-containing beverages.[193] It has shown also good results by the assessment of health risks of its use as food container and its degradation by enzymatic hydrolysis.[151, 194]

The demand of **7** or its esters (like **40**) in the polymer industry has brought great attention to the oxidation/oxidative esterification of HMF. There are several reports about the use of heterogeneous catalysts in the oxidation of HMF to **7**, using different metals,[195, 196] combinations of them,[197, 198] and also several types of supports.[199-201]

There are two ways in which FDCA is used as starting material in the polymer synthesis, the first way involves the preparation of an ester (e.g. **40**) and after that a transesterification reaction is made to obtain the desired products, and the second way using it in a two stage polyesterification. The advantage of having **40** as a starting material is that the step for the esterification of FDCA is avoided, and it's possible to proceed to the transesterification step directly.[61] Another advantage is that in general, the polyesters obtained from **40** are colourless (indicative of less decomposition in

the polymerization process), and the reaction proceeds at higher rates than using FDCA as starting material.[202]
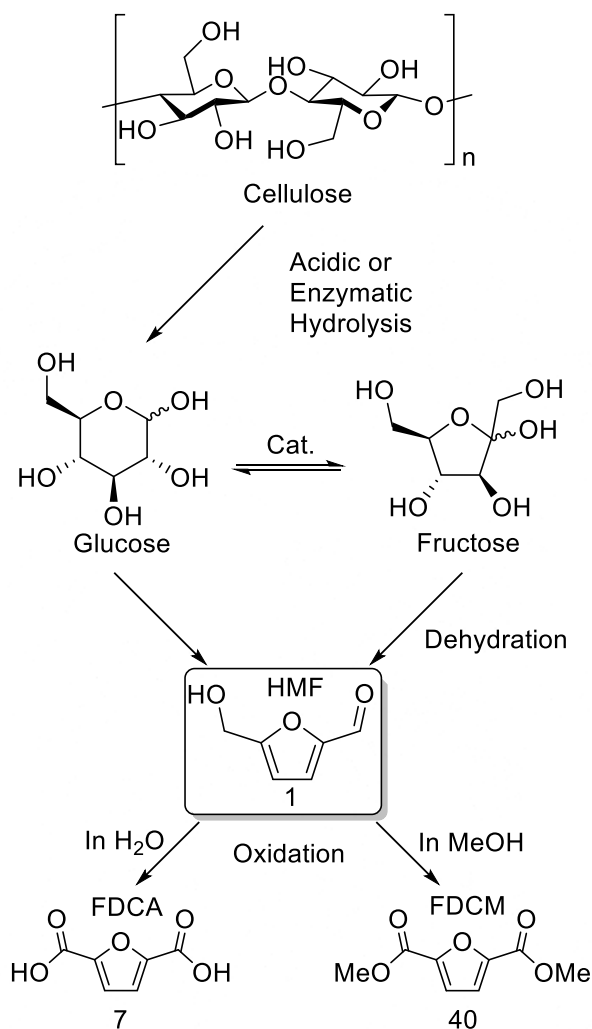
Scheme 2.1. Production of HMF and derivatives from biomass
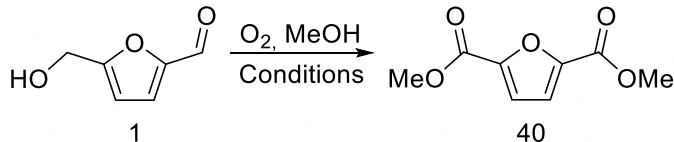
There are only a few reports of the oxidative esterification of HMF. Recently, Xu et al. reported the use of cobalt oxide supported in nitrogen-doped carbon (CoO_x-N@C) catalysts using MnO_2 as stoichiometric additive with 96% yield of **40** (Table 2.1 Entry 1).[203] Fu et al. reported the use of Co_xO_y-N@C in combination with a porous potassium/manganese oxide ($KMn_8O_{16}.nH_2O$), obtaining full conversion but no appreciable selectivity to one specific product (Table 2.1 Entry 2).[204] Corma et al. reported the use Au nanoparticles supported in ceria obtaining full conversion and selectivity to **40** (Table 2.1 Entry 3). [205] Later on, Manzoli et al. also reported that Au nanoparticles supported in zirconia fully convert HMF, showing only 32% selectivity to **40** (Table 2.1 Entry 4).[206]

All the reported systems require high pressures of oxygen and high temperatures to achieve full conversion or selectivity.

Recently, Fu et al. reported the oxidative esterification of HMF to **40** using a trimetallic system (Pd, Co and Bi) under mild conditions with high selectivity, using high metal loadings(up to 10% each metal) in heterogeneous and homogeneous way (Table 2.1 entry 5).[207]

Table 2.1. Comparison between reported systems for the synthesis of FDCM (**40**) via oxidative esterification of HMF (**1**).

HO—[furan]—CHO →(O$_2$, MeOH, Conditions)→ MeO$_2$C—[furan]—CO$_2$Me

1 → 40

Entry	Ref.	Catalyst(s)	$P\,O_2$ (Bar)	Temp. (°C)/Time (h)	Conv./Select. (%)
1	203	CoO_x-N@C + MnO_2	6	100/12	100/96
2	204	Co_xO_y-N@C + KMn_8O_{16}	10	100/6	99/53
3	205	Au@CeO$_2$	10	130/5	100/99
4	206	Au@ZrO$_2$	3	130/5	100/32
5	207	PdCoBi@C	1	60/14	99/96
6	This work	Co_xO_y-N@C + Ru@C	1(Air)	50/16	100/99

Herein, we report the aerobic oxidative esterification of HMF to FDCM (**40**), made by a cooperative reaction using the heterogeneous catalyst mixture of Co_xO_y supported on nitrogeneous carbon (Co_xO_y-N@C)[208, 209] and commercially available ruthenium on carbon (Ru@C) under mild conditions (Table 2.1 Entry 6). The independent performance of each catalyst was studied along with the effect of oxygen availability in the system. Moreover, an increase in the speed of the reaction was achieved using perfluorinated compounds (PFC's) as they show excellent gas solubility.[210] This synergistic bimetallic approach yields, to the best of our knowledge, the highest selectivity towards FDCM (**40**) under the mildest conditions so far.

2.2 Experimental Section

2.2.1 Synthesis and Characterization of the Co_xO_y-N@C Catalyst

The catalyst has been prepared according to the previously reported procedure:[208, 209] A mixture of $Co(OAc)_2.4H_2O$ (corresponds to 3 wt% Co) and 1,10-phenanthroline (Co:phenanthroline = 1:2 mole ratio) in ethanol was stirred for 20-30 minutes at room temperature. Then, vulcan XC72R carbon powder was added and the whole reaction mixture was stirred at 60 °C for 5-6 hours. The reaction mixture was cooled to room temperature and ethanol was removed slowly under vacuum. The remaining solid sample obtained was dried at 60 °C for 12 hours. The dried sample was grinded to a powder. Then, the grinded powder was pyrolyzed at 800 °C for 2 hours in argon atmosphere and cooled to room temperature. Elemental analysis of Co-Phenanthroline/C (Wt%): C = 89.68, H = 0.199, N = 2.70, Co = 3.05. XPS data of Co-Phenanthroline/C (Atom%): C = 92.38, N = 2.80, Co = 0.61, O = 4.02

2.2.2 Catalytic Oxidation of HMF

All the oxidative esterification reactions were performed in an oven dried Schlenk tube. All the reagents (HMF, Base, Catalyst and 4 mL of MeOH) and a magnetic stirrer were added to the tube. To the Schlenk tube a condenser was coupled and to the top of if a balloon filled with Air was attached. Air was used as the oxidant. After flushing the system with Air for a while, it was closed and heating and stirring started. At the end of the reaction time (16h) the catalyst was filtered off, and the solution was analyzed by GC. Conversion and Yields were determined by GC-FID. The identification of the products was made by GC-MS and NMR.

When MPFB solvent or mixtures with it were used, the solvent was bubbled with oxygen or air previous usage. After the reactions the MPFB solvent or mixtures were fully recovered and reused.

2.2.3 Kinetic Measurements

The kinetic measurements were made in similar experimental conditions as the previously described using a custom made Schlenk tube, by following the disappearance/appearance of the IR peak corresponding to carbonyl group of **2** (1678 cm^{-1}) using the Mettler Toledo ReactIR 15 Equipment.

2.2.4　EPR Measurements

For detection radical intermediates in catalytic oxidation of HMF (**1**), a sample was taken after 3 h of a reaction and mixed with 100 μL of 600 mM DMPO (Dojindo) as spin trap in H_2O at 50 °C under bubbling of O_2. Then 50 μL of the reaction solution were transferred into a microcapillary glass tube (Hirschmann) and measured immediately at room temp (20 °C).

2.3 Results and Discussion

2.3.1　Catalyst Screening and optimization

A series of different heterogeneous metal catalysts with known activity in oxidation reactions[195, 196, 211, 212] were tested for the oxidation of **1** in methanol to produce in all cases a mixture of products (**8**, **40**, **41** and **42**, Scheme 2.2 and Table 2.2). The highest conversion of **1** was achieved with the cobalt oxide catalysts Co_xO_y-N@C (>99% and 95%, entries 1 and 2), followed by supported ruthenium, Ru@C (75%, entry 4). Even though catalytic activity for Pt, Pd and Fe oxide was previously reported for HMF oxidation,[196, 211, 212] under the tested conditions both conversion and selectivity were poor (entries 3, 5 and 6). There was no significant difference in the conversion achieved when using cobalt catalysts with different metal loadings (entries 1 and 2) so we decided to continue the studies with the one with the lower Co content. The observed low yield of products containing the formyl group (**8** and **42**) suggests a higher selectivity of this catalyst towards the conversion of the aldehyde (to ester) than of alcohol (to aldehyde). In fact, after optimizing the reaction conditions, the cobalt catalyst delivers almost quantitatively **41** as the major product (Scheme 2.3, A). Conversely, the ruthenium catalyst yields to a completely different product distribution; being selective towards the dialdehyde **8** (Table 2.2 entry 4). The selectivity of ruthenium catalysts towards the oxidation of alcohols[213] including HMF[214] was previously reported. Hence, we hypothesized that the two catalysts might operate synergistically in the oxidative esterification of **1** via orthogonal pathways (A and B, Scheme 2.2) to yield to the desired diester **40**.
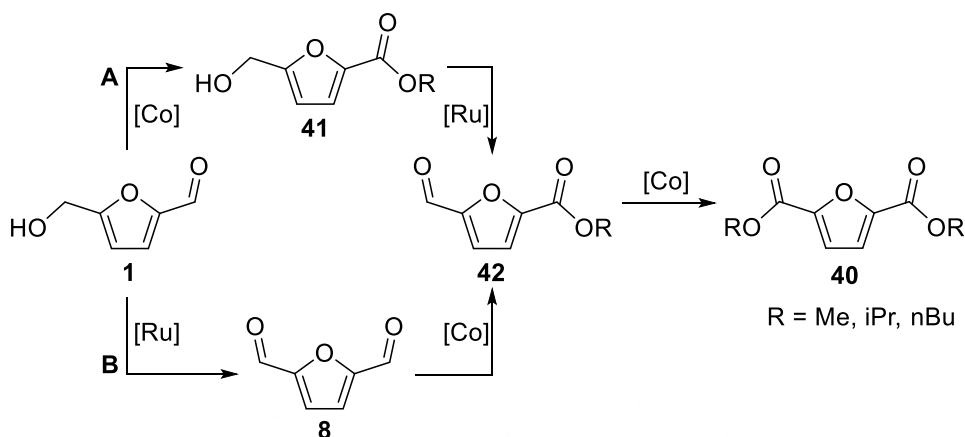
Scheme 2.2. Reaction pathways for the oxidative esterification of HMF (**1**)

Table 2.2. Catalyst screening for the oxidative esterification of HMF (**1**) in methanol

Entry	Catalyst	Conv. (%)	Product selectivity (%) (R=Me)			
			40	41	8	42
1	Co_xO_y-N@C (3,8% Co)	>99	14	69	trace	17
2	Co_xO_y-N@C (5,8% Co)	95	24	71	5	-
3	Pt@C (10% Pt)	trace	trace	trace	-	-
4	Ru@C (5% Ru)	75	3	-	63	34
5	Pd@C (10% Pd)	26[a]	2	14	38	15
6	Fe_2O_3-N@C (2,8% Fe)	28	8	17	15	19

*0.5 mmol HMF, 0.2 equiv. K_2CO_3, 25 mg Cat., 4 mL MeOH, Air as oxidant, 50 °C, 18h. [a] 5-methyl-2-furfural was detected as a product (32% selectivity).

Having this mechanistic insight, and under the assumption that the ruthenium catalyst will help improving the selectivity towards the diester (**40**) by fostering the oxidation of the alcohol moiety of **1**, both catalysts (Co_xO_y-N@C and Ru@C) were combined, leading to the desired product (**40**) quantitatively (Scheme 2.3, path B).

Different experiments using varying proportions of each catalyst were done (Table S1) to find the optimum mixture composition. As a result, the amount of cobalt catalyst could be reduced to a half of its initial amount (Scheme 2.3, A) thanks to the synergistic effect brought by the use of the ruthenium as co-catalyst.
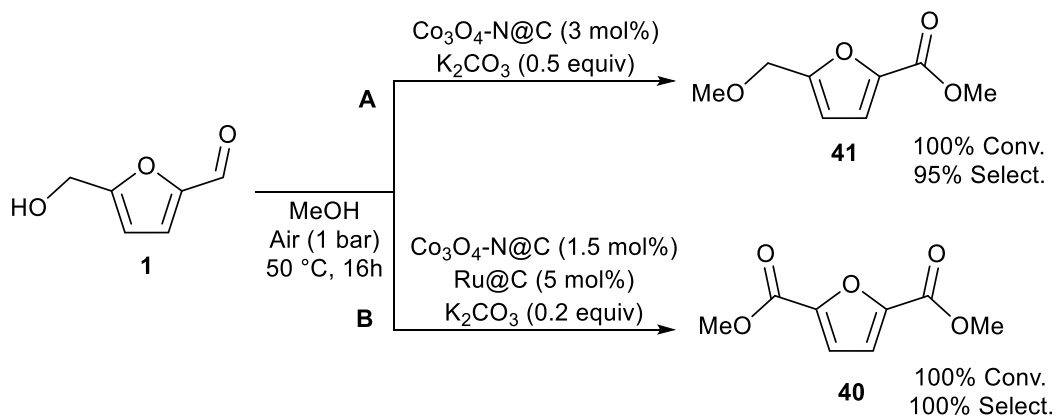
Scheme 2.3. Reaction conditions for the selective oxidative esterification of HMF (**1**)

To gain further insight into the catalytic process, tests without base where conducted (Table S2), showing that it is needed for the cobalt catalyst to turn-over. As it is know that base promotes hemiacetal formation,[215] this observation suggests that the cobalt catalyst is responsible for the oxidation of the hemiacetal formed between the aldehyde and methanol. When the reaction with both catalysts without base was carried out, the conversion was twice as much as the one obtained with the ruthenium alone pointing out, once again, the synergetic cooperation between both catalysts.

Other alcohols were also screened as nucleophiles under our reaction conditions (Table 2.3). As previously discussed in the literature, the mechanism of esterification involves the formation of a hemiacetal intermediary, which is subsequently oxidized.[209] Structural changes might result in variations in the basicity and nucleophilicity of the alcohols, affecting the formation of the hemiacetal intermediary, and hence the overall conversion. Isopropanol gave a poor conversion of HMF and no ester products were observed, suggesting that the formation of the hemiacetal intermediary was not possible (Table 2.3 entry 2). In the case of primary alcohols like ethanol and butanol, good conversions were achieved, with selectivity towards the ester products and to the complete oxidative esterification of HMF (Table 2.3 entries 1 and 3). In the case of butanol, an increase in the reaction temperature resulted in an increase of the conversion of HMF maintaining the product distribution (Table 2.3 entry 4). Such difference in conversion can be attributed to the drastic viscosity changes at the used temperatures, which has direct effects on the kinetics of the reaction (1-Butanol viscosity; at 50 °C 1.4 mPa.s; at 80 °C 0.8 mPa.s; data obtained from the provider).

Table 2.3. Alcohol screening for the oxidative esterification of HMF (**1**)

Entry	Solvent	Conv.	Product selectivity (%)			
			40	41	8	42
1	EtOH	86	10	4	10	76
2	iPrOH	1,5	-	100	-	-
3	nBuOH	55	-	5	24	71
4	nBuOH (80 °C)	90	3	trace	21	76

*0.5 mmol HMF, 0.2 equiv. K_2CO_3, 25 mg Cat., 4 mL Solvent, Air as oxidant, 50 °C, 18h. [a]The ester fragments contain the respective alkylic chain of the alcohol used as solvent.

Additionally, catalyst recycling experiments were performed (See Appendix). The recycling was made by centrifugation, decantation and thorough washing of the catalyst. After the first catalytic cycle, partial deactivation of Co_xO_y-N@C was observed, while Ru@C showed activity detriment only after the fourth cycle (Figure S10). Importantly, HMF was fully converted in every catalytic run, although with different product selectivity. Unfortunately, it was not possible to regain the catalysts' selectivity by the used recovery methods.

2.3.2 Fate of the catalysts

XPS measurements were performed to the fresh and used catalysts (see Appendix), as a way of seeing what happens to the catalyst after the reaction period was finished. The used catalysts were analyzed after one use. The elementary analysis from Ru@C shows no significant difference in the ruthenium content, and the chemical composition also remains similar (aprox. 60% Ru metal and 40% RuO_x). On the other side, changes in the cobalt catalyst could be measured, the nitrogen and cobalt content remains similar and the oxygen content increases from 3 to 5%. When the chemical composition was checked, changes in the nitrogen species were observed; a decrease from 64 to 60% of the Pyridinic N-bound to metal was measured. These species are described as responsible of the catalytic activity of the cobalt catalyst, and the loss of selectivity is a direct consequence of the decreased presence of these species.[216] When the catalysts are recycled these cumulative changes affect its performance; as observed in the recycling experiment, the selectivity was diminished.

2.3.3   Kinectic studies

To gain further insight on the role of each catalyst, kinetic experiments on the oxidation of furfuryl alcohol (**43**) and furfural (**2**) with each separate catalyst were carried out.

As seen in Table 2.4, the product distributions suggest that Co_xO_y-N@C achieves a fast conversion of the aldehyde whilst its activity for the oxidation of the alcohol is low. This was confirmed by the almost quantitative conversion of **2** to **44**, even at higher substrate loadings (Table 2.4, entries 2 and 3). Interestingly, a yield of 13% of **44** was obtained under argon atmosphere, meaning that the presence of gaseous oxygen is not necessary for the cobalt catalyst to oxidize the substrate. This is in agreement with previous reports that show that the oxygen atoms from the metal oxide can be responsible of the oxidation until the metal is completely reduced.[217]

On the other hand, Ru@C selectively converts furfuryl alcohol to furfural with moderate yields (40% of **2**, Table 2.4, entry 5) without the formation of the ester **44**. No conversion was observed in the absence of oxygen (Table 4, entry7).Thus, the results confirm that the ruthenium catalyst oxidizes only the alcohol moiety, while the cobalt oxide converts the aldehyde to the desired ester.

Table 2.4. Independent performance of Co_xO_y-N@C and Ru@C catalysts on the aerobic oxidation of furfuryl alcohol (**43**) and furfural (**2**).

Entry	Catalyst	Substrate	Conv.	Products (%)	
				2	44
1	Co_xO_y-N@C	43	11	12	85
2	Co_xO_y-N@C	2	98	-	100
3	Co_xO_y-N@C	2	80	-	100
4	Co_xO_y-N@C	2	13	-	100
5	Ru@C	43	46	100	-
6	Ru@C	2	-	-	-
7	Ru@C	43	-	-	-

*0.5 mmol Substrate, 0.2 equiv. K_2CO_3, 1.5 mol % Cat., 4 mL MeOH, Air as oxidant, 50 °C, 18h. [a] 1.0 mmol substrate. [b] Argon atmosphere

Furthermore, kinetic analysis of the oxidation of **43** by Ru@C and the oxidative esterification of **2** by Co_xO_y-N@C were performed via in situ IR measurements at different temperatures (Figure 2.1). Changes in temperature showed different effects on the reaction rate, being decreased either at higher or lower temperatures. On one hand, by performing the reaction at 60 °C, the availability of oxygen in the solution is diminished, hence decreasing the reaction rate.[218] On the other hand, when the temperature is decreased to 40 °C, even though there is more oxygen dissolved, the lower amount of (thermal) energy available results in the catalyst' slower turn-over. In all cases, the reaction showed first-order dependence on the substrate.

Figure 2.1. Kinetic profiles at different temperatures for the oxidative esterification of furfural (**2**) in methanol using Co_xO_y-N@C as catalysts and air as oxidant. (40° C k = 0.030±5 h^{-1}; 50 °C k = 0.158±3 h^{-1}; 60 °C k = 0.075±1 h^{-1}).

2.3.4 Oxygen solubility

In order to assess the effect of increased oxygen availability in solution, the kinetic profiles under O_2 atmosphere were measured (Figure 2.2 and Figure S8). As expected, the dilution effect was diminished and no significant difference between the reaction rates at 40 °C and 50 °C was observed. The highest rate was achieved at 60 °C. In comparison to air, the use of pure oxygen as oxidant not only increases the reaction rate in most of the cases (Table S3), but also leads the reaction to completion.

With the aim of circumventing the oxygen solubility limitation under mild reactions conditions, methoxyperfluorobutane (MPFB) was added to the reactions as co-solvent. MPFB have high oxygen solubility (72.7 % v/v). Importantly, fluoroethers have low toxicity, and very low potential, making them attractive to the industry.[210] Full conversion was achieved when a 1:1 mixture of MeOH:MPFB

was used, showing not only the tolerance of the catalysts towards this solvent, but more importantly, a marked increase of the reaction rate was observed, from 0.115 ± 2 h^{-1} to 0.281 ± 7 h^{-1} (Figure 2.2).[219] Moreover, conversion of 85% was observed after 4.5 h, a significant reduction in comparison with the 12 h needed using only MeOH as solvent.

Conversely, the determination of the reaction kinetics for the ruthenium catalyzed oxidation of **43** to **2** proved to be more challenging. Attempts to linearize the reaction profiles to the traditional kinetic equations were not successful. Nonetheless, assuming a Langmuir-Hinshelwood mechanism as suggested by Nie,[214] an apparent zero order dependence in substrate was found from the initial rates (Figure S38). Alternatively, the graphical method reported by Burés was applied,[220, 221] suggesting, by approximation, an apparent zero-order kinetics related to the catalyst (Figure S37).
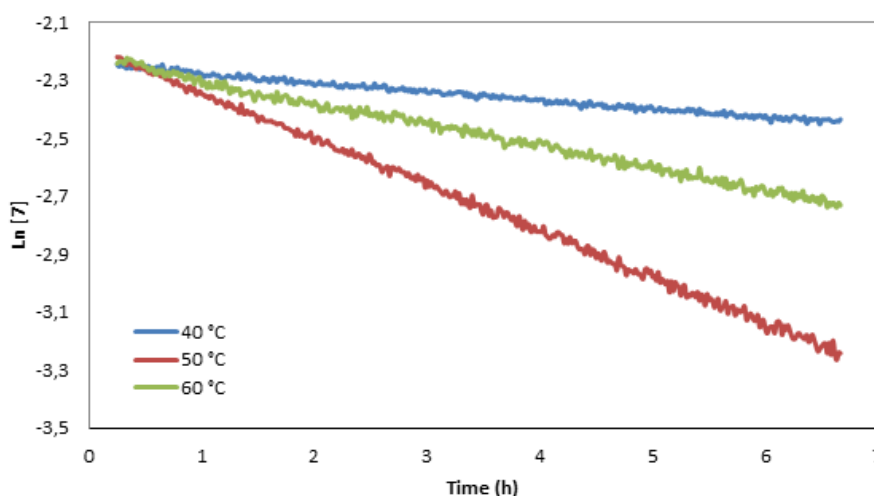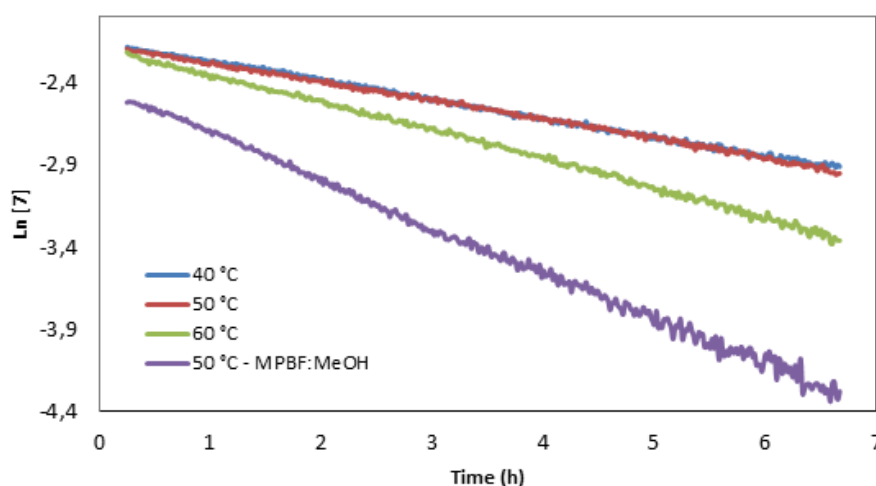

Figure 2.2. Kinetic profiles at different temperatures for the oxidative esterification of furfural (**2**) in methanol and a MPBF:MeOH mixture using Co_xO_y-N@C as catalysts and oxygen as oxidant. (40° C k = 0.115 ± 2 h^{-1}; 50 °C k = 0.115 ± 2 h^{-1}; 60 °C k = 0.174 ± 3 h^{-1}; 50° C MPBF/MeOH mixture k = 0.281 ± 7 h^{-1}).

2.3.5   Mechanism proposal

Based on these results and taking into account previous reports in the literature we propose the reaction pathway presented in scheme 2.4, where the synergetic interaction between both catalysts is explained.

The alcohol oxidation takes place at the ruthenium catalyst, most likely at the surface [Ru]-OH species.[222, 223] It starts with the formation of [Ru]-Alcoholate species by ligand exchange (Scheme 2.4, A), following a β-hydride elimination to form the aldehyde intermediate and [Ru]-H species

(Scheme 2.4, B). Then the hydride species is re-oxidized (Scheme 2.4, C) and upon releasing of oxygen the active [Ru]-OH sites are regenerated (Scheme 2.4, D).
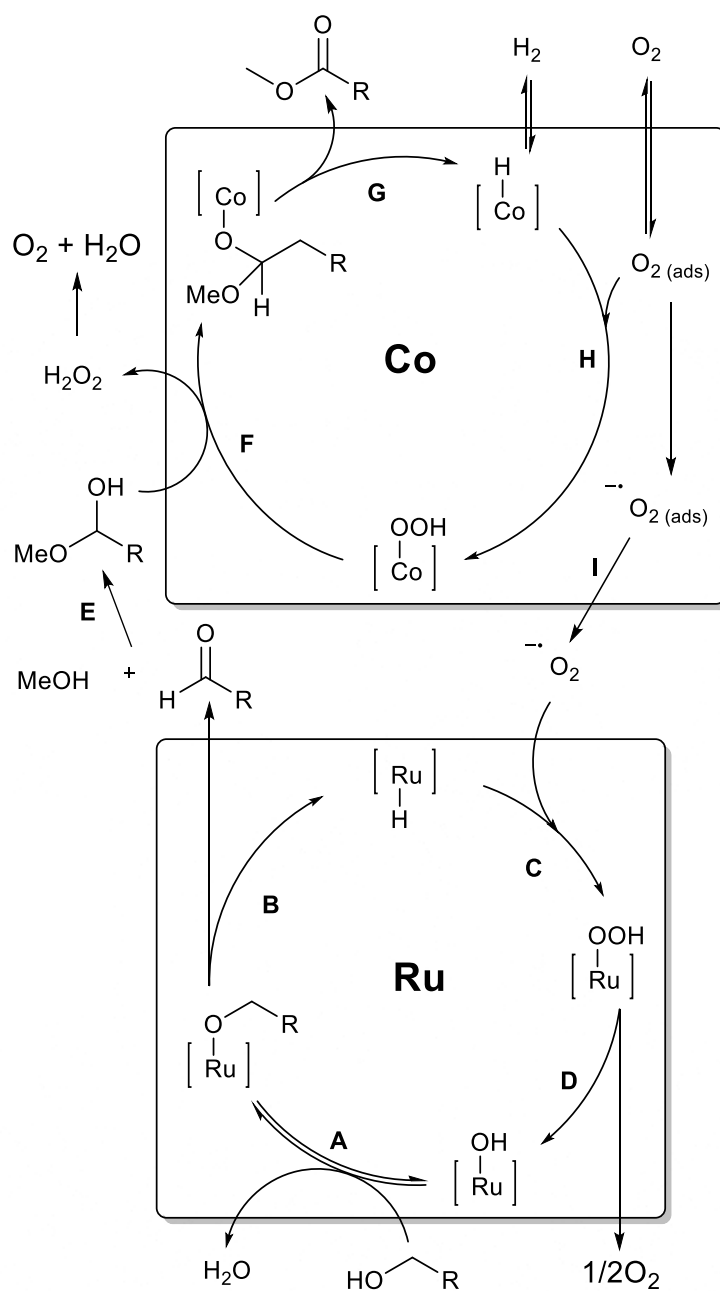
Scheme 2.4. Mechanism proposed for the synergetic bimetallic oxidative esterification of alcohols.

Once in solution, the formed aldehyde reacts with the alcohol to form a hemiacetal in basic media (Scheme 2.4, E). Metal-alcoholate species shall thus be formed at the Cobalt catalyst surface, analogous to was recently observed is a similar system by Stahl and co-workers (Scheme 2.4, F).[224] Then β-hydride elimination takes place to form the ester product along with surface [Co]-H species

(Scheme 2.4, G). More specifically at the [Co]-N sites of the catalyst (from the nitrogen doping), as they are responsible for the catalytic activity (See Appendix for a complete characterization of the catalyst).[216]

A hint on the presence of Cobalt hydrides is given by the detection of gaseous hydrogen in the headspace of a closed reaction setup (see Appendix, Figure S41). Taking into account that this catalyst has shown to be active in hydrogenation reactions,[216] one can expect to see the liberation of H_2 from the [Co]-H species simply as a consequence of the microscopic reversibility principle. The closing step of the cycle is the oxidation of the [Co]-H by the adsorbed oxygen species (Scheme 2.4, H). It is known that on most metal surfaces, adsorbed oxygen ($O_{2(ads)}$) can easily gain electrons from the metal core, resulting in the formation of adsorbed superoxo species ($^{..}O_{2(ads)}$).[225] It has been also documented that in the cobalt catalyst the activation of oxygen is performed both at the Co-N$_x$ and Co-O$_x$ sites.[226]

We were able to detect the formation of superoxide by EPR spectroscopy. The measurements were performed using 5,5-dimethyl-1-pyrroline N-oxide (DMPO) as a spin trap from which the corresponding DMPO-OOH adduct is detected,[227, 228] revealing the formation of superoxide radical (Figure 2.3). These experiments show the formation of superoxide in the presence of the cobalt catalyst but not with the ruthenium catalyst. Interestingly, when both catalysts are present, the signal of the superoxide loses intensity, suggesting that the superoxide is being quenched by ruthenium catalyst. This interaction can be responsible for the improved conversion shown before (see table S2 entry 3).

Thus, we propose that the synergy observed between both catalysts is due to the formation of superoxide species by the cobalt catalyst (Scheme 2.4, I) which upon desorption, is consumed in the reoxidation of the [Ru]-H facilitating this commonly difficult step (Scheme 2.4, C). The catalysis performed by ruthenium benefits from the superoxide formation by the cobalt catalysis, and the later benefits from the increased presence of aldehyde delivered by the alcohol oxidation at the ruthenium catalyst. Thanks to this synergy, we were able to perform the complete oxidative esterification of HMF with quantitative yields.
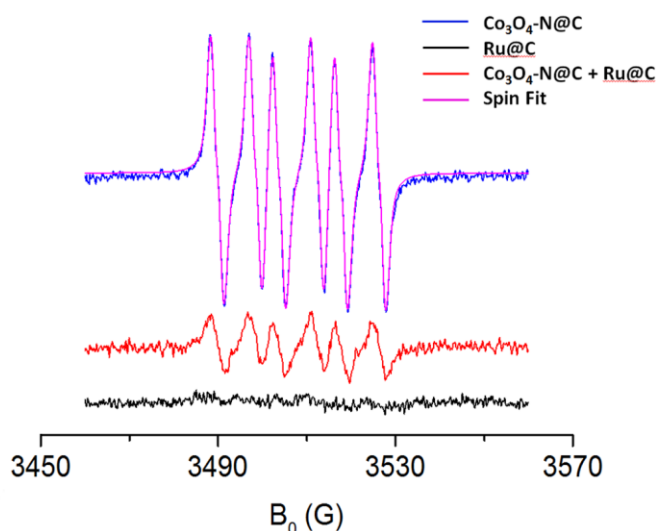
Figure 2.3. EPR measurements of different catalytic solutions for the oxidation of HMF (1) in the presence of DMPO showing the characteristic signals of the DMPO-OOH spin adduct. The DMPO-OOH signal at g = 2.006 was simulated using SpinFit (Bruker) with the spin Hamiltonian parameters hyperfine splitting αN = 13.73, $\alpha H\beta$ = 8.03 and $\alpha H\gamma$ = 1.51 G (the hyperfine splitting of $\alpha H\gamma$ is not resolved due to the line broadening but it can be clearly seen from the 2nd derivative of the EPR signal, see appendix).

2.4 Conclusions

Given its inherent reactivity, the selective oxidation of HMF (**1**) is a challenge. Herewith, we report the selective oxidative esterification of HMF to the esters **40** and **41** with excellent to quantitative yields under mild conditions. This was achieved by the use of a bimetallic catalytic system containing Ru@C and Co_xO_y-N@C catalysts working in synergy. Such effect seems to be related to the formation of superoxide radicals at the cobalt surface which are in turn used for the catalytic turn-over at the ruthenium sites. The kinetics of the oxidation of the alcohol moiety by Ru@C follow an apparent order zero on catalyst and substrate. In contrast, the esterification of the aldehyde moiety at Co_xO_y-N@C shows a first order dependence on the substrate. We demonstrated that the rate of the reaction is limited by the solubility of oxygen by using pure O_2 instead of air and by increasing the solubility of the gas using a perfluoroester (MPFB) as a co-solvent.

To the best of our knowledge, this is the first report of the use mixture of cobalt and ruthenium catalysts in oxidative esterification reactions and gives the best yields and conversions for HMF under the mildest conditions reported so far.

3 Oxidative Esterification of 5-Hydroxymethylfurfural under flow conditions using a bimetallic Co/Ru catalyst[b]

3.1 Introduction

Nowadays, the necessity to reduce society's dependence in oil derivatives makes obtaining platform chemicals from renewable sources a highly relevant topic. The use of biomass derived platform chemicals is a step forward in achieving a sustainable circular economy,[190] bringing molecules like 5-hydroxymethylfurfural (HMF, **1**) to the spotlight.[14] And even more the synthesis of furan based polymers,[61] were polyethylene furanoate (PEF) stands as a promising substitute of polyethylene terephtalate (PET),[151, 193, 194] being 100% produced from renewable sources.

The biomass-based production route of PEF commonly starts with acidic or enzymatic hydrolysis of cellulose to obtain C_6-sugars (e.g. glucose, fructose), from which dimethyl-2,5-furandicarboxylate (FDCM, **40**) and ethylene glycol (EG) can be synthesized. HMF is obtained by the dehydration of sugars (preferably fructose);[229] and from its oxidative esterification in MeOH, FDCM can be obtained. EtOH is obtained from the fermentation of sugars,[230] which is dehydrated to synthesize ethylene.[231] By the established industrial oxidation, ethylene is converted into EG. Finally, PEF is synthesized by a 2-stage polymerization between FDCM and EG (See scheme 3.1).[202]

In order to make PEF economically viable, the production of FDCM or analogs (e.g. 2,5-furandicarboxilic acid (FDCA)) must be improved, either by catalyst development or by using new synthetic techniques. FDCM is a better starting monomer than FDCA because is easier to purify, it has shown more stability during the polymerization process and increased rates of reaction.[202] Taking this into consideration, FDCM was chosen as synthetic target.

The use of oxygen gas as ultimate oxidant in organic synthesis is an attractive goal as it is readily available and non-toxic. Nevertheless, is usage is limited due to safety concerns and the poor solubility of oxygen in liquids.[218] Such concerns have high influence when a process is in the scale up phase. Microflow conditions presents itself as an alternative in increasing safety, do to smaller reactor volumes the severity of an accident is minimized, also the accumulation of hazardous/unstable intermediaries is minimized. The possibility of accurately dose gases and the

---

[b] The work presented in this chapter was published in ChemCatChem, 2020, DOI: 10.1002/cctc.202000205, see appendix.

lack of headspace (e.g. batch conditions/reactors) reduce significantly the risks of accidents.[168, 170, 232]
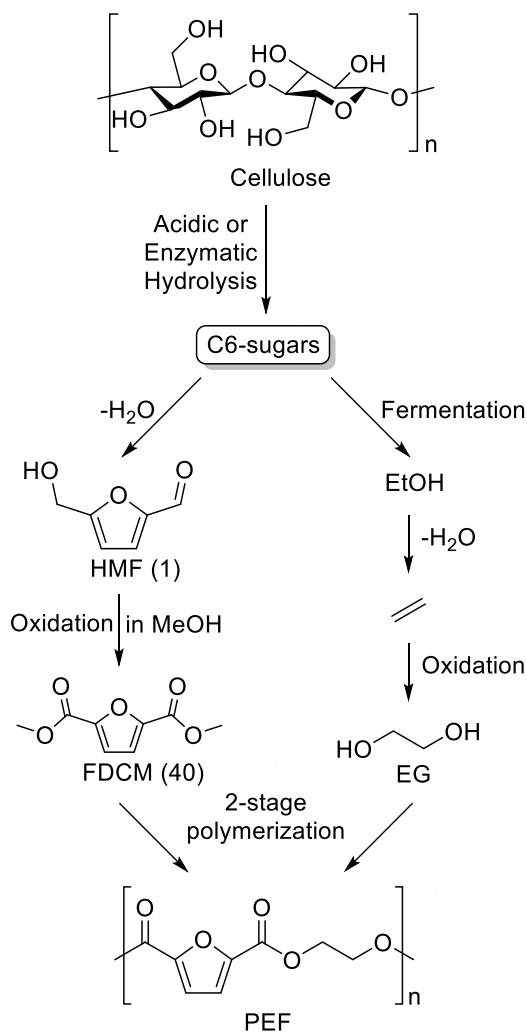
Scheme 3.1. Production of PEF from biomass.

Under microflow conditions, as a consequence of the reduced size component, different physical conditions are optimized to a higher level compared to the standard laboratory and industrial conditions (e.g. mass and heat transfer, mixing, etc.).[233, 234] More importantly, mass transfer limitations of working with low solubility gases like oxygen.[235] The development of processes under flow conditions allows the possibility of a scale up with relative easiness.[236]

In this chapter the development of a bimetallic catalyst, containing cobalt and ruthenium supported on carbon and being able to operate under the up to date commercially available technology, will be discussed. Also, its application for the first oxidative esterification of HMF under flow conditions to produce FDCM with very high conversions and good selectivity.

3.2 Experimental Section

3.2.1 Synthesis of the catalysts

3.2.1.1 *RuOx-N@C-powder catalyst*

[Ru(p-cymene)Cl$_2$]$_2$ (154.6 mg, 0.26 mmol, corresponds to 5% Ru) and 1,10-Phenantroline (83.0 mg, 0.46 mmol) were mixed in Ethanol (50 mL) for 30 min. The desired carbon (759.3 mg) was added to the solution and heated to reflux at 100 °C for 4 hours. The solvent was evaporated and the resulting solid thoroughly dried overnight at 60 °C under high vacuum. The black solid obtained was then pyrolized at 800 °C for 2 hours in argon atmosphere and cooled to room temperature.

Elemental analysis (Wt %): C= 76.27, H= 0.332, N= 0.588, Ru= 5.51.

3.2.1.2 *Co$_x$O$_y$ + RuOx-N@C-powder catalyst*

Co(OAc)$_2$.4H$_2$O (160.6 mg, 0.64 mmol, corresponds to 3% wt Co) and [Ru(p-cymene)Cl$_2$]$_2$ (154.6 mg, 0.26 mmol, corresponds to 5% wt Ru) were dissolved in 50 mL MeOH, after 5 min of vigorous stirring 1,10-Phenantroline (315.0 mg, 1.75 mmol) was added. The solution was stirred for 30 min and carbon powder (412 mg) was added, then heated to reflux at 100 °C for 4 hours. The solvent was evaporated and the resulting solid thoroughly dried overnight at 60 °C under high vacuum. The black solid obtained was then pyrolized at 800 °C for 2 hours in argon atmosphere and cooled to room temperature.

Elemental analysis (Wt %): C= 70.08, H= 0.575, N= 1.633, Co= 4.83, Ru= 4.48.

3.2.1.3 *Co$_x$O$_y$-N@C catalysts*

Co(OAc)$_2$.4H$_2$O (380.4 mg, 1.53 mmol, corresponds to 3% wt Co) and 1,10-Phenantroline (550.5 mg, 3.06 mmol) were mixed in Ethanol (150 mL) for 30 min. The desired carbon (2069.1 mg) was added to the solution and heated to reflux at 100 °C for 4 hours. The solvent was evaporated and the resulting solid thoroughly dried overnight at 60 °C under high vacuum. The black solid obtained was then pyrolized at 800 °C for 2 hours in argon atmosphere and cooled to room temperature.

-20+40 mesh particle size (C-irregular): Elemental analysis (Wt %): C= 72.75, H= 0.477, N= 1.745, Co= 2.23. XPS data (atom %): C= 90.1, O= 5.9, N= 2.1, Si= 0.8, S= 0.2, Co= 0.6.

0.8 mm pellets (C-pellets): Elemental analysis (Wt %): C= 85.40, H= 0.3954, N= 3.961, Co= 2.34.

3.2.1.4   *RuO$_x$-N@C catalysts*

[Ru(p-cymene)Cl$_2$]$_2$ (463.8 mg, 0.74 mmol, corresponds to 5% wt Ru) and 1,10-Phenantroline (266.7 mg, 1.48 mmol) were mixed in Ethanol (150 mL) for 30 min. The desired carbon (2269.5 mg) was added to the solution and heated to reflux at 100 °C for 4 hours. The solvent was evaporated and the resulting solid thoroughly dried overnight at 60 °C under high vacuum. The black solid obtained was then pyrolized at 800 °C for 2 hours in argon atmosphere and cooled to room temperature.

-20+40 mesh particle size(C-irregular): Elemental analysis (Wt %): C= 65.40, H= 0.4507, N= 1.167, Ru= 2.46. XPS data (atom %): C= 89.2, O= 6.9, N= 0.9, Si= 0.7, S= 0.3, Ru= 1.8.

0.8 mm pellets (C-pellets): Elemental analysis analysis (Wt %): C= 83.12, H= 0.4507, N= 0.850, Ru= 1.79.

3.2.1.5   *Bimetallic Co$_x$O$_y$-N + RuO$_x$-N@C catalysts*

[Ru(p-cymene)Cl$_2$]$_2$ (231.9 mg, 0.38 mmol, corresponds to 5% wt Ru) and 1,10-Phenantroline (133.3 mg, 0.74 mmol) were mixed in Ethanol (75 mL) for 30 min. The previously prepared Co$_x$O$_y$-N@C catalyst (1143.8 mg) was added to the solution and heated to reflux at 100 °C for 4 hours. The solvent was evaporated and the resulting solid thoroughly dried overnight at 60 °C under high vacuum. The black solid obtained was then pyrolized at 800 °C for 2 hours in argon atmosphere and cooled to room temperature.

-20+40 mesh particle size (C-irregular): Elemental analysis (Wt %): C= 68.86, H= 0.5722, N= 1.746, Co= 1.70, Ru= 2.34. XPS data (atom %): C= 88.3, O= 6.9, N= 1.3, Si= 0.5, S= 0.2, Co= 1.3, Ru= 1.3.

0.8 mm pellets (C-pellets): Elemental analysis (Wt %): C= 72.35, H= 0.1247, N= 1.789, Co= 1.48, Ru= 0.56.

3.2.1.6   *Bimetallic RuO$_x$-N + Co$_x$O$_y$-N@C catalysts*

Co(OAc)$_2$.4H$_2$O (190.2 mg, 0.765 mmol, corresponds to 3% wt Co) and 1,10-Phenantroline (275.3 mg, 1.53 mmol) were mixed in Ethanol (75 mL) for 30 min. The previously prepared RuO$_x$-N@C catalyst (1034.5 mg) was added to the solution and heated to reflux at 100 °C for 4 hours. The solvent was evaporated and the resulting solid thoroughly dried overnight at 60 °C under high vacuum. The black solid obtained was then pyrolized at 800 °C for 2 hours in argon atmosphere and cooled to room temperature.

-20+40 mesh particle size (C-irregular): Elemental analysis (Wt %): C= 85.33, H= 0.6427; N= 3.007, Co= 1.58, Ru= 2.17. XPS data (atom %): C= 86.0, O= 7.7, N= 1.9, Si= 0.6, S= 0.4, Co= 1.3, Ru= 1.7.

0.8 mm pellets (C-pellets): Elemental analysis (Wt %): C= 54.11, H= 0.0802, N= 1.770, Co= 1.26, Ru= 1.20.

3.2.2   Flow microreactor

All the reactions were carried out using the Modular MicroReaction System (MMRS) from Ehrfeld Mikrotechnik. The solution was pumped with a HPLC pump (Knauer). The oxygen flow was controlled with an EL-FLOW Mass Flow Controller from Bronkhorst. For the gas/liquid mixing a multilamination mixer was used, a Cartridge Reactor F200 with temperature indicator was used. The total volume of the setup was ~7-8 mL.

3.2.3   Oxidative Esterification of HMF

A desired amount of K_2CO_3 was let to dissolve in MeOH overnight at room temperature under vigorous stirring, once the K_2CO_3 was completely dissolved HMF was added, additional MeOH was added until a solution with the concentration of 0.125 M in HMF and 0.025 M in K_2CO_3 was reached. 600 mg of catalyst was loaded into the cartridge of the reactor; then the heating and a flow of MeOH and oxygen were started. Once the temperature, pressure and flows (liquid and gas) in the system were stable (after ~45-60 min) the HMF/ K_2CO_3 solution was pumped through and the reaction was started. The solution coming at the end of the setup was collected and analyzed by gas chromatography.

3.2.4   Isolation of compounds

An automated flash chromatography system with UV detection was used (CombiFlashRf from Teledyne ISCO), using a silica column and heptane/ethyl acetate as solvents. The solvent flow was set up to 30mL/min. The solvent setup was configured as follows, from start to min 20 the concentration increased from 0% to 45% ethyl acetate; the mixture was kept to min 32, and from min 32 to min 42 the concentration increased from 45% to 100% ethyl acetate; which was kept flowing until the column was completely washed. The compounds obtained were analyzed by NMR and GC-MS.

3.3 Results and discussion

3.3.1 Explorative experiments towards bimetallic catalysts

As shown in Scheme 3.2, the oxidative esterification of HMF (**1**) to produce FDCM (**40**) can be achieved in a divergent, multistep process. HMF is converted in a first step to **41** or **8**, from which **42** is obtained and a final aldehyde esterification leads to the desired **40**. Conversion and selectivity depends on the catalyst used and its activity, as demonstrated in the oxidation of HMF to FDCA (**7**).[237]
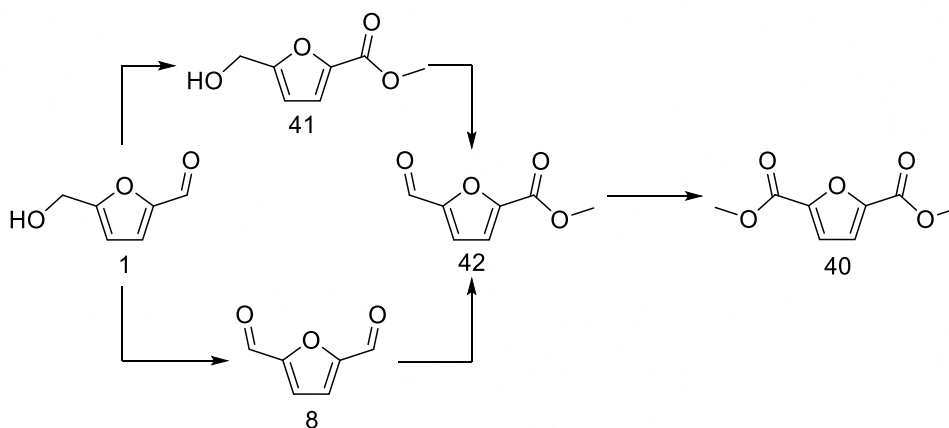
Scheme 3.2. Reaction pathway for the oxidative esterification of HMF (**1**)

In the previous chapter, the batch oxidative esterification of HMF to **40** using a mixture of a self-made Co_xO_y-N@C and commercial Ru@C catalyst was discussed.[238] In order to incorporate both metals in the same support, nitrogen doped RuO_x-N@C-powder was prepared and tested.

The RuO_x-N@C-powder showed a similar activity as its counterpart, the commercial Ru@C. A conversion of 60% was achieved, with a selectivity of 76% to 8. (See table 3.1 entry 1). With this result the bimetallic Co_xO_y + RuOx-N@C-powder was prepared by simultaneous impregnation of both metals, which was also tested (See table 3.1 entry 2).

The results were promising, >99% of HMF conversion was achieved with selectivities of 38% towards FDCM (**40**), 47% to **41**, and 8% toward **42**. Already knowing the limitations of the batch reactions, we moved on to perform the reaction in a flow regime.

Table 3.1. Explorative experiments using powder catalysts

Entry	Catalyst	Conv. (%)	Product Selectivity				
			40	41	8	42	Others
1	RuO_x-N@C-powder	60	-	-	76	24	-
2	Co_xO_y + RuO_x-N@C-powder	>99	38	47	-	8	7

*Reaction conditions: 0.5 mmol HMF, 0.2 equiv K_2CO_3, 50 mg cat,4 mL MeOH, Air as oxidant, 50 °C 18h. Procedure described in 2.2.2.

3.3.2 Explorative reactions in flow regime

When powder catalysts analogous to those used in the aforementioned batch experiments were used in the microflow reactor, technical problems arose. The fine catalyst particles packed in the cartridge led to an increase of the system pressure above the maximum input pressure of oxygen. As a consequence, oxygen could not be fed into the system anymore. In an attempt to avoid this problem, the powdered catalyst was mixed with glass spheres and glass wool, alas, unsuccessfully. Layering of the catalyst with glass spheres led to an improvement, although the catalyst particles were too small to be contained in the cartridge, and small amounts of catalyst were collected along with the product on the system outlet. Also increased temperature conditions were not ideal, the HMF decomposed at 150 °C causing clogging of the system.

3.3.3 Oxidative esterification in flow conditions

Therefore, a series of new catalysts were synthesized; based on the type of carbon support and in the order in which the metals are impregnated on them. Carbon particles sized -20+40 mesh (irregular shape) and cylindrical pellets (~0,8 mm diameter) were selected, which will be called C-irregular and C-pellets respectively from now on (see figure 3.1).

This change allowed to obtain the desired reactor operating conditions, and to prevent the catalyst loss. The catalyst screening was focused on the conversion of HMF and the selectivity shown towards **40** and the intermediaries **41**, **8** and **42**.
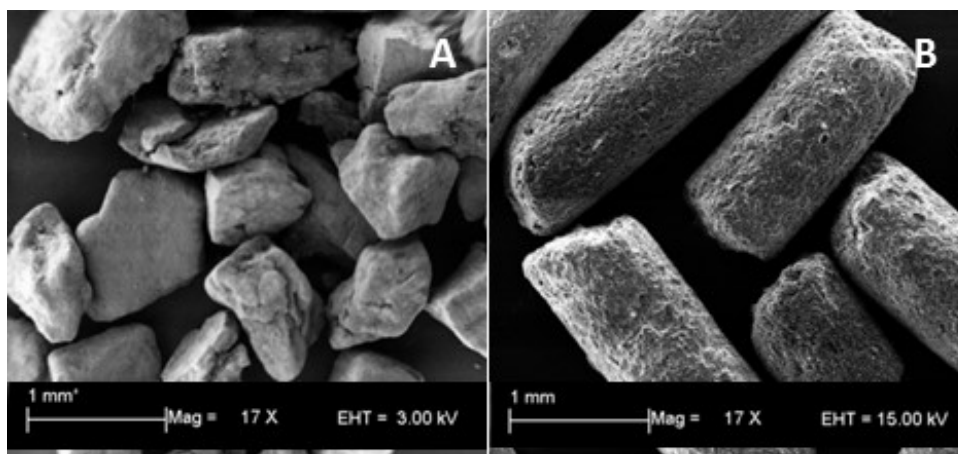
Figure 3.1. SEM images of C-irregular(A) and C-pellets (B)

3.3.3.1 *Microreactor setup*

In the explorative experiments not only problems related to the catalyst and substrate appeared but also related to the setup (e.g. starting procedure, stabilization of the reaction parameters, etc). All the problems were solved and a configuration of the micro reactor setup as seen in Scheme 3.3 was used. It begins with having gas and liquid phases separated. In the liquid part a selector valve allows to choose from clean solvent or substrate solution. The two phases (gas and liquid) were mixed, and afterwards the mixture goes into the reactor. Then the solution is cooled down in a water/ice bath and collected to analyze. The setup contains a pressure gauge, as well as a temperature indicator. The reactor is heated with a fittet thermostat. Additionally, for safety reasons a pressure release valve was used. The mixer used is based in the multilamination principle which provides the ideal conditions for gas/liquid mixing.[239]

3.3.3.1 *Catalyst screening*

As presented in Table 3.2 when the Co_xO_y-N@C catalysts were used (entries 1 and 5) selectivity (up to 73%) towards **41** was observed for both types of supports. The Co_xO_y-N@C-irregular catalyst (entry 5) shows an excellent 92% conversion of HMF and poor selectivity of 18% towards **40**, in comparison Co_xO_y-N@C-pellets (entry 1) only shows a 57% conversion and 4% selectivity towards **40**. In the case of the RuO_x-N@C catalysts (entries 2 and 6), selectivity towards **8** was observed. On the contrary to the Co_xO_y-N@C catalysts; conversion up to 60% was obtained with RuO_x-N@C-pellets (entry 2) and just 35% with RuO_x-N@C-irregular (entry 6). The latter also show the highest amount of side products of the catalyst screening, up to 31%. For the cobalt catalyst the best support seemed to be C-irregular and surprisingly for the ruthenium one C-pellets. Up to this point the reactivity and selectivity of the catalysts is similar to what was observed before.

48
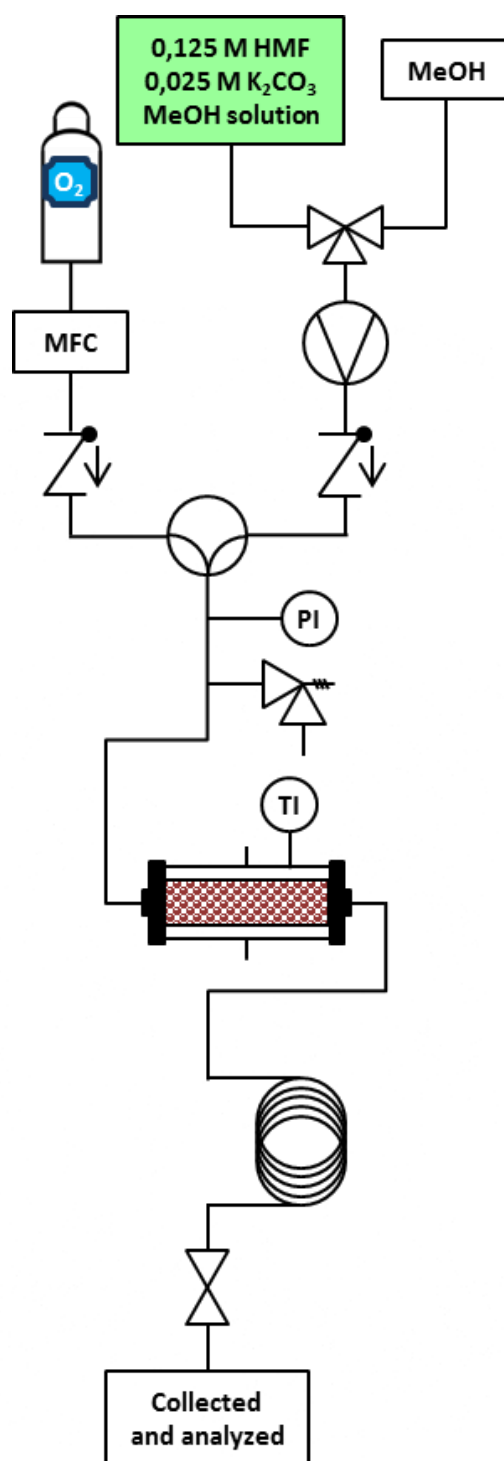
Scheme 3.3. Flow diagram of the microreactor setup used

Must be highlighted that, nitrogen doping of the ruthenium over carbon has no hindering effect of the catalytic activity. The commercial Ru@C is prepared by reduction in H_2 atmosphere,[240] and the RuO_x-N@C is pyrolyzed in argon atmosphere. This change in the preparation method allow the

possibility of simplifying the synthesis of the catalysts, by removing the difficulty of preparing a bimetallic catalyst with metallic Ru and Co-oxide. Also important, the change of support didn't suppress the catalytic activity.

Table 3.2. Catalyst Screening

Entry	Catalyst	Conv. (%)	Product Selectivity (%)				
			40	41	8	42	Others
1	Co_xO_y-N@C-pellets	57	4	72	12	-	12
2	RuO_x-N@C-pellets	60	4	-	66	25	5
3	Co_xO_y-N + RuO_x-N@C-pellets	44	5	46	20	-	29
4	RuO_x-N + Co_xO_y-N@C-pellets	66	15	52	11	-	22
5	Co_xO_y-N@C-irregular	92	18	63	4	-	15
6	RuO_x-N@C-irregular	35	3	-	54	11	31
7	Co_xO_y-N + RuO_x-N@C-irregular	98	57	20	1	1	21
8	RuO_x-N + Co_xO_y-N@C-irregular	73	27	45	8	-	20
9	Mixture entry 5 – entry 6	62	15	50	11	1	23

*Reaction conditions: 600 mg cat. loading, 0.2mL/min of a MeOH solution of 0.125 M HMF and 0.025 M K_2CO_3, 1.4 mL/min of oxygen, reactor temperature: 62°C, autogenous pressure, residence time in reactor: 10 min.

In the case of Co_xO_y-N + RuO_x-N@C catalysts (entries 3 and 7) remarkable differences in conversion and selectivity were observed. Using C-pellets as support (entry 3) gave only 44% conversion with selectivity toward products **41** and **8** of 46% and 20% respectively. On other side, C-irregular (entry 7) as support gave the best results of the catalyst screening; where conversion up to 98% was achieved and selectivity of 57% towards the desired product **40**. In addition, RuO_x-N + Co_xO_y-N@C catalysts (entries 4 and 8) show moderate to good conversions, 66% for C-pellets (entry 4) and 73% for C-Irregular (entry 8). And selectivities of 52% and 45% for **41** and 15% and 27% for **40** respectively. The catalytic performance of mixing Co_xO_y-N@C-irregular and RuO_x-N@C-irregular (entry 9) was also checked. 62% conversion was obtained with selectivities of 50% and 15% towards **41** and **40** respectively. This result confirms that the presence of cobalt and ruthenium in the same support (entry 7) represents an improvement. In comparison to the test performed with each metal by its own, the metal amount used was reduced 50% and 62% conversion was obtained, with 50%

and 15% selectivity towards **41** and **40** respectively. Confirming that the synergy observed in batch reactions is also present under flow regime.

3.3.3.2   *Activity profiles*

The most promising reaction progress for the Co_xO_y-N + RuO_x-N@C-irregular catalyst is shown in Figure 3.2, remarkably, the selectivity towards **40** increases with the time. Within the timeframe of the experiment a steady state in conversion (>95% HMF conversion after 100 min) was achieved but not in selectivity. Selectivity towards **41** is on its highest at min 40 (>35%) and constantly decreases to 20% until min 180. Similar behavior is observed for **8** and byproducts (Others). The decrease in selectivity for some molecules coincides with the increase in selectivity towards **40**. Also, an unexpected product (**45**) (see figure 3.2 and scheme 3.4) formed in relevant amounts (up to 20% selectivity).
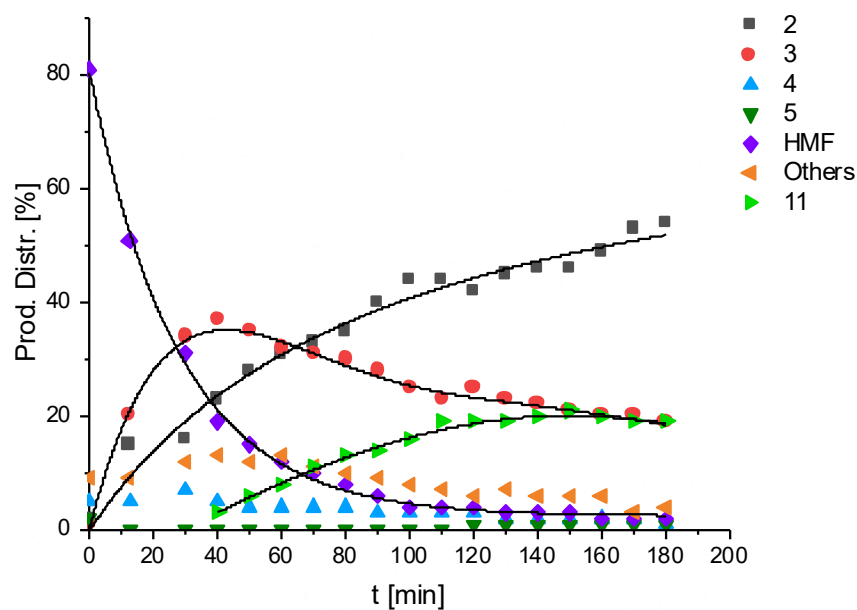
Figure 3.2. Reaction progress over time when Co_xO_y-N + RuO_x-N@C-irregular was tested.

As show in table 3.2, in all experiments side products could be detected (identified as Others). The identified compounds can be seen in Scheme 3.4.
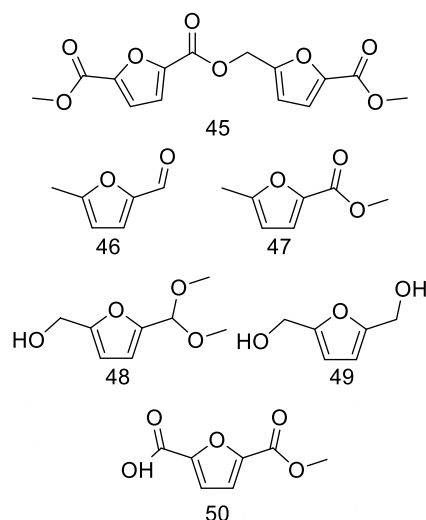
Scheme 3.4. Byproducts detected during the catalyst screening.

Compound **46** is present in the starting solution of HMF, presumably a decomposition compound formed in basic conditions; from which compound **47** is naturally obtained after passing through the setup. Compound **48** could be detected at the first samples collected in each experiment, indicating the acidic character of the catalysts at the first stages of the experiments; acetals are normally formed under acidic conditions. Compound **49** is a side product coming from the hydrogenation of HMF, as we demonstrated before, hydrogen gas was detected in the headspace of batch reactions which could be the starting step of a transfer hydrogenation.[238] A partially esterificated FDCA (**7**) was detected **50** which its formation is presumably from the partial hydrolysis of FDCM. A compound with molecular mass and fragmentation patterns fitting to **45** was detected, this suggests that esterification between intermediaries **41** and **42** is possible under the reaction conditions.

3.3.4   Catalyst characterization

3.3.4.1   *N₂ Physisoprtion (BET measurements)*

As a general remark, the cobalt containing catalysts with C-irregular as support are more active in the conversion of HMF (Table 3.2 entries 5, 7 and 8) with a higher selectivity towards **40**. In the search for an explanation to this fact BET measurements were done to the raw supports and to the prepared catalysts (see Table 3.3).

Table 3.3. BET Measurements

Entry	Catalyst	Surface area (m^2/g)	Micropore area (m^2/g)	External surface area (m^2/g)
1	C-pellets	1178.2693	1125.1873	53.0820
2	Co_xO_y-N@C-pellets	678.8927	647.5312	31.3615
3	RuO_x-N@C-pellets	695.7680	660.1688	35.5993
4	Co_xO_y-N + RuO_x-N@C-pellets	546.9071	513.2515	33.6556
5	RuO_x-N + Co_xO_y-N@C-pellets	463.7652	436.8284	36.9341
6	C-irregular	562.7351	372.7956	189.9395
7	Co_xO_y-N@C-irregular	128.4905	5.0698	123.4206
8	RuO_x-N@C-irregular	226.8789	76.5092	150.3697
9	Co_xO_y-N + RuO_x-N@C-irregular	174.9132	51.4183	123.4949
10	RuO_x-N + Co_xO_y-N@C-irregular	129.3743	29.1868	100.1874

The results show that there is a marked difference in the surface area of each raw support (entries 1 and 6). C-pellets have more than twice the surface area of C-irregular, 1178.9897 m^2/g and 562.7351 m^2/g respectively. After the first impregnation and pyrolysis, the surface area is drastically reduced: more than 40 % for the C-pellets catalysts (entries 2 and 3), more than 75% for Co_xO_y-N@C-irregular (entry 7) and 60% for the RuO_x-N@C-irregular catalyst (entry 8). The measurements after the second impregnation and pyrolysis show the same trend in the case of the C-pellet catalysts (entries 4 and 5). Co_xO_y-N + RuO_x-N@C-pellets lose 19% of the starting surface area and, RuO_x-N + Co_xO_y-N@C-pellets loses 33%. On other side, RuO_x-N + Co_xO_y-N@C-irregular lose 43% (entry 10). Surprisingly Co_xO_y-N + RuO_x-N@C-irregular (entry 9) presents an increase, having almost 140% the surface area the initial material had.

When the porosity of the materials (micropore area and external surface area) was studied, could be observed that the C-pellet materials present a micropore:mesopore ratio of about 18:1 in comparison to 1:3 for the C-irregular ones. This is an important feature because in the conditions in which the experiments were performed porosity plays an important role in the diffusion of the substrate in the catalysts; which have direct consequences on the conversion.[241] The better reactivity of C-irregular catalysts can be correlated with the abundance of mesopores in its structure in comparison to the C-pellet catalysts. The surface area provided by mesopores in the C-irregular materials is evidently higher; almost 4 times more than the C-pellets materials. Having a residence time of only 10 min, it is important that the substrate can easily diffuse into the catalysts' pores. It

is know that micropores don't take part in the catalytic conversion of bulky molecules, because the active places within them can't be reached by the substrates, making them useless and therefore a non-active surface in the catalysts.[242] For the residence time set in our experiments, the presence of mesopores is an important feature, it makes the process less diffusion limited and also they are accessible to the bulky substrates.[243]

3.3.4.2   *XRD, XPS and elemental analysis*

Also, XDR measurements of all the catalysts were done (See Supp. Info). Diffraction patterns of all the catalysts supported on C-pellets shows broad bands and low intensity peaks, which is evidence of a lack of crystallinity.[244] Conversely, the C-irregular catalysts show crystallinity. The Co_xO_y-N@C-irregular shows the same diffraction pattern as the Co_xO_y-N@C powder catalysts we previously used,[209, 238] meaning that the particles in the new catalyst are similar to the powder analog. Co_xO_y-N@C-irregular contains Co metal, CoO and Co_3O_4. More interestingly, Co_xO_y-N + RuO_x-N@C-irregular catalyst it was possible to confirm the presence of Co metal, but it was not possible to assign some diffraction peaks. Also, the diffraction pattern is not comparable with RuO_x-N + Co_xO_y-N@C-irregular. This shows that the order of addition of the metals have an influence in the type of catalyst obtained. The metal species obtained in both Co_xO_y-N + RuO_x-N@C-irregular and RuO_x-N + Co_xO_y-N@C-irregular are different.

In order to better understand the nature of the surface of the C-irregular catalysts XPS characterization of them was performed. As expected, 3 different species of nitrogen were found. Pyridinic N-Metal, Pyrrolic N and Ammonia N (See Table 3.4).

Table 3.4. Nitrogen species detected by XPS

Entry	Catalyst	Nitrogen species (%)		
		Pyridinic N (M-N)	Pyrrolic N	Ammon N
1	Co_xO_y-N@C-irregular	58	35	7
2	RuO_x-N@C-irregular	39	40	21
3	Co_xO_y-N + RuO_x-N@C-irregular	40	37	23
4	RuO_x-N + Co_xO_y-N@C-irregular	46	34	20

The data in table 3.4 show that nitrogen doped catalysts were effectively produced, and that the Pyridinic N bound to metal specie is the more abundant one, an important fact that improves catalytic activity.[216]

Two ruthenium species are present in the surface, not only Ru^0 but also Ru^{4+} was detected. All the samples contained mainly ~70% Ru^0 and ~30% Ru. On the other side; after a modification of the Auger parameter it was possible to detect Co^{3+} in Co_xO_y-N@C-irregular, and both Co^{2+} and Co^{3+} in the bimetallic catalysts. Due to the low content of Cobalt, quantification of the Cobalt species was not possible.

A comparison of the traditional elemental analysis and the elemental analysis of the surface (by XPS) shows that the metallic species are located mostly in the surface of the material (see Table 3.5).

Table 3.5. Comparison of elemental analysis

Entry	Catalyst	Location	Metal (wt %)	
			Co	Ru
1	Co_xO_y-N@C-irregular	Bulk	2.23	-
		Surface	2.78	-
2	RuO_x-N@C-irregular	Bulk	-	2.46
		Surface	-	12.94
3	Co_xO_y-N + RuO_x-N@C-irregular	Bulk	1.70	2.34
		Surface	5.40	9.27
4	RuO_x-N + Co_xO_y-N@C-irregular	Bulk	1.58	2.17
		Surface	5.24	11.76

*Surface elemental analysis derived from identification of >99,6% of atoms by XPS

Co_xO_y-N@C-irregular is the starting material to synthesize Co_xO_y-N + RuO_x-N@C-irregular. The comparison between the 2 elemental analyses (entries 1 and 3) allow us to see a migration process of the cobalt from the bulk to the surface of the material; most likely fostered by the incorporation of the ruthenium. This result is supported by the increase in porosity observed for this catalyst; in which the mesoporous quantity remains similar but the micropore quantity increases in relation to the starting material. The migration of cobalt (Ostwald ripening) through the bulk creates new micropores.[245, 246] A similar process was observed by Jones et al. in which during pyrolysis of Co/Cu

bimetallic catalysts copper atoms migrate through the bulk to form Co-core Cu-shell particles increasing the amount of micropores in the material.[247]

This migration process is not observed for ruthenium in the synthesis of RuO_x-N + Co_xO_y-N@C-irregular. And as we can see in entries 2, 3 and 4, the ruthenium remains mostly on the surface of the material. In comparison, the cobalt in Co_xO_y-N@C-irregular is distributed in a homogenous fashion. This difference is due to the temperature at which the pyrolysis is made; the Co atoms have enough energy to migrate in the bulk (i.e., lower Tamman temperature) but not the Ru ones.[248, 249]

Performing the reaction under flow regime proved to be a good improvement. In batch conditions full conversion to FDCM (**40**) is achieved in 18 h, representing a production of 0,03 mmol/h; in comparison, under flow conditions (table 2 entry 6) in the last hour of the experiment >96% conversion of HMF was obtained (1.44 mmol/h) and a selectivity to FDCM of 44-54%, which represents a production of 0.47 mmol/h. The production of **40** was greatly increased, >15-fold compared to batch conditions.

In comparison, the cobalt in Co_xO_y-N@C-irregular is distributed in a homogenous fashion. This difference is due to the temperature at which the pyrolysis is made; the Co atoms have enough energy to migrate in the bulk (i.e., lower Tamman temperature) but not the Ru ones.[248, 249]

Performing the reaction under flow regime proved to be a good improvement: in batch conditions full conversion to **40** is achieved in 18h, representing a production of 0,03 mmol/h; in comparison, under flow conditions (table 2 entry 6) in the last hour of the experiment >96% conversion of HMF was obtained (1.44 mmol/h) and a selectivity to **40** of 44-54%, which represents a production of 0.47 mmol/h. Hence, the production of **40** under flow could be increased >15-fold compared to batch conditions.

3.4 Conclusions

The chemical modification of HMF is a challenge due to its reactivity. Herewith, we report the oxidative esterification of HMF to FDCM under flow regime showing excellent conversion (98%) and good selectivity towards **40** (57%). We were able to circumvent technical issues, by changing the catalyst support, obtaining Co_xO_y-N + RuO_x-N@C-irregular as the best catalyst. The higher mesoporous surface related to the C-pellets catalysts is an important feature that provides improvement in conversion and selectivity. Overall, under flow regime, a >15-fold increase on the production of **40** was obtained in comparison to batch conditions.

To the best of our knowledge this is the first report of oxidative esterification of HMF to **40** under flow conditions.

4 Valorization of Furfural biobased molecules through carbene catalysis

4.1 Introduction

Nowadays, the use of organocatalysts represents an alternative to traditional metal catalyzed reactions. The use of metals and their depletion is avoided. Consequently, the toxicity related to their use is removed, making organocatalysts potential candidates for application in the pharmaceutical industry. Other benefits are: the lack of sensitivity to moisture and oxygen, their low cost, the possible use of mild conditions and their compatibility with several functional groups that could be sensitive in other processes.[250, 251]

Catalysis by N-heterocyclic carbenes (NHCs) has developed to a valuable tool for the formation of C-C bonds and C-heteroatom bonds. The nucleophilic nature of NHCs has led to its application as organocatalysts, mostly where carbonyl groups are involved. The majority of these processes start with the nucleophilic attack of the carbene into a carbonyl group from the substrate to form the Breslow intermediate, which is said to be the starting intermediate in the NHC catalyzed reactions (see scheme 4.1).[252, 253]

The first example of these type of reactions can be traced back to 1943 when Ukai et al. reported the dimerization of aldehydes to benzoins catalyzed by a thiazolium salt.[254] Breslow proposed that the mechanism of this process relies on the amphiphilic nature of the NHC catalyst generated in situ. He also proposed the structure now called "Breslow intermediate". It is formed after the nucleophilic attack of the NHC on the aldehyde followed by proton transfer. The aldehydic proton is rendered acidic by negative induction effect of the cationic azolium group, which fosters the proton transfer.[255] Although experimental evidence of its formation has been reported,[256] the isolation of the Breslow intermediate was elusive for long time. In 2018, Berkessel et al. reported for the first time the isolation and characterization by NMR and X-ray analysis of the Breslow intermediate formed between 2,6-diisopropylphenyl-benzimidazolin-2-ylidene and 2,4-Bis(trifluoromethyl)benzaldehyde.[257]

During the course of the NHC catalyzed reactions the natural reactivity of the aldehyde's carbonyl group is inverted (normally referred as "umpolung"), and the usually electrophilic carbonyl carbon acts as a temporary nucleophile.[258] The reactivity of α,β-unsaturated aldehydes can also be

altered, as they possess a conjugated π system which by conjugated umpolung can suffer a nucleophilic attack at the β-position.[259] Other reaction pathways of Breslow intermediates which do not involve the umpolung of the carbonyl group are also known. Elimination of a leaving group in the α-position on the aldehyde as well as in situ oxidation can generate acyl azolium salts, expanding the possibilities for more type of reactions (see Scheme 4.1).[260]
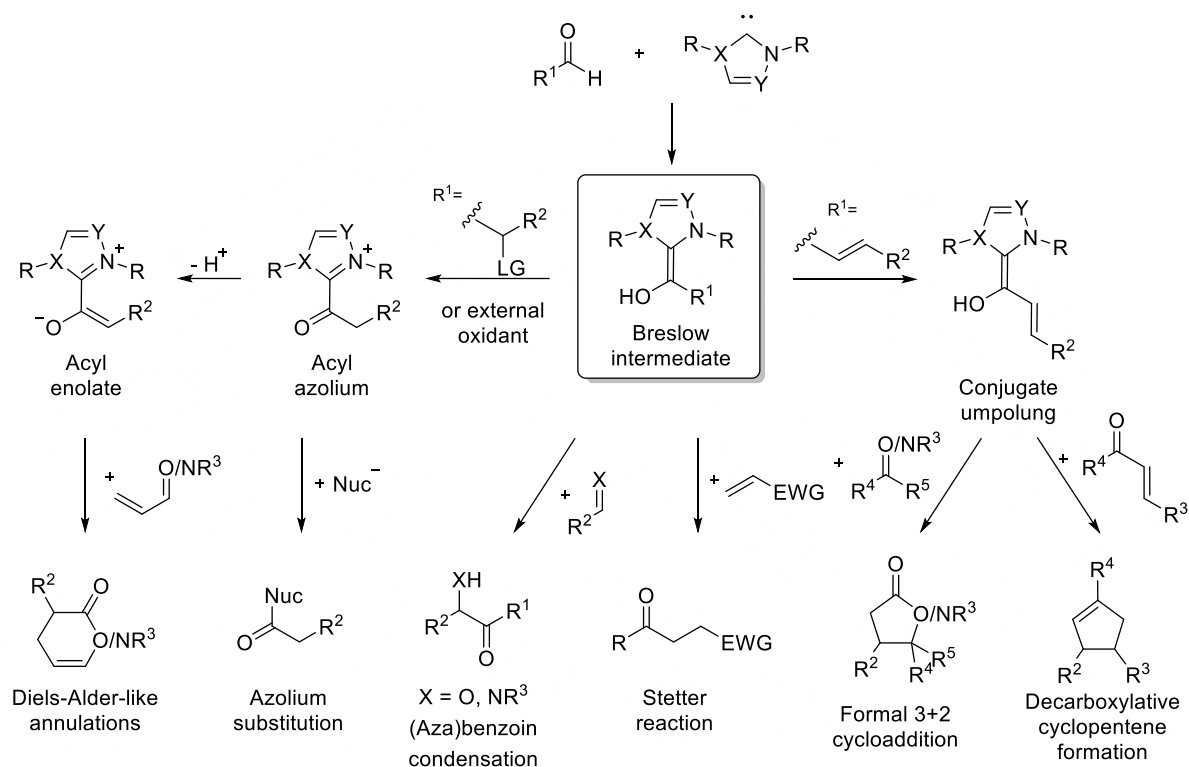
Scheme 4.1. NHC catalyzed reactions of aldehydes .[252]

The present work is focused on the use of the oxidative pathway where azolium salts are formed, which allows the formation of esters and amides. The goal of the study was to find sustainable methodologies for the valorization of biobased furfurals.

In 2008 Scheidt et al. reported the oxidative esterification of alkylic aldehydes catalyzed by N-Heterocyclic carbenes. 10% mol 1,4-dimethyl-4H-1,2,4-triazol-1-ium iodide(**NHC-1**) was used as catalyst, primary and secondary alcohols(mostly MeOH) and 5 equiv. of MnO_2 as oxidant with 74-99% yield (see scheme 4.2) were employed.[261]

In 2013, Studer et al. reported the cooperative N-heterocyclic carbene and ruthenium redox catalysis in the oxidative esterification using air as final oxidant. $Ru(bpz)_3(PF_6)_2$ was used as redox catalyst in the single electron transfer (SET) oxidation of the generated Breslow intermediate upon reaction of the carbene with the aldehyde. Benzaldehyde, functionalized benzaldehydes,

heteroaromatic aldehydes and α,β-insaturated aldehydes, benzyl alcohol, MeOH, EtOH, nPrOH, allyl alcohol and propargyl alcohol were used as substrates. Yields ranged from 15% to 80%. They also demonstrated that carboxylic acids form in moderate to high yields in the absence of the redox catalyst (see scheme 4.3).[262]
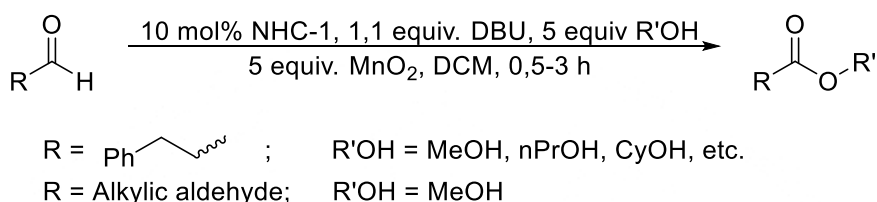
Scheme 4.2. N-Heterocyclic carbene catalyzed oxidation of alkylic aldehydes.**[261]**
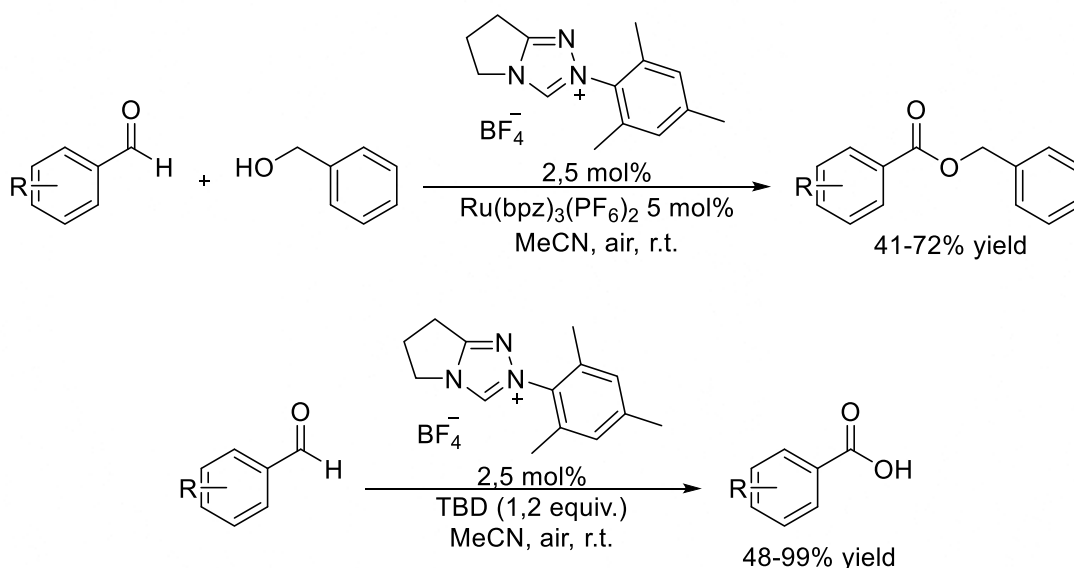
Scheme 4.3. Cooperative oxidative esterification of aldehydes with air.[262]

In the same year, Connon et al. reported the NHC-catalyzed esterification of aldehydes in air without the need of additives of co-catalysts. Only aromatic and heteroaromatic aldehydes could be converted in moderate to good yields (see scheme 4.4).[263]
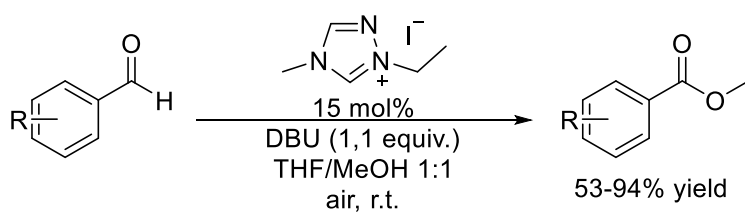
Scheme 4.4. NHC catalyzed aerobic aldehyde esterification without additives or cocatalysts.[263]

In 2014, Studer et al. reported the carbene catalyzed oxidative esterification of aliphatic aldehydes with moderate to good yields. Rb_2CO_3 was used as base and additive, to foster the proton transfer that enables the formation of the Breslow intermediate (see scheme 4.5).[264]
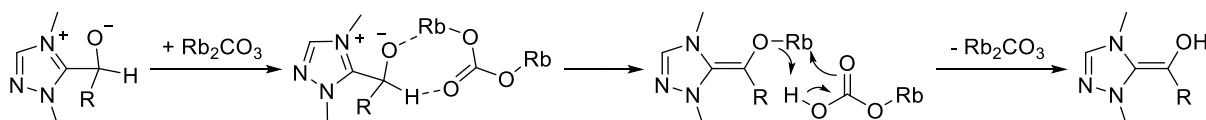
Scheme 4.5. Activation mechanism by Rb_2Co_3 proposed by Studer et al.[264]

In 2017, Chung et al. used a poly(thiazolium) Iodide and phenazine to perform the esterification of aldehydes with alcohols. The use of a polymeric catalyst and phenazine enabled the possibility of recovery and reuse of both catalyst and oxidant (see scheme 4.6).[265]
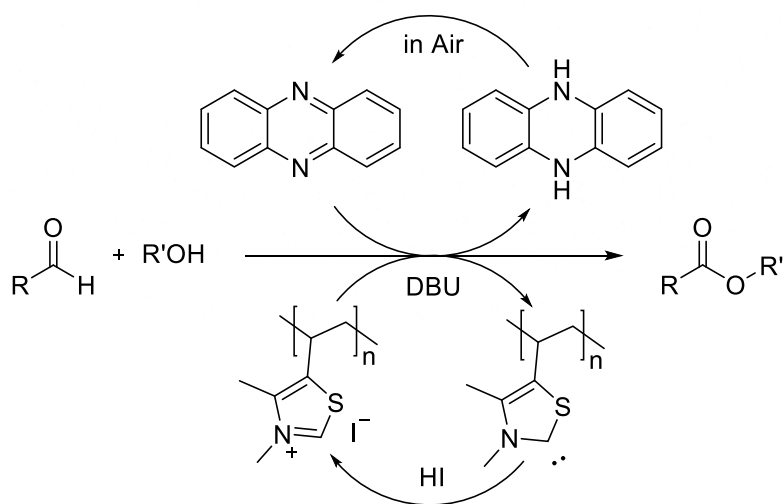
Scheme 4.6. Esterification of aldehydes catalyzed by a Poly(thiazolium)iodide.[265]

Carbene catalysis has previously been used in the self-coupling of HMF and the cross coupling of HMF and Furfural among the efforts to produce diesel and alkane fuels from biomass.[266, 267] In 2014 Chen et al. reported an integrated catalytic process for conversion and upgrade of biomass feedstocks into nC_{12} alkane for fuel purposes. It comprises 3 steps in which the first is the semi continuous carbene catalyzed conversion of biomass to HMF. The second step is the NHC-catalyzed self-coupling to produce 5,5'-dihydroxymethyl furoin. And a final step of hydrodeoxygenation to produce liquid hydrocarbon fuel by a bifunctional catalytic system which is composed of 78% alkanes.[268] The same group in 2016 reported the synthesis of polyol monomers through NHC catalyzed cross coupling of HMF.[269] Later that year in a similar fashion, the NHC-catalyzed cross coupling of HMF and furfural was reported by the same group.[270] The valorization of HMF and furfural in these reports is based in the carbene catalyzed benzoin-type condensation, more specifically the furoin condensation which is a formal C-C coupling reaction.

Based on the demonstrated potential of the catalytic application of NHC's, the production of new HMF derivatives established as the goal of this chapter; more specifically the esterification of HMF with diols to produce new furan-based monomers. Synthetic and mechanistic aspects will be addressed, as well as an exploration of NHC-catalyzed amidation of aldehydes.

4.2 Experimental section

4.2.1 Synthesis of NHC precursors

4.2.1.1 *Synthesis of 1,4-dimethyl-4H-1,2,4-triazol-1-ium iodide NHC-1.*

Procedure 1: A solution of 1-methyl-1,2,4-triazole (20 mmol, 1.66 g) and methyl iodide (40 mmol, 5.68 g) in MeCN (30 mL) was heated to reflux for 3h. After cooling down, the solvent was evaporated and the remaining solid was washed with Et_2O. The final product was obtained as a grayish solid (3.78 g, 84 % yield).

Procedure 2: 1-methyl-1,2,4-triazole (43.34 mmol, 3.6 g) and methyl iodide (86.68 mmol, 12.3 g) were stirred in an oven-dried Schlenk flask. After 3 days a white solid was obtained (9.75 g, >99% yield) and used without further purification.

4.2.1.2   *Synthesis of 3,4-dimethyl-5-vinylthiazol-3-ium iodide NHC-2*

A solution of 4-methyl-5-vinylthiazole (4.32 mmol, 541 mg) and methyl iodide (28.09 mmol, 4 g) in MeOH (35mL) was heated to 70 °C for 24 hours under vigorous stirring. The solvent was evaporated, and the residue purified by flash chromatography (silica, CH_2Cl_2/MeOH 10:1). The carbene precursor was obtained as brown sticky crystals (364 mg, 32% yield).

4.2.2   Carbene-catalyzed oxidative esterification

4.2.2.1   *Procedures*

Procedure A: The NHC precursor was added to a 10 mL Schlenk tube and placed under inert atmosphere by at least 3x vacuum/argon cycles. A freeze pump thaw degassed solution of base and aldehyde was added, followed by the oxidant and finally the alcohol. The reaction was kept under vigorous stirring and in inert atmosphere overnight at room temp.

Procedure B: The NHC precursor was added to a 10 mL Schlenk tube and placed under inert atmosphere by at least 3x vacuum/argon cycles. A freeze-pump-thaw degassed solution of base was added and after 30 min stirring the aldehyde was added, followed by oxidant and finally alcohol. The reaction was kept under vigorous stirring and in inert atmosphere overnight at room temp.

Procedure C: The NHC precursor and the oxidant were added to a 10 mL Schlenk tube and placed under inert atmosphere by at least 3x vacuum/argon cycles. A freeze-pump-thaw degassed solution of base and aldehyde was added and immediately followed by alcohol. The reaction was kept under vigorous stirring and in inert atmosphere overnight at room temp.

Procedure D: The NHC precursor and the oxidant were added to a 10 mL Schlenk tube and placed under inert atmosphere by at least 3x vacuum/argon cycles. Base was added in a small fraction of freeze-pump-thaw degassed solvent and after 30 min stirring, a solution of aldehyde and alcohol made with the rest of the solvent was added dropwise. The reaction was kept under vigorous stirring and in inert atmosphere overnight at room temp.

Procedure E: Under inert atmosphere, NHC precursor and base were dissolved in 1 mL DCM and after 15 min added dropwise to 6,5 mL DCM solution containing the aldehyde, alcohol and oxidant. The reaction was kept under vigorous stirring and in inert atmosphere overnight at room temp.

Procedure F: The NHC precursor and the oxidant were added to a 10 mL Schlenk tube and placed under inert atmosphere by at least 3x vacuum/argon cycles. A freeze-pump-thaw degassed solution of base and aldehyde was added and immediately followed by alcohol. To the Schlenk tube an oxygen filled balloon was coupled, the system was saturated of oxygen and the reaction was kept under vigorous stirring overnight at room temp.

4.2.2.2   *Reaction work up*

In case a heterogeneous oxidant was used, it was filtered off and washed with the used solvent, volatiles were evaporated, and the remaining oil was re-dissolved in DCM (10 mL). Extractions with water (10 mL x 3) were made, the organic phase was collected and dried with Na_2SO_4 and analyzed by GC. Isolation of the desired products was made in an automated flash chromatography system with UV detection was used (CombiFlashRf from Teledyne ISCO), using a silica column and heptane/ethyl acetate as solvents. The solvent flow was set up to 30mL/min. The solvent setup was configured as follows; from start to min 2 pure heptane was used and starting from min 2 to min 5 concentration of ethyl acetate was increased from 0% to 100%. It was kept until no signal was detected. The fractions collected were analyzed by NMR and GC-MS.

4.2.2.3   *NMR quantification*

After overnight reaction the solvent was evaporated; the remaining oil was re-dissolved in deuterated solvent. The oil was analyzed, followed by in-situ liquid extraction on the NMR tube a new spectrum was taken from which yields were quantified using mesitylene as internal standard.

4.2.3   Carbene-catalyzed oxidative amidation

4.2.3.1   *Procedure*

The NHC precursor and oxidant were added to a 10 mL Schlenk tube and placed under inert atmosphere by at least 3x vacuum/argon cycles. A freeze-pump-thaw degassed solution of base was added and after 30 min stirring the aldehyde was added, followed the amine. To the Schlenk an oxygen-filled balloon was coupled, the system was saturated of oxygen and the reaction was kept under vigorous stirring overnight at room temp.

4.2.3.2   *Reaction work up*

In case a heterogeneous oxidant was used, it was filtered off and washed with the used solvent, solvent was evaporated, and the remaining oil was analyzed by GC. Isolation of the desired products was made in an automated flash chromatography system with UV detection was used

(CombiFlashRf from Teledyne ISCO), using a silica column and heptane/ethyl acetate as solvents. The solvent flow was set up to 30mL/min. The solvent setup was configured as follows; from start to min 2 pure heptane was used and starting from min 2 to min 5 concentration of ethyl acetate was increased from 0% until the desired amount was reached.

4.2.3.3 *NMR quantification*

In case a heterogeneous oxidant was used, it was filtered off and washed with the used solvent, followed by evaporation; the remaining oil was re-dissolved in deuterated solvent. The oil was analyzed by NMR, after an in-situ liquid extraction on the NMR tube a new spectrum was taken from which yields were quantified using mesitylene as internal standard.

4.3 Results and discussion

After exploring the metal catalyzed oxidative esterification of HMF (**1**) and having tried the reaction with diols without success (see chapter 2) we moved on to the carbene-catalyzed esterification of aldehydes as a way to synthesize new polyester monomers directly from HMF (see scheme 4.7), and as the same time its valorization in order to avoid the drawbacks inherent of handling HMF (e.g. stability, pH sensitivity, heat sensitivity, etc).
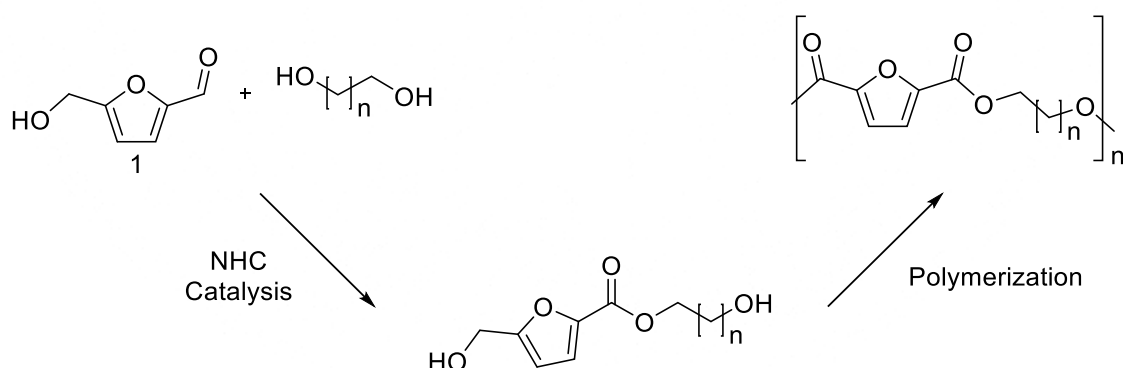
Scheme 4.7 General reaction to furan based diols as intermediaries for polymer synthesis.

The study began with the test of several reaction conditions based on previous reports of carbene-catalyzed oxidative esterification of aldehydes.[261-265, 271, 272] And as a model substrates, **1** and 1,6-Hexanediol (**51**) were selected. 1,4-dimethyl-4H-1,2,4-triazol-1-ium iodide (**NHC-1**) and 3,4-dimethyl-5-vinylthiazol-3-ium iodide (**NHC-2**) were selected as model NHC's, the first because its

66

demonstrated catalytic activity and the second because its core is present in nature (e.g Thiamine or vitamin B_1(see scheme 4.8)), and the synthetic goal was 6-hydroxyhexyl 5-(hydroxymethyl)furan-2-carboxylate (**52**).
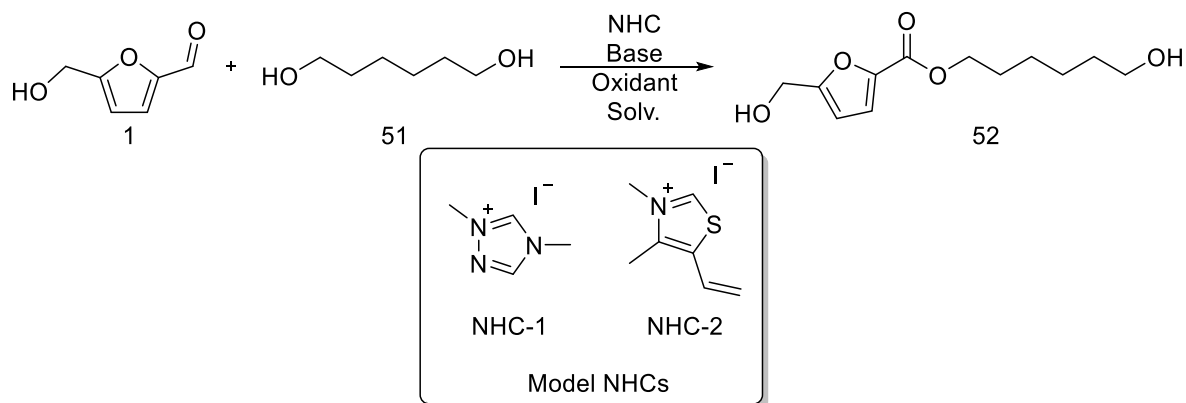
Scheme 4.8 Model reaction

4.3.1 Reaction screening and optimization

Preliminary tests were performed using different bases (TBD, DBU and 1,8-Bis(tetramethylguanidino)naphthalene), oxidation catalysts (phenazine, Ru@C and MnO_2), NHCs (1,4-dimethyl-4H-1,2,4-triazol-1-ium iodide **NHC-1** and 3,4-dimethyl-5-vinylthiazol-3-ium iodide **NHC-2**, (see scheme), solvents (DCM, THF, DMSO, DMF, MeCN) and reaction setups, until the desired product **52** was detected and isolated (see scheme 4.9).
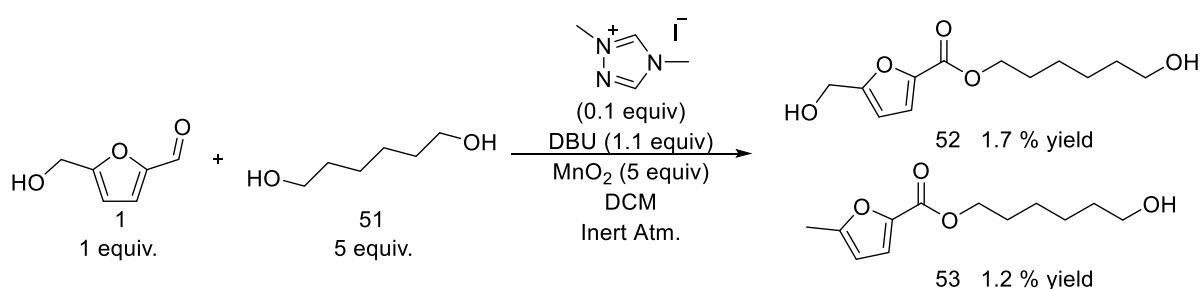
Scheme 4.9. Conditions in which the desired product was detected.

Surprisingly, not only the desired diol (**52**) was detected, but also 6-hydroxyhexyl 5-methylfuran-2-carboxylate (**53**) was isolated, a deoxygenated analog which lost the –OH functionality from the HMF backbone is seen. Based on these conditions, optimization towards synthesizing the desired diol was performed.

As can be seen in table 4.1, reduction in the amount of **51** resulted in a yield increase of **52** to 13% without changing so much the yield of **53** (entry 2). Therefore, the following reactions were done with a 1:1 mol ratio of HMF:1,6-hexanediol. Increase in the amount of catalyst from 10 mol% to 20 mol% had an adverse effect, as it diminished the yield of **52** and increased **53** from 1.4% to 9.7% (entry 3). On the other side, the increase in the amount of base increased the yield of **53** and had no effect on **52** (entry 4). THF, MeCN and DMF were tested (entries 5, 6 and 7) and lower yields of **52** were measured (8%, 8% and 9% respectively). Therefore, DCM remained as the solvent used. Additionally, other NHCs were tested; a bulky one (**NHC-3**) was tested without any improvement towards the desired products (entry 8). The influence of the counterion in the carbene precursors was assessed (**NHC-4, NHC-5** and **NHC-6**, entries 9, 10 and 11), and it could be determined that triflimide works as the best counterion in comparison to chloride and tetrafluoroborate. The yields of **52** were 11%, 7% and 16% respectively.
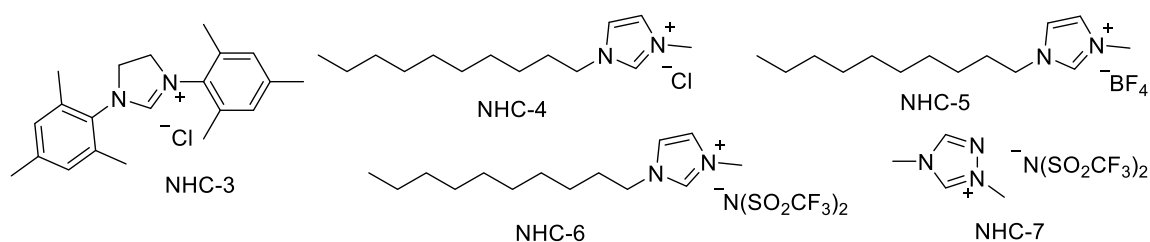
Scheme 4.10. Additional NHCs tested

Therefore, 1,4-dimethyl-4H-1,2,4-triazol-1-ium bis((trifluoromethyl)sulfonyl)amide (**NHC-7**) was prepared by treating **NHC-1** with Silver bis(trifluoromethanesulfonyl)imide. The results obtained with this carbene precursor were the best so far, 28% yield of **52** was achieved (table 4.1 entry 13). Additionally, it was combined with the use of MnO_2 in catalytic amounts and oxygen as terminal oxidant (see Scheme 4.11). Without the presence of co-catalyst (MnO_2) the esterification product could not be detected.

Table 4.1. Optimization towards furan containing diol

Entry	Conditions[a]	Yield (%)	
		52	53
1	5 equiv. 1,6-Hexanediol	1.7	1.2
2	-	13	1.4
3	0,2 equiv. NHC	9	9.7
4	2 equiv. DBU	13	9
5	THF as solvent	8	6.8
6	MeCN as Solvent	8	4.2
7	DMF as solvent	9	7.7
8	NHC-3 as catalyst	6	3.4
9	NHC-4 as catalyst	11	11
10	NHC-5 as catalyst	7	3
11	NHC-6 as catalyst	16	7
12[b]	0,2 equiv. MnO_2 in Oxygen atm.	13	9
13[b]	0,2 equiv. MnO_2 in Oxygen atm. and NHC-7 as catalyst	28	13

Procedure C was used. [a] Condition changed to the reaction scheme presented on the top of the table. [b] Procedure F was used.
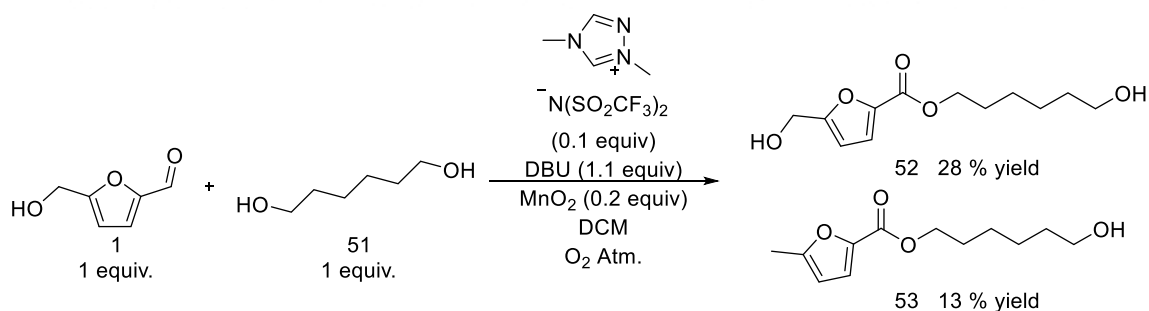
Scheme 4.11. Optimized conditions for the carbene catalyzed oxidative esterification of HMF

The use of MnO_2 in catalytic amounts should be highlighted as it is traditionally used in huge excess (from 5:1 to 500:1, MnO_2:substrate weight ratio).[273] It was used by Scheidt et al. in the

carbene-catalyzed oxidative esterification of unactivated aldehydes in a molar ratio 5:1.[261] Its role as catalyst will be further discussed in section 4.3.2.

In all the performed experiments, the formation of a black insoluble solid was observed which is presumed to be the polymerization of HMF into humins or poly-HMFCA as reported by Massi et al.[274]. The different procedures used (section 4.2.2.1) probed useless in order to avoid its formation (e.g. Simultaneous addition of base and aldehyde (Procedure A), pre-formation of the free NHC (Procedure B), formation of the free NHC in presence of the oxidation catalyst (Procedure C and D)).

4.3.2 Mechanistic insights and proposal

Traditionally, oxidative NHC-catalyzed reactions rely on the formation of an initial transient benzylic alcohol/alcoholate, followed by conversion to the nucleophilic NHC aldehyde adduct (Breslow intermediate) and oxidation of it. [261, 264] The oxidation event can either result in the formation of an electrophilic acyl azolium ion via transfer of two electrons to the oxidant (see scheme 4.12, path A: oxidation) or alternatively afford an azolium carboxylate species by oxygen atom transfer from the oxidant (see scheme 4.12, path B: oxygenation).[275] Path A leads to esterification products and Path B leads to oxidation products (e.g. carboxylic acids).

Based on the experimental evidence, a catalytic cycle is proposed (see scheme 4.13). The first step is the deprotonation of the carbene precursor which reacts with HMF. Two transient "benzylic" alcohols are formed (Scheme 4.13, A.1 and B.1), both reacting in two different ways.
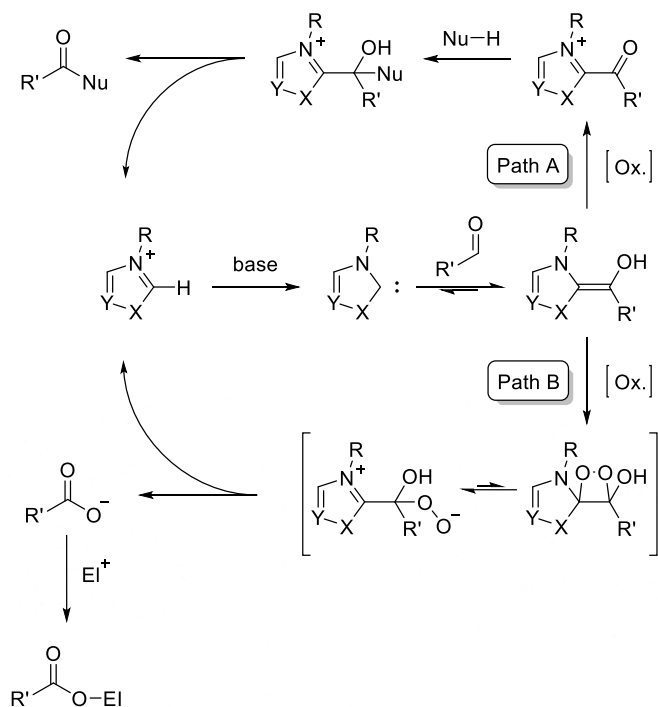
Scheme 4.12. General mechanism for the carbene catalyzed oxidation of aldehydes[275]
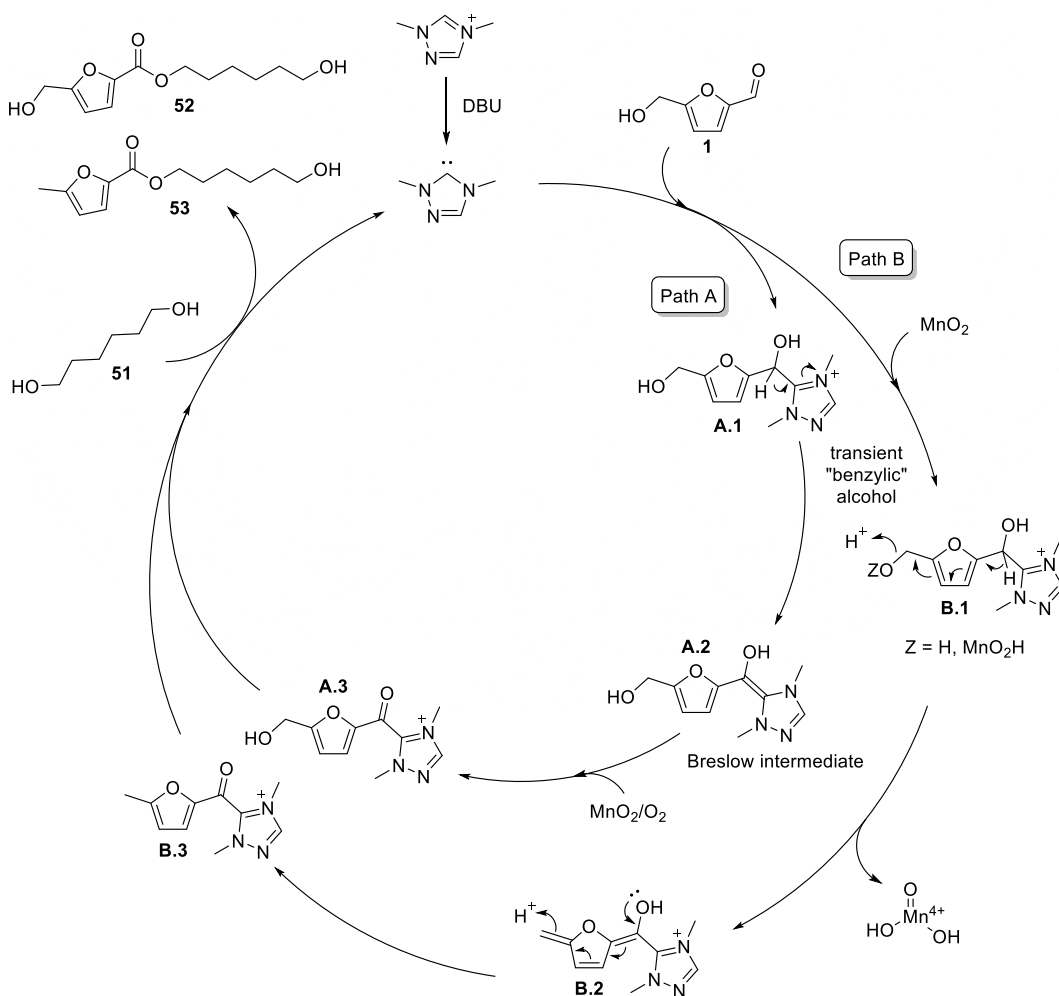
Scheme 4.13. Proposed mechanism for the carbene catalyzed oxidative esterification of HMF

Through Path A (inner circle) by 1,2-proton transfer the respective Breslow intermediate is formed (**A.2**) and further oxidation leads to the intermediate acyl triazolium ion (**A.3**) of the desired product **52**. Through Path B (outer circle) the formation mechanism of **53** can be explained. After the transient "benzylic" alcohol (**B.1**) is formed, the loss of the alcohol functionality proceeds through electron resonance (**B.2**) allowed by the presence of the furan ring. The furan ring acts as an electronic bridge between both ends of the molecule. This process was also observed by Zhao et al.[276] Also, the loss is presumably fostered by the previous formation of a manganese ester (Scheme 4.13 fragment Z of **B.1**) which works as a bulky and suitable leaving group. Formation of such type of esters is widely described in the oxidation of alcohols to aldehydes using MnO_2 as oxidizing agent.[277-279] After the loss of the alcohol moiety, the molecule rearranges to form the acyl triazolium intermediate (**B.3**) of **53**. Further interaction of the acyl triazolium ions (**A.3** and **B.3**) with 1,6-hexanediol leads to the formation of the esterification products and regenerates the NHC to restart the cycle.

4.3.3 Esterification of Furfural

In order to gain more insight on reaction mechanism the system was simplified by changing the starting substrates. Furfural (**2**) was used as substrate to maintain the furan ring moiety, which seems to influence the mechanism and product selectivity. Butanol (**54**) was selected as the alcohol to keep similarity to the alkyl chain in 1,6-hexanediol. When the reaction was performed under the same conditions as the ones used previously (see table 4.2) 48% of butyl furoate (**55**) was isolated (entry 1). Changing to an air atmosphere reduced the yield to 35% (entry 2). Oxygen concentration is a limiting factor in the rate of the reaction.

Changes in the amount of base and the atmosphere used to run the reaction changed the yields, and also for the first time side products were detected (table 4.2 entries 3 and 4). Furfuric acid (**56**) could be detected as major side product when the base was reduced to 0.15 equiv. and air atmosphere was used, indicating that an oxygenative process occurred (see scheme 4.11 path b) and that **54** was not participating in the reaction. In comparison, when oxygen atmosphere and 0,15 equiv of base were used; the major product was the **58** (72% yield) followed by **57** (11 %). The formation of dimer (**57**) and trimer (**58**) can be explained by the mechanism presented by Connon et al.[271] In which they propose that the intermediate which undergoes oxidation is benzoin instead of the Breslow intermediate (see scheme 4.14).

Table 4.2. Esterification of Furfural

Entry	Conditions[a]	Yield (%)			
		55	56	57	58
1	-	48[b]	-	-	-
2	Air as terminal oxidant	35[b]	-	-	-
3[c]	0,15 equiv. DBU, Air as terminal oxidant	10	23	11	10
4[c]	0,15 equiv. DBU, O_2 as terminal oxidant	5	2	11	72
5[d]	Inert atm.	5	-	1	1

[a]Condition changed to the reaction scheme on top of the table. [b]Isolated yields. [c]Yields by GC-MS and NMR. [d]Mass relations

The catalytic cycle begins with the formation of the Breslow intermediate (C) between the free carbene (A) and the aldehyde (B). Further reaction with another aldehyde molecule forms the benzoin intermediate (D), which in presence of base and oxygen is oxidized to benzil (E). The formed electrophilic diketone (E) is attacked by the NHC and an alcoholate specie (F) is formed, this reacts with the alcohol and releases the NHC and the desired product (G). Also, in the absence of an alcohol the benzoin (D) can react as a nucleophile with an NHC activated diketone (E) to form the hydroacylation product (H). This molecule in the presence of base and alcohol breaks apart to form the desired molecule (G) and benzoin (D). On other side the diketone (E) may react with a Breslow intermediate (C) in an alcoholate fashion to form a trimeric intermediary (I) and in the presence of base and alcohol breaks into the ester (G) and benzoin (D). In this case, a furoin intermediate should be responsible for the formation of dimer **57** and trimer **58** of furfural.
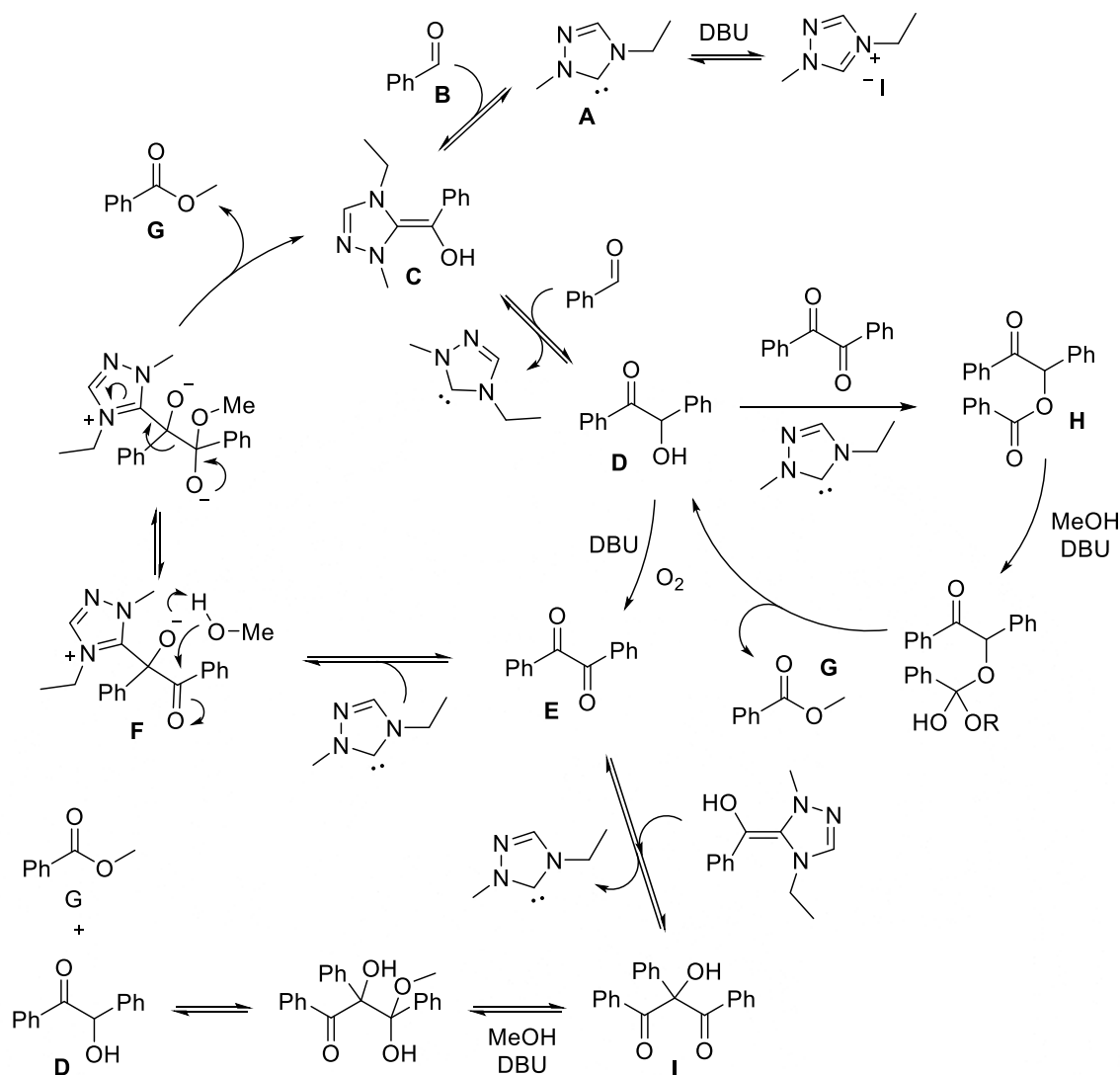
Scheme 4.14 Oxidative esterification mechanism proposed by Connon et al.[271]

The reaction is sensible to the amount of base used; a lack of base and oxygen allowed the detection of the respective diketone **57** and trimer **58** formed from **2**. Also, the results suggest that the base plays a role in the last steps on the catalytic cycle where butanol must interact with the intermediates to form the desired butyl furoate **55**. The products obtained indicates that more than one mechanism is in action. The variability observed in the product distribution shows a high degree of sensitivity of the reaction, respect to the stoichiometry of the reagents used. Moreover, the results obtained in the esterification of HMF and furfural shows that the reactivity imposed by the presence of the furan ring increases the difficulty in controlling the reaction.

4.3.4   Esterification of Benzaldehyde
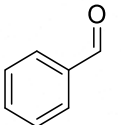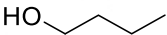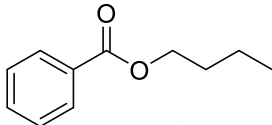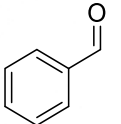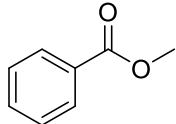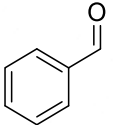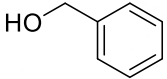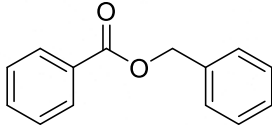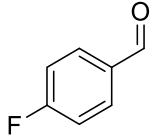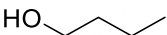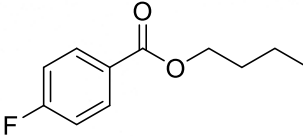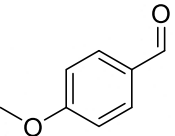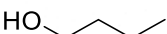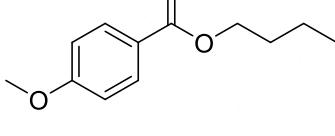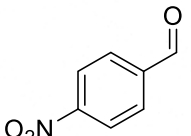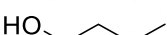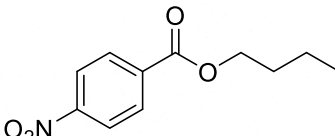
The esterification of benzaldehyde was made for comparison (as shown in table 4.2 entry 1). By using air or oxygen only, a yield of 22% of the desired ester (butyl benzoate) was obtained. Also, benzyl alcohol and allyl alcohol were tested, obtaining 37% and 23% yields of their respective esters. The improvement seen when benzyl alcohol is used is mostly attributed to the last steps of the reaction (as seen in the catalytic cycle in scheme 4.14) in which the electronic movement is stabilized and promoted by the presence of a phenyl ring. Also, its pKa value, higher than butanol (pKa: 15.4 Benzyl alcohol, 16.1 butanol), indicates that the −OH group is deprotonated easier, resulting in the promotion of proton transfer and nucleophilic attack, therefore increasing the yield of the final ester. The acidity of allyl alcohol is similar to benzyl alcohol (pKa: 15.5) but the obtained yield is similar to the one observed when butanol was used, indicating that the presence of the phenyl ring in the alcohol is more influential than the acidity of it.

Recently, Massi et al.[274] reported the aerobic oxidation of 5-hydroxymethylfurfural to 5-hydroxymethyl-2-furancarboxylic acid and its derivatives by heterogeneous NHC catalysis. They screened different oxidants, being Iron(II) phthalocyanine the most suitable. In their work they try unsuccessfully to avoid the polycondensation of HMF by driving the reaction towards an oxygenative pathway, the −OH group from HMF works as a good nucleophile necessary for the oxidative pathway to occur. When Iron(II) phthalocyanine (5 mol%) was used instead of MnO_2 (20 mol%), the yield of butyl benzoate was increased to 43%. The improved yield in reduced amount of co-catalyst suggests better performance and higher oxidation power than MnO_2. Iron(II) phthalocyanine has been used as an electron transfer mediator (ETM) for the activation of oxygen in biomimetic catalytic oxidations.[280] Sudén et al. reported the valorization of glycerol in which on reaction step is the oxidative esterification of cinnamaldehydes with carbonated glycerol using Iron(II) phthalocyanine in catalytical amounts as ETM and oxygen activator.[281] Sadly when it was used in the esterification of HMF, similar results as those reported by Massi et al. were obtained. Attempts to further optimize the formation of butyl benzoate were unsuccessful.

When methanol and benzylic alcohol were used, a remarkable increase in the yield was observed; 64% and 68% of the respective esters were obtained. A similar trend is observed when MnO_2 was the oxidant, pointing out the higher oxidation capabilities of Iron(II) phthalocyanine.

In order to understand the electronic effects that substrates confer to the system, different substrates were tested, as can be seen in table 4.3.

Table 4.3. Substrate screening

| Entry	Aldehyde	Alcohol	Product	Yield (%)*
1				29
2				52
3				37
4				19
5				15
6				61

Procedure C was followed, 1.5 mmol aldehyde scale, THF as solvent. *Yield calculated by NMR analysis of the resulting oil after solvent evaporation, mesitylen as internal standard was used.

When the reaction is performed in THF the yield suffers a 14% reduction (table 4.3 entry 1), indicating the presence of solvent effects. Although both solvents are polar aprotic, the free electron pairs of the oxygen in THF can work as Lewis bases. THF may form a Lewis adduct with the alcohol, which might hinder the interaction of the alcohol with the Aldehyde-NHC intermediaries formed (see scheme 4.14, F). This interaction is necessary as a final step to form the final ester

product. This effect was also observed with methanol and benzylic alcohol (table 4.3 entries 2 and 3), for which reduced yields were also obtained. Electron donating groups (EDG) in *para* position like fluoro and methoxy hamper the reaction to yield only 19% and 15% respectively. In comparison a strong electron withdrawing group (EWG) like nitro boosts the reaction, furnishing the product in a yield of 61%. An EDG deactivates the aldehyde towards esterification meanwhile an EWG activates it. This is due to the electronic effects conferred by the substituents; EDG's makes the carbonyl group less electrophilic, therefore less susceptible to a nucleophilic attack. The opposite occurs with EWG's which makes the carbonyl group more electrophilic favoring a nucleophilic attack.

4.3.5 Amidation of aldehydes

At the same time, an exploration on the oxidative amidation of aldehydes was made. Furfural (**2**), n-Hexylamine (**59**) and pyrrolidine (**60**) were used as model substrates. When the primary amine was used 33% of amide product (**61**) could be isolated, on the contrary to the secondary amine from which amidation product (**62**) could not be detected (see scheme 4.15). The yield of amide could be increased up to 37% when 1,1 equivalents of DBU were used.
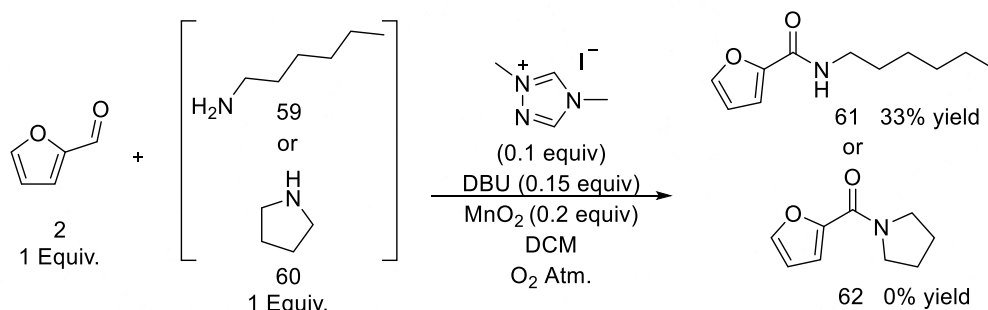
Scheme 4.15. Explorative carbene-catalized amidation of furfural

Massi et al. reported the NHC catalyzed oxidative polymerization of HMF using iron phthalocyanine as oxidation co-catalyst to suppress the oxygenative pathway by reaction with the Breslow intermediate.[274] When iron phthalocyanine (0,05 equiv) was used the yield of **61** was reduced to 23%, and also 27% of imine (**63**) condensation product was detected. Sadly when HMF was used as substrate neither amide nor imine was detected, similar as to the reported by Massi et al. in which they could not suppress the polycondensation of HMF.
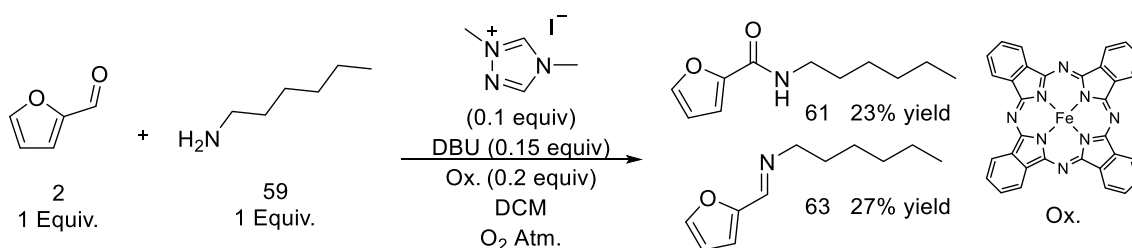
Scheme 4.16. Amidation using an ETM as oxidation catalyst

Based on the report by Connon et al.[282] benzaldehyde was selected as model substrate for the amidation reaction, and the previous used NHC's (see table 4.1) were tested. Surprisingly yields of 3-12% amide and 63-75% imine were obtained in air atmosphere. For comparison, reactions with the same NHC (*H*-1,2,4-Triazolium, 1,4-dimethyl-, iodide) and oxidation co-catalyst (MnO$_2$) were performed under inert, air and oxygen atmosphere, 12%, 14% and 24% amide yield was obtained respectively. Therefore, the following experiments were done in oxygen atmosphere. The necessity of a co-catalyst as suggested by Connon et al.[282] was also surveyed. Reactions using 0,2 equiv of imidazole as base catalyst were made obtaining a 4% increase in the yield of N-hexylbenzamide. A maximum of 29% amide yield was obtained with the use of the co-catalyst and iron phthalocyanine as oxidation co-catalyst (see table 4.4 entries 1 and 2). Contrary to what Connon et al. reported, under similar conditions neither amidation using pyrrolidine was observed nor were good yields obtained. THF as solvent reduced the yield to 25% (table 4.4 entry 3).

Under these conditions other substrates were tested, when benzylamine was used just 13% of the desired amide was obtained (entry 6). On the other side, a secondary amine like tetrahydroisoquinoline yielded 75% of amide product (entry 7). And finally furfural and n-Hexylamine as substrates yielded 34% of the desired amide (entry 8); which represents a mild increase in comparison to the explorative experiment.

In general, in all the reactions under oxygen atmosphere an imine byproduct can be detected in similar or higher amount than the desired amide in air atmosphere. Also, when THF was used as solvent the selectivity towards the imine product was increased. THF is a water miscible solvent which better promotes the condensation reaction between the aldehyde and the primary amine. A competitive reaction between condensation and oxidative amidation is happening. This is confirmed when n-Hexylamine and Tetrahydroisoquinoline yields are compared, the yield towards amide product for the secondary amine are more than twice the one for the primary amine (see table entries 1). Although 75% of amide product was obtained with Tetrahydroisoquinoline no amide was detected when pyrrolidine was used.

Table 4.4. Optimization and substrate screening

Entry	Aldehyde	Amine	Product	Yield (%)*
1				29
2[a]				25
3[b]				25
4[c]				28
5[d]				14
6				13
7				75
8				34

1.5 mmol aldehyde scale. *Yield reported after NMR analysis of the resulting oil after solvent evaporation, mesitylen as internal standard was used. [a] without co-cat. [b] THF as solvent. [c] 0.2 equiv. MnO$_2$ as oxidant. [d] 0.2 equiv. MnO$_2$ as oxidant and inert atm.

4.4 Final considerations

Valorization of biobased furfural molecules (HMF or furfural) in a controlled way through carbene catalysis probed to be challenging. Esterification and amidation seems to be reactions that work in a more complex way than expected. The results obtained in this study show that more than one mechanism might be operating at the same time. Additional to the mechanisms previously presented, radical species could be detected in oxygen free atmospheres by EPR. SET processes occur in carbene catalyzed reactions during the formation of the Breslow intermediate; and its existence is accompanied by its corresponding Breslow-like radical.[283]

Carbene catalyzed self-coupling of HMF and Furfural as single and mixed substrates have been reported in high yields.[267] These reactions follow the benzoin condensation mechanism. And as said previously, Massi et al. couldn't suppress polycondensation of HMF and poly-HMF had to be used as intermediary for the obtention of the final desired products.[274]

Most of the reports for carbene-catalyzed amidation are not covering an extended substrate scope which could make them a general procedure. Sundén et al. reports the N-acylation of indoles with moderate to good results.[284] Ma et al. reports the N-acylation of sulfonamides under oxidative conditions.[285] Yetra et al. synthesized N-acyl 2-aminobenzothiazoles.[286] In these cases the substrate scope limits itself to certain type of amine and to a certain type of aldehyde (benzaldehyde as main backbone). Application of the same conditions to other substrates might not give the same yields.

Alcohol or amine substrates have to be used in excess in order to achieve the desired product in high yields. The base usually needed to form the carbene species from its respective starting salts have to be used in stoichiometric amounts related to substrate. It was not possible to apply the atom-economy principle of green chemistry to obtain good yields.

Nevertheless, a deeper mechanistic insight in this challenging transformation was acquired which allowed the proposal of the reaction mechanism that explains the formation of the desired new ester and the major side product detected, the application of MnO_2 as oxidation catalyst and oxygen as terminal oxidant was performed. Current efforts to reach synthetic scale of **52** and other analogs using different diols (e.g ethyleneglycol, 1,3-propanediol, 1,4-butanediol) are being made.

5 Conclusions and Outlook

The selective oxidative esterification of HMF to the esters **2** and **3** with excellent to quantitative yields under mild conditions was achieved using a bimetallic catalytic system containing Ru@C and Co_xO_y-N@C catalysts working in synergy. EPR measurements shows that such effect seems to be related to the formation of superoxide radicals at the cobalt surface which are in turn used for the catalytic turn-over at the ruthenium sites. A mechanistic proposal was made in which the synergy of the catalysts is explained.

The kinetics of the oxidation of the alcohol moiety by Ru@C follow an apparent order zero on catalyst and substrate. In contrast, the esterification of the aldehyde moiety at Co_xO_y-N@C shows a first order dependence on the substrate. Additionally, the rate of the reaction is limited by the solubility of oxygen. Using pure O_2 instead of air and by increasing the solubility of the gas using a perfluoroester (MPFB) as a co-solvent increased the rate of the reaction.

To the best of our knowledge, this is the first report on the combination of cobalt and ruthenium catalysts for oxidative esterification. Moreover, it gives the best yields and conversions for HMF under the mildest conditions reported so far.

Flow conditions were used to reduce the mass transfer limitations in oxygen solubility. Technical issues were solved by developing new catalysts on supports suitable for the microreactor conditions. The reactor temperature must be kept low to prevent decomposition of HMF. Carbon particles sized -20+40 mesh (irregular shape – C-irregular) and cylindrical pellets (~0.8 mm diameter – C-pellets) were selected with which different nitrogen doped Co/Ru catalysts were prepared. Co_xO_y-N + RuO_x-N@C-irregular catalyst showed the more promising reactivity, 98% HMF conversion and 57% selectivity towards FDCM was achieved. Catalyst preparation, unique particle composition and the mesoporosity of the support are key to its activity. Overall, under flow regime, a >15-fold increase on the production of FDCM was obtained in comparison to batch conditions Further experiments and analysis might be required to fully understand the behavior of the new prepared catalysts.

New catalytic systems (in batch and in flow regime) were developed considering the principles of green chemistry and engineering. Air/Oxygen was used as oxidant, methanol was the primary solvent used, a perfluorinated solvent with low environmental persistence was used and recycled. Low pressures and temperatures were enough to achieve better conversion rates.

Here we report the first continuous micro flow synthesis of **2**, which nowadays is an important platform molecule in the development of furan-based polymers (Polyesters, polyamides, etc.). The development of a continuous process like the one in this work is relevant for the industry, and to achieve the Sustainable Development Goals (SDGs) set by the United Nations.

Synthesis of the new furan-based diol **52** was achieved through carbene catalysis. Carbene, base, oxidation catalyst and atmosphere conditions were screened. The best system was achieved with NHC-7, DBU, MnO_2 as oxidation catalyst in oxygen atmosphere, from which 28% of **52** was obtained.

A mechanistic proposal was made in which the formation of **52** and the main side product **53** was explained. Deeper mechanism exploration experiments showed a complex behavior of the reaction, as the results diverge from what is reported in the literature. Electronic properties of the substrates are important. EDG's deactivates the aldehyde meanwhile EWG's activates it. Also, chain length of the alcohols is important, where short chain yield more product than long chain alcohols.

Efforts to increase the yield of the reaction must be carried on as it represents a new synthetic route for **52** and its analogs, which could be used as monomer in the synthesis of polyesters. Furthermore, the catalytic system could be used to prepare tailor-made monomers for the polymer industry.

In a similar way, amidation was explored. The esterification process had to be adapted to amidation, in which the oxidation catalyst was changed from MnO_2 to Iron(II) phtalocyanine and Imidazole as co-catalyst was used. When primary amines are used, amidation of the aldehyde competes with condensation in which the corresponding imine by-product was detected. Using tetrahydroisoquinoline increased the yield significantly (up to 75%), more than twice the yield obtained with n-hexylamine. Suppression of the condensation reaction was a significant improvement.

The limited supply of fossil resources forces but moreover the climate and environmental situation of nowadays push us to find new ways to obtain chemicals from renewable sources and to substitute the oil-based that are part of our everyday life. This work represents a step further in the field of sustainable chemistry. A new heterogeneous catalyst system with low energy consumption was developed to oxidize a biobased renewable molecule with air. Possible industrial use was tested by performing the oxidation in flow micro reactor conditions. An organocatalytic approach was tested to synthesize new biobased diols that can be the potential starting materials in the polymer synthesis. Abundant metals like cobalt, iron and manganese were used in the catalytic systems.

The application of the principles of sustainability, neutral CO_2 emissions, green chemistry and engineering are the guidelines to reduce the impact of human activity in the environment, and to keep it healthy for the generations to come. Is our duty to keep a sustained and continued effort on applying and achieving them.

6 Scientific Contributions

Parts of this work has been published in peer reviewed journals and presented in conferences.

6.1 Publications

- **Salazar, A.,** Linke, A., Eckelt R., Quade, A., Kragl, U., Mejía, E., **Oxidative esterification of 5-Hydroxymethylfurfural under flow conditions using a bimetallic Co/Ru catalyst.** *Chemcatchem, DOI:* 10.1002/cctc.202000205*, **2020**.*

- **Salazar, A.,** Hünemörder, P., Rabeah, J., Quade, A., Jagadeesh, R. V., Mejía, E., **Synergetic Bimetallic Oxidative Esterification of 5-Hydroxymethylfurfural (HMF) under mild conditions.** *ACS Sustainable Chemistry & Engineering,* **2019**, 7, 14, 12061-12068.

6.2 Congresses and Conferences

2019   **Oral Presentation**: *4th Green and Sustainable Chemistry Conference*, Dresden, Germany.

"Synergetic bimetallic oxidative esterification of 5-Hydroxymethylfurfural (HMF) under mild conditions"

Poster presentation: *Hanse Chemistry Symposium 2019, Rostock, Germany.*

"Mechanism of the Synergetic bimetallic oxidative esterification of 5-Hydroxymethylfurfural (HMF)"

Poster presentation: *Posterparty 2019, JungChemikerForum GDCh,* Rostock, Deutschland.

"5-Hydroxymethylfurfural to FDCM: oxidative esterification under flow conditions using a bimetallic Co/Ru catalyst"

2018   **Oral** and **Poster presentation**: *2nd RoHan DAAD SDG Workshop "Catalysis towards Sustainable Chemical Industry"*, Hanoi, Vietnam.

"Carbene/Manganese catalyzed oxidative esterification of 5-Hydroxymethylfurfural"

Oral presentation: *Klausurtagung der Abteilung Technische und Analytische Chemie*, Universität Rostock**,** Wismar, Deutschland.

"Catalysis in Biomass Valorization"

Poster presentation: *28th International Conference on Organometallic Chemistry - ICOMC*, Florenz, Italien.

"Carbene/Manganese catalyzed oxidative esterification of 5-Hydroxymethylfurfural"

2017 **Poster presentation**: *2nd International Symposium on Synthesis and Catalysis - YSiSiCat*, Evora, Portugal.

"Synergetic bimetallic oxidative esterification of 5-Hydroxymethylfurfural (HMF) under mild conditions"

7 References

1.   Robinson, P. R.; Hsu, C. S., Petroleum and Its Products. In *Handbook of Industrial Chemistry and Biotechnology*, Springer: 2017; pp 13-106.
2.   *World Energy Resources 2016*; World Energy Council: 2016; p 44.
3.   Schellnhuber, H. J.; Rahmstorf, S.; Winkelmann, R., Why the right climate target was agreed in Paris. *Nat. Clim. Change* **2016,** *6*, 649.
4.   Hansen, G.; Stone, D., Assessing the observed impact of anthropogenic climate change. *Nat. Clim. Change* **2015,** *6*, 532.
5.   European Commission on Circular Economy. https://ec.europa.eu/environment/circular-economy/index_en.htm.
6.   Sauvé, S.; Bernard, S.; Sloan, P., Environmental sciences, sustainable development and circular economy: Alternative concepts for trans-disciplinary research. *Environmental Development* **2016,** *17*, 48-56.
7.   Vinoth Kumar, R.; Pakshirajan, K.; Pugazhenthi, G., Chapter 3 - Petroleum Versus Biorefinery-Based Platform Chemicals. In *Platform Chemical Biorefinery*, Kaur Brar, S.; Jyoti Sarma, S.; Pakshirajan, K., Eds. Elsevier: Amsterdam, 2016; pp 33-53.
8.   Sanders, J.; Scott, E.; Weusthuis, R.; Mooibroek, H., Bio-Refinery as the Bio-Inspired Process to Bulk Chemicals. *Macromol. Biosci.* **2007,** *7* (2), 105-117.
9.   Bals, B. D.; Dale, B. E., Developing a model for assessing biomass processing technologies within a local biomass processing depot. *Bioresour. Technol.* **2012,** *106*, 161-169.
10.   Parikh, J.; Channiwala, S. A.; Ghosal, G. K., A correlation for calculating elemental composition from proximate analysis of biomass materials. *Fuel* **2007,** *86* (12), 1710-1719.
11.   Shen, J.; Zhu, S.; Liu, X.; Zhang, H.; Tan, J., The prediction of elemental composition of biomass based on proximate analysis. *Energy Convers. Manage.* **2010,** *51* (5), 983-987.
12.   Saleh, S. B.; Flensborg, J. P.; Shoulaifar, T. K.; Sárossy, Z.; Hansen, B. B.; Egsgaard, H.; DeMartini, N.; Jensen, P. A.; Glarborg, P.; Dam-Johansen, K., Release of Chlorine and Sulfur during Biomass Torrefaction and Pyrolysis. *Energy Fuels* **2014,** *28* (6), 3738-3746.
13.   Demirbas, A.; Alidrisi, H.; Balubaid, M. A., API Gravity, Sulfur Content, and Desulfurization of Crude Oil. *Pet. Sci. Technol.* **2015,** *33* (1), 93-101.
14.   de Vries, J. G., Catalytic Conversion of Renewable Resources into Bulk and Fine Chemicals. *Chem. Rec.* **2016,** *16* (6), 2783-2796.
15.   Gupta, K.; Rai, R. K.; Singh, S. K., Metal Catalysts for the Efficient Transformation of Biomass-derived HMF and Furfural to Value Added Chemicals. *ChemCatChem* **2018,** *10* (11), 2326-2349.
16.   Huang, X.-F.; Santhanam, N.; Badri, D. V.; Hunter, W. J.; Manter, D. K.; Decker, S. R.; Vivanco, J. M.; Reardon, K. F., Isolation and characterization of lignin-degrading bacteria from rainforest soils. *Biotechnol. Bioeng.* **2013,** *110* (6), 1616-1626.
17.   Ahmed, S.; Rahman, M. S.; Hasan, M. M.; Paul, N.; Sajib, A. A., Microbial degradation of lignocellulosic biomass: discovery of novel natural lignocellulolytic bacteria. *BioTechnologia* **2018,** *99* (2), 137-146.
18.   Khan, T. S.; Mubeen, U., Wheat straw: a pragmatic overview. *Curr. Res. J. Biol. Sci.* **2012,** *4* (6), 673-675.
19.   Zugenmaier, P., Conformation and packing of various crystalline cellulose fibers. *Prog. Polym. Sci.* **2001,** *26* (9), 1341-1417.
20.   Bajpai, P., Chapter 2 - Wood and Fiber Fundamentals. In *Biermann's Handbook of Pulp and Paper (Third Edition)*, Bajpai, P., Ed. Elsevier: 2018; pp 19-74.

21.   Sun, Z.;   Fridrich, B.;   de Santi, A.;   Elangovan, S.;   Barta, K., Bright Side of Lignin Depolymerization: Toward New Platform Chemicals. *Chem. Rev.* **2018,** *118* (2), 614-678.

22.   Kleinert, T.; v. Tayenthal, K., Über neuere Versuche zur Trennung von Cellulose und Inkrusten verschiedener Hölzer. *Angew. Chem.* **1931,** *44* (39), 788-791.

23.   Chakar, F. S.; Ragauskas, A. J., Review of current and future softwood kraft lignin process chemistry. *Ind. Crops Prod.* **2004,** *20* (2), 131-141.

24.   Lora, J., Chapter 10 - Industrial Commercial Lignins: Sources, Properties and Applications. In *Monomers, Polymers and Composites from Renewable Resources*, Belgacem, M. N.; Gandini, A., Eds. Elsevier: Amsterdam, 2008; pp 225-241.

25.   Kim, J. S.;   Lee, Y. Y.;   Kim, T. H., A review on alkaline pretreatment technology for bioconversion of lignocellulosic biomass. *Bioresour. Technol.* **2016,** *199*, 42-48.

26.   Bunzel, M.; Schüßler, A.; Tchetseubu Saha, G., Chemical Characterization of Klason Lignin Preparations from Plant-Based Foods. *J. Agric. Food Chem.* **2011,** *59* (23), 12506-12513.

27.   Chatel, G.; Rogers, R. D., Review: Oxidation of Lignin Using Ionic Liquids—An Innovative Strategy To Produce Renewable Chemicals. *ACS Sustainable Chem. Eng.* **2014,** *2* (3), 322-339.

28.   Brosse, N.;   Hussin, M. H.;   Rahim, A. A., Organosolv Processes. In *Biorefineries*, Wagemann, K.; Tippkötter, N., Eds. Springer, Cham: 2017; pp 153-176.

29.   Llevot, A.;   Grau, E.;   Carlotti, S.;   Grelier, S.; Cramail, H., From Lignin-derived Aromatic Compounds to Novel Biobased Polymers. *Macromol. Rapid Commun.* **2016,** *37* (1), 9-28.

30.   Chio, C.;   Sain, M.; Qin, W., Lignin utilization: A review of lignin depolymerization from various aspects. *Renewable Sustainable Energy Rev.* **2019,** *107*, 232-249.

31.   Xu, R.;   Zhang, K.;   Liu, P.;   Han, H.;   Zhao, S.;   Kakade, A.;   Khan, A.;   Du, D.; Li, X., Lignin depolymerization and utilization by bacteria. *Bioresour. Technol.* **2018,** *269*, 557-566.

32.   Dessbesell, L.;   Yuan, Z.;   Leitch, M.;   Paleologou, M.;   Pulkki, R.; Xu, C. C., Capacity Design of a Kraft Lignin Biorefinery for Production of Biophenol via a Proprietary Low-Temperature/Low-Pressure Lignin Depolymerization Process. *ACS Sustainable Chem. Eng.* **2018,** *6* (7), 9293-9303.

33.   Pu, L.; Wang, X.; Cao, Q.; Liu, B.; Liu, H.; Han, Y.; Sun, G.; Li, Y.; Zhou, J., Novel Nonprecious Metal Loading Multi-Metal Oxide Catalysts for Lignin Depolymerization. *Energy Fuels* **2019,** *33* (7), 6491-6500.

34.   Kong-Win Chang, J.;   Duret, X.;   Berberi, V.;   Zahedi-Niaki, H.; Lavoie, J.-M., Two-Step Thermochemical Cellulose Hydrolysis With Partial Neutralization for Glucose Production. *Front. Chem.* **2018,** *6* (117).

35.   Delbecq, F.;   Wang, Y.;   Muralidhara, A.;   El Ouardi, K.;   Marlair, G.; Len, C., Hydrolysis of Hemicellulose and Derivatives—A Review of Recent Advances in the Production of Furfural. *Front. Chem.* **2018,** *6* (146).

36.   Liu, B.; Zhang, Z., Catalytic Conversion of Biomass into Chemicals and Fuels over Magnetic Catalysts. *ACS Catal.* **2016,** *6* (1), 326-338.

37.   Zhou, P.; Zhang, Z., One-pot catalytic conversion of carbohydrates into furfural and 5-hydroxymethylfurfural. *Catal. Sci. Technol.* **2016,** *6* (11), 3694-3712.

38.   van Zandvoort, I.;   Wang, Y.;   Rasrendra, C. B.;   van Eck, E. R. H.;   Bruijnincx, P. C. A.;   Heeres, H. J.; Weckhuysen, B. M., Formation, Molecular Structure, and Morphology of Humins in Biomass Conversion: Influence of Feedstock and Processing Conditions. *ChemSusChem* **2013,** *6* (9), 1745-1758.

39.   Kroh, L. W., Caramelisation in food and beverages. *Food Chem.* **1994,** *51* (4), 373-379.

40.   Martins, S. I. F. S.; Van Boekel, M. A. J. S., Kinetics of the glucose/glycine Maillard reaction pathways: influences of pH and reactant initial concentrations. *Food Chem.* **2005,** *92* (3), 437-448.

41.   van Boekel, M. A. J. S., Kinetic aspects of the Maillard reaction: a critical review. *Food / Nahrung* **2001,** *45* (3), 150-159.

42.   Kong, F.;   Lee, B. H.;   Wei, K., 5-Hydroxymethylfurfural mitigates lipopolysaccharide-stimulated inflammation via suppression of MAPK, NF-кb and mTOR activation in RAW 264.7 cells. *Molecules* **2019,** *24* (2), 275/1-275/16.

43.   Li, M.-M.; Wu, L.-Y.; Zhao, T.; Wu, K.-W.; Xiong, L.; Zhu, L.-L.; Fan, M., The protective role of 5-hydroxymethyl-2-furfural (5-HMF) against acute hypobaric hypoxia. *Cell Stress Chaperones* **2011,** *16* (5), 529-537.

44.   Li, Y.-X.; Li, Y.; Qian, Z.-J.; Kim, M.-M.; Kim, S.-K., In vitro antioxidant activity of 5-HMF isolated from marine red alga Laurencia undulata in free radical mediated oxidative systems. *J. Microbiol. Biotechnol.* **2009,** *19* (11), 1319-1327.

45.   Authority, E. F. S., Opinion of the Scientific Panel on food additives, flavourings, processing aids and materials in contact with food (AFC) related to Flavouring Group Evaluation 13 (FGE.13); Furfuryl and furan derivatives with and without additional side-chain substituents and heteroatoms from chemical group 14 (Commission Regulation (EC) No 1565/2000 of 18. *EFSA J.* **2005,** *3* (7), 215.

46.   Capuano, E.; Fogliano, V., Acrylamide and 5-hydroxymethylfurfural (HMF): A review on metabolism, toxicity, occurrence in food and mitigation strategies. *LWT--Food Sci. Technol.* **2011,** *44* (4), 793-810.

47.   Abraham, K.; Guertler, R.; Berg, K.; Heinemeyer, G.; Lampen, A.; Appel, K. E., Toxicology and risk assessment of 5-Hydroxymethylfurfural in food. *Mol. Nutr. Food Res.* **2011,** *55* (5), 667-678.

48.   Ventura, S. P. M.; de Morais, P.; Coelho, J. A. S.; Sintra, T.; Coutinho, J. A. P.; Afonso, C. A. M., Evaluating the toxicity of biomass derived platform chemicals. *Green Chem.* **2016,** *18* (17), 4733-4742.

49.   Bozell, J. J.; Petersen, G. R., Technology development for the production of biobased products from biorefinery carbohydrates-the US Department of Energy's "Top 10" revisited. *Green Chem.* **2010,** *12* (4), 539-554.

50.   van Putten, R.-J.; van der Waal, J. C.; de Jong, E.; Rasrendra, C. B.; Heeres, H. J.; de Vries, J. G., Hydroxymethylfurfural, A Versatile Platform Chemical Made from Renewable Resources. *Chem. Rev.* **2013,** *113* (3), 1499-1597.

51.   Moreau, C.; Belgacem, M. N.; Gandini, A., Recent Catalytic Advances in the Chemistry of Substituted Furans from Carbohydrates and in the Ensuing Polymers. *Top. Catal.* **2004,** *27* (1), 11-30.

52.   Ståhlberg, T.; Rodriguez-Rodriguez, S.; Fristrup, P.; Riisager, A., Metal-Free Dehydration of Glucose to 5-(Hydroxymethyl)furfural in Ionic Liquids with Boric Acid as a Promoter. *Chem. - Eur. J.* **2011,** *17* (5), 1456-1464.

53.   Moreau, C.; Durand, R.; Razigade, S.; Duhamet, J.; Faugeras, P.; Rivalier, P.; Ros, P.; Avignon, G., Dehydration of fructose to 5-hydroxymethylfurfural over H-mordenites. *Applied Catalysis A: General* **1996,** *145* (1), 211-224.

54.   Hu, L.; Zhao, G.; Hao, W.; Tang, X.; Sun, Y.; Lin, L.; Liu, S., Catalytic conversion of biomass-derived carbohydrates into fuels and chemicals via furanic aldehydes. *RSC Adv.* **2012,** *2* (30), 11184-11206.

55.   Kunnikuruvan, S.; Nair, N. N., Mechanistic Insights into the Brønsted Acid-Catalyzed Dehydration of β-d-Glucose to 5-Hydroxymethylfurfural under Ambient and Subcritical Conditions. *ACS Catal.* **2019,** *9* (8), 7250-7263.

56.   Hoang, T. M. C.; van Eck, E. R. H.; Bula, W. P.; Gardeniers, J. G. E.; Lefferts, L.; Seshan, K., Humin based by-products from biomass processing as a potential carbonaceous source for synthesis gas production. *Green Chem.* **2015,** *17* (2), 959-972.

57.   Vuyyuru, K. R.; Strasser, P., Oxidation of biomass derived 5-hydroxymethylfurfural using heterogeneous and electrochemical catalysis. *Catal. Today* **2012,** *195* (1), 144-154.

58.   Chacón-Huete, F.; Messina, C.; Chen, F.; Cuccia, L.; Ottenwaelder, X.; Forgione, P., Solvent-free mechanochemical oxidation and reduction of biomass-derived 5-hydroxymethyl furfural. *Green Chem.* **2018,** *20* (23), 5261-5265.

59.   Ventura, M.; Lobefaro, F.; de Giglio, E.; Distaso, M.; Nocito, F.; Dibenedetto, A., Selective Aerobic Oxidation of 5-Hydroxymethylfurfural to 2,5-Diformylfuran or 2-Formyl-5-furancarboxylic Acid in Water by using MgO·CeO2 Mixed Oxides as Catalysts. *ChemSusChem* **2018,** *11* (8), 1305-1315.

60.   Kim, M.; Su, Y.; Fukuoka, A.; Hensen, E. J. M.; Nakajima, K., Aerobic Oxidation of 5-(Hydroxymethyl)furfural Cyclic Acetal Enables Selective Furan-2,5-dicarboxylic Acid Formation with CeO2-Supported Gold Catalyst. *Angew. Chem., Int. Ed.* **2018,** *57* (27), 8235-8239.

61.   Sousa, A. F.; Vilela, C.; Fonseca, A. C.; Matos, M.; Freire, C. S. R.; Gruter, G.-J. M.; Coelho, J. F. J.; Silvestre, A. J. D., Biobased polyesters and other polymers from 2,5-furandicarboxylic acid: a tribute to furan excellency. *Polym. Chem.* **2015,** *6* (33), 5961-5983.

62.   Kucherov, F. A.; Romashov, L. V.; Galkin, K. I.; Ananikov, V. P., Chemical Transformations of Biomass-Derived C6-Furanic Platform Chemicals for Sustainable Energy Research, Materials Science, and Synthetic Building Blocks. *ACS Sustainable Chem. Eng.* **2018,** *6* (7), 8064-8092.

63.   Gupta, D.; Saha, B., Carbon nanosphere supported Ru catalyst for the synthesis of renewable herbicide and chemicals. *Catal. Commun.* **2017,** *100*, 206-209.

64.   Townsend, T. M.; Kirby, C.; Ruff, A.; O'Connor, A. R., Transfer hydrogenation of aromatic and linear aldehydes catalyzed using Cp*Ir(pyridinesulfonamide)Cl complexes under base-free conditions. *J. Organomet. Chem.* **2017,** *843*, 7-13.

65.   Kucherov, F. A.; Galkin, K. I.; Gordeev, E. G.; Ananikov, V. P., Efficient route for the construction of polycyclic systems from bioderived HMF. *Green Chem.* **2017,** *19* (20), 4858-4864.

66.   De Vries, J. G.; Teddy; Phua, P. H.; Melian Cabrera, I. V.; Heeres, H. J. Preparation of caprolactone, caprolactam, 2,5-tetrahydrofuran-dimethanol, 1,6-hexanediol or 1,2,6-hexanetriol from 5-hydroxymethyl-2-furfuraldehyde. US9199961B2, 2015.

67.   Yang, Y.; Liu, Q.; Li, D.; Tan, J.; Zhang, Q.; Wang, C.; Ma, L., Selective hydrodeoxygenation of 5-hydroxymethylfurfural to 2,5-dimethylfuran on Ru–MoOx/C catalysts. *RSC Adv.* **2017,** *7* (27), 16311-16318.

68.   Duan, Y.; Zheng, M.; Li, D.; Deng, D.; Ma, L.-F.; Yang, Y., Conversion of HMF to methyl cyclopentenolone using Pd/Nb2O5 and Ca–Al catalysts via a two-step procedure. *Green Chem.* **2017,** *19* (21), 5103-5113.

69.   Yoshii, K.; Yamada, A. Method for the preparation of tetrahydrofuran compound. WO2013133208A1, 2013.

70.   Luo, J.; Monai, M.; Wang, C.; Lee, J. D.; Duchoň, T.; Dvořák, F.; Matolín, V.; Murray, C. B.; Fornasiero, P.; Gorte, R. J., Unraveling the surface state and composition of highly selective nanocrystalline Ni–Cu alloy catalysts for hydrodeoxygenation of HMF. *Catal. Sci. Technol.* **2017,** *7* (8), 1735-1743.

71.   Insyani, R.; Verma, D.; Kim, S. M.; Kim, J., Direct one-pot conversion of monosaccharides into high-yield 2,5-dimethylfuran over a multifunctional Pd/Zr-based metal–organic framework@sulfonated graphene oxide catalyst. *Green Chem.* **2017,** *19* (11), 2482-2490.

72.   Mitra, J.; Zhou, X.; Rauchfuss, T., Pd/C-catalyzed reactions of HMF: decarbonylation, hydrogenation, and hydrogenolysis. *Green Chem.* **2015,** *17* (1), 307-313.

73.   Maniar, D.; Jiang, Y.; Woortman, A. J. J.; van Dijken, J.; Loos, K., Furan-Based Copolyesters from Renewable Resources: Enzymatic Synthesis and Properties. *ChemSusChem* **2019,** *12* (5), 990-999.

74.   Brandvold, T. A.; Buchbinder, A. M.; Iwamoto, N.; Abrevaya, H.; Do, P. T. M. Processes and catalysts for conversion of 2,5-dimethylfuran derivatives to terephthalate. US9321714B1, 2016.

75.   Wang, B.; Gruter, G. J. M.; Dam, M. A.; Kriegel, R. M. Process for the preparation of benzene derivatives from furan derivatives. WO2014065657A1, 2014.

76.   Pacheco, J. J.; Labinger, J. A.; Sessions, A. L.; Davis, M. E., Route to Renewable PET: Reaction Pathways and Energetics of Diels–Alder and Dehydrative Aromatization Reactions Between Ethylene and Biomass-Derived Furans Catalyzed by Lewis Acid Molecular Sieves. *ACS Catal.* **2015,** *5* (10), 5904-5913.

77.   Yang, W.; Sen, A., One-Step Catalytic Transformation of Carbohydrates and Cellulosic Biomass to 2,5-Dimethyltetrahydrofuran for Liquid Fuels. *ChemSusChem* **2010,** *3* (5), 597-603.

78.   Sousa, A. F.; Matos, M.; Freire, C. S. R.; Silvestre, A. J. D.; Coelho, J. F. J., New copolyesters derived from terephthalic and 2,5-furandicarboxylic acids: A step forward in the development of biobased polyesters. *Polymer* **2013,** *54* (2), 513-519.

79.   Matos, M.; Sousa, A. F.; Fonseca, A. C.; Freire, C. S. R.; Coelho, J. F. J.; Silvestre, A. J. D., A New Generation of Furanic Copolyesters with Enhanced Degradability: Poly(ethylene 2,5-furandicarboxylate)-co-poly(lactic acid) Copolyesters. *Macromol. Chem. Phys.* **2014,** *215* (22), 2175-2184.

80.   Papageorgiou, G. Z.; Papageorgiou, D. G.; Terzopoulou, Z.; Bikiaris, D. N., Production of bio-based 2,5-furan dicarboxylate polyesters: Recent progress and critical aspects in their synthesis and thermal properties. *Eur. Polym. J.* **2016,** *83*, 202-229.

81.   Carlos Morales-Huerta, J.; Martínez de Ilarduya, A.; Muñoz-Guerra, S., Poly(alkylene 2,5-furandicarboxylate)s (PEF and PBF) by ring opening polymerization. *Polymer* **2016,** *87*, 148-158.

82.   Pfister, D.; Storti, G.; Tancini, F.; Costa, L. I.; Morbidelli, M., Synthesis and Ring-Opening Polymerization of Cyclic Butylene 2,5-Furandicarboxylate. *Macromol. Chem. Phys.* **2015,** *216* (21), 2141-2146.

83.   Thiyagarajan, S.; Vogelzang, W.; J. I. Knoop, R.; Frissen, A. E.; van Haveren, J.; van Es, D. S., Biobased furandicarboxylic acids (FDCAs): effects of isomeric substitution on polyester synthesis and properties. *Green Chem.* **2014,** *16* (4), 1957-1966.

84.   Gruter, G.-J. M.; Sipos, L.; Dam, M. A., Accelerating research into bio-based FDCA-polyesters by using small scale parallel film reactors. *Comb. Chem. High Throughput Screening* **2012,** *15* (2), 180-188.

85.   Özcan, L.; Yalçın, P.; Alagöz, O.; Yurdakal, S., Selective photoelectrocatalytic oxidation of 5-(hydroxymethyl)-2-furaldehyde in water by using Pt loaded nanotube structure of TiO2 on Ti photoanodes. *Catal. Today* **2017,** *281*, 205-213.

86.   Sibi, M. P.; Sermadurai, S.; Zimmermann, N.; Serum, E.; Ma, G.; Moorthy, R.; Kalliokoski, K. Preparation of novel monomers from biomass. WO2016022943A2, 2016.

87.   Donoeva, B.; Masoud, N.; de Jongh, P. E., Carbon Support Surface Effects in the Gold-Catalyzed Oxidation of 5-Hydroxymethylfurfural. *ACS Catal.* **2017,** *7* (7), 4581-4591.

88.   Zhang, X.-Y.; Zong, M.-H.; Li, N., Whole-cell biocatalytic selective oxidation of 5-hydroxymethylfurfural to 5-hydroxymethyl-2-furancarboxylic acid. *Green Chem.* **2017,** *19* (19), 4544-4551.

89.   Jia, H.-Y.; Zong, M.-H.; Yu, H.-L.; Li, N., Dehydrogenase-Catalyzed Oxidation of Furanics: Exploitation of Hemoglobin Catalytic Promiscuity. *ChemSusChem* **2017,** *10* (18), 3524-3528.

90.   Chen, C.-T.; Nguyen, C. V.; Wang, Z.-Y.; Bando, Y.; Yamauchi, Y.; Bazziz, M. T. S.; Fatehmulla, A.; Farooq, W. A.; Yoshikawa, T.; Masuda, T.; Wu, K. C.-W., Hydrogen Peroxide Assisted Selective Oxidation of 5-Hydroxymethylfurfural in Water under Mild Conditions. *ChemCatChem* **2018,** *10* (2), 361-365.

91.   Wang, K.-F.; Liu, C.-l.; Sui, K.-y.; Guo, C.; Liu, C.-Z., Efficient Catalytic Oxidation of 5-Hydroxymethylfurfural to 2,5-Furandicarboxylic Acid by Magnetic Laccase Catalyst. *ChemBioChem* **2018,** *19* (7), 654-659.

92.   Pezzetta, C.; Veiros, L. F.; Oble, J.; Poli, G., Murai Reaction on Furfural Derivatives Enabled by Removable N,N′-Bidentate Directing Groups. *Chem. - Eur. J.* **2017,** *23* (35), 8385-8389.

93.   Xu, G. G.; Pagare, P. P.; Ghatge, M. S.; Safo, R. P.; Gazi, A.; Chen, Q.; David, T.; Alabbas, A. B.; Musayev, F. N.; Venitz, J.; Zhang, Y.; Safo, M. K.; Abdulmalik, O., Design, Synthesis, and Biological Evaluation of Ester and Ether Derivatives of Antisickling Agent 5-HMF for the Treatment of Sickle Cell Disease. *Mol. Pharmaceutics* **2017,** *14* (10), 3499-3511.

94.   Romashov, L. V.; Ananikov, V. P., Alkynylation of Bio-Based 5-Hydroxymethylfurfural to Connect Biomass Processing with Conjugated Polymers and Furanic Pharmaceuticals. *Chem. - Asian J.* **2017,** *12* (20), 2652-2655.

95.   Arias, K. S.; Garcia-Ortiz, A.; Climent, M. J.; Corma, A.; Iborra, S., Mutual Valorization of 5-Hydroxymethylfurfural and Glycerol into Valuable Diol Monomers with Solid Acid Catalysts. *ACS Sustainable Chem. Eng.* **2018,** *6* (3), 4239-4245.

96.   Shinde, S.; Rode, C., Cascade Reductive Etherification of Bioderived Aldehydes over Zr-Based Catalysts. *ChemSusChem* **2017,** *10* (20), 4090-4101.

97.   Liu, Q.; Zhang, C.; Shi, N.; Zhang, X.; Wang, C.; Ma, L., Production of renewable long-chained cycloalkanes from biomass-derived furfurals and cyclic ketones. *RSC Adv.* **2018,** *8* (25), 13686-13696.

98.   Li, S.; Chen, F.; Li, N.; Wang, W.; Sheng, X.; Wang, A.; Cong, Y.; Wang, X.; Zhang, T., Synthesis of Renewable Triketones, Diketones, and Jet-Fuel Range Cycloalkanes with 5-Hydroxymethylfurfural and Ketones. *ChemSusChem* **2017,** *10* (4), 711-719.

99.   Han, M.; Liu, X.; Zhang, X.; Pang, Y.; Xu, P.; Guo, J.; Liu, Y.; Zhang, S.; Ji, S., 5-Hydroxymethyl-2-vinylfuran: a biomass-based solvent-free adhesive. *Green Chem.* **2017,** *19* (3), 722-728.

100.   Xu, Y.-J.; Shi, J.; Wu, W.-P.; Zhu, R.; Li, X.-L.; Deng, J.; Fu, Y., Effect of Cp*Iridium(III) Complex and acid co-catalyst on conversion of furfural compounds to cyclopentanones or straight chain ketones. *Applied Catalysis A: General* **2017,** *543*, 266-273.

101.   Wozniak, B.; Spannenberg, A.; Li, Y.; Hinze, S.; de Vries, J. G., Cyclopentanone Derivatives from 5-Hydroxymethylfurfural via 1-Hydroxyhexane-2,5-dione as Intermediate. *ChemSusChem* **2018,** *11* (2), 356-359.

102.   Wozniak, B.; Li, Y.; Hinze, S.; Tin, S.; de Vries, J. G., Efficient Synthesis of Biomass-Derived N-Substituted 2-Hydroxymethyl-5-Methyl-Pyrroles in Two Steps from 5-Hydroxymethylfurfural. *Eur. J. Org. Chem.* **2018,** *2018* (17), 2009-2012.

103.   Buntara, T.; Noel, S.; Phua, P. H.; Melián-Cabrera, I.; de Vries, J. G.; Heeres, H. J., Caprolactam from Renewable Resources: Catalytic Conversion of 5-Hydroxymethylfurfural into Caprolactone. *Angew. Chem., Int. Ed.* **2011,** *50* (31), 7083-7087.

104.   Li, X.; Ho, B.; Lim, D. S. W.; Zhang, Y., Highly efficient formic acid-mediated oxidation of renewable furfural to maleic acid with H2O2. *Green Chem.* **2017,** *19* (4), 914-918.

105.   Ventura, M.; Williamson, D.; Lobefaro, F.; Jones, M. D.; Mattia, D.; Nocito, F.; Aresta, M.; Dibenedetto, A., Sustainable Synthesis of Oxalic and Succinic Acid through Aerobic Oxidation of C6 Polyols Under Mild Conditions. *ChemSusChem* **2018,** *11* (6), 1073-1081.

106.   Li, X.; Jia, X.; Ma, J.; Xu, Y.; Huang, Y.; Xu, J., Catalytic Amidation of 5-Hydroxymethylfurfural to 2,5-Furandicarboxamide over Alkali Manganese Oxides. *Chin. J. Chem.* **2017,** *35* (6), 984-990.

107.   Li, X.; Ma, J.; Jia, X.; Xia, F.; Huang, Y.; Xu, Y.; Xu, J., Al-Doping Promoted Aerobic Amidation of 5-Hydroxymethylfurfural to 2,5-Furandicarboxamide over Cryptomelane. *ACS Sustainable Chem. Eng.* **2018,** *6* (6), 8048-8054.

108.   Kang, S.; Fu, J.; Zhang, G., From lignocellulosic biomass to levulinic acid: A review on acid-catalyzed hydrolysis. *Renewable Sustainable Energy Rev.* **2018,** *94*, 340-362.

109.   Stadler, B. M.; Wulf, C.; Werner, T.; Tin, S.; de Vries, J. G., Catalytic Approaches to Monomers for Polymers Based on Renewables. *ACS Catal.* **2019**, 8012-8067.

110.   Zhang, X.; Fevre, M.; Jones, G. O.; Waymouth, R. M., Catalysis as an Enabling Science for Sustainable Polymers. *Chem. Rev.* **2018,** *118* (2), 839-885.

111.   Ragauskas, A. J.; Williams, C. K.; Davison, B. H.; Britovsek, G.; Cairney, J.; Eckert, C. A.; Frederick, W. J.; Hallett, J. P.; Leak, D. J.; Liotta, C. L.; Mielenz, J. R.; Murphy, R.; Templer, R.; Tschaplinski, T., The Path Forward for Biofuels and Biomaterials. *Science* **2006,** *311* (5760), 484-489.

112.   Fittig, R., Mittheilungen aus dem chemischen Institut der Universität Strassburg. *Ber. Dtsch. Chem. Ges.* **1876,** *9* (2), 1189-1199.

113.   Poulopoulou, N.; Pipertzis, A.; Kasmi, N.; Bikiaris, D. N.; Papageorgiou, D. G.; Floudas, G.; Papageorgiou, G. Z., Green polymeric materials: On the dynamic homogeneity and miscibility of furan-based polyester blends. *Polymer* **2019,** *174*, 187-199.

114.   Kim, M.; Su, Y.; Aoshima, T.; Fukuoka, A.; Hensen, E. J. M.; Nakajima, K., Effective Strategy for High-Yield Furan Dicarboxylate Production for Biobased Polyester Applications. *ACS Catal.* **2019,** *9* (5), 4277-4285.

115.   Chebbi, Y.; Kasmi, N.; Majdoub, M.; Cerruti, P.; Scarinzi, G.; Malinconico, M.; Dal Poggetto, G.; Papageorgiou, G. Z.; Bikiaris, D. N., Synthesis, Characterization, and Biodegradability of Novel Fully Biobased Poly(decamethylene-co-isosorbide 2,5-furandicarboxylate) Copolyesters with Enhanced Mechanical Properties. *ACS Sustainable Chem. Eng.* **2019,** *7* (5), 5501-5514.

116.   Wang, X.; Wang, Q.; Liu, S.; Wang, G., Synthesis and characterization of poly(isosorbide-co-butylene 2,5-furandicarboxylate) copolyesters. *Eur. Polym. J.* **2019,** *115*, 70-75.

117.   Kasmi, N.; Poulopoulou, N.; Terzopoulou, Z.; Papageorgiou, D. G.; Bikiaris, D. N.; Papageorgiou, G. Z., Sustainable thermoplastics from renewable resources: Thermal behavior of poly(1,4-cyclohexane dimethylene 2,5-furandicarboxylate). *Eur. Polym. J.* **2019,** *112*, 1-14.

118.   Xie, H.; Wu, L.; Li, B.-G.; Dubois, P., Modification of Poly(ethylene 2,5-furandicarboxylate) with Biobased 1,5-Pentanediol: Significantly Toughened Copolyesters Retaining High Tensile Strength and O2 Barrier Property. *Biomacromolecules* **2019,** *20* (1), 353-364.

119.   Zhang, D.; Dumont, M.-J., Advances in polymer precursors and bio-based polymers synthesized from 5-hydroxymethylfurfural. *J. Polym. Sci., Part A: Polym. Chem.* **2017,** *55* (9), 1478-1492.

120.   Wilsens, C. H. R. M.; Rastogi, S.; Veld, M. A. J.; Klop, E. A.; Noordover, B. A. J. Liquid crystalline furandicarboxylic acid-based aromatic polyesters. WO2013092667A1, 2013.

121.   Wilsens, C. H. R. M.; Noordover, B. A. J.; Rastogi, S., Aromatic thermotropic polyesters based on 2,5-furandicarboxylic acid and vanillic acid. *Polymer* **2014,** *55* (10), 2432-2439.

122.   Wilsens, C. H. R. M.; Verhoeven, J. M. G. A.; Noordover, B. A. J.; Hansen, M. R.; Auhl, D.; Rastogi, S., Thermotropic Polyesters from 2,5-Furandicarboxylic Acid and Vanillic Acid: Synthesis, Thermal Properties, Melt Behavior, and Mechanical Performance. *Macromolecules* **2014,** *47* (10), 3306-3316.

123.   Sousa, A. F.; Fonseca, A. C.; Serra, A. C.; Freire, C. S. R.; Silvestre, A. J. D.; Coelho, J. F. J., New unsaturated copolyesters based on 2,5-furandicarboxylic acid and their crosslinked derivatives. *Polym. Chem.* **2016,** *7* (5), 1049-1058.

124.   Gubbels, E.; Jasinska-Walc, L.; Noordover, B. A. J.; Koning, C. E., Linear and branched polyester resins based on dimethyl-2,5-furandicarboxylate for coating applications. *Eur. Polym. J.* **2013,** *49* (10), 3188-3198.

125.   Yeh, I.-C.; Rinderspacher, B. C.; Andzelm, J. W.; Cureton, L. T.; La Scala, J., Computational study of thermal and mechanical properties of nylons and bio-based furan polyamides. *Polymer* **2014,** *55* (1), 166-174.

126.   Endah, Y. K.; Han, S. H.; Kim, J. H.; Kim, N.-K.; Kim, W. N.; Lee, H.-S.; Lee, H., Solid-state polymerization and characterization of a copolyamide based on adipic acid, 1,4-butanediamine, and 2,5-furandicarboxylic acid. *J. Appl. Polym. Sci.* **2016,** *133* (18).

127.   Amarasekara, A. S.; Green, D.; Williams, L. D., Renewable resources based polymers: Synthesis and characterization of 2,5-diformylfuran–urea resin. *Eur. Polym. J.* **2009,** *45* (2), 595-598.

128.   Wilsens, C. H. R. M.; Deshmukh, Y. S.; Noordover, B. A. J.; Rastogi, S., Influence of the 2,5-Furandicarboxamide Moiety on Hydrogen Bonding in Aliphatic–Aromatic Poly(ester amide)s. *Macromolecules* **2014,** *47* (18), 6196-6206.

129.   Wilsens, C. H. R. M.; Wullems, N. J. M.; Gubbels, E.; Yao, Y.; Rastogi, S.; Noordover, B. A. J., Synthesis, kinetics, and characterization of bio-based thermosets obtained through polymerization of a 2,5-furandicarboxylic acid-based bis(2-oxazoline) with sebacic acid. *Polym. Chem.* **2015,** *6* (14), 2707-2716.

130.   Deng, J.; Liu, X.; Li, C.; Jiang, Y.; Zhu, J., Synthesis and properties of a bio-based epoxy resin from 2,5-furandicarboxylic acid (FDCA). *RSC Adv.* **2015,** *5* (21), 15930-15939.

131.   James Drewitt; Lincoln, J. Polyesters from Heterocyclic Components. 1947.

132.   Gandini, A.; Silvestre, A. J. D.; Pascoal Neto, C.; Sousa, A. F.; Gomes, M., The furan counterpart of poly(ethylene terephthalate): an alternative material based on renewable resources. *J. Polym. Sci., Part A: Polym. Chem.* **2008,** *47* (1), 295-298.

133.   Collias, D. I.; Harris, A. M.; Nagpal, V.; Cottrell, I. W.; Schultheis, M. W., Biobased Terephthalic Acid Technologies: A Literature Review. *Ind. Biotechnol.* **2014,** *10* (2), 91-105.

134.   Tachibana, Y.; Kimura, S.; Kasuya, K.-i., Synthesis and Verification of Biobased Terephthalic Acid from Furfural. *Sci. Rep.* **2015,** *5*, 8249.

135.   Miller, K. K.; Zhang, P.; Nishizawa-Brennen, Y.; Frost, J. W., Synthesis of Biobased Terephthalic Acid from Cycloaddition of Isoprene with Acrylic Acid. *ACS Sustainable Chem. Eng.* **2014,** *2* (8), 2053-2056.

136. Vilela, C.; Sousa, A. F.; Fonseca, A. C.; Serra, A. C.; Coelho, J. F. J.; Freire, C. S. R.; Silvestre, A. J. D., The quest for sustainable polyesters – insights into the future. *Polym. Chem.* **2014,** *5* (9), 3119-3141.

137. Eerhart, A. J. J. E.; Faaij, A. P. C.; Patel, M. K., Replacing fossil based PET with biobased PEF; process analysis, energy and GHG balance. *Energy Environ. Sci.* **2012,** *5* (4), 6407-6422.

138. Gomes, M.; Gandini, A.; Silvestre, A. J. D.; Reis, B., Synthesis and characterization of poly(2,5-furan dicarboxylate)s based on a variety of diols. *J. Polym. Sci., Part A: Polym. Chem.* **2011,** *49* (17), 3759-3768.

139. Muñoz de Diego, C.; Dam, M. A.; Gruter, G. J. M. Methods for production of 2,5-furandicarboxylic acid and dialkyl 2,5-furandicarboxylates. WO2011043661A1, 2011.

140. de Jong, E.; Dam, M. A.; Sipos, L.; Gruter, G. J. M., Furandicarboxylic Acid (FDCA), A Versatile Building Block for a Very Interesting Class of Polyesters. In *Biobased Monomers, Polymers, and Materials*, American Chemical Society: 2012; Vol. 1105, pp 1-13.

141. Knoop, R. J. I.; Vogelzang, W.; van Haveren, J.; van Es, D. S., High molecular weight poly(ethylene-2,5-furanoate); critical aspects in synthesis and mechanical property determination. *J. Polym. Sci., Part A: Polym. Chem.* **2013,** *51* (19), 4191-4199.

142. Sipos, L. Preparation of polyesters containing 2,5-furandicarboxylate moieties within the polymer backbone. WO2010077133A1, 2010.

143. Jiang, M.; Liu, Q.; Zhang, Q.; Ye, C.; Zhou, G., A series of furan-aromatic polyesters synthesized via direct esterification method based on renewable resources. *J. Polym. Sci., Part A: Polym. Chem.* **2012,** *50* (5), 1026-1036.

144. Burgess, S. K.; Karvan, O.; Johnson, J. R.; Kriegel, R. M.; Koros, W. J., Oxygen sorption and transport in amorphous poly(ethylene furanoate). *Polymer* **2014,** *55* (18), 4748-4756.

145. Burgess, S. K.; Mikkilineni, D. S.; Yu, D. B.; Kim, D. J.; Mubarak, C. R.; Kriegel, R. M.; Koros, W. J., Water sorption in poly(ethylene furanoate) compared to poly(ethylene terephthalate). Part 1: Equilibrium sorption. *Polymer* **2014,** *55* (26), 6861-6869.

146. Burgess, S. K.; Mikkilineni, D. S.; Yu, D. B.; Kim, D. J.; Mubarak, C. R.; Kriegel, R. M.; Koros, W. J., Water sorption in poly(ethylene furanoate) compared to poly(ethylene terephthalate). Part 2: Kinetic sorption. *Polymer* **2014,** *55* (26), 6870-6882.

147. Burgess, S. K.; Wenz, G. B.; Kriegel, R. M.; Koros, W. J., Penetrant transport in semicrystalline poly(ethylene furanoate). *Polymer* **2016,** *98*, 305-310.

148. Burgess, S. K.; Kriegel, R. M.; Koros, W. J., Carbon Dioxide Sorption and Transport in Amorphous Poly(ethylene furanoate). *Macromolecules* **2015,** *48* (7), 2184-2193.

149. Saywell, C.; Mai, S.; Capelas Romeu, C.; Legramanti Neves, J. C. Process for the production of poly(ethylene 2,5-furandicarboxylate) from 2,5-furandicarboxylic acid and use thereof, polyester compound and blends thereof. FR2985260A1, 2013.

150. Sipos, L.; Olson, M. L. Process for the depolymerization of a furandicarboxylate containing polyester. WO2012091573A1, 2012.

151. Pellis, A.; Haernvall, K.; Pichler, C. M.; Ghazaryan, G.; Breinbauer, R.; Guebitz, G. M., Enzymatic hydrolysis of poly(ethylene furanoate). *J. Biotechnol.* **2016,** *235*, 47-53.

152. Ribitsch, D.; Yebra, A. O.; Zitzenbacher, S.; Wu, J.; Nowitsch, S.; Steinkellner, G.; Greimel, K.; Doliska, A.; Oberdorfer, G.; Gruber, C. C.; Gruber, K.; Schwab, H.; Stana-Kleinschek, K.; Acero, E. H.; Guebitz, G. M., Fusion of Binding Domains to Thermobifida cellulosilytica Cutinase to Tune Sorption Characteristics and Enhancing PET Hydrolysis. *Biomacromolecules* **2013,** *14* (6), 1769-1776.

153. Herrero Acero, E.; Ribitsch, D.; Steinkellner, G.; Gruber, K.; Greimel, K.; Eiteljoerg, I.; Trotscha, E.; Wei, R.; Zimmermann, W.; Zinn, M.; Cavaco-Paulo, A.; Freddi, G.; Schwab, H.; Guebitz, G., Enzymatic Surface Hydrolysis of PET: Effect of Structural Diversity on Kinetic Properties of Cutinases from Thermobifida. *Macromolecules* **2011,** *44* (12), 4632-4640.

154. Jiang, Y.; Liu, W.; Zou, H.; Cheng, T.; Tian, N.; Xian, M., Microbial production of short chain diols. *Microb. Cell Fact.* **2014,** *13* (1), 165.

155. Toogood, H. S.; Scrutton, N. S., Retooling microorganisms for the fermentative production of alcohols. *Curr. Opin. Biotechnol.* **2018,** *50*, 1-10.

156.   Tsanaktsis, V.; Papageorgiou, G. Z.; Bikiaris, D. N., A facile method to synthesize high-molecular-weight biobased polyesters from 2,5-furandicarboxylic acid and long-chain diols. *J. Polym. Sci., Part A: Polym. Chem.* **2015,** *53* (22), 2617-2632.

157.   Papageorgiou, G. Z.; Tsanaktsis, V.; Papageorgiou, D. G.; Exarhopoulos, S.; Papageorgiou, M.; Bikiaris, D. N., Evaluation of polyesters from renewable resources as alternatives to the current fossil-based polymers. Phase transitions of poly(butylene 2,5-furan-dicarboxylate). *Polymer* **2014,** *55* (16), 3846-3858.

158.   Ma, J.; Yu, X.; Xu, J.; Pang, Y., Synthesis and crystallinity of poly(butylene 2,5-furandicarboxylate). *Polymer* **2012,** *53* (19), 4145-4151.

159.   Zhu, J.; Cai, J.; Xie, W.; Chen, P.-H.; Gazzano, M.; Scandola, M.; Gross, R. A., Poly(butylene 2,5-furan dicarboxylate), a Biobased Alternative to PBT: Synthesis, Physical Properties, and Crystal Structure. *Macromolecules* **2013,** *46* (3), 796-804.

160.   Gao, L.; Zhuge, W.; Feng, X.; Sun, W.; Sun, X.; Zheng, G., Co/rGO synthesized via the alcohol-thermal method as a heterogeneous catalyst for the highly efficient oxidation of ethylbenzene with oxygen. *New J. Chem.* **2019,** *43* (21), 8189-8194.

161.   Ma, J.; Pang, Y.; Wang, M.; Xu, J.; Ma, H.; Nie, X., The copolymerization reactivity of diols with 2,5-furandicarboxylic acid for furan-based copolyester materials. *J. Mater. Chem.* **2012,** *22* (8), 3457-3461.

162.   Terzopoulou, Z.; Tsanaktsis, V.; Bikiaris, D. N.; Exarhopoulos, S.; Papageorgiou, D. G.; Papageorgiou, G. Z., Biobased poly(ethylene furanoate-co-ethylene succinate) copolyesters: solid state structure, melting point depression and biodegradability. *RSC Adv.* **2016,** *6* (87), 84003-84015.

163.   Hong, S.; Min, K.-D.; Nam, B.-U.; Park, O. O., High molecular weight bio furan-based co-polyesters for food packaging applications: synthesis, characterization and solid-state polymerization. *Green Chem.* **2016,** *18* (19), 5142-5150.

164.   Sousa, A. F.; Coelho, J. F. J.; Silvestre, A. J. D., Renewable-based poly((ether)ester)s from 2,5-furandicarboxylic acid. *Polymer* **2016,** *98*, 129-135.

165.   Wang, J.; Liu, X.; Zhang, Y.; Liu, F.; Zhu, J., Modification of poly(ethylene 2,5-furandicarboxylate) with 1,4-cyclohexanedimethylene: Influence of composition on mechanical and barrier properties. *Polymer* **2016,** *103*, 1-8.

166.   Anastas, P.; Eghbali, N., Green Chemistry: Principles and Practice. *Chem. Soc. Rev.* **2010,** *39* (1), 301-312.

167.   Anastas, P. T.; Zimmerman, J. B., Peer Reviewed: Design Through the 12 Principles of Green Engineering. *Environ. Sci. Technol.* **2003,** *37* (5), 94A-101A.

168.   Dallinger, D.; Kappe, C. O., Why flow means green – Evaluating the merits of continuous processing in the context of sustainability. *Current Opinion in Green and Sustainable Chemistry* **2017,** *7*, 6-12.

169.   Lee, S. L.; O'Connor, T. F.; Yang, X.; Cruz, C. N.; Chatterjee, S.; Madurawe, R. D.; Moore, C. M. V.; Yu, L. X.; Woodcock, J., Modernizing Pharmaceutical Manufacturing: from Batch to Continuous Production. *J. Pharm. Sci. Innovation* **2015,** *10* (3), 191-199.

170.   Kockmann, N.; Thenée, P.; Fleischer-Trebes, C.; Laudadio, G.; Noël, T., Safety assessment in development and operation of modular continuous-flow processes. *React. Chem. Eng.* **2017,** *2* (3), 258-280.

171.   Mallia, C. J.; Baxendale, I. R., The Use of Gases in Flow Synthesis. *Org. Process Res. Dev.* **2016,** *20* (2), 327-360.

172.   Gutmann, B.; Kappe, C. O., Forbidden chemistries go flow in API synthesis. *Chim. Oggi* **2015,** *33* (3), 18-24.

173.   May, S. A.; Johnson, M. D.; Buser, J. Y.; Campbell, A. N.; Frank, S. A.; Haeberle, B. D.; Hoffman, P. C.; Lambertus, G. R.; McFarland, A. D.; Moher, E. D.; White, T. D.; Hurley, D. D.; Corrigan, A. P.; Gowran, O.; Kerrigan, N. G.; Kissane, M. G.; Lynch, R. R.; Sheehan, P.; Spencer, R. D.; Pulley, S. R.; Stout, J. R., Development and Manufacturing GMP Scale-Up of a Continuous Ir-Catalyzed Homogeneous Reductive Amination Reaction. *Org. Process Res. Dev.* **2016,** *20* (11), 1870-1898.

174.   Holladay, J. E.; White, J. F.; Bozell, J. J.; Johnson, D. *Top Value-Added Chemicals from Biomass - Volume II—Results of Screening for Potential Candidates from Biorefinery Lignin*; United States, 2007-10-01, 2007.

175.   Gérardy, R.; Emmanuel, N.; Toupy, T.; Kassin, V.-E.; Tshibalonza, N. N.; Schmitz, M.; Monbaliu, J.-C. M., Continuous Flow Organic Chemistry: Successes and Pitfalls at the Interface with Current Societal Challenges. *Eur. J. Org. Chem.* **2018,** *2018* (20-21), 2301-2351.

176.   EU-28: Biofuels Annual. USDA Foreign Agricultural Service: 2017.

177.   Vardon, D. R.; Settle, A. E.; Vorotnikov, V.; Menart, M. J.; Eaton, T. R.; Unocic, K. A.; Steirer, K. X.; Wood, K. N.; Cleveland, N. S.; Moyer, K. E.; Michener, W. E.; Beckham, G. T., Ru-Sn/AC for the Aqueous-Phase Reduction of Succinic Acid to 1,4-Butanediol under Continuous Process Conditions. *ACS Catal.* **2017,** *7* (9), 6207-6219.

178.   Gérardy, R.; Winter, M.; Horn, C. R.; Vizza, A.; Van Hecke, K.; Monbaliu, J.-C. M., Continuous-Flow Preparation of γ-Butyrolactone Scaffolds from Renewable Fumaric and Itaconic Acids under Photosensitized Conditions. *Org. Process Res. Dev.* **2017,** *21* (12), 2012-2017.

179.   Aellig, C.; Jenny, F.; Scholz, D.; Wolf, P.; Giovinazzo, I.; Kollhoff, F.; Hermans, I., Combined 1,4-butanediol lactonization and transfer hydrogenation/hydrogenolysis of furfural-derivatives under continuous flow conditions. *Catal. Sci. Technol.* **2014,** *4* (8), 2326-2331.

180.   Scholz, D.; Aellig, C.; Hermans, I., Catalytic Transfer Hydrogenation/Hydrogenolysis for Reductive Upgrading of Furfural and 5-(Hydroxymethyl)furfural. *ChemSusChem* **2014,** *7* (1), 268-275.

181.   Wang, X.; Liang, X.; Li, J.; Li, Q., Catalytic hydrogenolysis of biomass-derived 5-hydroxymethylfurfural to biofuel 2, 5-dimethylfuran. *Applied Catalysis A: General* **2019,** *576*, 85-95.

182.   Kumalaputri, A. J.; Bottari, G.; Erne, P. M.; Heeres, H. J.; Barta, K., Tunable and Selective Conversion of 5-HMF to 2,5-Furandimethanol and 2,5-Dimethylfuran over Copper-Doped Porous Metal Oxides. *ChemSusChem* **2014,** *7* (8), 2266-2275.

183.   Lewis, J. D.; Van de Vyver, S.; Crisci, A. J.; Gunther, W. R.; Michaelis, V. K.; Griffin, R. G.; Román-Leshkov, Y., A Continuous Flow Strategy for the Coupled Transfer Hydrogenation and Etherification of 5-(Hydroxymethyl)furfural using Lewis Acid Zeolites. *ChemSusChem* **2014,** *7* (8), 2255-2265.

184.   Luo, J.; Yu, J.; Gorte, R. J.; Mahmoud, E.; Vlachos, D. G.; Smith, M. A., The effect of oxide acidity on HMF etherification. *Catal. Sci. Technol.* **2014,** *4* (9), 3074-3081.

185.   Xiao, B.; Zheng, M.; Li, X.; Pang, J.; Sun, R.; Wang, H.; Pang, X.; Wang, A.; Wang, X.; Zhang, T., Synthesis of 1,6-hexanediol from HMF over double-layered catalysts of Pd/SiO2 + Ir–ReOx/SiO2 in a fixed-bed reactor. *Green Chem.* **2016,** *18* (7), 2175-2184.

186.   Lilga, M. A.; Hallen, R. T.; Gray, M., Production of Oxidized Derivatives of 5-Hydroxymethylfurfural (HMF). *Top. Catal.* **2010,** *53* (15), 1264-1269.

187.   Aellig, C.; Scholz, D.; Conrad, S.; Hermans, I., Intensification of TEMPO-mediated aerobic alcohol oxidations under three-phase flow conditions. *Green Chem.* **2013,** *15* (7), 1975-1980.

188.   Ambreen, N.; Kumar, R.; Wirth, T., Hypervalent iodine/TEMPO-mediated oxidation in flow systems: a fast and efficient protocol for alcohol oxidation. *Beilstein J. Org. Chem.* **2013,** *9*, 1437-1442.

189.   Liguori, F.; Barbaro, P.; Calisi, N., Continuous-Flow Oxidation of HMF to FDCA by Resin-Supported Platinum Catalysts in Neat Water. *ChemSusChem* **2019,** *12* (12), 2558-2563.

190.   Clark, J. H.; Farmer, T. J.; Herrero-Davila, L.; Sherwood, J., Circular economy design considerations for research and process development in the chemical sciences. *Green Chem.* **2016,** *18* (14), 3914-3934.

191.   Eerhart, A. J. J. E.; Huijgen, W. J. J.; Grisel, R. J. H.; van der Waal, J. C.; de Jong, E.; de Sousa Dias, A.; Faaij, A. P. C.; Patel, M. K., Fuels and plastics from lignocellulosic biomass via the furan pathway; a technical analysis. *RSC Adv.* **2014,** *4* (7), 3536-3549.

192.   Delidovich, I.; Hausoul, P. J. C.; Deng, L.; Pfützenreuter, R.; Rose, M.; Palkovits, R., Alternative Monomers Based on Lignocellulose and Their Use for Polymer Production. *Chem. Rev.* **2016,** *116* (3), 1540-1599.

193.   Burgess, S. K.; Leisen, J. E.; Kraftschik, B. E.; Mubarak, C. R.; Kriegel, R. M.; Koros, W. J., Chain Mobility, Thermal, and Mechanical Properties of Poly(ethylene furanoate) Compared to Poly(ethylene terephthalate). *Macromolecules* **2014,** *47* (4), 1383-1391.

194.   Efsa Panel on Food Contact Materials, E. F.; Processing, A., Scientific Opinion on the safety assessment of the substance, furan-2, 5-dicarboxylic acid, CAS No 3238-40-2, for use in food contact materials. *EFSA J.* **2014,** *12* (10), 3866-3874.

195.   Yi, G.; Teong, S. P.; Zhang, Y., Base-free conversion of 5-hydroxymethylfurfural to 2,5-furandicarboxylic acid over a Ru/C catalyst. *Green Chem.* **2016,** *18* (4), 979-983.

196.   Wang, Y.; Yu, K.; Lei, D.; Si, W.; Feng, Y.; Lou, L.-L.; Liu, S., Basicity-Tuned Hydrotalcite-Supported Pd Catalysts for Aerobic Oxidation of 5-Hydroxymethyl-2-furfural under Mild Conditions. *ACS Sustainable Chem. Eng.* **2016,** *4* (9), 4752-4761.

197.   Gui, Z.; Cao, W.; Saravanamurugan, S.; Riisager, A.; Chen, L.; Qi, Z., Efficient Aerobic Oxidation of 5-Hydroxymethylfurfural in Aqueous Media with Au–Pd Supported on Zinc Hydroxycarbonate. *ChemCatChem* **2016,** *8* (23), 3636-3643.

198.   Tong, X.; Yu, L.; Chen, H.; Zhuang, X.; Liao, S.; Cui, H., Highly efficient and selective oxidation of 5-hydroxymethylfurfural by molecular oxygen in the presence of Cu-MnO2 catalyst. *Catal. Commun.* **2017,** *90*, 91-94.

199.   Mishra, D. K.; Lee, H. J.; Kim, J.; Lee, H.-S.; Cho, J. K.; Suh, Y.-W.; Yi, Y.; Kim, Y. J., MnCo2O4 spinel supported ruthenium catalyst for air-oxidation of HMF to FDCA under aqueous phase and base-free conditions. *Green Chem.* **2017,** *19* (7), 1619-1623.

200.   Ait Rass, H.; Essayem, N.; Besson, M., Selective Aerobic Oxidation of 5-HMF into 2,5-Furandicarboxylic Acid with Pt Catalysts Supported on TiO2- and ZrO2-Based Supports. *ChemSusChem* **2015,** *8* (7), 1206-1217.

201.   Artz, J.; Palkovits, R., Base-Free Aqueous-Phase Oxidation of 5-Hydroxymethylfurfural over Ruthenium Catalysts Supported on Covalent Triazine Frameworks. *ChemSusChem* **2015,** *8* (22), 3832-3838.

202.   Gert-Jan, M. G.; Laszlo, S.; Matheus Adrianus, D., Accelerating Research into Bio-Based FDCA-Polyesters by Using Small Scale Parallel Film Reactors. *Comb. Chem. High Throughput Screening* **2012,** *15* (2), 180-188.

203.   Sun, Y.; Ma, H.; Jia, X.; Ma, J.; Luo, Y.; Gao, J.; Xu, J., A High-Performance Base-Metal Approach for the Oxidative Esterification of 5-Hydroxymethylfurfural. *ChemCatChem* **2016,** *8* (18), 2907-2911.

204.   Deng, J.; Song, H.-J.; Cui, M.-S.; Du, Y.-P.; Fu, Y., Aerobic Oxidation of Hydroxymethylfurfural and Furfural by Using Heterogeneous CoxOy–N@C Catalysts. *ChemSusChem* **2014,** *7* (12), 3334-3340.

205.   Casanova, O.; Iborra, S.; Corma, A., Biomass into chemicals: One pot-base free oxidative esterification of 5-hydroxymethyl-2-furfural into 2,5-dimethylfuroate with gold on nanoparticulated ceria. *J. Catal.* **2009,** *265* (1), 109-116.

206.   Menegazzo, F.; Signoretto, M.; Marchese, D.; Pinna, F.; Manzoli, M., Structure–activity relationships of Au/ZrO2 catalysts for 5-hydroxymethylfurfural oxidative esterification: Effects of zirconia sulphation on gold dispersion, position and shape. *J. Catal.* **2015,** *326*, 1-8.

207.   Li, F.; Li, X.-L.; Li, C.; Shi, J.; Fu, Y., Aerobic oxidative esterification of 5-hydroxymethylfurfural to dimethyl furan-2,5-dicarboxylate by using homogeneous and heterogeneous PdCoBi/C catalysts under atmospheric oxygen. *Green Chem.* **2018,** *20* (13), 3050-3058.

208.   Westerhaus, F. A.; Jagadeesh, R. V.; Wienhofer, G.; Pohl, M. M.; Radnik, J.; Surkus, A. E.; Rabeah, J.; Junge, K.; Junge, H.; Nielsen, M.; Bruckner, A.; Beller, M., Heterogenized cobalt oxide catalysts for nitroarene reduction by pyrolysis of molecularly defined complexes. *Nat. Chem.* **2013,** *5* (6), 537-43.

209.   Jagadeesh, R. V.; Junge, H.; Pohl, M.-M.; Radnik, J.; Brückner, A.; Beller, M., Selective Oxidation of Alcohols to Esters Using Heterogeneous Co3O4–N@C Catalysts under Mild Conditions. *J. Am. Chem. Soc.* **2013,** *135* (29), 10776-10782.

210.	Costello, M. G.; Flynn, R. M.; Owens, J. G., Fluoroethers and Fluoroamines. In *Kirk-Othmer Encyclopedia of Chemical Technology*, John Wiley & Sons, Inc.: 2000.

211.	Han, X.; Geng, L.; Guo, Y.; Jia, R.; Liu, X.; Zhang, Y.; Wang, Y., Base-free aerobic oxidation of 5-hydroxymethylfurfural to 2,5-furandicarboxylic acid over a Pt/C-O-Mg catalyst. *Green Chem.* **2016,** *18* (6), 1597-1604.

212.	Geng, L.; Zheng, B.; Wang, X.; Zhang, W.; Wu, S.; Jia, M.; Yan, W.; Liu, G., Fe3O4 Nanoparticles Anchored on Carbon Serve the Dual Role of Catalyst and Magnetically Recoverable Entity in the Aerobic Oxidation of Alcohols. *ChemCatChem* **2016,** *8* (4), 805-811.

213.	Ray, R.; Chandra, S.; Maiti, D.; Lahiri, G. K., Simple and Efficient Ruthenium-Catalyzed Oxidation of Primary Alcohols with Molecular Oxygen. *Chem. - Eur. J.* **2016,** *22* (26), 8814-8822.

214.	Nie, J.; Xie, J.; Liu, H., Efficient aerobic oxidation of 5-hydroxymethylfurfural to 2,5-diformylfuran on supported Ru catalysts. *J. Catal.* **2013,** *301*, 83-91.

215.	Li, Y.; Wang, L.; Yan, R.; Han, J.; Zhang, S., Promoting effects of MgO, (NH4)2SO4 or MoO3 modification in oxidative esterification of methacrolein over Au/Ce0.6Zr0.4O2-based catalysts. *Catal. Sci. Technol.* **2016,** *6* (14), 5453-5463.

216.	Formenti, D.; Ferretti, F.; Topf, C.; Surkus, A.-E.; Pohl, M.-M.; Radnik, J.; Schneider, M.; Junge, K.; Beller, M.; Ragaini, F., Co-based heterogeneous catalysts from well-defined α-diimine complexes: Discussing the role of nitrogen. *J. Catal.* **2017,** *351*, 79-89.

217.	Moro-oka, Y.; Ueda, W.; Lee, K.-H., The role of bulk oxide ion in the catalytic oxidation reaction over metal oxide catalyst. *J. Mol. Catal. A: Chem.* **2003,** *199* (1), 139-148.

218.	Battino, R.; Rettich, T. R.; Tominaga, T., The solubility of oxygen and ozone in liquids. *J. Phys. Chem. Ref. Data* **1983,** *12* (2), 163-78.

219.	When the mixture MeOH:MPBF was used, the first minutes of the reaction couln't be measured precisely since oxygen solubility changes drastically from roon temperature (24 °C) to the reaction temperature, generating bubbles that interfere with the measurements.

220.	Bures, J., A Simple Graphical Method to Determine the Order of a Reaction in Catalyst. *Angew. Chem., Int. Ed.* **2016,** *55* (6), 2028-2031.

221.	Bures, J., Variable Time Normalization Analysis: General Graphical Elucidation of Reaction Orders from Concentration Profiles. *Angew. Chem., Int. Ed.* **2016,** *55* (52), 16084-16087.

222.	Yamaguchi, K.; Mizuno, N., Supported Ruthenium Catalyst for the Heterogeneous Oxidation of Alcohols with Molecular Oxygen. *Angew. Chem., Int. Ed.* **2002,** *41* (23), 4538-4542.

223.	Yamaguchi, K.; Mizuno, N., Scope, Kinetics, and Mechanistic Aspects of Aerobic Oxidations Catalyzed by Ruthenium Supported on Alumina. *Chem. - Eur. J.* **2003,** *9* (18), 4353-4361.

224.	Mannel, D. S.; King, J.; Preger, Y.; Ahmed, M. S.; Root, T. W.; Stahl, S. S., Mechanistic Insights into Aerobic Oxidative Methyl Esterification of Primary Alcohols with Heterogeneous PdBiTe Catalysts. *ACS Catal.* **2018,** *8* (2), 1038-1047.

225.	Li, C.; Domen, K.; Maruya, K.; Onishi, T., Dioxygen adsorption on well-outgassed and partially reduced cerium oxide studied by FT-IR. *J. Am. Chem. Soc.* **1989,** *111* (20), 7683-7687.

226.	Eisenberg, D.; Slot, T. K.; Rothenberg, G., Understanding Oxygen Activation on Metal- and Nitrogen-Codoped Carbon Catalysts. *ACS Catal.* **2018,** *8* (9), 8618-8629.

227.	Xiao, J.; Rabeah, J.; Yang, J.; Xie, Y.; Cao, H.; Brückner, A., Fast Electron Transfer and •OH Formation: Key Features for High Activity in Visible-Light-Driven Ozonation with C3N4 Catalysts. *ACS Catal.* **2017,** *7* (9), 6198-6206.

228.	Makino, K.; Hagiwara, T.; Murakami, A., A mini review: Fundamental aspects of spin trapping with DMPO. *International Journal of Radiation Applications and Instrumentation. Part C. Radiation Physics and Chemistry* **1991,** *37* (5), 657-665.

229.	Lin, F.; Wang, K.; Gao, L.; Guo, X., Efficient conversion of fructose to 5-hydroxymethylfurfural by functionalized γ-Al2O3 beads. *Appl. Organomet. Chem.* **2019,** *33* (5), e4821.

230.	Fromanger, R.; Guillouet, S. E.; Uribelarrea, J. L.; Molina-Jouve, C.; Cameleyre, X., Effect of controlled oxygen limitation on Candida shehatae physiology for ethanol production from xylose and glucose. *J. Ind. Microbiol. Biotechnol.* **2010,** *37* (5), 437-45.

231. Mohsenzadeh, A.; Zamani, A.; Taherzadeh, M. J., Bioethylene Production from Ethanol: A Review and Techno-economical Evaluation. *ChemBioEng Rev.* **2017,** *4* (2), 75-91.

232. Gutmann, B.; Cantillo, D.; Kappe, C. O., Continuous-Flow Technology-A Tool for the Safe Manufacturing of Active Pharmaceutical Ingredients. *Angew. Chem., Int. Ed.* **2015,** *54* (23), 6688-6728.

233. Plutschack, M. B.; Pieber, B.; Gilmore, K.; Seeberger, P. H., The Hitchhiker's Guide to Flow Chemistry. *Chem. Rev.* **2017,** *117* (18), 11796-11893.

234. Gemoets, H. P. L.; Su, Y.; Shang, M.; Hessel, V.; Luque, R.; Noël, T., Liquid phase oxidation chemistry in continuous-flow microreactors. *Chem. Soc. Rev.* **2016,** *45* (1), 83-117.

235. Hone, C. A.; Kappe, C. O., The Use of Molecular Oxygen for Liquid Phase Aerobic Oxidations in Continuous Flow. *Top. Curr. Chem.* **2018,** *377* (1), 2.

236. Hessel, V.; Löb, P.; Löwe, H., Industrial Microreactor Process Development up to Production. In *Microreactors in Organic Synthesis and Catalysis*, Wirth, T., Ed. Wiley: 2008; pp 211-275.

237. Sajid, M.; Zhao, X.; Liu, D., Production of 2,5-furandicarboxylic acid (FDCA) from 5-hydroxymethylfurfural (HMF): recent progress focusing on the chemical-catalytic routes. *Green Chem.* **2018**.

238. Salazar, A.; Hünemörder, P.; Rabeah, J.; Quade, A.; Jagadeesh, R. V.; Mejia, E., Synergetic Bimetallic Oxidative Esterification of 5-Hydroxymethylfurfural under Mild Conditions. *ACS Sustainable Chem. Eng.* **2019**.

239. Gruenewald, M.; Heck, J., Modular Process Engineering: New Challenges for Apparatus Engineering Development. *Chem. Ing. Tech.* **2015,** *87* (9), 1185-1193.

240. Kluson, P.; Cerveny, L.; Had, J., Preparation and properties of ruthenium supported catalysts. *Catal. Lett.* **1994,** *23* (3-4), 299-12.

241. Santen, R. A. v., Physical Chemistry, Elementary Kinetics. In *Modern Heterogeneous Catalysis*, 2017; pp 59-116.

242. Perego, C.; Carati, A.; Ingallina, P.; Mantegazza, M. A.; Bellussi, G., Production of titanium containing molecular sieves and their application in catalysis. *Appl. Catal., A* **2001,** *221* (1-2), 63-72.

243. Perego, C.; Millini, R., Porous materials in catalysis: challenges for mesoporous materials. *Chem. Soc. Rev.* **2013,** *42* (9), 3956-3976.

244. Cullity, B. D. S., S.R., *Elements of X-Ray Diffraction*. 3rd ed.; Pearson: 2013; p 696.

245. Hansen, T. W.; DeLaRiva, A. T.; Challa, S. R.; Datye, A. K., Sintering of Catalytic Nanoparticles: Particle Migration or Ostwald Ripening? *Acc. Chem. Res.* **2013,** *46* (8), 1720-1730.

246. Harris, P. J. F., Growth and structure of supported metal catalyst particles. *Int. Mater. Rev.* **1995,** *40* (3), 97-115.

247. Golub, K. W.; Sulmonetti, T. P.; Darunte, L. A.; Shealy, M. S.; Jones, C. W., Metal–Organic-Framework-Derived Co/Cu–Carbon Nanoparticle Catalysts for Furfural Hydrogenation. *ACS Appl. Nano Mater.* **2019**.

248. Moulijn, J. A.; van Diepen, A. E.; Kapteijn, F., Catalyst deactivation: is it predictable?: What to do? *Applied Catalysis A: General* **2001,** *212* (1), 3-16.

249. Argyle, M. D.; Bartholomew, C. H., Heterogeneous Catalyst Deactivation and Regeneration: A Review. *Catalysts* **2015,** *5* (1), 145-269.

250. Introduction: Organocatalysis – From Biomimetic Concepts to Powerful Methods for Asymmetric Synthesis. In *Asymmetric Organocatalysis*, pp 1-8.

251. Oliveira, V. d. G.; Cardoso, M. F. d. C.; Forezi, L. d. S. M., Organocatalysis: A Brief Overview on Its Evolution and Applications. *Catalysts* **2018,** *8* (12), 605.

252. Hopkinson, M. N.; Richter, C.; Schedler, M.; Glorius, F., An overview of N-heterocyclic carbenes. *Nature* **2014,** *510*, 485.

253. Flanigan, D. M.; Romanov-Michailidis, F.; White, N. A.; Rovis, T., Organocatalytic Reactions Enabled by N-Heterocyclic Carbenes. *Chem. Rev.* **2015,** *115* (17), 9307-9387.

254. Ukai, T.; Tanaka, R.; Dokawa, T., A new catalyst for acyloin condensation. *J. Pharm. Soc. Jpn.* **1943,** *42*, 296-300.

255. Breslow, R., On the Mechanism of Thiamine Action. IV.1 Evidence from Studies on Model Systems. *J. Am. Chem. Soc.* **1958,** *80* (14), 3719-3726.

256. Berkessel, A.; Elfert, S.; Yatham, V. R.; Neudörfl, J.-M.; Schlörer, N. E.; Teles, J. H., Umpolung by N-Heterocyclic Carbenes: Generation and Reactivity of the Elusive 2,2-Diamino Enols (Breslow Intermediates). *Angew. Chem., Int. Ed.* **2012,** *51* (49), 12370-12374.

257. Paul, M.; Sudkaow, P.; Wessels, A.; Schlörer, N. E.; Neudörfl, J.-M.; Berkessel, A., Breslow Intermediates from Aromatic N-Heterocyclic Carbenes (Benzimidazolin-2-ylidenes, Thiazolin-2-ylidenes). *Angew. Chem., Int. Ed.* **2018,** *57* (27), 8310-8315.

258. Bugaut, X.; Glorius, F., Organocatalytic umpolung: N-heterocyclic carbenes and beyond. *Chem. Soc. Rev.* **2012,** *41* (9), 3511-3522.

259. Jiang, Y.; Chen, W.; Lu, W., N-Heterocyclic carbene catalyzed conjugate umpolung reactions leading to coumarin derivatives. *RSC Adv.* **2012,** *2* (4), 1540-1546.

260. Vora, H. U.; Wheeler, P.; Rovis, T., Exploiting Acyl and Enol Azolium Intermediates via N-Hetero- cyclic Carbene-Catalyzed Reactions of α-Reducible Aldehydes. *Adv. Synth. Catal.* **2012,** *354* (9), 1617-1639.

261. Maki, B. E.; Scheidt, K. A., N-Heterocyclic Carbene-Catalyzed Oxidation of Unactivated Aldehydes to Esters. *Org. Lett.* **2008,** *10* (19), 4331-4334.

262. Zhao, J.; Mück-Lichtenfeld, C.; Studer, A., Cooperative N-Heterocyclic Carbene (NHC) and Ruthenium Redox Catalysis: Oxidative Esterification of Aldehydes with Air as the Terminal Oxidant. *Adv. Synth. Catal.* **2013,** *355* (6), 1098-1106.

263. Delany, E. G.; Fagan, C.-L.; Gundala, S.; Mari, A.; Broja, T.; Zeitler, K.; Connon, S. J., NHC-catalysed aerobic aldehyde-esterifications with alcohols: no additives or cocatalysts required. *Chem. Commun.* **2013,** *49* (58), 6510-6512.

264. Samanta, R. C.; Studer, A., N-heterocyclic carbene catalysed oxidative esterification of aliphatic aldehydes. *Org. Chem. Front.* **2014,** *1* (8), 936-939.

265. Chun, S.; Chung, Y. K., Transition-Metal-Free Poly(thiazolium) Iodide/1,8-Diazabicyclo[5.4.0]undec-7-ene/Phenazine-Catalyzed Esterification of Aldehydes with Alcohols. *Org. Lett.* **2017,** *19* (14), 3787-3790.

266. Liu, D.; Chen, E. Y. X., Diesel and Alkane Fuels From Biomass by Organocatalysis and Metal–Acid Tandem Catalysis. *ChemSusChem* **2013,** *6* (12), 2236-2239.

267. Zang, H.; Wang, K.; Zhang, M.; Xie, R.; Wang, L.; Chen, E. Y. X., Catalytic coupling of biomass-derived aldehydes into intermediates for biofuels and materials. *Catal. Sci. Technol.* **2018,** *8* (7), 1777-1798.

268. Liu, D.; Chen, E. Y. X., Integrated Catalytic Process for Biomass Conversion and Upgrading to C12 Furoin and Alkane Fuel. *ACS Catal.* **2014,** *4* (5), 1302-1310.

269. Mou, Z.; Feng, S.; Chen, E. Y. X., Bio-based difuranic polyol monomers and their derived linear and cross-linked polyurethanes. *Polym. Chem.* **2016,** *7* (8), 1593-1602.

270. Wilson, J.; Chen, E. Y. X., Organocatalytic Cross-Coupling of Biofuranics to Multifunctional Difuranic C11 Building Blocks. *ACS Sustainable Chem. Eng.* **2016,** *4* (9), 4927-4936.

271. Delany, E. G.; Fagan, C.-L.; Gundala, S.; Zeitler, K.; Connon, S. J., Aerobic oxidation of NHC-catalysed aldehyde esterifications with alcohols: benzoin, not the Breslow intermediate, undergoes oxidation. *Chem. Commun.* **2013,** *49* (58), 6513-6515.

272. Kiran, I. N. C.; Lalwani, K.; Sudalai, A., N-Heterocyclic carbene catalyzed esterification of aromatic aldehydes with alcohols under aerobic conditions. *RSC Adv.* **2013,** *3* (6), 1695-1698.

273. Manganese Dioxide. In *Encyclopedia of Reagents for Organic Synthesis*.

274. Brandolese, A.; Ragno, D.; Di Carmine, G.; Bernardi, T.; Bortolini, O.; Giovannini, P. P.; Pandoli, O. G.; Altomare, A.; Massi, A., Aerobic oxidation of 5-hydroxymethylfurfural to 5-hydroxymethyl-2-furancarboxylic acid and its derivatives by heterogeneous NHC-catalysis. *Org. Biomol. Chem.* **2018,** *16* (46), 8955-8964.

275. Knappke, C. E. I.; Imami, A.; Jacobi von Wangelin, A., Oxidative N-Heterocyclic Carbene Catalysis. *ChemCatChem* **2012,** *4* (7), 937-941.

276.   Zhang, Z.; Liu, W.; Xie, H.; Zhao, Z. K., An Unexpected Reaction between 5-Hydroxymethylfurfural and Imidazolium-Based Ionic Liquids at High Temperatures. *Molecules* **2011,** *16* (10), 8463-8474.

277.   Fatiadi, A. J., Active Manganese Dioxide Oxidation in Organic Chemistry - Part I. *Synthesis* **1976,** *1976* (02), 65-104.

278.   Fatiadi, A. J., Active Manganese Dioxide Oxidation in Organic Chemistry - Part II. *Synthesis* **1976,** *1976* (03), 133-167.

279.   Fatiadi, A. J., The Oxidation of Organic Compounds by Active Manganese Dioxide. In *Organic Syntheses by Oxidation with Metal Compounds*, Mijs, W. J.; de Jonge, C. R. H. I., Eds. Springer US: Boston, MA, 1986; pp 119-260.

280.   Piera, J.; Bäckvall, J.-E., Catalytic Oxidation of Organic Substrates by Molecular Oxygen and Hydrogen Peroxide by Multistep Electron Transfer—A Biomimetic Approach. *Angew. Chem., Int. Ed.* **2008,** *47* (19), 3506-3523.

281.   Axelsson, A.; Antoine-Michard, A.; Sundén, H., Organocatalytic valorisation of glycerol via a dual NHC-catalysed telescoped reaction. *Green Chem.* **2017,** *19* (11), 2477-2481.

282.   Kumar, V.; Connon, S. J., Direct, efficient NHC-catalysed aldehyde oxidative amidation: in situ formed benzils as unconventional acylating agents. *Chem. Commun.* **2017,** *53* (73), 10212-10215.

283.   Rehbein, J.; Ruser, S.-M.; Phan, J., NHC-catalysed benzoin condensation – is it all down to the Breslow intermediate? *Chem. Sci.* **2015,** *6* (10), 6013-6018.

284.   Ta, L.; Sundén, H., Oxidative organocatalytic chemoselective N-acylation of heterocycles with aromatic and conjugated aldehydes. *Chem. Commun.* **2018,** *54* (5), 531-534.

285.   Zheng, C.; Liu, X.; Ma, C., Organocatalytic Direct N-Acylation of Amides with Aldehydes under Oxidative Conditions. *J. Org. Chem.* **2017,** *82* (13), 6940-6945.

286.   Premaletha, S.; Ghosh, A.; Joseph, S.; Yetra, S. R.; Biju, A. T., Facile synthesis of N-acyl 2-aminobenzothiazoles by NHC-catalyzed direct oxidative amidation of aldehydes. *Chem. Commun.* **2017,** *53* (9), 1478-1481.

8 Appendix

8.1 Paper 1

Synergetic Bimetallic Oxidative Esterification of 5-Hydroxymethylfurfural under Mild Conditions

Abel Salazar, Paul Hünemörder, Jabor Rabeah, Antje Quade, Rajenahally V. Jagadeesh and Esteban Mejia.
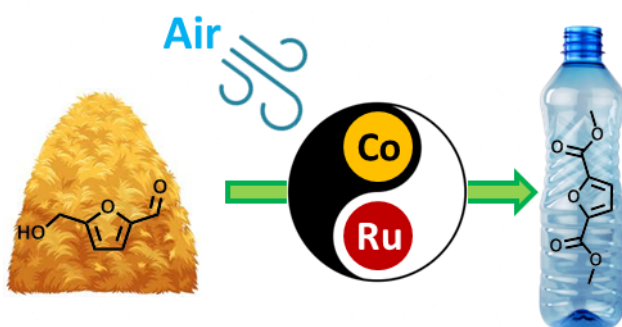
Synopsis

A mixture of Ru@C and Co$_3$O$_4$-N@C catalyse the oxidative esterification of 5-hydroxymethylfurfural under mild conditions showing a unique cooperative mechanism of action.

Synergetic Bimetallic Oxidative Esterification of 5-Hydroxymethylfurfural under Mild Conditions

Abel Salazar,[†] Paul Hünemörder,[†] Jabor Rabeah,[†] Antje Quade,[‡] Rajenahally V. Jagadeesh,[†] and Esteban Mejia*[,†]

[†]Leibniz-Institute für Katalyse e.V., Albert-Einstein-Straße 29A, 18059, Rostock, Germany
[‡]Leibniz-Institut für Plasmaforschung und Technologie e.V-INP-Greifswald, 17489, Greifswald, Germany

Ⓢ *Supporting Information*

ABSTRACT: 5-Hydroxymethylfurfural (HMF) has become a benchmark chemical as it can be obtained by the processing of renewable biomass, making its downstream modification an important topic both in industry and academia. Finding catalytic processes for the selective derivatization of HMF is challenging due to its reactivity, hence mild conditions are needed. Here we report the selective oxidative esterification of HMF to methyl 5-(hydroxymethyl)furan-2-carboxylate and to dimethyl furan-2,5-dicarboxylate (FDCM) under mild conditions using oxygen (from air) as oxidant. A synergetic effect between the used catalysts, cobalt oxide over nitrogen-doped carbon, and ruthenium over carbon catalysts was observed by catalytic and electron paramagnetic resonance measurements. Kinetic analysis revealed a first order dependence on substrate for the cobalt catalyst and an apparent zero order for the ruthenium catalysts. The conversion rates were improved by the use of perfluoroether as solvent, proving that the oxygen diffusion is the limiting factor in the system.

KEYWORDS: *Cooperative effects, Oxidation, Heterogeneous catalysis, Biomass, Radicals, Oxygen, Fluorine*
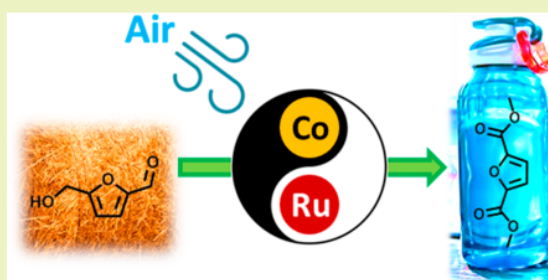
INTRODUCTION

The use of biomass-derived chemicals is nowadays a very relevant topic, since these, coming from renewable sources, can be incorporated in a circular, sustainable economy.[1] Special focus has been given to the conversion of agricultural waste into useful chemical commodities.[2] Among these products, 5-hydroxymethylfurfural (HMF, **1**) is of special interest; it can be synthesized by the dehydration of C₆-sugars (e.g., fructose or glucose), which in turn can be obtained from lignocellulose materials from the agro and food industries (Scheme 1).[3] Among other applications, HMF is the precursor of 2,5-furandicarboxylic acid (FDCA) and its methyl ester derivative (FDCM, **2**).[4] Both can be used as monomers for the production of furan-based polyesters,[5] like poly(ethylene-furanoate) (PEF), which is the furanic analogue of poly-(ethylene-terephthalate) (PET).[6] There is special interest in PEF as it has shown better gas containing properties than PET, an advantage in the storage of CO₂-containing beverages.[7] It has shown also good results by the assessment of health risks of its use as food container and its degradation by enzymatic hydrolysis.[8,9]

The demand of FDCA or its esters (such as **2**) in the polymer industry has brought great attention to the oxidation/oxidative esterification of HMF. There are several reports about the use of heterogeneous catalysts in the oxidation of HMF to FDCA. These reports mention different metals,[10,11]

combinations of them,[12,13] and also several types of supports.[14−16]

There are two ways in which FDCA is used as the starting material in the polymer synthesis. The first way involves the preparation of an ester (e.g., **2**) and after that, a trans-esterification reaction is made to obtain the desired products. The second way is to use the FDCA in a two-stage polyesterification. The advantage of having **2** as a starting material is that the step for the esterification of FDCA is avoided, and it is possible to proceed to the transesterification step directly.[6] Another advantage is that in general, the polyesters obtained from **2** are colorless (indicative of less decomposition in the polymerization process), and the reaction proceeds at higher rates than those using FDCA as starting material.[17]

There are only a few reports of the oxidative esterification of HMF. Recently, Xu et al. reported the use of cobalt oxide supported in nitrogen-doped carbon (CoO$_x$−N@C) catalysts using MnO₂ as a stoichiometric additive with 96% yield of **2** (Table 1 entry 1).[18] Fu et al. reported the use of Co$_x$O$_y$−N@C in combination with a porous potassium/manganese oxide (KMn₈O₁₆·nH₂O), obtaining full conversion but no appreci-

105

Scheme 1. Production of HMF and Derivatives from Biomass
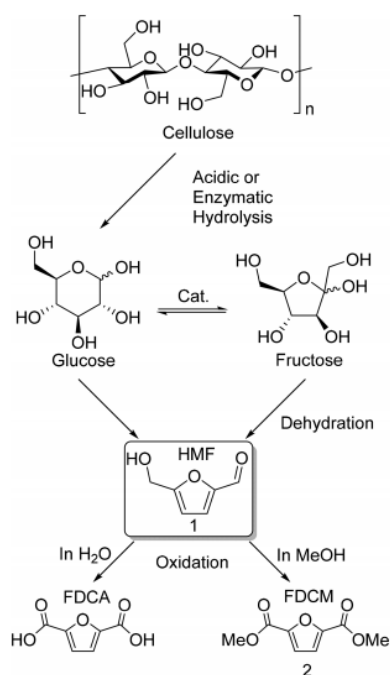
Table 1. Comparison between Reported Systems for the Synthesis of FDCM (2) via Oxidative Esterification of HMF (1)

entry	ref	catalyst(s)	$P\ O_2$ (bar)	temp (°C)/ time (h)	convn/ select (%)
1	18	CoO_x–N@C + MnO_2	6	100/12	100/96
2	19	Co_xO_y–N@C + KMn_8O_{16}	10	100/6	99/53
3	20	$Au@CeO_2$	10	130/5	100/99
4	21	$Au@ZrO_2$	3	130/5	100/32
5	22	PdCoBi@C	1	60/14	99/96
6	this work	Co_xO_y–N@C + Ru@C	1 (air)	50/16	100/99

able selectivity to one specific product (Table 1 entry 2).[19] Corma et al. reported the use of Au nanoparticles supported in ceria obtaining full conversion and selectivity to **2** (Table 1 entry 3).[20] Later on, Manzoli et al. also reported that Au nanoparticles supported in zirconia fully convert HMF, showing only 32% selectivity to **2** (Table 1 entry 4).[21] All these reported systems require high pressures of oxygen and high temperatures to achieve full conversion or selectivity.

Recently, Fu et al. reported the oxidative esterification of HMF to **2** using a trimetallic system (Pd, Co, and Bi) under mild conditions with high selectivity, using high metal loadings (up to 10% each metal) in heterogeneous and homogeneous systems (Table 1 entry 5).[22]

Herein, we report the aerobic oxidative esterification of HMF to FDCM (**2**), made by a cooperative reaction using the heterogeneous catalyst mixture of Co_xO_y supported on nitrogeneous carbon (Co_xO_y–N@C)[23,24] and commercially available ruthenium on carbon (Ru@C) under mild conditions (Table 1 entry 6). The independent performance of each catalyst was studied along with the effect of oxygen availability in the system. Moreover, an increase in the speed of the reaction was achieved using perfluorinated compounds (PFCs) as they show excellent gas solubility.[25] This synergistic bimetallic approach yields, to the best of our knowledge, the highest selectivity toward FDCM (**2**) under the mildest conditions so far.

■ EXPERIMENTAL SECTION

General Experimental Details. 5-hydroxymethylfurfural (98%) was purchased from Fluorochem Ltd. and stored under refrigeration. Furfuryl alcohol (98%) and 2-furfuraldehyde (99%) were purchased from Acros Organics. Methanol, ethanol, isopropyl alcohol and *n*-butanol were purchased from Fischer Scientific and used as received. Oxygen (99,99%) was purchased from Linde. Ultrahigh purity ($\geq$99.0%) DMPO was purchased from Dojindo, stored under refrigeration, and used as received. Ru@C (5% Ru) was purchased from Alfa Aesar. $Co(OAc)_2 \cdot 4H_2O$ was purchased from Abcr GmbH. 1,10-Phenantroline and methoxyperfluorobutane were purchased from Sigma-Aldrich. The vulcan XC72R was purchased from Cabot Limited. The pyrolysis of the catalyst precursors were carried out in Centurion Neytech Qex Vacuum Furnace. ^1H and ^{13}C NMR spectra were recorded in $CDCl_3$ with a Bruker Avance 300 with a QNP probe head (^1H, 300 MHz; ^{13}C, 75 MHz), or with a Bruker Avance 400 (^1H, 400 MHz; ^{13}C, 100 MHz). The calibration of the spectra was carried out using residual solvent shifts ($CDCl_3$, ^1H = 7.26, ^{13}C = 77.16) and were reported as parts per million relative to $SiMe_4$. All the NMR samples were measured at 24 °C. GC analysis was performed on a Hewlett-Packard 6890 series chromatographer with MS and FID detectors. Time resolved measurements for kinetic purposes were recorded using a Mettler Toledo React IR 15 with a diamond window probe. The adsorption region measured was from 650 to 2500 cm^{-1}. Electron paramagnetic resonance (EPR) spectra were obtained on a Bruker ELEXSYS 500-10/12 cw-EPR spectrometer (X-band, about 9.85 GHz) with a microwave power of 6.9 mW, a modulation frequency of 100 kHz, and modulation amplitude up to 5G. Signal fitting were carried out by using the SpinFit program (Bruker). The elemental surface composition and chemical binding properties were analyzed by X-ray photoelectron spectroscopy (XPS) using an AXIS Ultra DLD electron spectrometer (Kratos Analytical, Manchester, UK). The spectra were recorded utilizing monochromatic X-rays Al $k\alpha$ (1486.6 eV) with a medium magnification (field of view 2) lens mode and with the slot mode selected.

Synthesis and Characterization of the Co_xO_y–N@C Catalyst. The catalyst was prepared according to the previously reported procedure:[23,24] A mixture of $Co(OAc)_2 \cdot 4H_2O$ (corresponds to 3 wt % Co) and 1,10-phenanthroline (Co/phenanthroline = 1:2 mol ratio) in ethanol was stirred for 20−30 min at room temperature. Then, vulcan XC72R carbon powder was added and the entire reaction mixture was stirred at 60 °C for 5−6 h. The reaction mixture was cooled to room temperature and ethanol was removed slowly under vacuum. The remaining solid sample obtained was dried at 60 °C for 12 h. The dried sample was ground to a powder. Then, the ground powder was pyrolyzed at 800 °C for 2 h in argon atmosphere and cooled to room temperature. The elemental analysis of Co−phenanthroline/C (wt %) yielded the following results: C = 89.68, H = 0.199, N = 2.70, and Co = 3.05. XPS analysis of Co−phenanthroline/C (atom %) yielded C = 92.4, N = 2.8, Co = 0.6, and O = 4.0.

Catalytic Oxidation of HMF. All the oxidative esterification reactions were performed in an oven-dried Schlenk tube. All the reagents (HMF, base, catalyst, and 4 mL of MeOH) and a magnetic stirrer were added to the tube. To the Schlenk tube a condenser was

106

coupled and to the top of if a balloon filled with air was attached. Air was used as the oxidant. After flushing the system with air for a while, it was closed and heating and stirring started. At the end of the reaction time (16 h) the catalyst was filtered off, and the solution was analyzed by GC. Conversion and yields were determined by GC-FID. The identification of the products was made by GC–MS and NMR.

When MPFB solvent or mixtures with it were used, the solvent was bubbled with oxygen or air. After the reactions, the MPFB solvent or mixtures were fully recovered and reused.

Kinetic Measurements. The kinetic measurements, obtained with Mettler Toledo ReactIR 15 Equipment, were made in similar experimental conditions as that previously described. A custom-made Schlenk tube was used, and the disappearance/appearance of the IR peak corresponded to the carbonyl group of **7** (1678 cm^{-1}).

EPR Measurements. For the detection of radical intermediates in the catalytic oxidation of HMF (**1**), a sample was taken after 3 h of reaction and mixed with 100 μL of 600 mM DMPO (Dojindo). The mixture was added to a spin trap in H$_2$O at 50 °C under bubbling O$_2$. Then 50 μL of the reaction solution was transferred into a microcapillary glass tube (Hirschmann) and measured immediately at room temp (20 °C).

■ RESULTS AND DISCUSSION

A series of different heterogeneous metal catalysts with known activity in oxidation reactions[10,11,26,27] were tested for the oxidation of **1** in methanol to produce in all cases a mixture of products (**2**, **3**, **4**, and **5**, Scheme 2 and Table 2). The highest

Scheme 2. Reaction Pathways for the Oxidative Esterification of HMF(1)
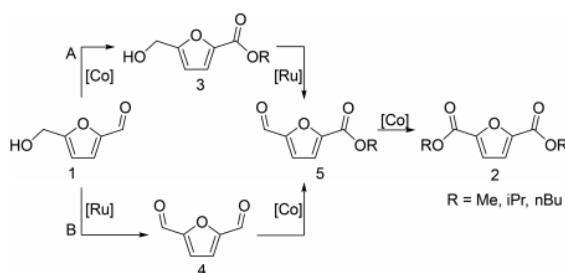
Table 2. Catalyst Screening for the Oxidative Esterification of HMF (1) in Methanol^a

			product selectivity (%) (R = Me)			
entry	catalyst	convn (%)	2	3	4	5
1	Co$_x$O$_y$–N@C (3.8% Co)	>99	14	69	trace	17
2	Co$_x$O$_y$–N@C (5.8% Co)	95	24	71	5	
3	Pt@C (10% Pt)	trace	trace	trace		
4	Ru@C (5% Ru)	75	3		63	34
5	Pd@C (10% Pd)	26^b	2	14	38	15
6	Fe$_2$O$_3$–N@C (2.8% Fe)	28	8	17	15	19

^{a}Reaction conditions: 0.5 mmol HMF, 0.2 equiv K$_2$CO$_3$, 25 mg of cat., 4 mL of MeOH, air as oxidant, 50 °C, 18 h. ^{b}5-Methyl-2-furfural was detected as a product (32% selectivity).

conversion of **1** was achieved with the cobalt oxide catalysts Co$_x$O$_y$–N@C (>99% and 95%, entries 1 and 2), followed by supported ruthenium, Ru@C (75%, entry 4). Even though catalytic activity for Pt, Pd, and Fe oxide was previously

reported for HMF oxidation,[11,26,27] under the tested conditions both conversion and selectivity were poor (entries 3, 5, and 6). There was no significant difference in the conversion achieved when using cobalt catalysts with different metal loadings (entries 1 and 2) so we decided to continue the studies with the one with the lower Co content. The observed low yield of products containing the formyl group (**4** and **5**) suggests a higher selectivity of this catalyst toward the conversion of the aldehyde (to ester) than of alcohol (to aldehyde). In fact, after optimizing the reaction conditions, the cobalt catalyst delivers almost quantitatively **3** as the major product (Scheme 3A). Conversely, the ruthenium catalyst yields a completely different product distribution; being selective toward the dialdehyde **4** (Table 2 entry 4). The selectivity of ruthenium catalysts toward the oxidation of alcohols[28] including HMF[29] was previously reported. Hence, we hypothesized that the two catalysts might operate synergistically in the oxidative esterification of **1** via orthogonal pathways (paths A and B, Scheme 2) to yield to the desired diester **2**.

Having this mechanistic insight, and under the assumption that the ruthenium catalyst will help improving the selectivity toward the diester (**2**) by fostering the oxidation of the alcohol moiety of **1**, both catalysts (Co$_x$O$_y$–N@C and Ru@C) were combined, leading to the desired product (**2**) quantitatively (Scheme 3, path B).

Different experiments using varying proportions of each catalyst were done (Table S1) to find the optimum mixture composition. As a result, the amount of cobalt catalyst could be reduced to a half of its initial amount (Scheme 3A) thanks to the synergistic effect brought by the use of the ruthenium as cocatalyst.

To gain further insight into the catalytic process, tests without base were conducted (Table S2), showing that it is needed for the cobalt catalyst to turnover. As it is known that base promotes hemiacetal formation,[30] this observation suggests that the cobalt catalyst is responsible for the oxidation of the hemiacetal formed between the aldehyde and methanol. When the reaction with both catalysts without base was carried out, the conversion was twice as much as the one obtained with the ruthenium alone, pointing out, once again, the synergetic cooperation between both catalysts.

Other alcohols were also screened as nucleophiles under our reaction conditions (Table 3). As previously discussed in the literature, the mechanism of esterification involves the formation of a hemiacetal intermediary, which is subsequently oxidized.[24] Structural changes might result in variations in the basicity and nucleophilicity of the alcohols, affecting the formation of the hemiacetal intermediary, and hence the overall conversion. Isopropyl alcohol gave a poor conversion of HMF and no ester products were observed, suggesting that the formation of the hemiacetal intermediary was not possible (Table 3 entry 2). In the case of primary alcohols such as ethanol and butanol, good conversions were achieved, with selectivity toward the ester products and to the complete oxidative esterification of HMF (Table 3 entries 1 and 3). In the case of butanol, an increase in the reaction temperature resulted in an increase of the conversion of HMF maintaining the product distribution (Table 3 entry 4). Such a difference in conversion can be attributed to the drastic viscosity changes at the temperatures used, which has direct effects on the kinetics of the reaction (1-butanol viscosity: at 50 °C, 1.4 mPa·s; at 80 °C, 0.8 mPa·s; data obtained from the provider).

Scheme 3. Reaction Conditions for the Selective Oxidative Esterification of HMF
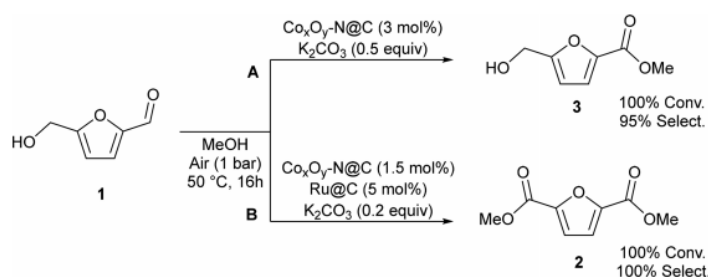
Table 3. Alcohol Screening for the Oxidative Esterification of HMF(1)[a]

entry	solvent	convn	2	3	4	5
			product selectivity[b]			
1	ethanol	86	10	4	10	76
2	isopropyl alcohol	1,5		100		
3	1-butanol	55		5	24	71
4	1-butanol (80 °C)	90	3	trace	21	76

[a]Reaction conditions: 0.5 mmol HMF, 0.2 equiv K_2CO_3, 25 mg of cat., 4 mL of solvent; air as oxidant; 50 °C; 18 h. [b]The ester fragments contain the respective alkylic chain of the alcohol used as solvent.

Additionally, catalyst recycling experiments were performed (see Supporting Information). The recycling was made by centrifugation, decantation and thorough washing of the catalyst. After the first catalytic cycle, partial deactivation of Co_xO_y–N@C was observed, while Ru@C showed activity detriment only after the fourth cycle (Figure S10). Importantly, HMF was fully converted in every catalytic run, although with different product selectivity. Unfortunately, it was not possible to regain the catalysts' selectivity by the recovery methods used.

XPS measurements were performed to the fresh and used catalysts (see Supporting Information), in order to assess the fate of the catalyst after the reaction was finished. The used catalysts were analyzed after a single use. The elementary analysis from Ru@C shows no significant difference in the ruthenium content, and the chemical composition also remains similar (aprox. 60% Ru metal and 40% RuOx).

On the other side, changes in the cobalt catalyst Co_xO_y–N@C could be observed: the nitrogen and cobalt content remained similar and the oxygen content increased from 3 to 5%. Changes in the nitrogen species were observed; a decrease from 64 to 60% of the pyridinic N-bound to metal was measured. These species are described as responsible for the catalytic activity of the cobalt catalyst, and the loss of selectivity is a direct consequence of the decreased presence of these species.[31] Successive recycling of the catalysts results in a cumulative detriment of the catalyst selectivity.

To gain further insight on the role of each catalyst, kinetic experiments on the oxidation of furfuryl alcohol (**6**) and furfural (**7**) with each separate catalyst were carried out.

As seen in Table 4, the product distributions suggest that Co_xO_y–N@C achieves a fast conversion of the aldehyde while its activity for the oxidation of the alcohol is low. This was confirmed by the almost quantitative conversion of **7** to **8**, even at higher substrate loadings (Table 4, entries 2 and 3). Interestingly, a yield of 13% of **8** was obtained under argon atmosphere, meaning that the presence of gaseous oxygen is

Table 4. Independent Performance of Co_xO_y–N@C and Ru@C Catalysts on the Aerobic Oxidation of Furfuryl Alcohol (6) and Furfural (7)[a]

entry	catalyst	substrate	convn	7	8
				products	
1	Co_xO_y–N@C	6	11	15	85
2	Co_xO_y–N@C	7	98		100
3	Co_xO_y–N@C	7[b]	80		100
4	Co_xO_y–N@C	7[c]	13		100
5	Ru@C	6	40	100	
6	Ru@C	7			
7	Ru@C	6[c]			

[a]Reaction conditions: 0.5 mmol substrate, 0.2 equiv K_2CO_3, 1.5 mol % cat., 4 mL of MeOH, air as oxidant; 50 °C; 18 h. [b]Substrate at 1.0 mmol. [c]Argon atmosphere.

not necessary for the cobalt catalyst to oxidize the substrate. This is in agreement with previous reports that show that the oxygen atoms from the metal oxide can be responsible for the oxidation until the metal is completely reduced.[32]

On the other hand, Ru@C selectively converts furfuryl alcohol to furfural with a moderate yields (40% of **7**, Table 4, entry 5) without the formation of the ester **8**. No conversion was observed in the absence of oxygen (Table 4, entry 7).

Thus, the results confirm that the ruthenium catalyst oxidizes only the alcohol moiety, while the cobalt oxide converts the aldehyde to the desired ester.

Furthermore, kinetic analysis of the oxidation of **6** by Ru@C and the oxidative esterification of **7** by Co_xO_y–N@C were performed via in situ IR measurements at different temperatures (Figure 1). Changes in temperature showed different effects on the reaction rate, being decreased either at higher or lower temperatures. On one hand, by performing the reaction at 60 °C, the availability of oxygen in the solution is diminished, hence decreasing the reaction rate.[33] On the other hand, when the temperature is decreased to 40 °C, even though there is more oxygen dissolved, the lower amount of (thermal) energy available results in the catalyst' slower turnover. In all cases, the reaction showed first-order dependence on the substrate.

To assess the effect of increased oxygen availability in solution, the kinetic profiles under O_2 atmosphere were measured (Figure 2 and Figure S8). As expected, the dilution effect was diminished and no significant difference between the

108

Research Article
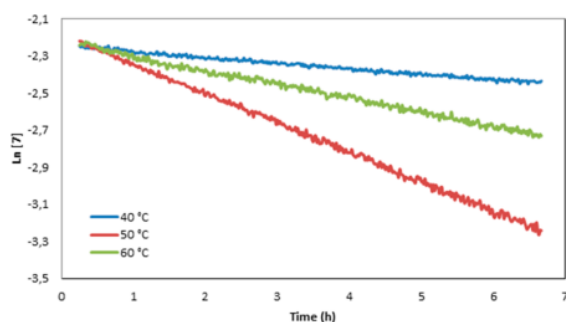
Figure 1. Kinetic profiles at different temperatures for the oxidative esterification of furfural (**7**) in methanol using Co_xO_y–N@C as catalysts and air as oxidant. (40 °C, k = 0.030 ± 5 h^{-1}; 50 °C, k = 0.158 ± 3 h^{-1}; 60 °C, k = 0.075 ± 1 h^{-1}).
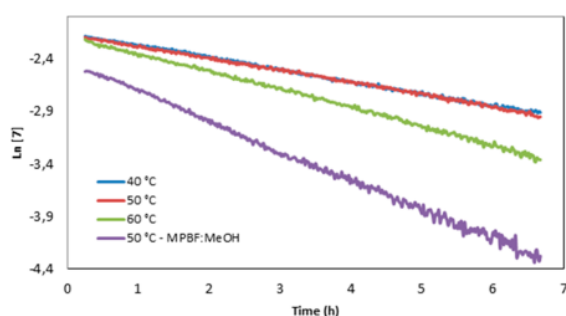
Figure 2. Kinetic profiles at different temperatures for the oxidative esterification of furfural (**7**) in methanol and a MPBF/MeOH mixture using Co_xO_y–N@C as catalysts and oxygen as oxidant. (40 °C, k = 0.115 ± 2 h^{-1}; 50 °C, k = 0.115 ± 2 h^{-1}; 60 °C, k = 0.174 ± 3 h^{-1}; 50 °C MPBF/MeOH mixture, k = 0.281 ± 7 h^{-1}).

reaction rates at 40 and 50 °C was observed. The highest rate was achieved at 60 °C. In comparison to air, the use of pure oxygen as oxidant not only increases the reaction rate in most of the cases (Table S3) but also leads the reaction to completion.

With the aim of circumventing the oxygen solubility limitation under mild reactions conditions, methoxyperfluor-obutane (MPFB) was added to the reactions as cosolvent. MPFB has high oxygen solubility (72.7% v/v). Importantly, fluoroethers have low toxicity, and very low potential, making them attractive to industry.[25] Full conversion was achieved when a 1:1 mixture of MeOH:/MPFB was used, showing the tolerance of the catalysts toward this solvent, but more importantly, a marked increase of the reaction rate was observed, from 0.115 ± 2 h^{-1} to 0.281 ± 7 h^{-1} (Figure 2).[34] Moreover, conversion of 85% was observed after 4.5 h, a significant reduction in comparison with the 12 h needed when only MeOH was used as solvent.

Conversely, the determination of the reaction kinetics for the ruthenium-catalyzed oxidation of **6** to **7** proved to be more challenging. Attempts to linearize the reaction profiles to the traditional kinetic equations were not successful. Nonetheless, assuming a Langmuir–Hinshelwood mechanism as suggested by Nie,[29] an apparent zero-order dependence in substrate was found from the initial rates (Figure S38). Alternatively, the graphical method reported by Burés was applied,[35,36]

suggesting, by approximation, an apparent zero-order kinetics related to the catalyst (Figure S37).

On the basis of these results and taking into account previous reports in the literature we propose the reaction pathway presented in Scheme 4, where the synergetic interaction between both catalysts is explained.

Scheme 4. Mechanism Proposed for the Synergetic Bimetallic Oxidative Esterification of Alcohols
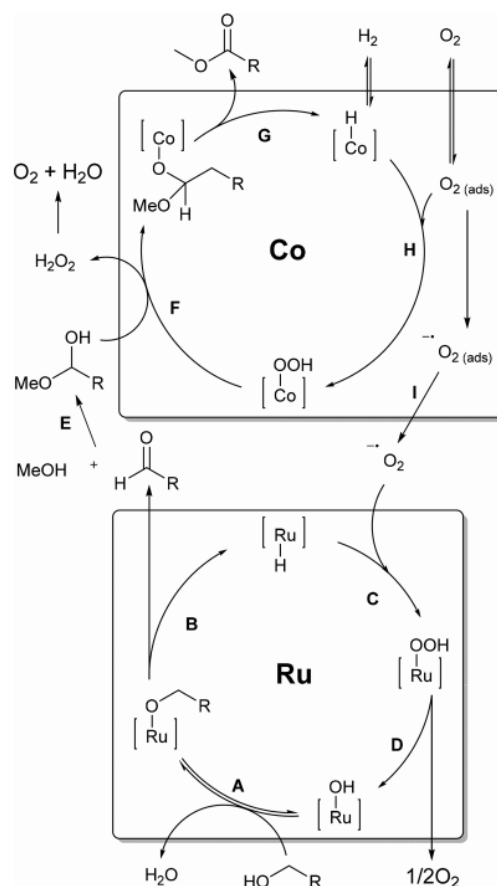
The alcohol oxidation takes place at the ruthenium catalyst, most likely at the surface [Ru]–OH species.[37,38] It starts with the formation of the [Ru]–alcoholate species by ligand exchange (Scheme 4A), following a β-hydride elimination to form the aldehyde intermediate and [Ru]–H species (Scheme 4B). Then the hydride species is reoxidized (Scheme 4C), and upon the release of oxygen the active [Ru]–OH sites are regenerated (Scheme 4D).

Once in solution, the formed aldehyde reacts with the alcohol to form a hemiacetal in basic media (Scheme 4E). Metal–alcoholate species shall thus be formed at the cobalt catalyst surface, analogous to that recently observed in a similar system by Stahl and co-workers (Scheme 4F).[39] Then β-hydride elimination takes place to form the ester product along with the surface [Co]–H species (Scheme 4G), more specifically at the [Co]–N sites of the catalyst (from the nitrogen doping), as they are responsible for the catalytic

activity (see Supporting Information for a complete characterization of the catalyst).[31] A hint of the presence of cobalt hydrides is given by the detection of gaseous hydrogen in the headspace of a closed reaction setup (see Supporting Information, Figure S41). Taking into account that this catalyst has been shown to be active in hydrogenation reactions,[31] one can expect to see the liberation of H_2 from the [Co]−H species simply as a consequence of the microscopic reversibility principle. The closing step of the cycle is the oxidation of [Co]−H by the adsorbed oxygen species (Scheme 4H). It is known that on most metal surfaces, adsorbed oxygen ($O_{2(ads)}$) can easily gain electrons from the metal core, resulting in the formation of the adsorbed superoxo species ($^{\bullet-}O_{2(ads)}$).[40] It has been also documented that in the cobalt catalyst the activation of oxygen is performed both at the Co−N_x and Co−O_x sites.[41]

We were able to detect the formation of superoxide by EPR spectroscopy. The measurements were performed using 5,5-dimethyl-1-pyrroline *N*-oxide (DMPO) as a spin trap from which the corresponding DMPO−OOH adduct is detected,[42,43] revealing the formation of superoxide radical (Figure 3). These experiments show the formation of
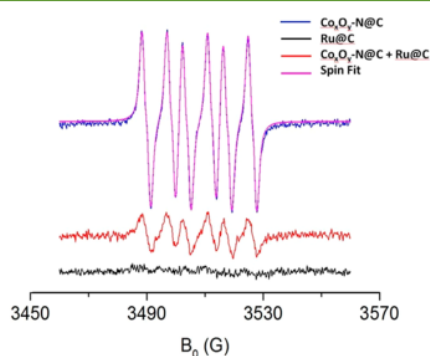
Figure 3. EPR measurements of different catalytic solutions for the oxidation of HMF (1) in the presence of DMPO showing the characteristic signals of the DMPO−OOH spin adduct. The DMPO−OOH signal at $g = 2.006$ was simulated using SpinFit (Bruker) with the spin Hamiltonian parameters hyperfine splitting $aN = 13.73$, $aH\beta = 8.03$ and $aH\gamma = 1.51$ G (the hyperfine splitting of $aH\gamma$ is not resolved due to the line broadening but it can be clearly seen from the second derivative of the EPR signal, Figure S40).

superoxide in the presence of the cobalt catalyst but not with the ruthenium catalyst. Interestingly, when both catalysts are present, the signal of the superoxide loses intensity, suggesting that the superoxide is being quenched by the ruthenium catalyst. This interaction can be responsible for the improved conversion shown before (see Table S2 entry 3).

Thus, we propose that the synergy observed between both catalysts is due to the formation of superoxide species by the cobalt catalyst (Scheme 4I) which upon desorption, is consumed in the reoxidation of the [Ru]-H facilitating this commonly difficult step (Scheme 4C). The catalysis performed by ruthenium benefits from the superoxide formation by the cobalt catalysis, and later benefits from the increased presence of aldehyde delivered by the alcohol oxidation at the ruthenium catalyst. Because of this synergy, we were able to perform the complete oxidative esterification of HMF with quantitative yields.

CONCLUSIONS

Given its inherent reactivity, the selective oxidation of HMF (**1**) is a challenge. Herewith, we report the selective oxidative esterification of HMF to the esters **2** and **3** with excellent to quantitative yields under mild conditions. This was achieved by the use of a bimetallic catalytic system containing Ru@C and Co_xO_y−N@C catalysts working in synergy. Such an effect seems to be related to the formation of superoxide radicals at the cobalt surface which are in turn used for the catalytic turnover at the ruthenium sites. The kinetics of the oxidation of the alcohol moiety by Ru@C follow an apparent zero-order on the catalyst and substrate. In contrast, the esterification of the aldehyde moiety at Co_xO_y−N@C shows a first-order dependence on the substrate. We demonstrated that the rate of the reaction is limited by the solubility of oxygen by using pure O_2 instead of air and by increasing the solubility of the gas using a perfluoroester (MPFB) as a cosolvent.

To the best of our knowledge, this is the first report of the the use of a mixture of cobalt and ruthenium catalysts in oxidative esterification reactions, and gives the best yields and conversions for HMF under the mildest conditions reported so far.

Since the solubility of oxygen is the limiting factor in the rate of the reaction, and taking into account the inherent safety risks posed by oxygen/organic solvents mixtures, efforts toward the implementation of microflow conditions for this reaction are currently underway in our laboratories. Microflow conditions overcome the mass-transport limitations and provide better and optimal conditions in the mixing of gases and liquids in comparison to batch conditions.

We hope that the findings in this paper provide a source of inspiration for the design of new heterogeneous catalysts for the chemical modification of biomass-derived substrates.

ASSOCIATED CONTENT

Ⓢ Supporting Information

The Supporting Information is available free of charge on the ACS Publications website at DOI: 10.1021/acssuschemeng.9b00914.

> Characterization of the Co_xO_y−N@C−catalyst (XRD, TEM, XPS, and EPR); investigation of reaction conditions; catalyst recycling investigations for the oxidative esterification of HMF; characterization of the esterification products (^{1}H NMR, ^{13}C NMR−^{1}H-COSY-NMR, ^{1}H−^{13}C-HMBC-NMR and MES-EI); determination of the order of reaction using Ru@C_i; calibration curve (GC) for the determination of 2-furfuraldehyde concentration; additional EPR spectra of DMPO−OOH and GC detection of H_2 (PDF)

AUTHOR INFORMATION

Corresponding Author
*E-mail: esteban.mejia@catalysis.de.
ORCID Ⓞ
Jabor Rabeah: 0000-0003-2162-0981
Rajenahally V. Jagadeesh: 0000-0001-6079-0962
Esteban Mejia: 0000-0002-4774-6884
Notes
The authors declare no competing financial interest.

110

ACS Sustainable Chemistry & Engineering

■ REFERENCES

(1) Clark, J. H.; Farmer, T. J.; Herrero-Davila, L.; Sherwood, J. Circular economy design considerations for research and process development in the chemical sciences. *Green Chem.* **2016**, *18* (14), 3914−3934.

(2) Eerhart, A. J. E.; Huijgen, W. J. J.; Grisel, R. J. H.; van der Waal, J. C.; de Jong, E.; de Sousa Dias, A.; Faaij, A. P. C.; Patel, M. K. Fuels and plastics from lignocellulosic biomass via the furan pathway; a technical analysis. *RSC Adv.* **2014**, *4* (7), 3536−3549.

(3) Delidovich, I.; Hausoul, P. J. C.; Deng, L.; Pfützenreuter, R.; Rose, M.; Palkovits, R. Alternative Monomers Based on Lignocellulose and Their Use for Polymer Production. *Chem. Rev.* **2016**, *116* (3), 1540−1599.

(4) Gupta, K.; Rai, R. K.; Singh, S. K. Metal Catalysts for the Efficient Transformation of Biomass-derived HMF and Furfural to Value Added Chemicals. *ChemCatChem* **2018**, *10* (11), 2326−2349.

(5) Papageorgiou, G. Z.; Papageorgiou, D. G.; Terzopoulou, Z.; Bikiaris, D. N. Production of bio-based 2,5-furan dicarboxylate polyesters: Recent progress and critical aspects in their synthesis and thermal properties. *Eur. Polym. J.* **2016**, *83*, 202−229.

(6) Sousa, A. F.; Vilela, C.; Fonseca, A. C.; Matos, M.; Freire, C. S. R.; Gruter, G.-J. M.; Coelho, J. F. J.; Silvestre, A. J. D. Biobased polyesters and other polymers from 2,5-furandicarboxylic acid: a tribute to furan excellency. *Polym. Chem.* **2015**, *6* (33), 5961−5983.

(7) Burgess, S. K.; Leisen, J. E.; Kraftschik, B. E.; Mubarak, C. R.; Kriegel, R. M.; Koros, W. J. Chain Mobility, Thermal, and Mechanical Properties of Poly(ethylene furanoate) Compared to Poly(ethylene terephthalate). *Macromolecules* **2014**, *47* (4), 1383−1391.

(8) EFSA Panel on Food Contact Materials. Scientific Opinion on the safety assessment of the substance, furan-2, 5-dicarboxylic acid, CAS No 3238-40-2, for use in food contact materials. *EFSA J.* **2014**, *12* (10), 3866−3874.

(9) Pellis, A.; Haernvall, K.; Pichler, C. M.; Ghazaryan, G.; Breinbauer, R.; Guebitz, G. M. Enzymatic hydrolysis of poly(ethylene furanoate). *J. Biotechnol.* **2016**, *235*, 47−53.

(10) Yi, G.; Teong, S. P.; Zhang, Y. Base-free conversion of 5-hydroxymethylfurfural to 2,5-furandicarboxylic acid over a Ru/C catalyst. *Green Chem.* **2016**, *18* (4), 979−983.

(11) Wang, Y.; Yu, K.; Lei, D.; Si, W.; Feng, Y.; Lou, L.-L.; Liu, S. Basicity-Tuned Hydrotalcite-Supported Pd Catalysts for Aerobic Oxidation of 5-Hydroxymethyl-2-furfural under Mild Conditions. *ACS Sustainable Chem. Eng.* **2016**, *4* (9), 4752−4761.

(12) Gui, Z.; Cao, W.; Saravanamurugan, S.; Riisager, A.; Chen, L.; Qi, Z. Efficient Aerobic Oxidation of 5-Hydroxymethylfurfural in Aqueous Media with Au-Pd Supported on Zinc Hydroxycarbonate. *ChemCatChem* **2016**, *8* (23), 3636−3643.

(13) Tong, X.; Yu, L.; Chen, H.; Zhuang, X.; Liao, S.; Cui, H. Highly efficient and selective oxidation of 5-hydroxymethylfurfural by molecular oxygen in the presence of Cu-MnO2 catalyst. *Catal. Commun.* **2017**, *90*, 91−94.

(14) Mishra, D. K.; Lee, H. J.; Kim, J.; Lee, H.-S.; Cho, J. K.; Suh, Y.-W.; Yi, Y.; Kim, Y. J. MnCo2O4 spinel supported ruthenium catalyst for air-oxidation of HMF to FDCA under aqueous phase and base-free conditions. *Green Chem.* **2017**, *19* (7), 1619−1623.

(15) Ait Rass, H.; Essayem, N.; Besson, M. Selective Aerobic Oxidation of 5-HMF into 2,5-Furandicarboxylic Acid with Pt

Catalysts Supported on TiO2- and ZrO2-Based Supports. *ChemSusChem* **2015**, *8* (7), 1206−1217.

(16) Artz, J.; Palkovits, R. Base-Free Aqueous-Phase Oxidation of 5-Hydroxymethylfurfural over Ruthenium Catalysts Supported on Covalent Triazine Frameworks. *ChemSusChem* **2015**, *8* (22), 3832−3838.

(17) Gert-Jan, M. G.; Laszlo, S.; Matheus Adrianus, D. Accelerating Research into Bio-Based FDCA-Polyesters by Using Small Scale Parallel Film Reactors. *Comb. Chem. High Throughput Screening* **2012**, *15* (2), 180−188.

(18) Sun, Y.; Ma, H.; Jia, X.; Ma, J.; Luo, Y.; Gao, J.; Xu, J. A High-Performance Base-Metal Approach for the Oxidative Esterification of 5-Hydroxymethylfurfural. *ChemCatChem* **2016**, *8* (18), 2907−2911.

(19) Deng, J.; Song, H.-J.; Cui, M.-S.; Du, Y.-P.; Fu, Y. Aerobic Oxidation of Hydroxymethylfurfural and Furfural by Using Heterogeneous CoxOy-N@C Catalysts. *ChemSusChem* **2014**, *7* (12), 3334−3340.

(20) Casanova, O.; Iborra, S.; Corma, A. Biomass into chemicals: One pot-base free oxidative esterification of 5-hydroxymethyl-2-furfural into 2,5-dimethylfuroate with gold on nanoparticulated ceria. *J. Catal.* **2009**, *265* (1), 109−116.

(21) Menegazzo, F.; Signoretto, M.; Marchese, D.; Pinna, F.; Manzoli, M. Structure-activity relationships of Au/ZrO2 catalysts for 5-hydroxymethylfurfural oxidative esterification: Effects of zirconia sulphation on gold dispersion, position and shape. *J. Catal.* **2015**, *326*, 1−8.

(22) Li, F.; Li, X.-L.; Li, C.; Shi, J.; Fu, Y. Aerobic oxidative esterification of 5-hydroxymethylfurfural to dimethyl furan-2,5-dicarboxylate by using homogeneous and heterogeneous PdCoBi/C catalysts under atmospheric oxygen. *Green Chem.* **2018**, *20* (13), 3050−3058.

(23) Westerhaus, F. A.; Jagadeesh, R. V.; Wienhofer, G.; Pohl, M. M.; Radnik, J.; Surkus, A. E.; Rabeah, J.; Junge, K.; Junge, H.; Nielsen, M.; Bruckner, A.; Beller, M. Heterogenized cobalt oxide catalysts for nitroarene reduction by pyrolysis of molecularly defined complexes. *Nat. Chem.* **2013**, *5* (6), 537−43.

(24) Jagadeesh, R. V.; Junge, H.; Pohl, M.-M.; Radnik, J.; Brückner, A.; Beller, M. Selective Oxidation of Alcohols to Esters Using Heterogeneous Co3O4-N@C Catalysts under Mild Conditions. *J. Am. Chem. Soc.* **2013**, *135* (29), 10776−10782.

(25) Costello, M. G.; Flynn, R. M.; Owens, J. G., Fluoroethers and Fluoroamines. In *Kirk-Othmer Encyclopedia of Chemical Technology*; John Wiley & Sons, Inc.: 2000.

(26) Han, X.; Geng, L.; Guo, Y.; Jia, R.; Liu, X.; Zhang, Y.; Wang, Y. Base-free aerobic oxidation of 5-hydroxymethylfurfural to 2,5-furandicarboxylic acid over a Pt/C-O-Mg catalyst. *Green Chem.* **2016**, *18* (6), 1597−1604.

(27) Geng, L.; Zheng, B.; Wang, X.; Zhang, W.; Wu, S.; Jia, M.; Yan, W.; Liu, G. Fe3O4 Nanoparticles Anchored on Carbon Serve the Dual Role of Catalyst and Magnetically Recoverable Entity in the Aerobic Oxidation of Alcohols. *ChemCatChem* **2016**, *8* (4), 805−811.

(28) Ray, R.; Chandra, S.; Maiti, D.; Lahiri, G. K. Simple and Efficient Ruthenium-Catalyzed Oxidation of Primary Alcohols with Molecular Oxygen. *Chem. - Eur. J.* **2016**, *22* (26), 8814−8822.

(29) Nie, J.; Xie, J.; Liu, H. Efficient aerobic oxidation of 5-hydroxymethylfurfural to 2,5-diformylfuran on supported Ru catalysts. *J. Catal.* **2013**, *301*, 83−91.

(30) Li, Y.; Wang, L.; Yan, R.; Han, J.; Zhang, S. Promoting effects of MgO, (NH4)2SO4 or MoO3 modification in oxidative esterification of methacrolein over Au/Ce0.6Zr0.4O2-based catalysts. *Catal. Sci. Technol.* **2016**, *6* (14), 5453−5463.

(31) Formenti, D.; Ferretti, F.; Topf, C.; Surkus, A.-E.; Pohl, M.-M.; Radnik, J.; Schneider, M.; Junge, K.; Beller, M.; Ragaini, F. Co-based heterogeneous catalysts from well-defined α-diimine complexes: Discussing the role of nitrogen. *J. Catal.* **2017**, *351*, 79−89.

(32) Moro-Oka, Y.; Ueda, W.; Lee, K.-H. The role of bulk oxide ion in the catalytic oxidation reaction over metal oxide catalyst. *J. Mol. Catal. A: Chem.* **2003**, *199* (1), 139−148.

(33) Battino, R.; Rettich, T. R.; Tominaga, T. The solubility of oxygen and ozone in liquids. *J. Phys. Chem. Ref. Data* **1983**, *12* (2), 163−78.

(34) When the mixture MeOH/MPBF was used, the first minutes of the reaction could not be measured precisely since oxygen solubility changes drastically from roon temperature (24 °C) to the reaction temperature, generating bubbles that interfere with the measurements.

(35) Bures, J. A Simple Graphical Method to Determine the Order of a Reaction in Catalyst. *Angew. Chem., Int. Ed.* **2016**, *55* (6), 2028−2031.

(36) Bures, J. Variable Time Normalization Analysis: General Graphical Elucidation of Reaction Orders from Concentration Profiles. *Angew. Chem., Int. Ed.* **2016**, *55* (52), 16084−16087.

(37) Yamaguchi, K.; Mizuno, N. Supported Ruthenium Catalyst for the Heterogeneous Oxidation of Alcohols with Molecular Oxygen. *Angew. Chem., Int. Ed.* **2002**, *41* (23), 4538−4542.

(38) Yamaguchi, K.; Mizuno, N. Scope, Kinetics, and Mechanistic Aspects of Aerobic Oxidations Catalyzed by Ruthenium Supported on Alumina. *Chem. - Eur. J.* **2003**, *9* (18), 4353−4361.

(39) Mannel, D. S.; King, J.; Preger, Y.; Ahmed, M. S.; Root, T. W.; Stahl, S. S. Mechanistic Insights into Aerobic Oxidative Methyl Esterification of Primary Alcohols with Heterogeneous PdBiTe Catalysts. *ACS Catal.* **2018**, *8* (2), 1038−1047.

(40) Li, C.; Domen, K.; Maruya, K.; Onishi, T. Dioxygen adsorption on well-outgassed and partially reduced cerium oxide studied by FT-IR. *J. Am. Chem. Soc.* **1989**, *111* (20), 7683−7687.

(41) Eisenberg, D.; Slot, T. K.; Rothenberg, G. Understanding Oxygen Activation on Metal- and Nitrogen-Codoped Carbon Catalysts. *ACS Catal.* **2018**, *8* (9), 8618−8629.

(42) Xiao, J.; Rabeah, J.; Yang, J.; Xie, Y.; Cao, H.; Brückner, A. Fast Electron Transfer and •OH Formation: Key Features for High Activity in Visible-Light-Driven Ozonation with C3N4 Catalysts. *ACS Catal.* **2017**, *7* (9), 6198−6206.

(43) Makino, K.; Hagiwara, T.; Murakami, A. A mini review: Fundamental aspects of spin trapping with DMPO. *International Journal of Radiation Applications and Instrumentation. Part C. Radiation Physics and Chemistry* **1991**, *37* (5), 657−665.

112

Supporting Information:

Synergetic Bimetallic Oxidative Esterification of 5-hydroxymethylfurfural (HMF) under mild conditions

Abel Salazar[†], Paul Hünemörder[†], Jabor Rabeah[†], Antje Quade[‡], Rajenahally V. Jagadeesh[†] and Esteban Mejía[†*]

[†] Leibniz-Institute for Catalysis, Albert-Einstein-Str. 29a, 18059 Rostock, Germany

[‡] Leibniz-Institute for Plasma Science and Technology – INP-Greifswald, 17489, Greifswald, Germany

E-mail: esteban.mejia@catalysis.de

Total number of pages: 34

Total number of figures: 46

Total number of tables: 8

Table of Contents

1. Characterization of the Co$_x$O$_y$-N@C-catalyst

1.1. XRD measurements of the Co$_x$O$_y$-N@C-catalyst

The XRD powder pattern was recorded on a Stoe STADI P diffractometer, equipped with a linear Position Sensitive Detector (PSD) using Cu Kα radiation (λ = 1.5406 Å). Processing and assignment of the powder patterns was done using the software WinXpow (Stoe) and the Powder Diffraction File (PDF) database of the International Centre of Diffraction Data (ICDD). The powder pattern of the catalyst shows two sharp peaks characteristic for metallic Co (Fig. S1) at 2Θ = 44.16° and 51.42° besides weak reflections at 2Θ = 36.35°, 36.89°, 42.47 and 61.52°. The peaks at 36.35°, 42.47°and 61.52° confirm the existence of CoO, whereas the peak at 36.89° and the features around 59° 65.5° point to small Co$_3$O$_4$ particles just above the detection limit of XRD, which were confirmed by TEM (see below).
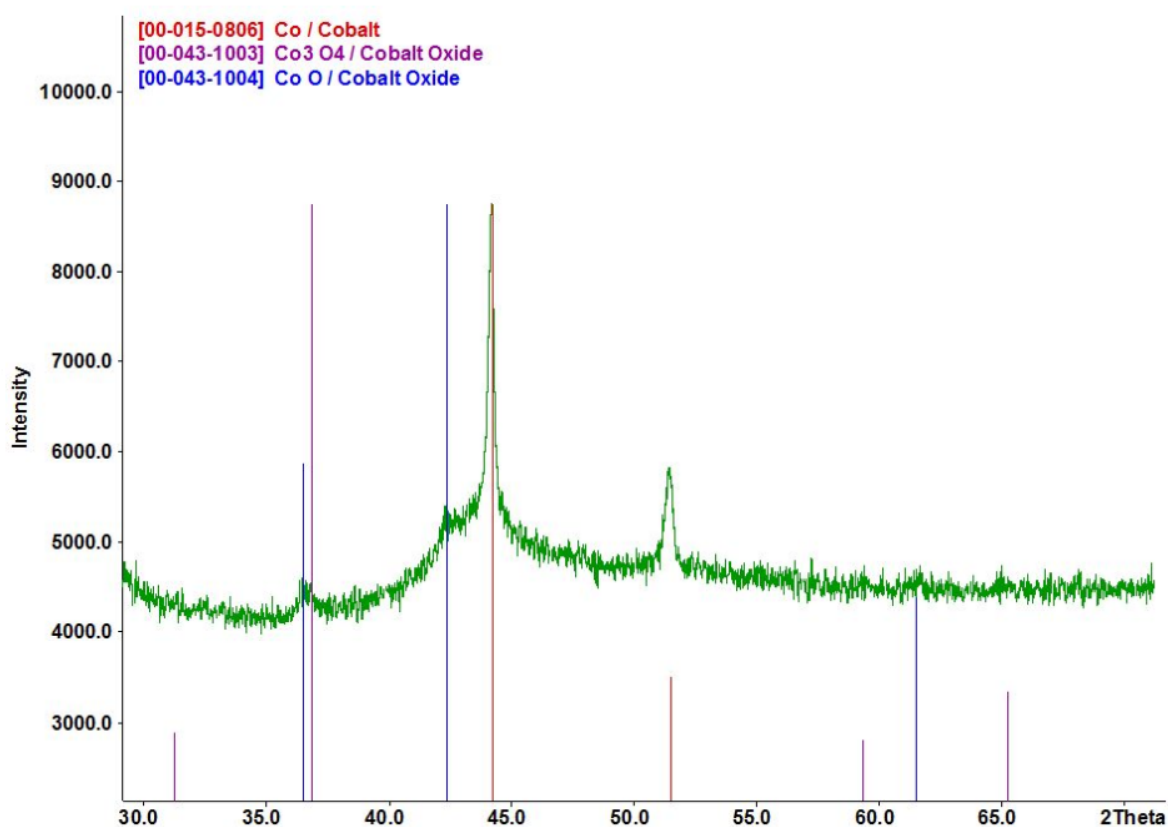
Figure S1. XRD powder pattern of the active cobalt catalyst. The PDF (Powder Diffraction Files) numbers are in brackets.

1.2. TEM measurements and images of the Co$_x$O$_y$-N@C-catalyst

The TEM measurements were performed at 200kV on a JEM-ARM200F (JEOL) which is aberration corrected by a CESCOR (CEOS) for the STEM applications. The microscope is equipped with a JED-2300 (JEOL) EDXS spectrometer for chemical analysis. The HAADF imaging was performed with spot size 6c and a 40μm condenser aperture. The sample was deposited on a holey carbon supported grid mesh 300 and transferred to the microscope. To image the full size spectra of Co$_3$O$_4$ particles, High Angle Annular Dark Field (HAADF) at a Cs corrected microscope was used. With a conventional TEM it was not possible to image the smallest particles due to the weak contrast. As shown in Figures S2, in the catalyst contains mainly small particles of 2-10 nm in size. By EDXS analysis, cobalt along with oxygen was detected in such particles (Fig. S2), suggesting that they consist of CoO and/or Co$_3$O$_4$. This agrees very well with the XRD pattern showing only very weak signals of CoO and Co$_3$O$_4$ (Fig. S1). Due to their small size, such particles are hardly visible by XRD.
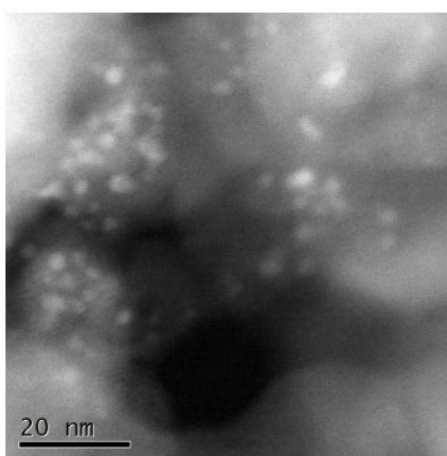
Figure S2-STEM-HAADF of Co- phenanthroline /C
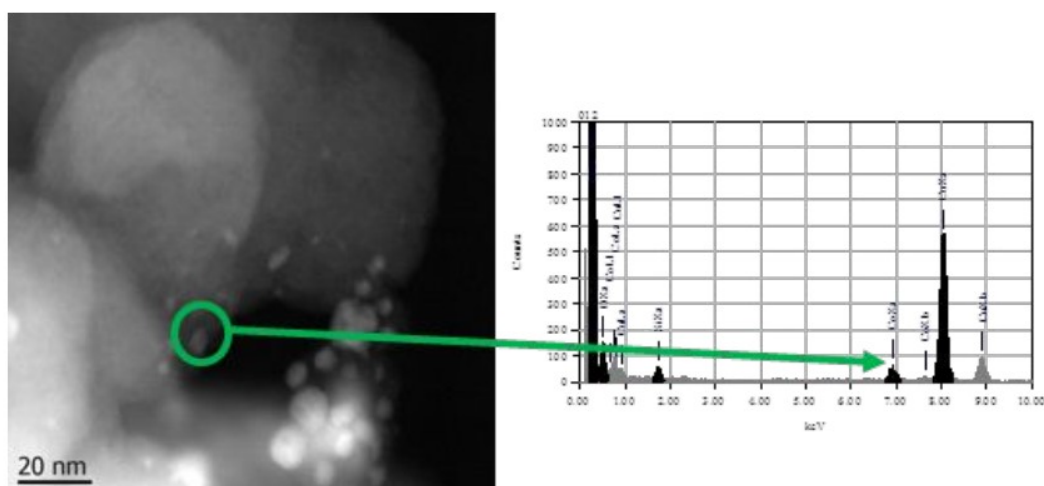
Figure. S3. EDX analysis (right) of the particle indicated in the left plot.

Besides the small particles shown in Fig. S2 and S3, there are also a few larger particles and agglomerates in a range of 20-80 nm and occasionally even larger structures up to 800 nm. As an example, one of these structures is shown in Fig. S4. EDXS mapping shows clearly that Co is concentrated in the core of such particles, while oxygen is enriched in the shell. Thus, those larger particles might consist of a Co core and a CoO and/or Co_3O_4 shell. In the XRD pattern (Fig. S1) these particles, though much less abundant than the small particles shown in Fig. S2, give rise to the sharp reflections for metallic Co. This is due to their much larger size and higher crystallinity.
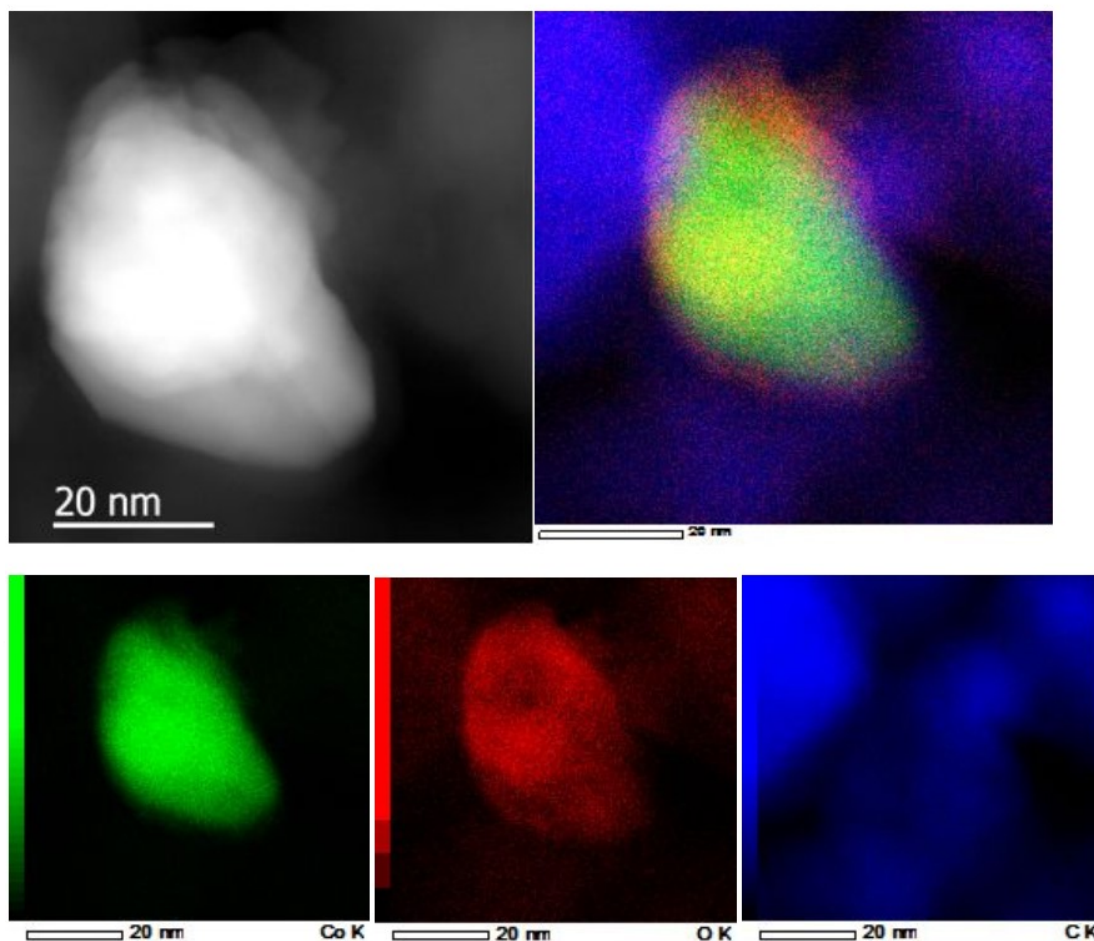
Figure S4. Micrograph and elemental mapping (green: Co; red: oxygen; blue: carbon (from the grid)

1.3. XPS data of the Co_xO_y-N@C-catalyst

To obtain further insight into the structure of the catalyst surface and especially into the role of nitrogen coming from the organic ligand, XPS investigations of N and Co species were carried out. Interestingly, three distinct peaks are observed in the N1s spectra of the Co_3O_4-N@C-catalyst with an electron binding energy of 399.0 eV, 400.8 eV and 402.3 eV (Figure S5). The lowest binding energy peak can be attributed to pyridine-type nitrogen, which is bound to a metal ion.[S1] The electron binding energy of 400.8 eV is characteristic for pyrrole-type nitrogen contributing two electrons to the carbon matrix. It is bound to a hydrogen atom. Such types of nitrogen are found after the carbonization of nitrogen-containing organic materials.[S2] Finally, the small peak at 402.3 eV is typical

S5

for ammonium species like NH_4^+ or $R\text{-}NH_3^+$.[S3] The ratio between all Co atoms and all N atoms in the near surface region is 1:4.7. Deconvolution reveals that around 64% of all N atoms are bound to the metal ions.
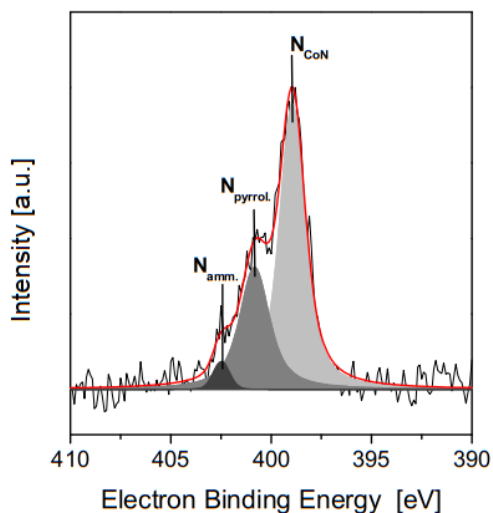
Figure S5. N1s spectrum of the catalyst. The different N1s state are labelled: N_{CoN} N bound to Co; $N_{pyrrol.}$: pyrrolic N; $N_{amm.}$: N of ammonium species

In the cobalt region, only peaks characteristic for oxidic Co are found (Fig. S6) with the typical binding energy of 780.4 eV of the $Co2p_{3/2}$ and 795.3 eV of the Co $2p_{1/2}$ electrons are found. Additionally, the satellite peaks at 786.7 eV and 802.8 eV are characteristic for oxidic Co, the relatively weak.satellites are typical for Co_3O_4. This oxidation state is further confirmed by the modified Auger parameter (α'=1552.7 eV). This agrees very well with TEM results, which suggest that the very small particles of 2-10 nm are oxidic (in line with XRD) and the bigger particles contain a Co core and a cobalt oxide shell. In the literature[S4] it is discussed, that CoO on the surface is not stable and therefore oxidized to Co_3O_4. Thus, it can be concluded that the surface of all Co-containing particles in the catalyst consists of Co_3O_4 while CoO and Co (reflected by XRD) might be enriched in the bulk.
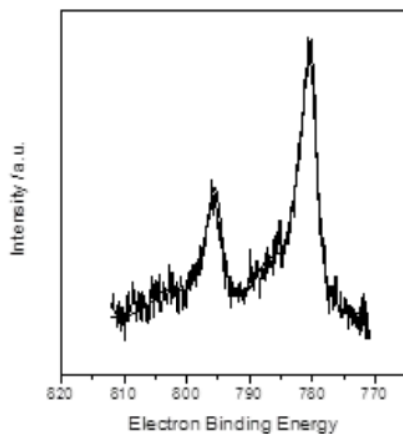
Figure S6. Co2p spectrum of the catalyst with the typical features of Co_3O_4.

1.4. EPR measurements of the catalyst

Besides XRD and TEM, EPR spectroscopy is another suitable method to gain information on the nature of Co containing particles. EPR spectra were recorded in X-band at 80 K and 290 K on a Bruker EMX CW-micro spectrometer equipped with an ER 4119HS-WI high-sensitivity cavity and a variable temperature control unit (microwave power: 6.64 mW, modulation frequency: 100 kHz, modulation amplitude: 1 G). The EPR spectrum of the active catalyst contains a broad signal at g = 2.12 (Fig. S7). The intensity of this signal increases slightly with rising temperature, which is characteristic for antiferromagnetic Co_3O_4 particles. The Neel temperature T_N above which bulk Co_3O_4 becomes paramagnetic is below 40 K.[S5,S6] Previously it was found that the temperature dependence of the EPR signal intensity reflects very sensitively the onset of anti-ferromagnetic ordering in Co_3O_4 and also in other antiferromagnetic oxide materials already well above T_N.[S7] In bulk Co_3O_4 the EPR intensity increased gradually up to 150 K and then remained constant up to 250 K before it started decreasing.[S6] The observed intensity behavior in Figure S7 is exactly in line with these previous results.

g = 2.12

T = 88 K
T = 290 K

B / G
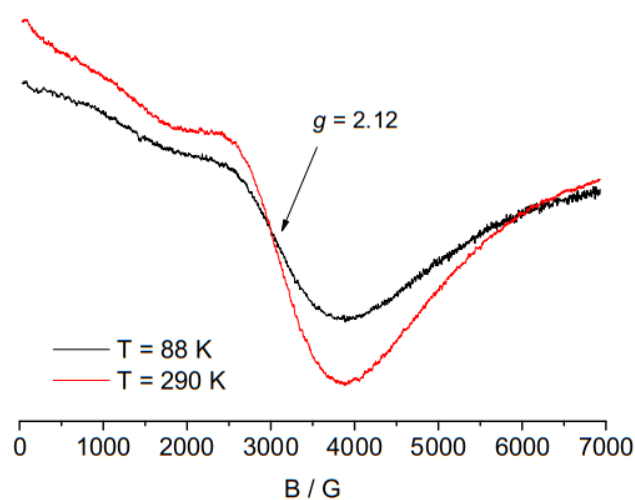
Figure S7. EPR spectra of the active cobalt catalyst recorded at 88 and 290 K.

The EPR signal at g = 2.12 is superimposed on a second very broad anisotropic signal, the positive lobe of which is cut off at B = 0. This suggests that the magnetic properties are not exactly the same for each particle. The reason may be different particle sizes (see below) and/or replacement of O by N in the coordination of Co (as observed by XPS see below). In contrast to Co_3O_4, CoO is not expected to contribute to the EPR spectrum since CoO is antiferromagnetic below $T_N \approx 293K$[S8] and thus EPR silent. Metallic Co is ferromagnetic up to a Curie temperature of 1120 °C[S9] and could in principle cause a ferromagnetic resonance signal, the intensity of which does not depend on temperature between 88 and 290 K. Such signal is not seen in Fig. 7 (possibly due to the very low amount of

S7

metallic particles in the catalyst as suggested by TEM), however, it cannot be excluded that it contributes to some extend to the background of the EPR spectrum.

2. Investigation of reaction conditions

2.1 Catalyst loading screening
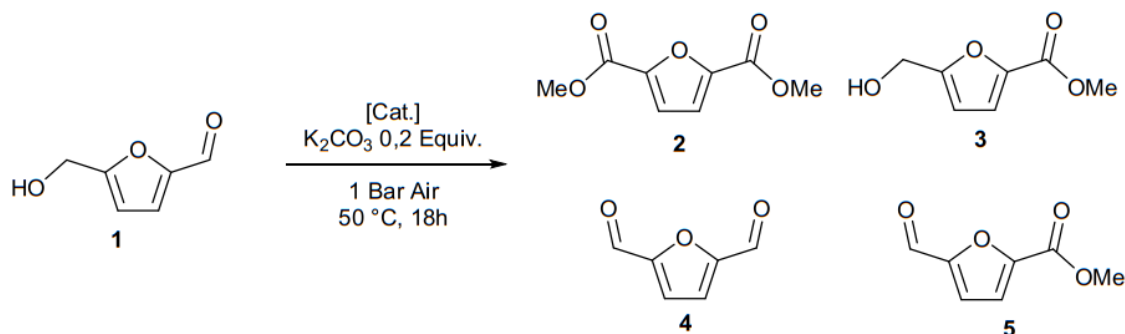
Table S1   Catalysts proportions screening

Entry	Catalyst Loading		Conv.	Products (R=Me)			
	CoₓOᵧ@N-C	Ru@C		2	3	4	5
1	3 mol %	5 mol %	>99	100	-	-	-
2	3 mol %	2,5 mol %	>99	73	18	-	9
3	1,5 mol %	5 mol %	>99	100	-	-	-

0,5 mmol HMF, 0,2 equiv. K_2CO_3, Cat, 4 mL MeOH, Air as oxidant, 50 °C, 18h.

2.2 Catalyst performance without base
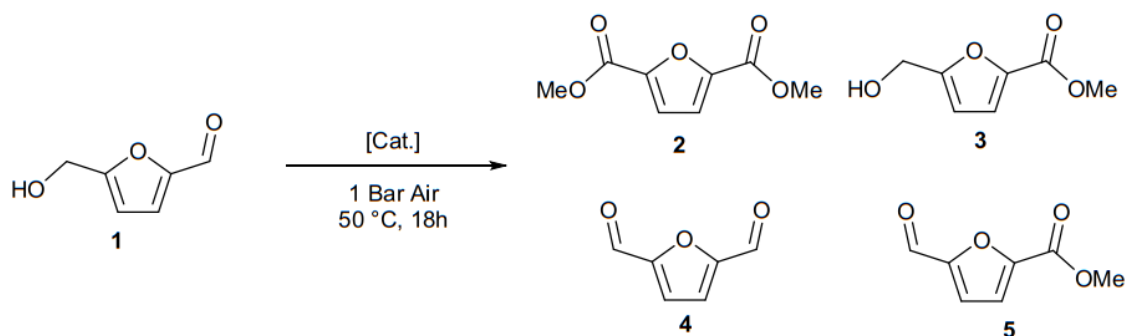
Table S2   Catalyst performance without base

Entry	Catalyst Loading		Conv.	Products (R=Me)			
	CoₓOᵧ@N-C	Ru@C		2	3	4	5
1	3 mol %	-	11	42	58	-	-
2	-	5 mol %	20	-	-	100	-
3	1,5 mol %	5 mol %	43	1	-*	80	10

0,5 mmol HMF, Cat., 4 mL MeOH, Air as oxidant, 50 °C, 18h.

2.3 Catalyst performance comparison using air and oxygen as oxidants
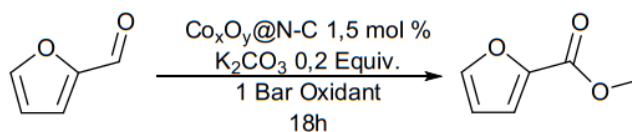
Table S3   Performance comparison between oxidants in the oxidative esterification of furfural in MeOH

Entry	Oxidant		Temp.	Time (h)
	Air	Oxygen	(°C)	70% conv.
1	✓		40	-*
2		✓	40	10
3	✓		50	7
4		✓	50	9
5	✓		60	17
6		✓	60	6,3

*70% conversion not reached.

0,5 mmol 2-Furfuraldehyde, 1,5% mol Cat, 4 mL MeOH, Ballon filled with oxidant, 18h.
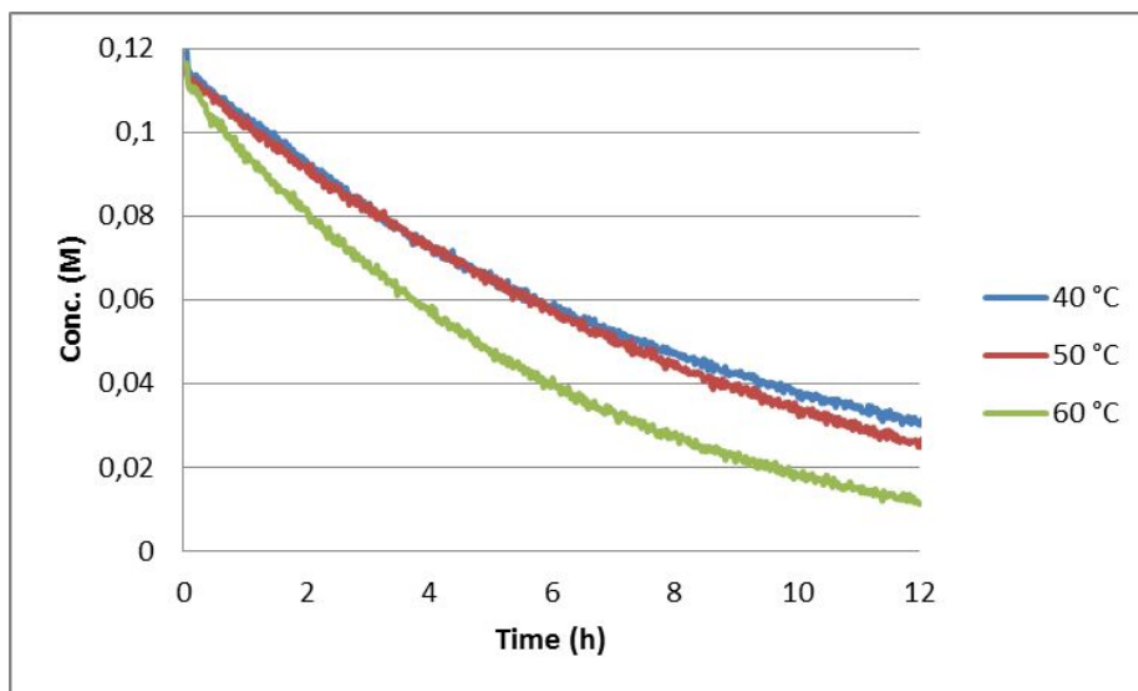
Figure S8. Kinetic profiles at different temperatures for the oxidative esterification of furfural (**7**) in methanol using Co_xO_y@N-C as catalysts and pure oxygen as oxidant.
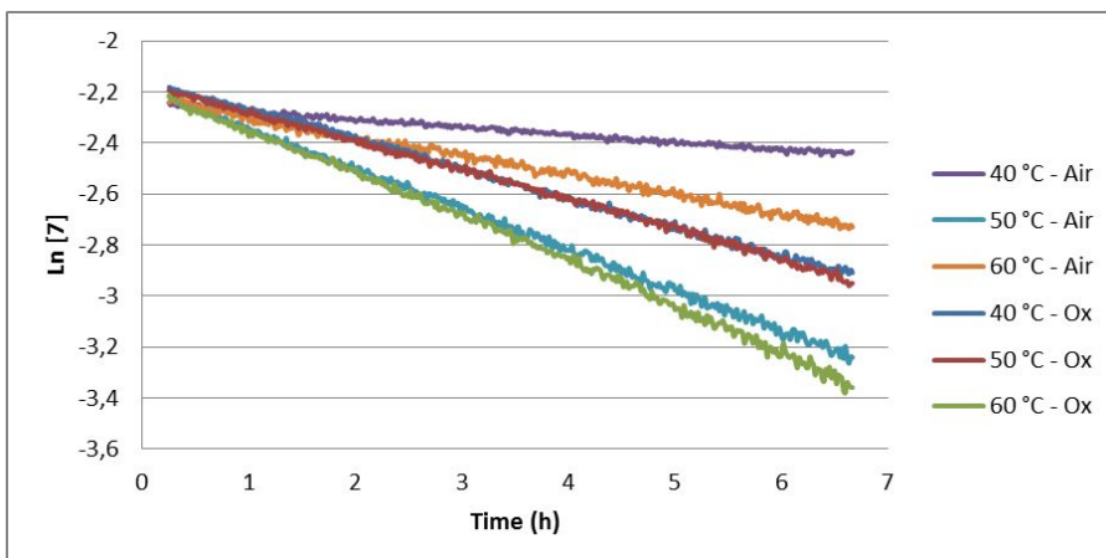
Figure S9. Linearized kinetic profiles at different temperatures for the oxidative esterification of furfural (**7**) in methanol using Co_xO_y@N-C as catalysts and, air and pure oxygen as oxidant.

Table S4 k values derived from linearization of the kinetic profiles

Entry	Oxidant		Temp.	k (h^{-1})
	Air	Oxygen	(°C)	
1	✓		40	0,0300±5
2		✓	40	0,155±2
3	✓		50	0,158±3
4		✓	50	0,155±2
5	✓		60	0,075±1
6		✓	60	0,174±1
7*		✓	50	0,2809±7

*A MPBF:MeOH mixture was used.

3. Catalyst Recycling – Oxidative Esterification of HMF

To an oven dried schlenk tube all the reagents were added (catalysts: Co_xO_y@N-C (12,5 mg) and Ru@C (50mg); 0,5 mmol HMF; 0,1 mmol K_2CO_3; 4 mL MeOH). To the schlenk tube a condenser was coupled and to the top of it a ballon filled with oxygen. After flushing with oxygen for a while, the system was closed and the heating (50 °C) and stirring started. After 16 h the reaction was transferred into a glass tube for centrifugation, after centrifugation the solution was decanted. The catalyst was washed, centrifuged and decanted 3 times with 2 mL MeOH. After that the used catalyst was transferred to a schlenk tube and a reaction with fresh reagents was performed. All the MeOH

solutions (after the reaction and after the washings) were collected and analyzed by GC to determine conversion and yields.

In all the catalytic runs the conversion of HMF was >99%
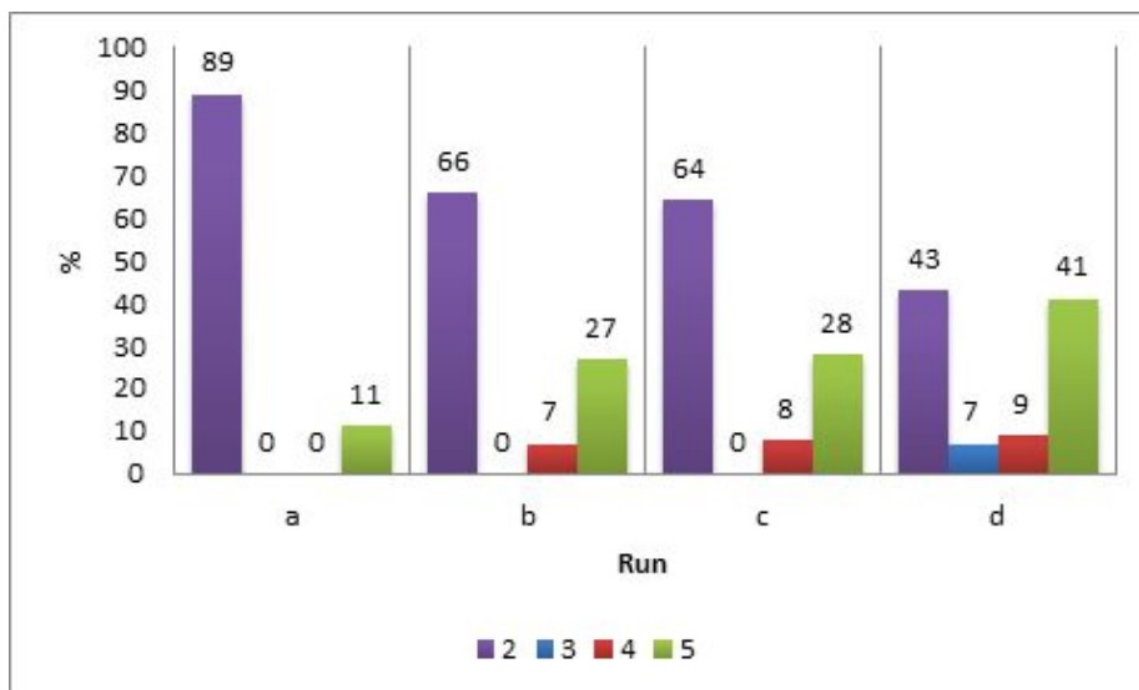
Figure S10. Recycling experiments with Co_xO_y@N-C and Ru@C (0,5 mmol HMF; 0,2 equiv K_2CO_3; 4 mL MeOH) at 50 °C with a balloon filled with oxygen.

3.1 XPS measurements of the used catalysts

XPS measurements of the catalysts were performed (before and after use (Figures S11 and S12)) to gain insight on what changes occur to the catalysts after one use.
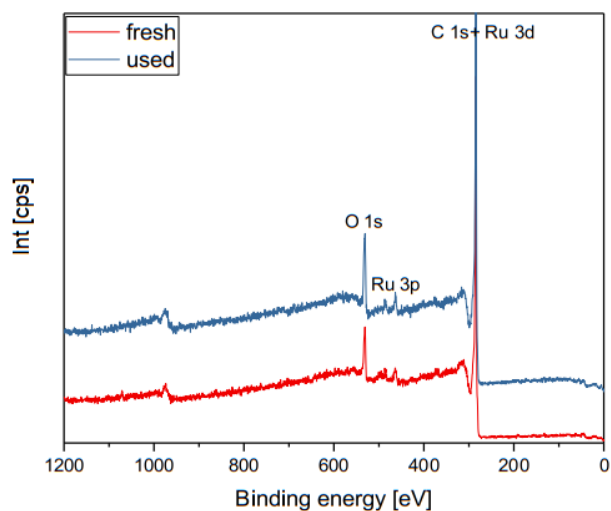
Figure S11. XPS survey scans of Ru@Ccatalysts (fresh and used).
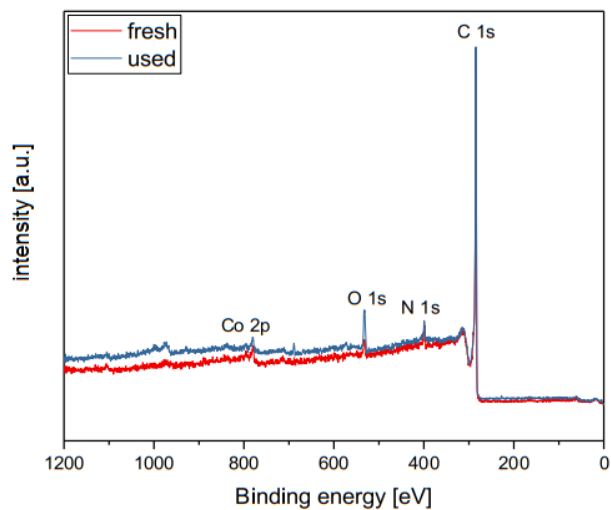
Figure S12. . XPS survey scans of Co_xO_y@N-C catalysts (fresh and used).

The elementary analysis from the Ru@C shows no significant difference between the fresh and used catalysts. (see Table S5).

Table S5   Elementary analysis by XPS of the commercial Ru@C catalyst.

Element	Content (at%)	
	Fresh	Used
Ru	2,2	2,0
O	8,7	6,2
C	88,8	89,8

Also the chemical composition of the catalyst remains similar after use. It is to remark that, the signal corresponding to ruthenium is very noisy, therefore making a precise identification between Ru metal and RuO_x very difficult. Although, a composition of 60% Ru metal and 40% RuO_x is estimated. (see figure S13).
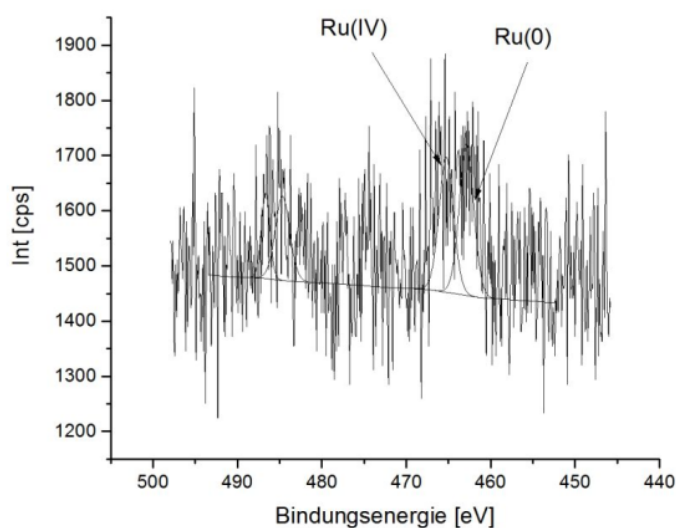
Figure S13. Ru region of the XPS measurements.

On other side, changes in the cobalt catalyst could be observed. The oxygen content in the catalyst increases from 3 to 5%, and the nitrogen and cobalt content remain similar. (See table S6) The intensity of the Co 2p-peaks are very low and an estimation of the oxidation state of Cobalt is difficult. After change of the Auger-Parameter, the measurement indicates the presence of Co_3O_4.

Table S6   Elementary analysis by XPS of the commercial $Co_xO_y@C$ catalyst

Element	Content (at%)	
	Fresh	Used
Co	1,1	0,7
N	4,1	4,7
O	2,7	5,4
C	92,0	89,1

The analysis of the chemical species of nitrogen changes after the reaction. The N1s-peak remains similar but the deconvolution shows changes in the amount of the components (See figures S14 and S15).

S13

125
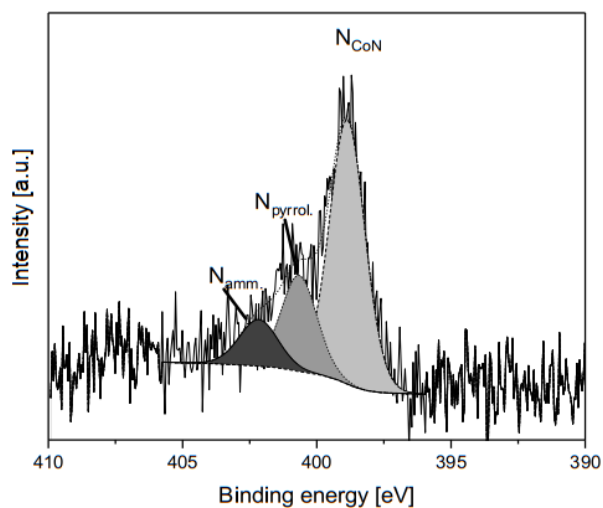
Figure S14. Nitrogen region from the XPS measurements of the fresh Co_xO_y-N@C catalyst
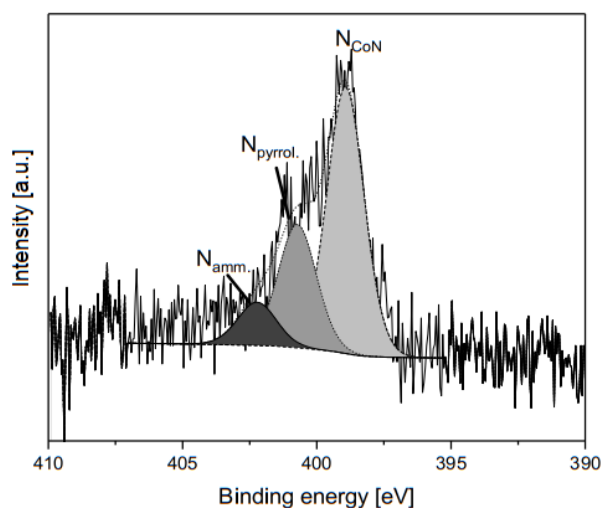
Figure S15. Nitrogen region from the XPS measurements of the used Co_xO_y-N@C catalyst

The catalytically active species of pyridinic N-bound (N_{CoN}) to metal is reduced from 64 to 60%, therefore explaining the lost in catalytic activity during the recycling experiments. Changes in the pyrrolic N and ammonium N were also observed. (see table S7).

Table S7   Nitrogen species in the fresh and used Co_xO_y-N@C catalyst.

Nitrogen species	Content (%)	
	Fresh	Used

Pyridinic N-bound to metal	~64	~60
Pyrrolic N	~25	~30
Ammonium N	~11	~10

4. Characterization of the Esterification products

4.1 Characterization of dimethyl furan-2,5-dicarboxylate (2)

^{1}H NMR (300 MHz, CDCl$_3$): δ = 7,17 ppm (-CH, 2H, s); 3,88 ppm (-OCH$_3$, 6H, s).^{13}C NMR (75 MHz, CDCl$_3$): δ = 158,45 ppm (C=O); 146,67 ppm (C arom); 118,53 ppm (CH arom); 52,45 ppm (-OCH$_3$). MS (GC-MS): m/z = 184[M$^+$], 153 (100%).
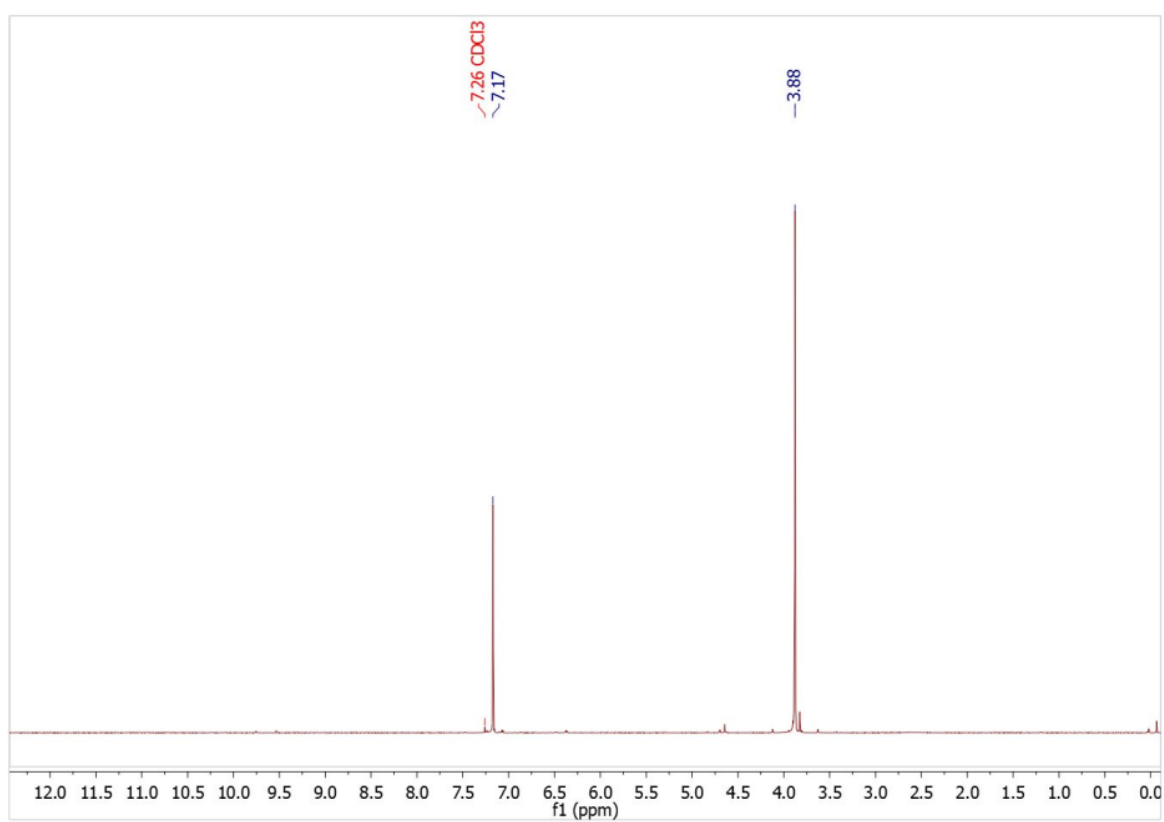
Figure S16. ^{1}H NMR (300 MHz) spectrum of 2 in CDCl$_3$
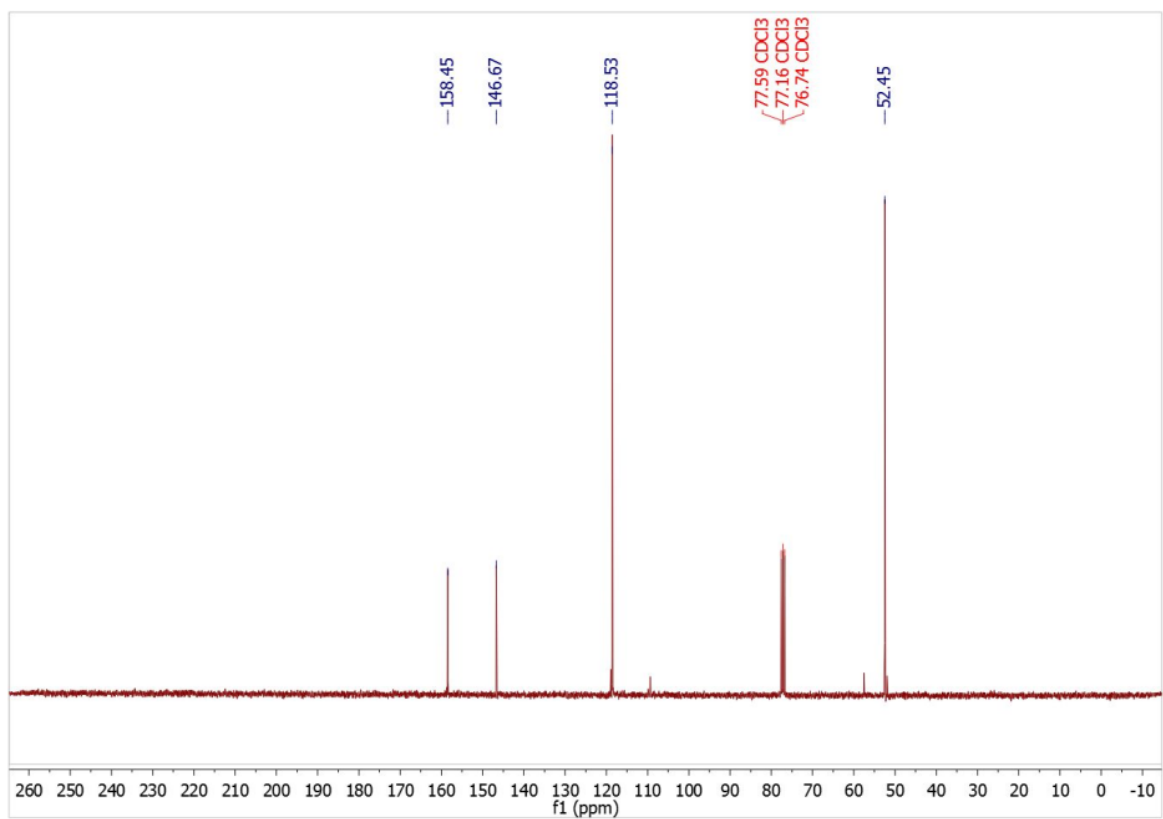
Figure S17. ^{13}C NMR (75 MHz) spectrum of 2 in CDCl$_3$
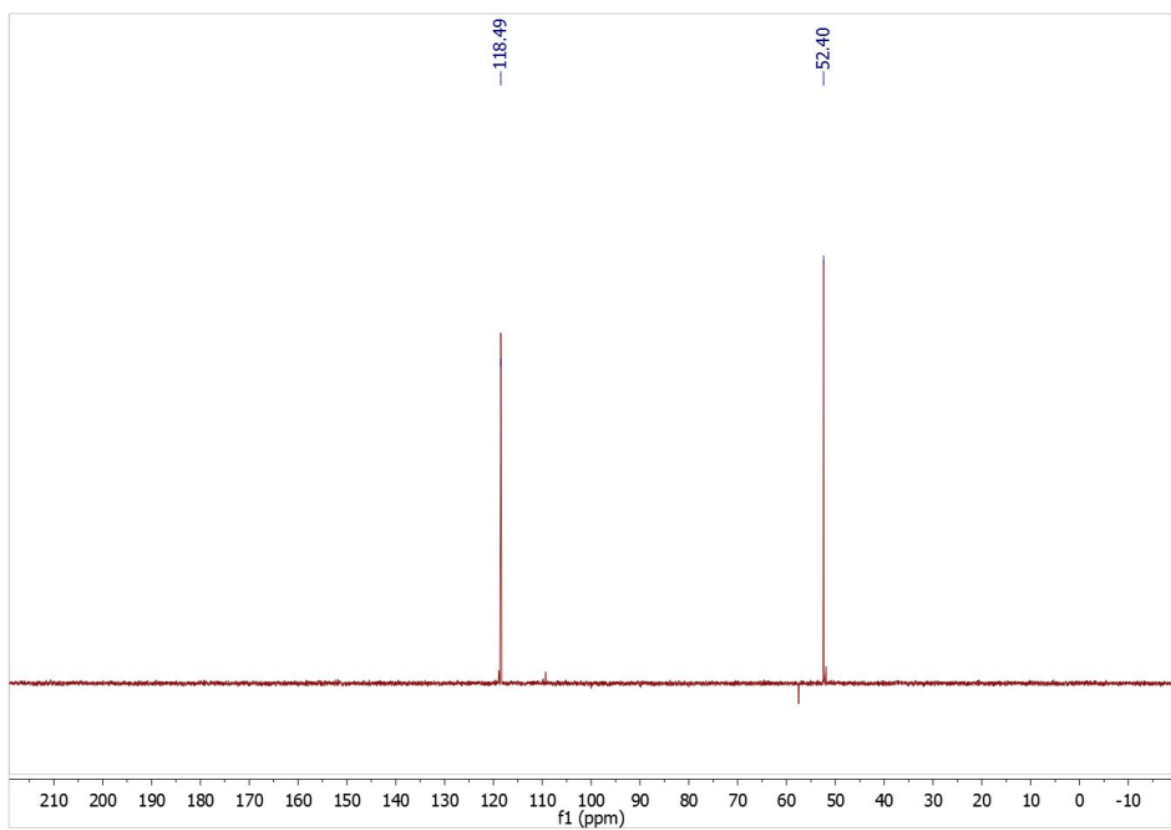
Figure S18. ^{13}C-DEPT NMR (75 MHz) spectrum of 2 in CDCl$_3$

S16

128
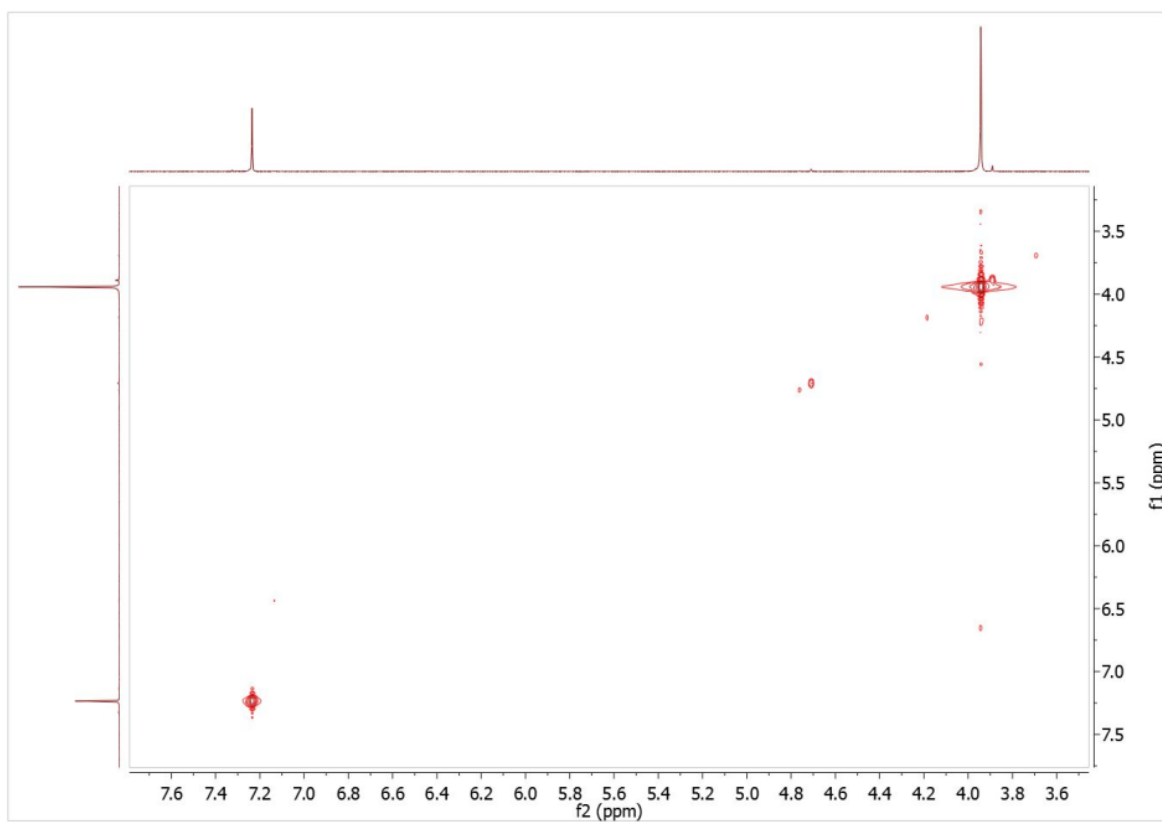
Figure S19. ^{1}H-COSY-NMR (300 MHz) spectrum of 2 in CDCl$_3$
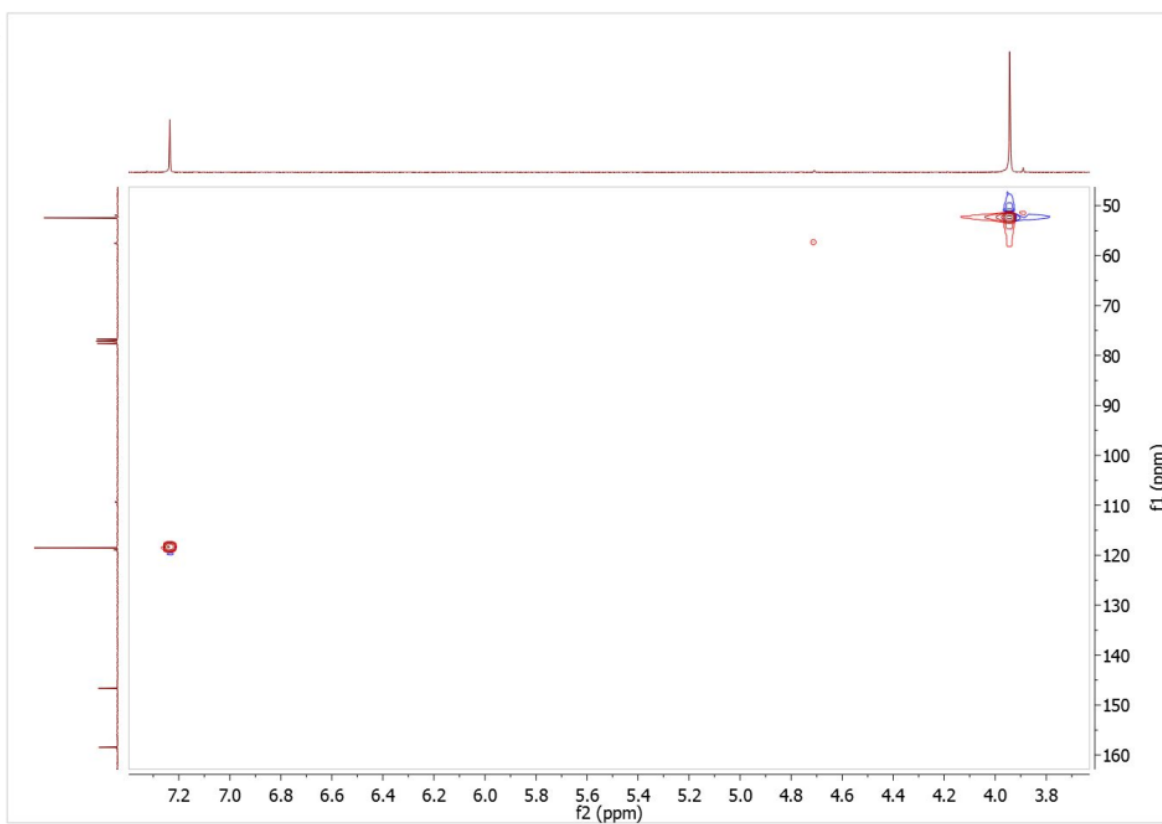
Figure S20. ^{1}H-^{13}C-HSQC- NMR (300 MHz; 75 MHz) spectrum of 2 in CDCl$_3$

S17
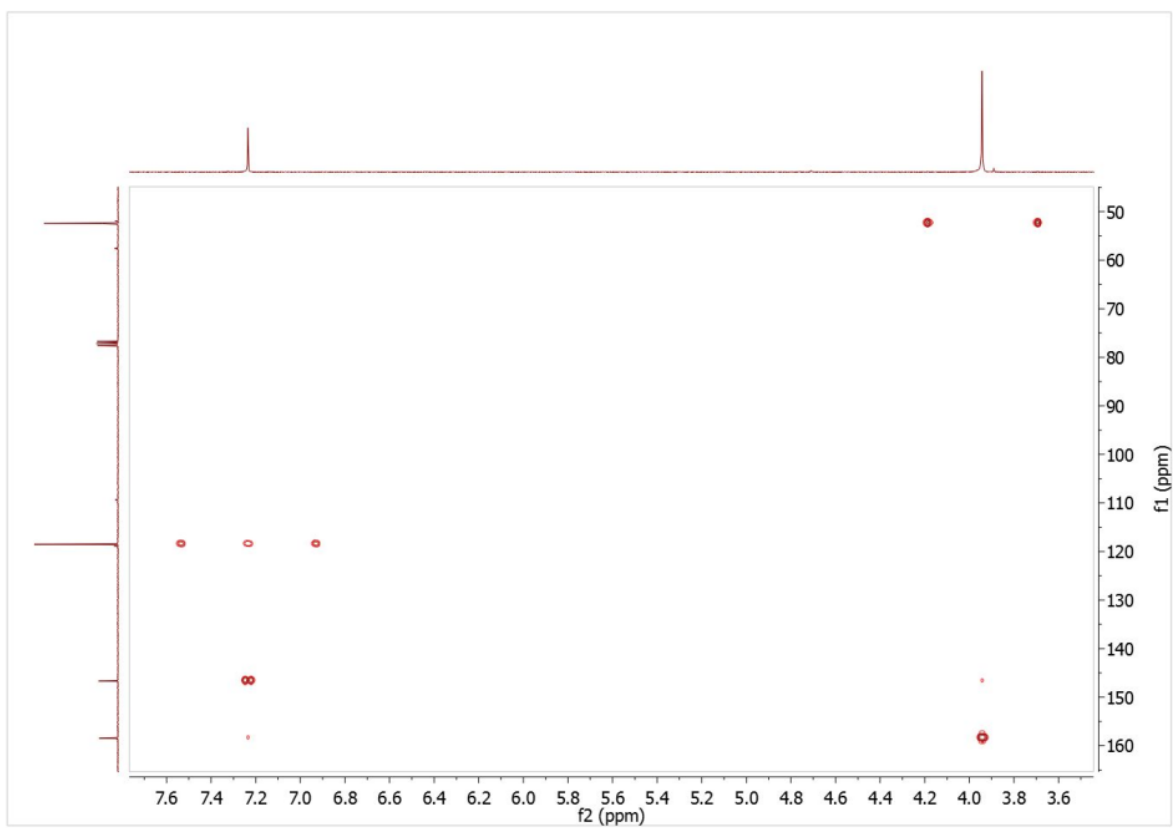
Figure S21. ^1H-^{13}C-HMBC- NMR (300 MHz; 75 MHz) spectrum of 2 in CDCl$_3$
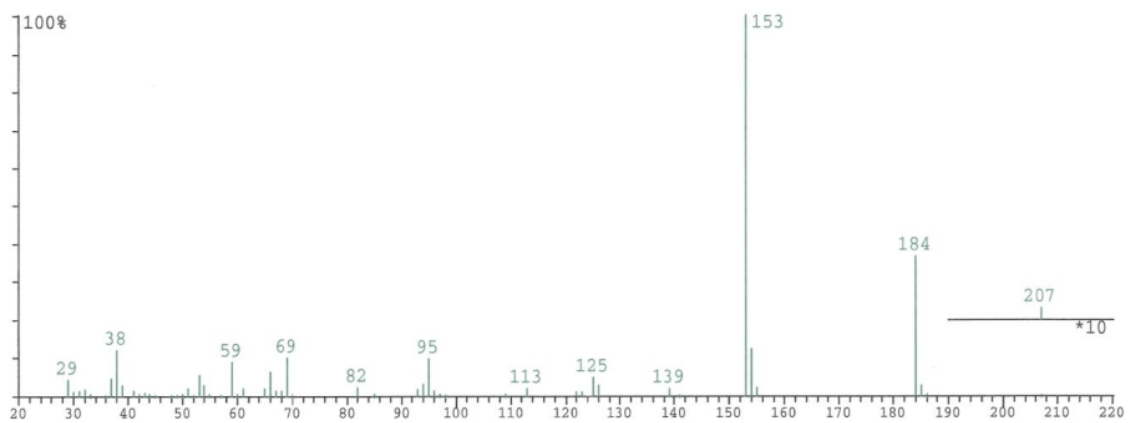
Figure S22. MS spectrum (EI) of 2

4.2 Characterization of methyl 5-(hydroxymethyl)furan-2-carboxylate (3)

^{1}H NMR (300 MHz, CDCl$_3$): δ = 7,09 ppm (-CH arom(alcohol side), 1H, d, *J* = 3,5 Hz); 6,38 ppm (-CH arom (ester side), 1H, d, *J* = 3,5 Hz); 4,63 ppm (CH$_2$, 2H, s); 3,85 ppm (-OCH$_3$, 3H, s).^{13}C NMR (75 MHz, CDCl$_3$): δ = 159,40 ppm (C=O); 158,76 ppm (C arom (alcohol side)); 143,94 ppm (C arom (ester side)); 119,04 ppm (CH arom (ester side)); 109,45 ppm (CH arom (alcohol side)); 57,45 ppm (CH$_2$); 52,06 ppm (-OCH$_3$). MS (GC-MS): m/z = 156[M$^+$], 97 (100%).
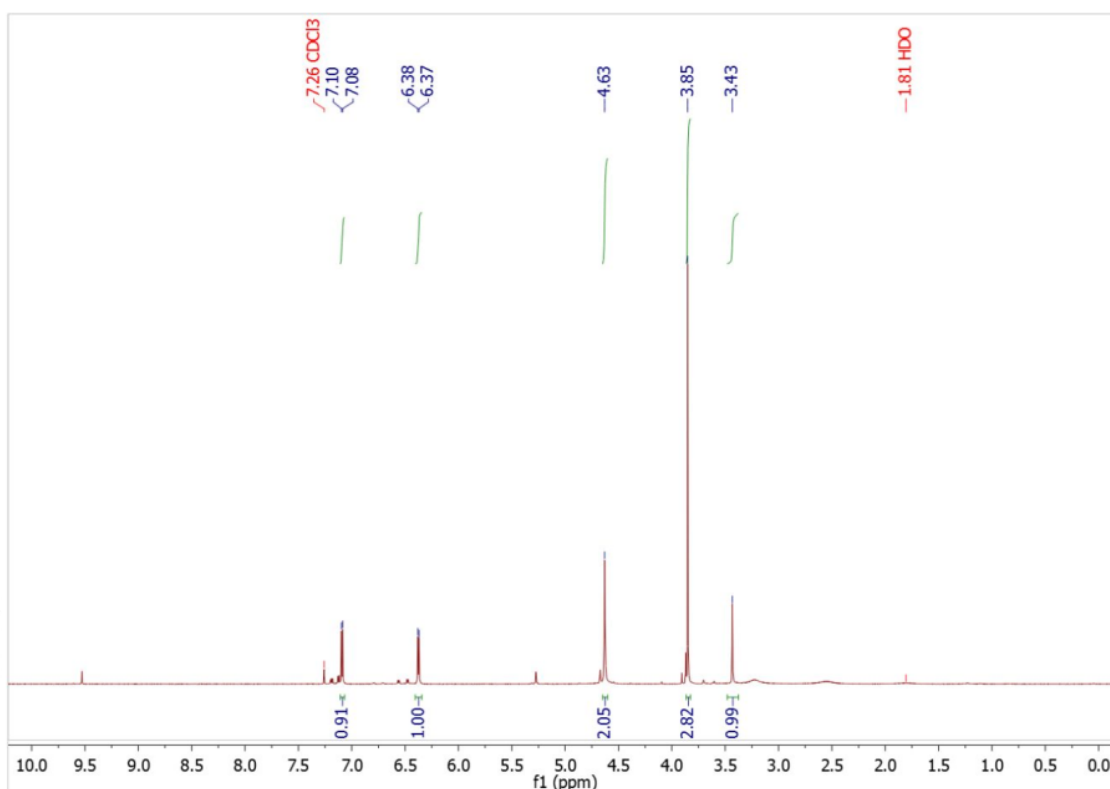
Figure S23. ^{1}H NMR (300 MHz) spectrum of 3 in CDCl$_3$
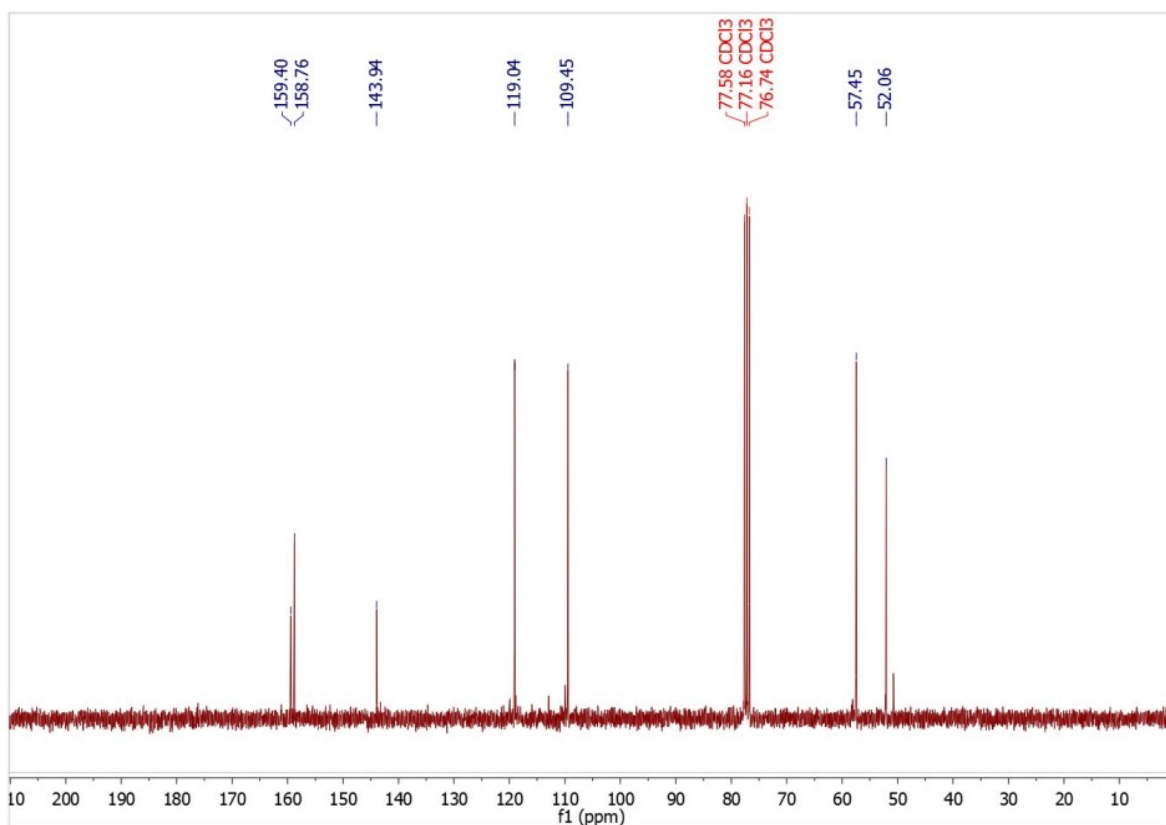
Figure S24. ^{13}C NMR (75 MHz) spectrum of 3 in $CDCl_3$
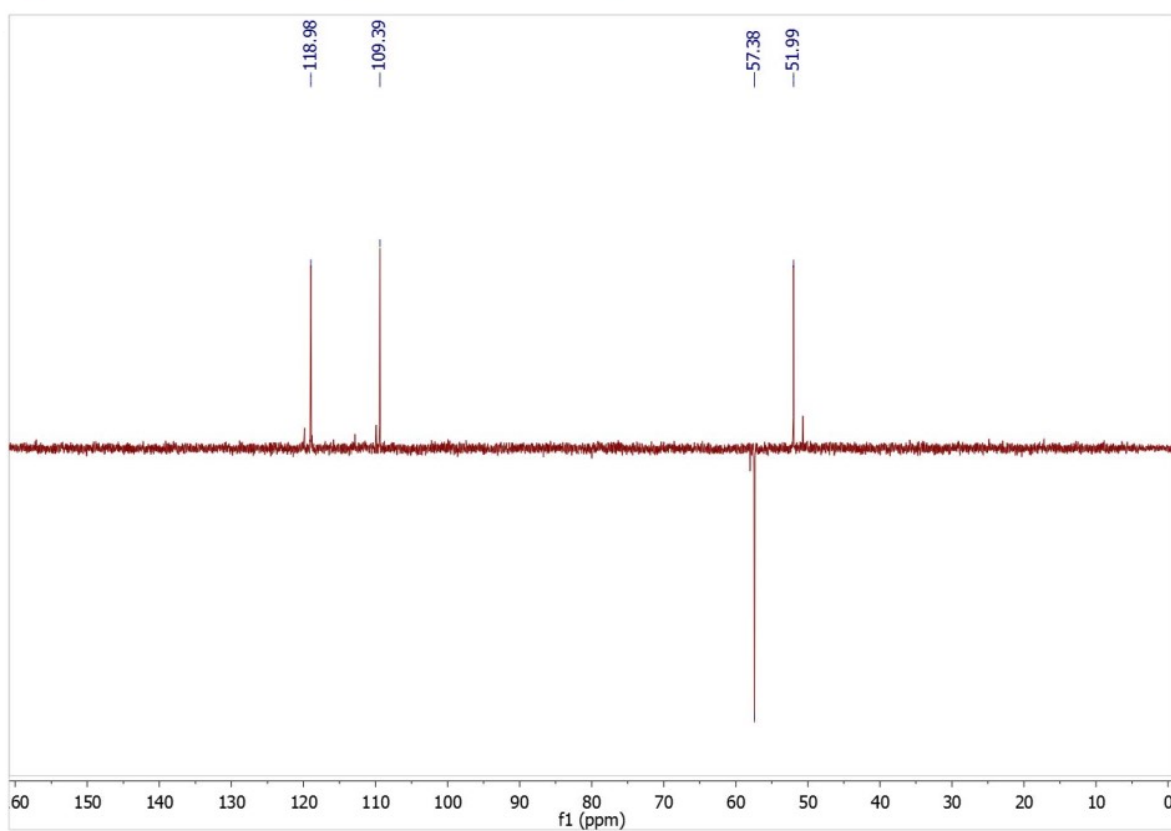
Figure S25. ^{13}C-DEPT NMR (75 MHz) spectrum of 3 in $CDCl_3$
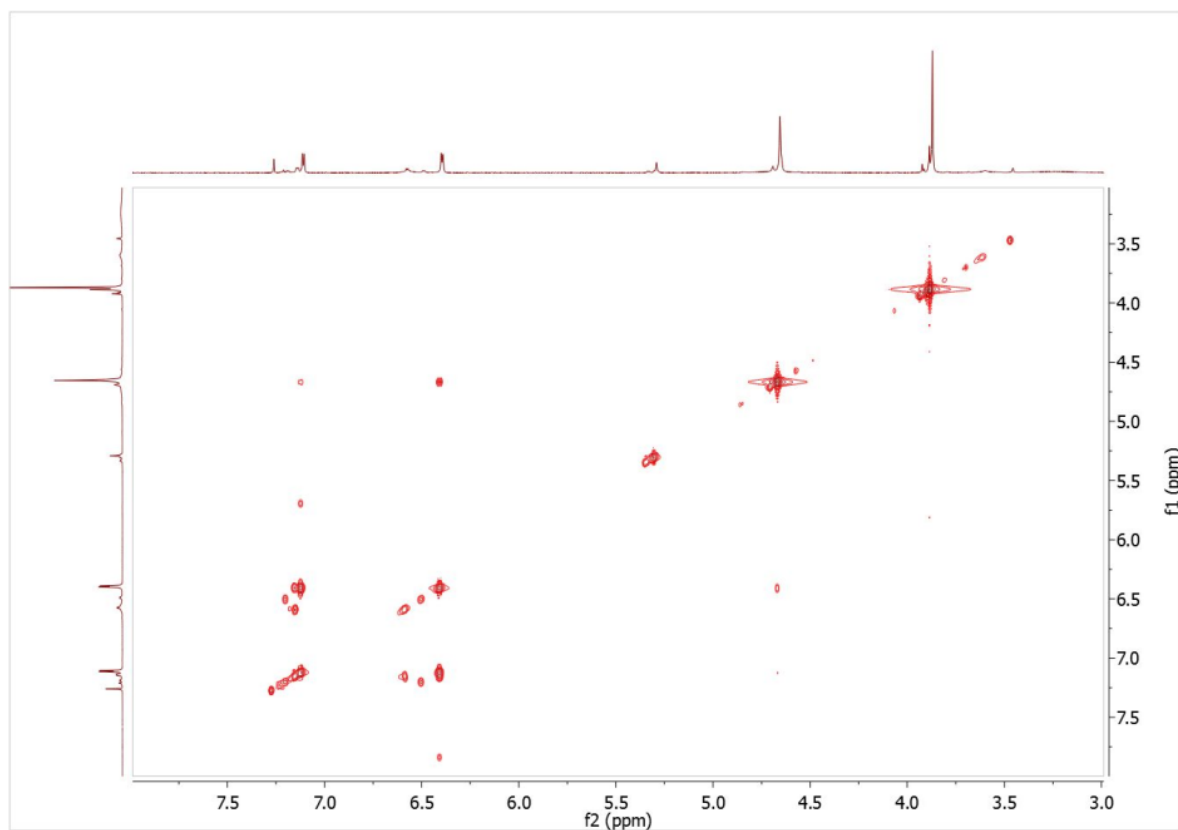
Figure S26. ^{1}H-COSY-NMR (400 MHz) spectrum of **3** in CDCl$_3$
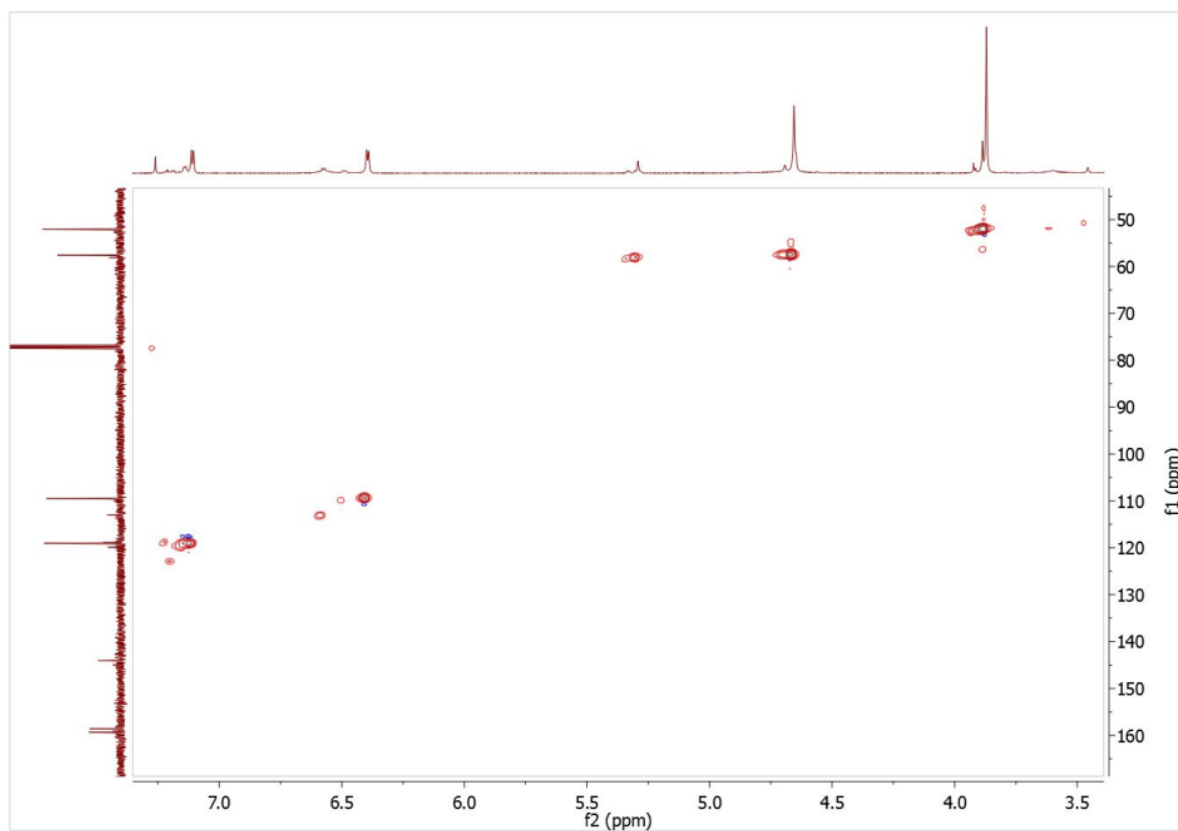
Figure S27. ^{1}H-^{13}C-HSQC- NMR (400 MHz; 101 MHz) spectrum of **3** in CDCl$_3$
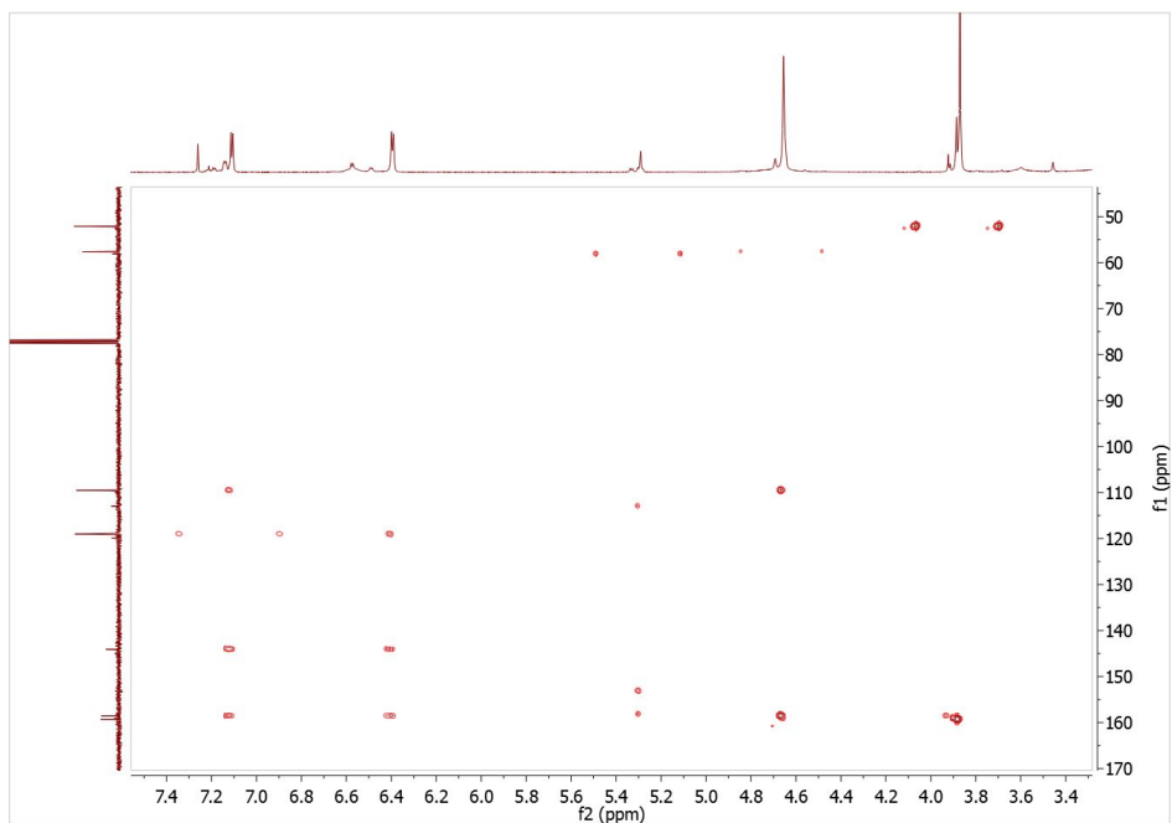
Figure S28. ^{1}H-^{13}C-HMBC- NMR (400 MHz; 101 MHz) spectrum of 3 in CDCl$_3$
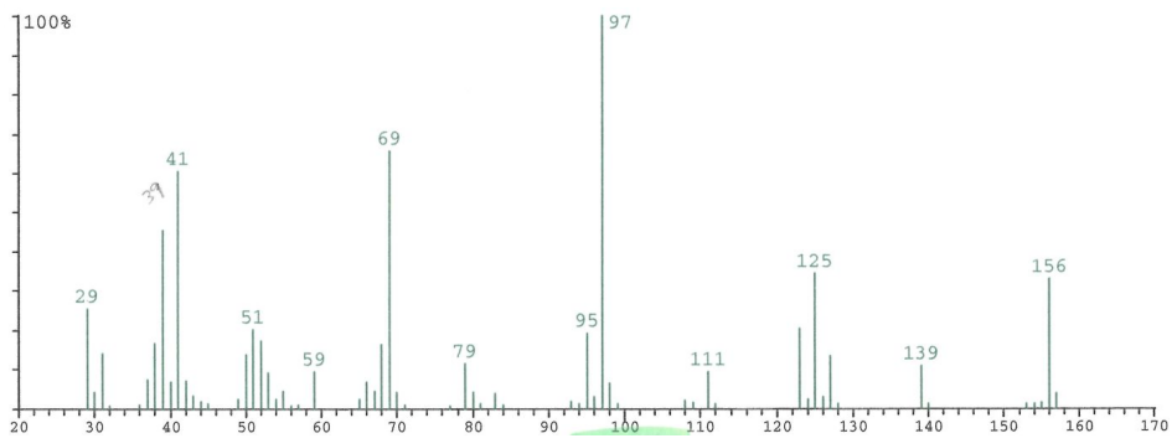
Figure S29. MS spectrum (EI) of 3

4.3 Characterization of furan-2,5-dicarbaldehyde (4)

^{1}H NMR (400 MHz, CDCl$_3$): δ = 9,81 ppm (-CHO), 2H, s); 7,32 ppm (-CH arom, 2H, s). ^{13}C NMR (75 MHz, CDCl$_3$): δ = 179,29 ppm (C=O, aldehyde); 154,26 ppm (C arom); 119,46 ppm (CH arom). MS (GC-MS): m/z = 124[M$^+$] (100%).
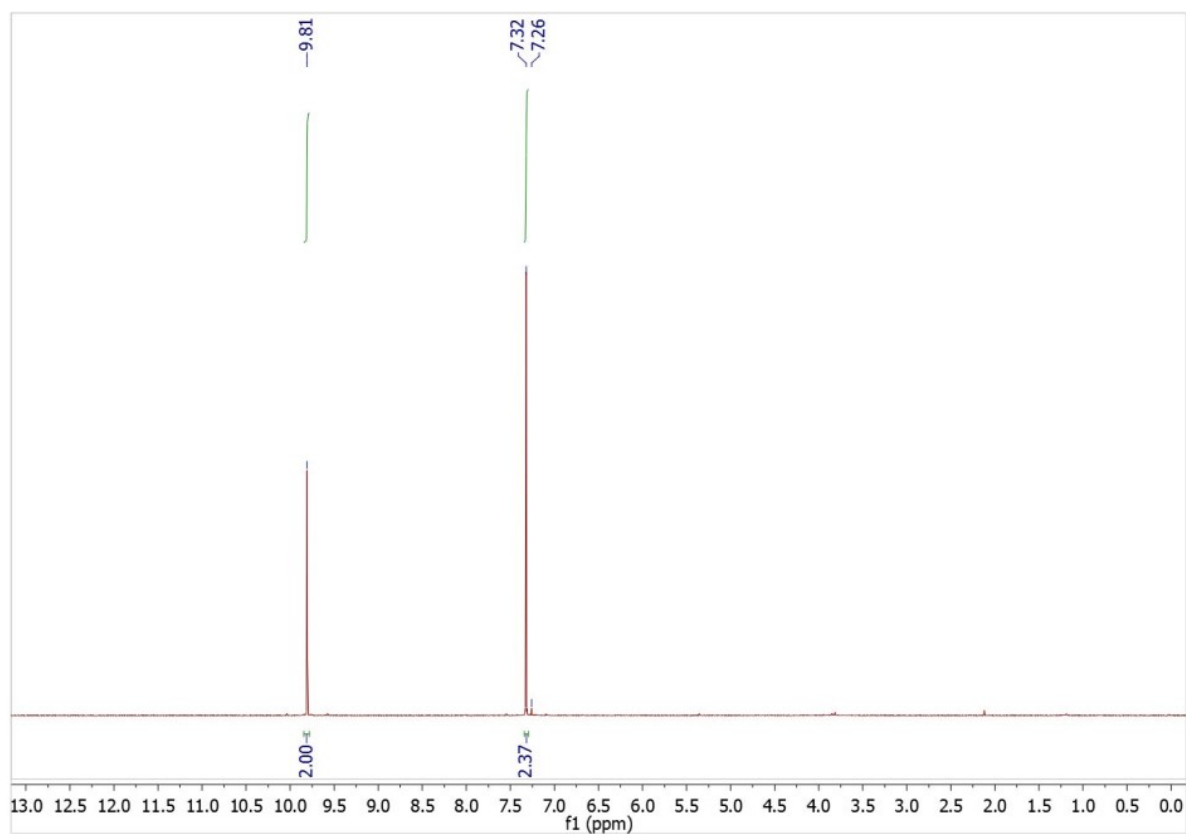
Figure S30. ¹H NMR (400 MHz) spectrum of 4 in CDCl₃
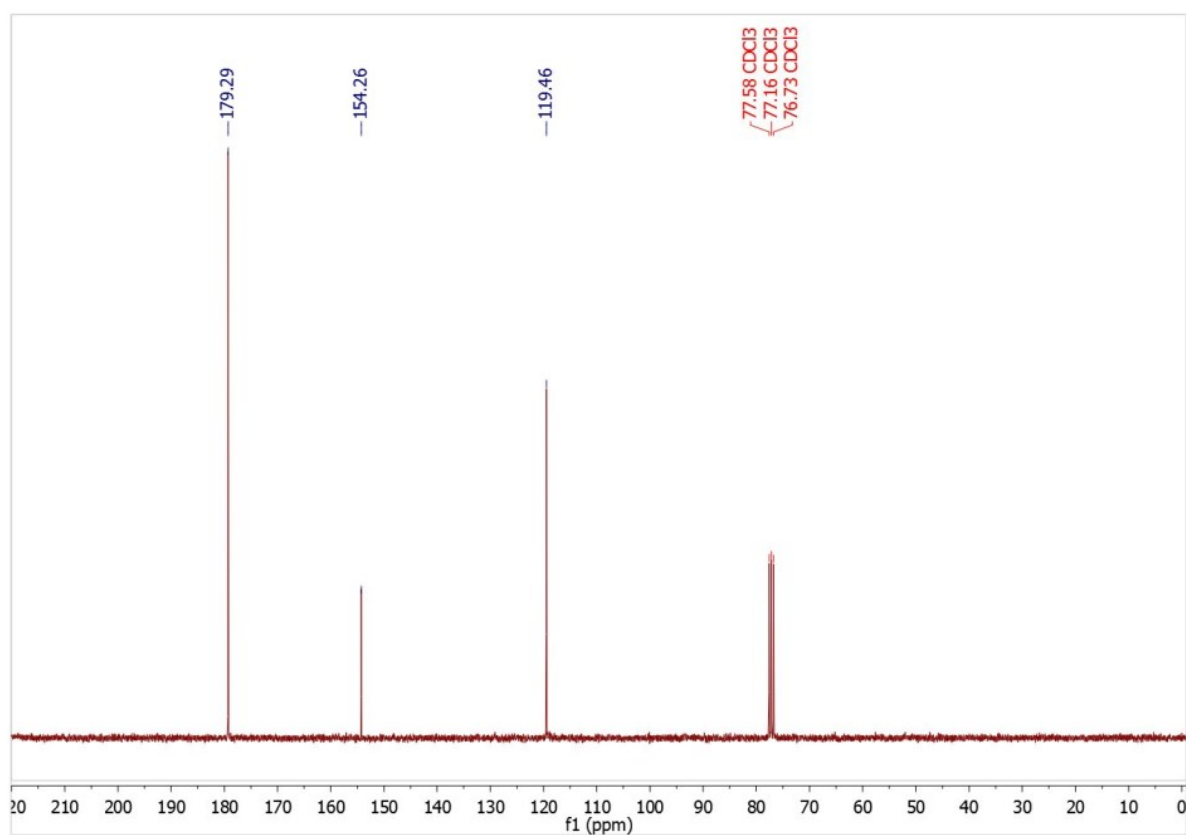
Figure S31. ¹³C NMR (75 MHz) spectrum of 4 in CDCl₃
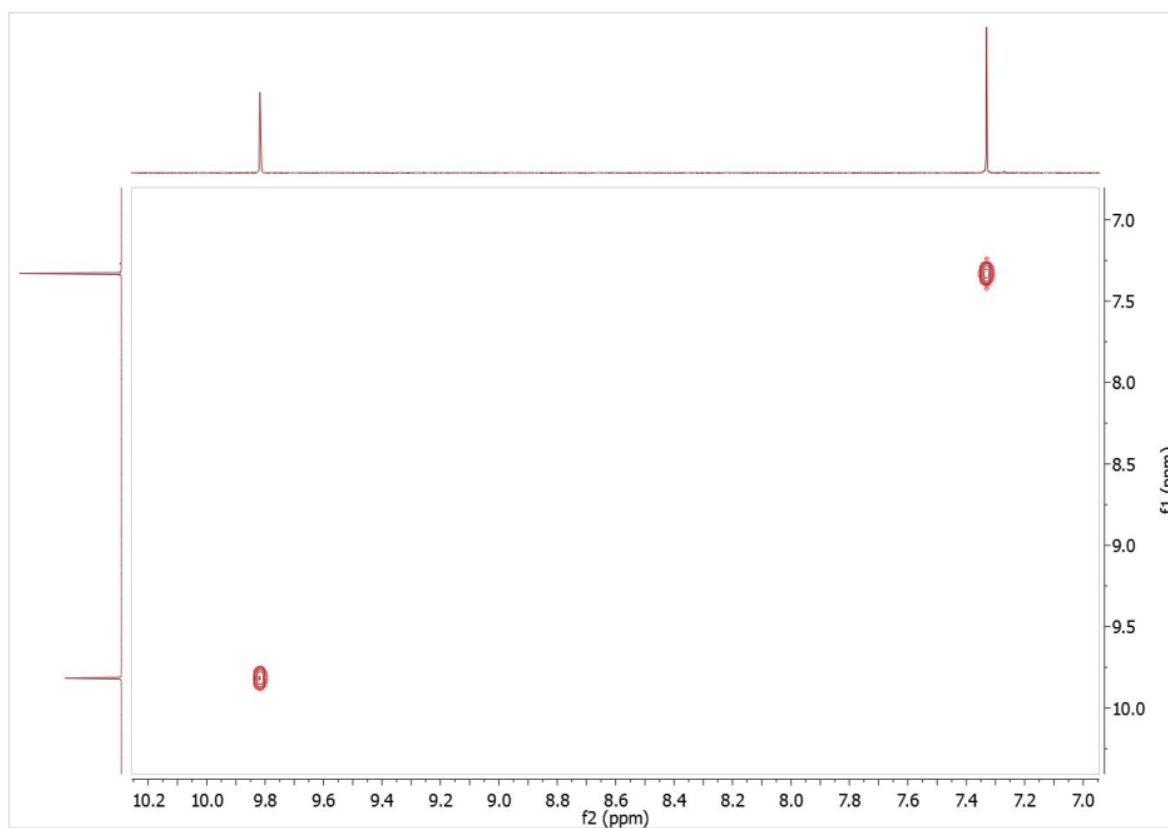
Figure S32. ^{1}H-COSY-NMR (400 MHz) spectrum of 4 in CDCl$_3$
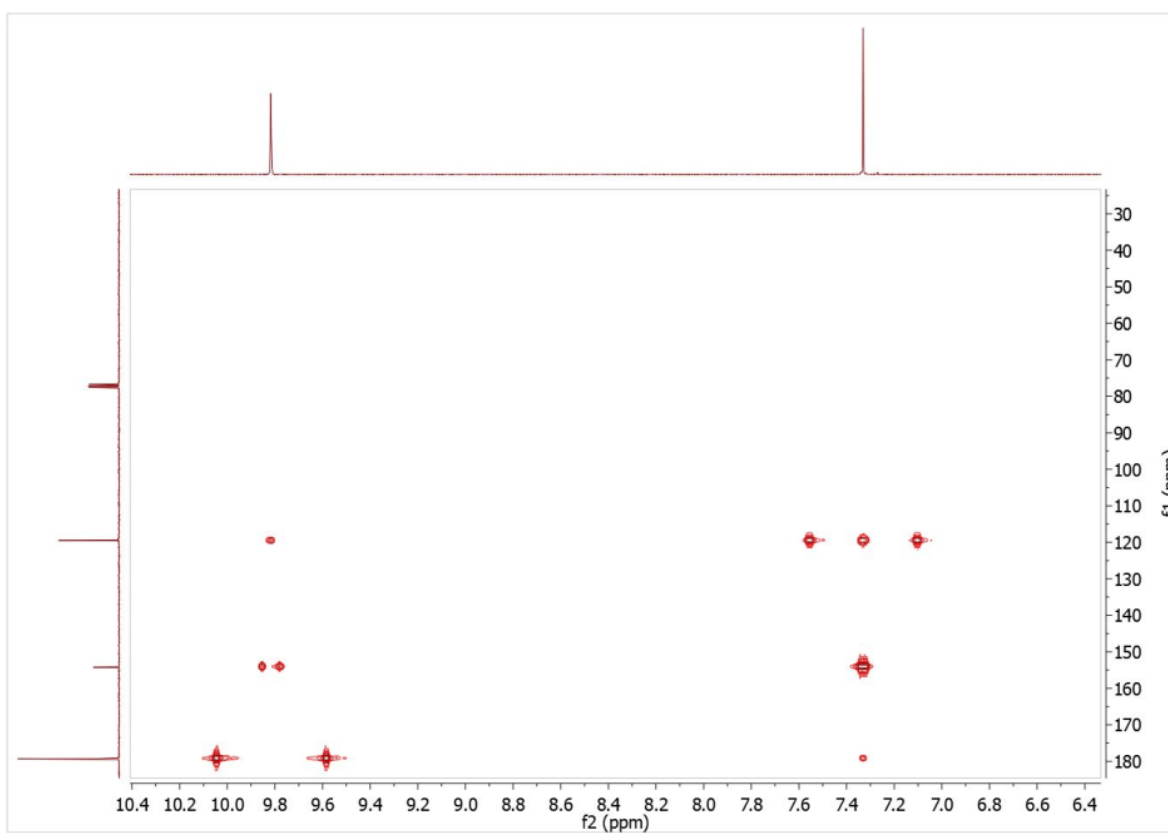
Figure S33. ^{1}H-^{13}C-HMBC- NMR (400 MHz; 101 MHz) spectrum of 3 in CDCl$_3$
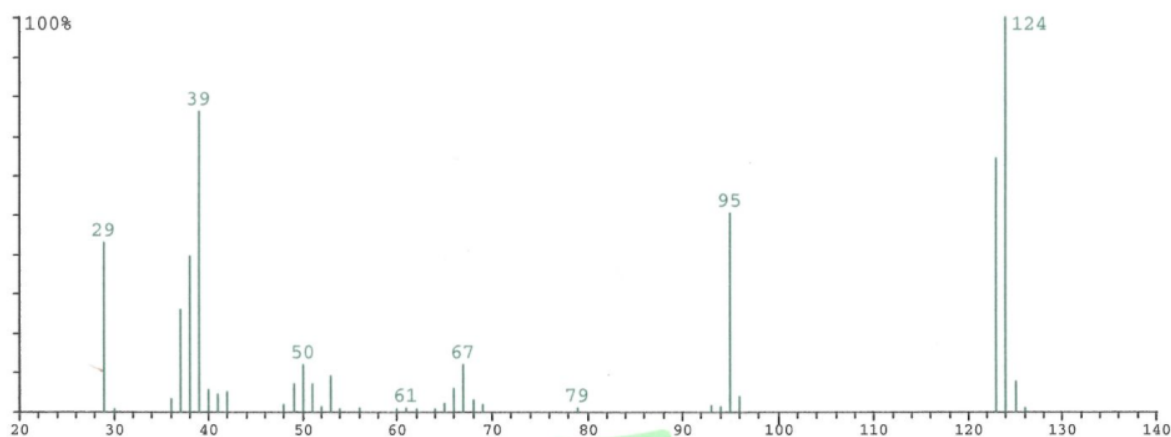
Figure S34. MS spectrum (EI) of 4

4.4 Characterization of methyl 5-formylfuran-2-dicarboxylate (5)

^{1}H NMR (400 MHz, CDCl$_3$): δ = 9,78 ppm (-CHO, 1H, s); 7,25 ppm (-CH arom, 2H, s); 3,92 ppm (-OCH$_3$, 3H, s). ^{13}C NMR (75 MHz, CDCl$_3$): δ = 179,06 ppm (C=O, aldehyde); 158,50 ppm (C=O, ester); 153,95 ppm (C arom (aldehyde side)); 147,72 ppm (C arom (ester side)); 118,78 ppm (CH arom); 52,69 ppm (-OCH$_3$). MS (GC-MS): m/z = 154[M$^+$], 123 (100%).
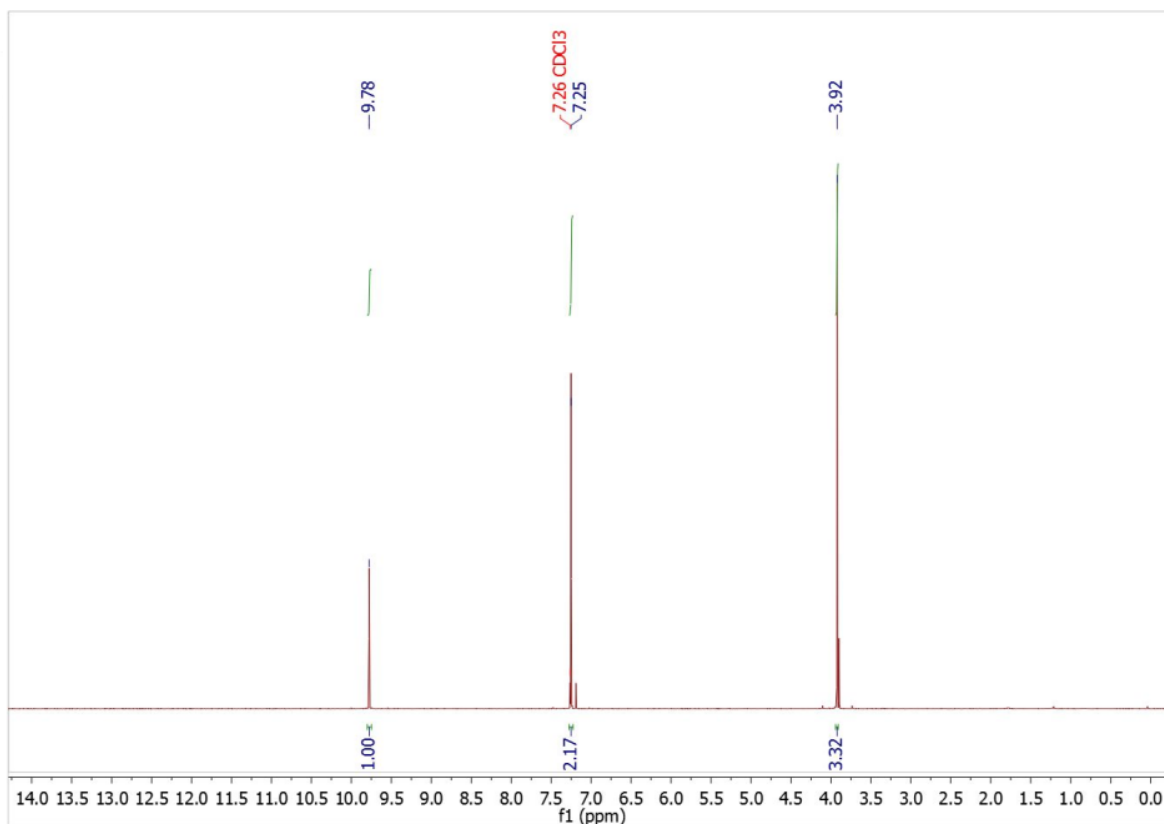
Figure S35. ^{1}H NMR (400 MHz) spectrum of 5 in CDCl$_3$

S25
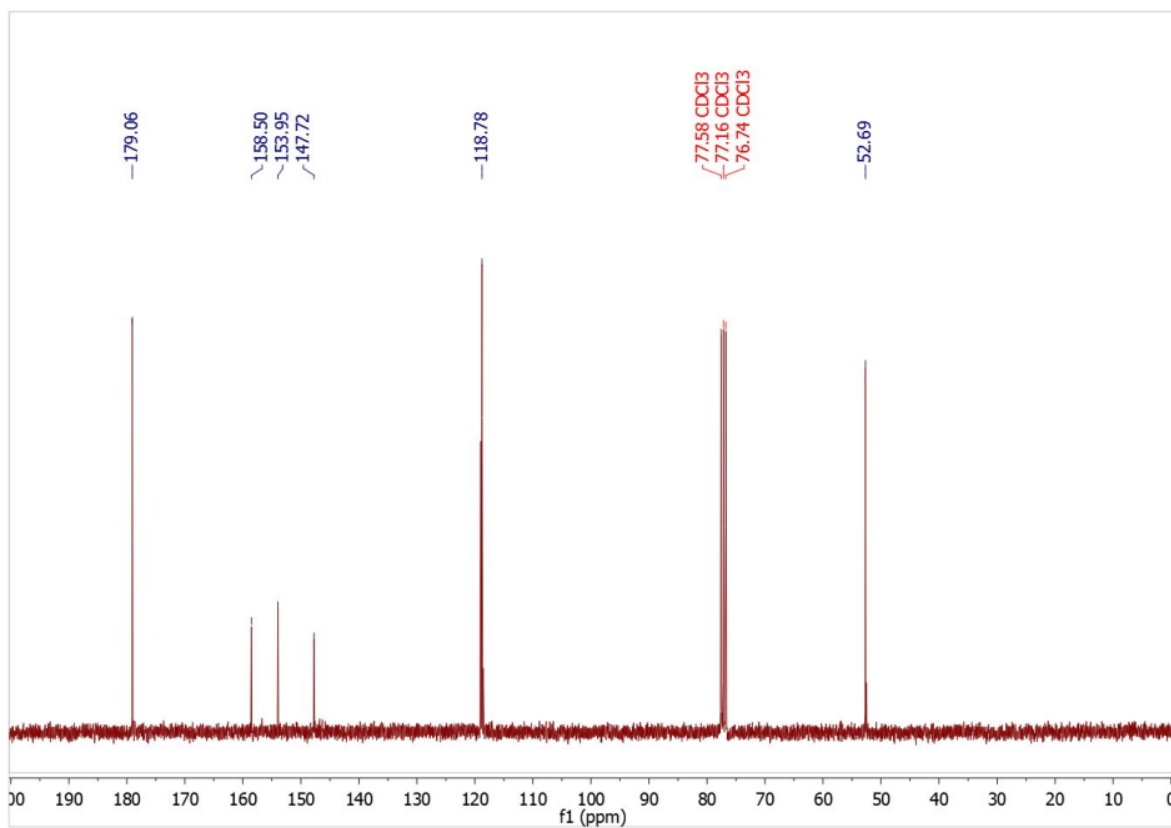
Figure S36. ^{13}C NMR (75 MHz) spectrum of 5 in CDCl$_3$
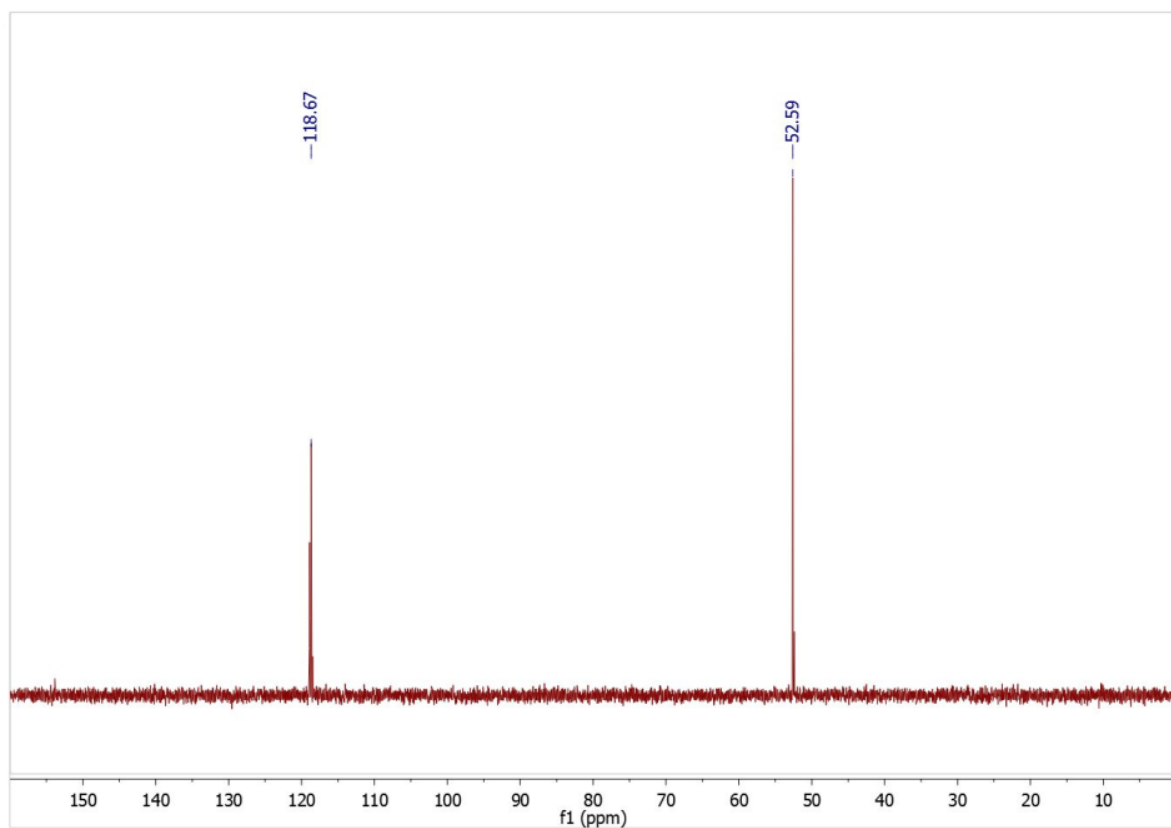
Figure S37. ^{13}C-DEPT NMR (75 MHz) spectrum of 5 in CDCl$_3$
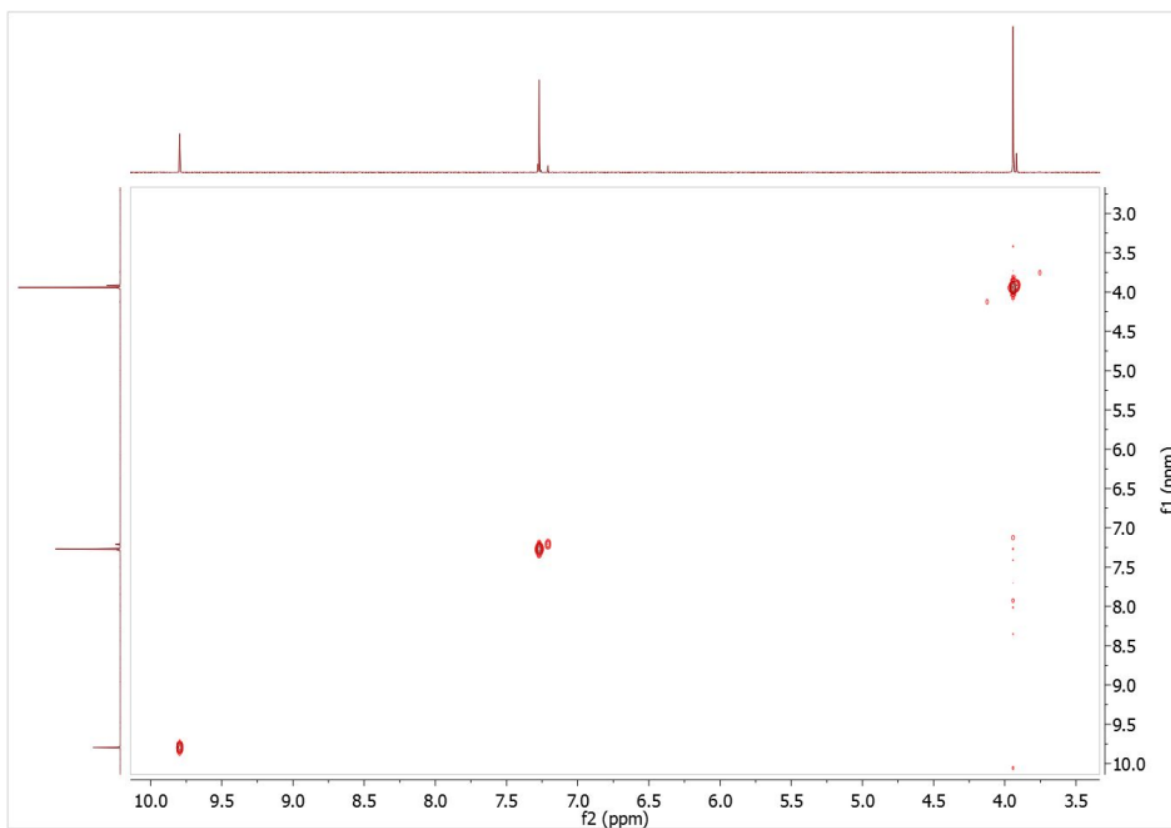
Figure S38. ^{1}H-COSY-NMR (400 MHz) spectrum of 5 in CDCl$_3$
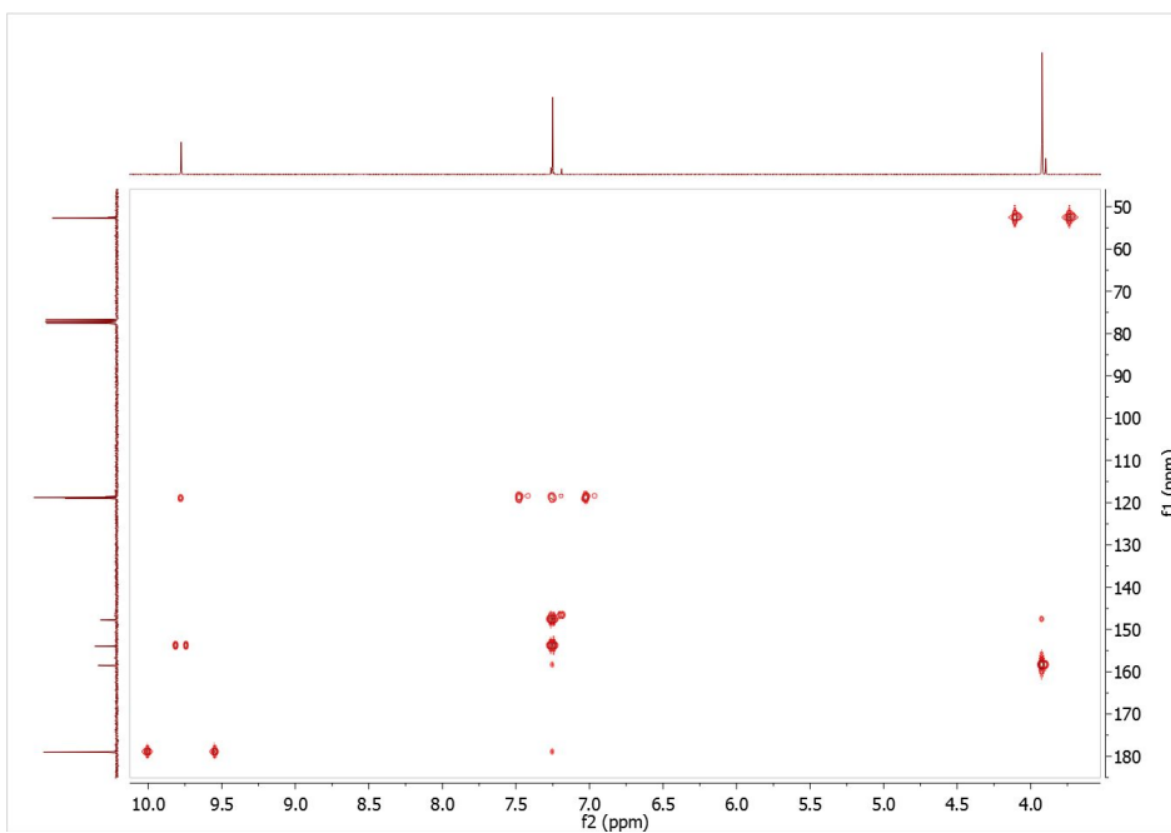
Figure S39. ^{1}H-^{13}C-HMBC- NMR (400 MHz; 101 MHz) spectrum of 5 in CDCl$_3$
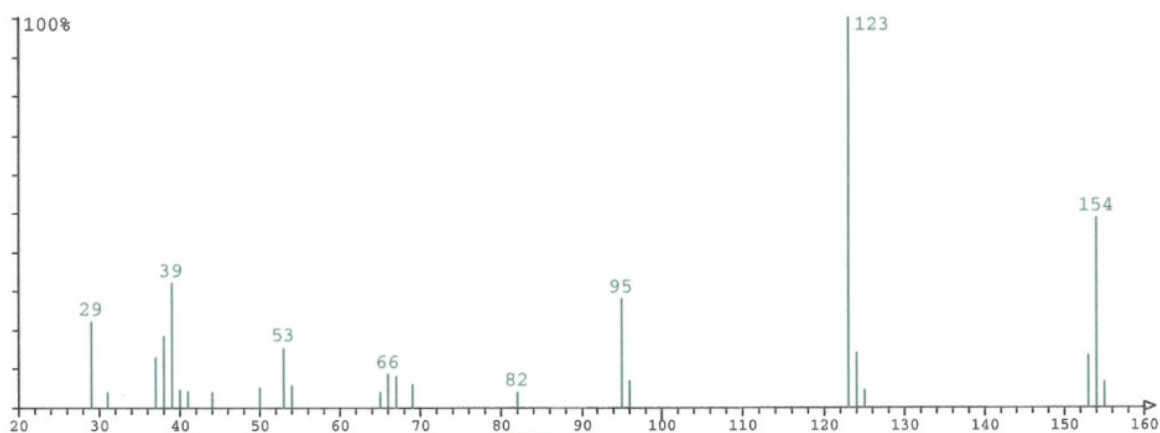
Figure S40. MS spectrum (EI) of 5

5. Determination of the order of reaction – Oxidation of 6 to 7 using Ru@C
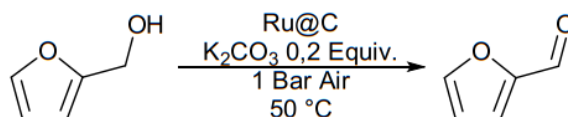
To determine the order of reaction related to the catalyst, the graphic method presented by Bures[S10] was applied. It consists in measuring the reaction profiles when different concentrations of catalyst are used (5 mol %(8,25mmol/L) and 10 mol %(16,5 mmol/L)) (See figure S41). Following, a data treatment is made to apply the method. The kinetic measurements were made using the Mettler Toledo React IR 15.
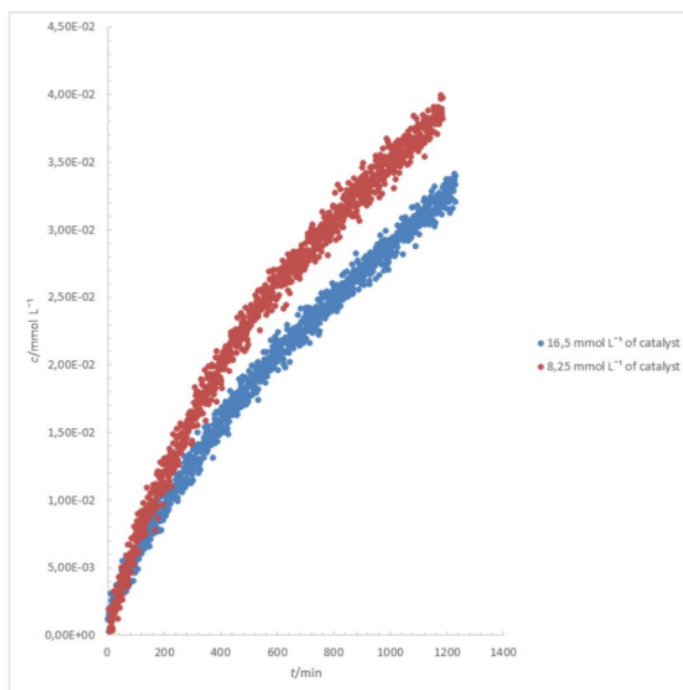
Figure S41. Reaction profiles of the oxidation of **6** at different catalyst concentrations (at 50 °C).

S28

140

The method consists in applying the following equation,

$$[A] = t[cat]^n$$

Where [A] is the concentration of the substrate, t is time, [cat] concentration of the catalyst and n the order of the reaction. $t[cat]^n$ represents a normalization of the time scale. The determination of the order of the reaction is made by changing the value of n simultaneously to both reaction profiles, until an overlapping is reached. Once the overlapping is achieved, the n value represents the order of the reaction.

After normalization of the time scale, complete overlapping was not achieved. (See figure S42). But as the exponent is being approximated to zero, the curves tend to overlap. This leads to the conclusion of an apparent order zero.

(a) Raised to the power of 1 (1. order)

(b) Raised to the power of 0,5 (half order)

(c) Raised to the power of 0,0001 (order approaches 0)
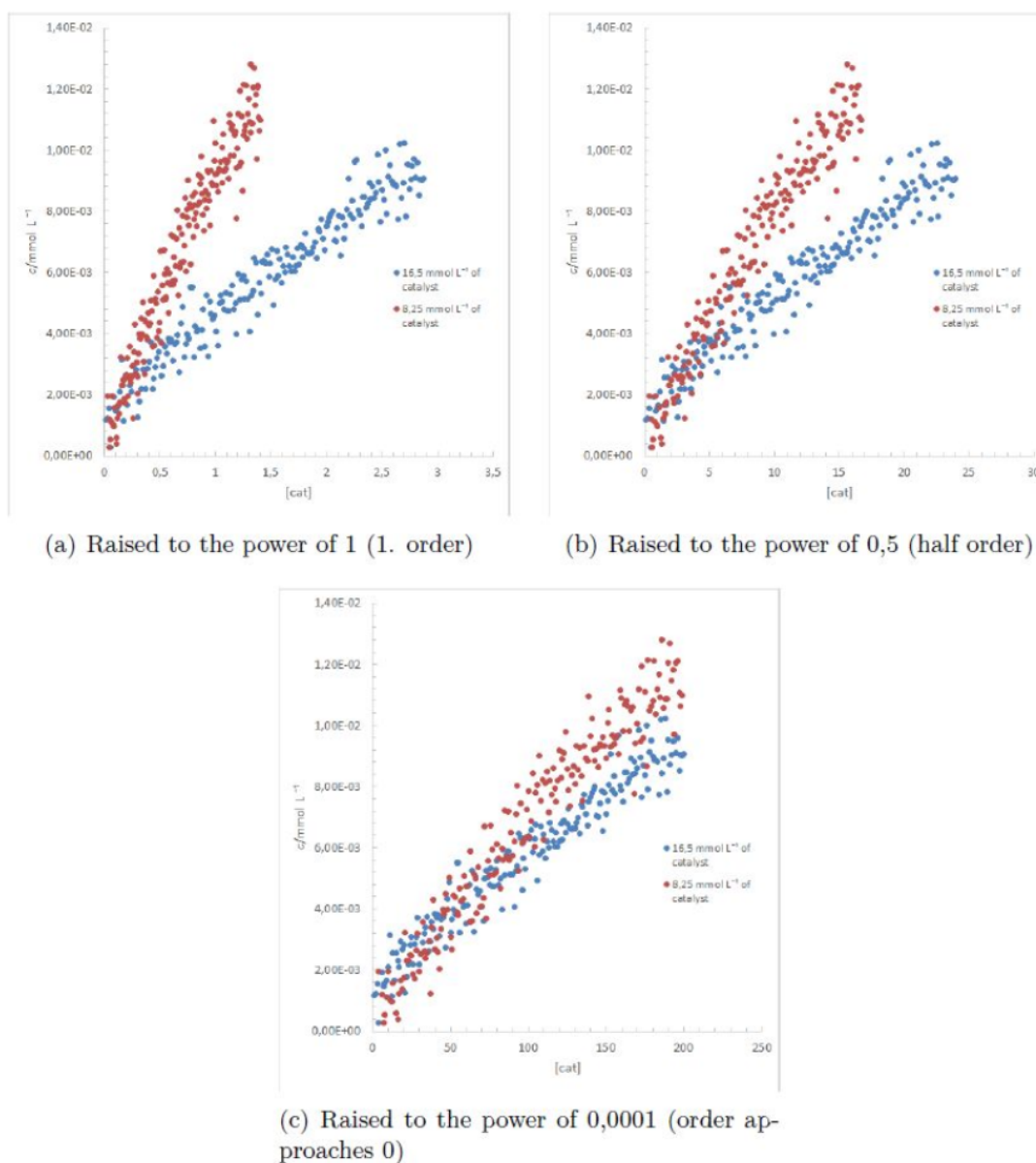
Figure S42. Graphical analysis to determine the reaction order in catalyst of the oxidation of **6** using Bures' Method.

Nie et al. investigated the kinetics of the oxidation of HMF to DFF and found that the reaction follows a Langmuir-Hinshelwood mechanism.[S11] This means that both substrate and dioxygen are adsorbed on the surface of the catalyst. Therein the substrate reacts to the product and water, which are then being desorbed from the surface of the catalyst.

Considering that the reaction is conducted under atmospheric pressure and the solubility of oxygen in MeOH is low at these conditions, the concentration of dioxygen in the solution might be the limiting factor of this reaction. The reaction of the substrate to the product is the rate determining step, as this requires the cleavage of a C-H-bond. Adsorption and desorption are in an equilibrium and very fast, rendering them negligible for reaction rate. This gives the following equation for the reaction rate:

$$\frac{\mathrm{d}\,[\mathrm{P}]}{\mathrm{d}\,t} = k_{\mathrm{R}} \theta_{\mathrm{A}} \theta_{\mathrm{B}}$$

Here [P] is the concentration of the product, kR the reaction constant and θ_{A} and θ_{B} the surface coverage of furfuryl alcohol and dioxygen. With the Langmuir-isotherm the following equation is obtained,

$$\frac{\mathrm{d}\,[\mathrm{P}]}{\mathrm{d}\,t} = \frac{k_{\mathrm{R}} K_{\mathrm{A}} [\mathrm{A}] K_{\mathrm{B}} [\mathrm{B}]}{(1 + K_{\mathrm{A}} [\mathrm{A}] + K_{\mathrm{B}} [\mathrm{B}])^2}$$

where K_{A} and K_{B} are the adsorption constants and [A] and [B] the concentration of furfuryl alcohol and dioxygen in the solution. Under the assumption that the concentration of dioxygen is steady over time, the constants in equation can be combined leading to:

$$\frac{\mathrm{d}\,[\mathrm{P}]}{\mathrm{d}\,t} = \frac{k_{\mathrm{R}}^* [\mathrm{A}]}{(k_{\mathrm{Q}} + K_{\mathrm{A}} [\mathrm{A}])^2}$$

With:

$$k_{\mathrm{R}}^* = k_{\mathrm{R}} K_{\mathrm{A}} K_{\mathrm{B}} [\mathrm{B}] \quad \text{and} \quad k_{\mathrm{Q}} = 1 + K_{\mathrm{B}} [\mathrm{B}]$$

This equation cannot be linearised. Therefore a non-linear regression has to be performed, which is not supported by the used regression software and thus not further investigated in this work. Instead the initial reaction constants for the first 200 min will be examined. The results for the reaction at 50°C are displayed in figure S43.
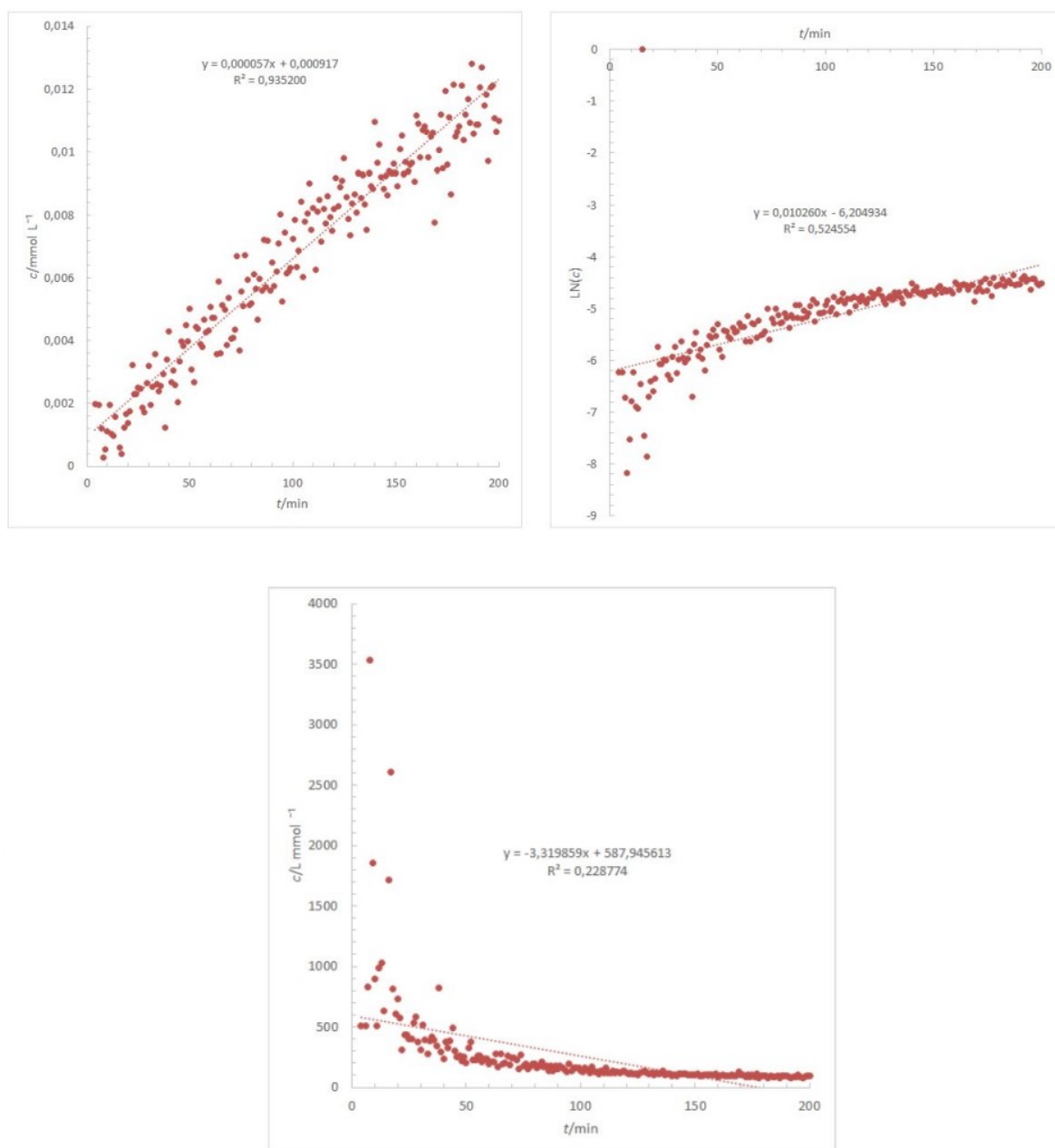
Figure S43. Linearisation for initial kinetics for the ruthenium catalized oxidation of **6** in MeOH at 50°C

6. Calibration curve for the determination of 2-Furfuraldehyde concentration

Solutions of 2-Furfuraldehyde in MeOH at different concentrations were made, and the response in the signal corresponding to the carbonyl group (1678 cm^{-1}) was measured using the React IR 15 (See Table S8).

Table S8   Data for calibration curve

Conc. (M)	Abs.
0,125	0,00714601
0,100	0,00574383
0,090	0,00518098
0,070	0,00399421
0,050	0,00287424
0,030	0,00176651
0,010	0,00051350

With the collected data a calibration curve was made (see Figure S44), which allowed us to confirm that the signal response has a linear response in the concentration range where the kinetic measurements were done.
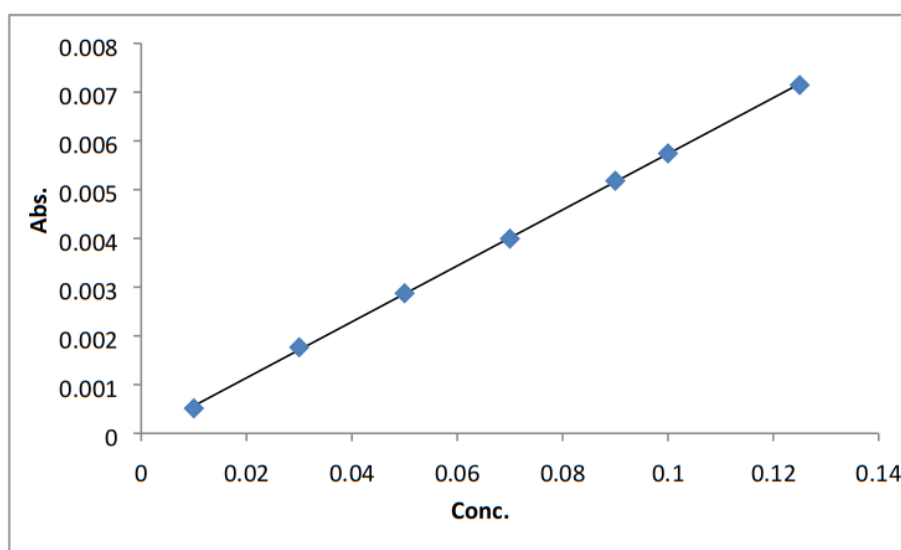
Figure S44. Calibration curve for the determination of 2-Furfuraldehyde concentration in the kinetic experiments

7. Additional EPR spectra
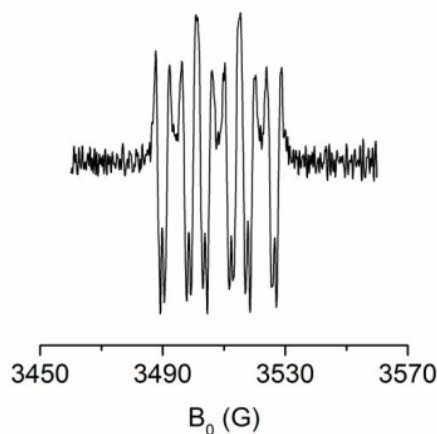
Figure S45. Second derivative EPR spectrum of DMPO-OOH spin adduct displayed in Figure 4 which clearly shows the hyperfine splitting from Hg.

8. Detection of H$_2$

All the reagents(HMF 0,5 mmol; K$_2$CO$_3$ 0,2 equiv.; 50 mg Ru@C(5% mol); 12,5 mg Co$_x$O$_y$@N-C and 4mL MeOH) were added to a 2-neck schlenk tube equipped with a magnetic stirrer. To one neck of the schlenk tube a condenser was coupled and to the top of if a balloon filled with Oxygen was attached. The second neck was sealed with an unused septum. The setup was flushed with oxygen, closed, heated to 50 °C and stirred. At the end of the reaction time (16h) keeping the system closed, a gas sample of the headspace was taken using a gas-tight syringe with a luer lock valve (before taking the sample the syringe was cleaned with 3 charge-discharge cycles of Argon).

The sample was analysed using a gas chromatograph equipped with a TCD detector (Agilent Technologies 6890N, carboxen 1000, external calibration).


```
RetTime Sig Type     Area      Amt/Area    Amount   Grp   Name
 [min]                                     [vol%]
-------|--|------|-----------|-----------|----------|--|----------------
  2.311  2 BP       9.91775  2.44721e-2  2.42708e-1  H2
  8.218  2 VB     3.34906e5  2.12017e-4  71.00590    Ar
 11.328  2             -          -          -       CO
 19.410  2             -          -          -       CH4
 25.864  2 PB    3088.99878  1.69146e-4  5.22493e-1  CO2

Totals :                                 71.77110
```
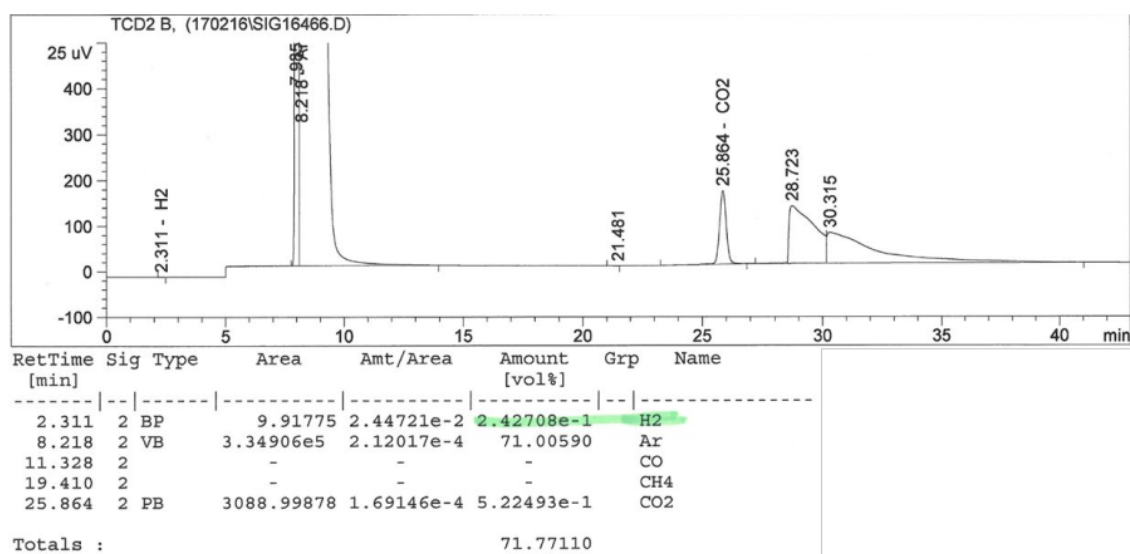
Figure S46. Analysis of the gas phase by GC-TCD

S33

9. References

(S1)   Casanovas, J.; Ricart, J. M. ; Rubio, J. ; Illas, E.; Jiménez-Mateos, J. M. *J. Am. Chem. Soc.* **1996**, *118,* 8071-8076.

(S2)   Pels, J. R.; Kapteijn, F.; Moulijn, J. A.; Zhu, Q.; Thomas, K. M. *Carbon*, **1995**, *33,* 1641-1653.

(S3)   Grünert, W.; Feldhaus, R.; Anders, K.; Shipiro, E. S.; Antoshin, G. V.; Minachev, K. M. *J. Electron. Spectrosc. Relat. Phenom.* **1986**, *40,* 187-192.

(S4)   Biesinger, M.C, Payne, B.P., Grosvenor, A.P., Lau, L.W.M., Gerson, A.R, Smart, R.St.C., Appl.Surf.Sci., **2011,** 257, 2717

(S5)   Angelov, S., Zhecheva, E. ; Stoyanova, R.; Atanasov, M.   *J. Phys. Chem. Solids,* **1990,** *51,* 1157.

(S6)   Dutta, P.; Seehra, M.S.; Thota, S; Kumar, J.   *J. Phys.: Condens. Matter*, **2008**, *20,* 15218

(S7)   Brückner, A.; Martin, A.; Steinfeldt, N.; Wolf, G.-U.; Lücke, B. *J. Chem. Soc., Faraday Trans.***1996,** *92,* 4257-4263.

(S8)   Wdowik, U. D.; Legut, D. *J. Phys. Chem. Solids,* **2008,** *69,* 1698-1703.

(S9)   Campbel, F. C.; "Elements of metallurgy and engineering alloys", Materials Park, Ohio: ASM International 2008, Chapter 29, p. 557.

(S10)   J. Bures, *Angew. Chem., Int. Ed.*, 2016, **55**, 2028-2031.

(S11)   J. Nie, J. Xie and H. Liu, *Journal of Catalysis*, 2013, **301**, 83-91

8.2 Paper 2

Oxidative Esterification of %-Hydroxymethylfurfural under Flow Conditions Using a Bimetallic Co/Ru Catalyst

Abel Salazar, Alexander Linke, Reinhard Eckelt, Dr. Antje Quade, Prof. Udo Kragl and Dr. Esteban Mejia.
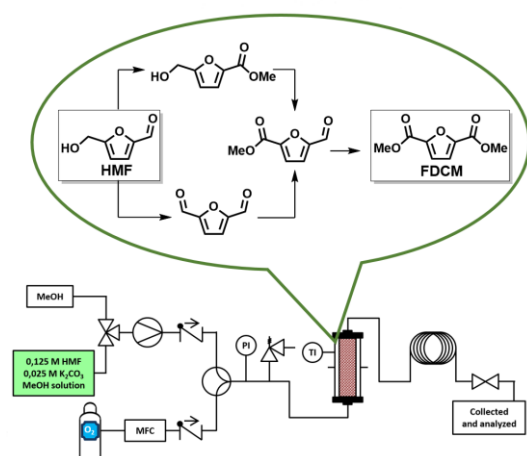
Synopsis

The first oxidative esterification of HMF under flow regime was achieved with excellent conversion (98 %) and good selectivity towards FDCM (57 %) using a heterogeneous bimetallic catalyst mixture based on Co_xO_y and RuO_x nanoparticles supported on mesoporous carbon. Overall, under flow regime, a >15-fold increase on the production of FDCM was obtained in comparison to batch conditions.

Oxidative Esterification of 5-Hydroxymethylfurfural under Flow Conditions Using a Bimetallic Co/Ru Catalyst

Abel Salazar,[a] Alexander Linke,[a] Reinhard Eckelt,[a] Antje Quade,[b] Udo Kragl,[c, d] and Esteban Mejía*[a]

Furanic di-carboxylate derivatives of 5-Hydroxymethylfurfural (HMF) are nowadays important in the polymer industry as they are used as building blocks for bio-based polyesters. The high reactivity of HMF compels to avoid harsh synthetic conditions. Therefore, developing mild catalytic processes for its selective oxidation is a challenging task. Herein, we report the first oxidative esterification of HMF to dimethyl furan-2,5-dicarboxylate (FDCM) under flow conditions using oxygen as oxidant.

For that purpose, a new series of nitrogen-doped carbon-supported bimetallic Co/Ru heterogeneous catalysts were prepared and characterized by XRD, XPS and N_2 physisorption. These analyses revealed that the porosity of the materials and order of impregnation of the metals to the carbon supports lead to varying catalytic activities. Under optimized conditions the flow reactor showed a 15-fold increase on the production of FDCM compared to batch conditions.

Introduction

Nowadays, obtaining platform chemicals from renewable sources is a highly relevant topic due to the necessity to reduce society's dependence in oil-derived resources. The use of biomass-derived platform chemicals is a step forward in achieving a sustainable circular economy,[1] bringing molecules like 5-hydroxymethylfurfural (HMF, **1**) to the spotlight.[2] HMF is the basis of furanic polymers,[3] where polyethylene furanoate (PEF) stands as a promising substitute of polyethylene terephthalate (PET), as it can be produced entirely from renewable sources.[4]

The biomass-based production of PEF (Scheme 1) commonly starts with acidic or enzymatic hydrolysis of cellulose to obtain C_6-sugars (e.g. glucose, fructose) from which dimethyl-2,5-furandicarboxylate (FDCM, **2**) and ethylenglycol (EG) can be synthesized. HMF is obtained by the dehydration of sugars

[a] A. Salazar, A. Linke, R. Eckelt, Dr. E. Mejía
Leibniz-Institute für Katalyse e. V.
Albert-Einstein-Straße 29A
18059 Rostock (Germany)
E-mail: esteban.mejia@catalysis.de
[b] Dr. A. Quade
Leibniz-Institut für Plasmaforschung und Technologie e. V.
Felix-Hausdorff-Str. 2
17489 Greifswald (Germany)
[c] Prof. U. Kragl
Institut für Chemie, Technische Chemie
Universität Rostock
Albert-Einstein-Straße 3A
18059 Rostock (Germany)
[d] Prof. U. Kragl
Department Life, Light and Matter
Universität Rostock
18051 Rostock (Germany)

Scheme 1. Production of polyethylene furanoate (PEF) from biomass.

(preferably fructose);[5] FDCM can be obtained from the oxidative esterification of HMF in MeOH, while EtOH is obtained from the fermentation of sugars,[6] and dehydrated to produce ethylene.[7] The latter can be converted into EG by various established industrial oxidation methods. Finally, PEF is synthesized by a 2-stage step-growth polymerization between FDCM and EG.[8]

In order to make PEF economically viable, the production of FDCM or its analogs (e.g. 2,5-furandicarboxilic acid, FDCA) must be improved, either by catalyst development or by using new synthetic methods. FDCM is a more promising monomer than FDCA since it is easier to purify, is more stable under polymerization conditions and shows increased reaction rates.[8] Taking this into consideration, we focused our efforts towards the synthesis of FDCM from HMF.

The use of oxygen gas as terminal oxidant in organic synthesis is an attractive goal as it is readily available and non-toxic.[9] Nevertheless, its usage has had limited spread due to safety concerns and the poor solubility of O_2 in most solvents.[10]

Microflow technologies are gaining increasing popularity in organic synthesis due to its improved safety, and the possibility to precisely control mass-transport and processing parameters. Hence, microflow reactors represent a safe alternative to batch systems since the smaller reactor volumes minimize the severity of an accident. At the same time, the accumulation of hazardous/unstable intermediaries is minimized. Moreover, the possibility to accurately dose gaseous reactants and the lack of a headspace (virtually unavoidable under batch conditions) reduce significantly the risks of accidents.[11] As a consequence of the reduced size components, different physical parameters can be optimized to a higher level under microflow conditions, compared to the standard laboratory and industrial batch conditions (e.g. mass and heat transfer, mixing, etc.).[12] More importantly, mass transfer limitations are reduced to the minimum,[13] which helps to circumvent the restrictions of working with low solubility gases like oxygen.[14] Last, but not least, the development of processes under microflow conditions allows the possibility of a scale-up with relative ease.[15]

Herein we report the development and characterization of carbon-supported bimetallic cobalt/ruthenium catalysts and their application in the first oxidative esterification of HMF under flow conditions, to produce FDCM with very high conversion and good selectivity.
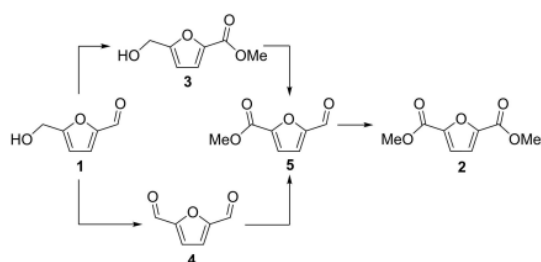
Results and Discussion

As shown in Scheme 2, the oxidative esterification of HMF (1) to produce FDCM (2) can be achieved in a divergent, multistep process. HMF is first converted either to methyl 5-(hydroxymethyl)furan-2-carboxylate (3) or to furan-2,5-dicarbaldehyde (4). Both 3 and 4 can be converted to methyl 5-formylfuran-2-dicarboxylate (5). Finally, aldehyde oxidative esterification leads to the desired product (2). Both conversion and selectivity depend on the catalyst used and its activity, as previously demonstrated in the oxidation of HMF to FDCA.[16]

In a previous work, we reported the aerobic oxidative esterification of 1 to 2 using a mixture of carbon-supported nitrogen-doped cobalt and commercial ruthenium catalysts (Co_xO_y–N@C and Ru@C) in a batch reactor.[17] In order to incorporate both metals in the same support, new powdered catalysts were prepared and explorative tests were done. The results were promising: > 99% of HMF conversion was achieved with a selectivity of 38% of 2, 47% of 3, and 8% of 5 (see Supp. Info). With this in mind and knowing the limitations of batch reactors, we moved on to perform the reaction in a flow regime.

The reactor setup is presented in Scheme 3. It begins with having both gas and liquid phases separated. In the liquid part, a selector valve allows to choose the feed from either pure solvent or substrate solution. The two phases (gas and liquid) are then mixed before going into the reactor. The mixer is based on the multilamination principle, providing the ideal conditions for gas/liquid mixing.[13] The setup contains a pressure gauge as well as a temperature indicator. The reactor is heated with a fitted thermostat. Additionally, for safety control, a pressure release valve was used. At the reactor outlet the product mixture is cooled down in a water/ice bath, and sampled for analysis.

When powdered catalysts (analogous to those used in the aforementioned batch experiments) were used in the microflow reactor, technical problems arose. The fine catalyst particles packed in the cartridge led to a pressure increase in the system above the maximum input pressure of oxygen. As a consequence, oxygen could not be fed into the system anymore. In an attempt to avoid this problem, the powdered catalyst was "diluted" with glass beads and glass wool, alas, unsuccessfully. Layering of the catalyst with glass spheres lead to a slight improvement, although the catalyst particles were too small to be contained in the cartridge and small amounts of catalyst were collected along with the product at the system outlet. Increased temperatures shown to be detrimental as well since 1 decomposes above 150 °C.

Therefore, a new series of nitrogen-doped Co and Ru-based catalysts was synthesized using different types of carbon supports, and changing the order in which the metals and ligands are impregnated into them. We selected carbon particles of irregular shape (−20 + 40 mesh) and cylindrical pellets (~0,8 mm diameter), which will be called from now on *C-irregular* and *C-pellets*, respectively (See figure 1). This simple changes in the supports' morphology allowed us to operate the reactor under the desired conditions and prevent catalyst loss.

Scheme 2. Divergent reaction pathways for the oxidative esterification of HMF (1) to produce FDCM (2).

150
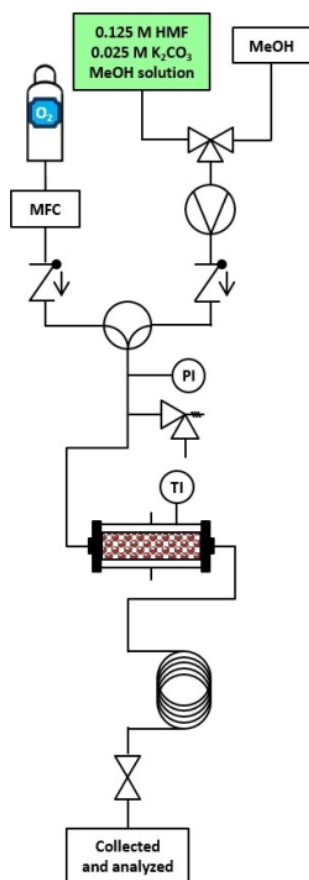
Scheme 3. Flow diagram of the microreactor setup used for the synthesis of FDCM (**2**) from HMF (**1**) under aerobic conditions.

Figure 1. SEM images of the carbon supports used. (A) particles of irregular shape (−20+40 mesh, C-irregular) and (B) cylindrical pellets (∼0,8 mm diameter, C-pellets).

Table 1. Catalyst screening for the oxidative esterification of HMF (1) under flow conditions.

Entry[a]	Catalyst	Conv. [%]	Product selectivity [%]				
			2	3	4	5	Others
1	Co$_x$O$_y$–N@C-pellets	57	4	72	12	-	12
2	RuO$_x$–N@C-pellets	60	4	–	66	25	5
3	Co$_x$O$_y$–N + RuO$_x$–N@C-pellets	44	5	46	20	–	29
4	RuO$_x$–N + Co$_x$O$_y$–N@C-pellets	66	15	52	11	–	22
5	Co$_x$O$_y$–N@C-irregular	92	18	63	4	–	15
6	RuO$_x$–N@C-irregular	35	3	-	54	11	31
7	Co$_x$O$_y$–N + RuO$_x$–N@C-irregular	98	57	20	1	1	21
8	RuO$_x$–N + Co$_x$O$_y$–N@C-irregular	73	27	45	8	–	20
9	Mixture entry 5 – entry 6	62	15	50	11	1	23

[a] Reaction conditions: 600 mg catalyst loading, 0.2 mL/min of a MeOH solution of 0.125 M HMF and 0.025 M K$_2$CO$_3$, 1,4 mL/min of oxygen, reactor temperature: 62 °C, autogenous pressure, residence time in reactor: 10 min.

The catalyst screening was focused on maximizing the conversion of **1** and the selectivity towards **2** above intermediates **3**, **4** and **5**. As presented in Table 1, when the cobalt-based catalysts were used (entries 1 and 5) selectivity (up to 73%) towards **3** was observed for both types of supports. The catalyst Co$_x$O$_y$–N@C-irregular (entry 5) showed an excellent conversion of **1** (92%) although only with poor selectivity towards **2** (18%). In comparison, Co$_x$O$_y$–N@C-pellets (entry 1) only showed a modest conversion (57%) and very poor selectivity (4%) towards **2**. In the case of the ruthenium-based catalysts, (entries 2 and 6), high selectivity towards **4** was observed. Contrary to the cobalt catalysts, conversion up to 60% was obtained with RuO$_x$–N@C-pellets (entry 2) and only 35% with RuO$_x$–N@C-irregular (entry 6). The latter also showed the highest amount of side products in the catalyst screening (up to 31%). For the cobalt catalysts, the best support seemed to be C-irregular and surprisingly, for the ruthenium, C-pellets. Up to this point, the reactivity and selectivity of the catalysts is similar

to what was observed previously in the batch reactor.[17] It must be highlighted that the nitrogen doping has no detrimental effect on the catalytic activity of the ruthenium catalysts. While commercial Ru@C is commonly prepared by reduction in H$_2$ atmosphere,[18] our RuO$_x$–N@C catalyst was made by pyrolysis under argon atmosphere, analogous to Co$_x$O$_y$–N@C. This change in the preparation method simplifies the synthesis of

the catalysts, removing the difficulty of preparing a bimetallic catalyst with different oxidation states. Importantly, the morphology changes of the support didn't affect the catalytic activity.

When a mixture of Co_xO_y–N and RuO_x–N@C catalysts was used (entries 3 and 7), remarkable differences in conversion and selectivity were observed. Using C-pellets as support (entry 3) a conversion of only 44% was observed, with selectivity toward products **3** and **4** of 46% and 20% respectively. On other side, C-irregular (entry 7) as support gave the best results of the catalyst screening, where conversion up to 98% was achieved with a selectivity of 57% towards the desired product **2**. In addition, RuO_x–N + Co_xO_y–N@C catalysts (entries 4 and 8) show moderate to good conversions, 66% for C-pellets (entry 4) and 73% for C-Irregular (entry 8) with selectivity of 52% and 45% for **3** and 15% and 27% for **2** respectively. We also checked the catalytic performance of a physical mixture of Co_xO_y–N@C-irregular and RuO_x–N@C-irregular (entry 9). 62% conversion was obtained with selectivity of 50% and 15% towards **3** and **2** respectively. This result confirms that the presence of cobalt and ruthenium in the same support (entry 7) results in an improvement in comparison to the test performed with each metal by its own, the metal amount used was reduced to the half and 62% conversion was obtained, with 50% and 15% selectivity towards **3** and **2** respectively, confirming that the synergy observed in batch reactions[17] is also present under a flow regime.

The reaction progress for the most promising catalyst, (Co_xO_y–N + RuO_x–N@C-irregular), is shown in Figure 2. Remarkably, the selectivity towards **2** increases with time. Within the timeframe of the experiment, a steady state in conversion (> 95% conversion of **1** after 100 min) was achieved, alas, with modest selectivity. Selectivity towards **3** is at its highest after 40 minutes (>35%) and constantly decreases to 20% after 180 minutes. Similar behavior is observed for **4** and other by-products. Also, an unexpected product (**11**) (Figure 2 and scheme 4) was formed in relevant amounts (up to 20%).
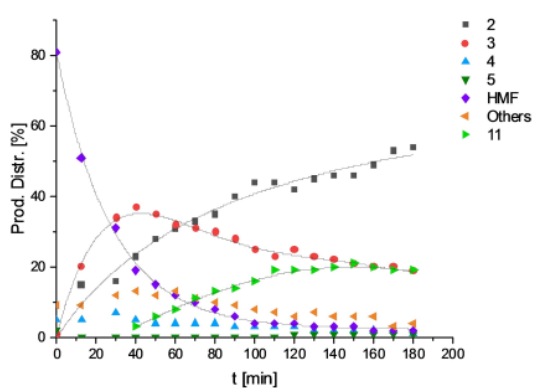
Figure 2. Reaction progress over time for the oxidative esterification of HMF using Co_xO_y–N + RuO_x–N@C-irregular as catalyst.
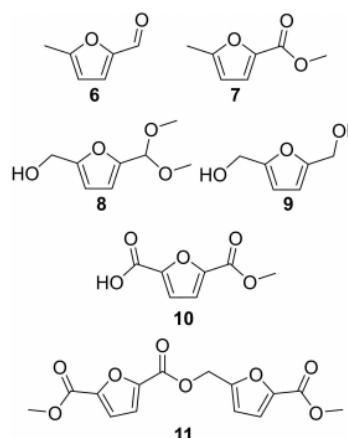
Scheme 4. By-products detected during the catalyst screening for the oxidative esterification of HMF under flow conditions.

As shown in table 1, side products could be detected in all experiments (labeled as "Others"). Those compounds that could be identified compounds are presented in Scheme 4.

5-methylfuran-2-carbaldehyde (**6**) is present in the starting solution of HMF, presumably as a decomposition product. From **6**, Methyl 5-methylfuran-2-carboxylate (**7**) would be obtained under the chosen reaction conditions. (5-(dimethoxymethyl) furan-2-yl)methanol (**8**) could be detected in the first samples collected in each experiment, indicating the acidic character of the catalysts at the first stages of the experiments, fostering the formation of acetals. Furan-2,5-diyldimethanol (**9**) is a side product arising from the eventual hydrogenation of **1** performed by the ruthenium catalysts. As we demonstrated before,[17] hydrogen gas was detected in the headspace of batch reactions, supporting this hypothesis. A mono-ester derivative of FDCA was detected, 5-(methoxycarbonyl)furan-2-carboxylic acid (**10**), which can arise from the partial hydrolysis of **2**. A compound with molecular mass and fragmentation patterns fitting to 2-((5-(methoxycarbonyl)furan-2-yl)methyl) 5-methyl furan-2,5-dicarboxylate (**11**) was also detected, suggesting that an esterification between **3** and **5** is possible under the reaction conditions.

As a general remark, the cobalt-containing catalysts having C-irregular as support are more active in the conversion of **1** (entries 5, 7 and 8) with a higher selectivity towards **2**. In the search for an explanation to this fact N_2 Physisorption analysis (BET measurements) were done on the raw supports and to the prepared catalysts (see Table 2).

The results show a marked difference in the surface area of each raw support (entries 1 and 6). C-pellets have more than twice the surface area of C-irregular, with 1178.3 m^2/g and 562.7 m^2/g, respectively. After the first impregnation and pyrolysis, the surface area is dramatically reduced: more than 40% for the C-pellets catalysts (entries 2 and 3), more than 75% for Co_xO_y–N@C-irregular (entry 7) and 60% for the RuO_x–N@C-

Table 2. N₂ Physisorption analysis for catalysts and supports.

Entry	Catalyst	Surface area [m²/g]	Micropore area [m²/g]	External surface area [m²/g]
1	C-pellets	1178.3	1125.2	53.1
2	Co$_x$O$_y$–N@C-pellets	678.9	647.5	31.4
3	RuO$_x$–N@C-pellets	695.8	660.2	35.6
4	Co$_x$O$_y$–N + RuO$_x$–N@C-pellets	546.9	513.2	33.7
5	RuO$_x$–N + Co$_x$O$_y$–N@C-pellets	463.7	436.8	26.9
6	C-irregular	562.7	372.8	189.9
7	Co$_x$O$_y$–N@C-irregular	128.5	5.1	123.4
8	RuO$_x$–N@C-irregular	226.9	76.5	150.4
9	Co$_x$O$_y$–N + RuO$_x$–N@C-irregular	174.9	51.4	123.5
10	RuO$_x$–N + Co$_x$O$_y$–N@C-irregular	129.4	29.2	100.2

irregular catalyst (entry 8). The measurements after the second impregnation and pyrolysis show the same trend as in the case of the C-pellet catalysts (entries 4 and 5). Co$_x$O$_y$–N + RuO$_x$–N@C-pellets loses 19% of the starting surface area while RuO$_x$–N + Co$_x$O$_y$–N@C-pellets loses 33%. In contrast, the surface area of RuO$_x$–N + Co$_x$O$_y$–N@C-irregular is reduced by 43% (entry 10). Surprisingly, Co$_x$O$_y$–N + RuO$_x$–N@C-irregular (entry 9) presents an increase of almost 40% of the surface area compared to the starting material (Co$_x$O$_y$–N@C-irregular).

When the porosity of the materials (micropore area and external surface area) was studied, it can be observed that the C-pellet materials present a micropore:mesopore ratio of about 18:1 in comparison to 1:3 for the C-irregular ones. This is an important feature because in the conditions in which the experiments were performed porosity plays an important role in the diffusion of the substrate in the catalysts, which has a direct consequence on the conversion.[19] The better reactivity of C-irregular catalysts can be correlated with the abundance of mesopores in its structure in comparison to the C-pellet catalysts. The surface area provided by mesopores in the C-irregular materials is evidently higher, almost 4 times more than the C-pellets materials. Having a residence time of only 10 min, it is important that the substrate can easily diffuse into the catalysts' pores. It is know that micropores don't take part in the catalytic conversion of bulky molecules because the active sites within them cannot be reached by the substrates This renders them useless and therefore constitute a non-active surface in the catalysts.[20] For the residence time set in our experiments, the presence of mesopores is an important feature, as they are accessible to the bulky substrates and make the process less diffusion-limited.[21]

Additionally, XRD measurements of all the catalysts were done (See Supp. Info). Diffraction patterns of the all the samples supported on C-pellets show broad bands and low intensity peaks, which is evidence of a lack of crystallinity.[22] Conversely, the C-irregular catalysts show crystallinity. The Co$_x$O$_y$–N@C-irregular shows the same diffraction pattern as the Co$_x$O$_y$–N@C powder catalysts we previously used,[17,23] meaning that the particles in the new catalyst are similar to the powder analogue.

Co$_x$O$_y$–N@C-irregular contains metallic cobalt, CoO and Co₃O₄. More interestingly, in the Co$_x$O$_y$–N + RuO$_x$–N@C-irregular catalyst it was possible to confirm the presence of metallic cobalt, but it was not possible to assign any refractions. Also, the diffraction pattern is not comparable with RuO$_x$–N + Co$_x$O$_y$–N@C-irregular. This shows that the order of addition of the metals has an influence in the type of catalyst obtained. The metal species present in both Co$_x$O$_y$–N + RuO$_x$–N@C-irregular and RuO$_x$–N + Co$_x$O$_y$–N@C-irregular are different.

In order gain a better understanding of the nature of the surface of the C-irregular catalysts, XPS characterization was performed. As expected, 3 different species of nitrogen were found. Pyridinic N-Metal, Pyrrolic N and Ammonia N (See Table 3).

The data in table 3 shows that we effectively produced nitrogen-doped catalysts and that the pyridinic nitrogen atoms bound to metal species is the more abundant type, an important fact that improves catalytic activity.[24]

Two ruthenium species are present at the surface, since not only Ru⁰ but also Ru⁴⁺ was detected. All the samples contained mainly ~70% Ru⁰ and ~30% Ru⁴⁺. On the other side; using the Co 2p-peak shapes and the modified Auger parameter the existence of Co³⁺ in Co$_x$O$_y$–N@C-irregular, and both Co²⁺ and Co³⁺ in the bimetallic catalysts can be anticipated. Due to the low content of cobalt, its quantification was not possible due to the low signal-to-noise ratio.

A comparison between bulk elemental analysis and the elemental analysis of the surface measured by XPS, shows that the metallic species are located mostly at the surface of the material (see Table 4).

Since Co$_x$O$_y$–N@C-irregular is the starting material to synthesize Co$_x$O$_y$–N + RuO$_x$–N@C-irregular, the comparison between both elemental analyses (entries 1 and 3) allow us to see

Table 3. Nitrogen species detected by XPS.

Entry	Catalyst	Nitrogen species [%]		
		Pyridinic N	Pyrrolic N	Ammon N
1	Co$_x$O$_y$–N@C-irregular	58	35	7
2	RuO$_x$–N@C-irregular	39	40	21
3	Co$_x$O$_y$–N + RuO$_x$–N@C-irregular	40	37	23
4	RuO$_x$–N + Co$_x$O$_y$–N@C-irregular	46	34	20

Table 4. Comparison of elemental analysis.

Entry	Catalyst	Location	Metal [wt%]	
			Co	Ru
1	Co$_x$O$_y$–N@C-irregular	bulk	2.23	–
		surface	2.78	–
2	RuO$_x$–N@C-irregular	bulk	–	2.46
		surface	–	12.94
3	Co$_x$O$_y$–N + RuO$_x$–N@C-irregular	bulk	1.70	2.34
		surface	5.40	9.27
4	RuO$_x$–N + Co$_x$O$_y$–N@C-irregular	bulk	1.58	2.17
		surface	5.24	11.76

[a] Surface elemental analysis derived from identification of >99,6% of atoms by XPS.

a migration process of the cobalt from the bulk to the surface of the material, most likely fostered by the incorporation of ruthenium. This result is supported by the increase in porosity observed for this catalyst: the mesoporous quantity remains similar but the micropore quantity increases in relation to the starting material. The migration of cobalt (Ostwald ripening) through the bulk creates new micropores.[25] A similar process was observed by Jones et al. in which, during pyrolysis of Co/Cu bimetallic catalysts, copper atoms migrate through the bulk to form Co-core Cu-shell particles increasing the amount of micropores in the material.[26]

This migration process is not observed for ruthenium in the synthesis of RuO_x–N + Co_xO_y–N@C-irregular. As can be seen in entries 2, 3 and 4, the ruthenium atoms remain mostly at the surface of the material. In comparison, the cobalt in Co_xO_y–N@C-irregular is distributed in a homogenous fashion. This difference is due to the temperature at which the pyrolysis is carried out; the Co atoms have enough energy to migrate in the bulk (i.e., lower Tamman temperature) but not the Ru ones.[27]

Performing the reaction under flow regime proved to be an improvement: in batch conditions full conversion to FDCM (**2**) is achieved in 18 h, representing a production of 0.03 mmol/h; in comparison, under flow conditions (Table 2 entry 6) in the last hour of the experiment > 96% conversion of HMF (**1**) was obtained (1.44 mmol/h) and a selectivity to **2** of 44–54%, which represents a production of 0.47 mmol/h. Hence, the production of **2** under flow could be increased > 15-fold compared to batch conditions.

Conclusions

The chemical modification of HMF is a challenge due to its inherent reactivity. Herewith, we report the oxidative esterification of HMF to FDCM under flow regime showing excellent conversion (98%) and good selectivity towards FDCM (57%). We were able to circumvent technical issues, by changing the catalyst support, identifying Co_xO_y–N + RuO_x–N@C-irregular as the best catalyst. The higher mesoporous surface related to the C-irregular catalysts is an important feature that provides improvement in conversion and selectivity.

Overall, under flow regime, a > 15-fold increase on the production of FDCM was obtained in comparison to batch conditions. To the best of our knowledge this is the first report of oxidative esterification of HMF to FDCM under flow conditions. Further optimization of the process and studies to understand the nature of the supported catalysts is currently ongoing in our labs.

We hope that the findings in this paper provide a source of inspiration for the implementation of micro flow conditions in traditional organic transformations, but especially in the chemical modification of biomass-derived substrates.

Experimental Section

General experimental details

5-hydroxymethylfurfural (98%) was purchased from Fluorochem Ltd. and kept stored in a fridge. Methanol was purchased from Fischer Scientific and used as received. Oxygen (99. 99%) was purchased from Linde. Co(OAc)$_2$·4H2O was purchased from Abcr GmbH. Di-μ-chlorobi(p-cymene)chlororuthenium(II) (98%) was purchased from Acros Organics. 1,10-Phenanthroline was purchased from SIGMA-ALDRICH. The activated carbons, −20 + 40 mesh (Art. Nr. 45478) and 0.8 mm pellets (Art. Nr. L16334), were purchased from Alfa Aesar. The pyrolisis of the catalyst precursors was carried out in Centurion™ Neytech Qex Vacuum Furnace following the procedure previously reported by Beller et al.[28] ^{1}H and ^{13}C NMR spectra were recorded in $CDCl_3$ and with a Bruker Avance 300 with a QNP probe head (^{1}H: 300 MHz; ^{13}C: 75 MHz), or with a Bruker Avance 400 (^{1}H: 400 MHz; ^{13}C: 100 MHz). The calibration of the spectra was carried out using residual solvent shifts ($CDCl_3$, ^{1}H = 7.26, ^{13}C = 77.16) and were reported as parts per million relative to $SiMe_4$. All the NMR samples were measured at 24°C. GC analysis was performed on a Hewlett-Packard 6890 Series chromatographer with MS and FID detectors. The elemental surface composition and chemical binding properties were analyzed by X-ray photoelectron spectroscopy (XPS) using an AXIS Ultra DLD electron spectrometer (Kratos Analytical, Manchester, UK). The spectra were recorded utilizing monochromatic X-rays Al kα (1486.6 eV) with a medium magnification (field of view 2) lens mode and with the slot mode selected. N_2 physisorption analyses were done with ASAP2010 instrument from Micromeritics (USA). The samples were pre-treated under Vacuum (0,001 mbar) at 400°C for at least 3 h. Isotherms were recorded under standard BET conditions with adsorption of N_2 at −196°C (cooling with liquid nitrogen). All calculations were done with ASAP2020 software V4.03 with standard parameters for BET, t-plot and BJH distribution. For micropore diameter and distribution the N_2-DFT model for slit pores with low regularisation was used. The SEM images of the carbon supports (C-pellets and C-irregular) were taken in a Carl Zeiss SUPRA 25 FESEM microscope operated by SmartSEM software.

Synthesis of the catalysts

RuOx–N@C-powder catalyst

[Ru(p-cymene)Cl$_2$]$_2$ (154.6 mg, 0.26 mmol, corresponds to 5% Ru) and 1,10-Phenanthroline (83.0 mg, 0.46 mmol) were mixed in ethanol (50 mL) for 30 min. The carbon (759.3 mg) was added to the solution and heated to reflux at 100°C for 4 hours. The solvent was evaporated and the resulting solid was thoroughly dried overnight at 60°C under high vacuum. The black solid obtained was then pyrolyzed at 800°C for 2 hours under argon atmosphere and cooled to room temperature. Elemental analysis (Wt%): C = 76.27, H = 0.332, N = 0.588, Ru = 5.51.

Co$_x$O$_y$ + RuOx–N@C-powder catalyst

Co(OAc)$_2$·4H$_2$O (160,6 mg, mmol, corresponds to 3% wt Co) and [Ru(p-cymene)Cl$_2$]$_2$ (154.6 mg, 0.26 mmol, corresponds to 5% wt Ru) were dissolved in 50 mL MeOH, after 5 min of vigorous stirring 1,10-phenanthroline (315.0 mg, mmol) was added. The solution was stirred for 30 min and carbon powder (412 mg) was added, then heated to reflux at 100°C for 4 hours. The solvent was evaporated and the resulting solid thoroughly dried overnight at 60°C under high vacuum. The black solid obtained was then pyrolyzed at 800°C for 2 hours in argon atmosphere and cooled to room

temperature. Elemental analysis (Wt%): $C = 70.08$, $H = 0.575$, $N = 1.633$, $Co = 4.83$, $Ru = 4.48$.

Co_xO_y–N@C catalysts

$Co(OAc)_2 \cdot 4H_2O$ (380.4 mg, 1.53 mmol, corresponds to 3% wt Co) and 1,10-Phenanthroline (550.5 mg, 3.06 mmol) were mixed in ethanol (150 mL) for 30 min. The desired carbon (2069.1 mg) was added to the solution and heated to reflux at 100 °C for 4 hours. The solvent was evaporated and the resulting solid thoroughly dried overnight at 60 °C under high vacuum. The black solid obtained was then pyrolyzed at 800 °C for 2 hours in argon atmosphere and cooled to room temperature. $-20 + 40$ mesh particle size (C-irregular): Elemental analysis (Wt%):$C = 72.75$, $H = 0.477$, $N = 1.745$, $Co = 2.23$. XPS data (atom %): $C = 90.1$, $O = 5.9$; $N = 2.1$, $Si = 0.8$; $S = 0.2$; $Co = 0.6$. 0,8 mm pellets (C-pellets): Elemental analysis (Wt%): $C = 85,40$, $H = 0,3954$, $N = 3,961$, $Co = 2,34$.

RuO_x–N@C catalysts

$[Ru(p\text{-cymene})Cl_2]_2$ (463.8 mg, 0.74 mmol, corresponds to 5% wt Ru) and 1,10-Phenanthroline (266.7 mg, 1.48 mmol) were mixed in ethanol (150 mL) for 30 min. The desired carbon (2269.5 mg) was added to the solution and heated to reflux at 100 °C for 4 hours. The solvent was evaporated and the resulting solid thoroughly dried overnight at 60 °C under high vacuum. The black solid obtained was then pyrolyzed at 800 °C for 2 hours in argon atmosphere and cooled to room temperature. $-20 + 40$ mesh particle size(C-irregular): Elemental analysis (Wt%): $C = 65.40$, $H = 0.4507$, $N = 1.167$, $Ru = 2.46$. XPS data (atom %): $C = 89.2$, $O = 6.9$, $N = 0.9$, $Si = 0.7$, $S = 0.3$; $Ru = 1.8$. 0,8 mm pellets (C-pellets): Elemental analysis analysis (Wt%): $C = 83.12$, $H = 0.4507$, $N = 0.850$, $Ru = 1.79$.

Bimetallic Co_xO_y–N + RuO_x–N@C catalysts

$[Ru(p\text{-cymene})Cl_2]_2$ (231.9 mg, 0.38 mmol, corresponds to 5% wt Ru) and 1,10-Phenanthroline (133.3 mg, 0.74 mmol) were mixed in ethanol (75 mL) for 30 min. The previously prepared Co_xO_y–N@C catalyst (1143.8 mg) was added to the solution and heated to reflux at 100 °C for 4 hours. The solvent was evaporated and the resulting solid thoroughly dried overnight at 60 °C under high vacuum. The black solid obtained was then pyrolyzed at 800 °C for 2 hours in argon atmosphere and cooled to room temperature. $-20 + 40$ mesh particle size (C-irregular): Elemental analysis (Wt%): $C = 68.86$, $H = 0.5722$, $N = 1.746$, $Co = 1.70$, $Ru = 2.34$. XPS data (atom %): $C = 88.3$, $O = 6.9$, $N = 1.3$, $Si = 0.5$, $S = 0.2$, $Co = 1.3$, $Ru = 1.3$. 0,8 mm pellets (C-pellets): Elemental analysis (Wt%): $C = 72.35$, $H = 0.1247$, $N = 1.789$, $Co = 1.48$, $Ru = 0.56$

Bimetallic RuO_x–N + Co_xO_y–N@C catalysts

$Co(OAc)_2 \cdot 4H_2O$ (190.2 mg, 0.765 mmol, corresponds to 3% wt Co) and 1,10-Phenanthroline (275.3 mg, 1.53 mmol) were mixed in ethanol (75 mL) for 30 min. The previously prepared RuO_x–N@C catalyst (1034.5 mg) was added to the solution and heated to reflux at 100 °C for 4 hours. The solvent was evaporated and the resulting solid thoroughly dried overnight at 60 °C under high vacuum. The black solid obtained was then pyrolyzed at 800 °C for 2 hours in argon atmosphere and cooled to room temperature. $-20 + 40$ mesh particle size (C-irregular): Elemental analysis (Wt%): $C = 85.33$, $H = 0.6427$, $N = 3.007$, $Co = 1.58$, $Ru = 2.17$. XPS data (atom %): $C = 86.0$, $O = 7.7$, $N = 1.9$, $Si = 0.6$, $S = 0.4$, $Co = 1.3$; $Ru = 1.7$.

0,8 mm pellets (C-pellets): Elemental analysis (Wt%): $C = 54.11$, $H = 0.0802$, $N = 1.770$, $Co = 1.26$, $Ru = 1.20$.

Flow microreactor setup

All the reactions were carried out using the Modular MicroReaction System (MMRS) from Ehrfeld Mikrotechnik. The solution was pumped with a HPLC-pump (Knauer). The oxygen flow was controlled with an EL-FLOW Mass Flow Controller from Bronkhorst, for the gas/liquid mixing a multilamination mixer was used. The catalyst was applied in a cartridge Reactor F200 with temperature indicator. The total volume of the setup was ~7–8 mL.

Oxidative esterification of HMF

A desired amount of K_2CO_3 was let to dissolve in MeOH overnight at room temperature under vigorous stirring, once the K_2CO_3 was completely dissolved HMF was added, additional MeOH was added until a solution with the concentration of 0.125 M in HMF and 0.025 M in K_2CO_3 was reached. 600 mg of catalyst was loaded into the cartridge of the reactor before the heating and a flow of MeOH and oxygen were started. Once the temperature, pressure and flows (liquid and gas) in the system were stable (after ~45–60 min) the HMF/K_2CO_3 solution was pumped through and the reaction started. The solution coming at the end of the setup was collected and analyzed by gas chromatography.

Isolation of compounds

An automated flash chromatography system with UV detection was used (CombiFlashRf from Teledyne ISCO), using a silica column and heptane/ethyl acetate as solvents. The solvent flow was set up to 30 mL/min. The solvent setup was configured as follows, from start to min 20 the concentration increased from 0% to 45% ethyl acetate; the mixture was kept to min 32, and from min 32 to min 42 the concentration increased from 45% to 100% ethyl acetate; which was kept flowing until the column was completely washed. The compounds obtained were analyzed by NMR and GC-MS.

Acknowledgements

Conflict of Interest

The authors declare no conflict of interest.

[1] J. H. Clark, T. J. Farmer, L. Herrero-Davila, J. Sherwood, *Green Chem.* **2016**, *18*, 3914–3934.

[2] J. G. de Vries, *Chem. Rec.* **2016**, *16*, 2783–2796.

[3] A. F. Sousa, C. Vilela, A. C. Fonseca, M. Matos, C. S. R. Freire, G.-J. M. Gruter, J. F. J. Coelho, A. J. D. Silvestre, *Polym. Chem.* **2015**, *6*, 5961–5983.

[4] a) S. K. Burgess, J. E. Leisen, B. E. Kraftschik, C. R. Mubarak, R. M. Kriegel, W. J. Koros, *Macromolecules* **2014**, *47*, 1383–1391; b) E. F. Efsa Panel on Food Contact Materials, A. Processing, *EFSA Journal* **2014**, *12*, 3866–3874; c) A. Pellis, K. Haernvall, C. M. Pichler, G. Ghazaryan, R. Breinbauer, G. M. Guebitz, *J. Biotechnol.* **2016**, *235*, 47–53.

[5] F. Lin, K. Wang, L. Gao, X. Guo, *Appl. Organomet. Chem.* **2019**, *33*, e4821.

[6] R. Fromanger, S. E. Guillouet, J. L. Uribelarrea, C. Molina-Jouve, X. Cameleyre, *J. Ind. Microbiol. Biotechnol.* **2010**, *37*, 437–445.

[7] A. Mohsenzadeh, A. Zamani, M. J. Taherzadeh, *ChemBioEng Rev.* **2017**, *4*, 75–91.

[8] M. G. Gert-Jan, S. Laszlo, D. Matheus Adrianus, *Comb. Chem. High Throughput Screening* **2012**, *15*, 180–188.

[9] a) L. Gao, W. Zhuge, X. Feng, W. Sun, X. Sun, G. Zheng, *New J. Chem.* **2019**, *43*, 8189–8194; b) I. Graca, S. Al-Shihri, D. Chadwick, *Appl. Catal. A* **2018**, *568*, 95–104.

[10] a) R. Battino, T. R. Rettich, T. Tominaga, *J. Phys. Chem. Ref. Data* **1983**, *12*, 163–178; b) P. M. Osterberg, J. K. Niemeier, C. J. Welch, J. M. Hawkins, J. R. Martinelli, T. E. Johnson, T. W. Root, S. S. Stahl, *Org. Process Res. Dev.* **2015**, *19*, 1537–1543.

[11] a) D. Dallinger, C. O. Kappe, *Curr. Opin. Green Sustainable Chem.* **2017**, *7*, 6–12; b) B. Gutmann, D. Cantillo, C. O. Kappe, *Angew. Chem. Int. Ed.* **2015**, *54*, 6688–6728; *Angew. Chem.* **2015**, *127*, 6788–6832; c) N. Kockmann, P. Thenée, C. Fleischer-Trebes, G. Laudadio, T. Noël, *React. Chem. Eng.* **2017**, *2*, 258–280.

[12] a) M. B. Plutschack, B. Pieber, K. Gilmore, P. H. Seeberger, *Chem. Rev.* **2017**, *117*, 11796–11893; b) H. P. L. Gemoets, Y. Su, M. Shang, V. Hessel, R. Luque, T. Noël, *Chem. Soc. Rev.* **2016**, *45*, 83–117.

[13] M. Gruenewald, J. Heck, *Chem. Ing. Tech.* **2015**, *87*, 1185–1193.

[14] C. A. Hone, C. O. Kappe, *Top. Curr. Chem.* **2018**, *377*, 2.

[15] V. Hessel, P. Löb, H. Löwe, in *Microreactors in Organic Synthesis and Catalysis* (Ed.: T. Wirth), Wiley, **2008**, pp. 211–275.

[16] M. Sajid, X. Zhao, D. Liu, *Green Chem.* **2018**.

[17] A. Salazar, P. Hünemörder, J. Rabeah, A. Quade, R. V. Jagadeesh, E. Mejia, *ACS Sustainable Chem. Eng.* **2019**, DOI: 10.1021/acssusche-meng.1029b00914.

[18] P. Kluson, L. Cerveny, J. Had, *Catal. Lett.* **1994**, *23*, 299–212.

[19] R. A. v. Santen, in *Modern Heterogeneous Catalysis*, **2017**, pp. 59–116.

[20] C. Perego, A. Carati, P. Ingallina, M. A. Mantegazza, G. Bellussi, *Appl. Catal. A* **2001**, *221*, 63–72.

[21] C. Perego, R. Millini, *Chem. Soc. Rev.* **2013**, *42*, 3956–3976.

[22] B. D. Cullity, S. R. Stock, *Elements of X-Ray Diffraction*, 3rd ed., Pearson, **2013**.

[23] R. V. Jagadeesh, H. Junge, M.-M. Pohl, J. Radnik, A. Brückner, M. Beller, *J. Am. Chem. Soc.* **2013**, *135*, 10776–10782.

[24] D. Formenti, F. Ferretti, C. Topf, A.-E. Surkus, M.-M. Pohl, J. Radnik, M. Schneider, K. Junge, M. Beller, F. Ragaini, *J. Catal.* **2017**, *351*, 79–89.

[25] a) T. W. Hansen, A. T. DeLaRiva, S. R. Challa, A. K. Datye, *Acc. Chem. Res.* **2013**, *46*, 1720–1730; b) P. J. F. Harris, *Int. Mater. Rev.* **1995**, *40*, 97–115.

[26] K. W. Golub, T. P. Sulmonetti, L. A. Darunte, M. S. Shealy, C. W. Jones, *ACS Appl. Nano Mater.* **2019**.

[27] a) J. A. Moulijn, A. E. van Diepen, F. Kapteijn, *Appl. Catal. A* **2001**, *212*, 3–16; b) M. D. Argyle, C. H. Bartholomew, *Catalysts* **2015**, *5*, 145–269.

[28] R. V. Jagadeesh, T. Stemmler, A.-E. Surkus, M. Bauer, M.-M. Pohl, J. Radnik, K. Junge, H. Junge, A. Bruckner, M. Beller, *Nat. Protoc.* **2015**, *10*, 916–926.

156

ChemCatChem

Supporting Information

Oxidative Esterification of 5-Hydroxymethylfurfural under Flow Conditions Using a Bimetallic Co/Ru Catalyst

Abel Salazar, Alexander Linke, Reinhard Eckelt, Antje Quade, Udo Kragl, and
Esteban Mejía*© 2020 The Authors. Published by Wiley-VCH Verlag GmbH & Co. KGaA.

Table of Contents

1. Explorative experiments using powder catalysts

With the goal of producing a bimetallic catalyst, nitrogen doped RuO_x-N@C-powder was prepared and tested. The RuO_x-N@C-powder showed a similar activity as its counterpart, the commercial Ru@C. A conversion of 60% was achieved, with a selectivity of 76% to 4. (See table 1 entry 1). With this result we prepared the bimetallic Co_xO_y + RuOx-N@C-powder by simultaneous impregnation of both metals, which was also tested (See table 1 entry 2). The results were promising, >99% of HMF conversion was achieved with selectivities of 38% towards FDCM (2), 47% to 3, and 8% toward 5.

Table S1. Explorative experiments using power catalysts

Entry	Catalyst	Conv.(%)	Product selectivity (%)				
			2	3	4	5	Others
1	RuO_x-N@C-powder	60	-	-	76	24	-
2	Co_xO_y + RuO_x-N@C-powder	>99	38	47	-	8	7

[a] Reaction conditions: 0,5 mmol HMF, 0,2 equiv K_2CO_3, 50 mg cat,4 mL MeOH, Air as oxidant, 50 °C 18h.

2. Reaction Profiles of the catalyst screening (table 2)
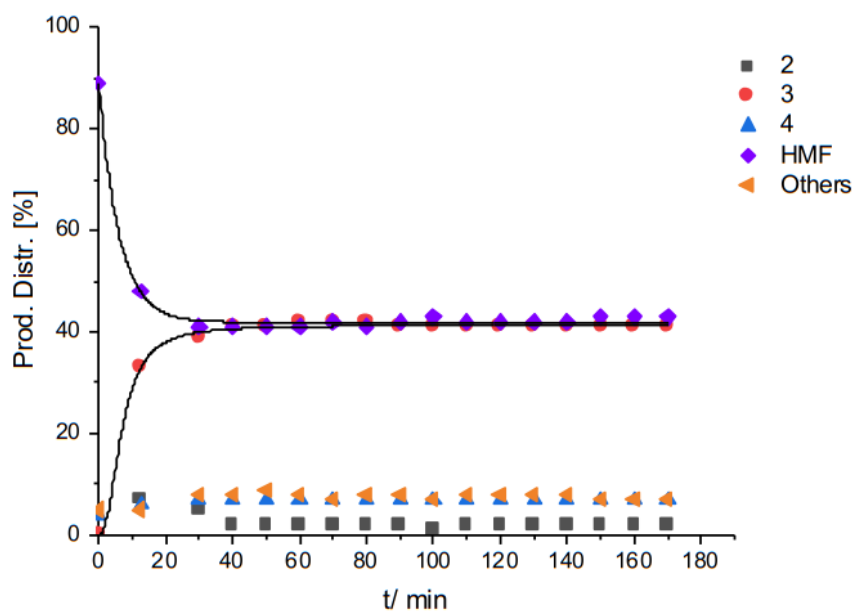
Figure S1. Product distribution vs. time for Co_xO_y-N@C-pellets catalyst (entry 1).
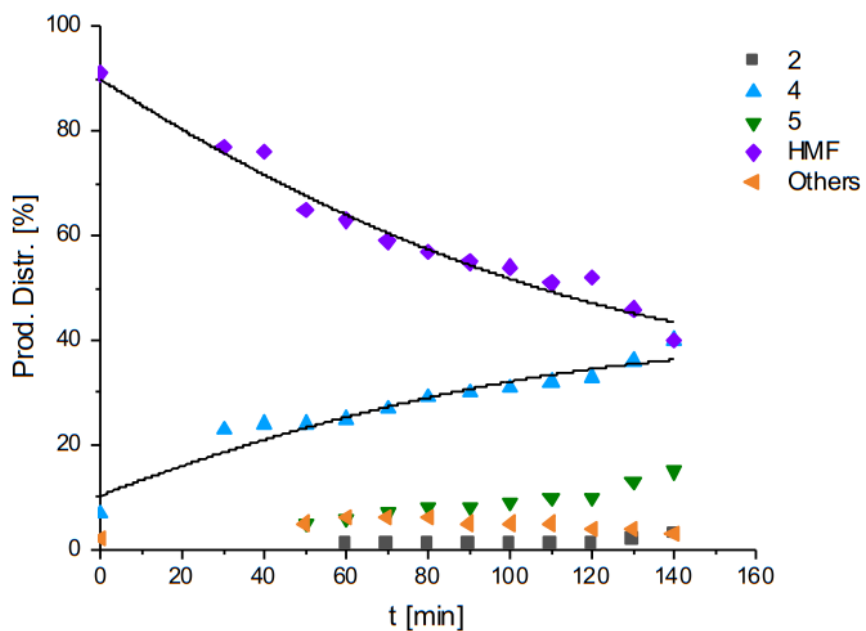
Figure S2. Product distribution vs. time for RuO_x-N@C-pellets catalyst (entry 2).
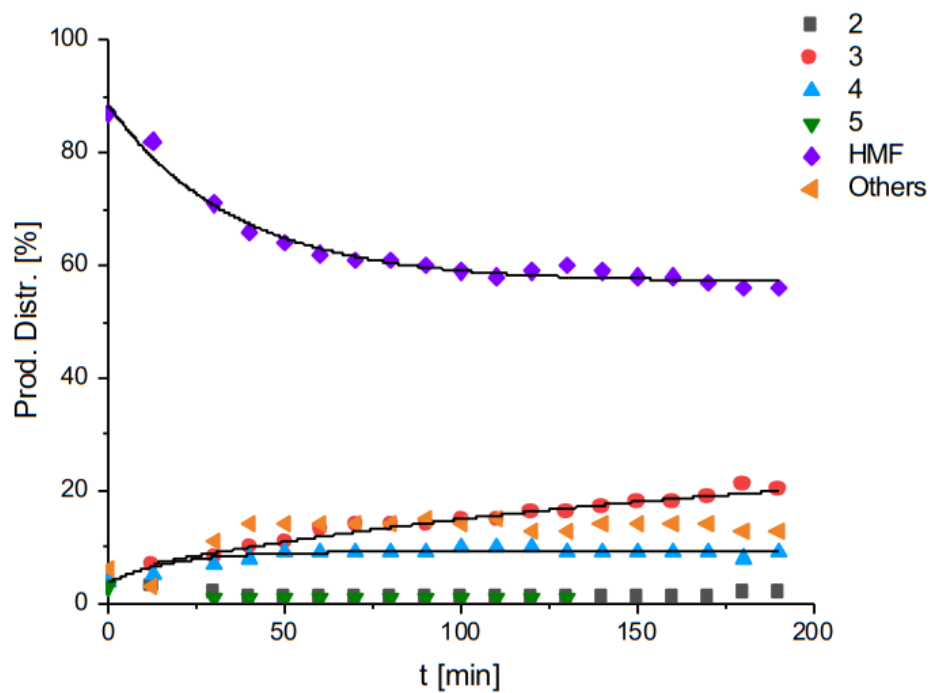
Figure S3. Product distribution vs. time for Co_xO_y-N + RuO_x-N@C-pellets catalyst (entry 3).
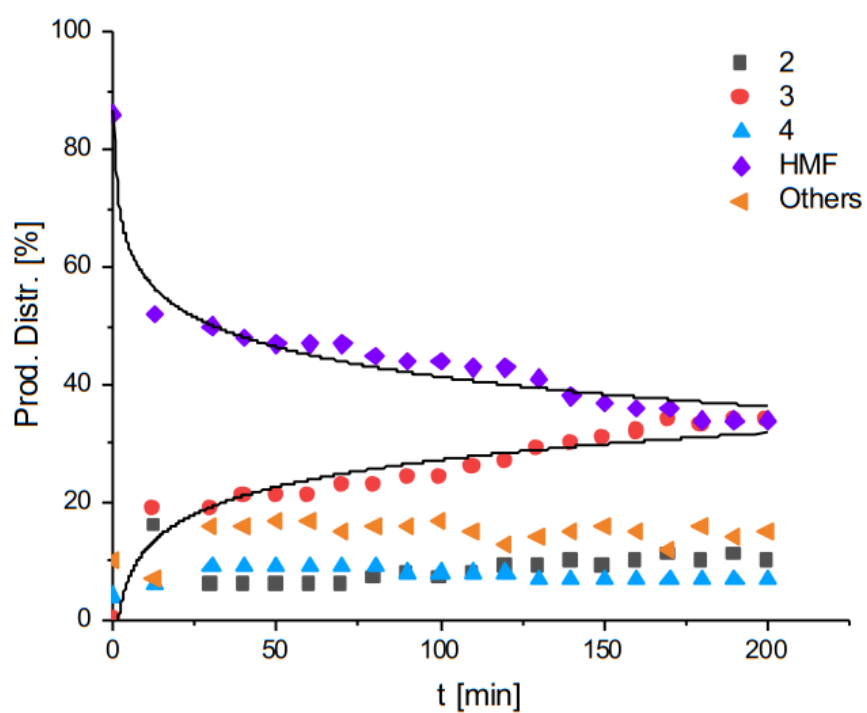
Figure S4. Product distribution vs. time for RuO_x-N + Co_xO_y-N@C-pellets (entry 4).
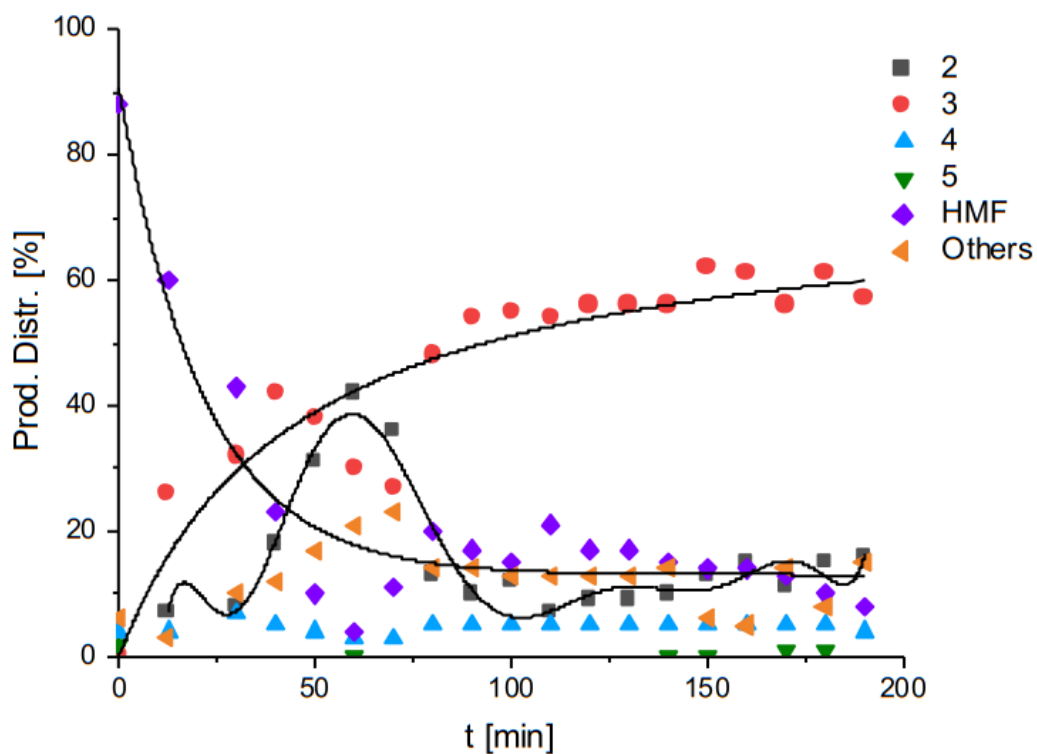
Figure S5. Product distribution vs. time for Co_xO_y-N@C-irregular catalyst (entry 5).
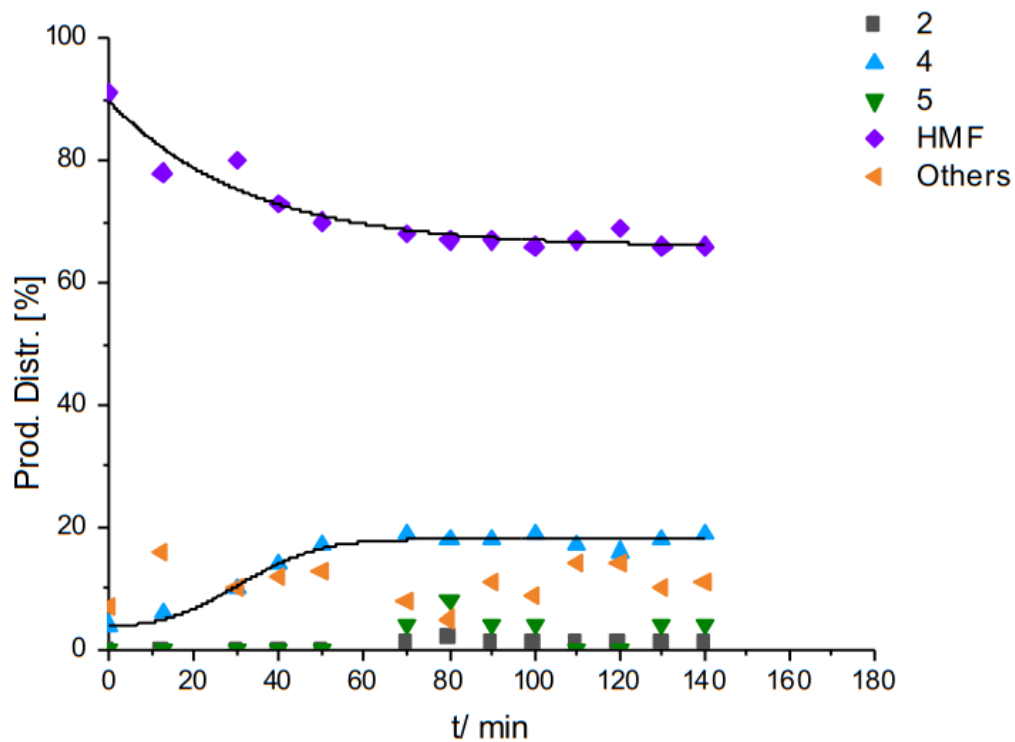
Figure S6. Product distribution vs. time for RuO_x-N@C-irregular catalyst (entry 6).
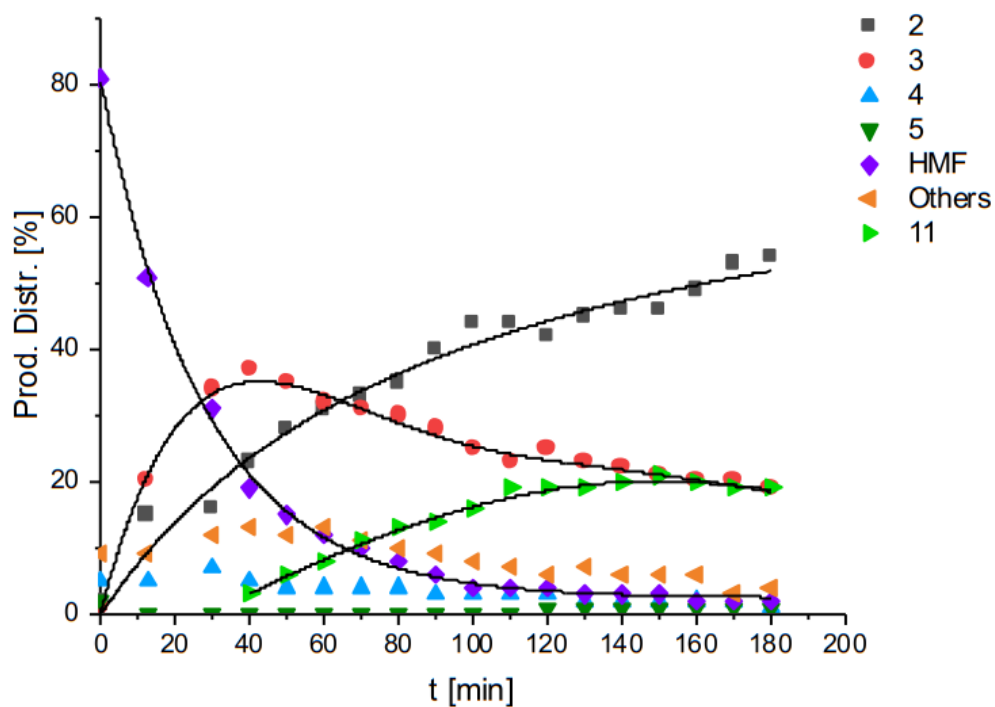
Figure S7. Product distribution vs. time for Co_xO_y-N + RuO_x-N@C-irregular catalyst (entry 7).
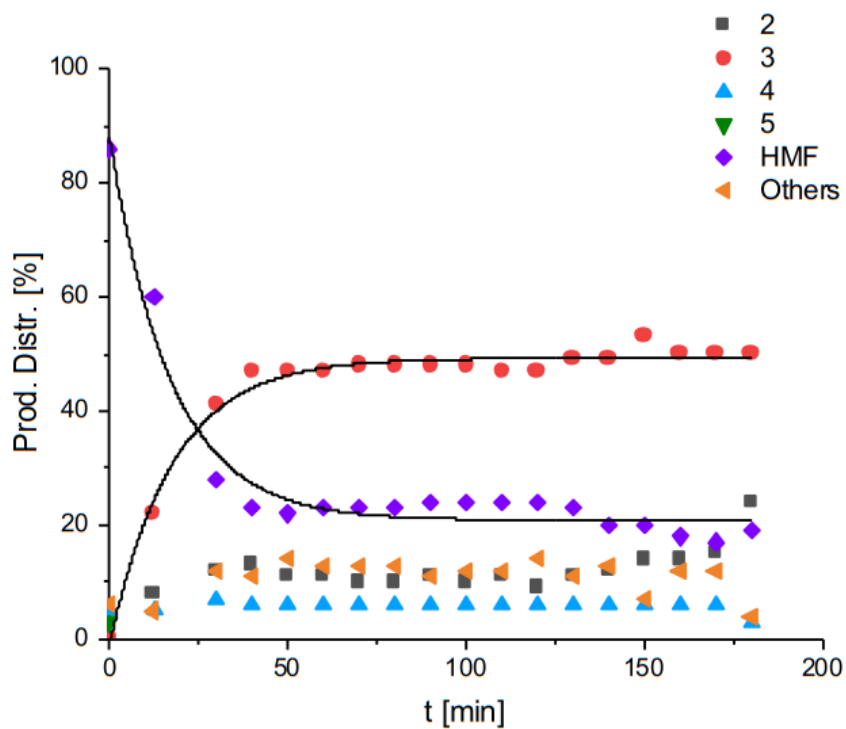
Figure S8. Product distribution vs. time for RuO_x-N + Co_xO_y-N@C-irregular (entry 8).
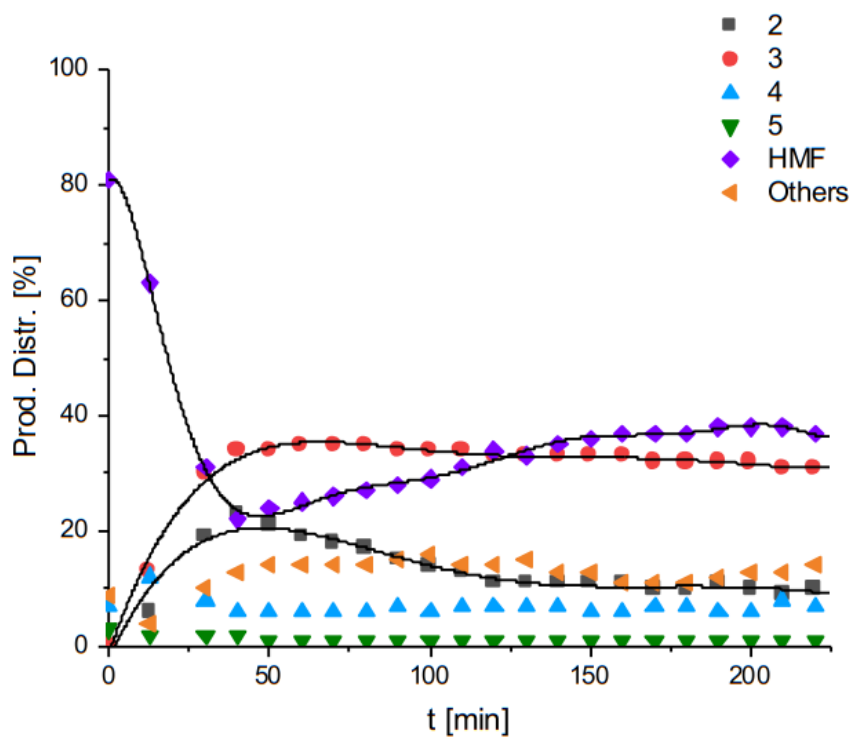
Figure S9. Product distribution vs. time for Mixture entry 5 - entry 6 catalyst (entry 9).

3. N₂ physisorption analysis

Table S2. Summary of physisorption data

Catalyst	Carbon	Co$_x$O$_y$-N@C	RuO$_x$-N@C	Co$_x$O$_y$-N + RuO$_x$-N@C	RuO$_x$-N + Co$_x$O$_y$-N@C	Carbon	Co$_x$O$_y$-N@C	RuO$_x$-N@C	Co$_x$O$_y$-N + RuO$_x$-N@C	RuO$_x$-N + Co$_x$O$_y$-N@C
Support			Pellets					irregular		
Single point area (m²/g)	1156.9897	665.6218	680.3401	536.4641	454.6599	546.8344	127.6486	222.9753	170.8559	129.6960
BET Surface Area (m²/g)	1178.2693	678.8927	695.7680	546.9071	463.7625	562.7351	128.4905	226.8789	174.9132	129.3743
t-plot Micropore Area (m²/g)	1125.1873	647.5312	660.1688	513.2515	436.8284	372.7956	5.0698	76.5092	51.4183	29.1868
t-Plot External Surface Area (m²/g)	53.0820	31.3615	35.5993	33.6556	26.9341	189.9395	123.4206	150.3697	123.4949	100.1874
t-Plot micropore volume (cm³/g)	0.605513	0.352456	0.363352	0.277833	0.231900	0.204849	0.015450	0.063366	0.041805	0.019541
BJH Desorption cumulative volume of pores between 2 nm and 100 nm (cm³/g)	0.264240	0.148993	0.153284	0.190158	0.148822	0.525496	0.339052	0.419892	0.339505	0.281297
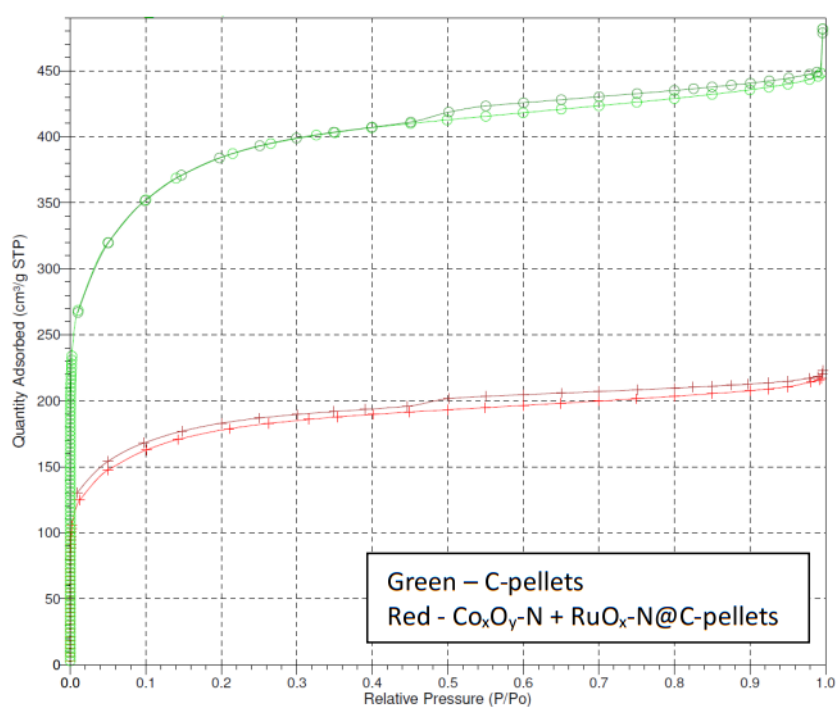
Figure S10. Representative example of the nitrogen physisorption isotherms of C-pellets materials.
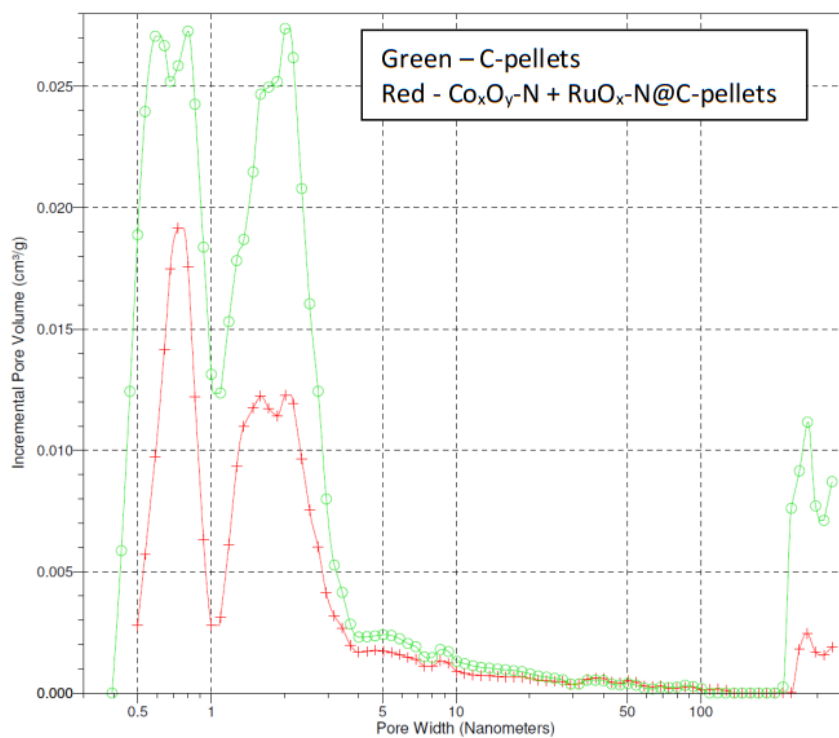
Figure S11. Representative example of the pore size vs pore volume in C-pellets materials.
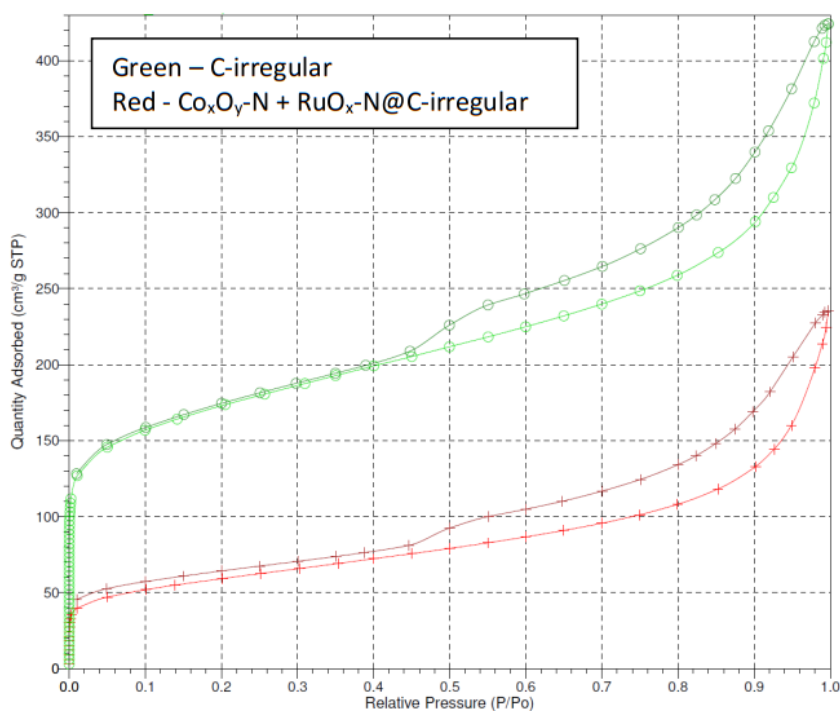
Figure S12. Representative example of the nitrogen physisorption isotherms of C-irregular materials.

S9

166
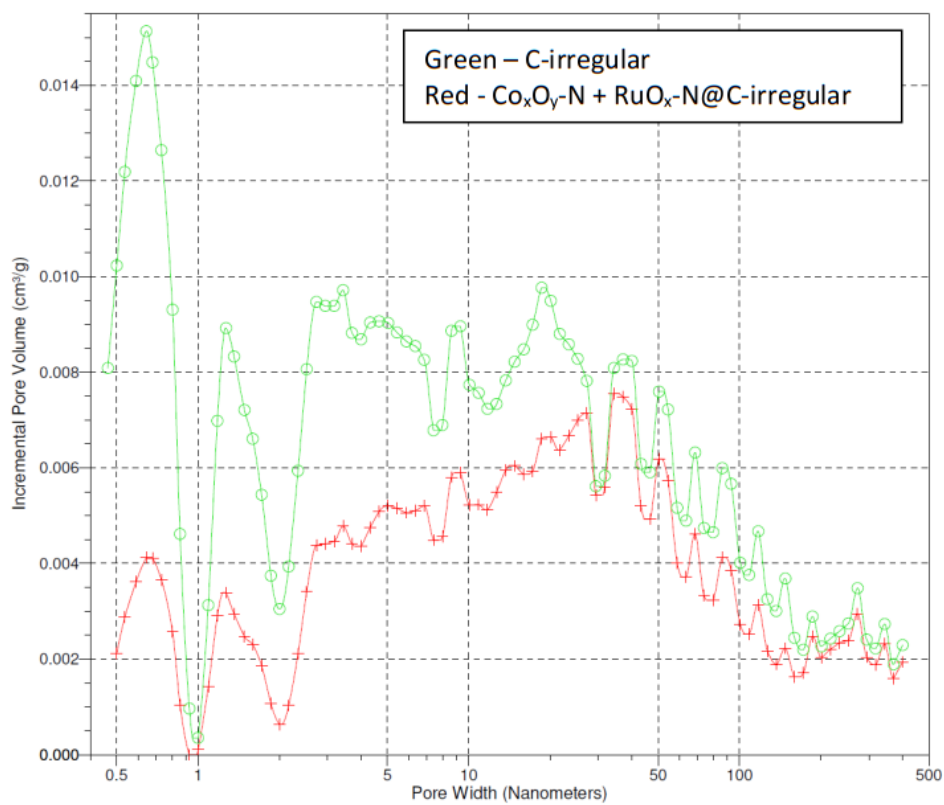
Figure S13. Representative example of the pore size vs pore volume in C-irregular materials.

4. XRD Measurements
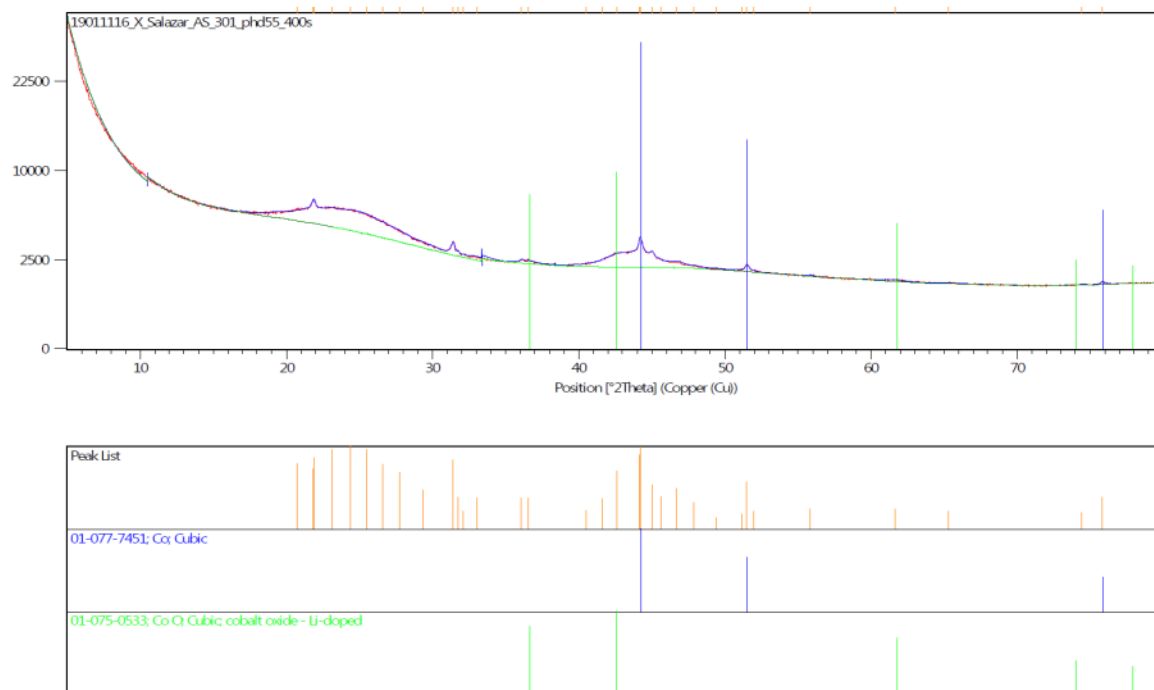
Figure S14. Diffraction pattern of Co_xO_y-N@C-pellets
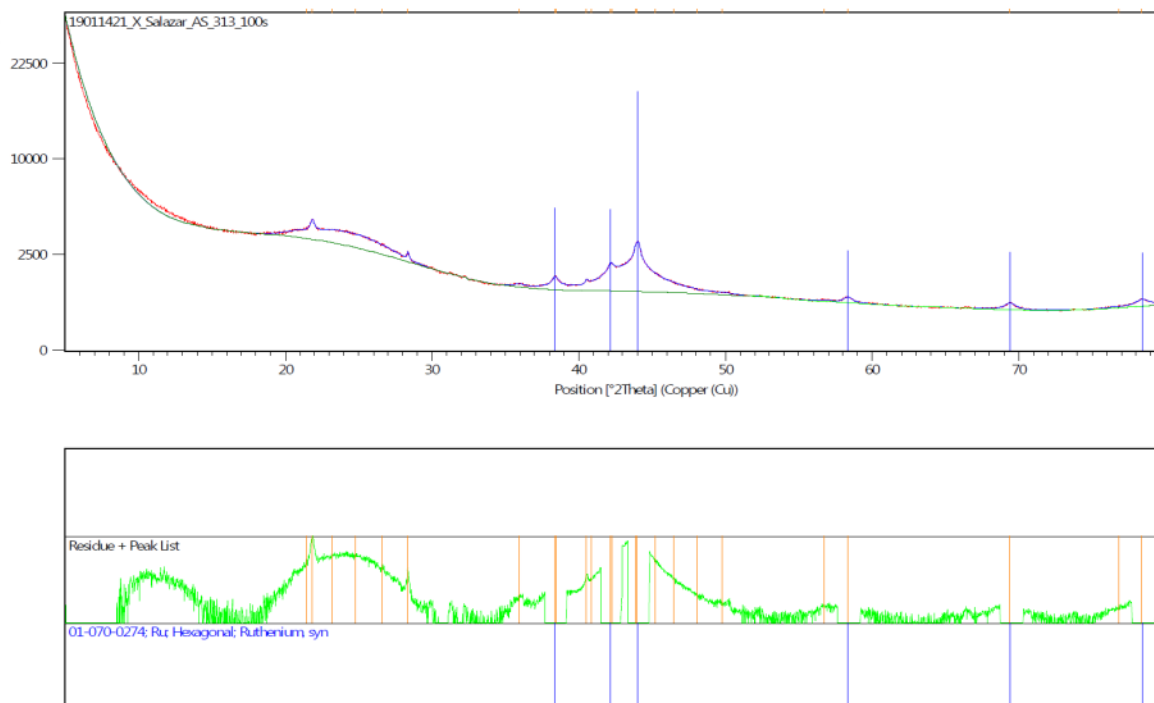
Figure S15. Diffraction pattern of RuO_x-N@C-pellets
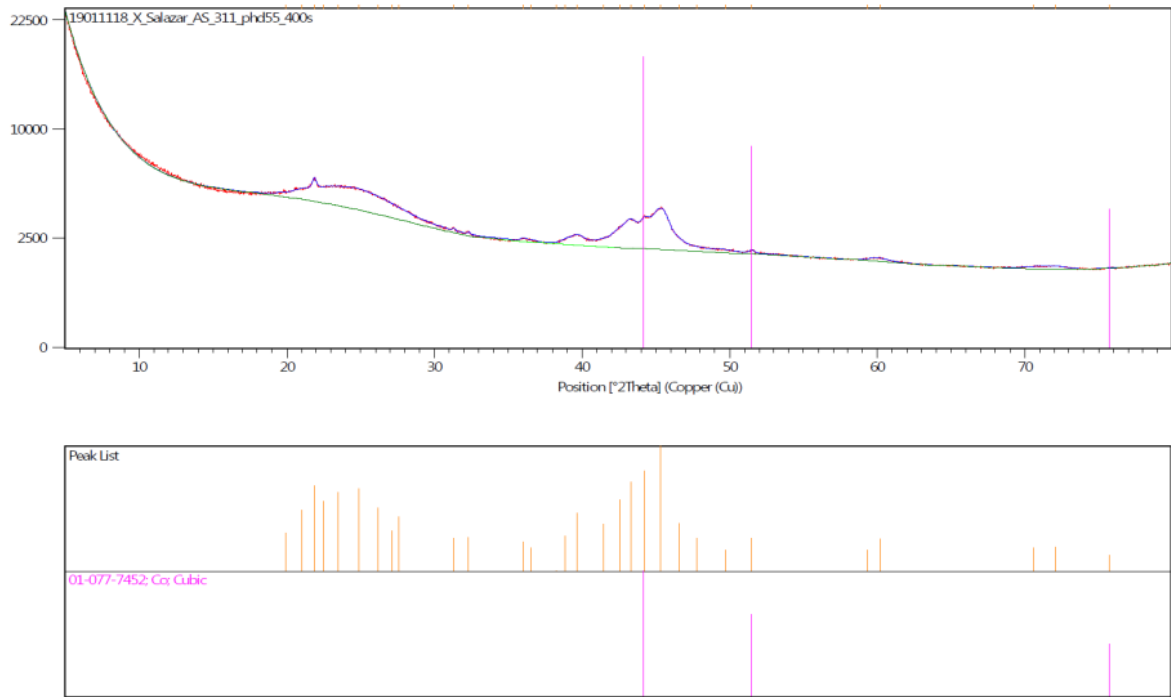
Figure S16. Diffraction pattern of Co_xO_y-N + RuO_x-N@C-pellets
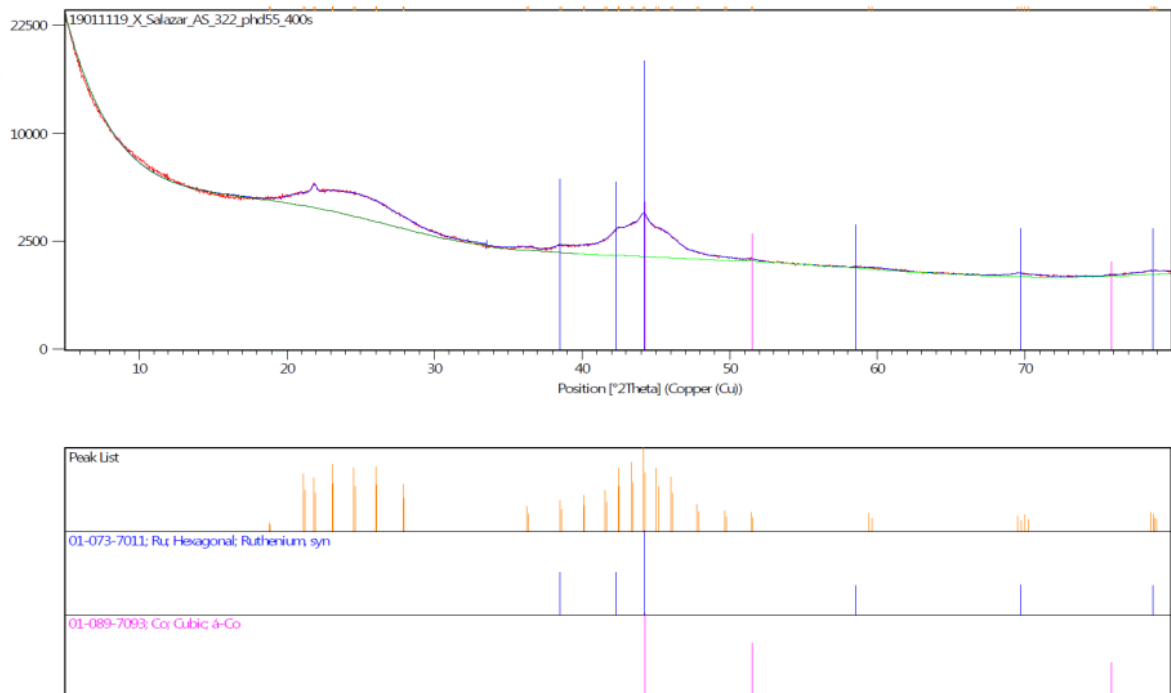
Figure S17. Diffraction pattern of RuO_x-N + Co_xO_y-N@C-pellets
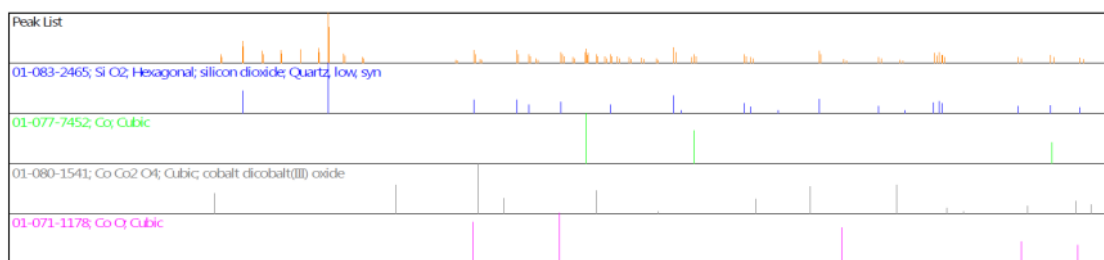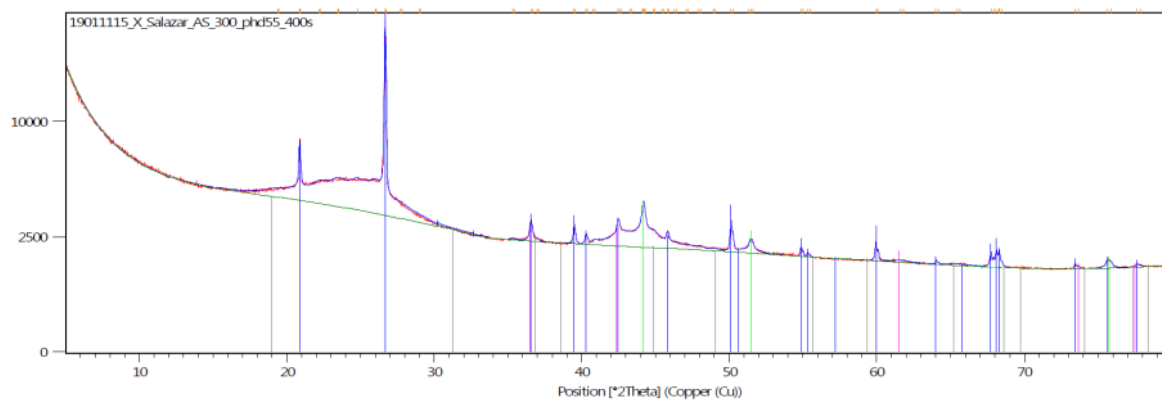
Figure S18. Diffraction pattern of Co_xO_y-N@C-irregular
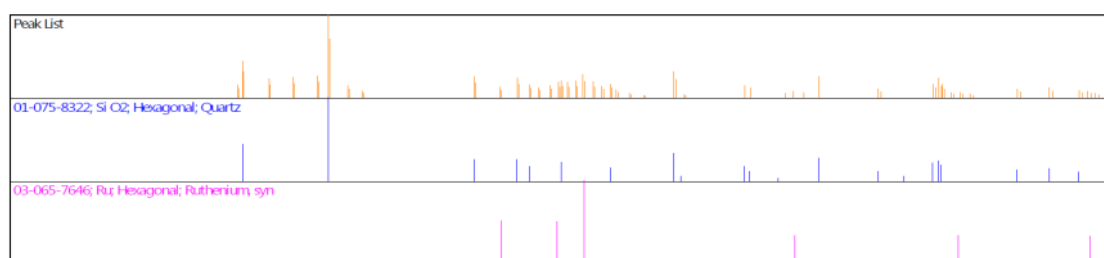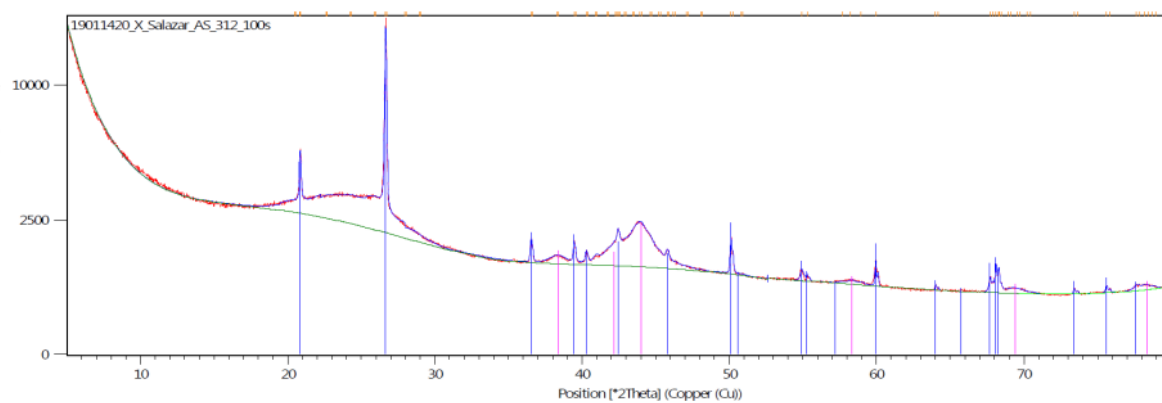
Figure S19. Diffraction pattern of RuO_x-N@C-irregular
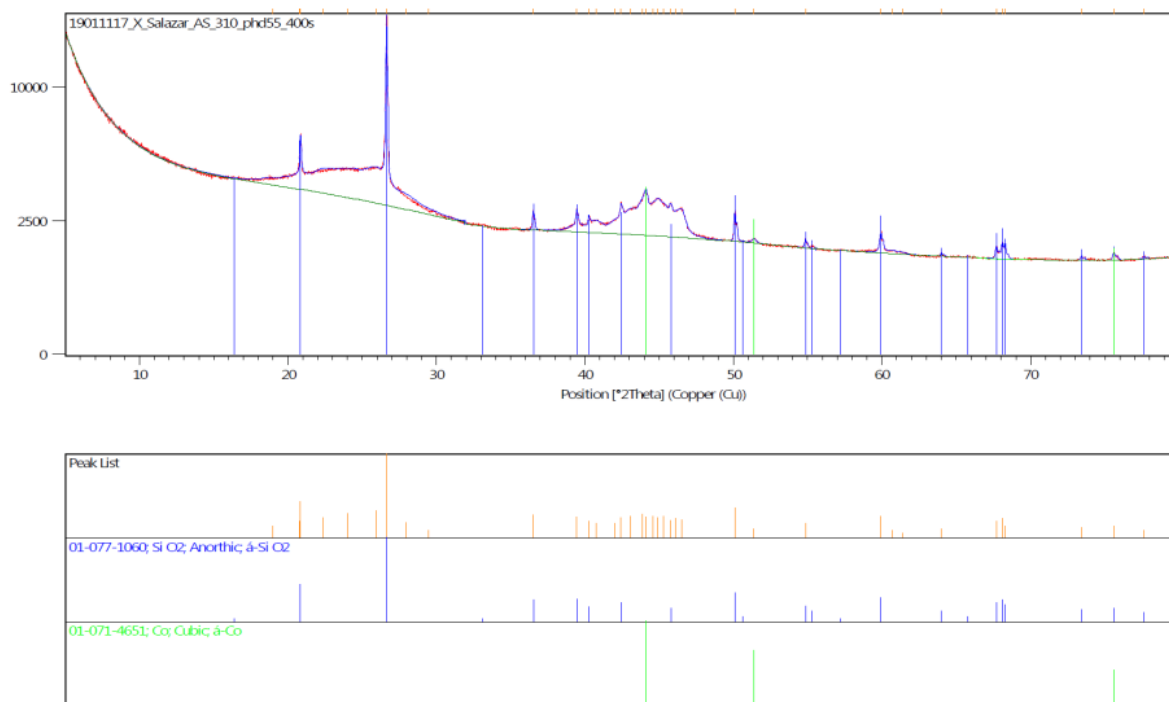
Figure S20. Diffraction pattern of Co_xO_y-N + RuO_x-N@C-irregular
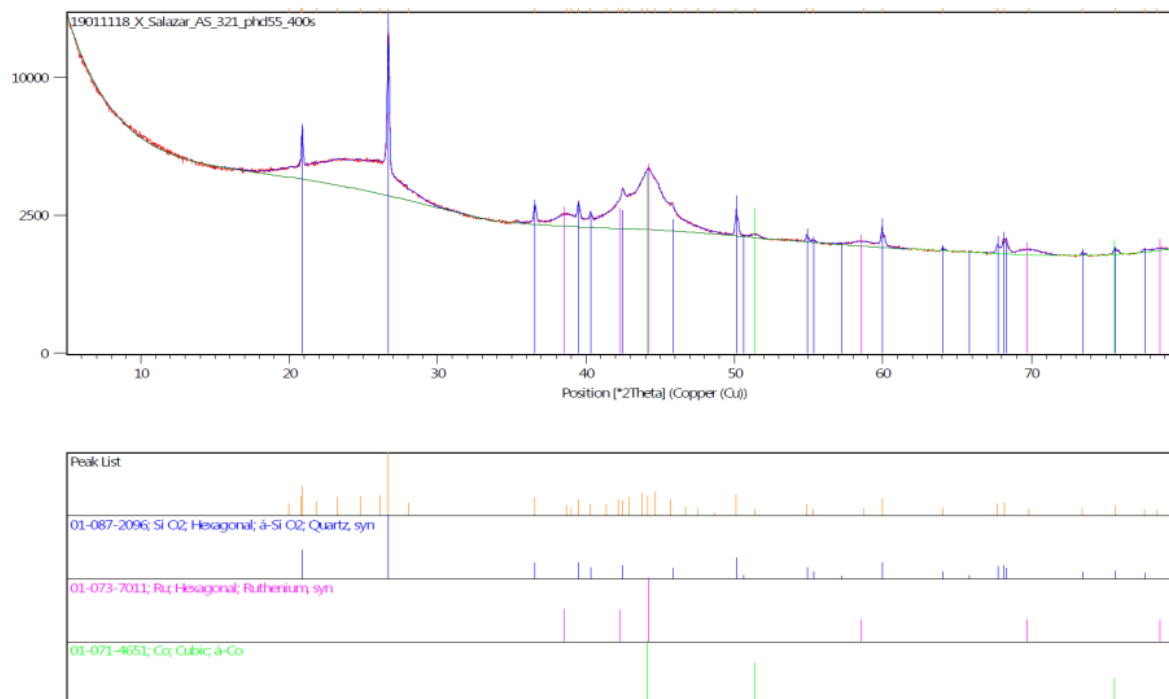
Figure S21. Diffraction pattern of RuO_x-N + Co_xO_y-N@C-irregular

5. XPS measurements of the C-irregular catalysts
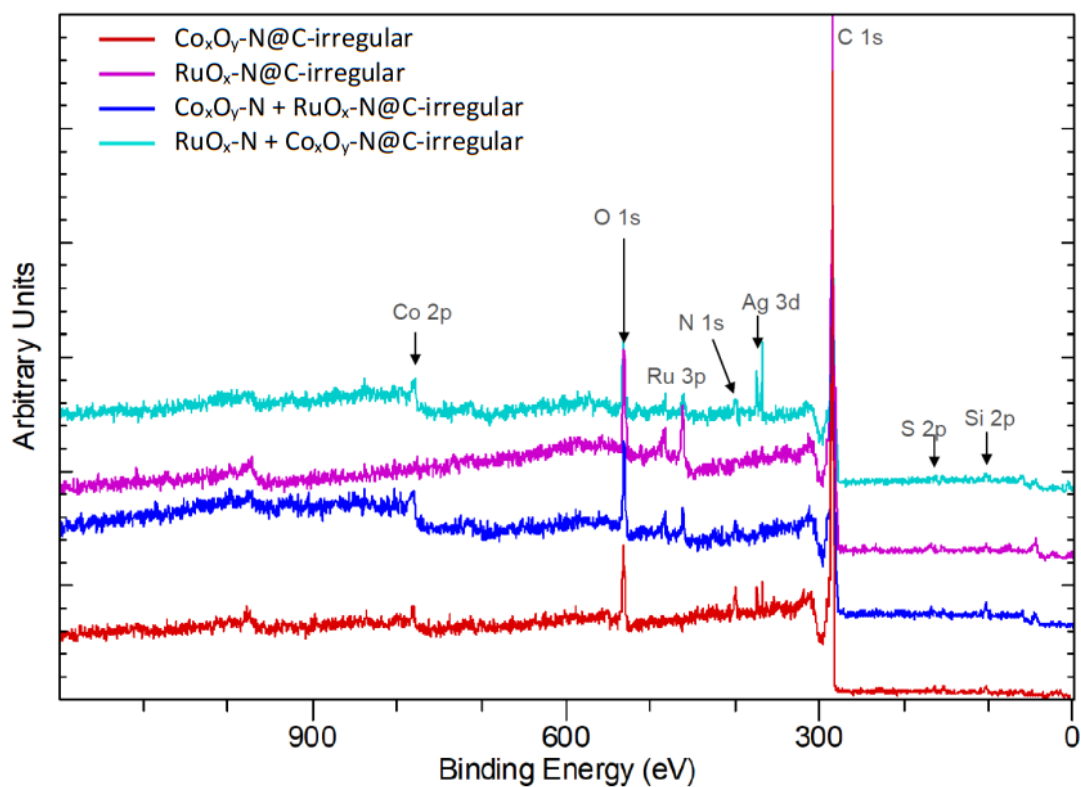
Figure S22. Survey scans of the C-irregular catalysts

Table S3. Elemental fraction [atom %] in the C-Irregular catalysts.

Element	Co_xO_y-N@C-irregular	Co_xO_y-N + RuO_x-N@C-irregular	RuO_x-N@C-irregular	RuO_x-N + Co_xO_y-N@C-irregular
C	90,1	88,3	89,2	86,0
O	5,9	6,9	6,9	7,7
N	2,1	1,3	0,9	1,9
Co	0,6	1,3	-	1,3
Ru	-	1,3	1,8	1,7
S	0,2	0,3	0,3	0,4
Si	0,8	0,5	0,7	0,6
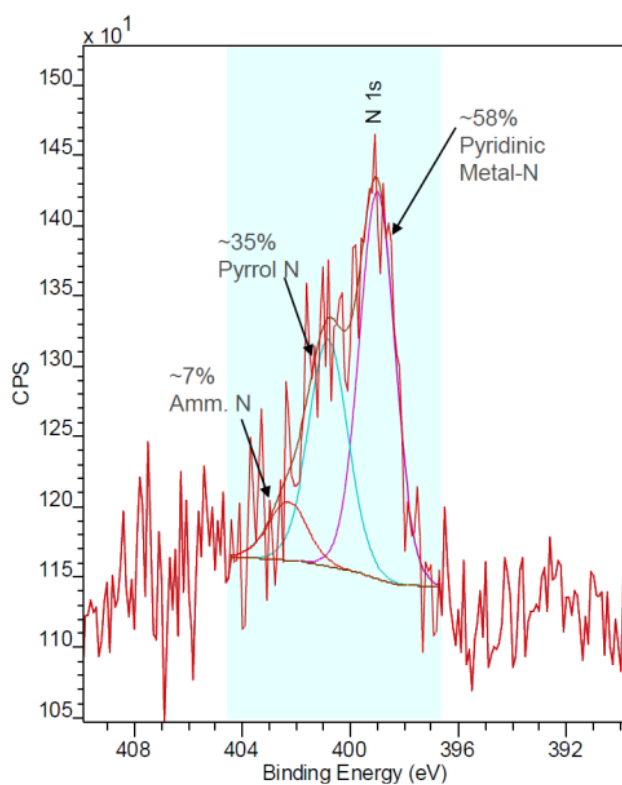
Figure S23. Representative example of the Nitrogen region of Co_xO_y-N@C-irregular catalyst
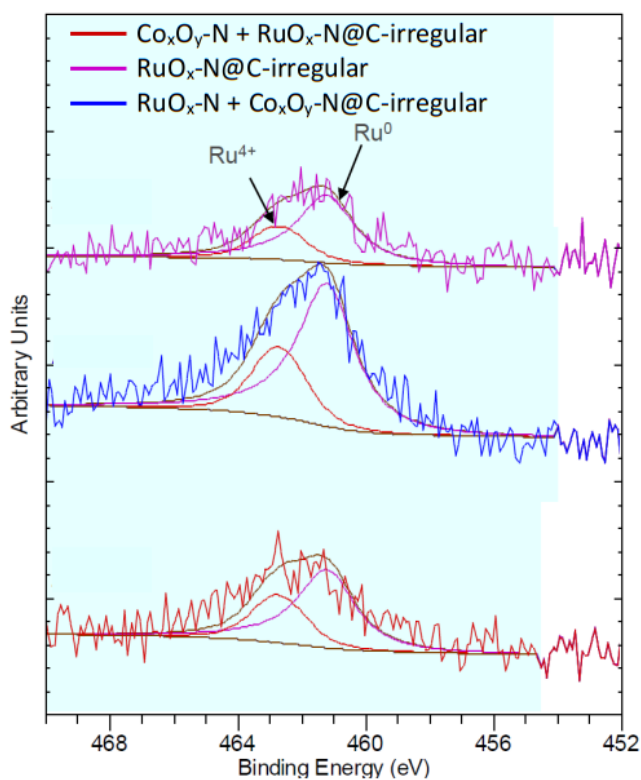
Figure S24. Ruthenium (Ru 3p) species in the catalysts
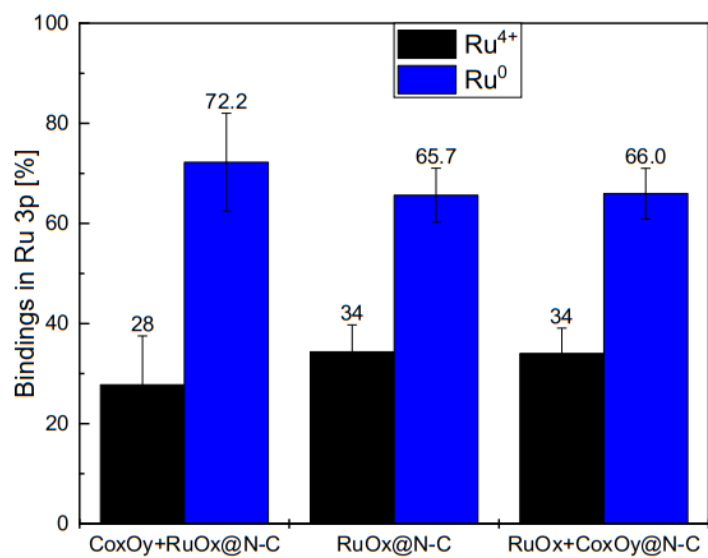
Figure S25. Quantification of the Ruthenium species

6. Characterization of the synthetic targets

6.1 Characterization of dimethyl furan-2,5-dicarboxylate (2)

^{1}H NMR (300 MHz, CDCl$_3$): δ = 7,17 ppm (-CH, 2H, s); 3,88 ppm (-OCH$_3$, 6H, s).^{13}C NMR (75 MHz, CDCl$_3$): δ = 158,45 ppm (C=O); 146,67 ppm (C arom); 118,53 ppm (CH arom); 52,45 ppm (-OCH$_3$). MS (GC-MS): m/z = 184[M$^+$], 153 (100%).
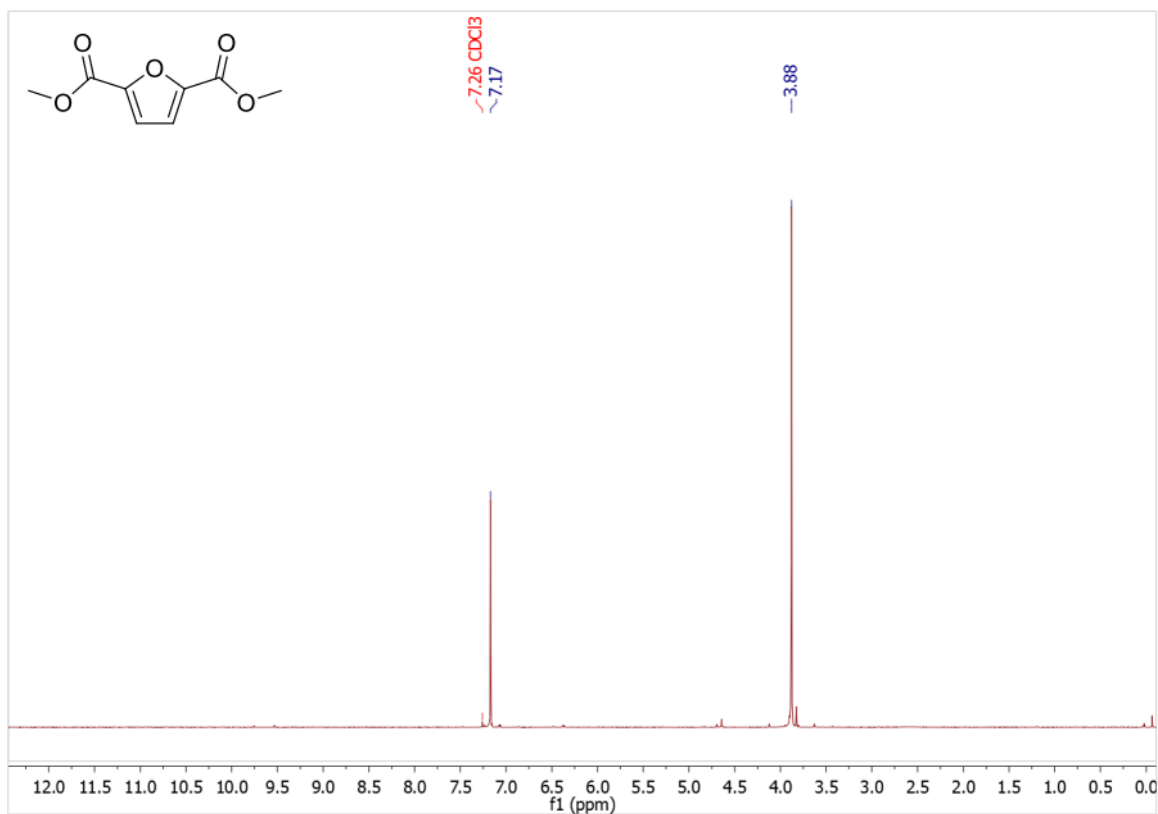
Figure S26. ^{1}H NMR (300 MHz) spectrum of 2 in CDCl$_3$
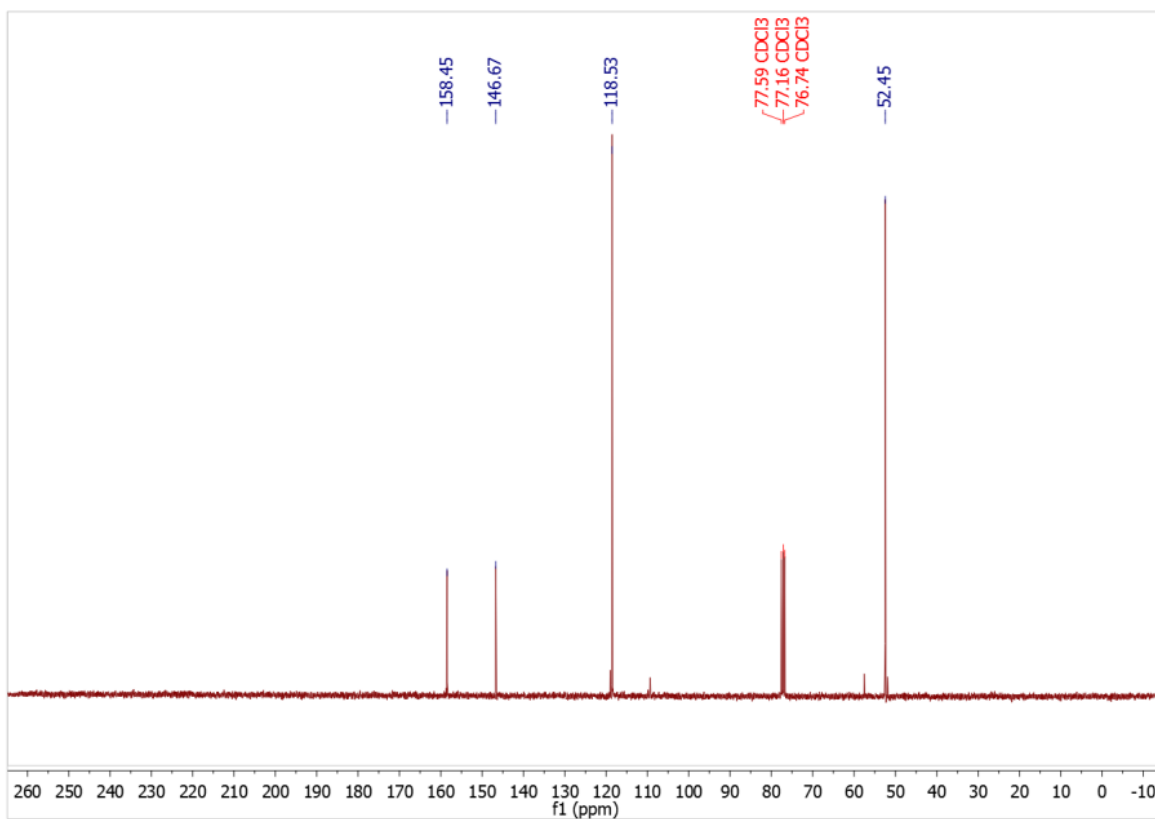
Figure S27. ^{13}C NMR (75 MHz) spectrum of 2 in CDCl$_3$
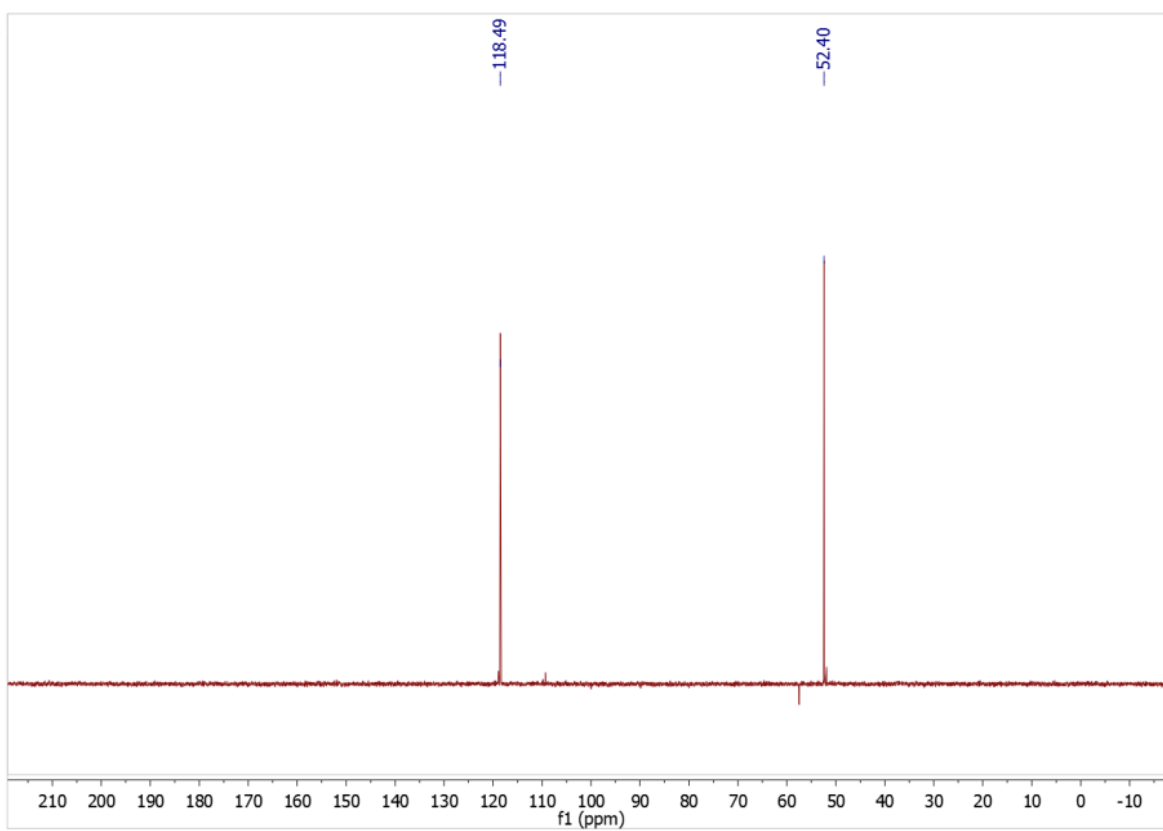
Figure S28. ^{13}C-DEPT NMR (75 MHz) spectrum of 2 in CDCl$_3$
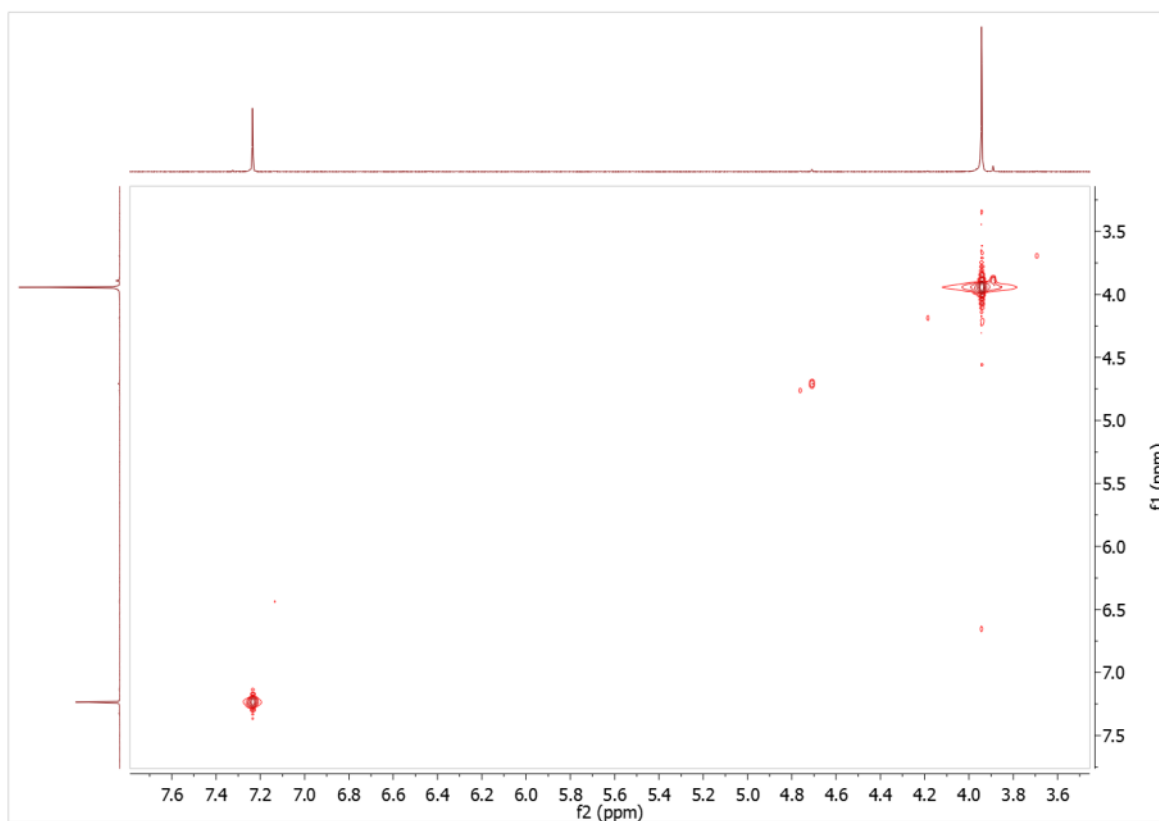
Figure S29. ¹H-COSY-NMR (300 MHz) spectrum of 2 in CDCl₃
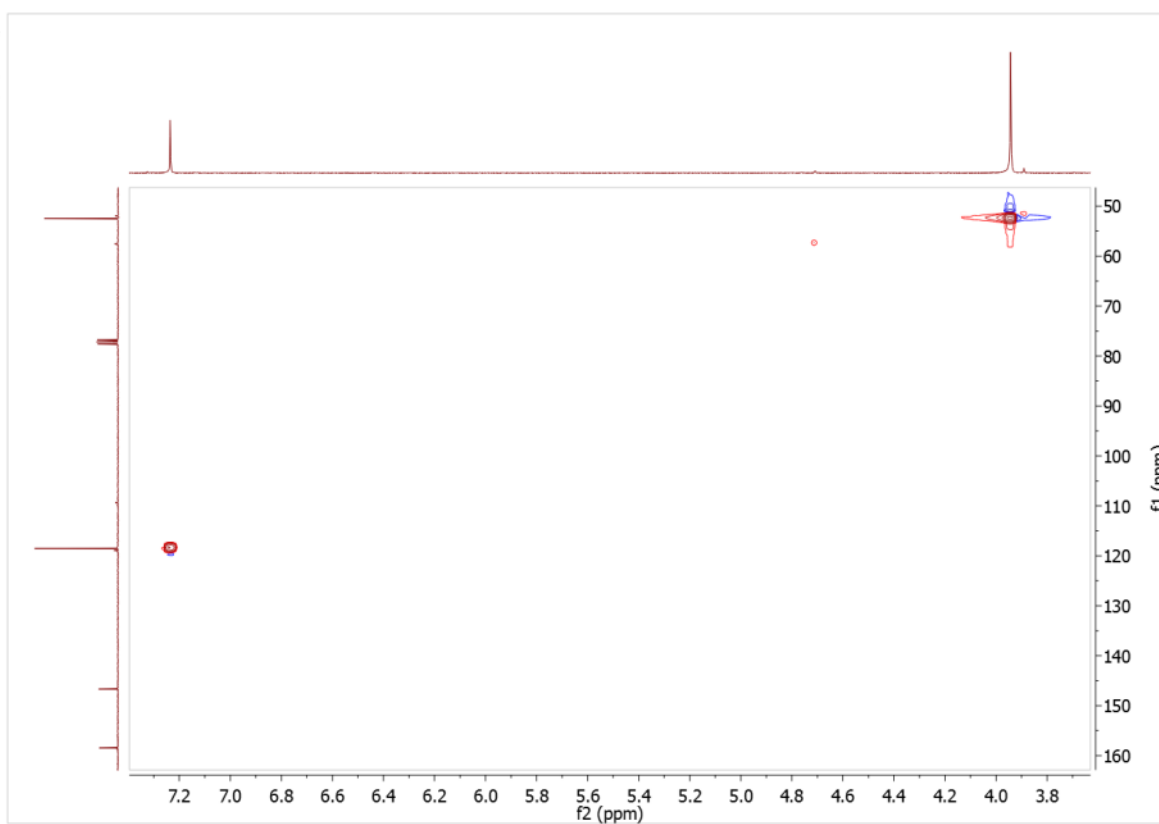
Figure S30. ¹H-¹³C-HSQC- NMR (300 MHz; 75 MHz) spectrum of 2 in CDCl₃
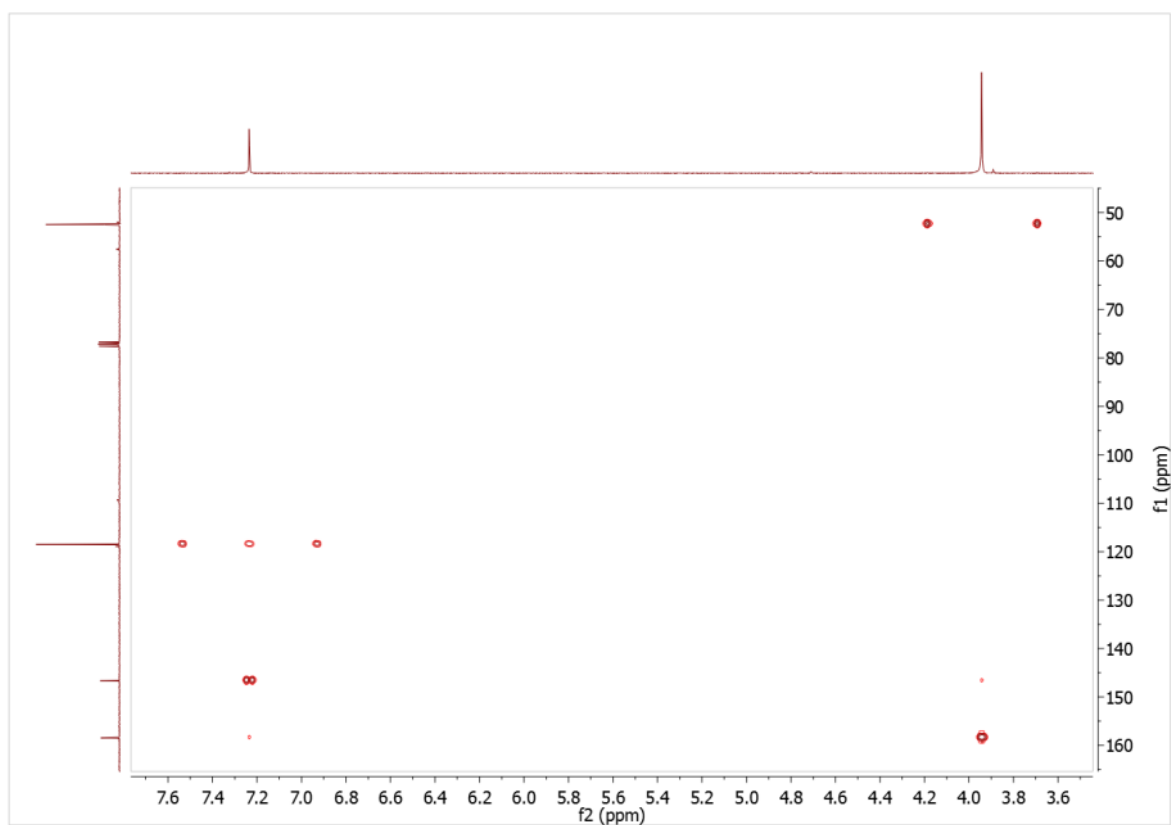
Figure S31. ^{1}H-^{13}C-HMBC- NMR (300 MHz; 75 MHz) spectrum of 2 in CDCl$_3$
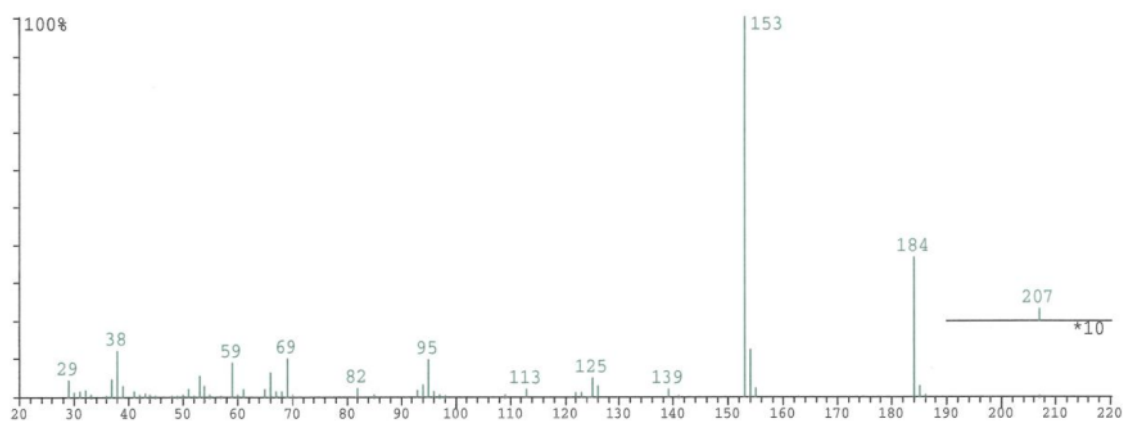
Figure S32. MS spectrum (EI) of 2

6.2 Characterization of methyl 5-(hydroxymethyl)furan-2-carboxylate (3)

^{1}H NMR (300 MHz, CDCl$_3$): δ = 7,09 ppm (-CH arom(alcohol side), 1H, d, *J* = 3,5 Hz); 6,38 ppm (-CH arom (ester side), 1H, d, *J* = 3,5 Hz); 4,63 ppm (CH$_2$, 2H, s); 3,85 ppm (-OCH$_3$, 3H, s).^{13}C NMR (75 MHz, CDCl$_3$): δ = 159,40 ppm (C=O); 158,76 ppm (C arom (alcohol side)); 143,94 ppm (C arom (ester side)); 119,04 ppm (CH arom (ester side)); 109,45 ppm (CH arom (alcohol side)); 57,45 ppm (CH$_2$); 52,06 ppm (-OCH$_3$). MS (GC-MS): m/z = 156[M$^+$], 97 (100%).
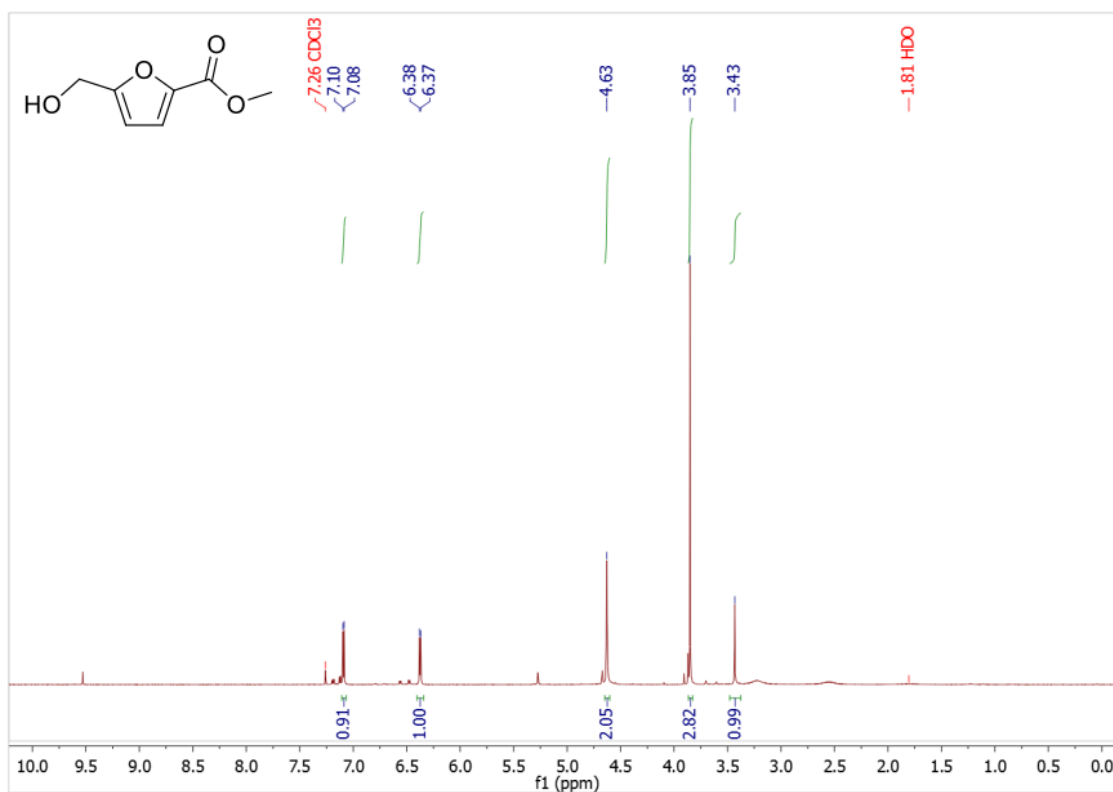
Figure S33. ^{1}H NMR (300 MHz) spectrum of 3 in CDCl$_3$
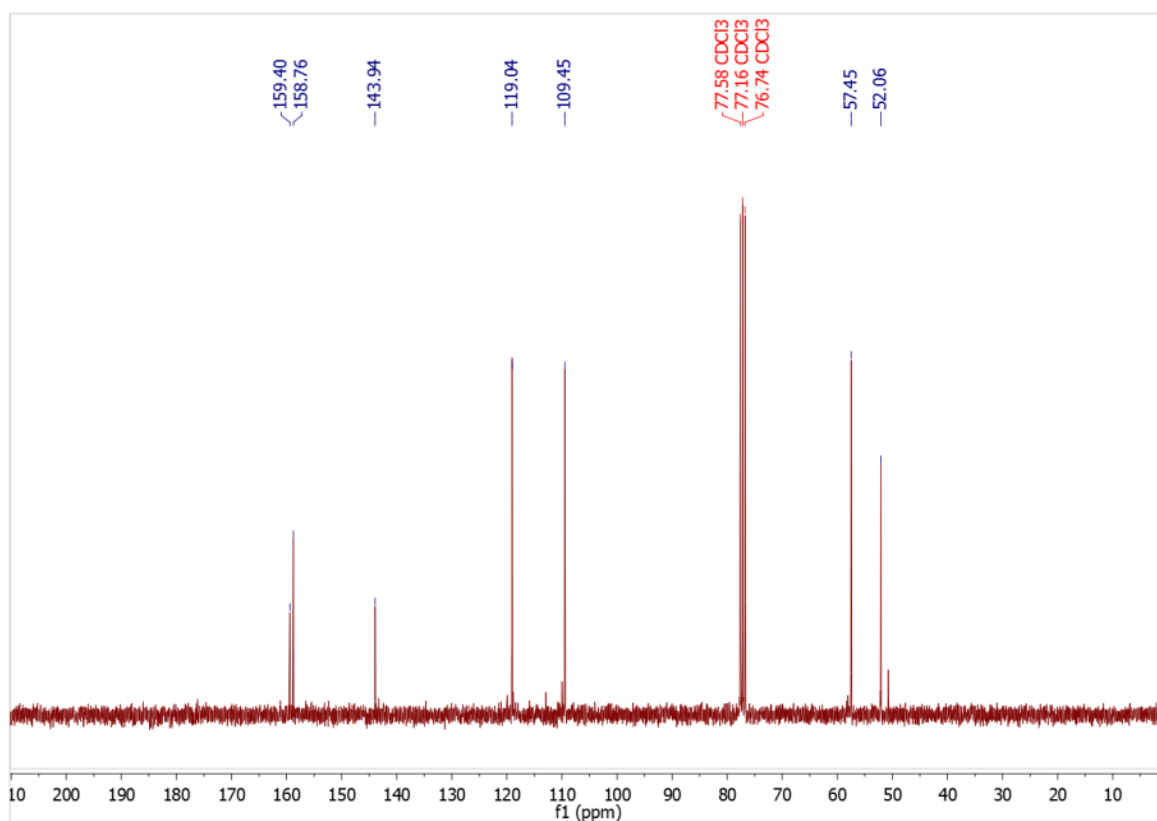
Figure S34. ^{13}C NMR (75 MHz) spectrum of **3** in CDCl$_3$
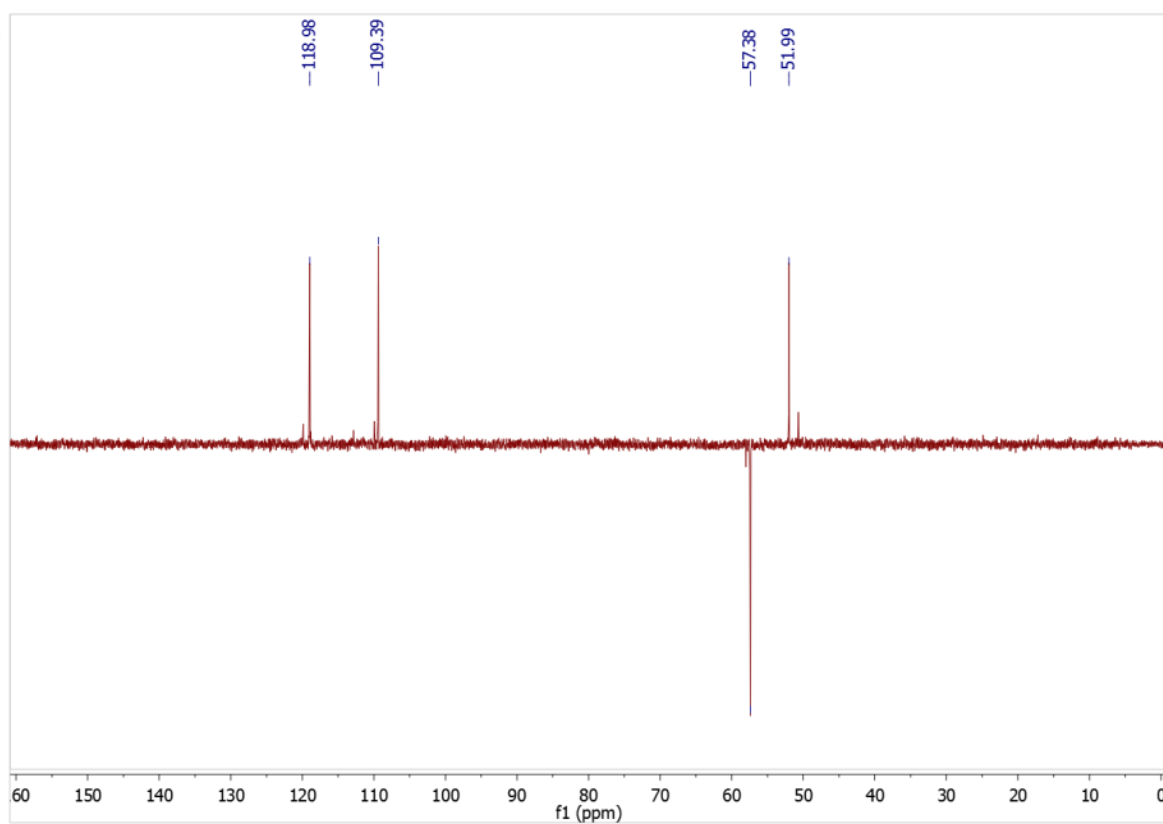
Figure S35. ^{13}C-DEPT NMR (75 MHz) spectrum of **3** in CDCl$_3$
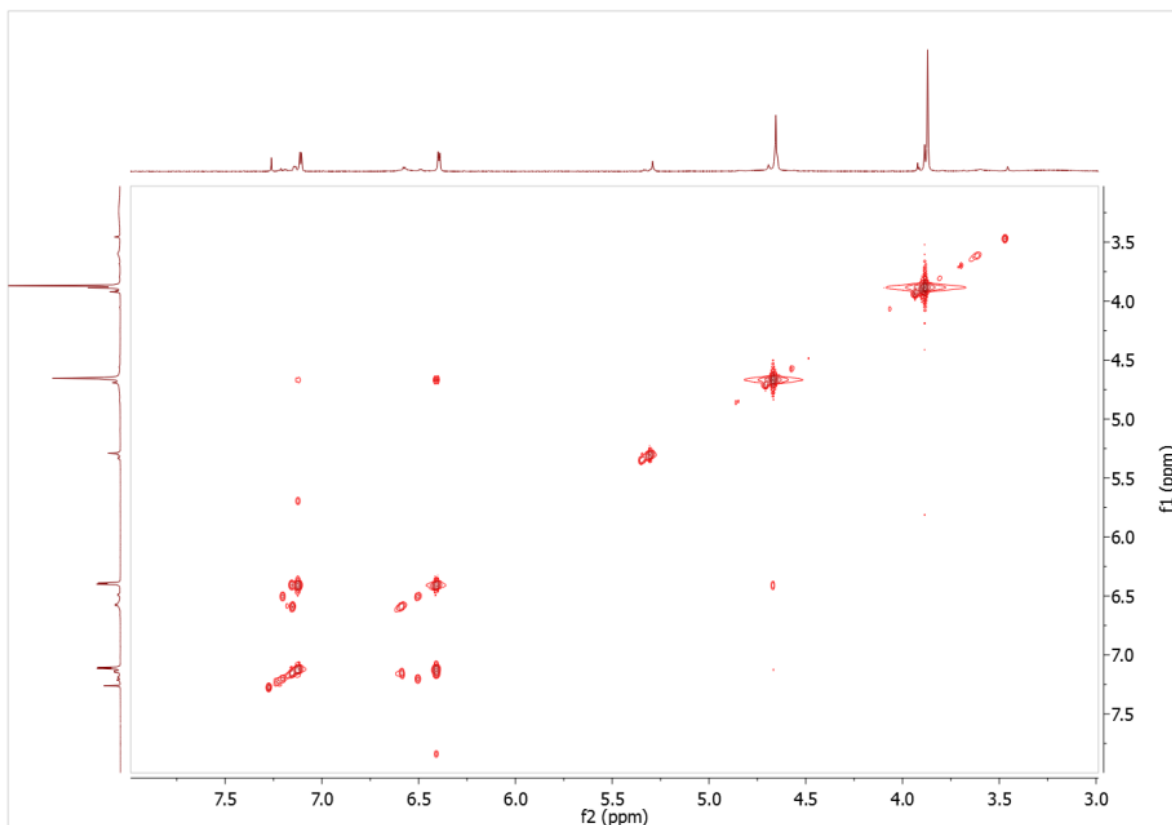
Figure S36. ^{1}H-COSY-NMR (400 MHz) spectrum of 3 in CDCl$_3$
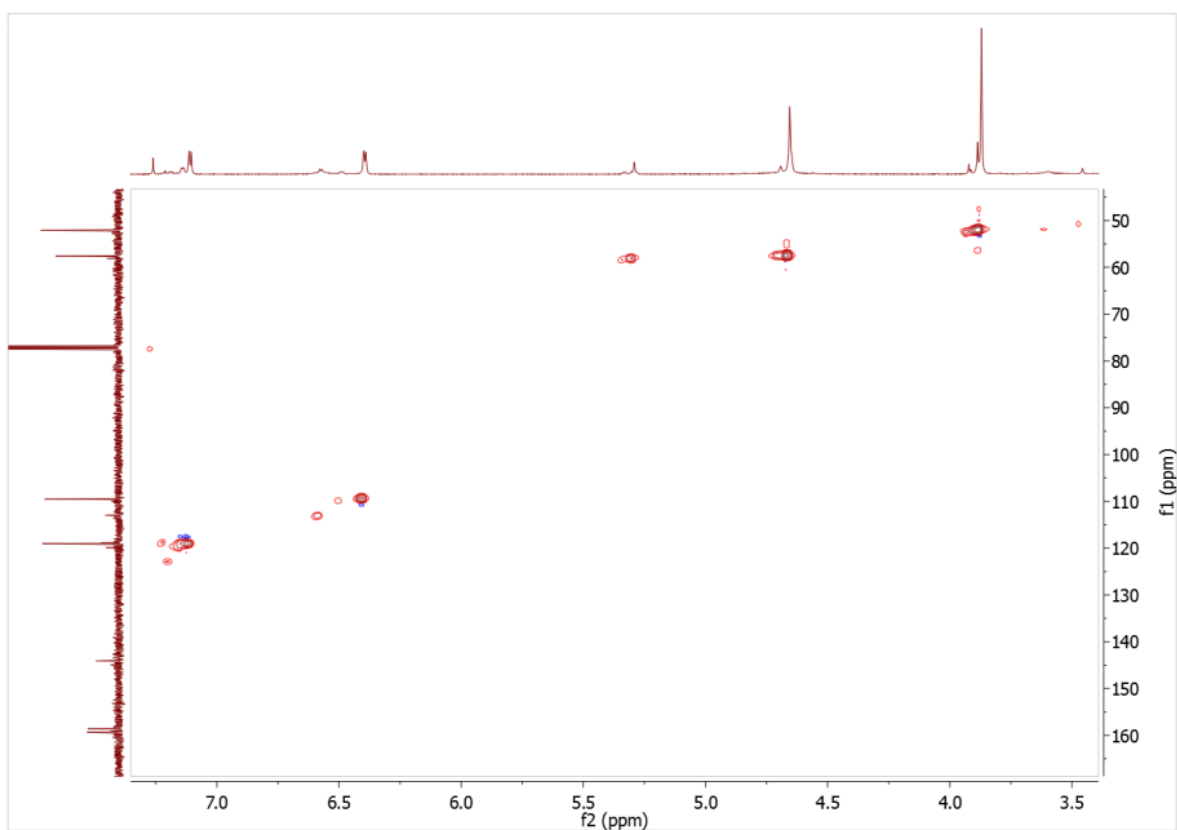
Figure S37. ^{1}H-^{13}C-HSQC- NMR (400 MHz; 101 MHz) spectrum of 3 in CDCl$_3$
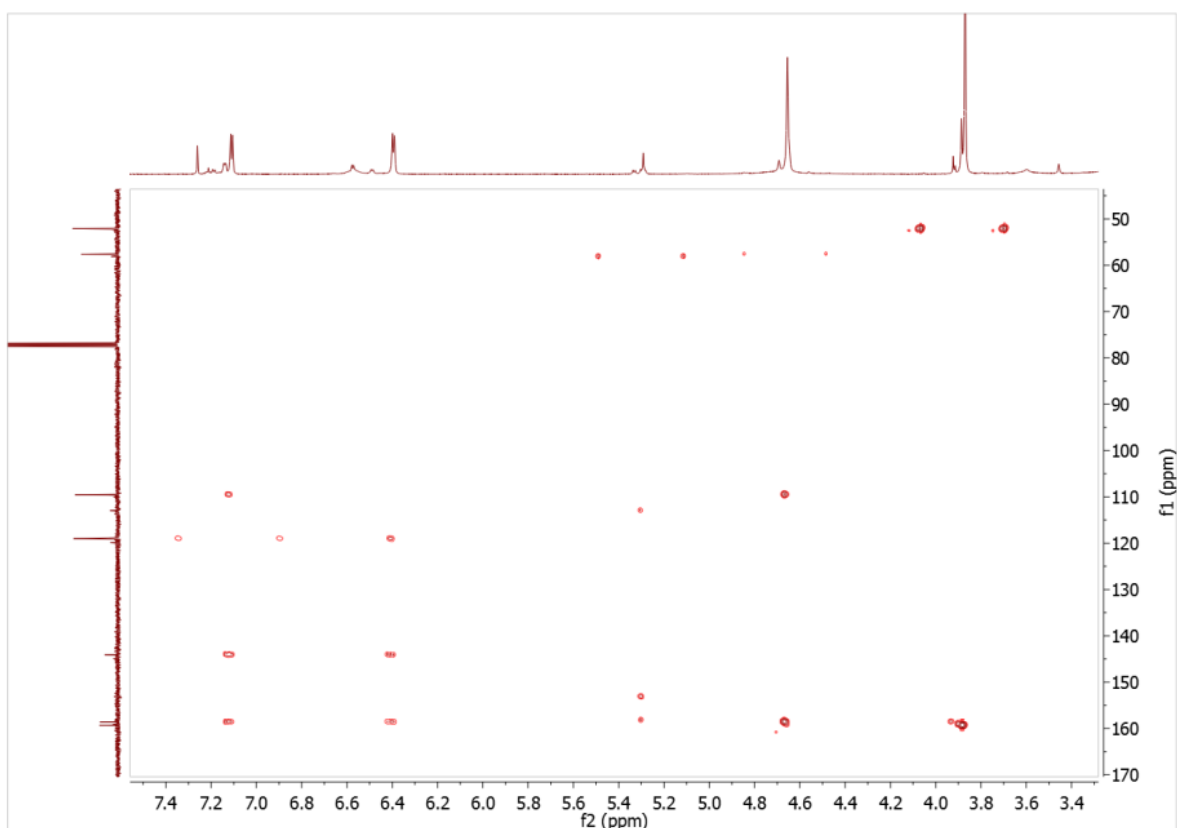
**Figure S38**. ^{1}H-^{13}C-HMBC- NMR (400 MHz; 101 MHz) spectrum of 3 in CDCl$_3$
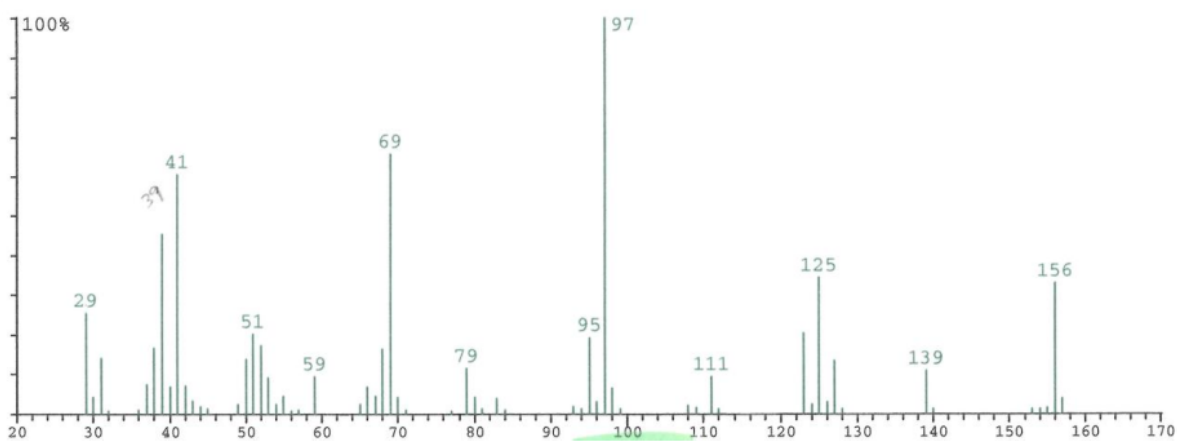
Figure S39. MS spectrum (EI) of 3

6.3 Characterization of furan-2,5-dicarbaldehyde (4)

^{1}H NMR (400 MHz, CDCl$_3$): δ = 9,81 ppm (-CHO), 2H, s); 7,32 ppm (-CH arom, 2H, s). ^{13}C NMR (75 MHz, CDCl$_3$): δ = 179,29 ppm (C=O, aldehyde); 154,26 ppm (C arom); 119,46 ppm (CH arom). MS (GC-MS): m/z = 124[M$^+$] (100%).
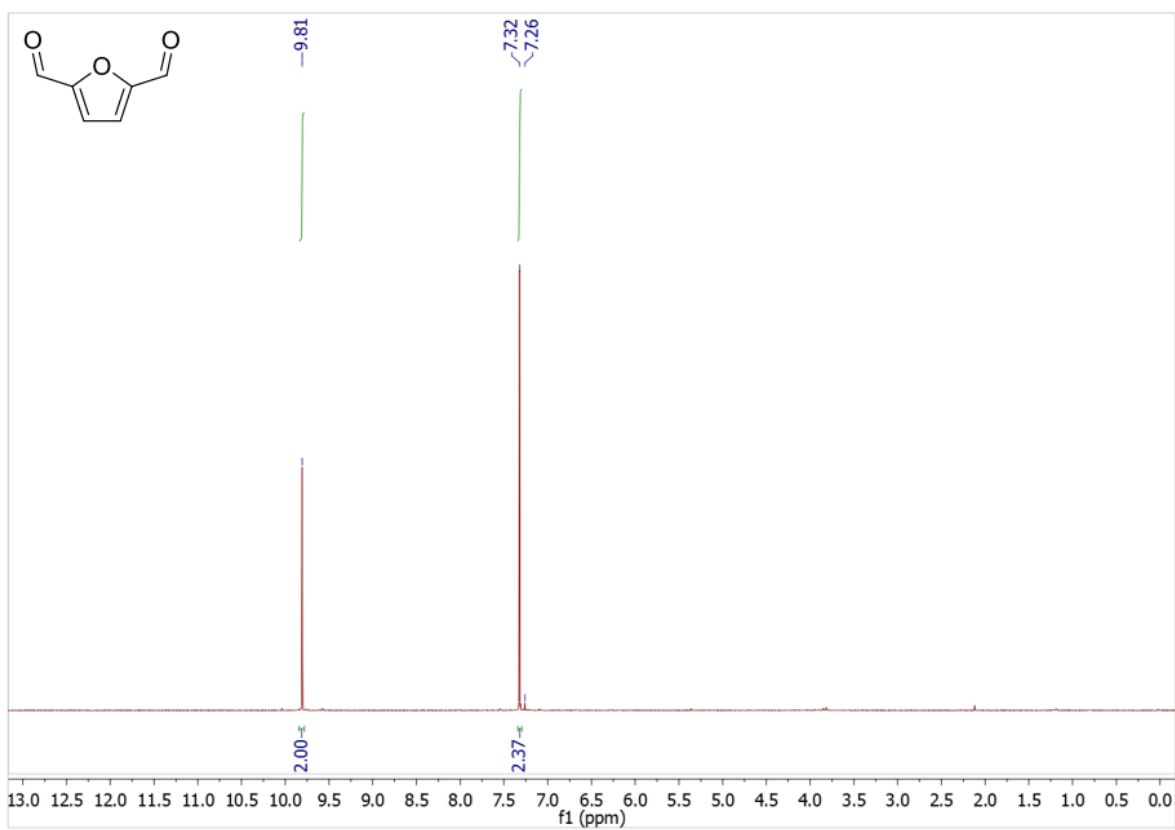
Figure S40. ^{1}H NMR (400 MHz) spectrum of 4 in CDCl$_3$
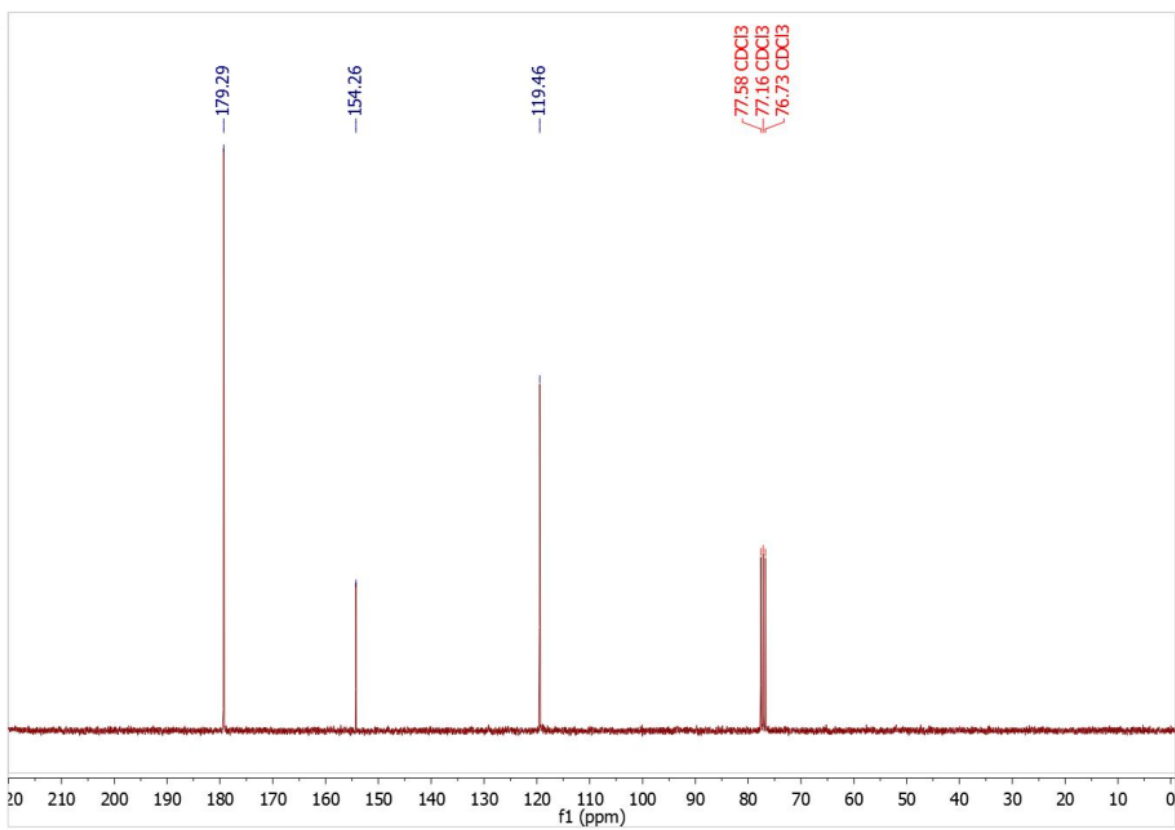
Figure S41. ^{13}C NMR (75 MHz) spectrum of 4 in CDCl$_3$
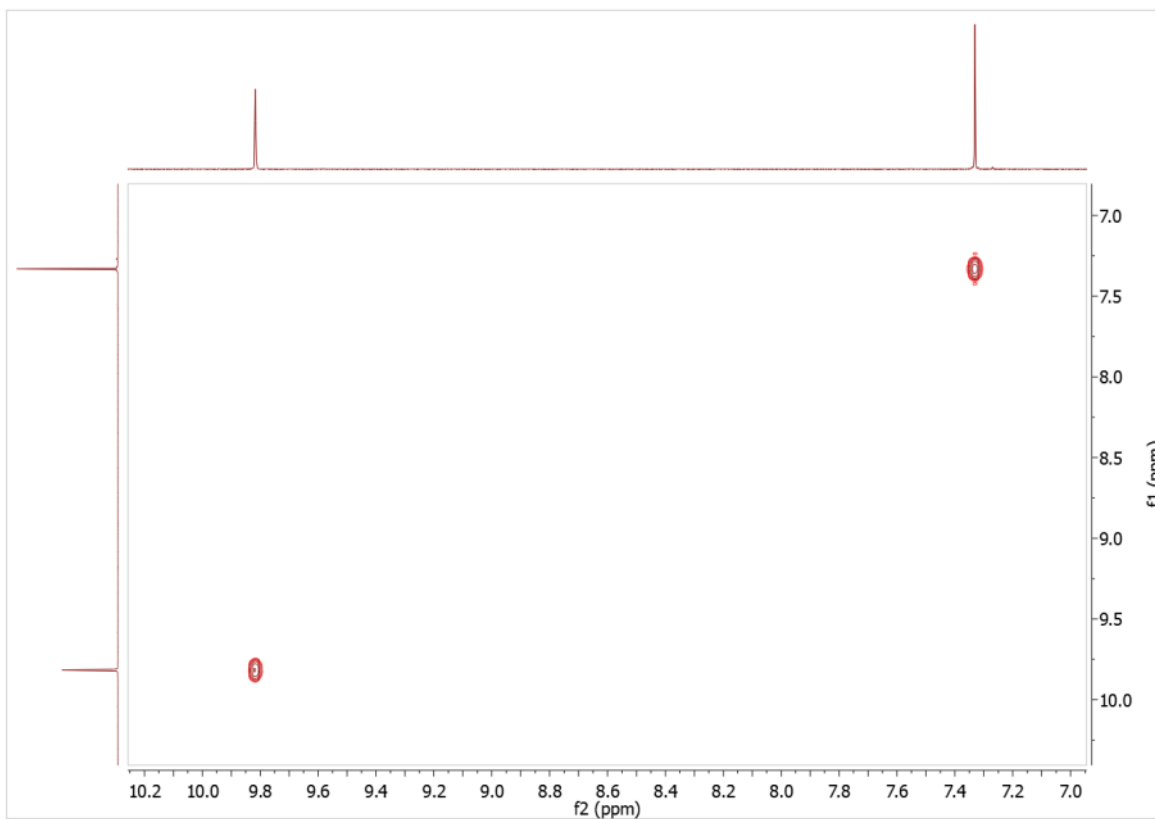
Figure S42. ^{1}H-COSY-NMR (400 MHz) spectrum of 4 in CDCl$_3$
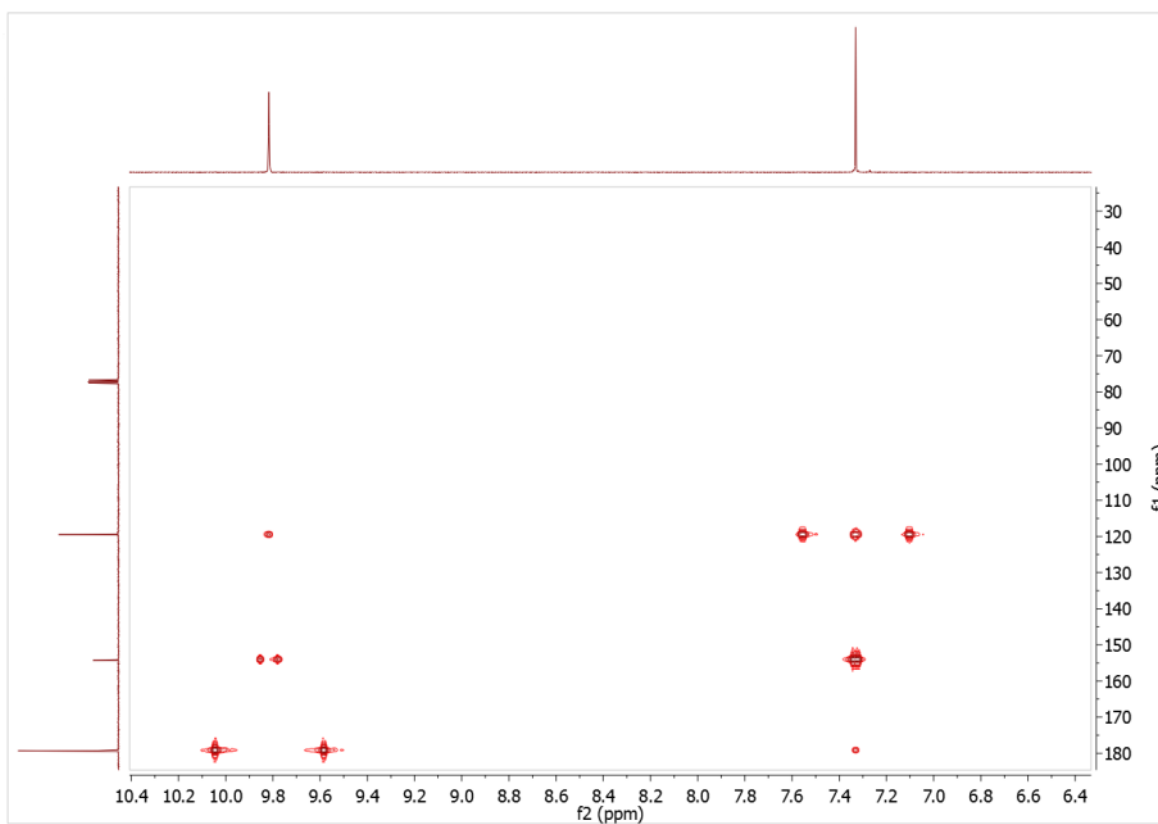
Figure S43. ^{1}H-^{13}C-HMBC- NMR (400 MHz; 101 MHz) spectrum of 3 in CDCl$_3$
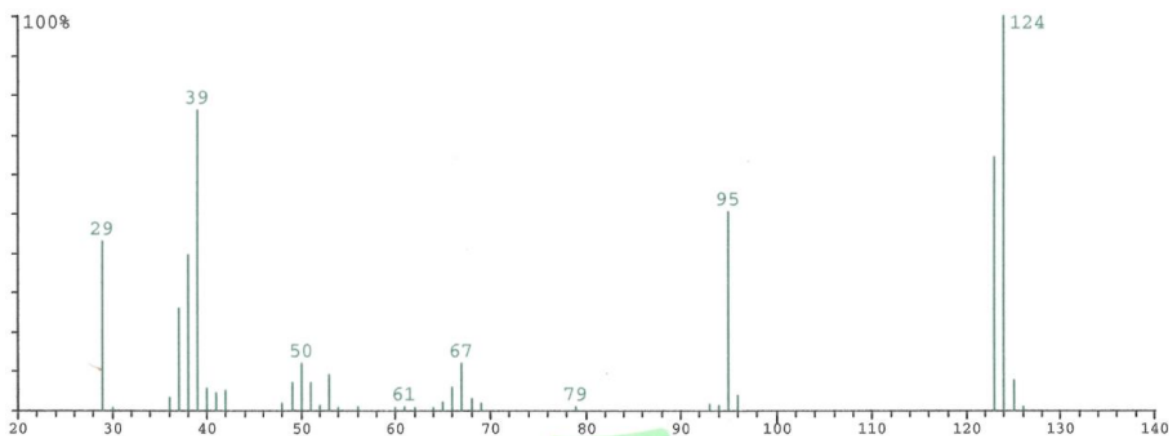
Figure S44. MS spectrum (EI) of 4

6.4 Characterization of methyl 5-formylfuran-2-dicarboxylate (5)

^{1}H NMR (400 MHz, CDCl$_3$): δ = 9,78 ppm (-CHO, 1H, s); 7,25 ppm (-CH arom, 2H, s); 3,92 ppm (-OCH$_3$, 3H, s). ^{13}C NMR (75 MHz, CDCl$_3$): δ = 179,06 ppm (C=O, aldehyde); 158,50 ppm (C=O, ester); 153,95 ppm (C arom (aldehyde side)); 147,72 ppm (C arom (ester side)); 118,78 ppm (CH arom); 52,69 ppm (-OCH$_3$). MS (GC-MS): m/z = 154[M$^+$], 123 (100%).
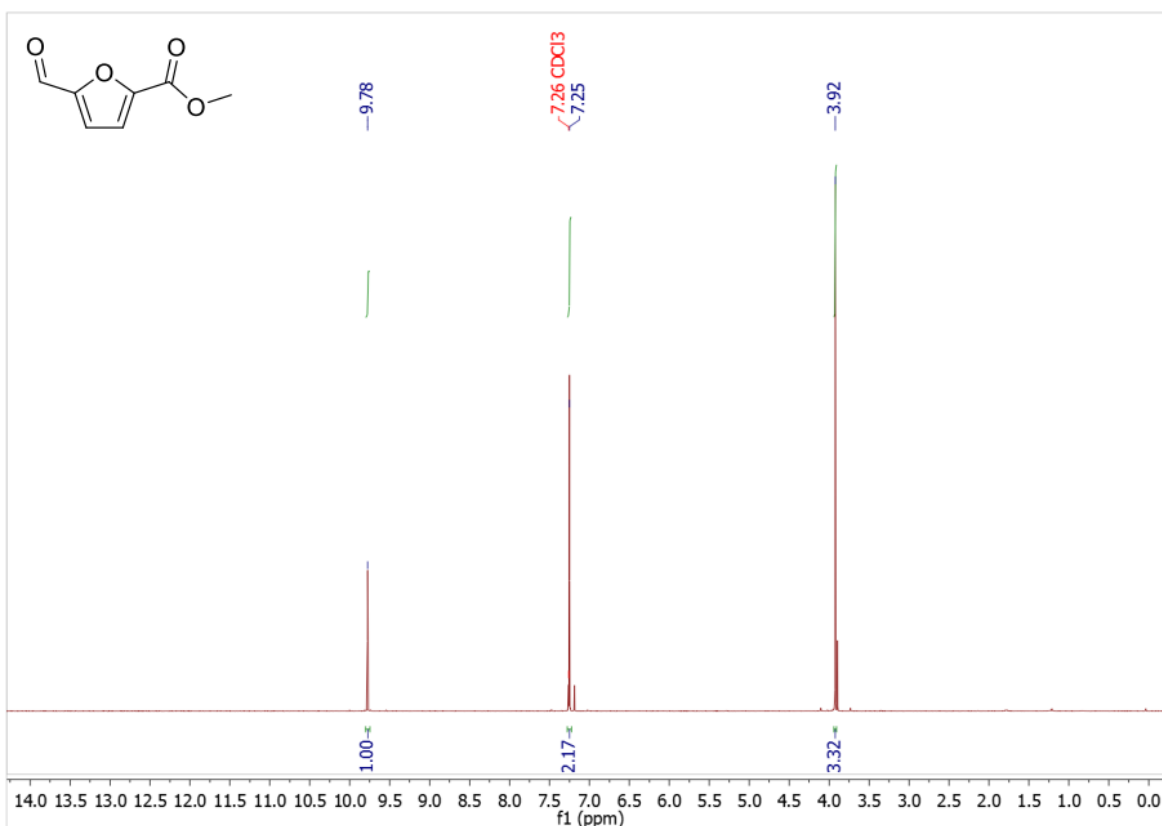
Figure S45. ^{1}H NMR (400 MHz) spectrum of 5 in CDCl$_3$
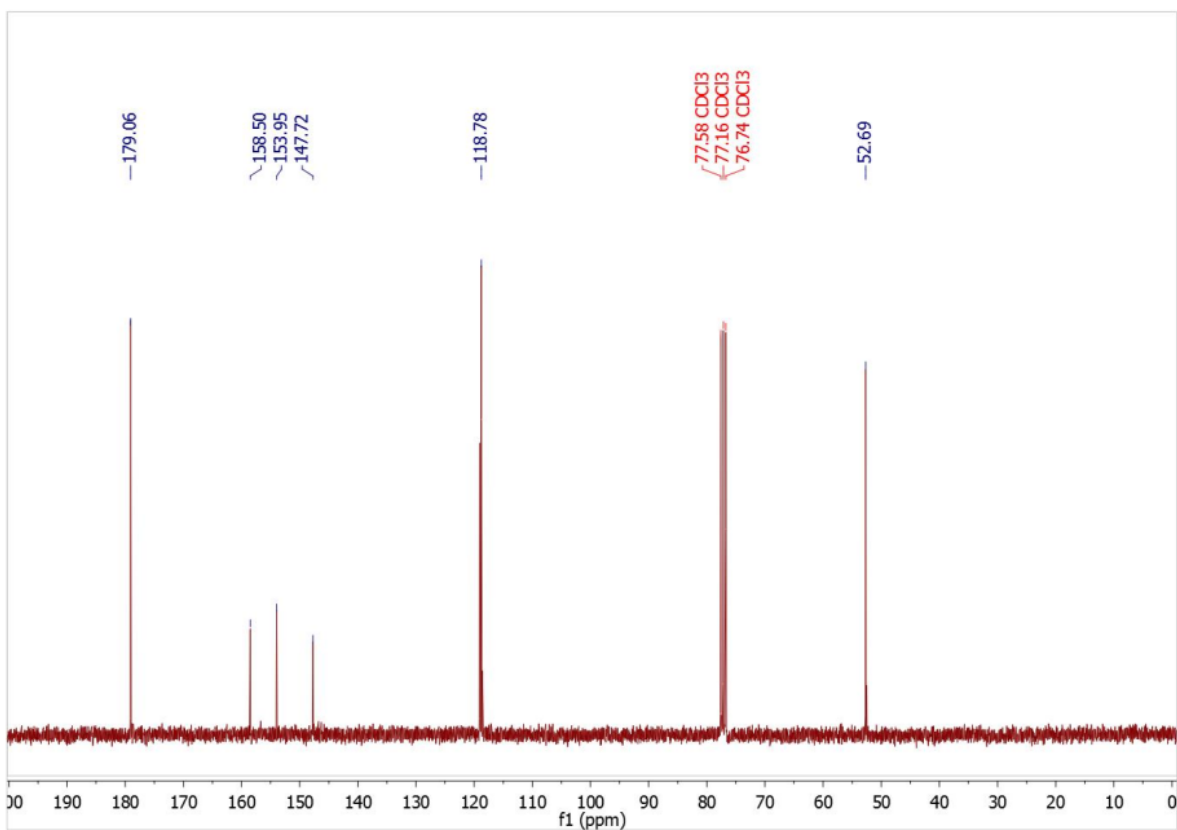
Figure S46. ^{13}C NMR (75 MHz) spectrum of **5** in CDCl$_3$
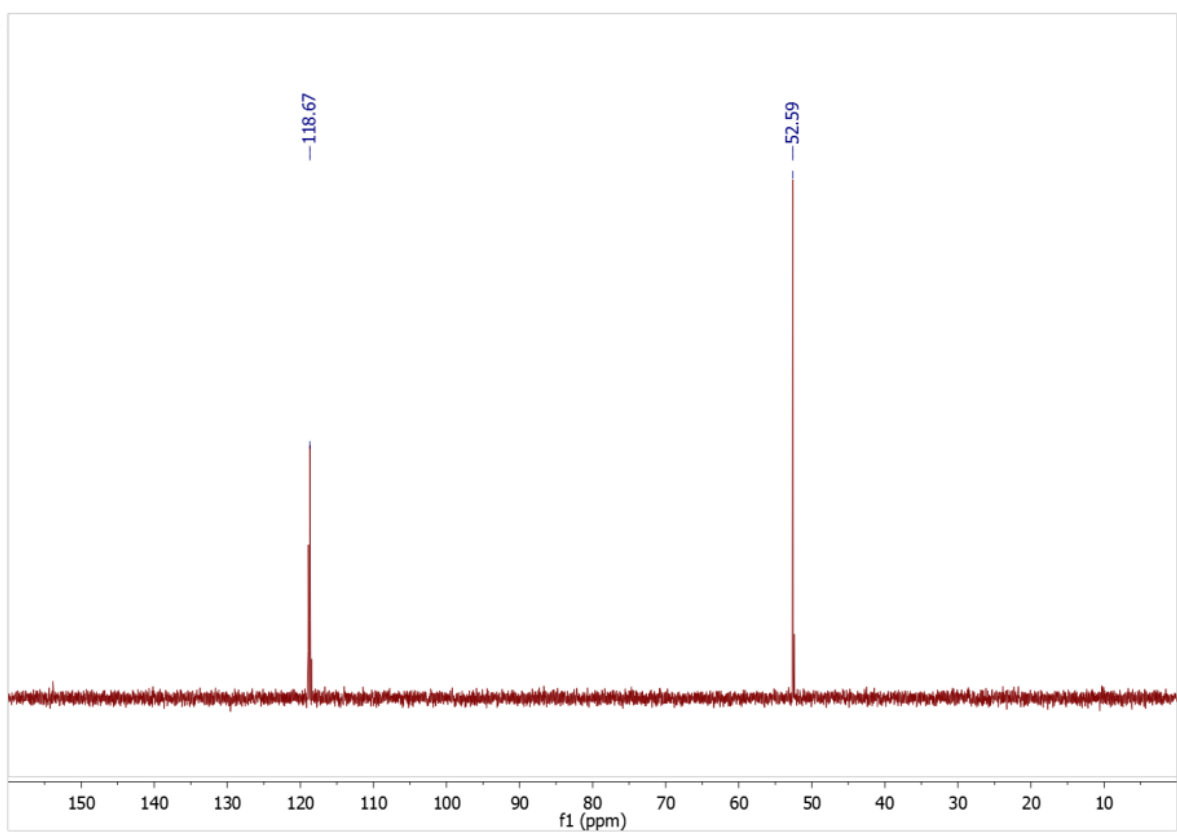
Figure S47. ^{13}C-DEPT NMR (75 MHz) spectrum of **5** in CDCl$_3$
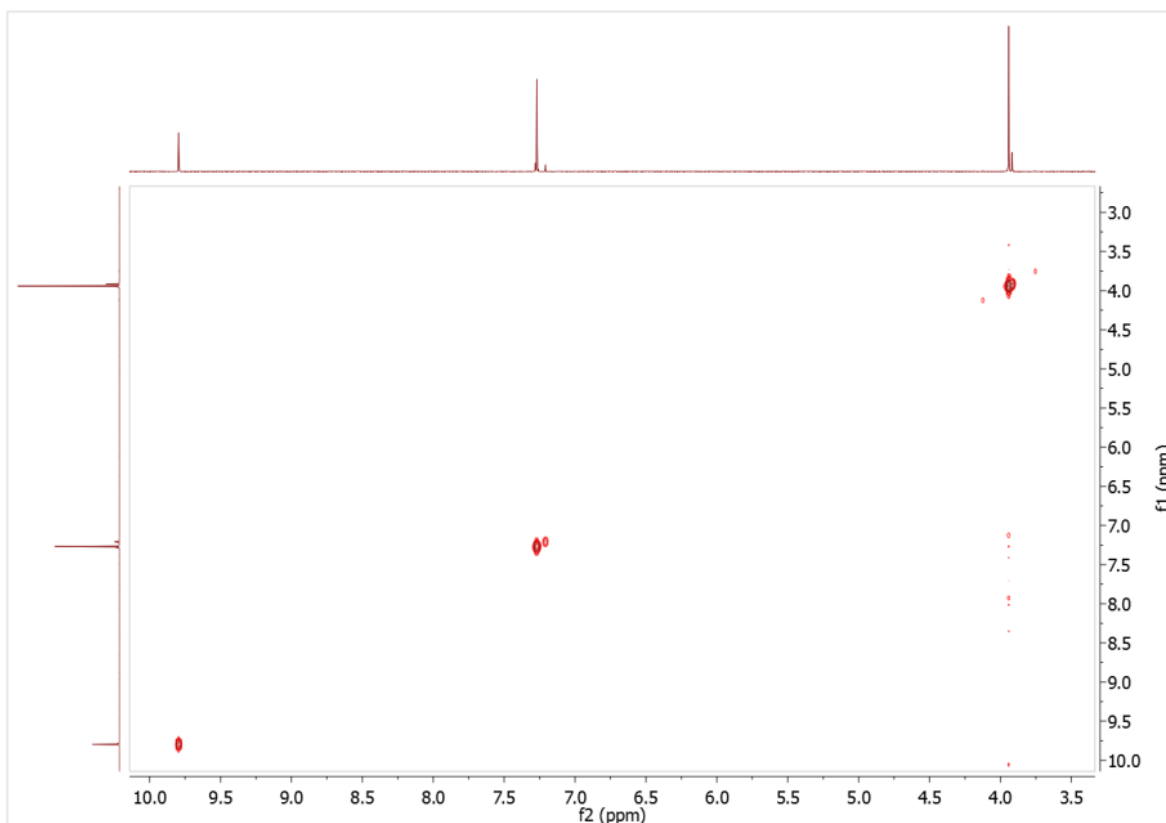
Figure S48. ^{1}H-COSY-NMR (400 MHz) spectrum of 5 in CDCl$_3$
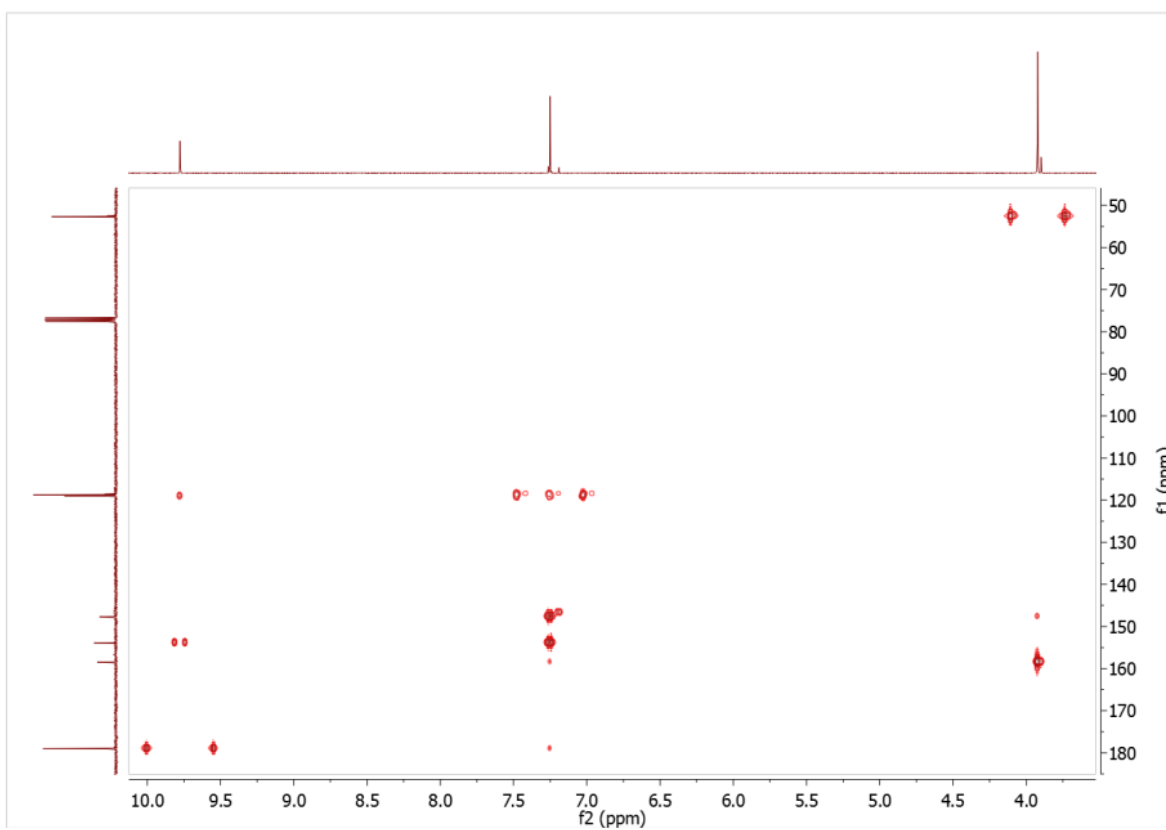
Figure S49. ^{1}H-^{13}C-HMBC- NMR (400 MHz; 101 MHz) spectrum of 5 in CDCl$_3$
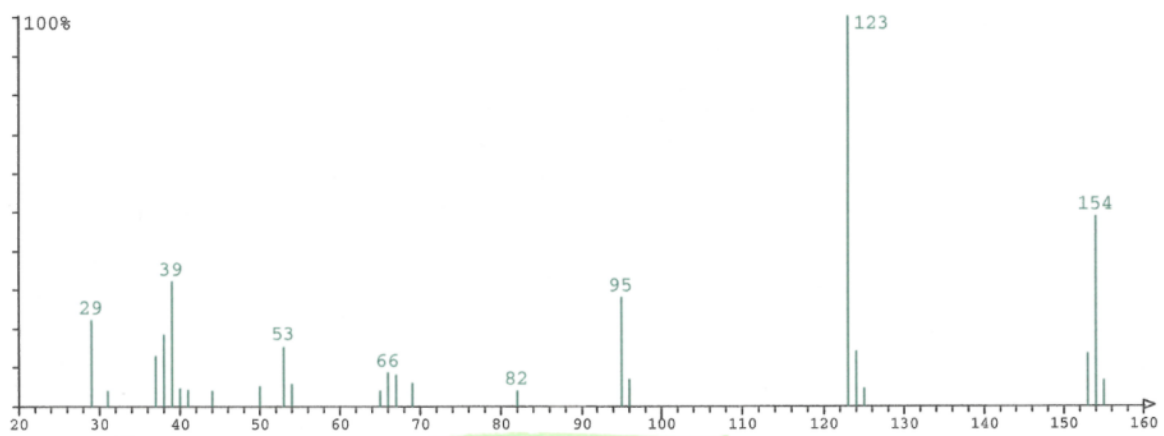
Figure S50. MS spectrum (EI) of 5

7. MS spectra of other compounds

The compounds named as "others" were identified by MS-spectra obtained from GC-MS analysis by comparison with other reports in the literature.

7.1 5-methylfuran-2-carbaldehyde (6) [1]
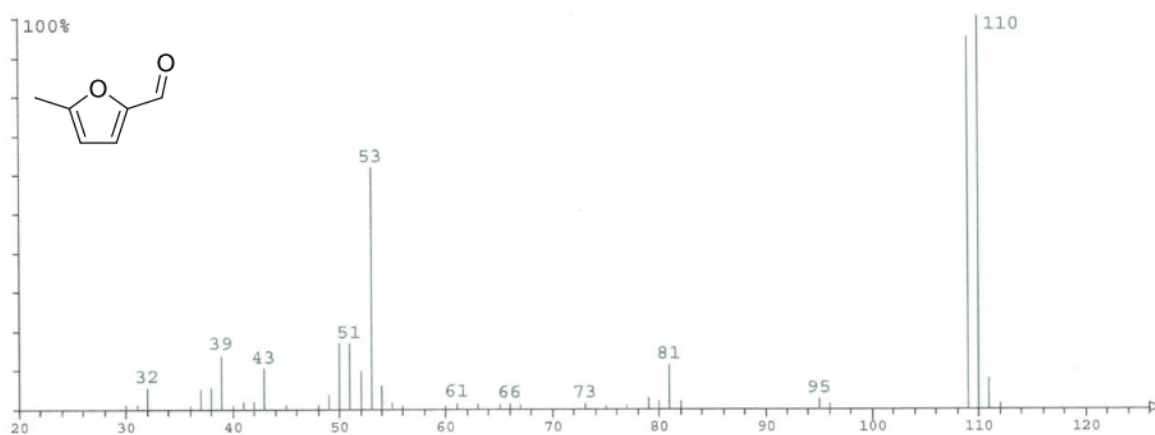
Figure S51. MS spectrum (EI) of 6

7.2 methyl 5-methylfuran-2-carboxylate (7) [2]
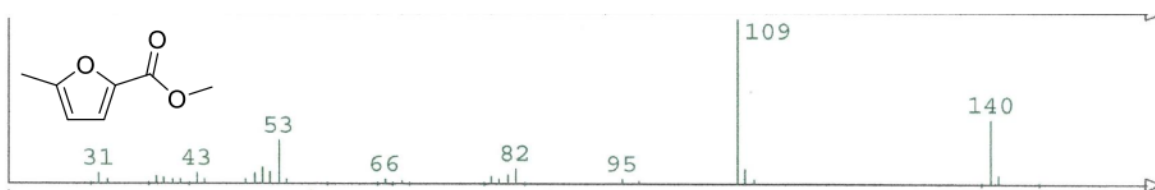
Figure S52. MS spectrum (EI) of 7

S32

7.3 (5-(dimethoxymethyl)furan-2-yl)methanol (8) [3]
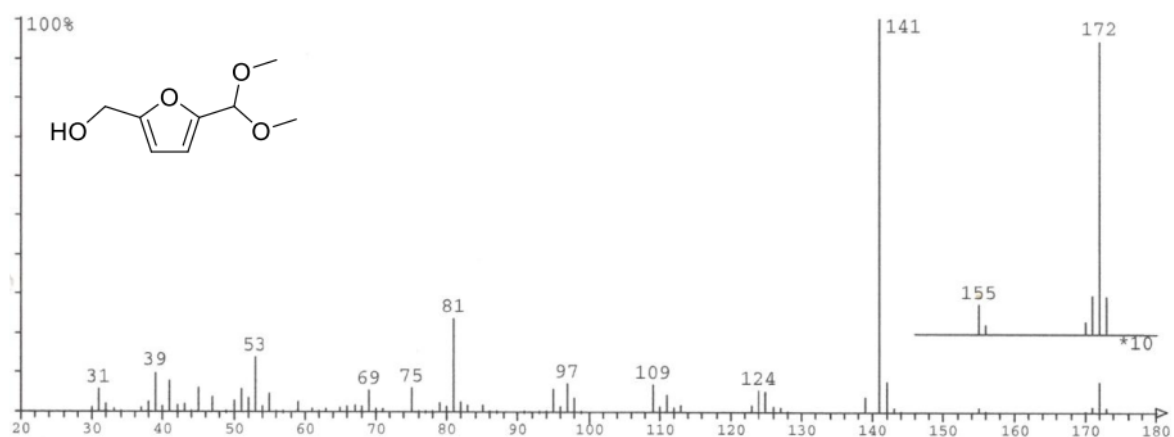
Figure S53. MS spectrum (EI) of 8

7.4 furan-2,5-diyldimethanol (9) [4]
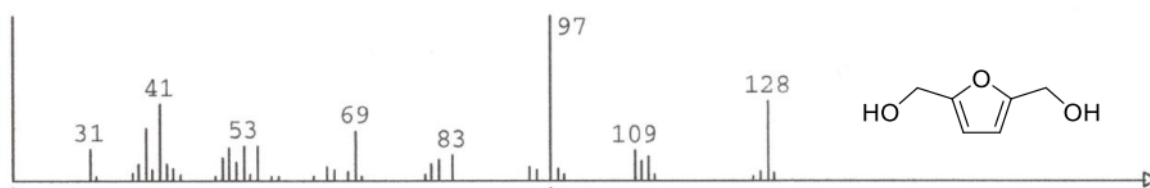
Figure S54. MS spectrum (EI) of 9

7.5 5-(methoxycarbonyl)furan-2-carboxylic acid (10) [5]
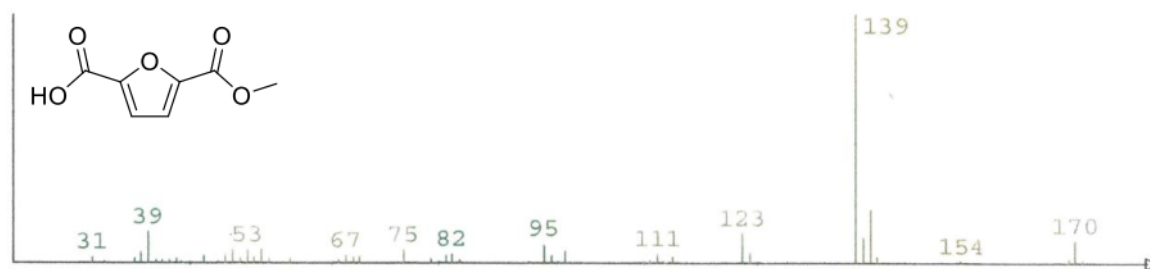
Figure S55. MS spectrum (EI) of 10

S33

190

7.6 2-((5-(methoxycarbonyl)furan-2-yl)methyl) 5-methyl furan-2,5-dicarboxylate (11)
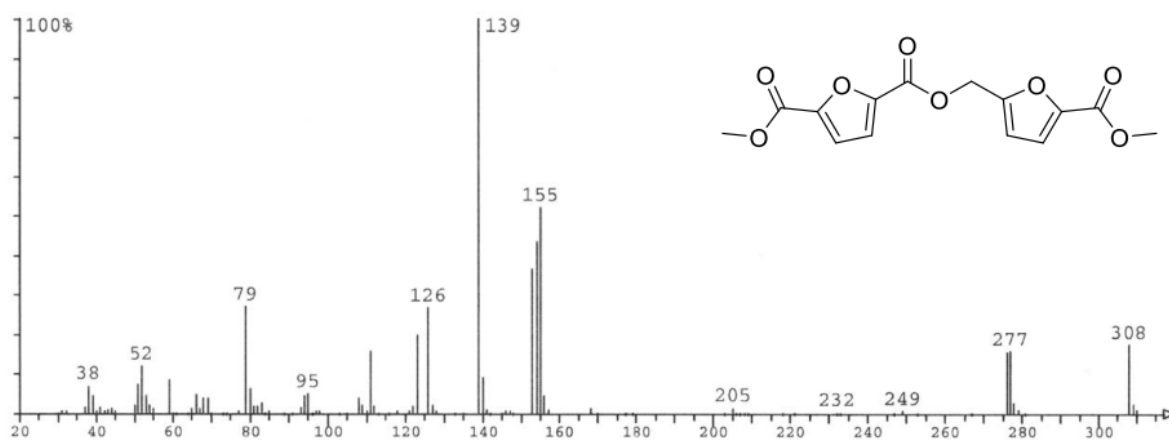
Figure S56. MS spectrum (EI) of 11

8 References

1.   Li, H.; Zhao, W.; Riisager, A.; Saravanamurugan, S.; Wang, Z.; Fang, Z.; Yang, S., A Pd-Catalyzed in situ domino process for mild and quantitative production of 2,5-dimethylfuran directly from carbohydrates. *Green Chemistry* **2017,** *19* (9), 2101-2106.

2.   Citron, C. A.; Rabe, P.; Dickschat, J. S., The Scent of Bacteria: Headspace Analysis for the Discovery of Natural Products. *Journal of Natural Products* **2012,** *75* (10), 1765-1776.

3.   Arias, K. S.; Al-Resayes, S. I.; Climent, M. J.; Corma, A.; Iborra, S., From Biomass to Chemicals: Synthesis of Precursors of Biodegradable Surfactants from 5-Hydroxymethylfurfural. *ChemSusChem* **2013,** *6* (1), 123-131.

4.   Zhou, S.; Dai, F.; Chen, Y.; Dang, C.; Zhang, C.; Liu, D.; Qi, H., Sustainable hydrothermal self-assembly of hafnium–lignosulfonate nanohybrids for highly efficient reductive upgrading of 5-hydroxymethylfurfural. *Green Chemistry* **2019,** *21* (6), 1421-1431.

5.   Kozlov, K. S.; Romashov, L. V.; Ananikov, V. P., A tunable precious metal-free system for selective oxidative esterification of biobased 5-(hydroxymethyl)furfural. *Green Chemistry* **2019,** *21* (12), 3464-3468.

8.3 Chapter 4

8.3.1 Characterization of NHC precursors

8.3.1.1 *Characterization of 1,4-dimethyl-4H-1,2,4-triazol-1-ium iodide (NHC-1)*

^{1}H NMR (300 MHz, CD$_3$CN) δ = 9.83 ppm (-CH, 1H, s), 8.74 ppm (-CH, 1H, s), 4.07 ppm (-CH$_3$, 3H, s), 3.94 ppm. ^{13}C NMR (75 MHz, CD$_3$CN) δ = 145.75 ppm(-CH), 143.66 ppm (-CH), 39.81 ppm (-CH$_3$), 35.27 ppm(-CH$_3$).
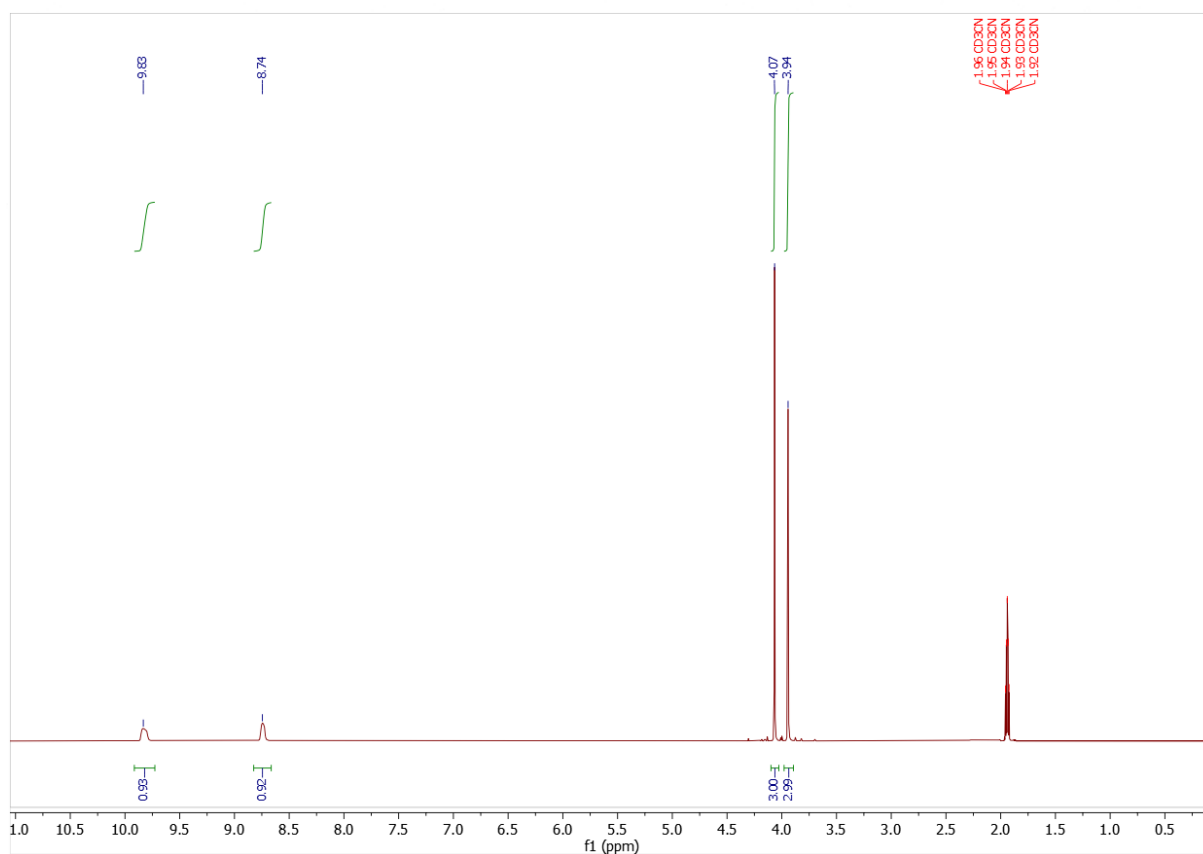
Figure A1. ^{1}H NMR (300 MHz) spectrum of NHC-1 in CD$_3$CN
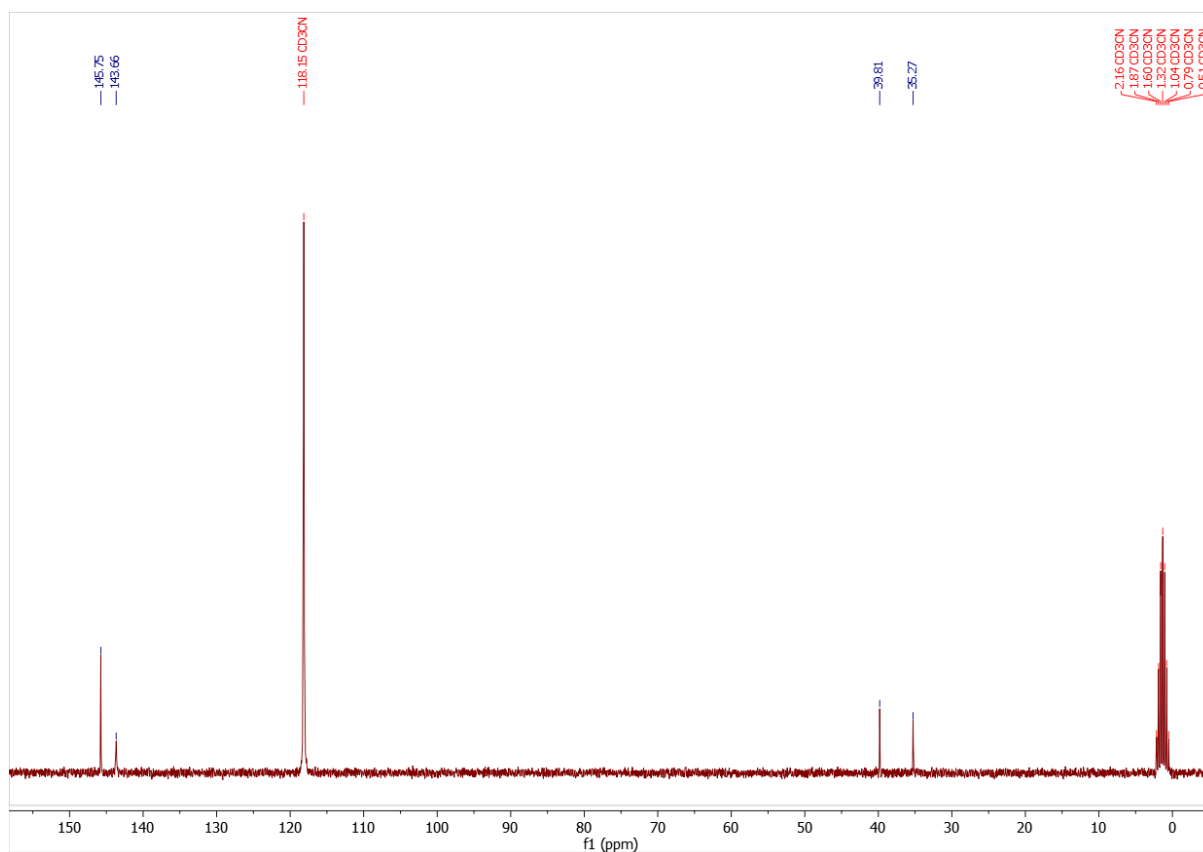
Figure A2. ^{13}C NMR (75 MHz) spectrum of NHC-1 in CD$_3$CN

8.3.1.2   *Characterization of 3,4-dimethyl-5-vinylthiazol-3-ium iodide (NHC-2)*

^{1}H NMR (300 MHz, MeOD) δ = 9.94 ppm (-CH, 1H, s), 7.02 ppm (-**CH**=CH$_2$, 1H, ddd, *J* = 17 Hz, 11 Hz, 0.7 Hz), 5.94 ppm(-CH=**CH$_2$**, 1H-trans, d, *J* = 17 Hz), 5.68 ppm (-CH=**CH$_2$**, 1H-cis, d, *J* = 11 Hz), 4.16 ppm (-CH$_3$, 3H, s), 2.58 ppm (-CH$_3$, 3H, s). ^{13}C NMR (75 MHz, MeOD) δ = 157.32 ppm (thiazol ring), 141.75 ppm (thiazol ring), 136.75 ppm (thiazol ring), 125.48 ppm (-vinyl), 122.14 ppm (-vinyl), 41.42 ppm (-CH$_3$), 11.89 ppm (-CH$_3$).
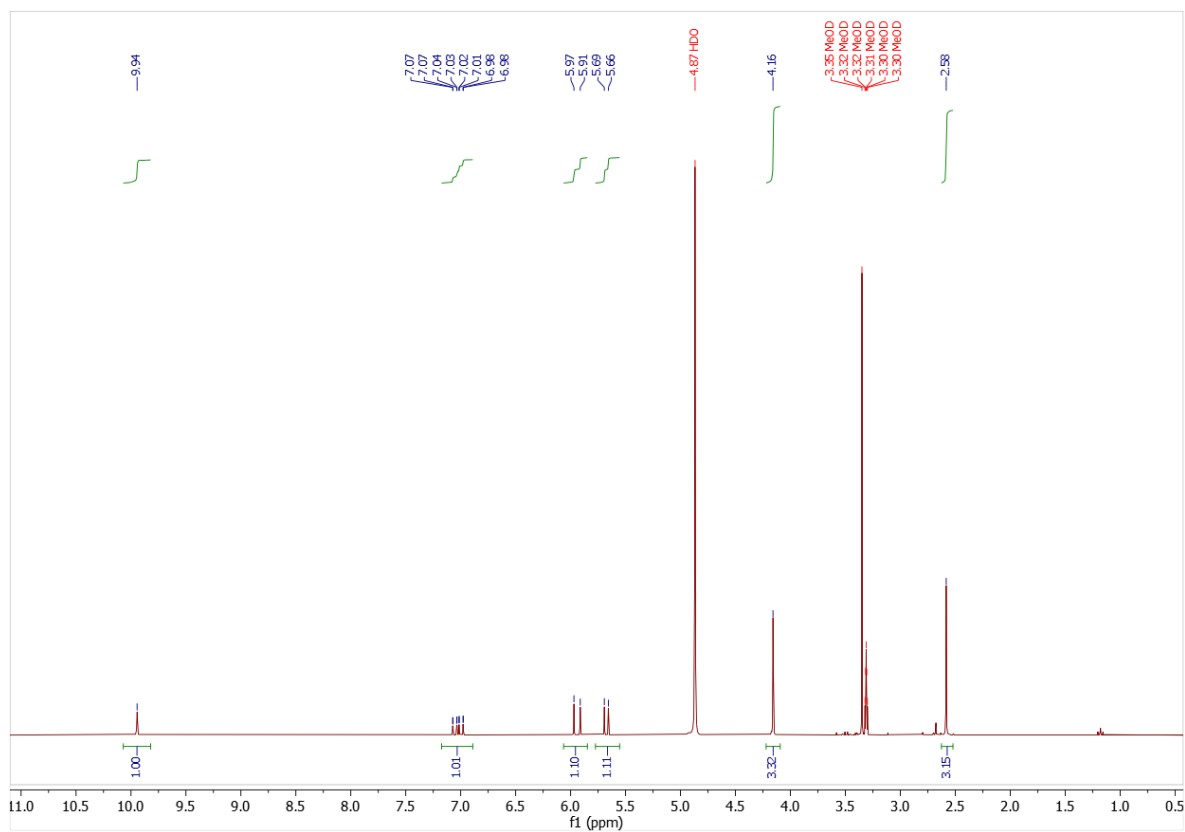
Figure A3. ^{1}H NMR (300 MHz) spectrum of NHC-2 in MeOD
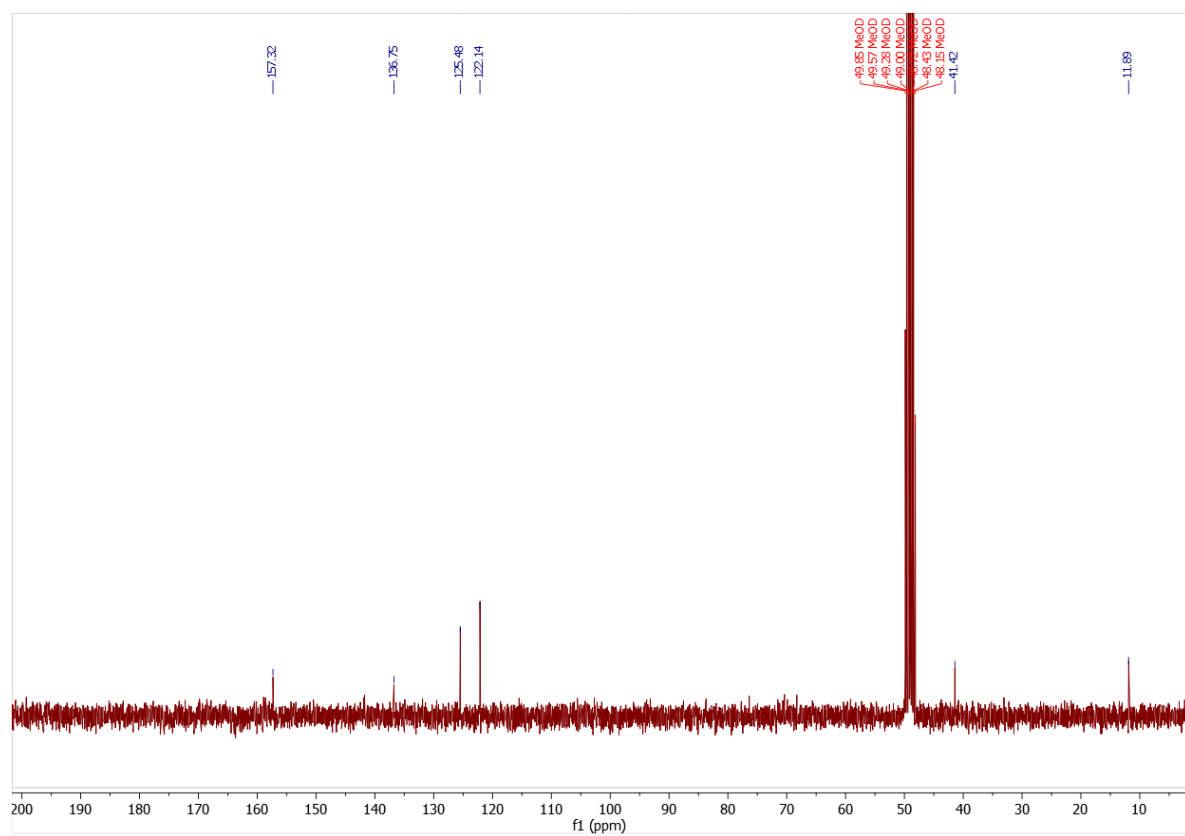
Figure A4. ^{13}C NMR (75 MHz) spectrum of NHC-2 in MeOD

8.3.1.3   Characterization of 1,4-dimethyl-4H-1,2,4-triazol-1-ium bis((trifluoromethyl)sulfonyl)amide (NHC-7)

^{1}H NMR (400 MHz, CD$_3$CN) δ = 9.17 ppm (-CH, 1H, s), 8.51 ppm (-CH, 1H, s), 4.04 ppm (-CH$_3$, 3H, s), 3.87 ppm (-CH$_3$, 3H, s). ^{13}C NMR (101 MHz, CH$_3$CN) δ = 145.95 ppm(-CH), 143.51 ppm (-CH), 120.89 ppm (-CF$_3$, q, J = 320.6 Hz), 39.78 ppm (-CH), 35.10 ppm (-CH).
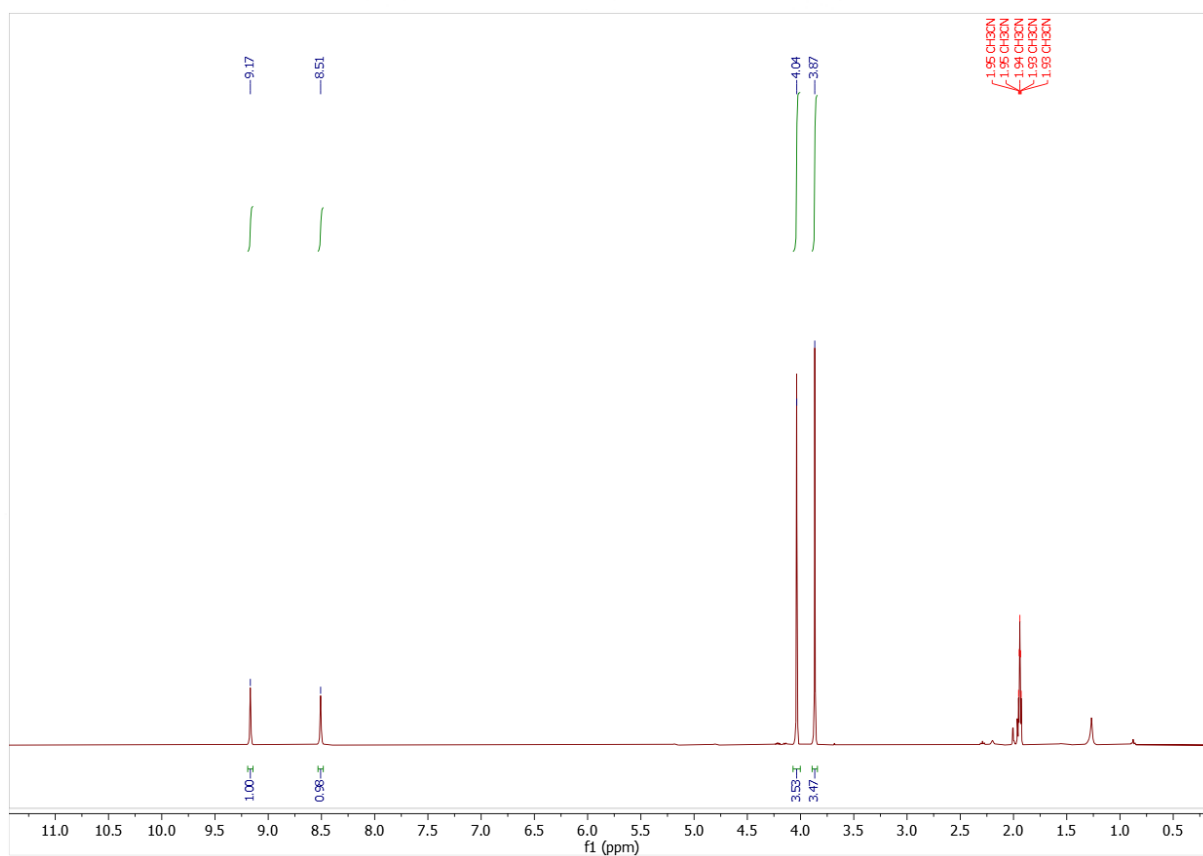
Figure A5. ^{1}H NMR (300 MHz) spectrum of NHC-7 in CD$_3$CN
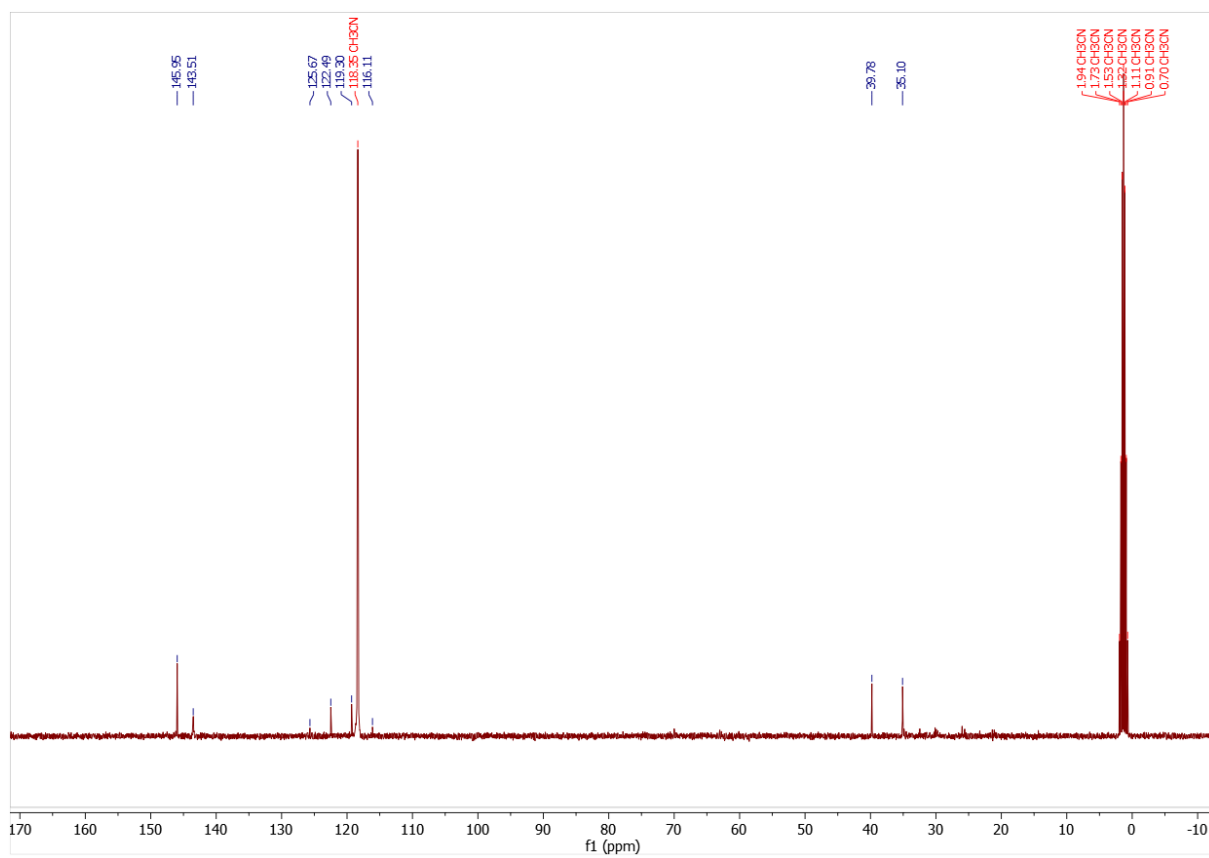
Figure A6. ^{13}C NMR (75 MHz) spectrum of NHC-7 in CD$_3$CN

8.3.2.1   *Characterization of 6-hydroxyhexyl 5-(hydroxymethyl)furan-2-carboxylate (52)*

^{1}H NMR (300 MHz, CDCl$_3$) δ = 7.11 ppm (-CH, 1H, d, *J* = 3.4 Hz), 6.40 ppm (-CH, 1H, d, *J* = 3.4 Hz), 4.65 ppm (-**CH$_2$**-OH, 2H, s), 4.29 ppm (-(CO)-O**CH$_2$**-, 2H, t), 3.64 ppm (t, *J* = 6.4 Hz, 3H), 1.83 − 1.67 (m, 3H), 1.64 − 1.53 (m, 3H), 1.52 − 1.33 (m, 6H). ^{13}C NMR (75 MHz, CDCl$_3$) δ = 159.04, 158.49, 144.40, 118.82, 109.52, 77.58, 77.16, 76.74, 65.15, 62.92, 57.61, 43.52, 32.59, 28.66, 25.86, 25.57, 25.44. MS (GC-MS): m/z = 242[M$^+$], 125 (100%).
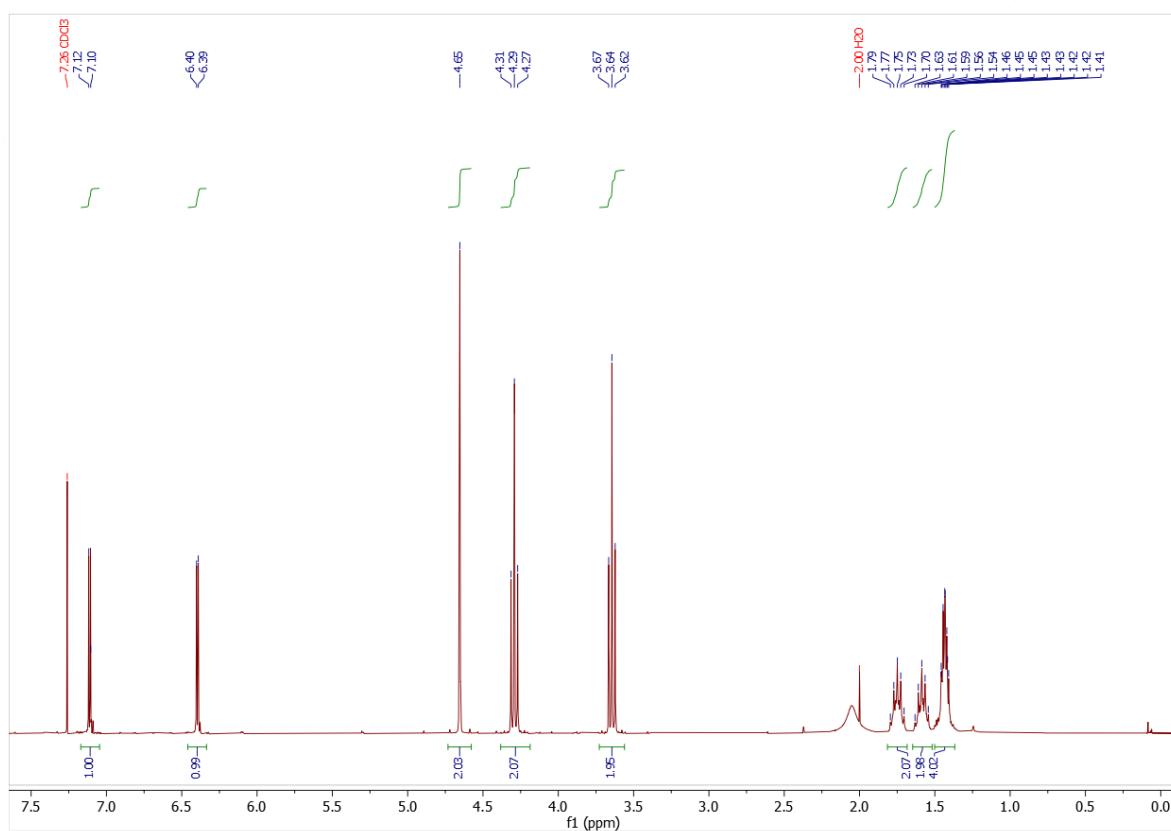
Figure A7. ^{1}H NMR (300 MHz) spectrum of 52 in CDCl$_3$
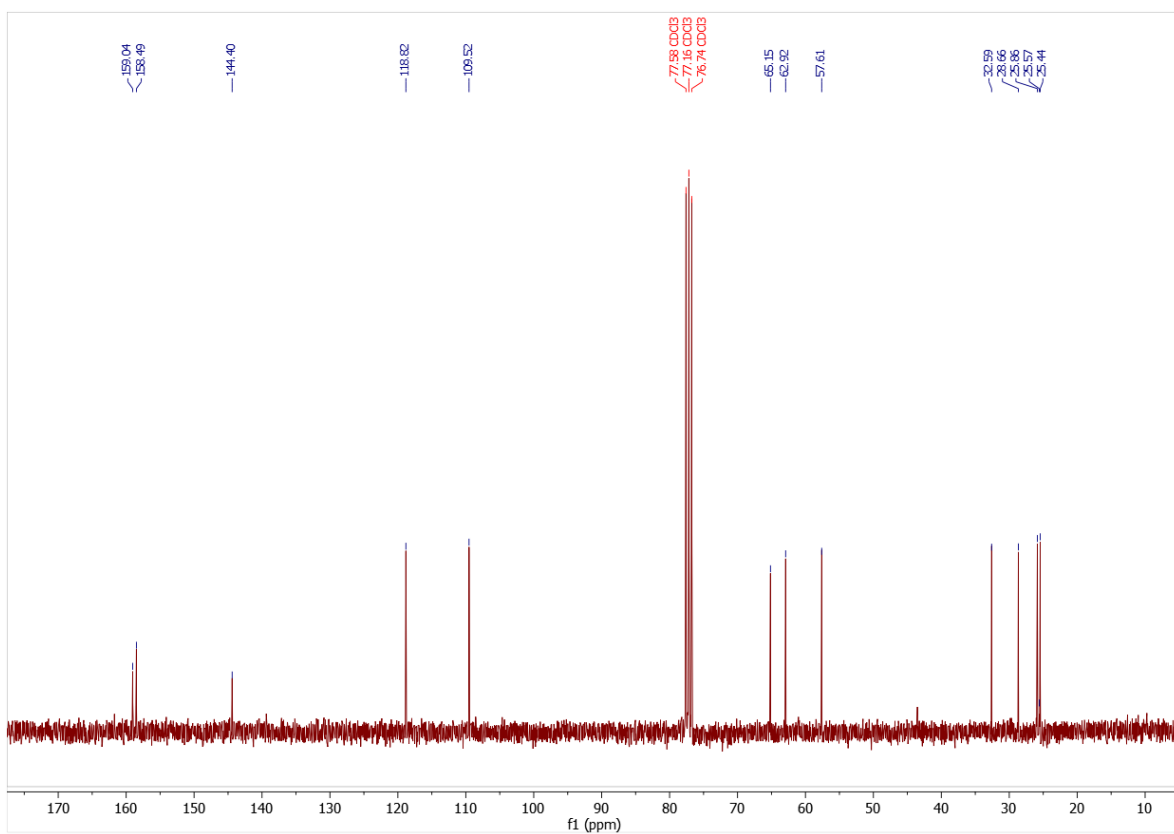
Figure A8. ^{13}C NMR (75 MHz) spectrum of 52 in CDCl$_3$
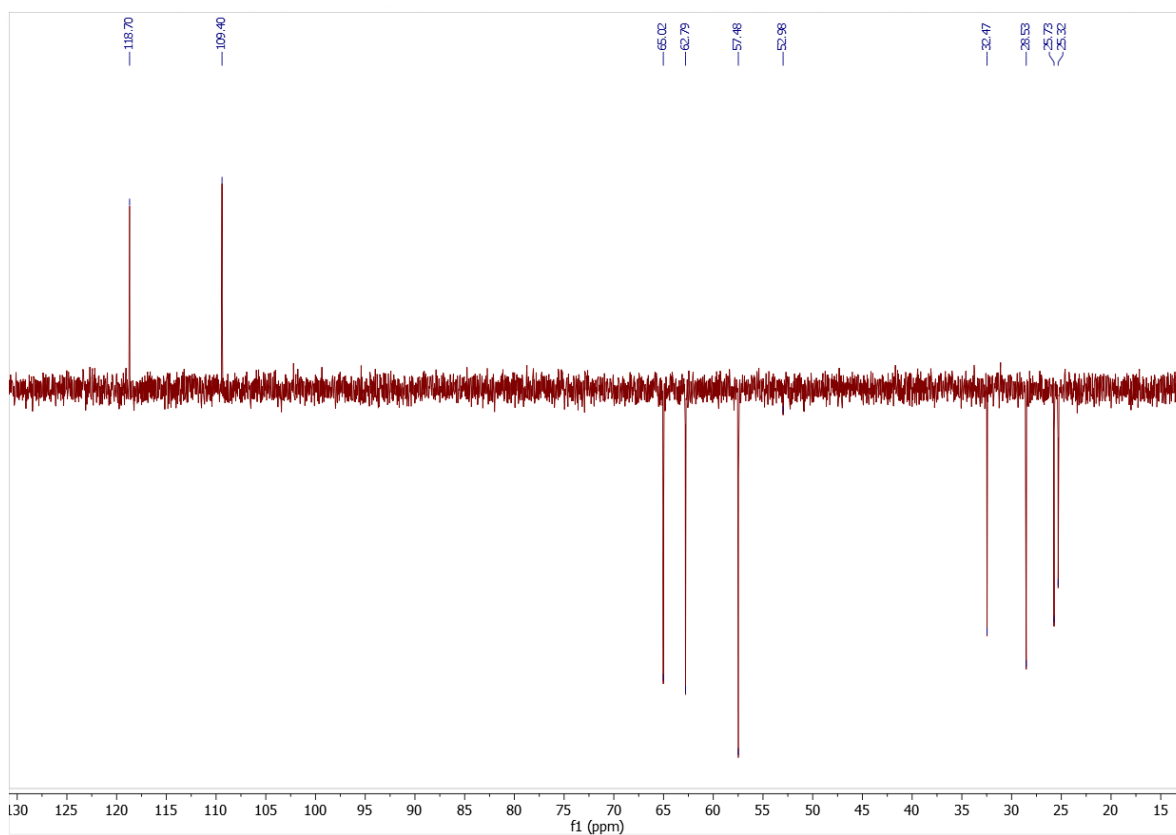
Figure A9. ^{13}C-DEPT NMR (75 MHz) spectrum of in CDCl$_3$
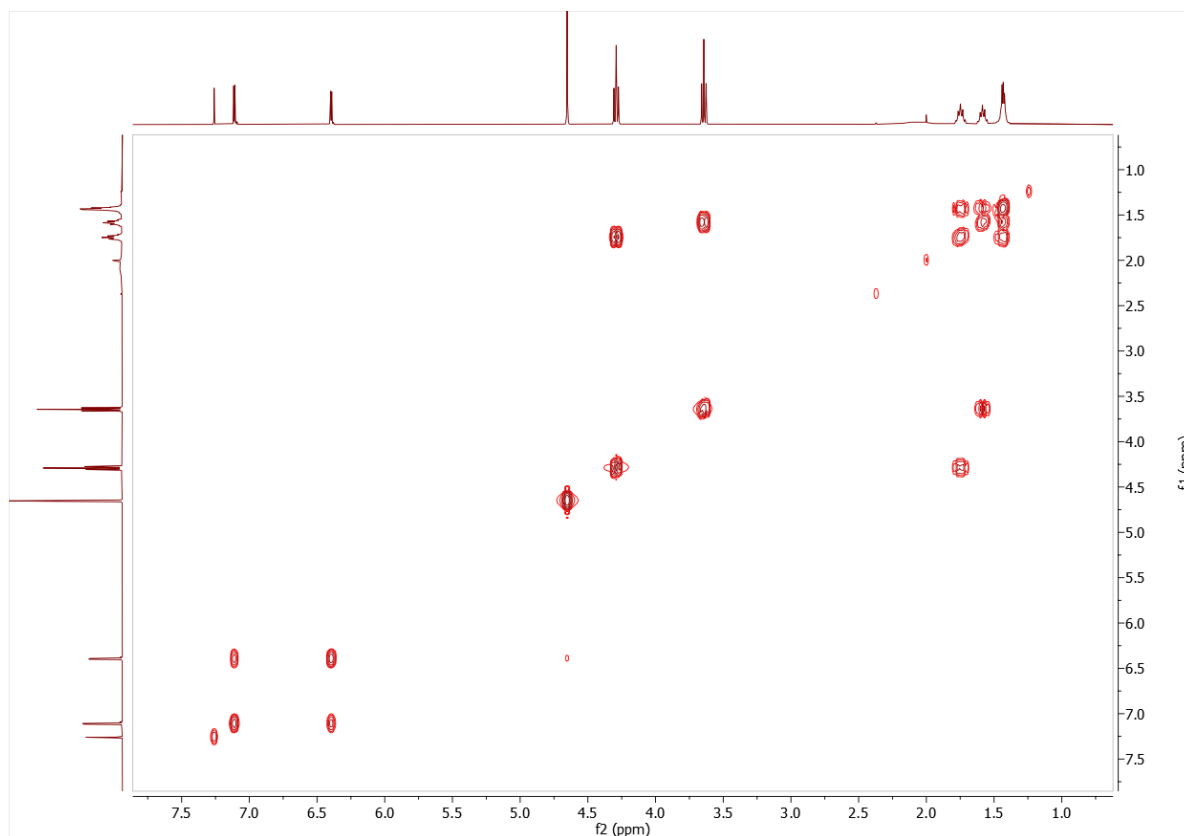
Figure A10. ^{1}H-COSY-NMR (300 MHz) spectrum of 52 in CDCl$_3$
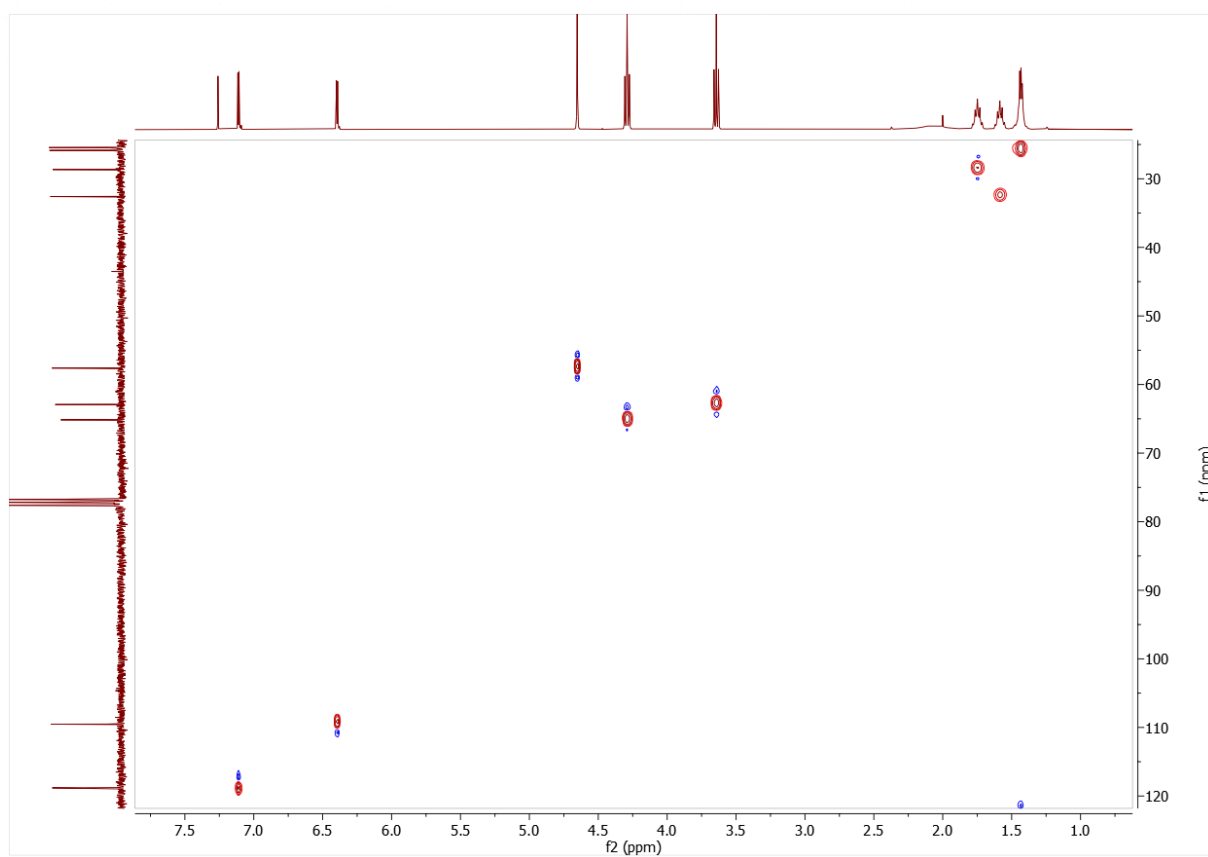
Figure A11. ^{1}H-^{13}C-HSQC- NMR (300 MHz; 75 MHz) spectrum of 52 in CDCl$_3$
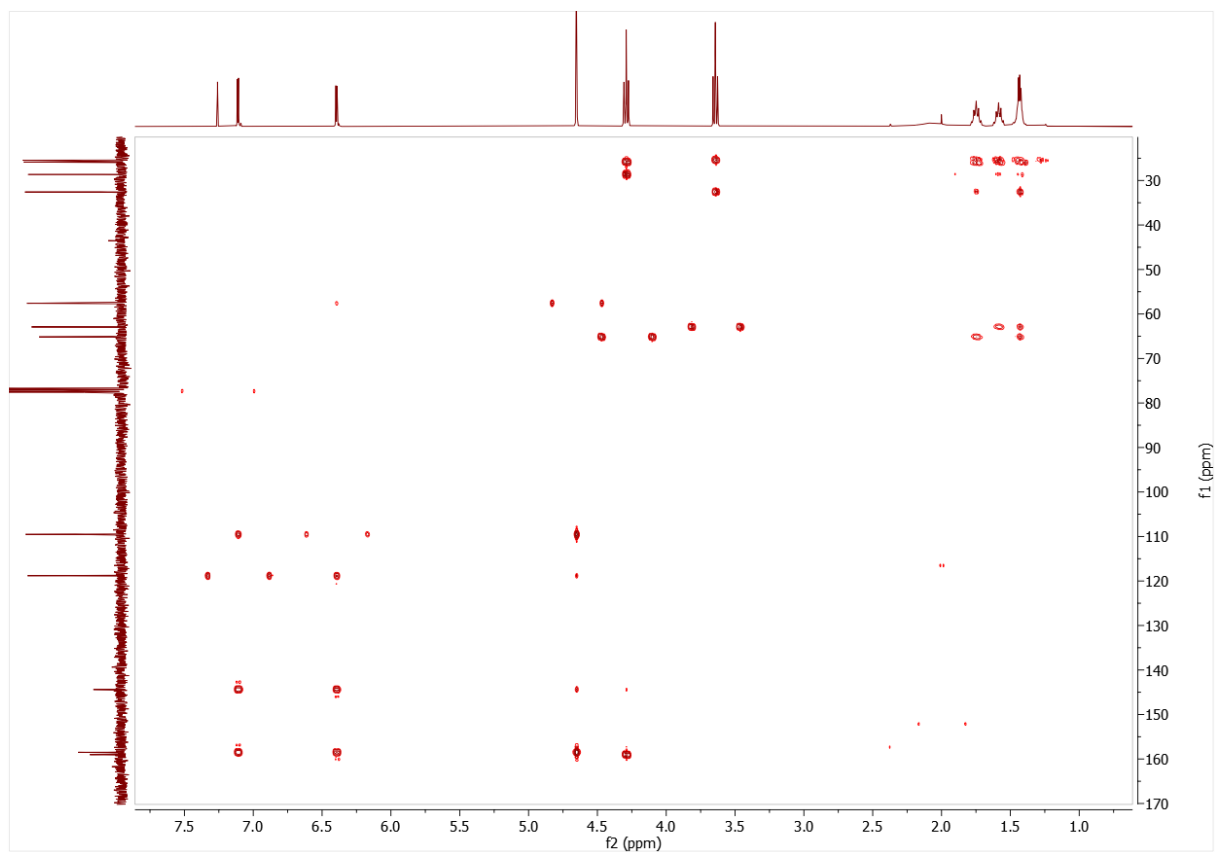
Figure A12. ^1H-^{13}C-HMBC- NMR (300 MHz; 75 MHz) spectrum of 52 in $CDCl_3$
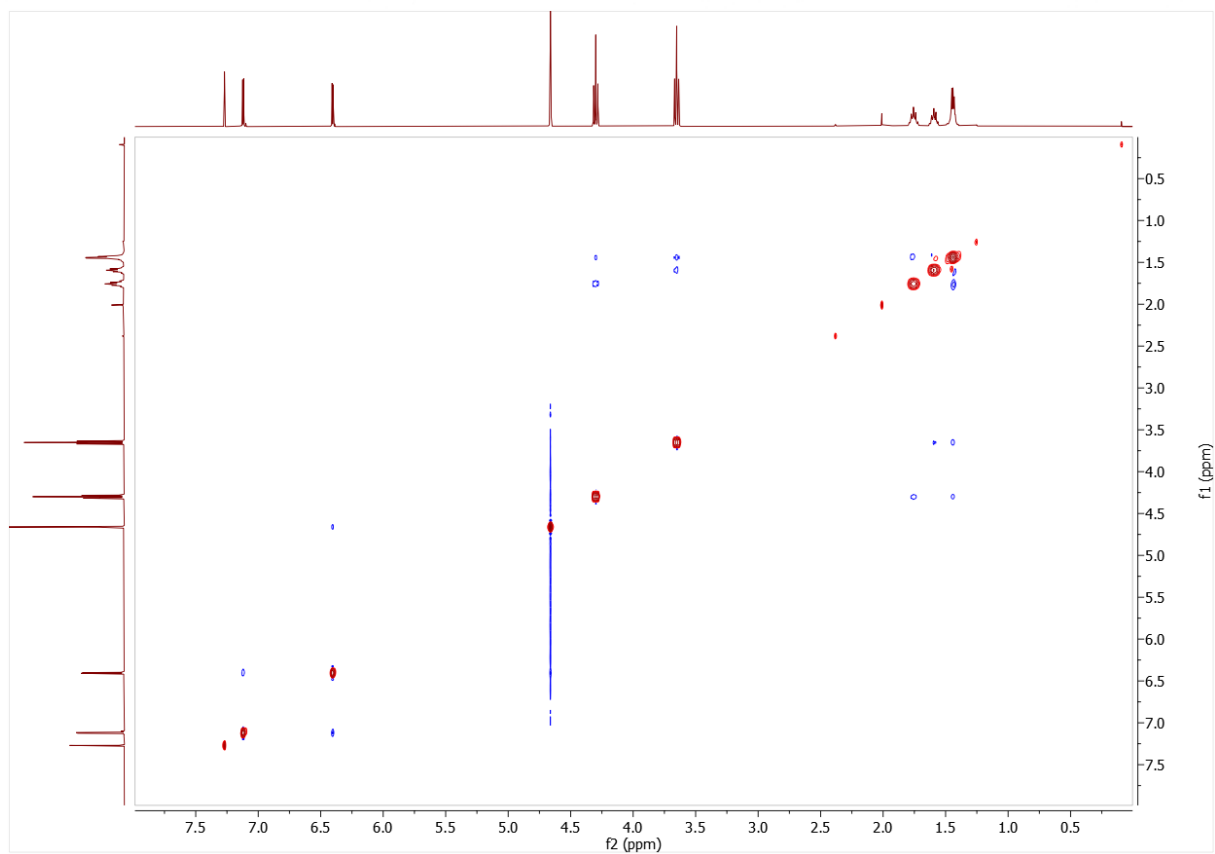
Figure A13. ^1H-NOESY-NMR (300 MHz) spectrum of 52 in $CDCl_3$
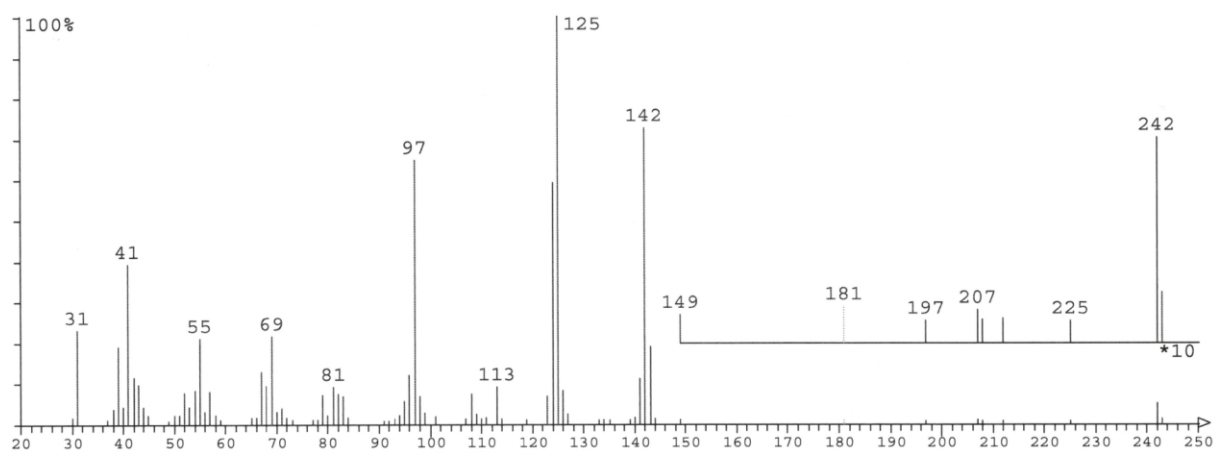
Figure A14. MS spectrum (EI) of 52

8.3.2.2   *Characterization of 6-hydroxyhexyl 5-methylfuran-2-carboxylate (53)*

^{1}H NMR (400 MHz, CDCl$_3$) δ = 7.06 ppm (-CH, 1H, d, *J* = 3.4 Hz), 6.10 ppm (-CH, 1H, d, *J* = 3.4 Hz), 4.28 ppm (-(CO)-O**CH$_2$**-, 2H, t), 3.65 ppm (HO-**CH$_2$**-, 2H, t), 2.39 ppm (CH$_3$, 3H, s), 1.82 – 1.68 ppm (-CH$_2$-, 2H, m), 1.60 – 1.55 ppm (-CH$_2$-, 2H, m), 1.52 – 1.35 ppm (-**CH$_2$**-**CH$_2$**-, 4H, m). ^{13}C NMR (101 MHz, CDCl$_3$) δ = 257.70, 159.11, 157.27, 143.31, 132.62, 119.37, 108.50, 106.07, 64.79, 62.97, 32.74, 28.86, 25.85, 25.52, 14.15. MS (GC-MS): m/z = 226[M$^+$], 126 (100%).
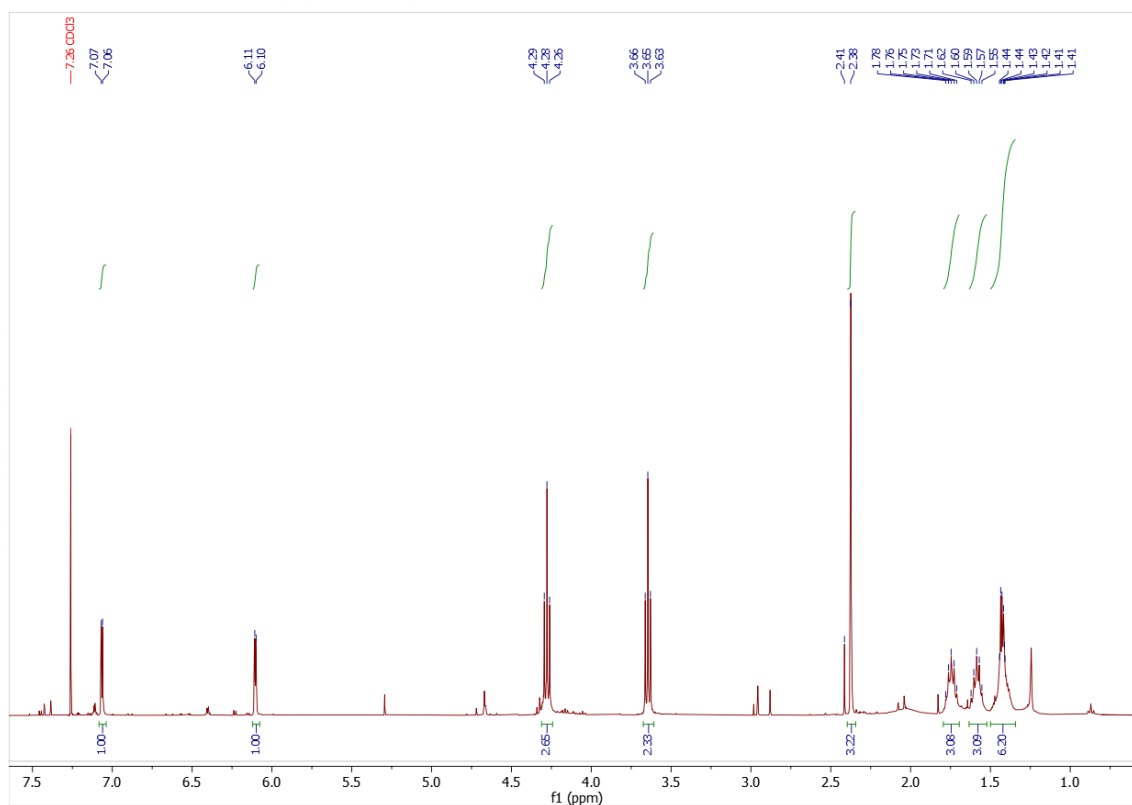
Figure A15. ^{1}H NMR (400 MHz) spectrum of 53 in CDCl$_3$
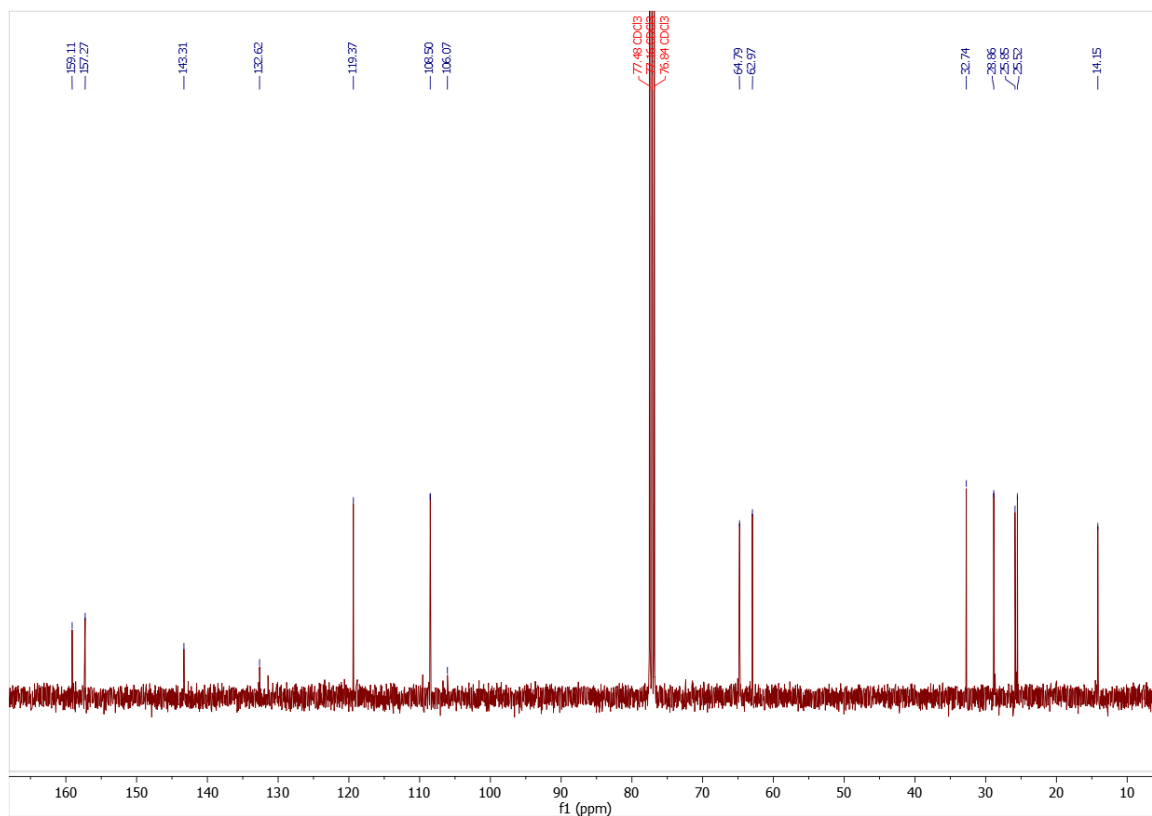
Figure A16. ^{13}C NMR (101 MHz) spectrum of 53 in CDCl$_3$
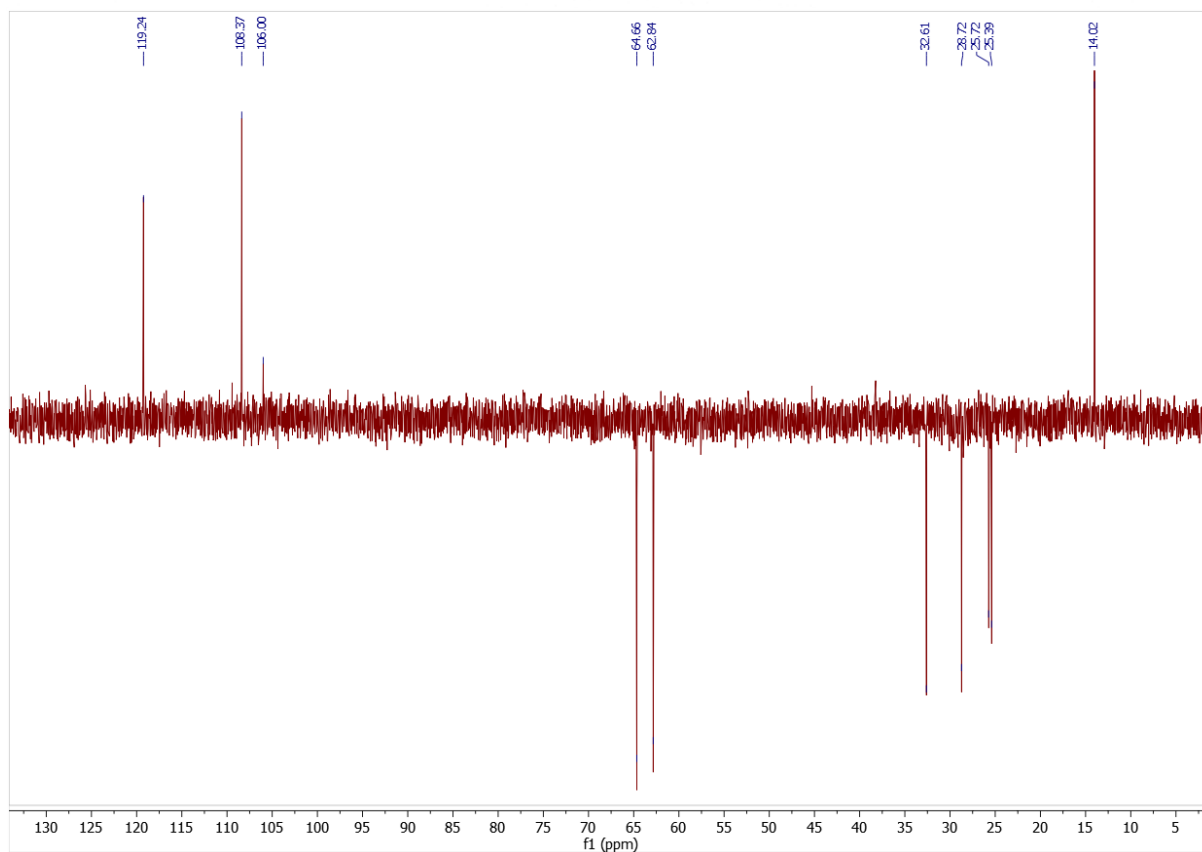
Figure A17. ^{13}C-DEPT NMR (101 MHz) spectrum of 53 in CDCl$_3$
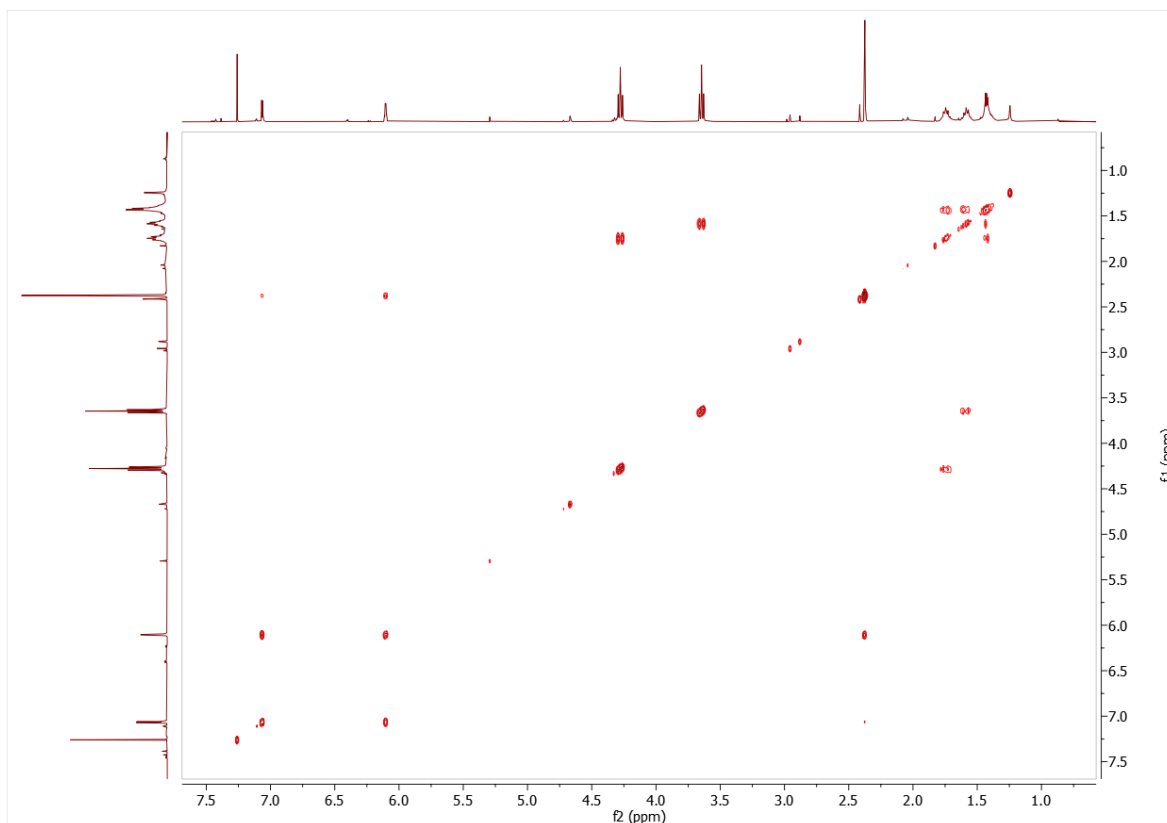
Figure A18. ^{1}H-COSY-NMR (400 MHz) spectrum of 53 in CDCl$_3$
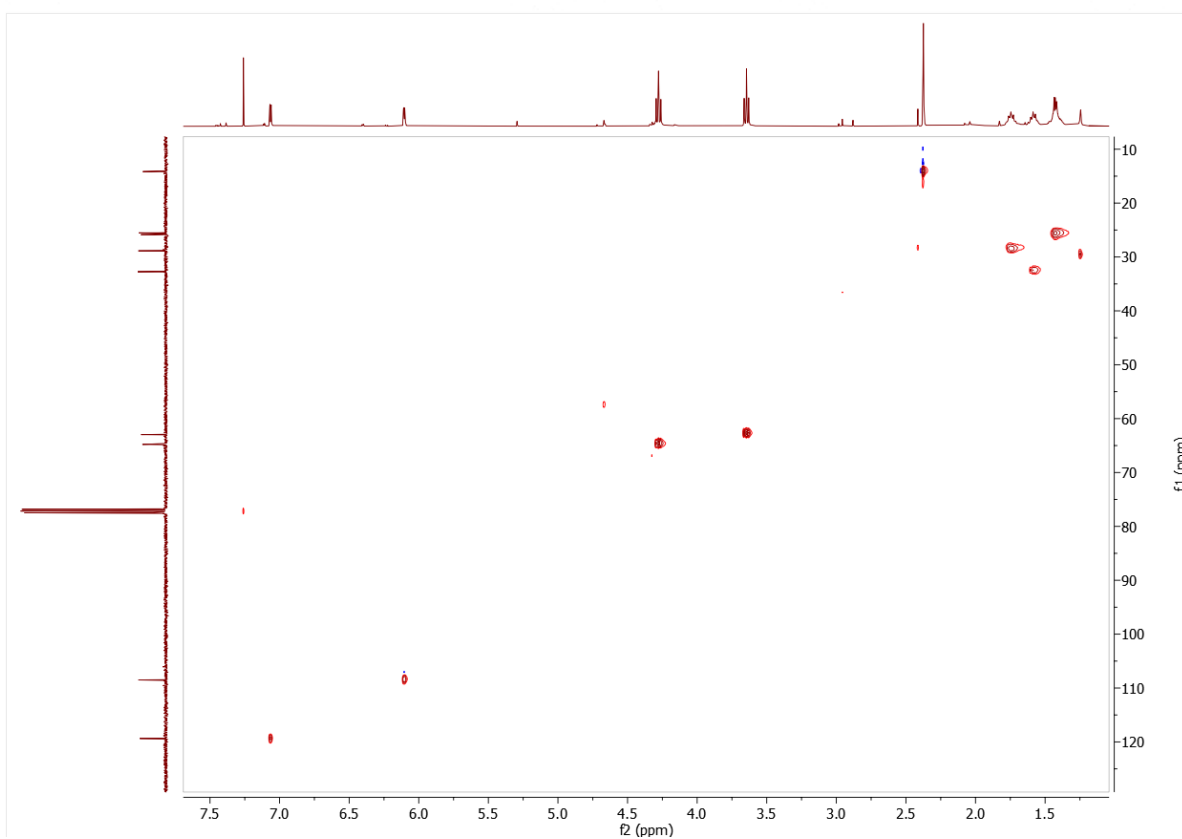
Figure A19. ^{1}H-^{13}C-HSQC- NMR (400 MHz; 101 MHz) spectrum of 53 in CDCl$_3$
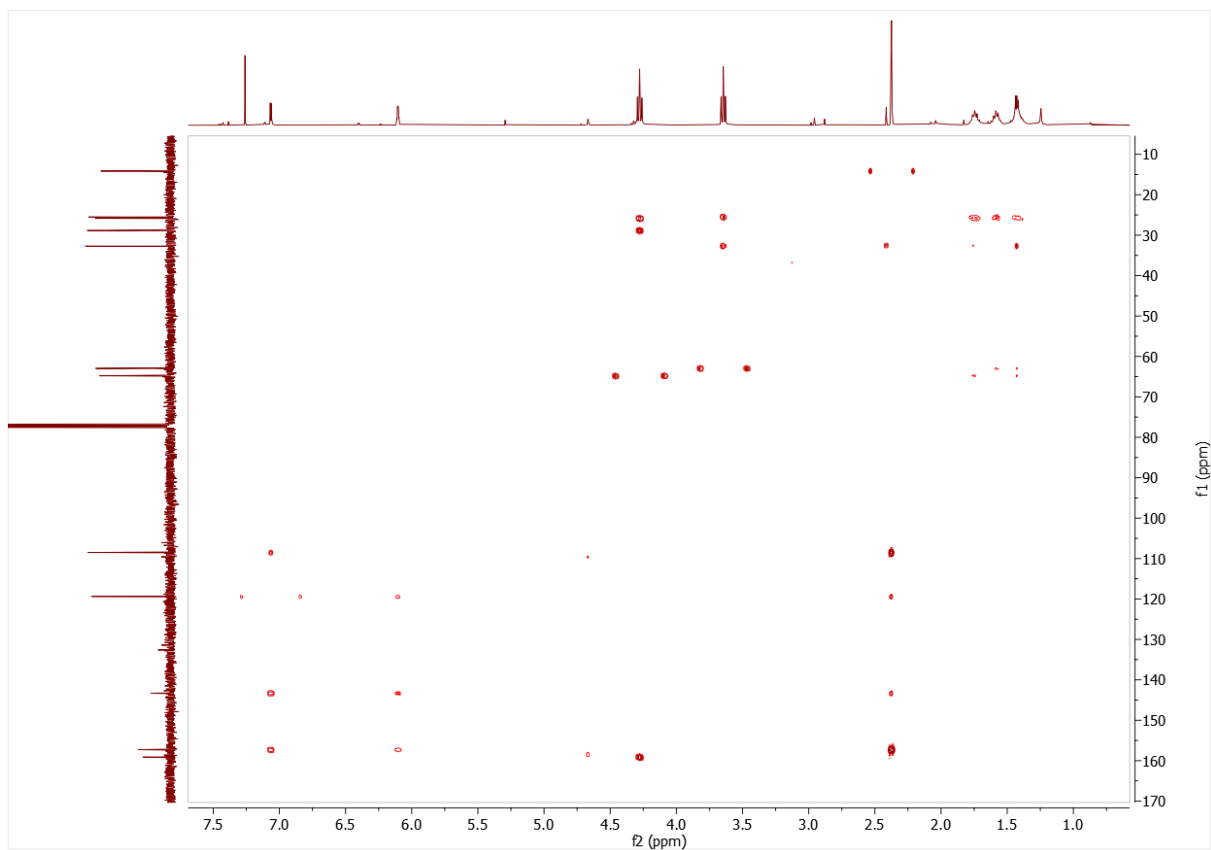
Figure A20. ^1H-^{13}C-HMBC- NMR (400 MHz; 101 MHz) spectrum of 53 in CDCl$_3$
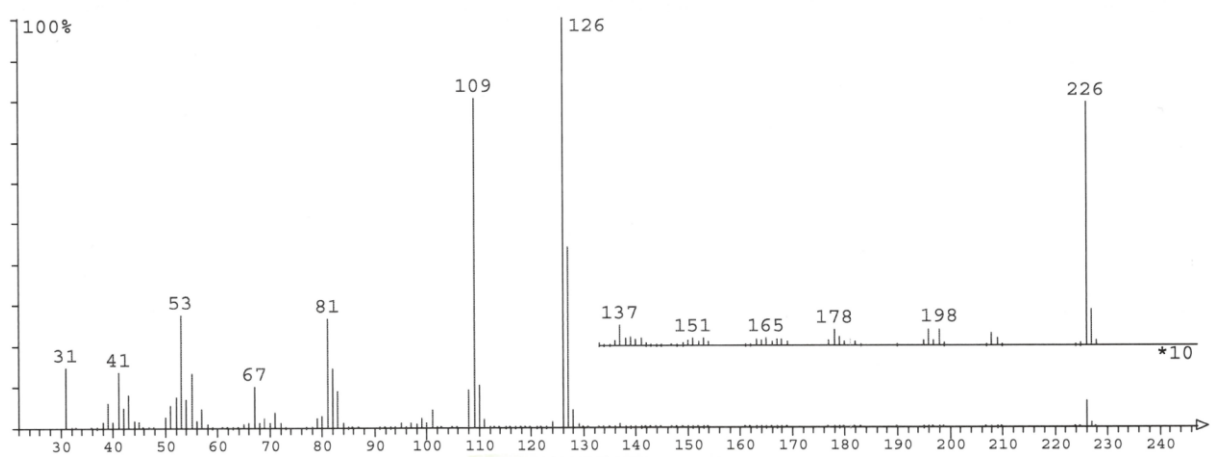
Figure A21. MS spectrum (EI) of 53

8.3.2.3   *Characterization of Butyl Furoate (55)*

^{1}H NMR (400 MHz, CDCl$_3$) δ = 7.56 ppm (-CH, 1H, dd), 7.15 ppm (-CH, 1H, dt), 6.48 ppm (-CH, 1H, dd), 4.29 ppm (-(CO)-O**CH$_2$**-, 2H, t), 1.71 ppm (-(CO)-OCH$_2$-**CH$_2$**-, 2H, quint), 1.44 ppm (-**CH$_2$**-CH$_3$, 2H, sext), 0.95 ppm (-CH$_2$-**CH$_3$**, 3H, t). ^{13}C NMR (101 MHz, CDCl$_3$) δ = 158.95 ppm (-(**C**O)-), 146.26 ppm (-**C**H$_{arom}$-), 145.00 ppm (-**C**$_{arom}$-), 117.76 ppm (-**C**H$_{arom}$-), 111.86 ppm (-**C**H$_{arom}$-), 64.90 ppm (-(CO)-O**CH$_2$**-), 30.83 ppm (-(CO)-OCH$_2$-**CH$_2$**-), 19.24 ppm (-**CH$_2$**-CH$_3$), 13.82 ppm (-CH$_2$-**CH$_3$**). MS (GC-MS): m/z = 168[M$^+$], 95 (100%).
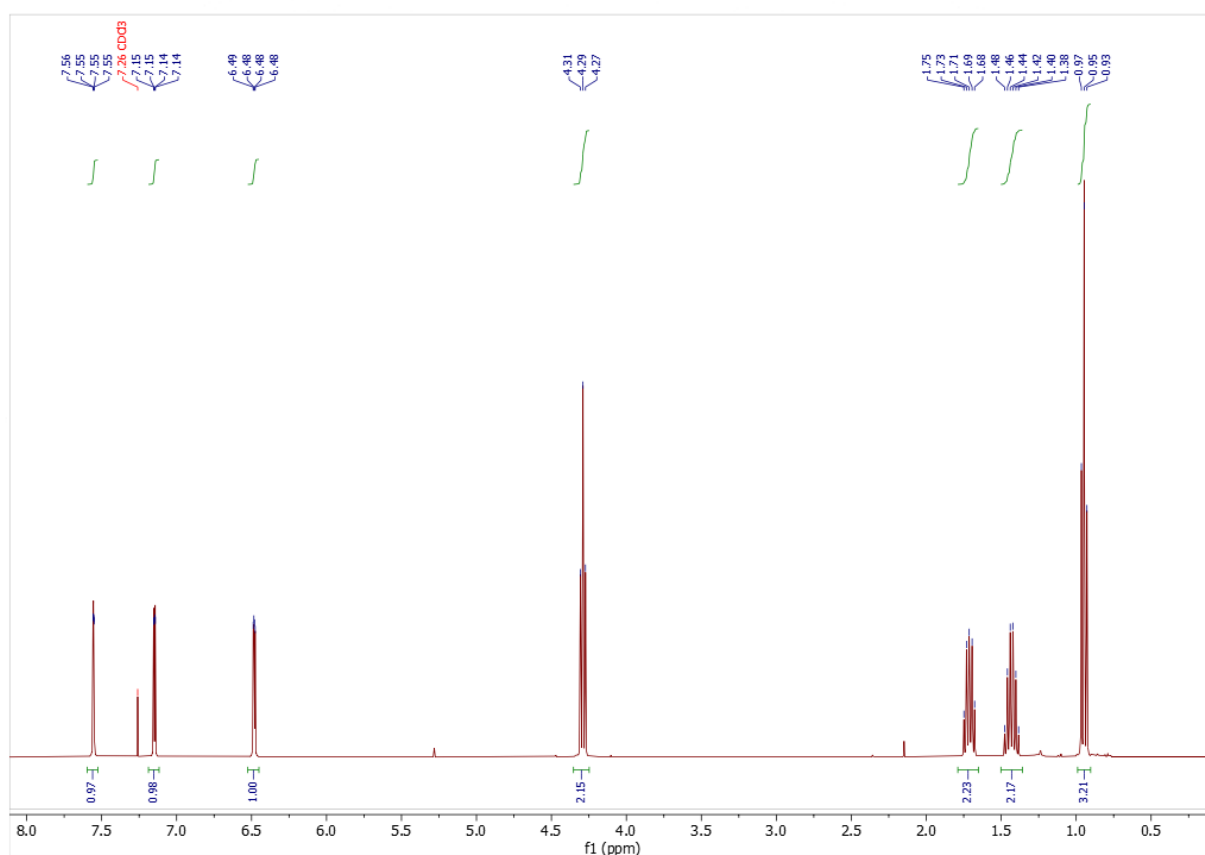
Figure A22. ^{1}H NMR (400 MHz) spectrum of 55 in CDCl$_3$
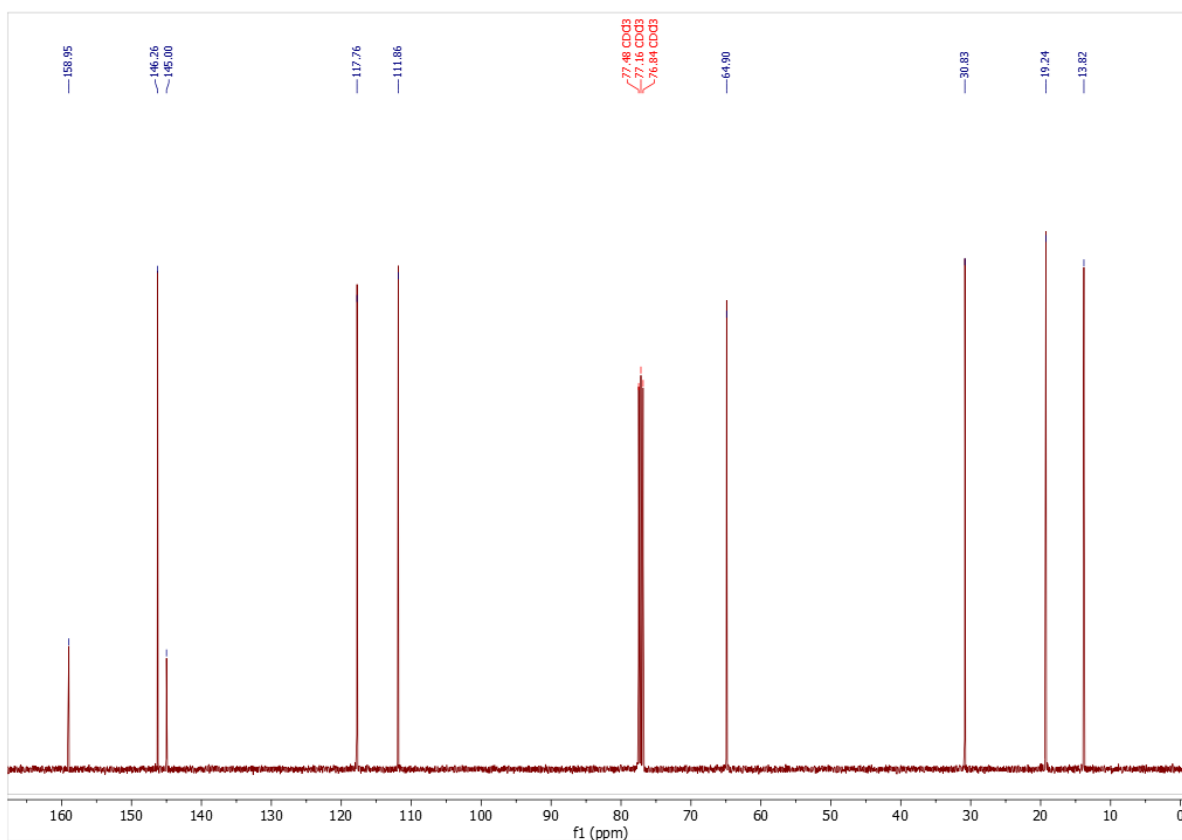
Figure A23. ^{13}C NMR (101 MHz) spectrum of 55 in CDCl$_3$
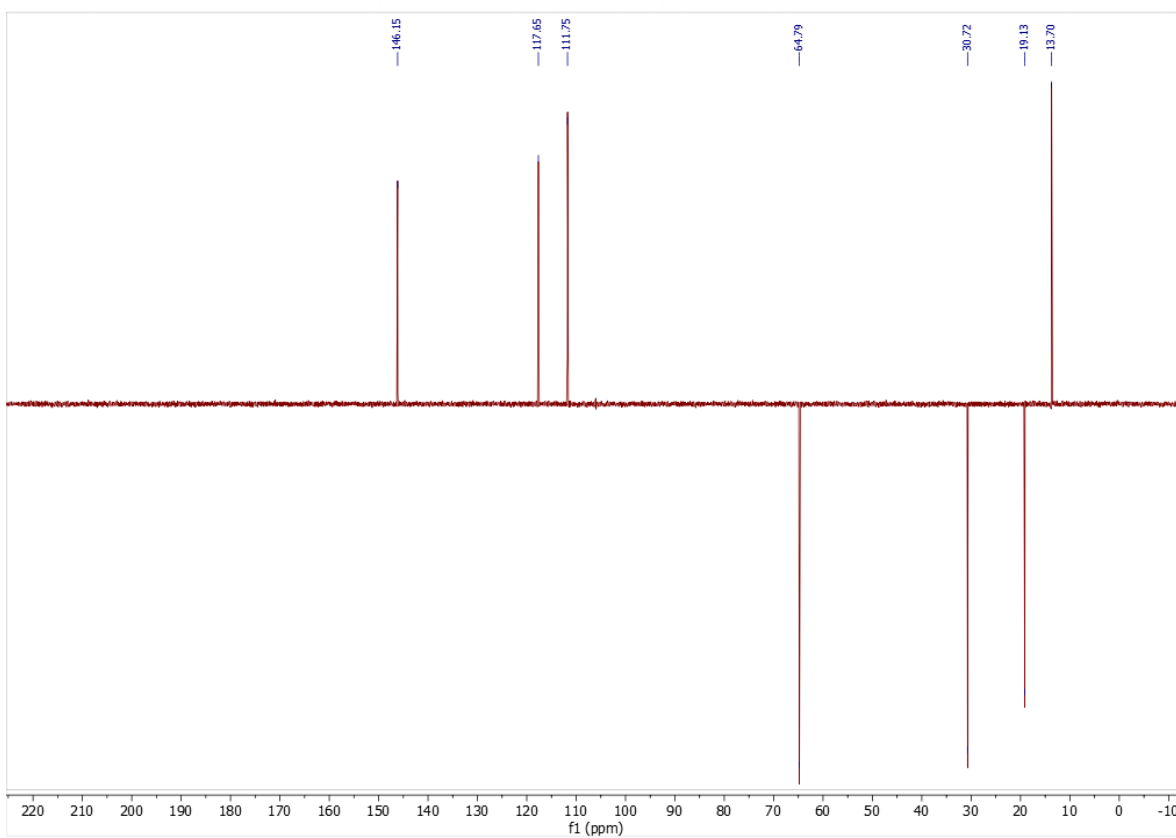
Figure A24. ^{13}C-DEPT NMR (101 MHz) spectrum of 55 in CDCl$_3$
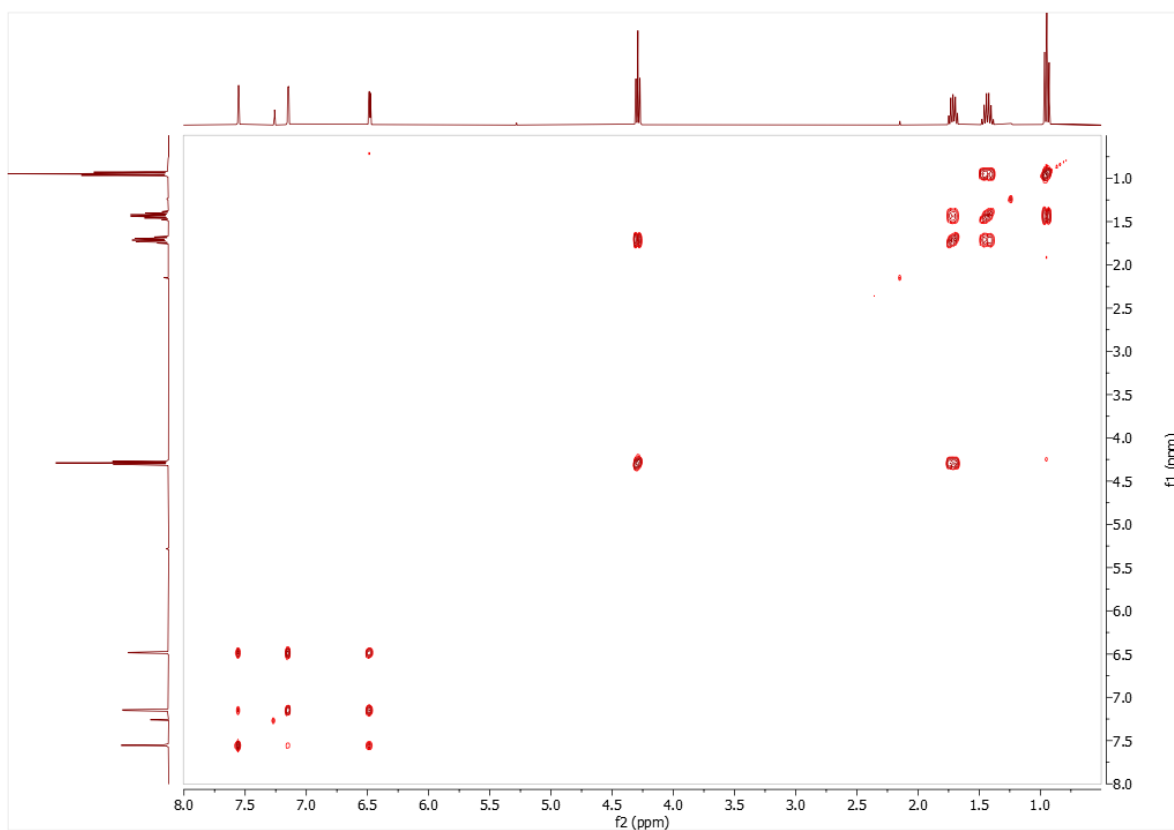
Figure A25. ^{1}H-COSY-NMR (400 MHz) spectrum of 55 in CDCl$_3$
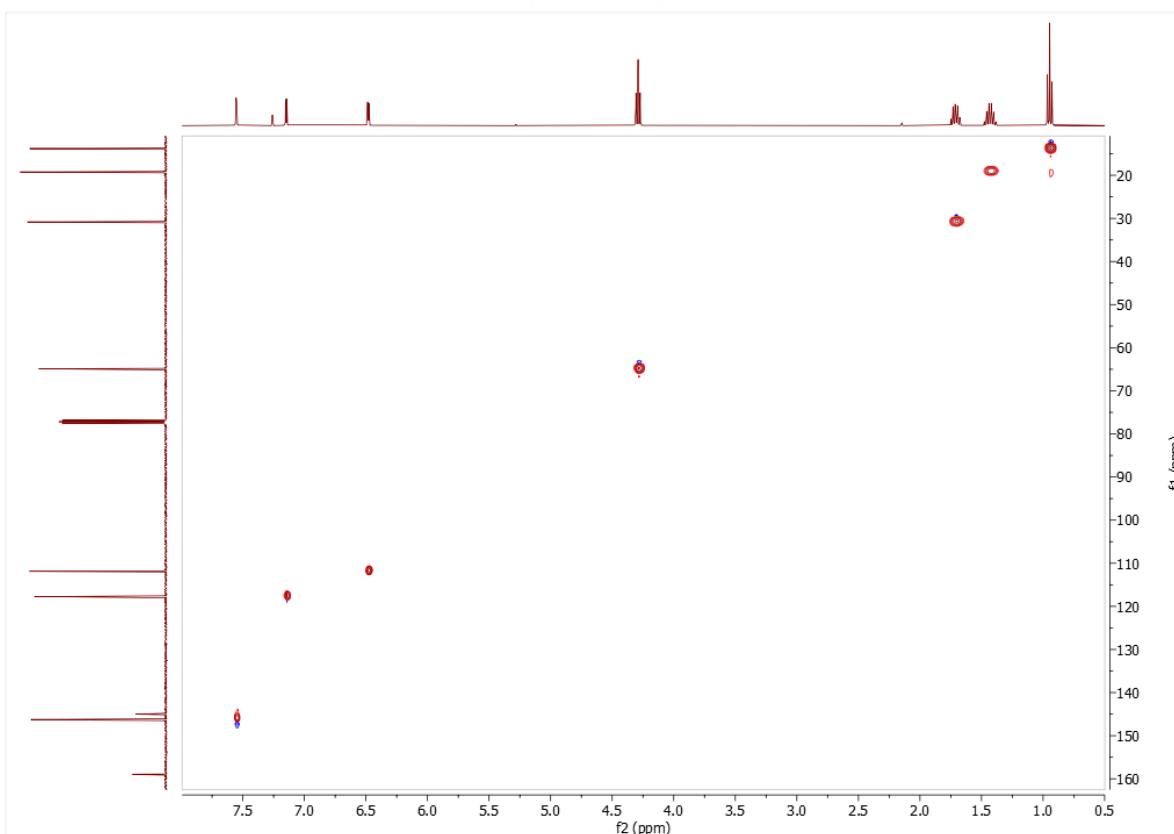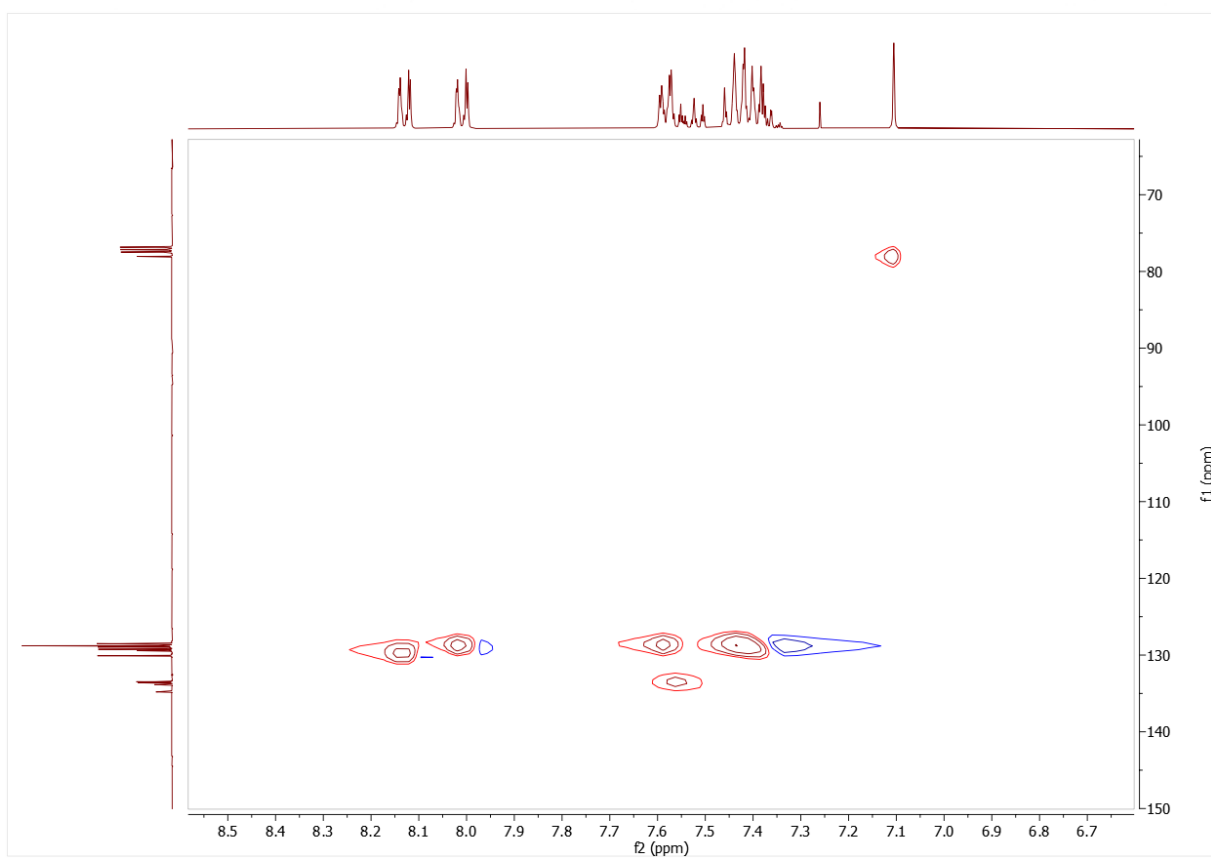

Figure A26. ^{1}H-^{13}C-HSQC- NMR (400 MHz; 101 MHz) spectrum of 55 in CDCl$_3$
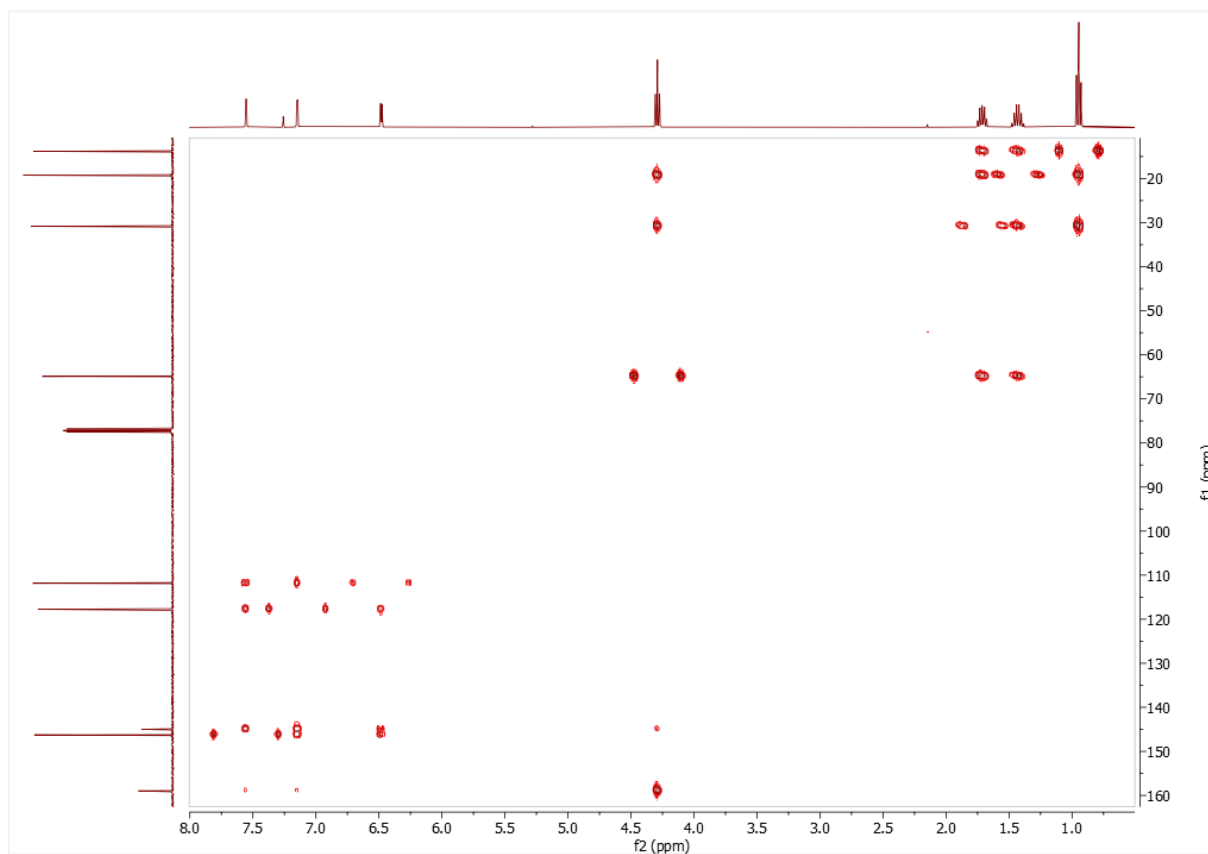
**Figure A27.** ^{1}H-^{13}C-HMBC- NMR (400 MHz; 101 MHz) spectrum of 55 in CDCl$_3$
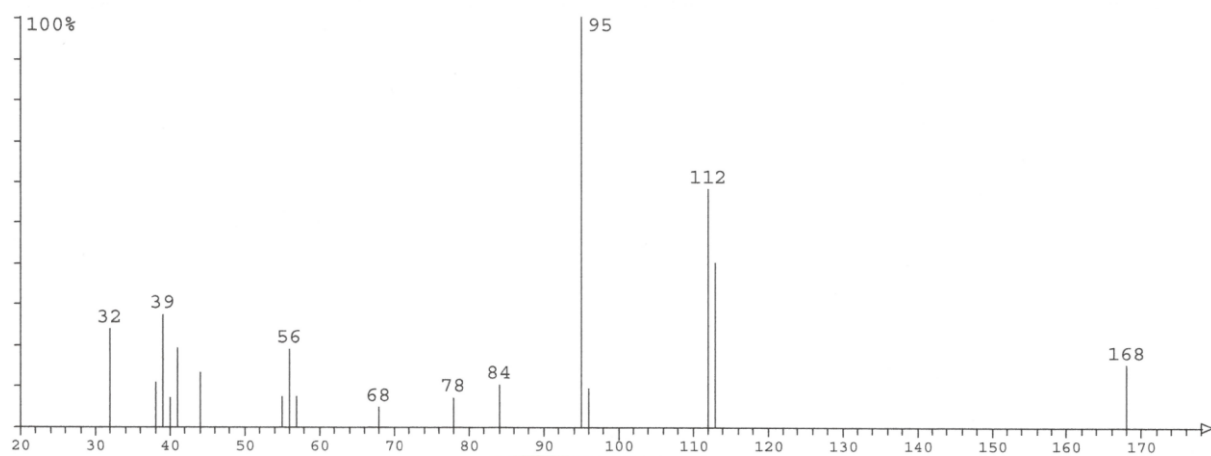
Figure A28. MS spectrum (EI) of 55

8.3.2.4   *Characterization of Butyl Benzoate*

^{1}H NMR (300 MHz, CDCl$_3$) δ = 8.05 ppm (-CH, 2H, m), 7.52 ppm (-CH, 1H, m), 7.42 ppm (-CH, 2H, m), 4.32 ppm (-(CO)-O**CH$_2$**-, 2H, t), 1.73 ppm (-(CO)-OCH$_2$-**CH$_2$**-, 2H, quint), 1.47 ppm (-**CH$_2$**-CH$_3$, 2H, sext), 0.97 ppm (-CH$_2$-**CH$_3$**, 3H, t). ^{13}C NMR (75 MHz, CDCl$_3$) δ = 166.68 ppm (-(**C**O)-), 132.81 ppm (-**C**H$_{arom}$-, para position), 130.58 ppm (-**C**$_{arom}$-), 129.56 ppm (-**C**H$_{arom}$-, orto position), 128.34 ppm (-**C**H$_{arom}$-, meta position), 64.84 ppm (-(CO)-O**CH$_2$**-), 30.83 ppm (-(CO)-OCH$_2$-**CH$_2$**-), 19.34 ppm (-**CH$_2$**-CH$_3$), 13.81 ppm (-CH$_2$-**CH$_3$**). MS (GC-MS): m/z = 178[M$^+$], 105 (100%).
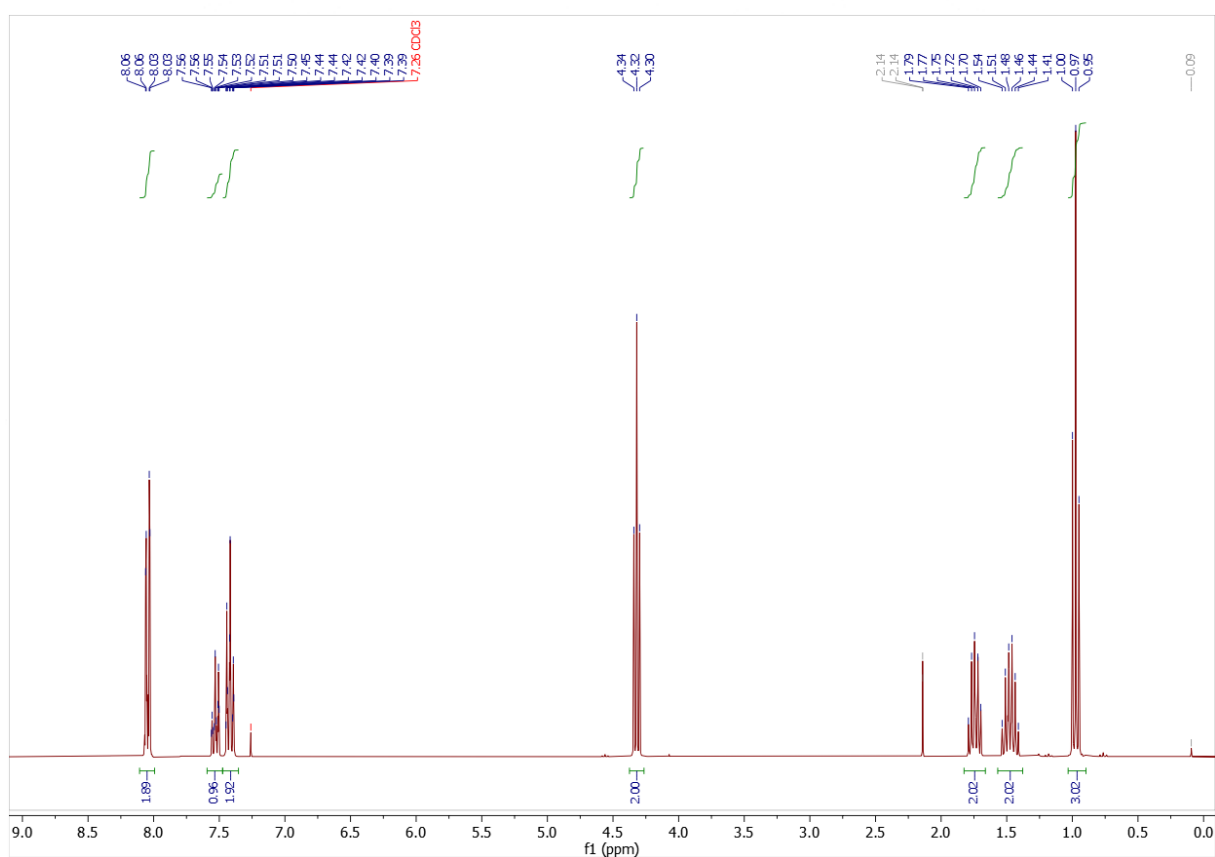
Figure A29. ^{1}H NMR (300 MHz) spectrum of butyl benzoate in CDCl$_3$
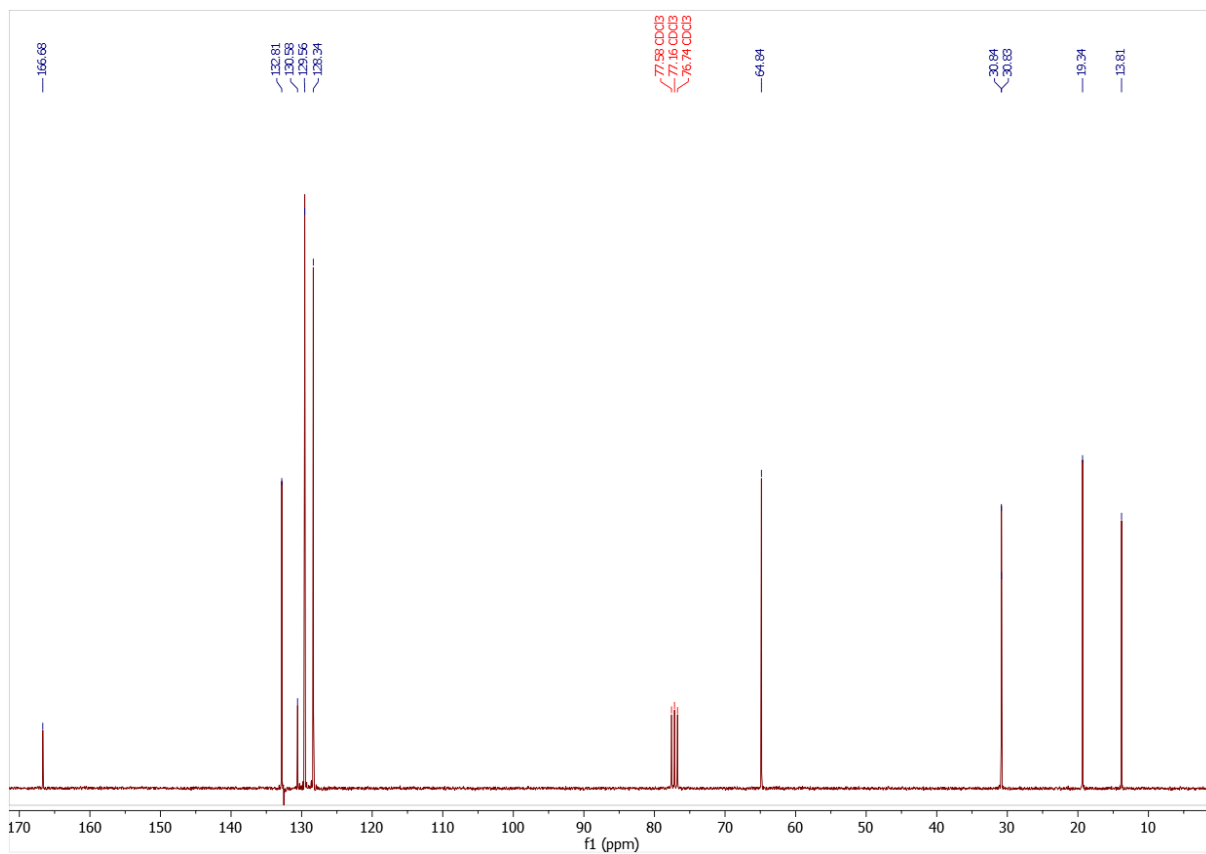
Figure A30. ^{13}C NMR (75 MHz) spectrum of butyl benzoate in CDCl$_3$
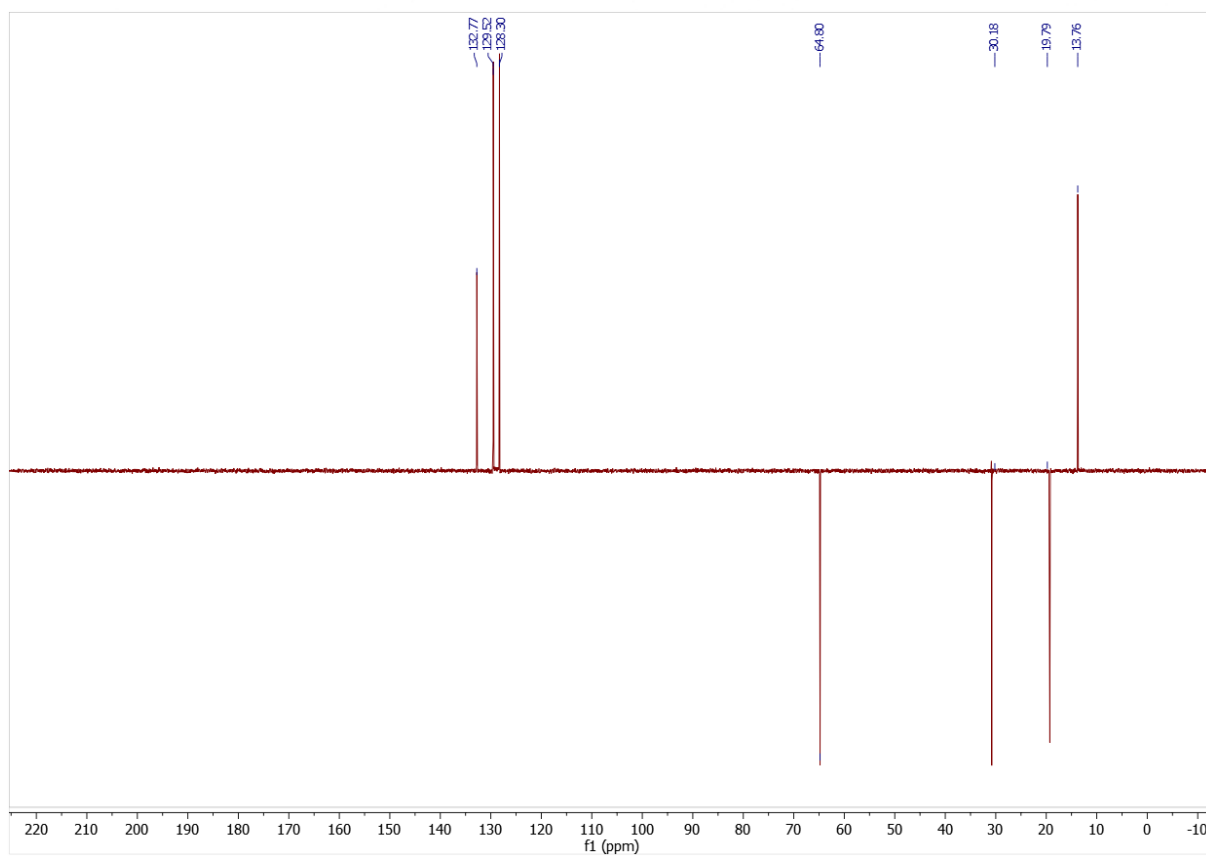
Figure A31. ^{13}C-DEPT NMR (75 MHz) spectrum of butyl benzoate in CDCl$_3$
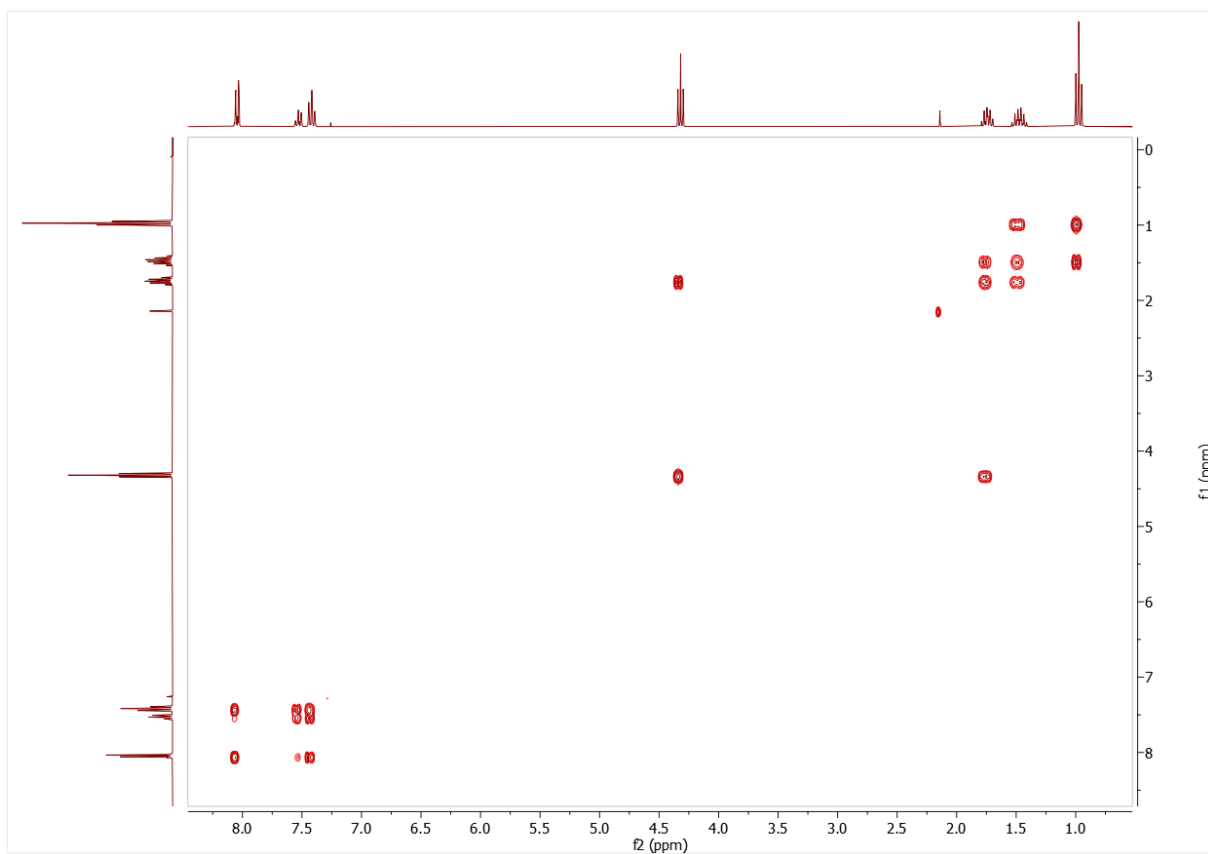
Figure A32. ^{1}H-COSY-NMR (400 MHz) spectrum of butyl benzoate in CDCl$_3$
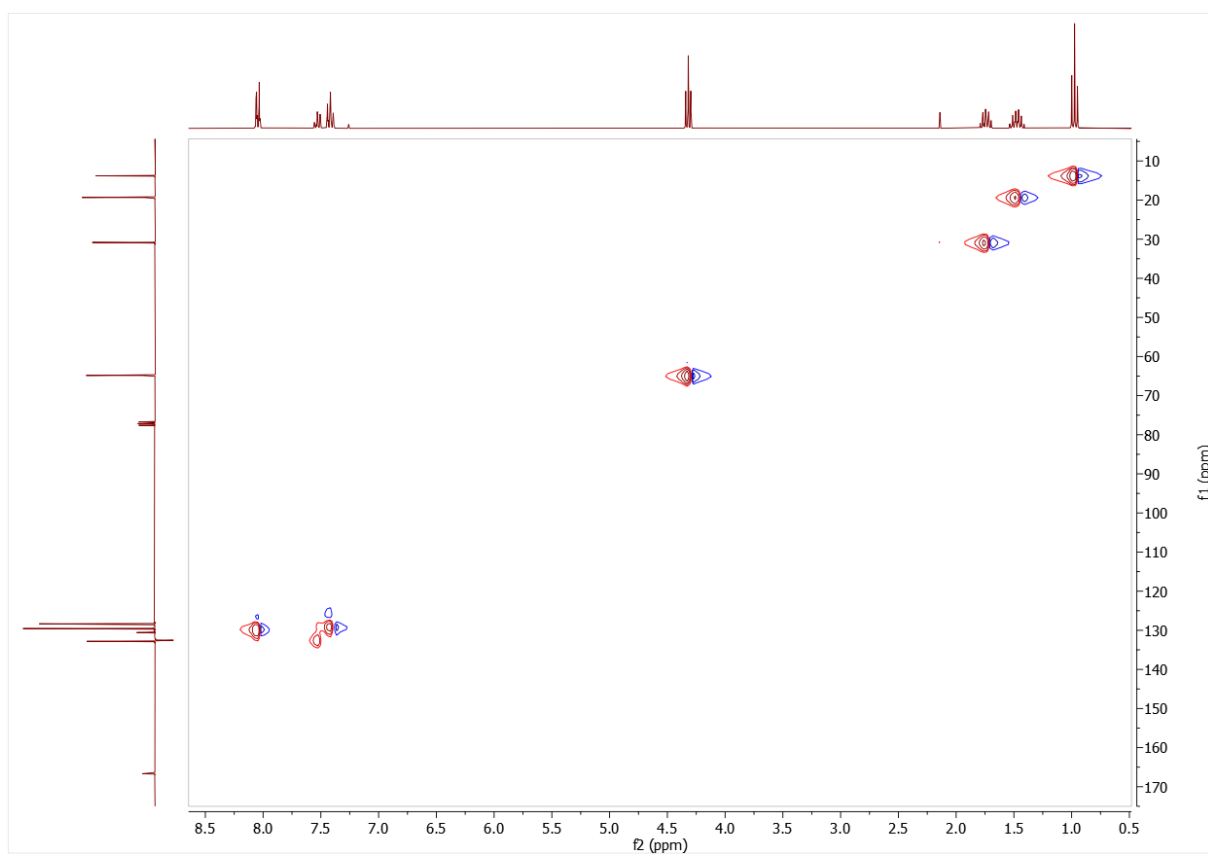
Figure A33. ^{1}H-^{13}C-HSQC- NMR (400 MHz; 101 MHz) spectrum of butyl benzoate in CDCl$_3$
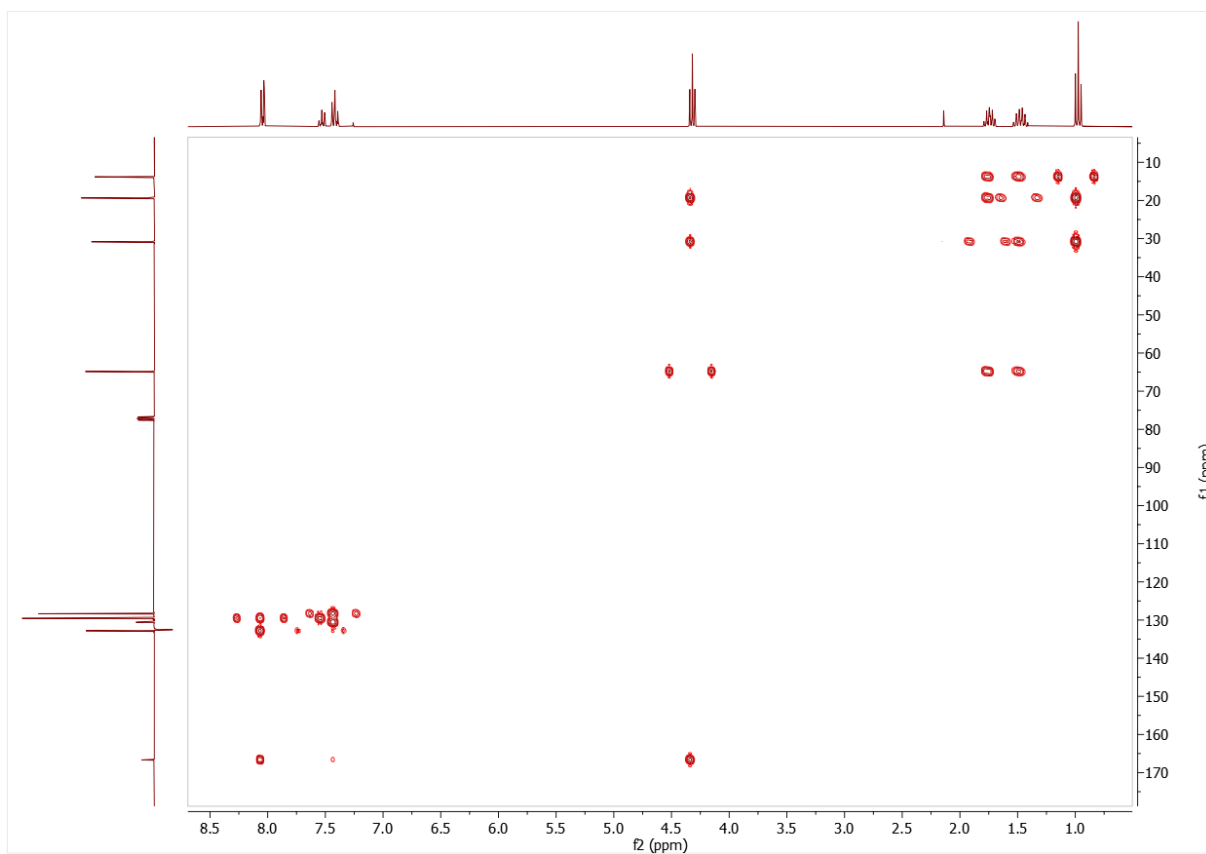
Figure A34. ^1H-^{13}C-HMBC- NMR (400 MHz; 101 MHz) spectrum of butyl benzoate in CDCl$_3$
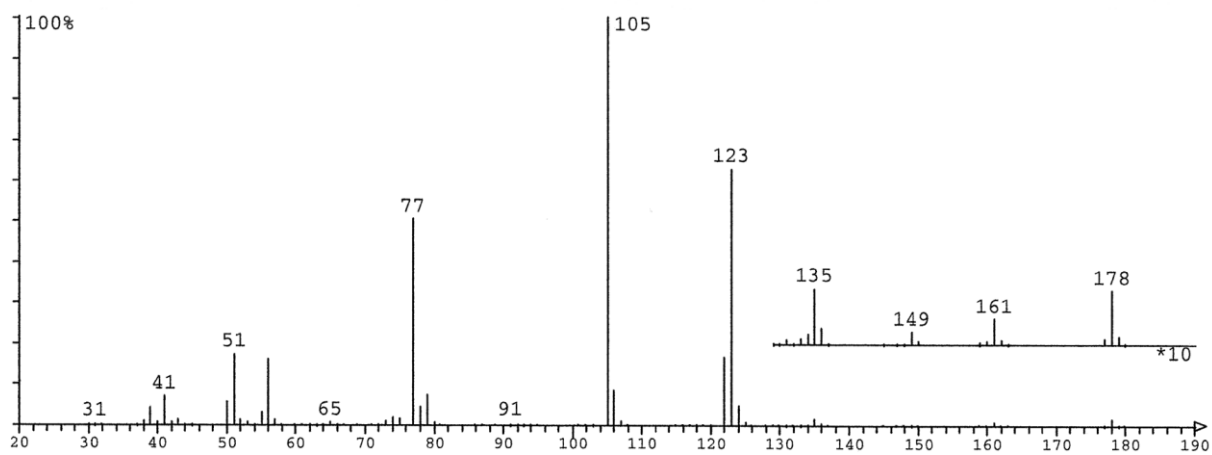
Figure A35. MS spectrum (EI) of butyl benzoate

214

8.3.2.5 *Characterization of Allyl Benzoate*

^{1}H NMR (400 MHz, CDCl$_3$) δ = 8.07 ppm (-CH, 2H, m), 7.56 ppm (-CH, 1H, m), 6.05 ppm (-CH$_2$-**CH**=CH$_2$, 1H, ddt, *J* = 17.2, 10.4, 5.6 Hz), 5.42 ppm (-CH$_2$-CH=**CH$_2$**, trans position, 1H, dq, *J* = 17.2, 1.6 Hz), 5.29 ppm (-CH$_2$-CH=**CH$_2$**, cis position, 1H, dq, *J* = 10.4, 1.3 Hz), 4.83 ppm (-**CH$_2$**-CH=CH$_2$, 2H, dt, *J* = 5.6, 1.5 Hz). ^{13}C NMR (101 MHz, CDCl$_3$) δ = 166.32 ppm (-(**C**O)-), 133.07 ppm (-**CH**$_{arom}$-, para position), 132.57 ppm (-**C**$_{arom}$-), 132.34 ppm (-CH$_2$-**CH**=CH$_2$), 130.26 ppm(-CH$_2$-**CH**=CH$_2$), 129.69 ppm (-**CH**$_{arom}$-, orto position), 128.45 ppm (-**CH**$_{arom}$-, meta position), 118.29 ppm (-CH$_2$-CH=**CH$_2$**), 65.62 ppm (-**CH$_2$**-CH=CH$_2$).
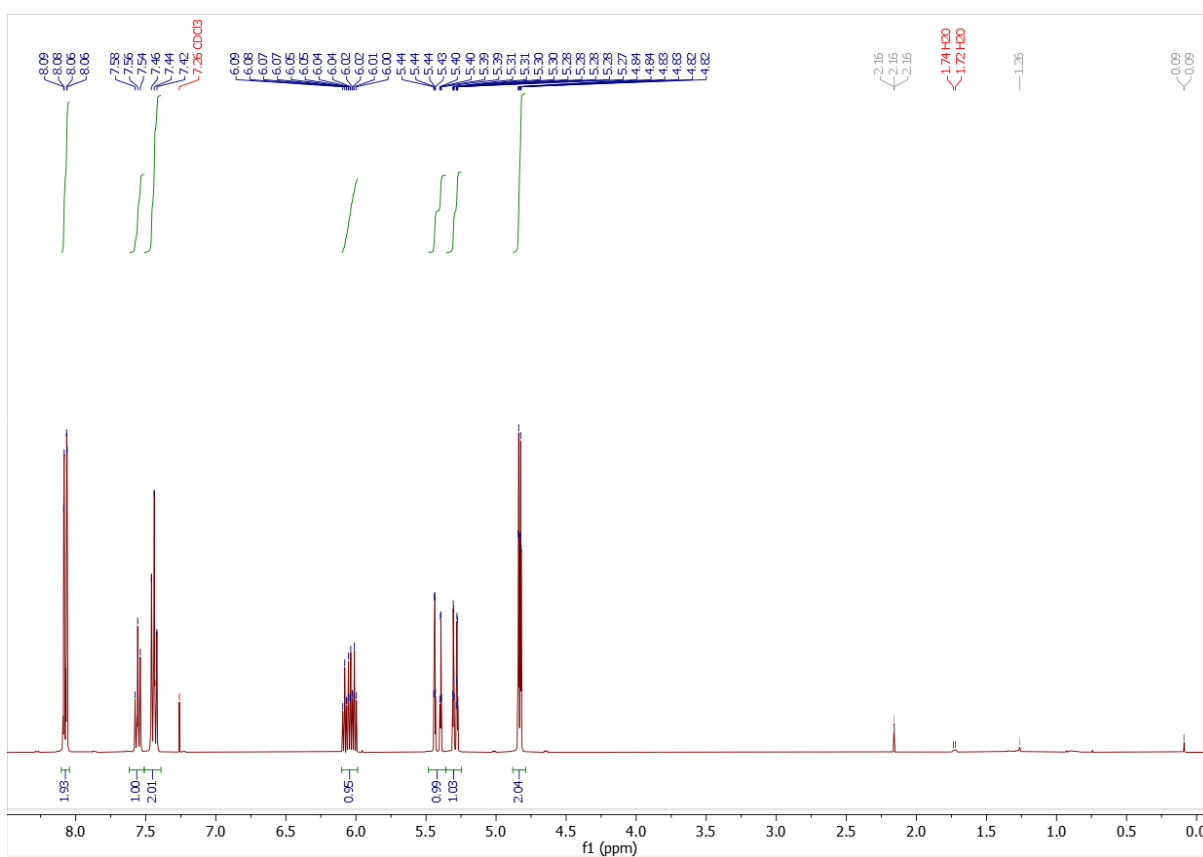
Figure A36. ^{1}H NMR (400 MHz) spectrum of allyl benzoate in CDCl$_3$
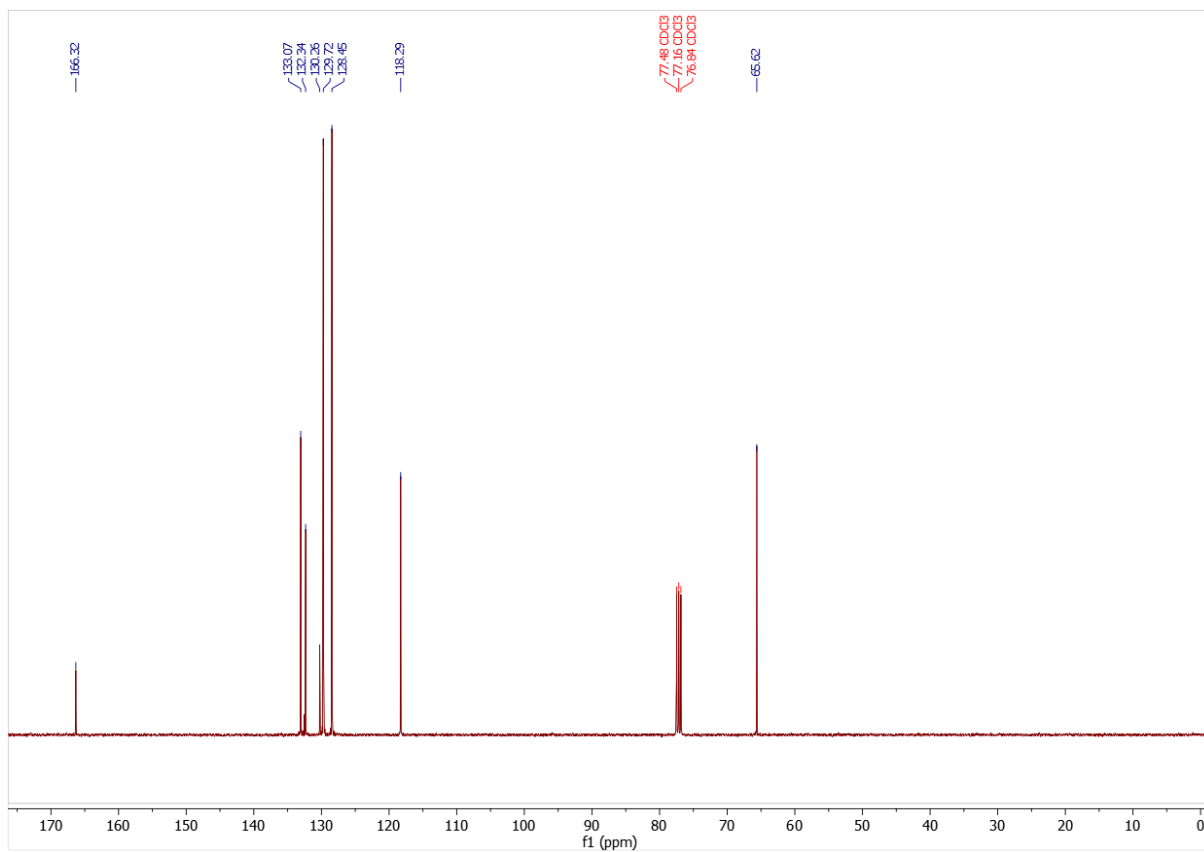
Figure A37. ^{13}C NMR (101 MHz) spectrum of 55 in CDCl$_3$
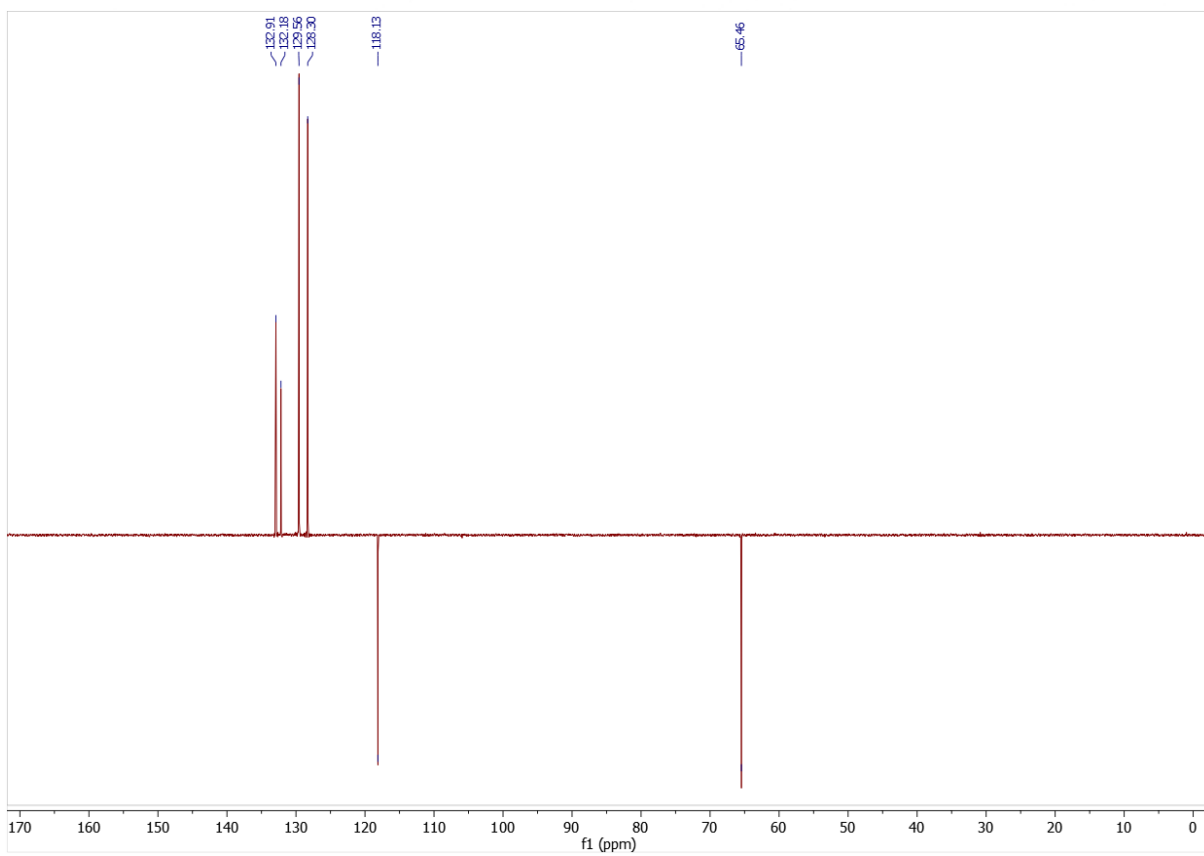
Figure A38. ^{13}C-DEPT NMR (101 MHz) spectrum of allyl benzoate in CDCl$_3$
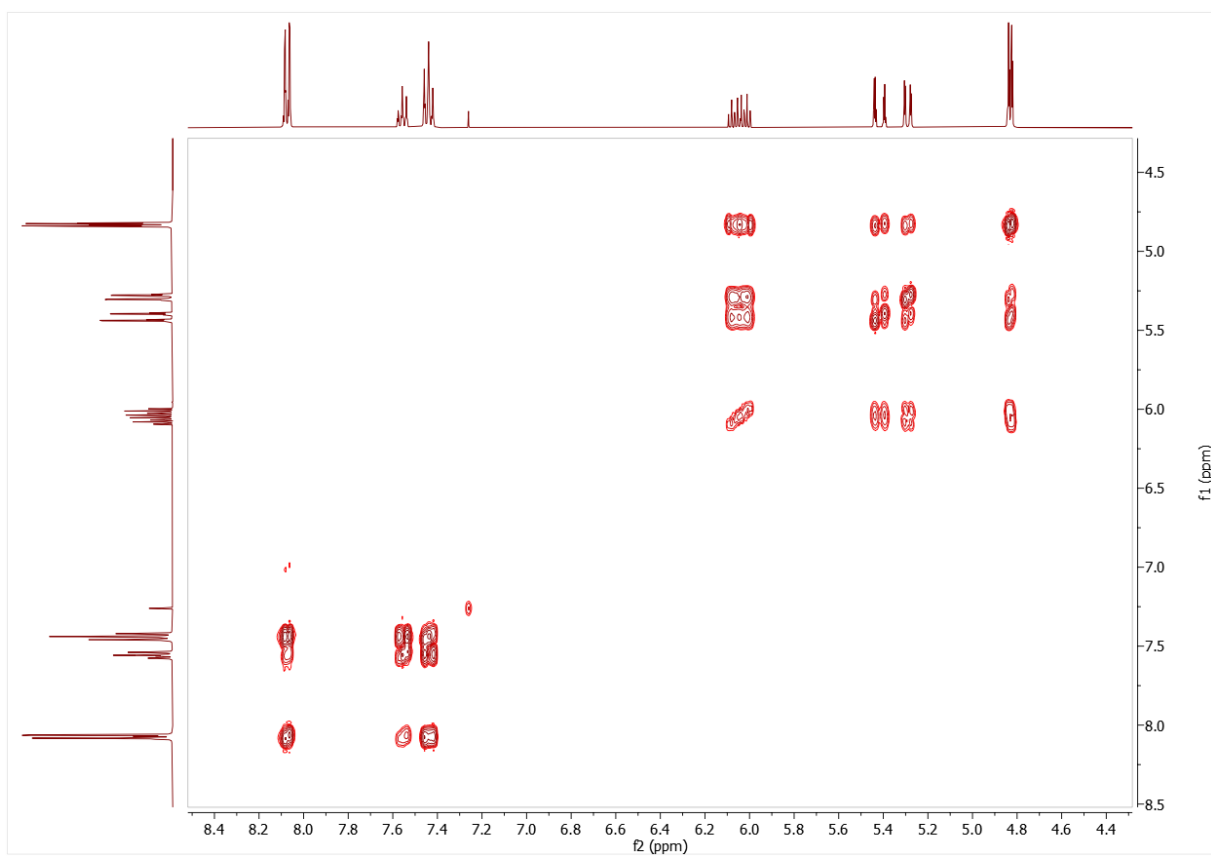
Figure A39. ^{1}H-COSY-NMR (400 MHz) spectrum of allyl bezoate in CDCl$_3$
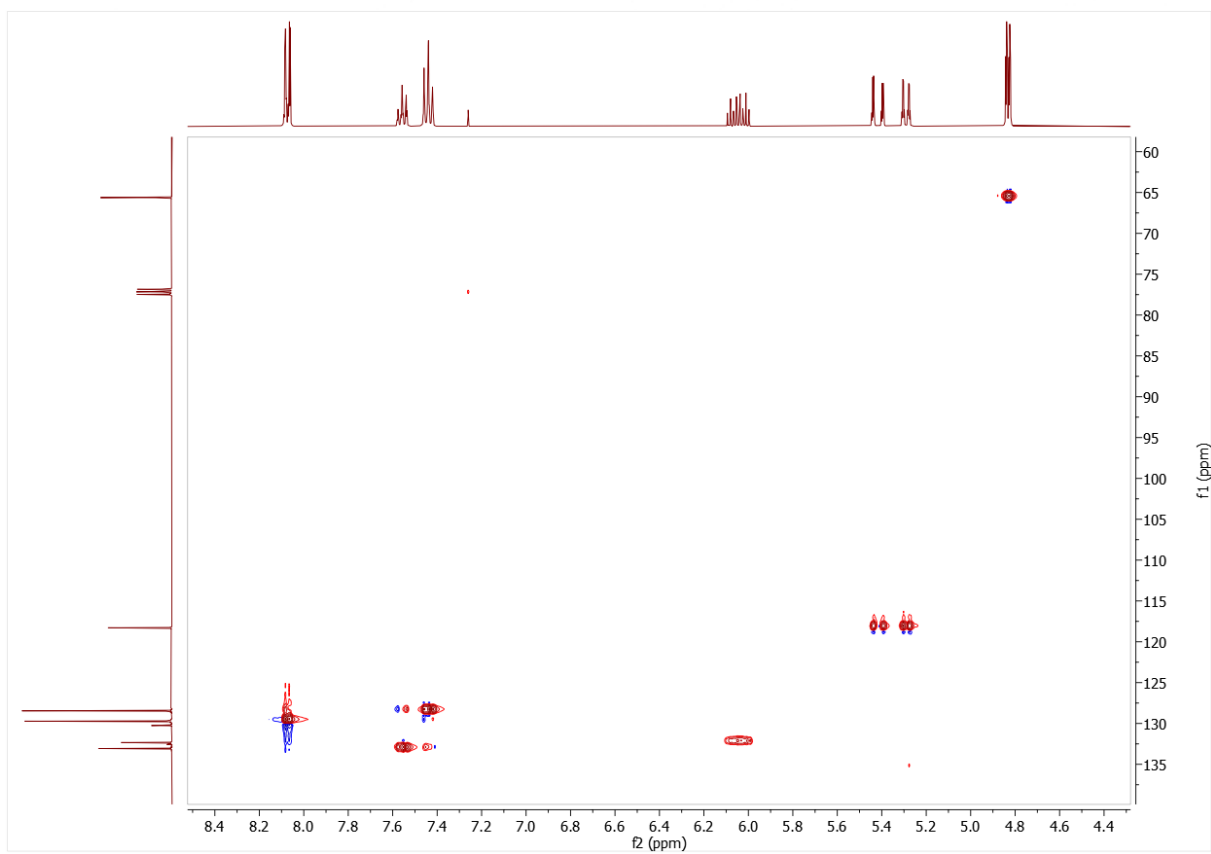
Figure A40. ^{1}H-^{13}C-HSQC- NMR (400 MHz; 101 MHz) spectrum of allyl benzoate in CDCl$_3$
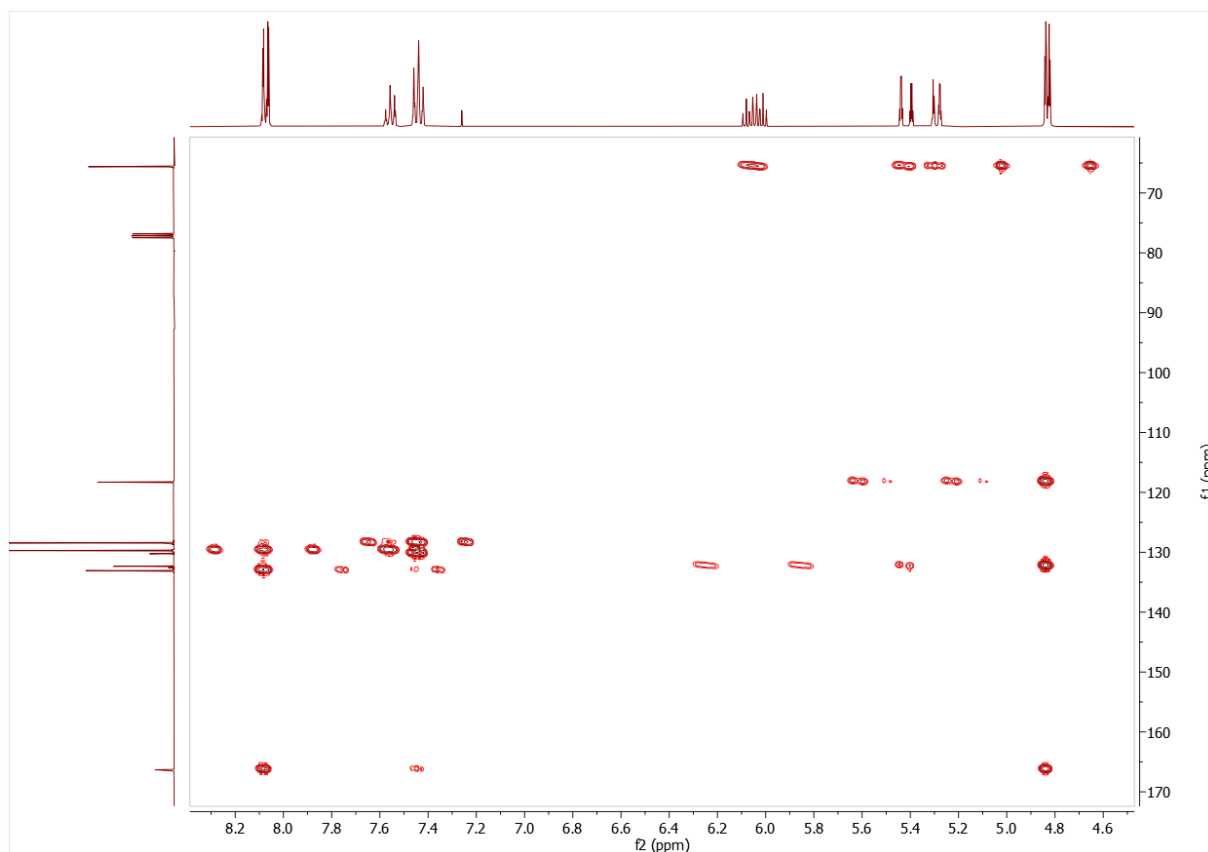
Figure A41. ^1H-^{13}C-HMBC- NMR (400 MHz; 101 MHz) spectrum of allyl benzoate in CDCl$_3$
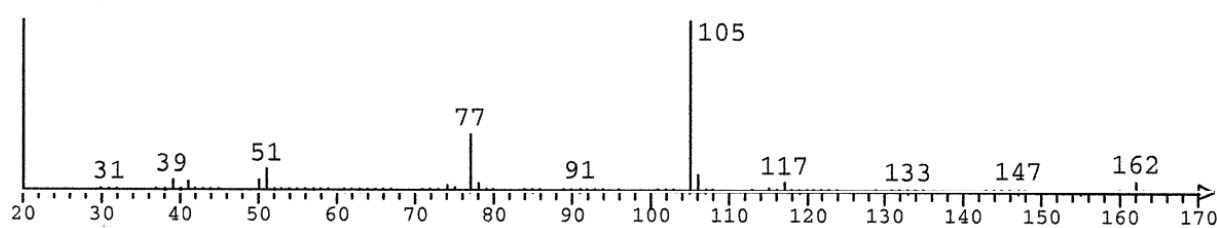
Figure A42. MS spectrum (EI) of allyl benzoate

8.3.2.6 *Characterization of Benzyl Benzoate*

^{1}H NMR (400 MHz, CDCl$_3$) δ = 8.16 ppm (-CH$_{arom}$-, para position benzoate side, 2H, m), 7.63 – 7.34 ppm (-CH$_{arom}$-, m, 8H), 5.42 ppm (-CH$_2$- s, 2H). ^{13}C NMR (75 MHz, CDCl$_3$) δ = 166.37 ppm (-(**C**O)-); 136.09 ppm (-**C**$_{arom}$-), 133.03 ppm (-**C**H$_{arom}$-), 130.15 (-**C**$_{arom}$-), 129.71 ppm (-**C**H$_{arom}$-), 128.61 ppm (-**C**H$_{arom}$-), 128.39 ppm (-**C**H$_{arom}$-), 128.25 ppm (-**C**H$_{arom}$-), 128.17 ppm (-**C**H$_{arom}$-), 66.68 ppm (-(CO)-O**CH$_2$**-).
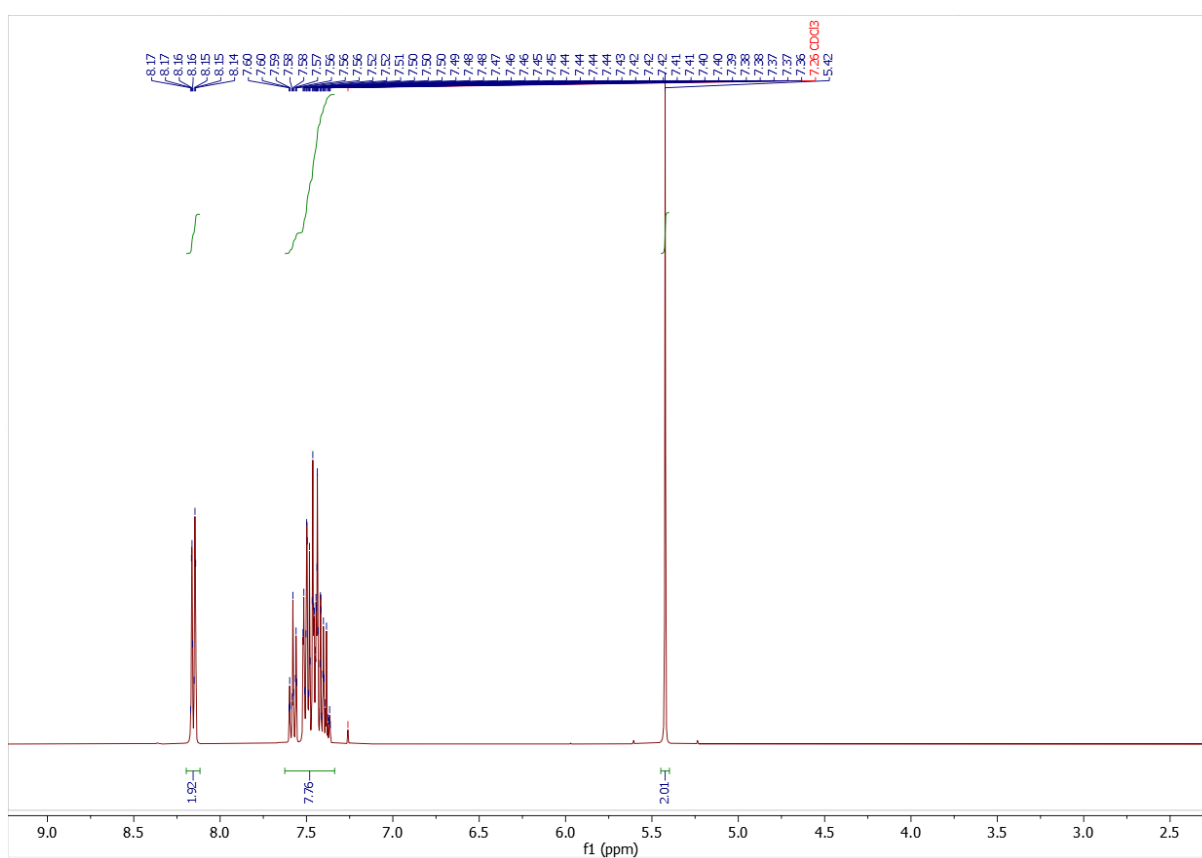
Figure A43. ^{1}H NMR (400 MHz) spectrum of benzyl benzoate in CDCl$_3$
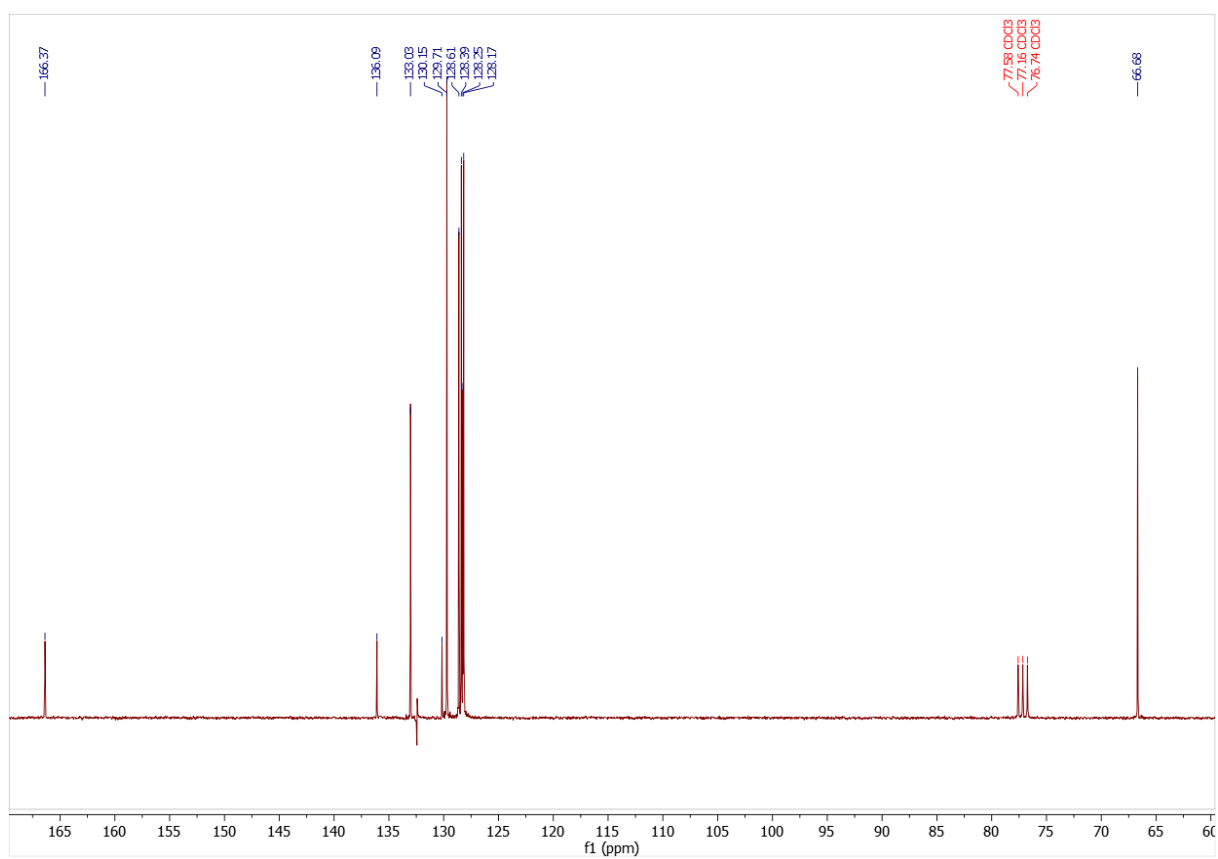
Figure A44. ^{13}C NMR (101 MHz) spectrum of benzyl benzoate in CDCl$_3$
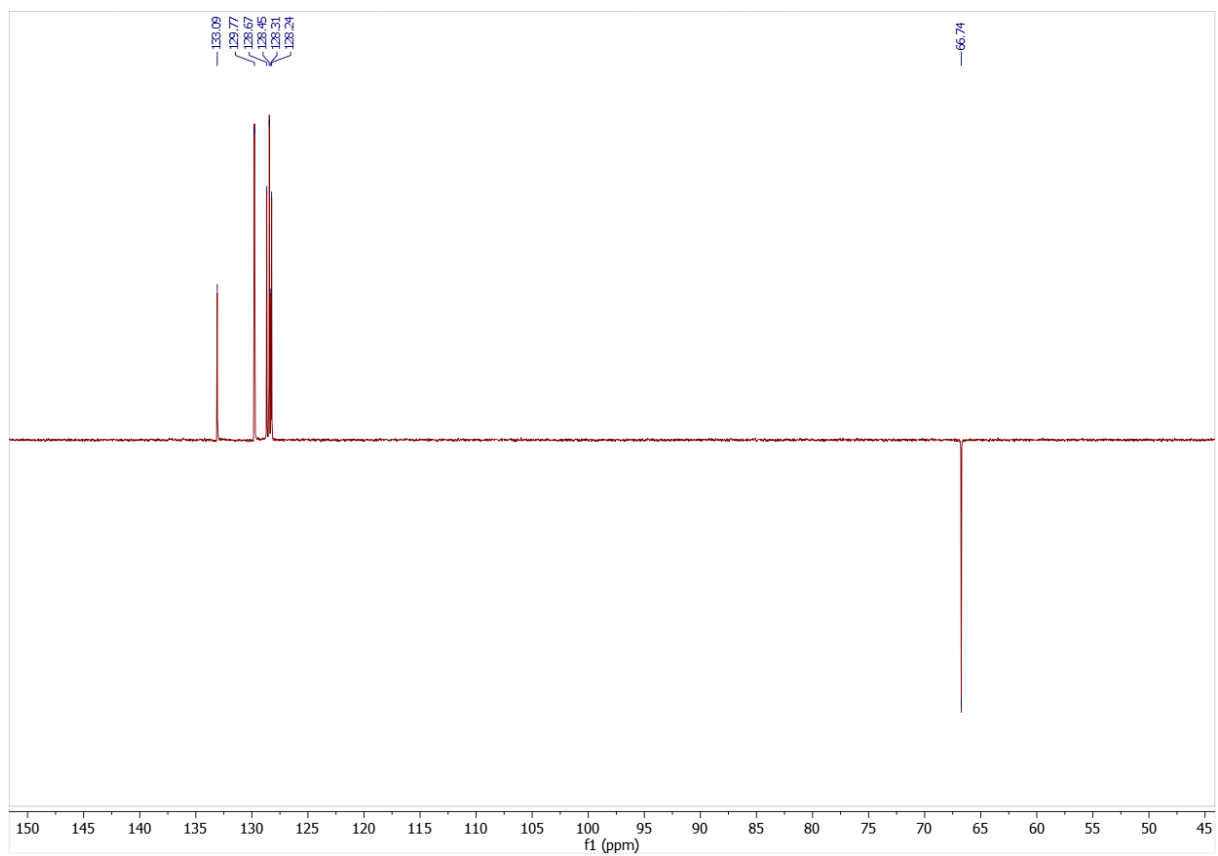
Figure A45. ^{13}C-DEPT NMR (101 MHz) spectrum of benzyl benzoate in CDCl$_3$
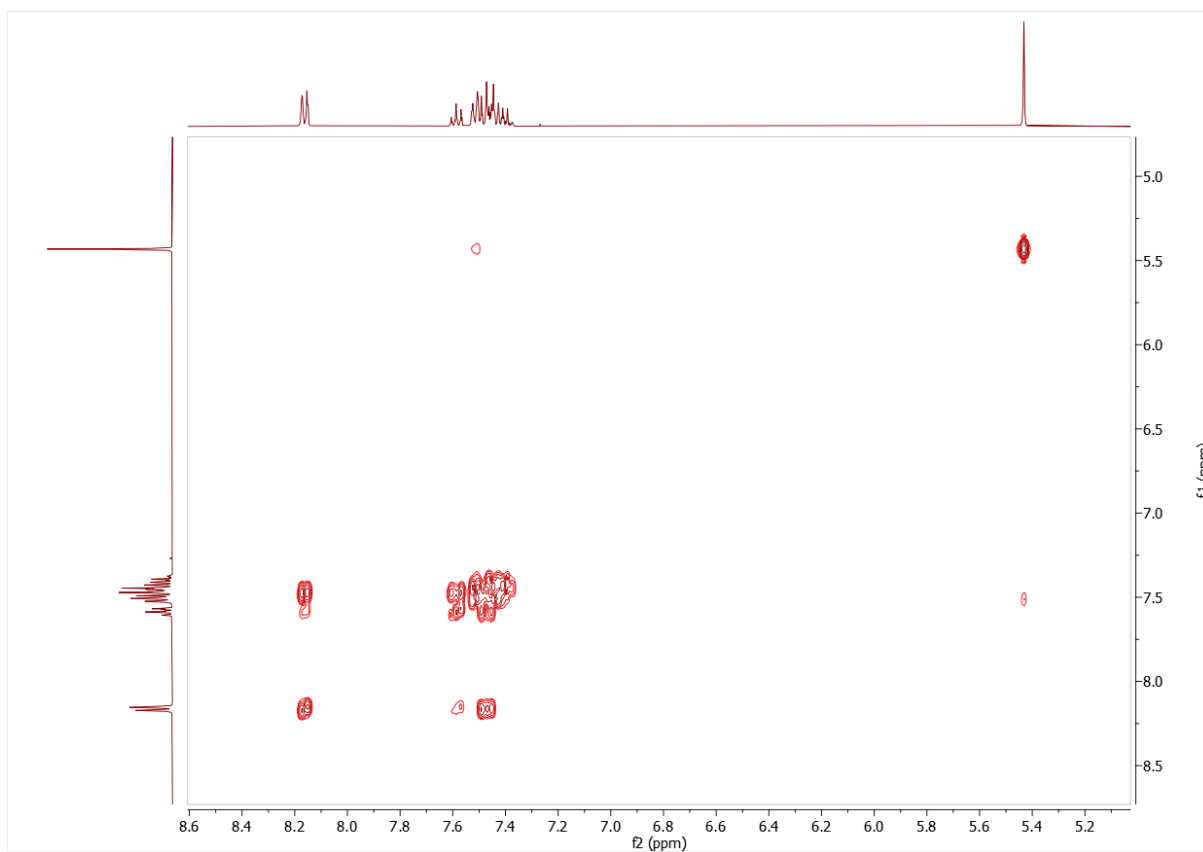
Figure A46. ¹H-COSY-NMR (300 MHz) spectrum of benzyl benzoate in CDCl₃
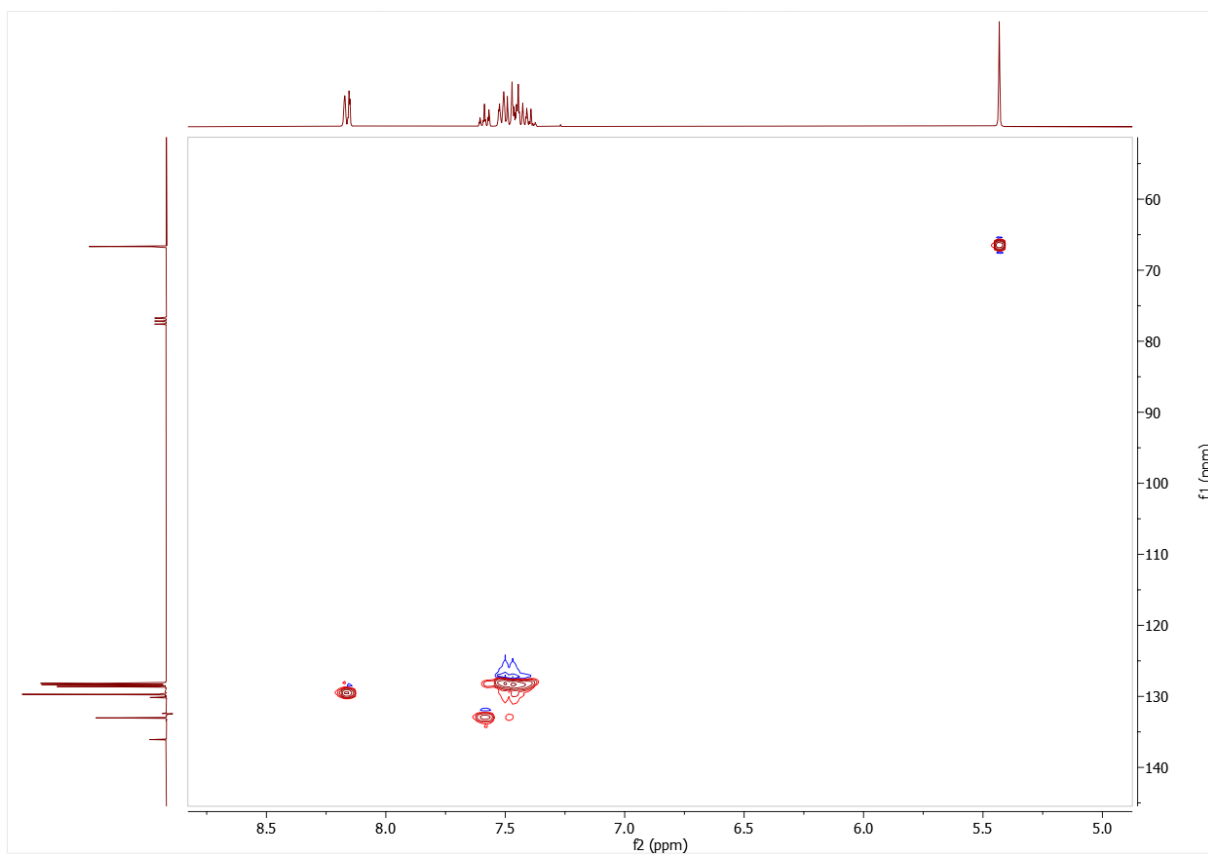
Figure A47. ¹H-¹³C-HSQC- NMR (400 MHz; 101 MHz) spectrum of benzyl benzoate in CDCl₃
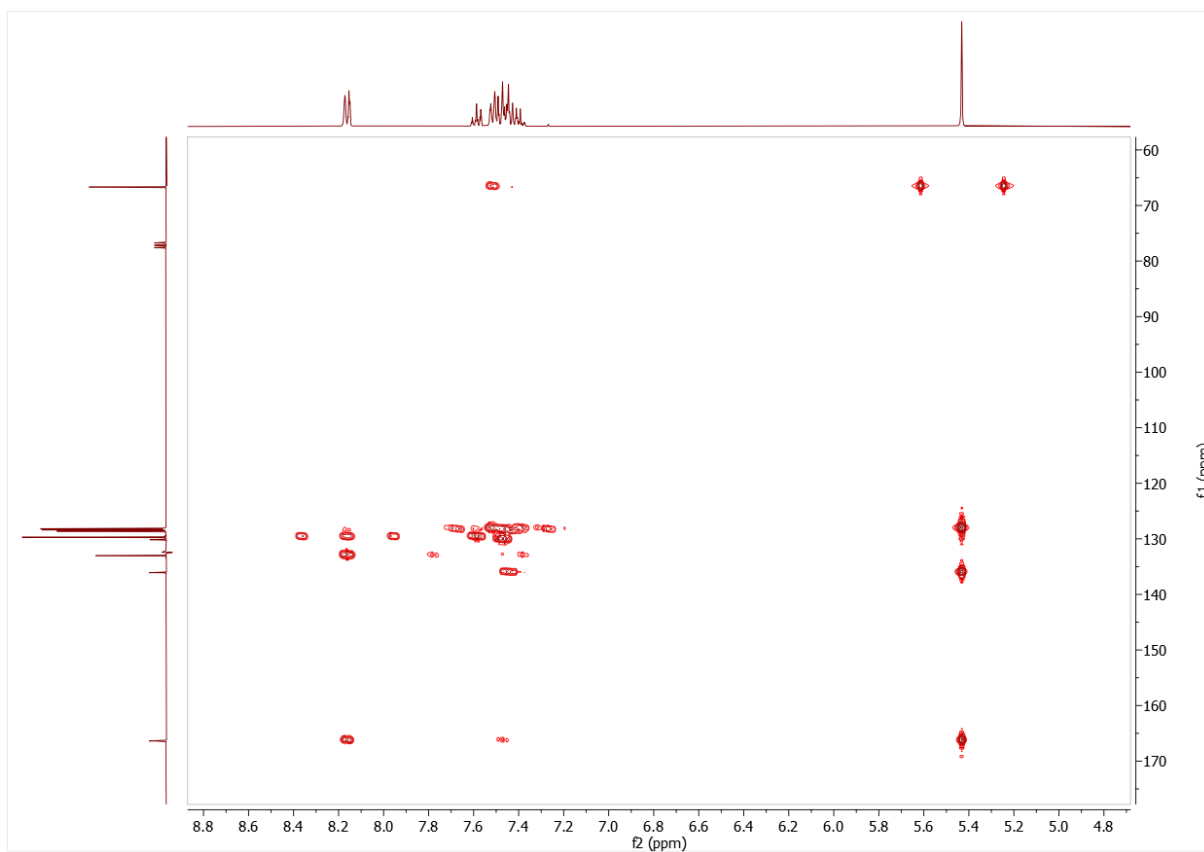
Figure A48. ^{1}H-^{13}C-HMBC- NMR (400 MHz; 101 MHz) spectrum of benzyl benzoate in CDCl$_3$
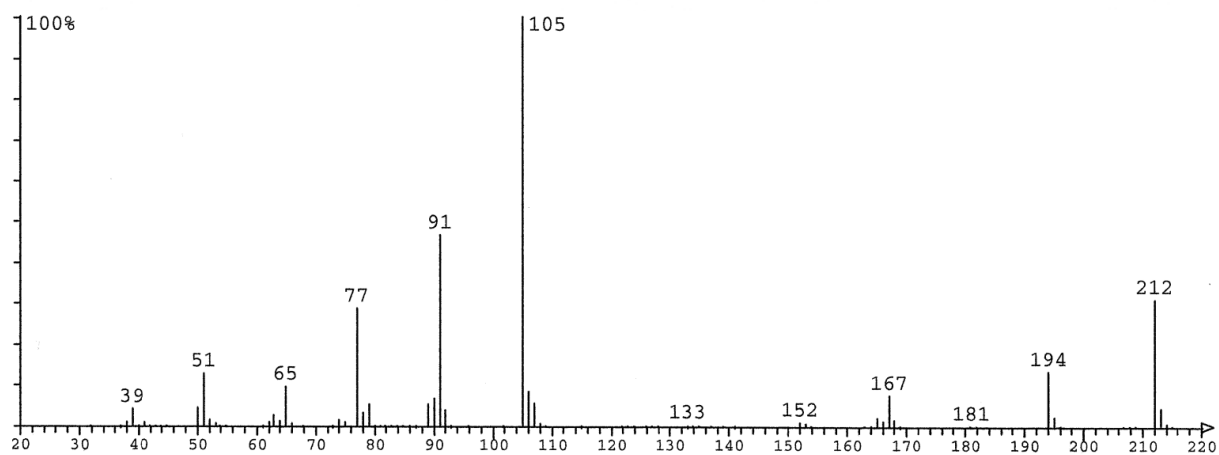
Figure A49. MS spectrum (EI) of allyl benzoate

8.3.2.7   *Characterization of 2-oxo-1,2-diphenylethyl benzoate (H)*

^{1}H NMR (400 MHz, CDCl$_3$) δ = 8.13 ppm (m, 2H), 8.01 ppm (m, 2H), 7.55 ppm (m, 4H), 7.41 ppm (m, 7H), 7.11 ppm (s, 1H). ^{13}C NMR (101 MHz, CDCl$_3$) δ = 193.79 ppm, 166.13 ppm, 134.80 ppm, 133.85 ppm, 133.61 ppm, 133.47 ppm, 130.09 ppm, 129.49 ppm, 129.43 ppm, 129.25 ppm, 128.96 ppm, 128.78 ppm, 128.51 ppm, 78.05 ppm (-**C**H$_{alkyl}$-). MS (GC-MS): m/z = 105[M$^+$], 316 (100%).
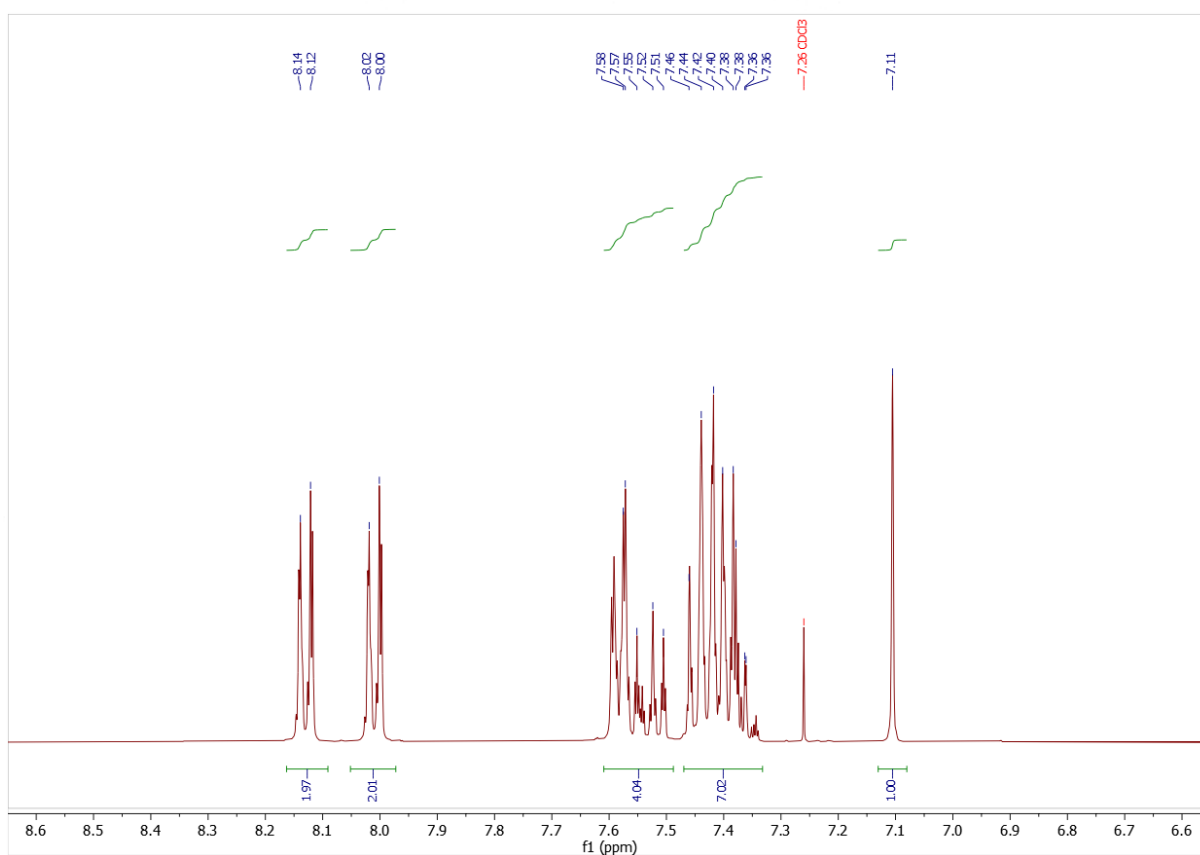
Figure A50. ^{1}H NMR (400 MHz) spectrum of H in CDCl$_3$
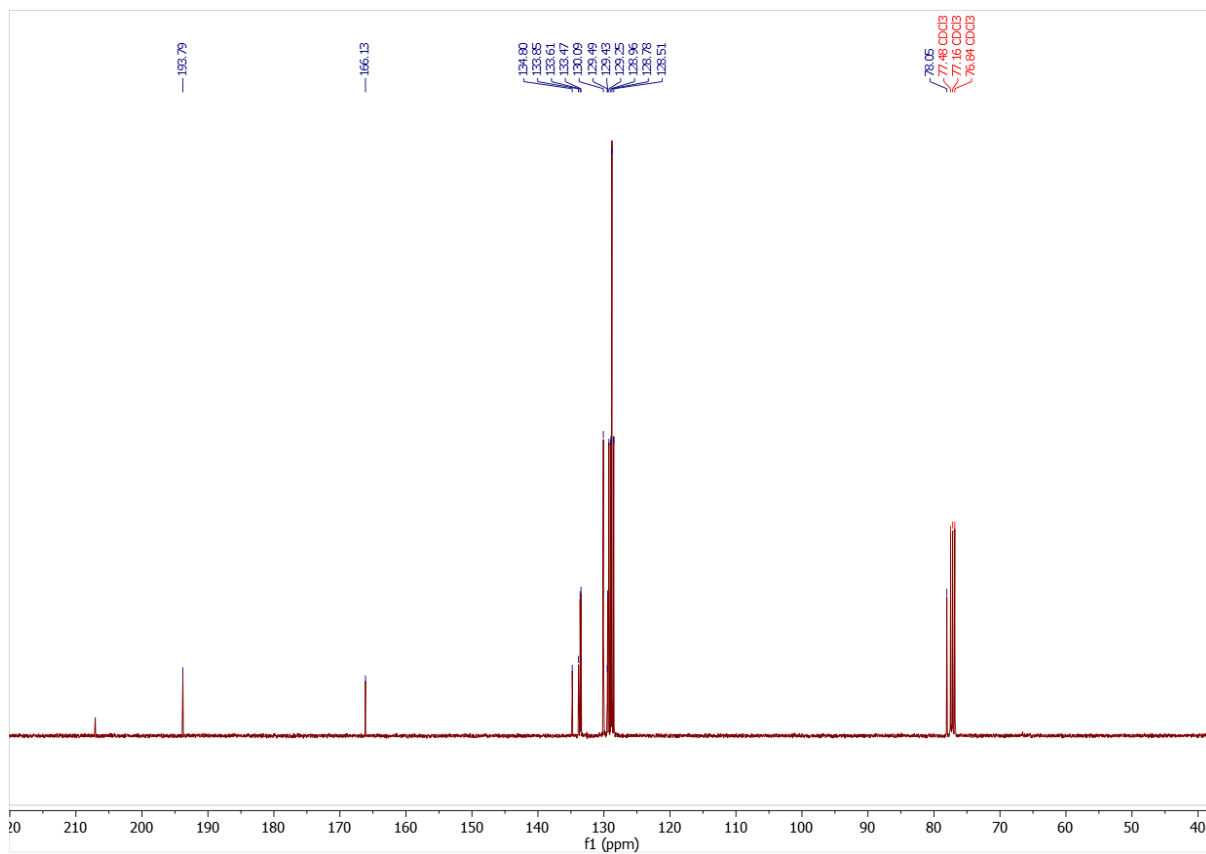
Figure A51. ^{13}C NMR (101 MHz) spectrum of H in $CDCl_3$
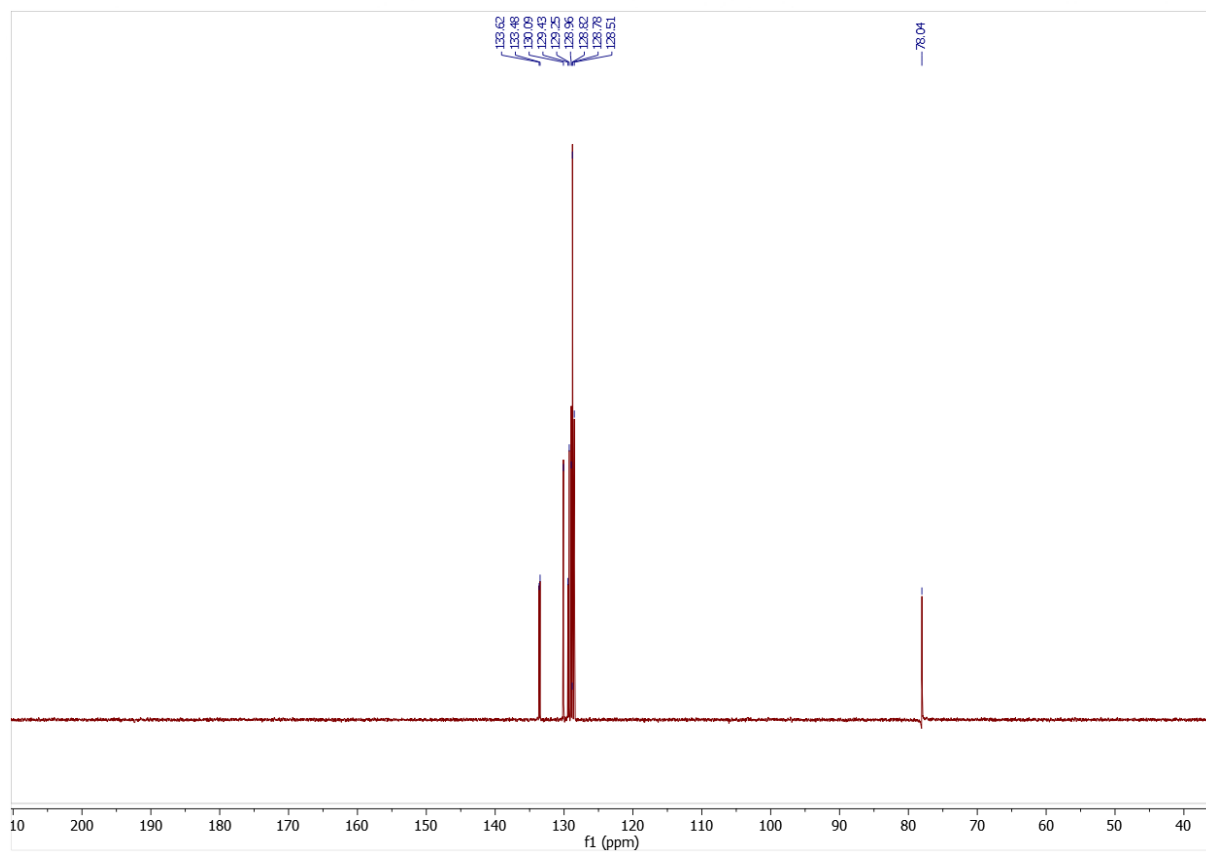
Figure A52. ^{13}C-DEPT NMR (101 MHz) spectrum of H in $CDCl_3$
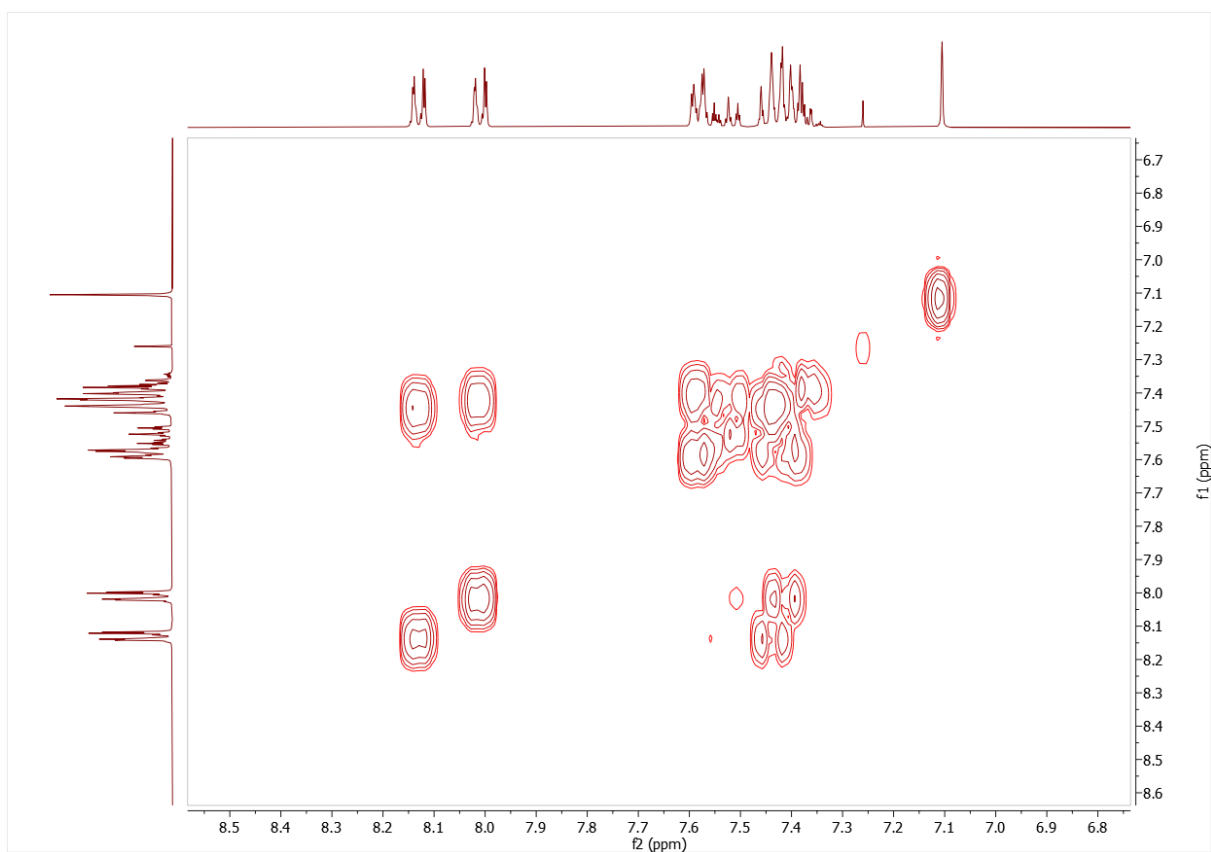
Figure A53. ^{1}H-COSY-NMR (400 MHz) spectrum of H in CDCl$_3$

Figure A54. ^{1}H-^{13}C-HSQC- NMR (400 MHz; 101 MHz) spectrum of H in CDCl$_3$
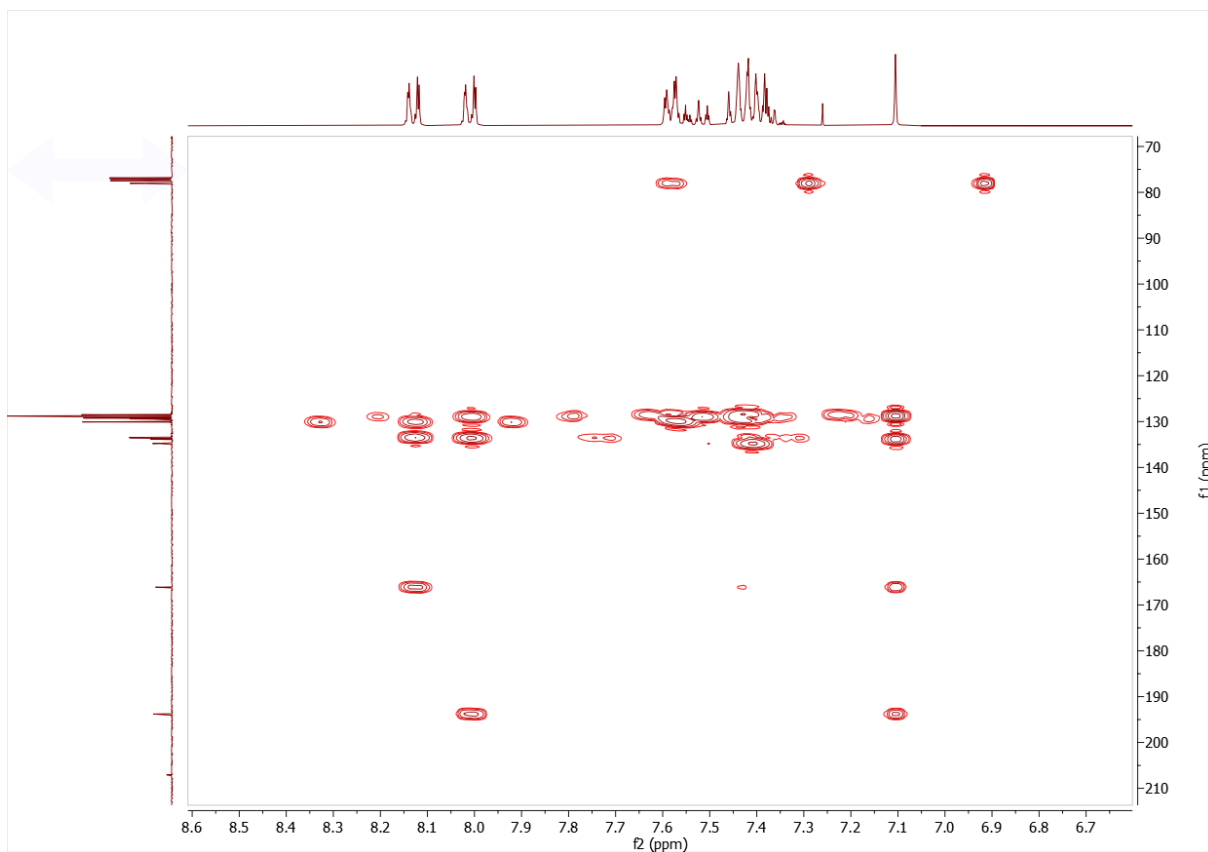
Figure A55. ^{1}H-^{13}C-HMBC- NMR (400 MHz; 101 MHz) spectrum of H in CDCl$_3$
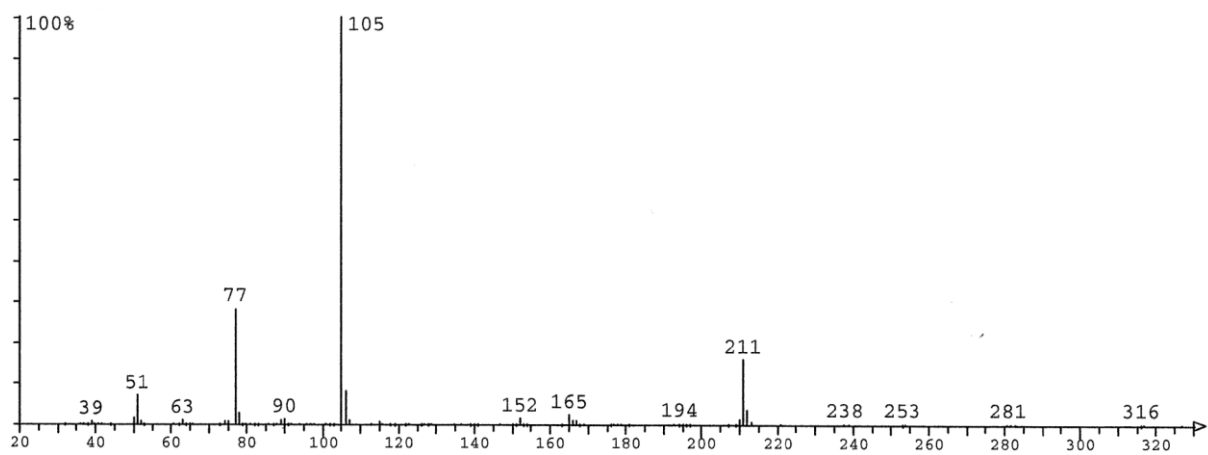
Figure A56. MS spectrum (EI) of H

8.3.3 Quantification by NMR of esterifications experients in table 4.3

8.3.3.1 *Butyl Benzoate (entry 1)*
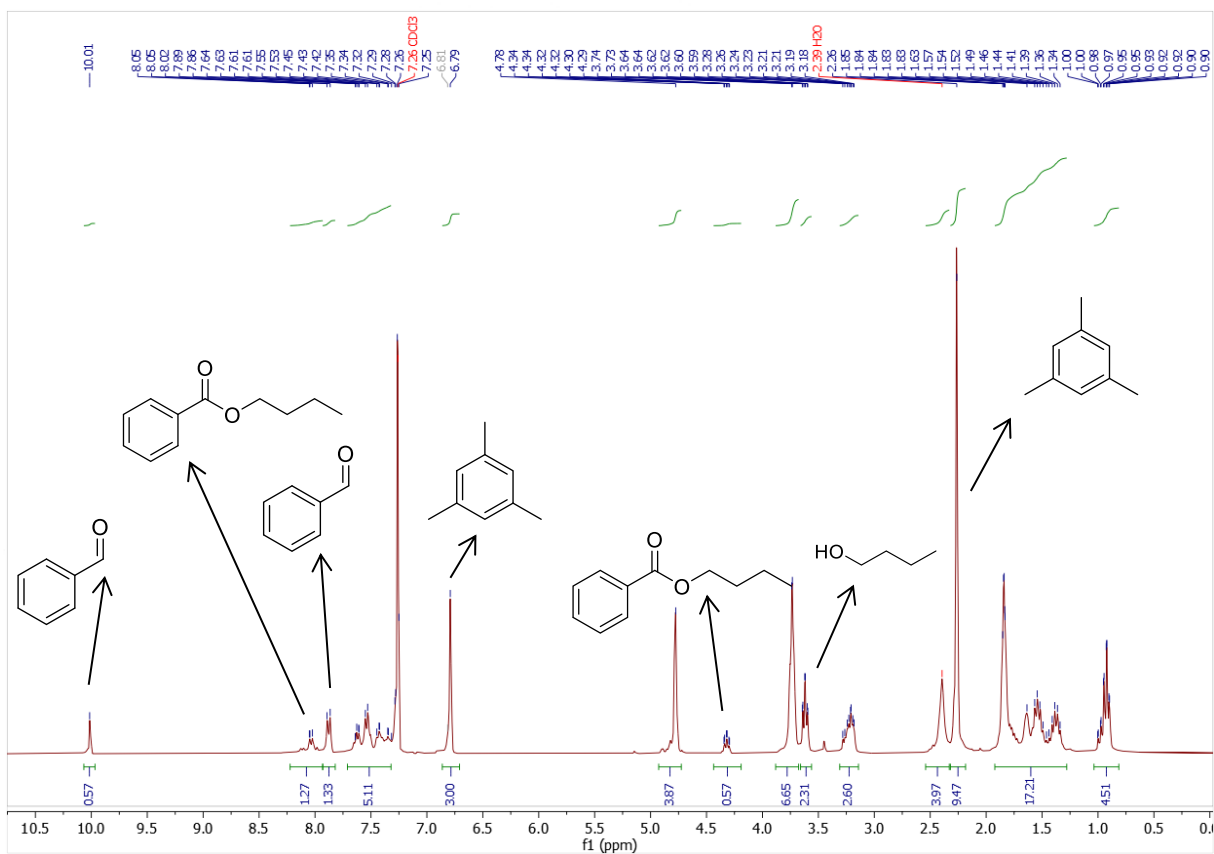
Figure A57. Quantification of Butyl Benzoate through ^{1}H NMR (300 MHz) spectrum of reaction mixture after water extraction in CDCl$_3$
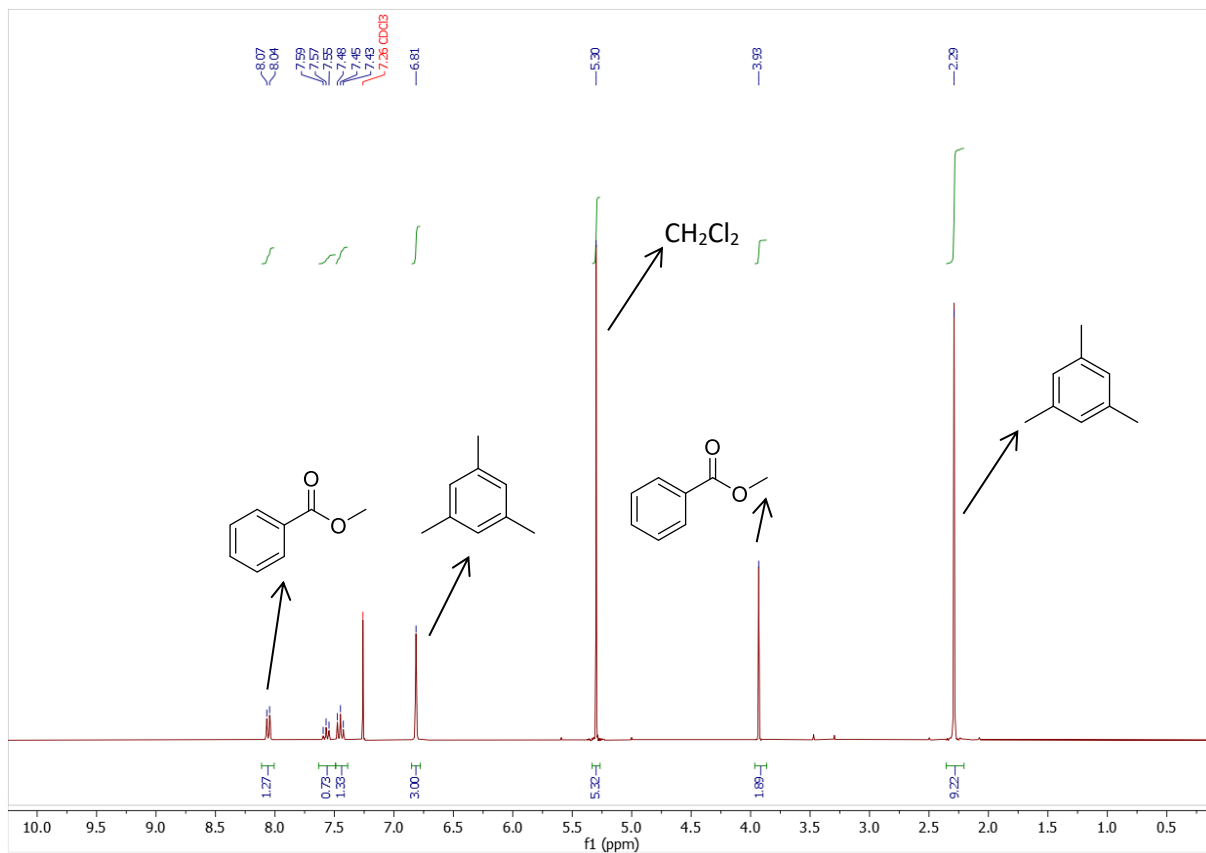
Figure A58. Quantification of Methyl Benzoate through ^{1}H NMR (300 MHz) spectrum of reaction mixture after water extraction in CDCl$_3$
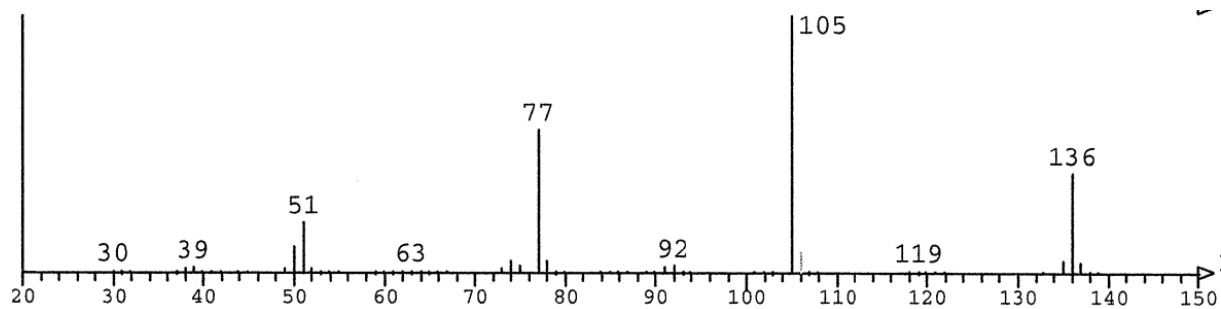
Figure A59. MS spectrum (EI) of methyl benzoate

8.3.3.3 *Benzyl Benzoate (entry 3)*
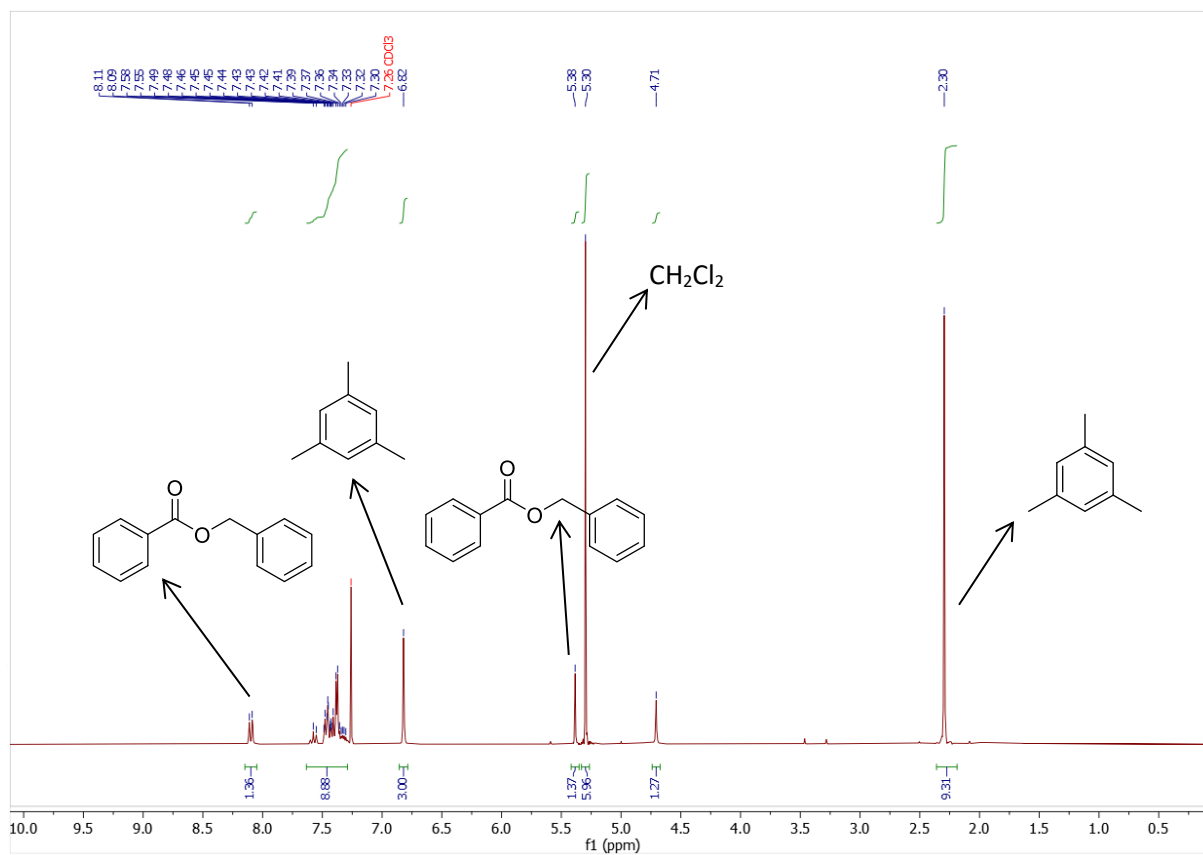
Figure A60. Quantification of Benzyl Benzoate through ^{1}H NMR (300 MHz) spectrum of reaction mixture after water extraction in CDCl$_3$

8.3.3.4   *Butyl 4-fluorobenzoate (entry 4)*
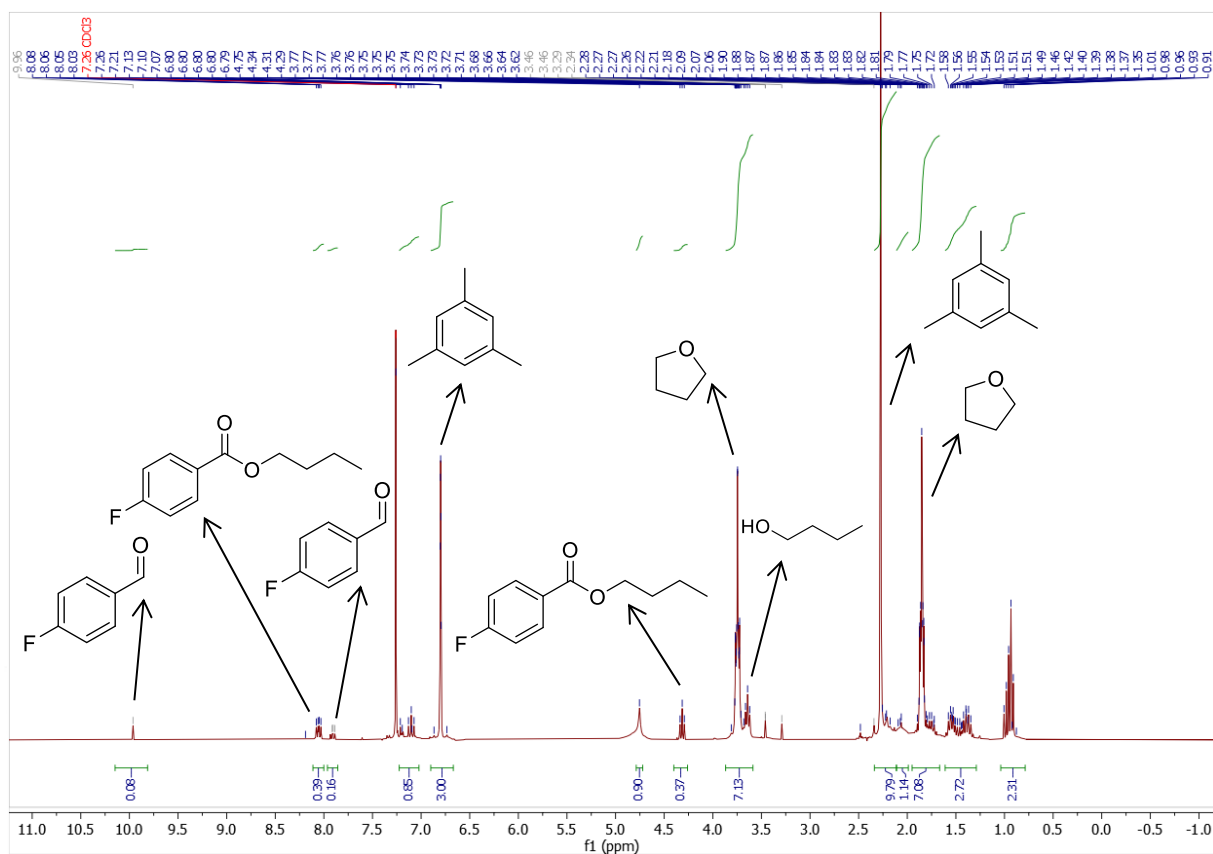
Figure A61. Quantification of Butyl 4-fluorobenzoate through ^{1}H NMR (300 MHz) spectrum of reaction mixture after water extraction in CDCl$_3$
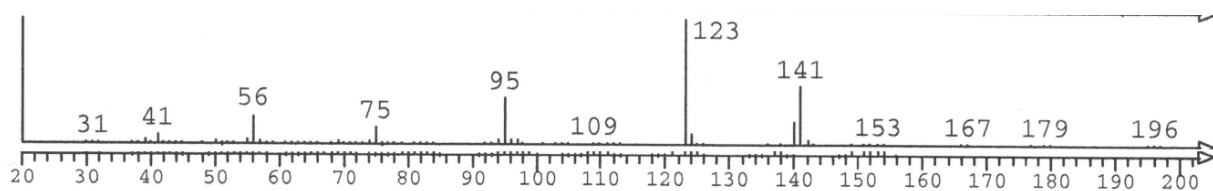
Figure A62. MS spectrum (EI) of butyl 4-fluorobenzoate

8.3.3.5 *Butyl 4-methoxybenzoate (entry 5)*
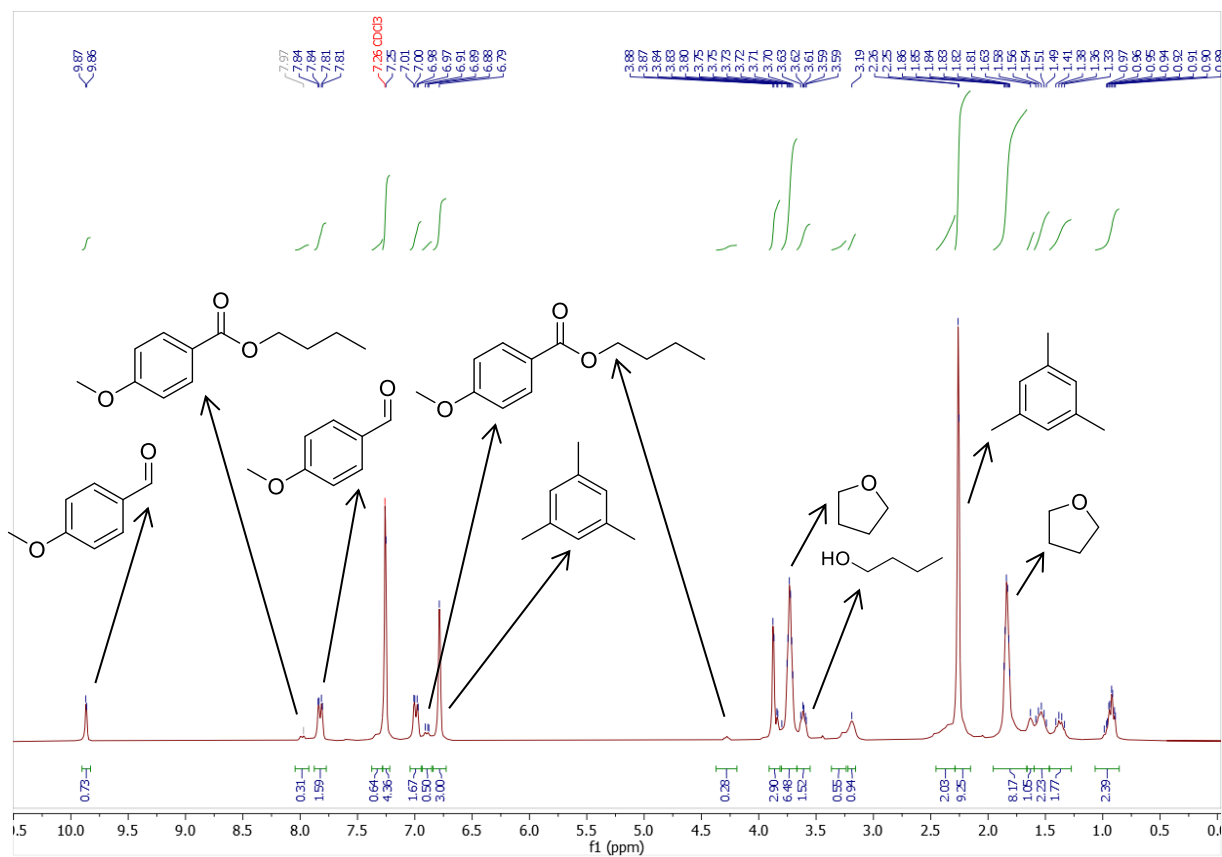
Figure A63. Quantification of Butyl 4-methoxybenzoate through ^{1}H NMR (300 MHz) spectrum of reaction mixture after water extraction in CDCl$_3$
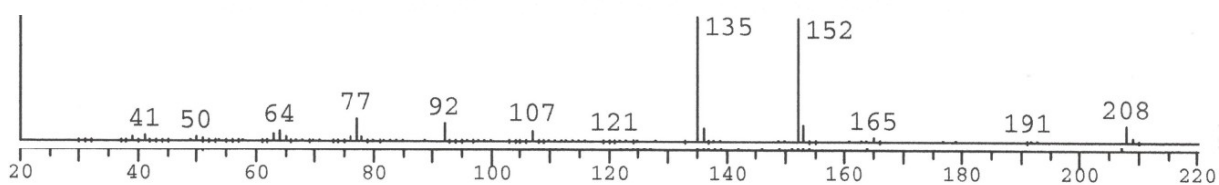
Figure A64. MS spectrum (EI) of butyl 4-methoxybenzoate

8.3.3.6   Butyl 4-nitrobenzoate (entry 6)
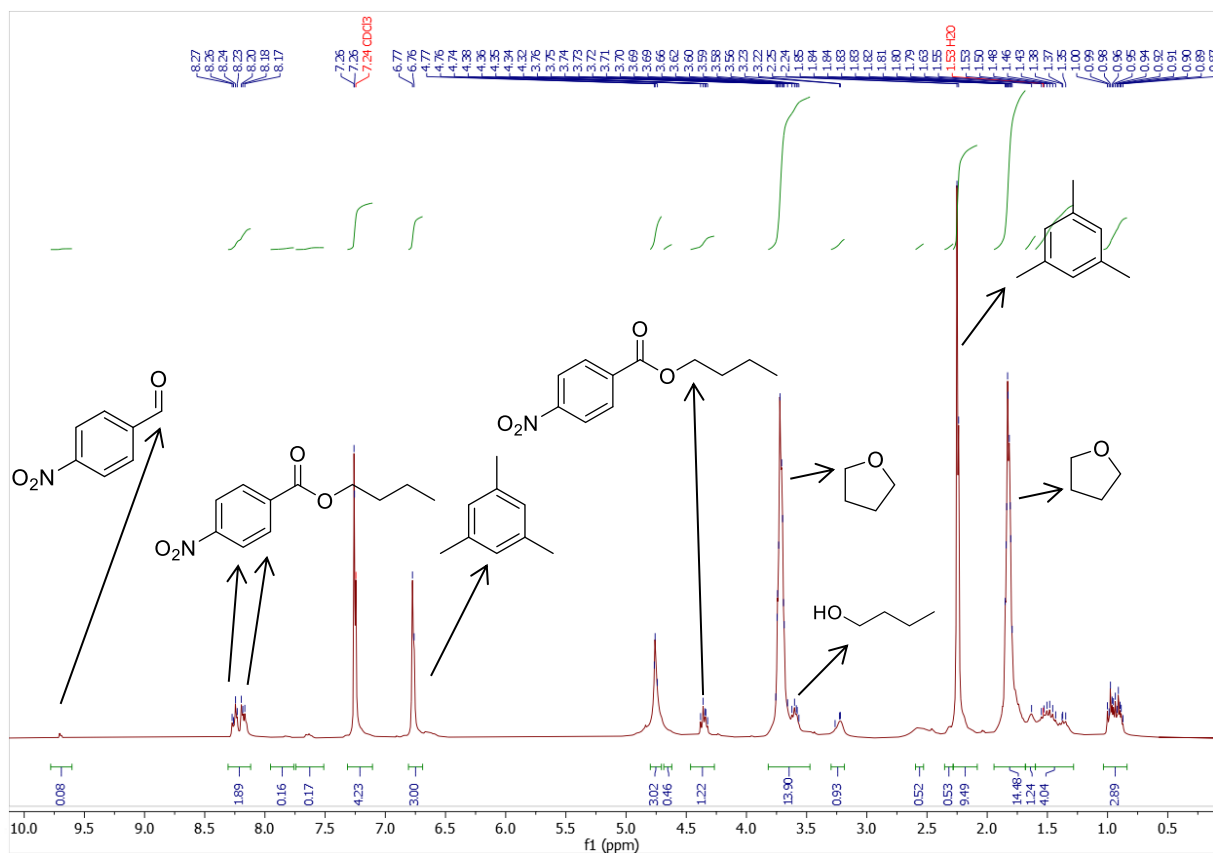
Figure A65. Quantification of Butyl 4-nitrobenzoate through ^{1}H NMR (300 MHz) spectrum of reaction mixture after water extraction in CDCl$_3$
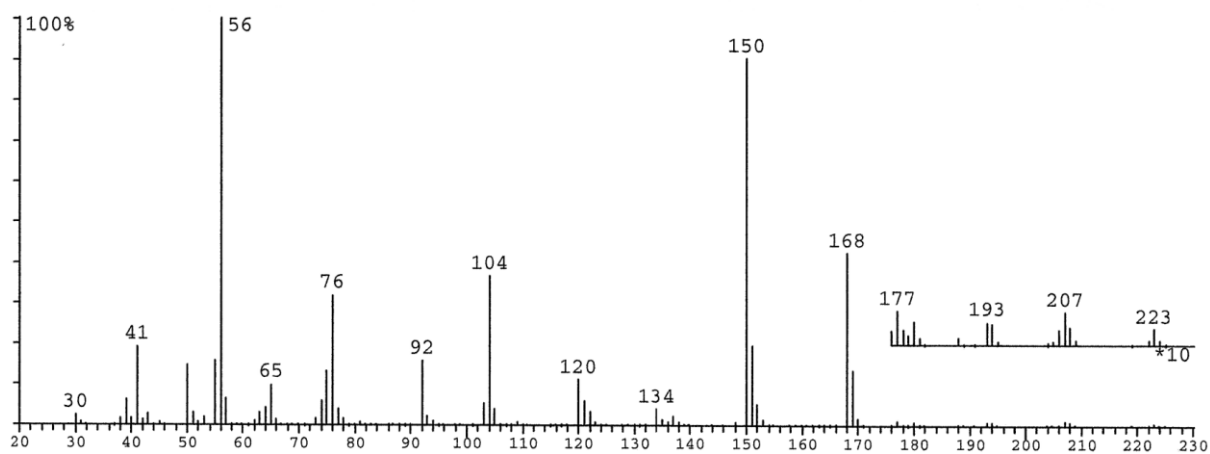
Figure A66. MS spectrum (EI) of butyl 4-nitrobenzoate

8.3.4 Characterization of amidation products

8.3.4.1 *Characterization of N-Hexylbenzamida*

^{1}H NMR (400 MHz, CDCl$_3$) δ = 7.76 ppm (-**CH**$_{arom}$-, orto position, d, 2H), 7.46 ppm (-**CH**$_{arom}$-, para position, t, 1H), 7.38 ppm (-**CH**$_{arom}$-, meta position, t, 2H), 6.44 ppm (-(CO)-**NH**-, s, 1H), 3.41 ppm (-(CO)-NH-**CH$_2$**-, q, 2H), 1.58 ppm (-NH-CH$_2$-**CH$_2$**-, p, 2H), 1.29 ppm (m, 6H), 0.86 ppm (-CH$_2$-**CH$_3$,** t, 3H).^{13}C NMR (75 MHz, CDCl$_3$) δ = 167.63 ppm (-(**C**O)-), 134.98 ppm (-**C**$_{arom}$-), 131.33 (-**CH**$_{arom}$-, para position), 128.58 ppm (-**CH**$_{arom}$-, meta position), 126.96 (-**CH**$_{arom}$-, orto position), 40.22 ppm (-(CO)-NH-**CH$_2$**-), 31.62 ppm (-**CH$_{2\text{-alkyl}}$**), 29.74 (-NH-CH$_2$-**CH$_2$**-), 26.78 ppm (-**CH$_{2\text{-alkyl}}$**), 22.66 ppm (-**CH$_{2\text{-alkyl}}$**), 14.12 ppm (-CH$_2$-**CH$_3$**). MS (GC-MS): m/z = 205[M$^+$], 105 (100%).
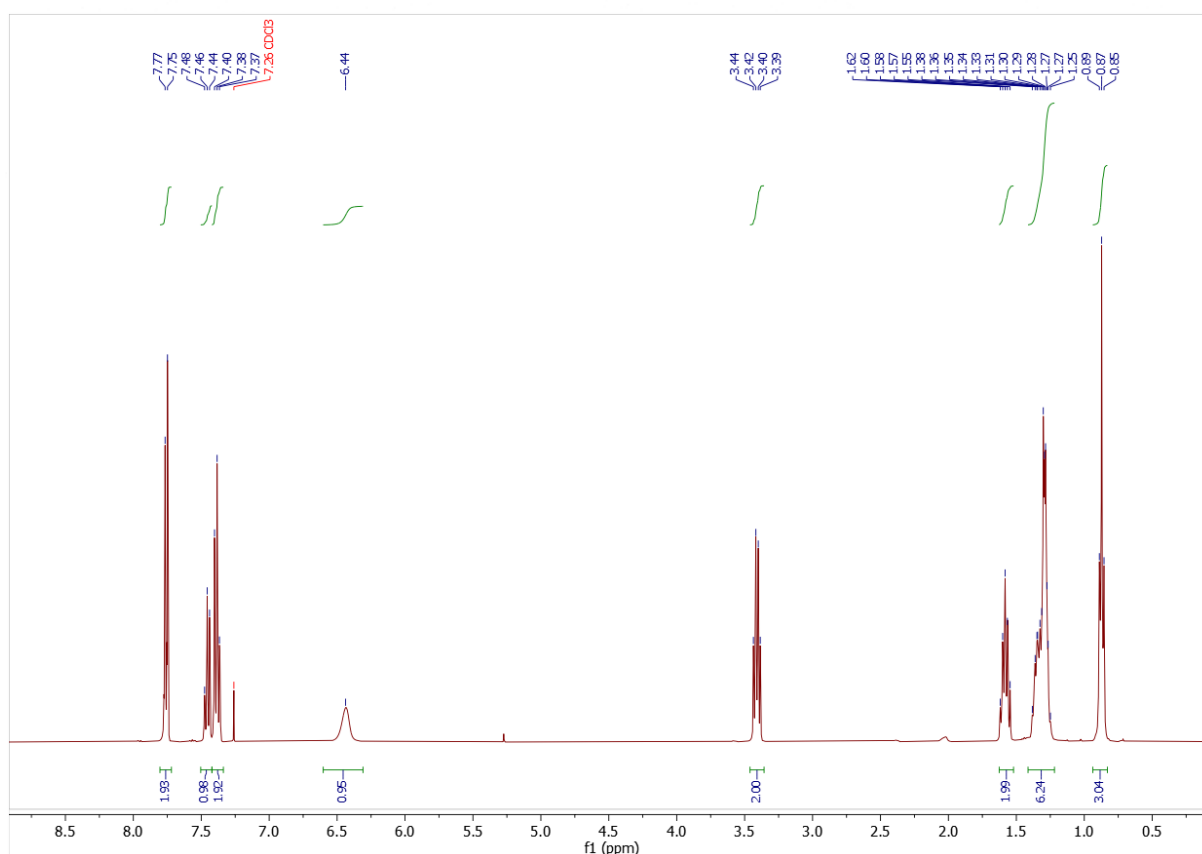
Figure A67. ^{1}H NMR (400 MHz) spectrum of N-Hexylbenzamida in CDCl$_3$
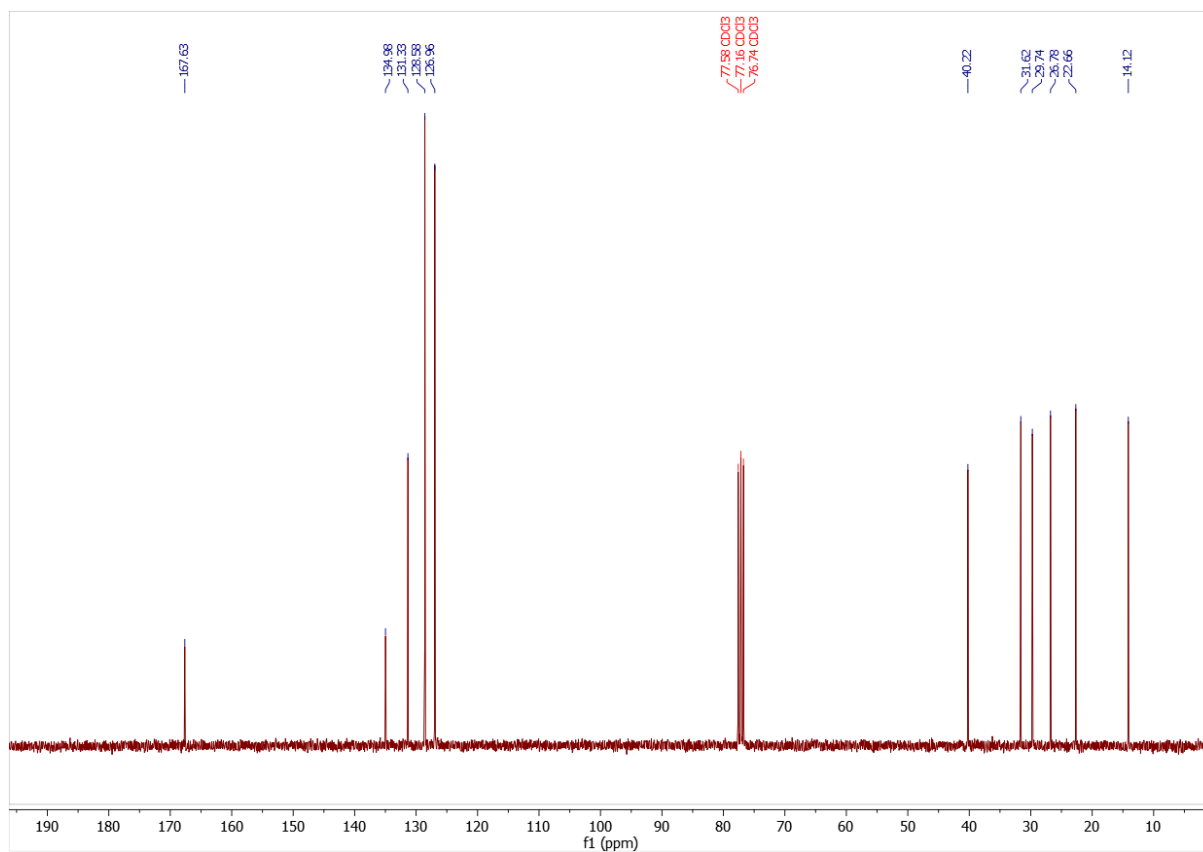
Figure A68. ^{13}C NMR (75 MHz) spectrum of N-Hexylbenzamida in CDCl$_3$
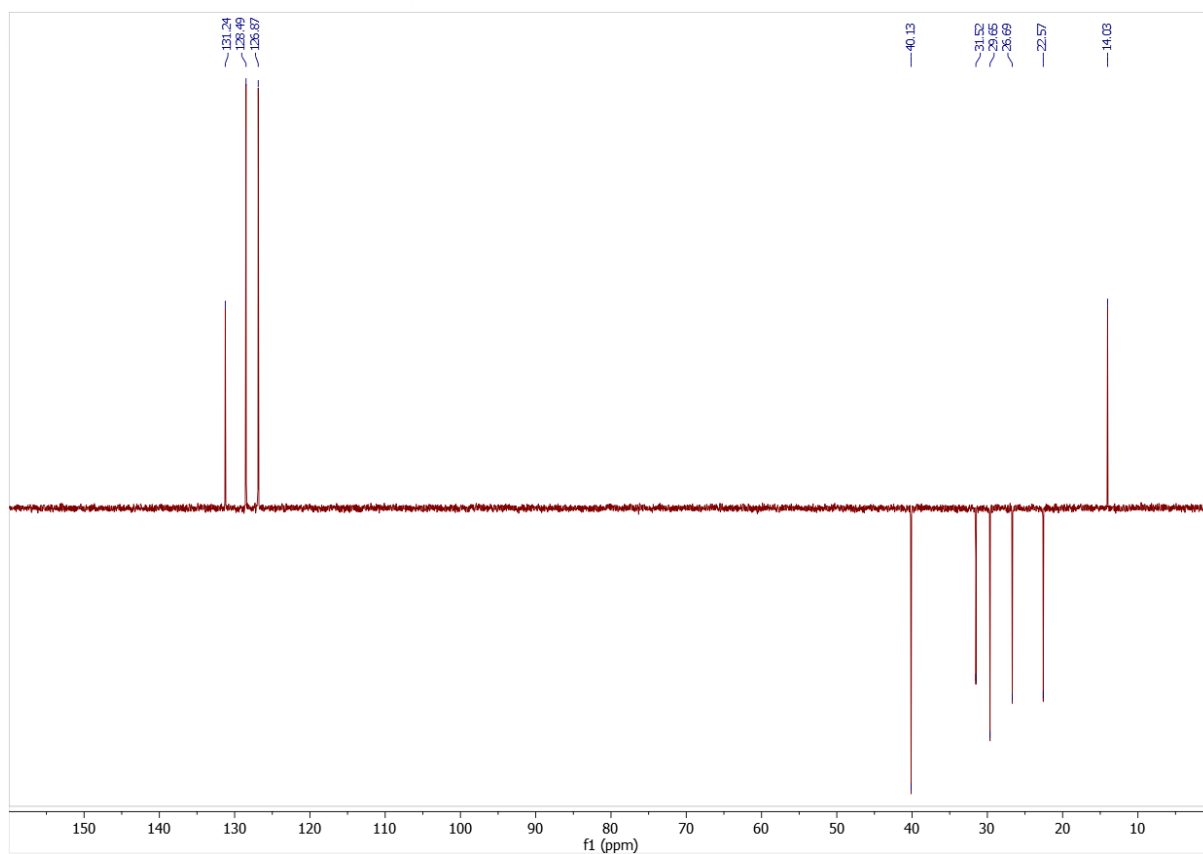
Figure A69. ^{13}C-DEPT NMR (75 MHz) spectrum of N-Hexylbenzamida in CDCl$_3$
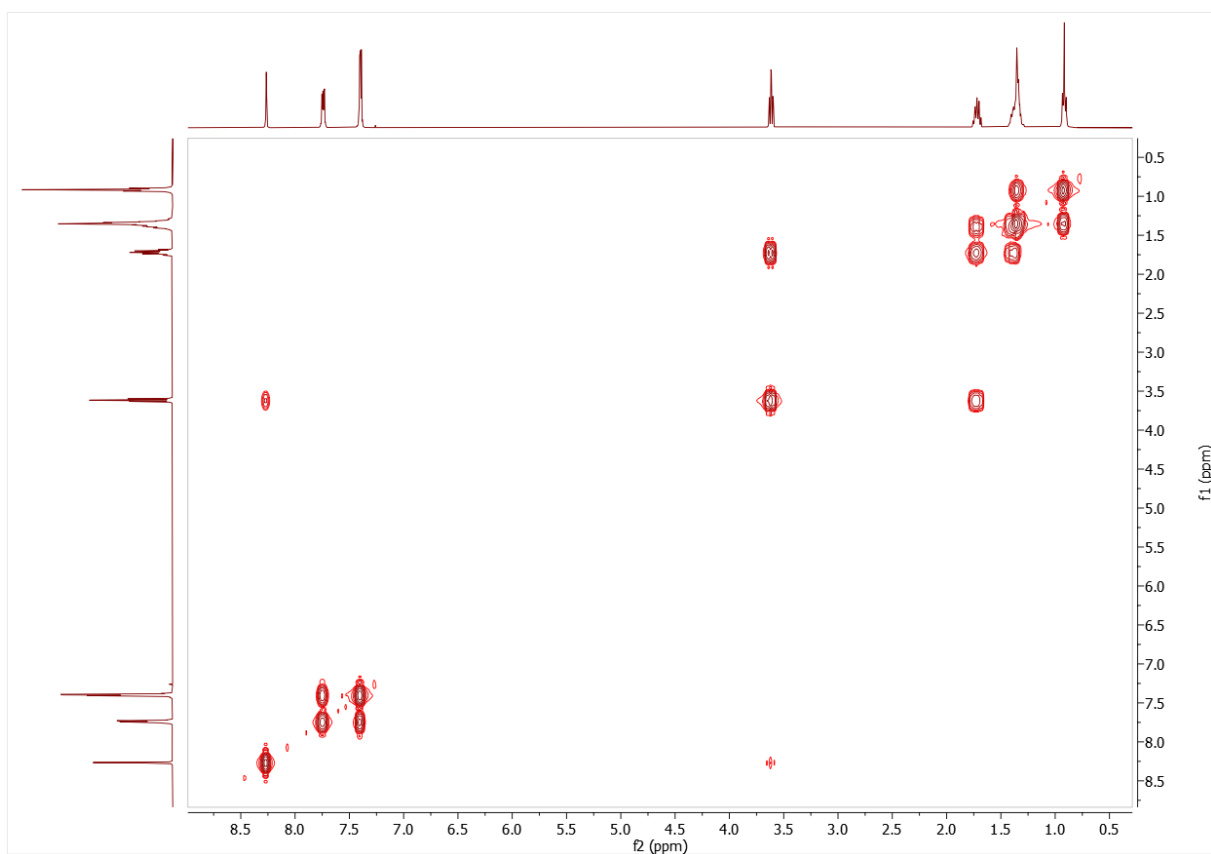
234
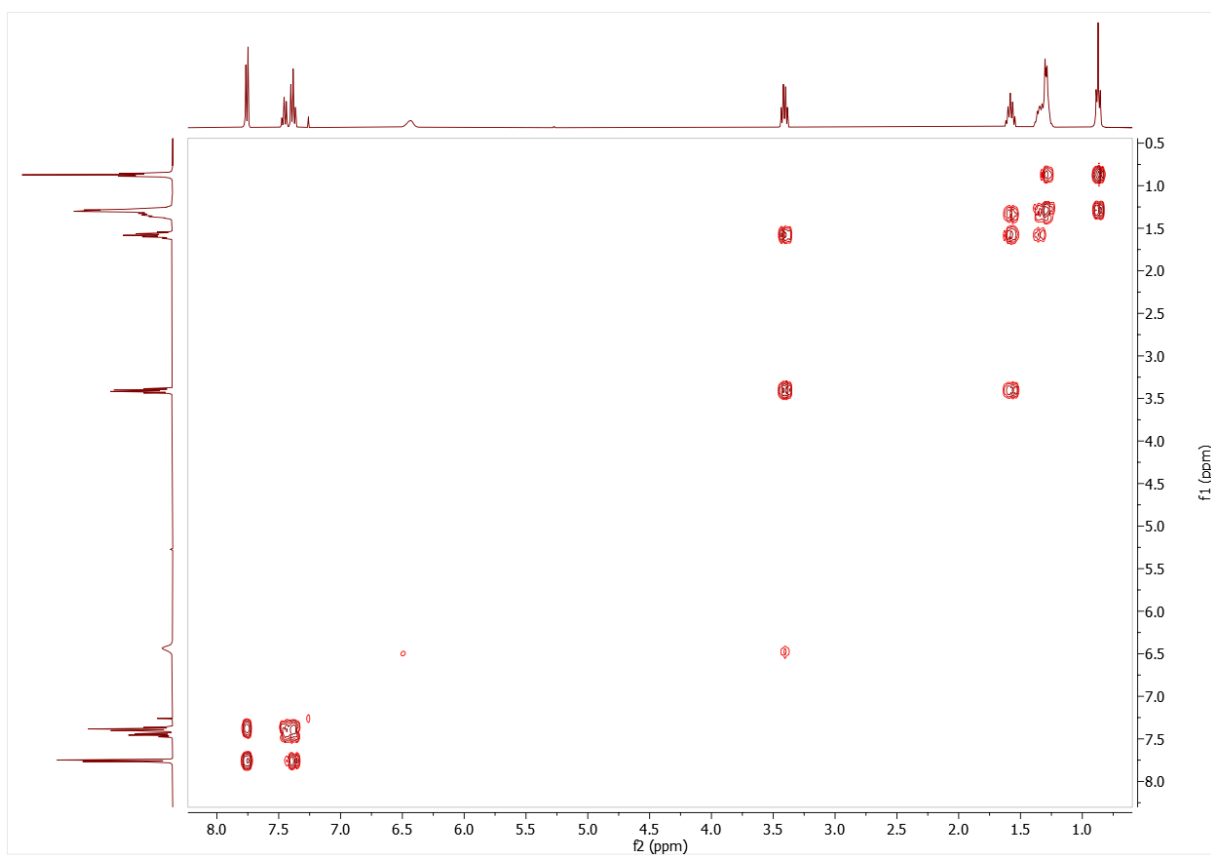
Figure A70. ^{1}H-COSY-NMR (400 MHz) spectrum of N-Hexylbenzamida in CDCl$_3$
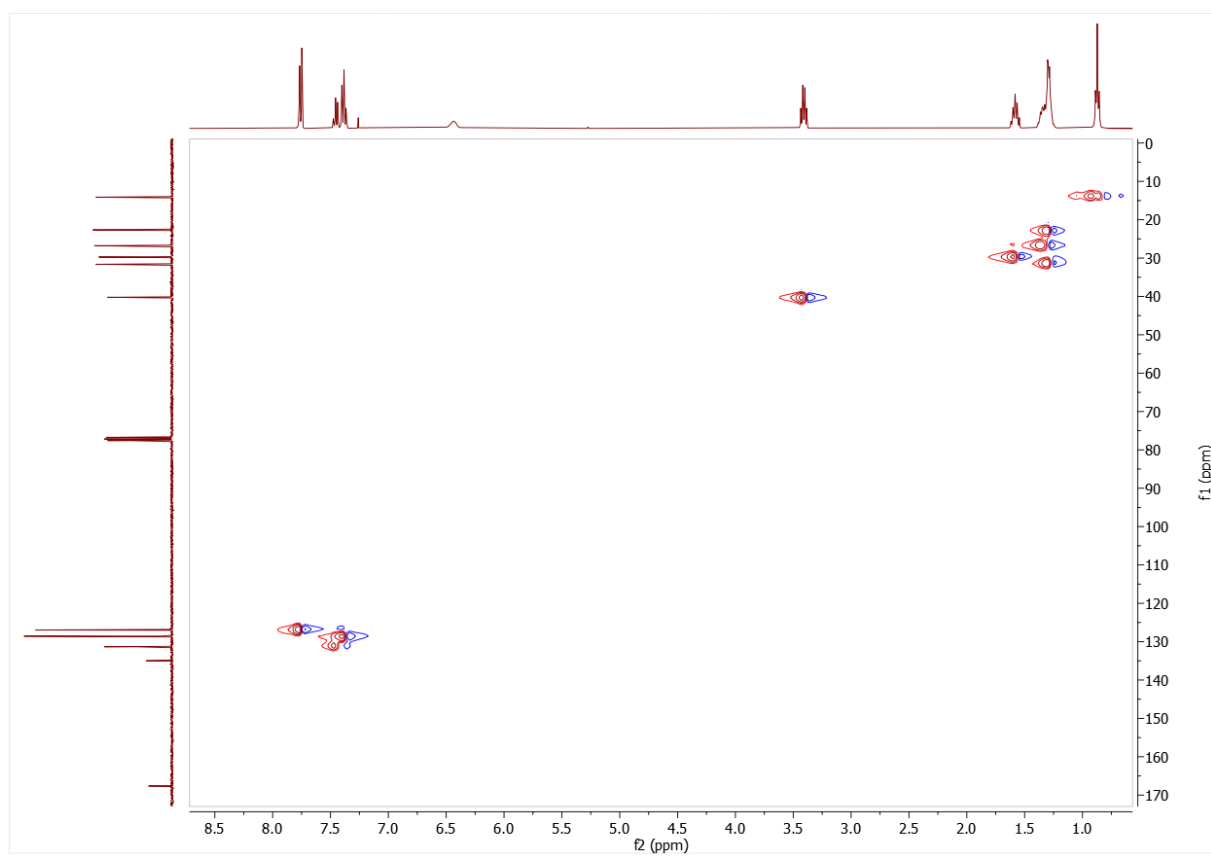
Figure A71. ^{1}H-^{13}C-HSQC- NMR (400 MHz; 101 MHz) spectrum of N-Hexylbenzamida in CDCl$_3$
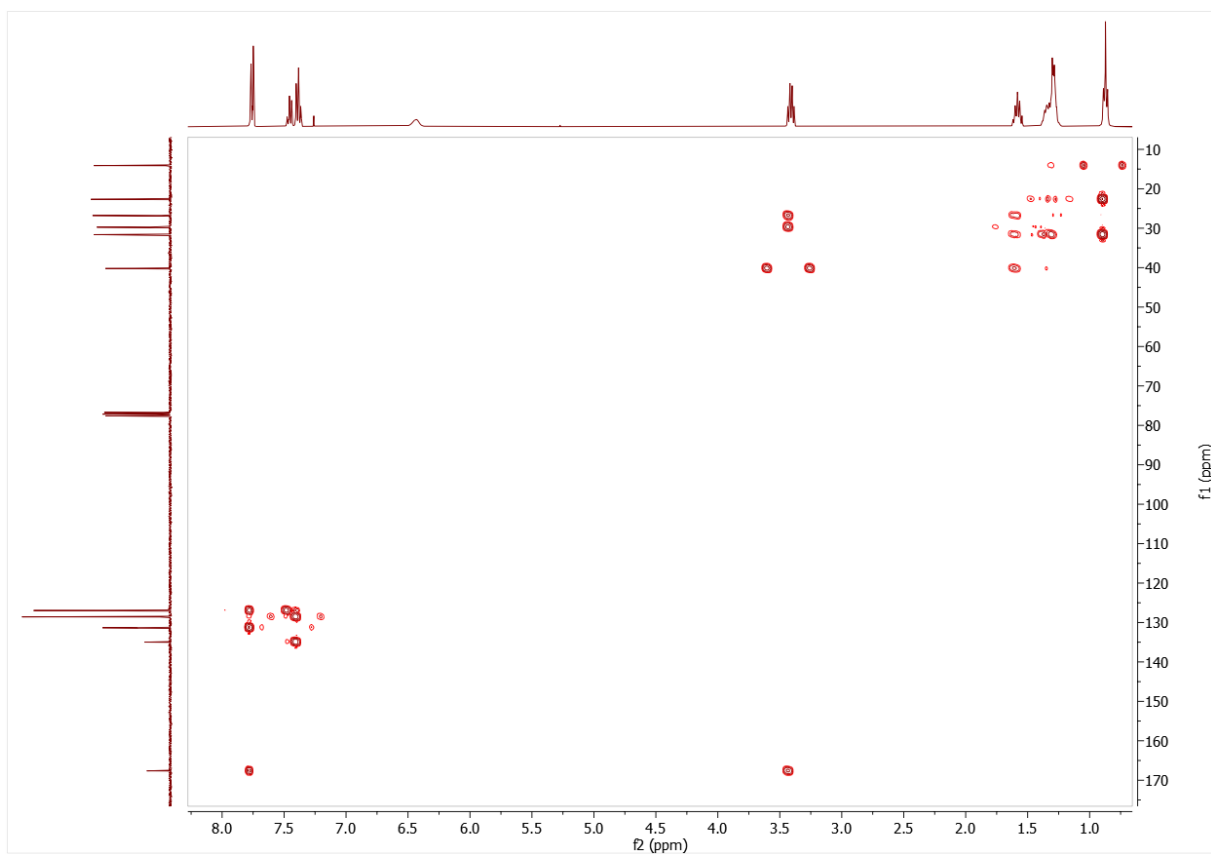
Figure A72. ^1H-^{13}C-HMBC- NMR (400 MHz; 101 MHz) spectrum of N-Hexylbenzamida in CDCl$_3$
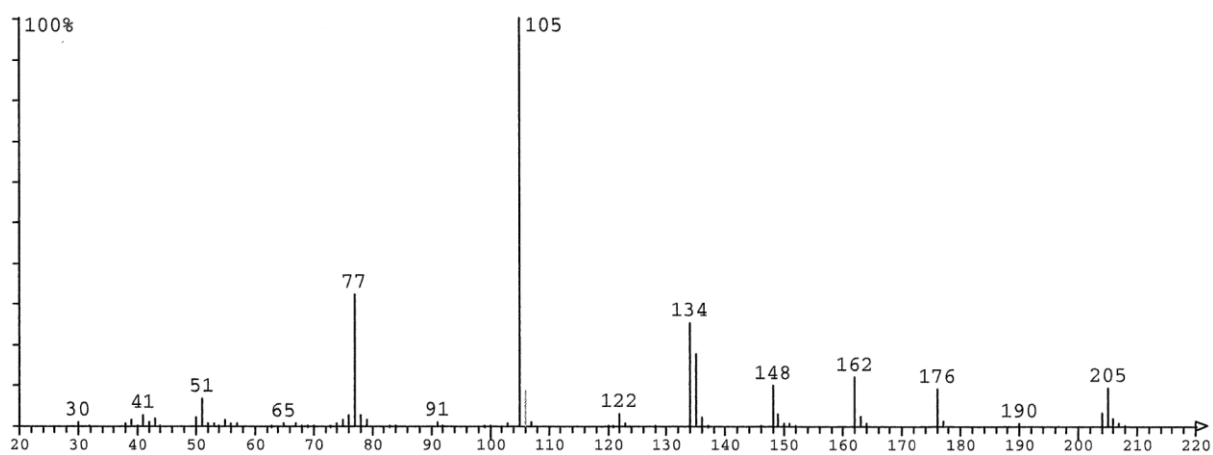
Figure A73. MS spectrum (EI) of N-hexylbenzamida

8.3.4.2   *Characterization of N-hexyl-1-phenylmethanimine*

^{1}H NMR (400 MHz, CDCl$_3$) δ = 8.27 ppm (-**CH**$_{imine}$, s, 1H), 7.74 ppm (-**CH**$_{arom}$-, orto position m, 2H), 7.40 ppm (-**CH**$_{arom}$-, meta and para positions, m, 3H), 3.62 ppm (=N-**CH$_2$**-, td, *J* = 7.0, 1.3 Hz, 2H), 1.71 ppm (=N-CH$_2$-**CH$_2$**-, m, 2H), 1.35 ppm (-**CH$_2$**-alkyl-, m, 6H), 0.92 ppm (-CH$_2$-**CH$_3$**, m, 3H). ^{13}C NMR (75 MHz, CDCl$_3$) δ = 160.60 ppm (-**CH**$_{imine}$), 136.41 ppm (-**C**$_{arom}$-), 130.39 ppm and 128.53 ppm (-**CH**$_{arom}$-, meta and para positions), 128.01 ppm (-**CH**$_{arom}$-, orto position), 61.83 (=N-**CH$_2$**-), 31.72 ppm (-**CH$_2$**-alkyl-), 30.94 ppm (=N-CH$_2$-**CH$_2$**-), 27.08 ppm (-**CH$_2$**-alkyl-), 22.66 ppm (-**CH$_2$**-alkyl-), 14.11 ppm (-CH$_2$-**CH$_3$**). MS (GC-MS): m/z = 189[M$^+$], 160 (100%).
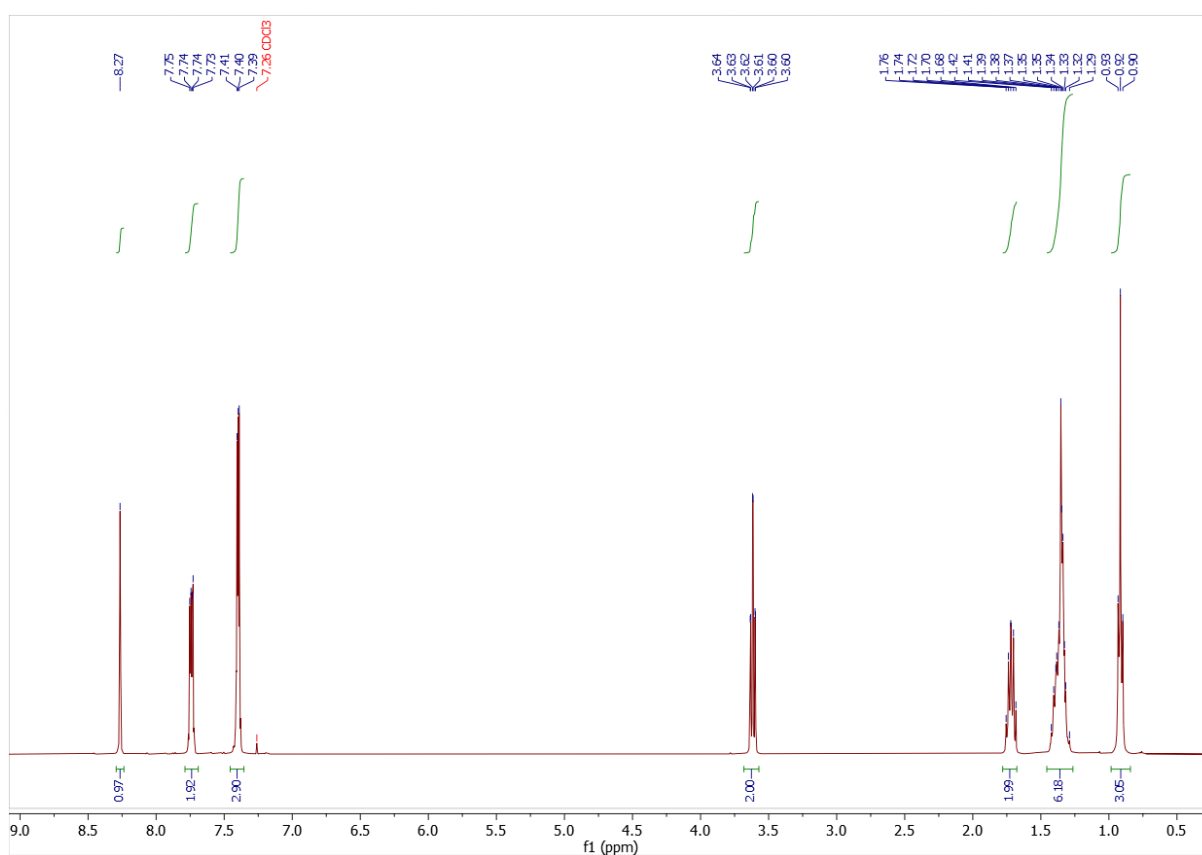
Figure A74. ^{1}H NMR (400 MHz) spectrum of N-hexyl-1-phenylmethanimine in CDCl$_3$
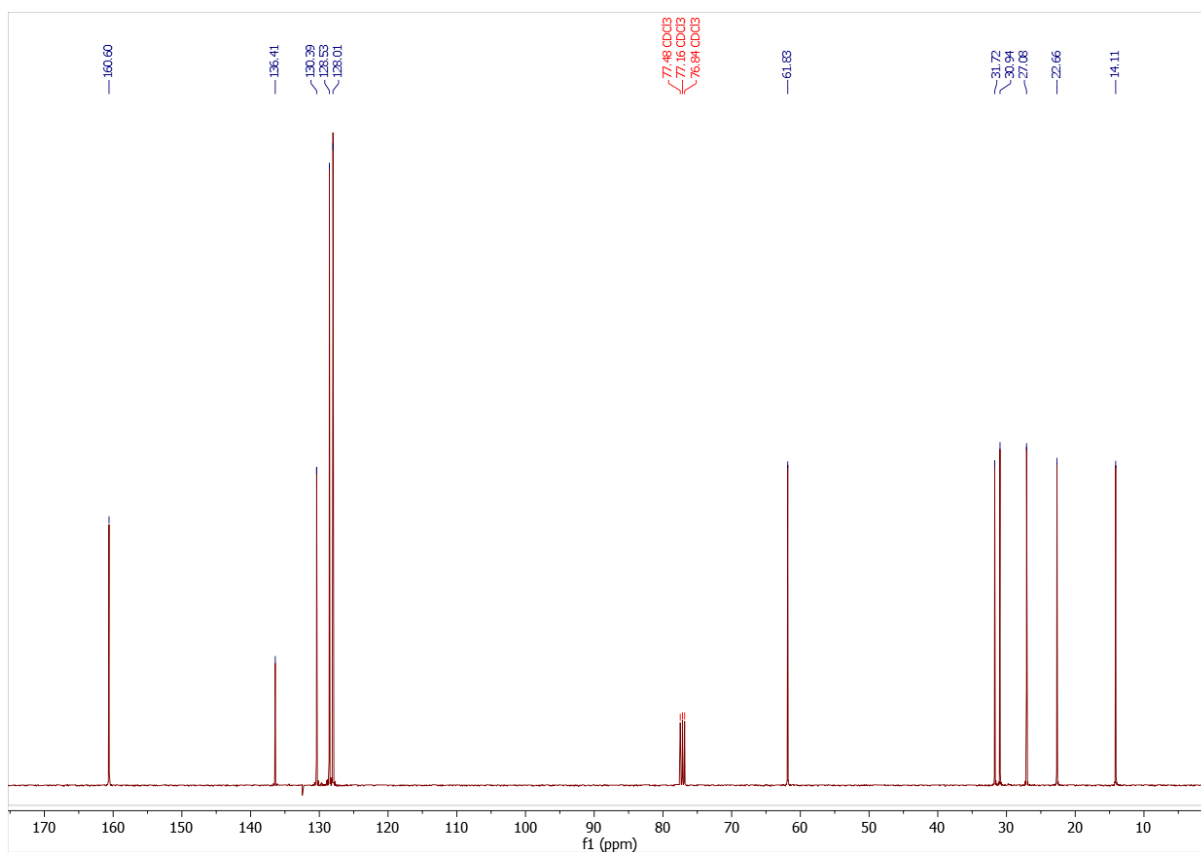
Figure A75. ^{13}C NMR (101 MHz) spectrum of 55 in CDCl$_3$
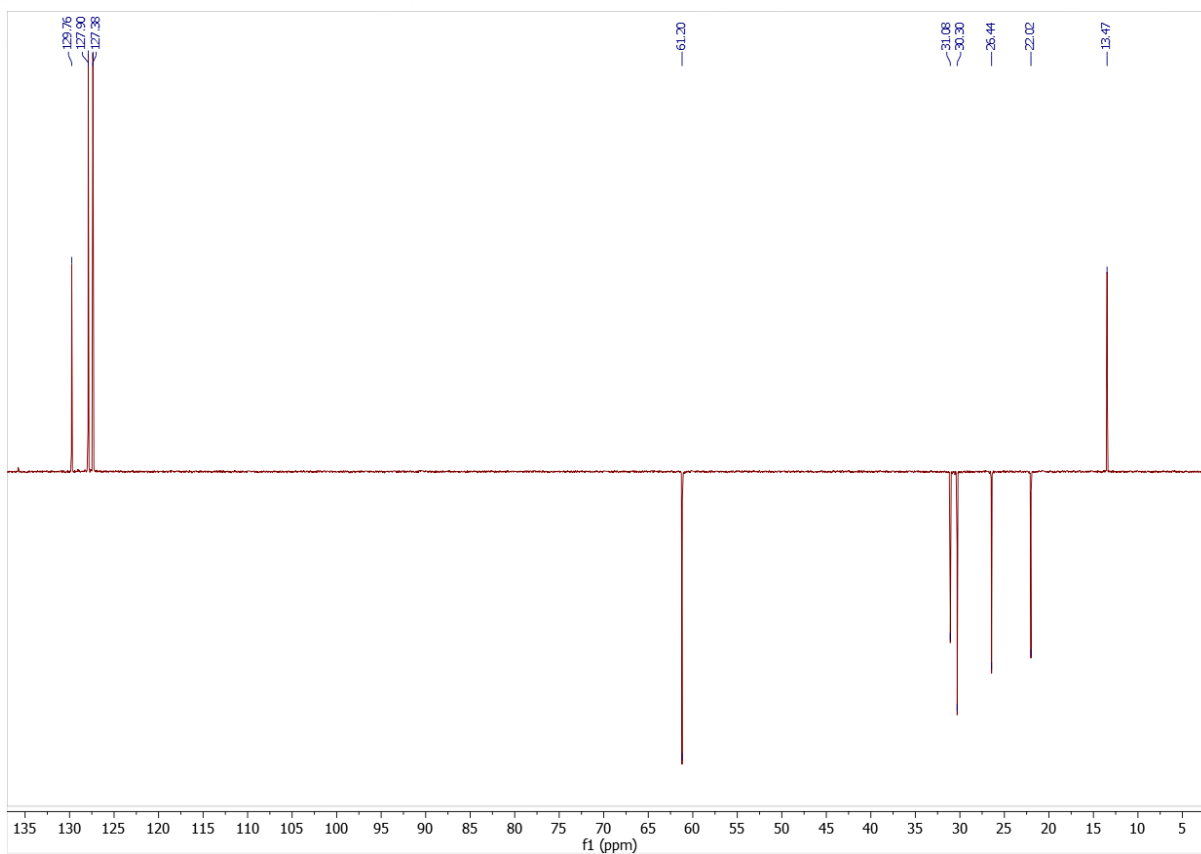
Figure A76. ^{13}C-DEPT NMR (101 MHz) spectrum of N-hexyl-1-phenylmethanimine in CDCl$_3$

Figure A77. ^{1}H-COSY-NMR (300 MHz) spectrum of N-hexyl-1-phenylmethanimine in CDCl$_3$
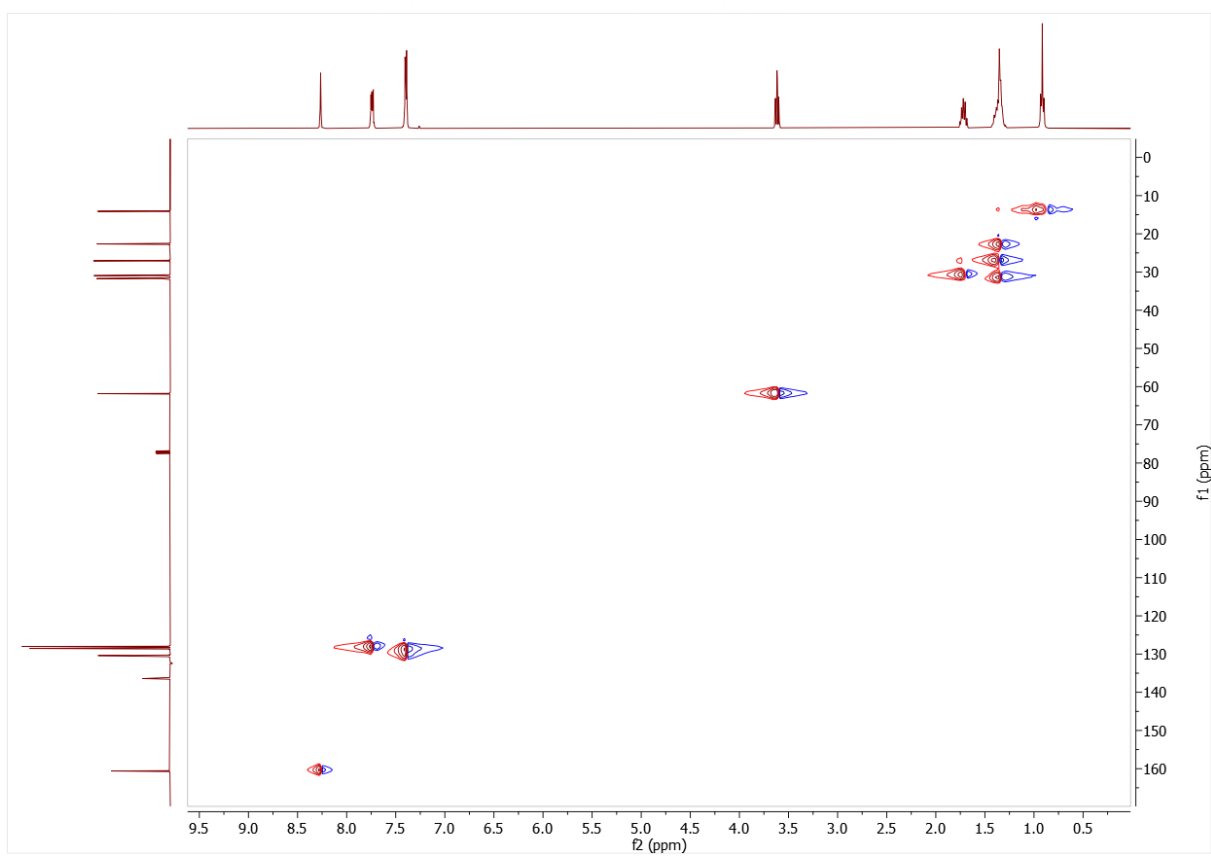
Figure A78. ^{1}H-^{13}C-HSQC- NMR (400 MHz; 101 MHz) spectrum of N-hexyl-1-phenylmethanimine in CDCl$_3$
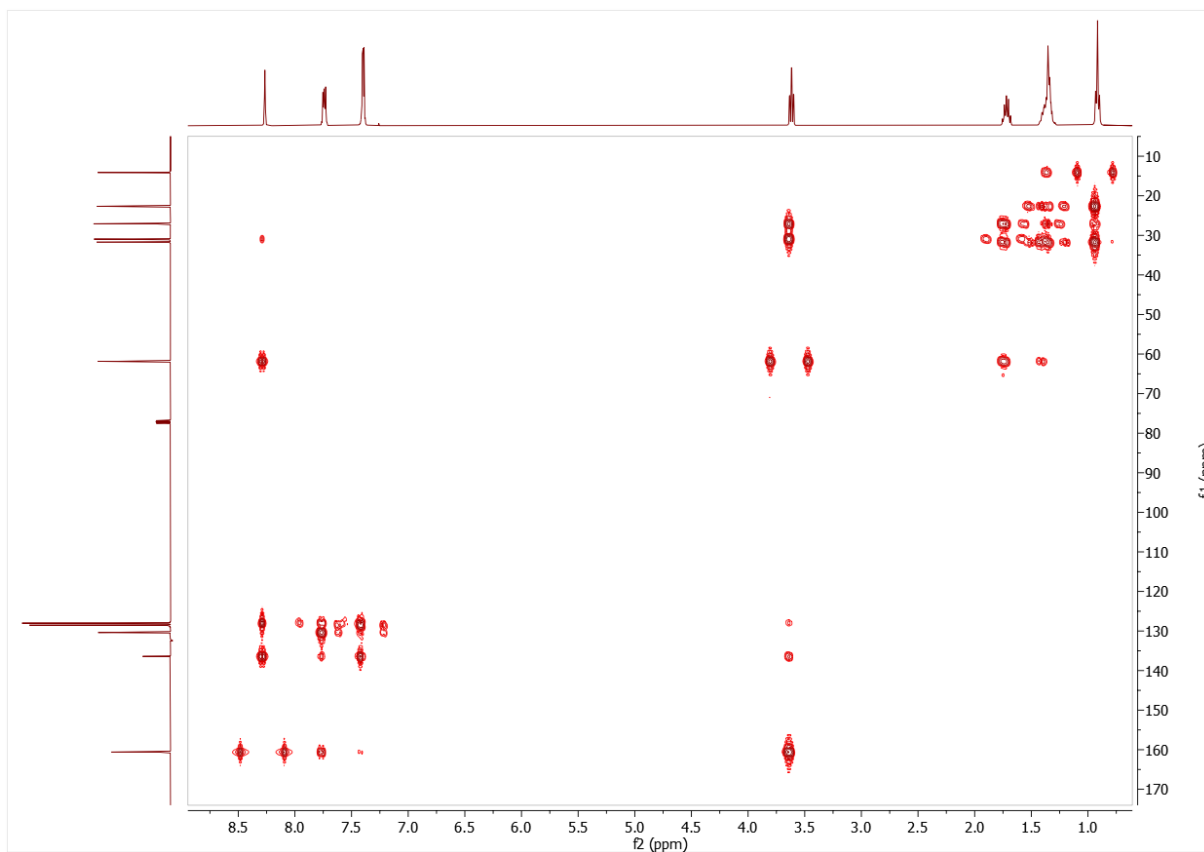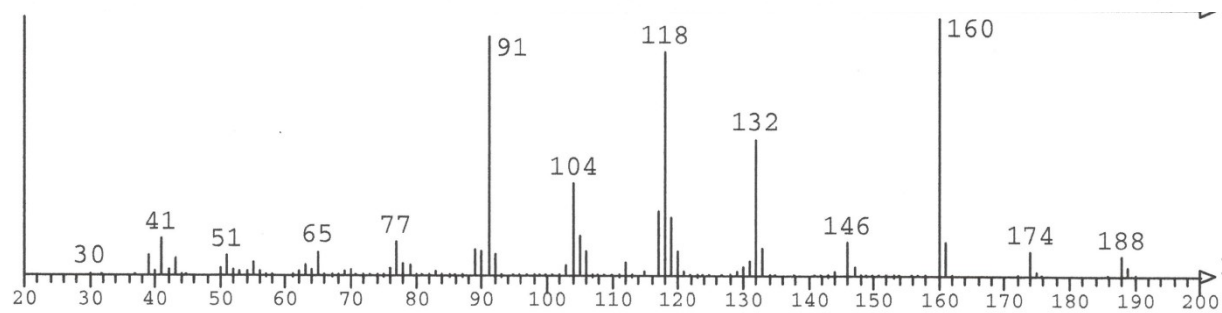
Figure A79. 1H-13C-HMBC- NMR (400 MHz; 101 MHz) spectrum of N-hexyl-1-phenylmethanimine in CDCl$_3$

Figure A80. MS spectrum (EI) of N-hexylbenzamida

8.3.5 Quantification by NMR of amidation experients in table 4.4

8.3.5.1 *N-Hexylbenzamida (example for entries 1 - 5)*
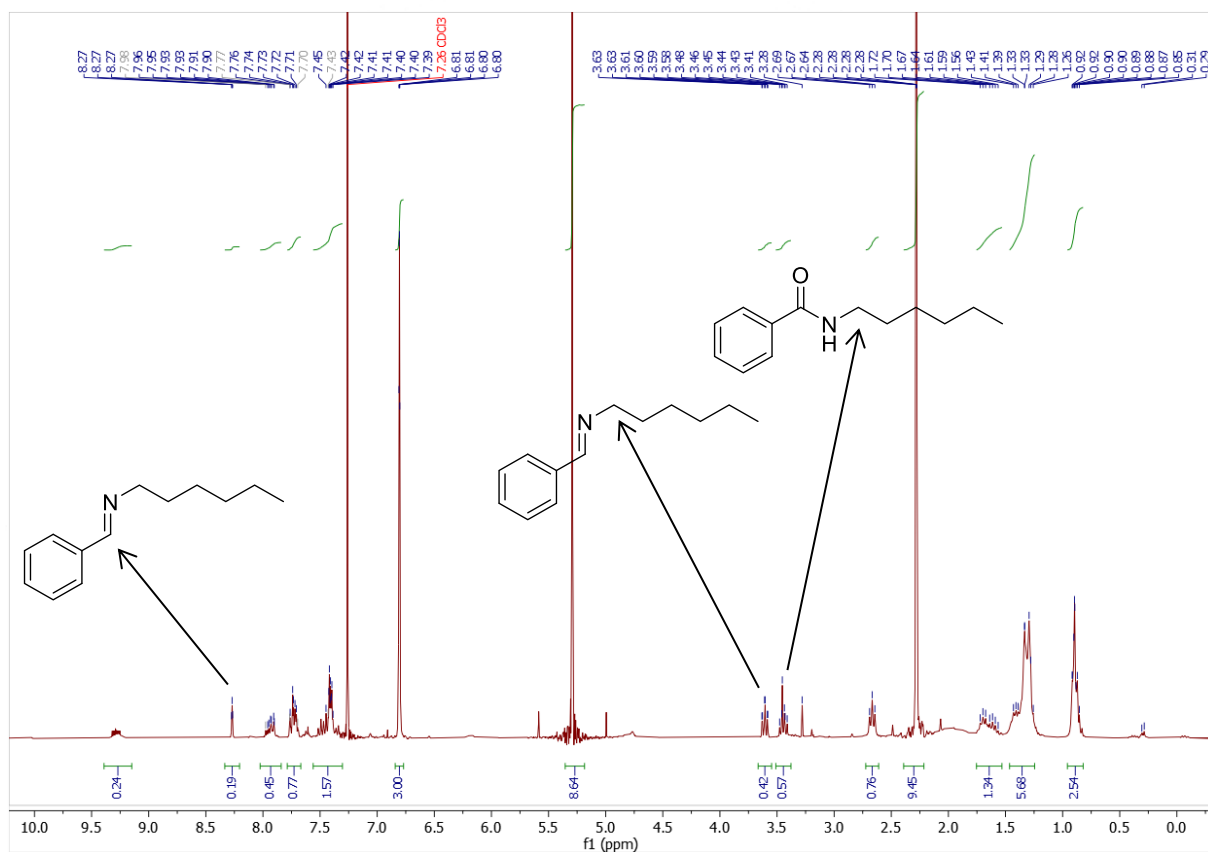
Figure A81. Quantification of N-Hexylbenzamida through ^{1}H NMR (300 MHz) spectrum of reaction mixture after water extraction in CDCl₃
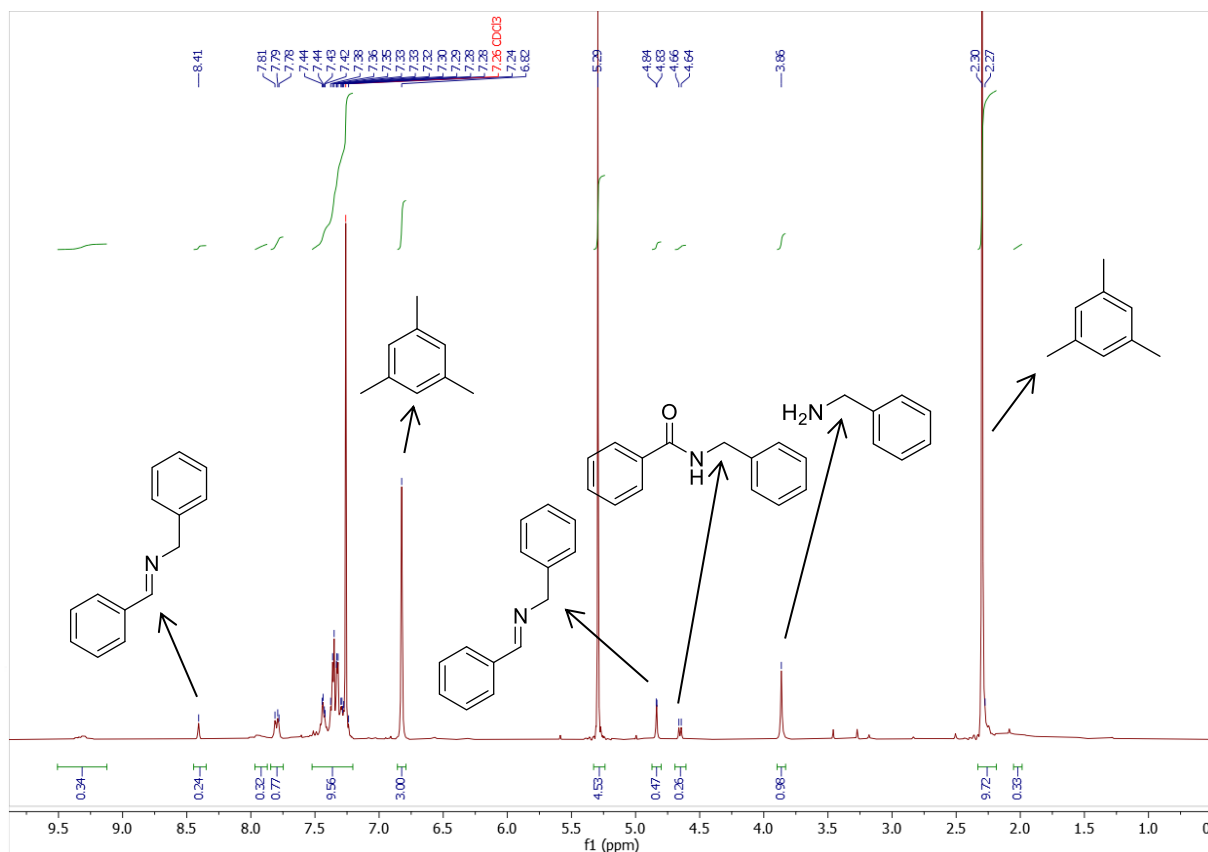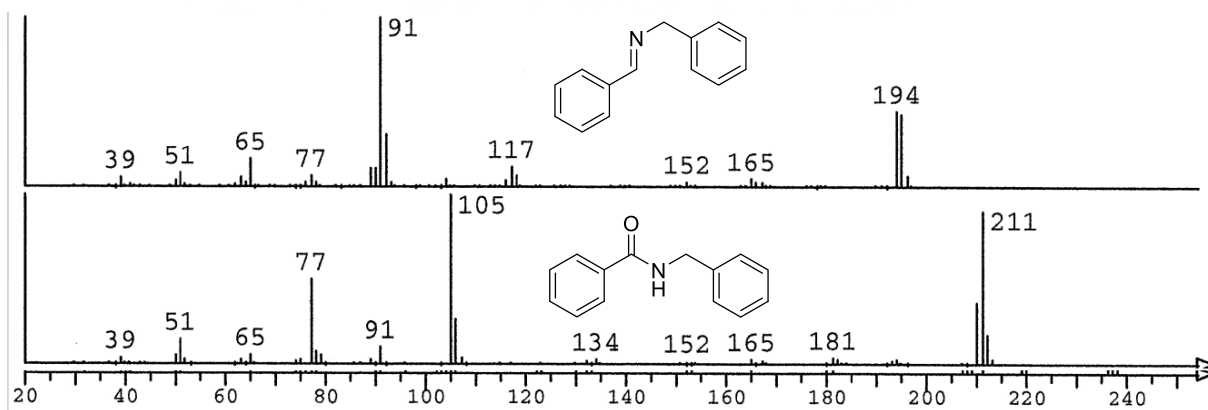
Figure A82. Quantification of N-Benzylbenzamida through ^{1}H NMR (300 MHz) spectrum of reaction mixture after water extraction in CDCl$_3$

Figure A83. MS spectrum (EI) of N-benzylbenzamida and N-benzyl-1-phenylmethanimine
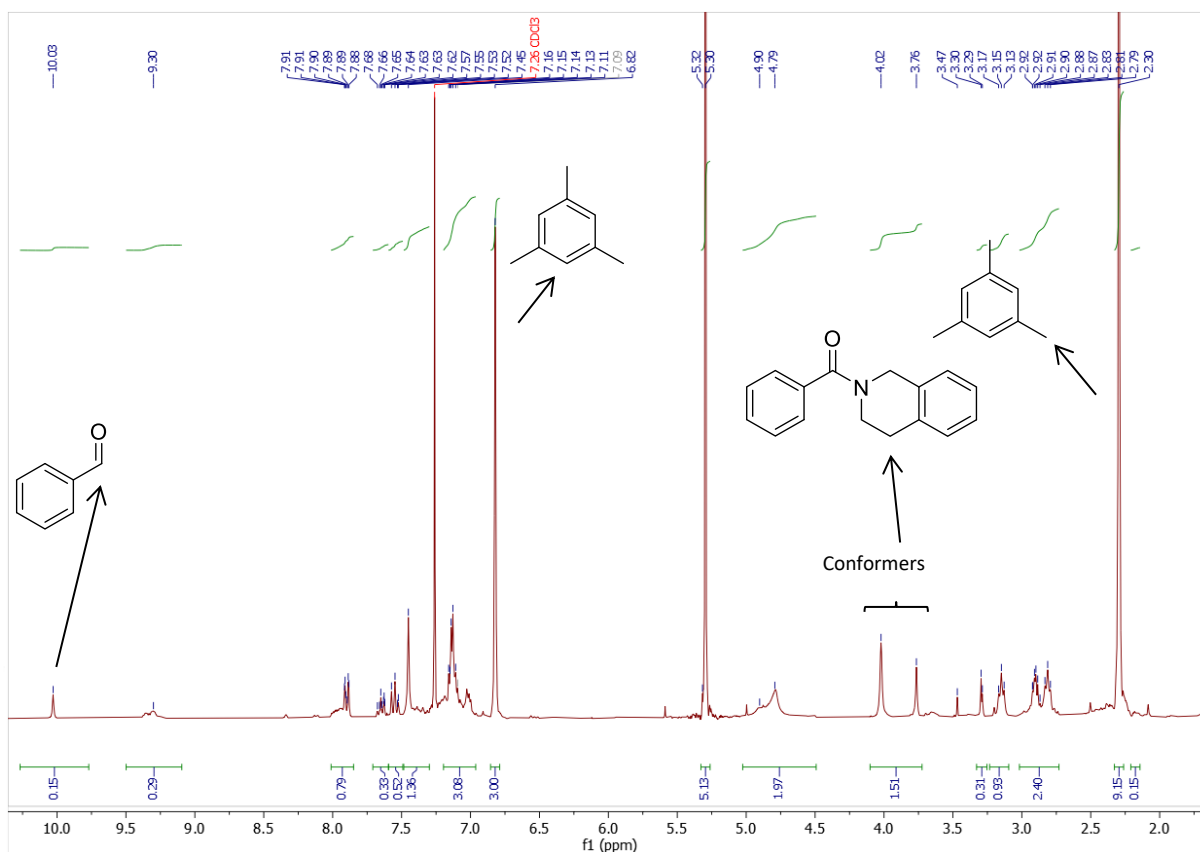
8.3.5.3   *N-Benzoyl-1,2,3,4-tetrahydroisoquinoline (entry 7)*

Figure A84. Quantification of N-Benzoyl-1,2,3,4-tetrahydroisoquinoline through ^{1}H NMR (300 MHz) spectrum of reaction mixture after water extraction in CDCl$_3$
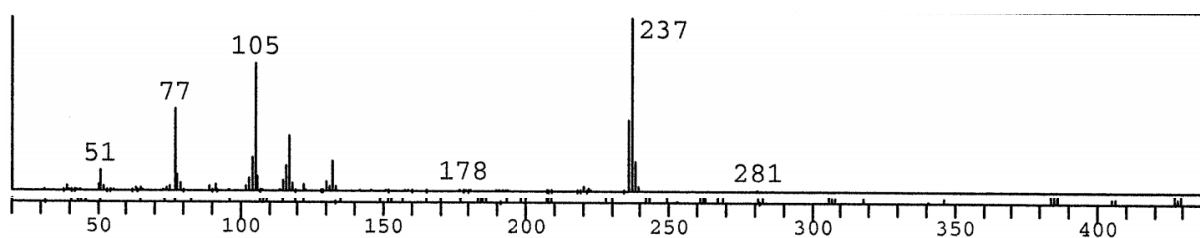

Figure A85. MS spectrum (EI) of N-Benzoyl-1,2,3,4-tetrahydroisoquinoline

8.3.5.4   *N-hexylfuran-2-carboxamide (entry 8)*

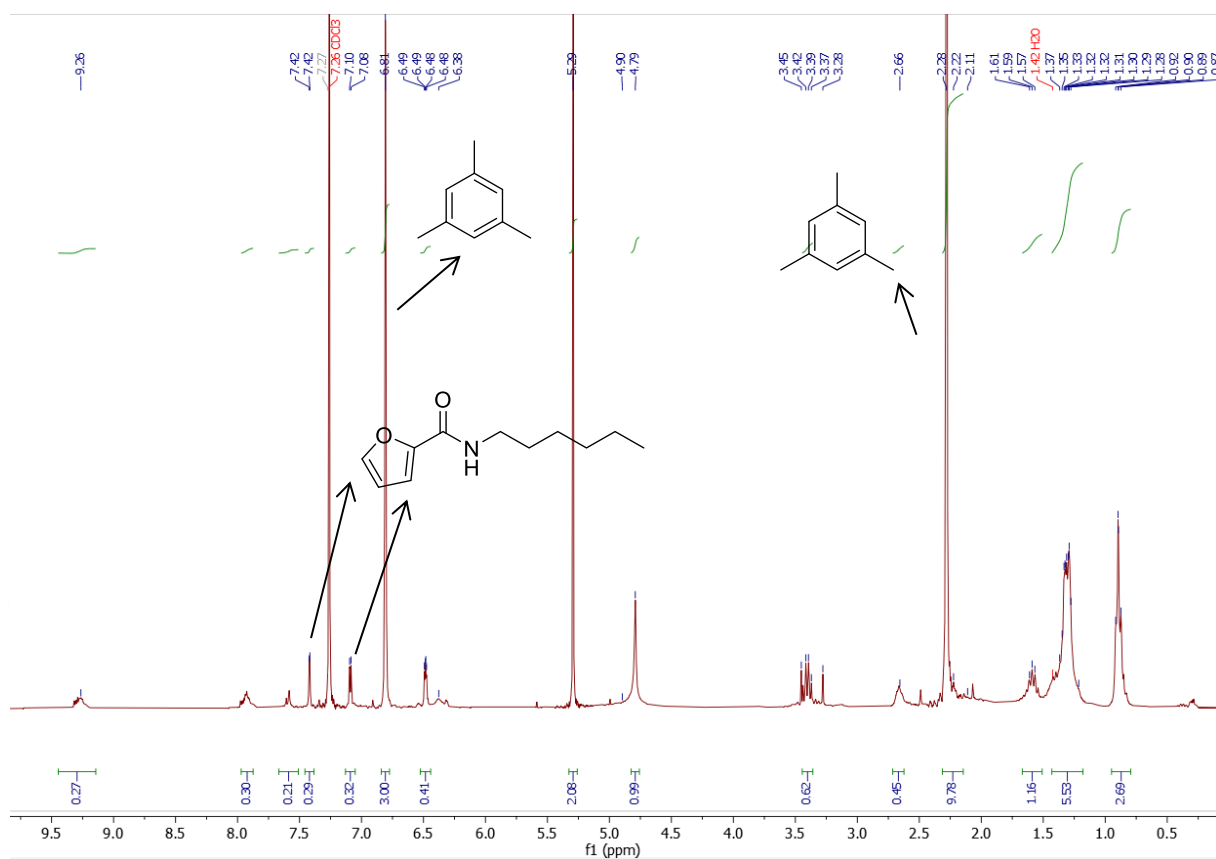**Figure A86.** Quantification of N-hexylfuran-2-carboxamide through ^{1}H NMR (300 MHz) spectrum of reaction mixture after water extraction in CDCl$_3$
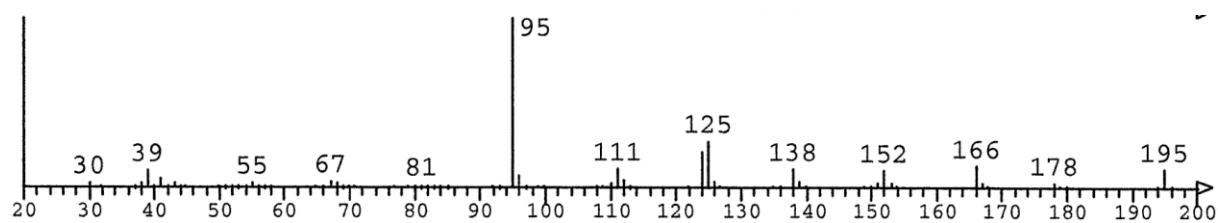

Figure A87. MS spectrum (EI) of N-hexylfuran-2-carboxamide